International Journal of
Molecular Sciences

Special Issue Reprint

Abiotic Stress Tolerance and Genetic Diversity in Plants, 2nd Edition

Edited by
Andrés J. Cortés

mdpi.com/journal/ijms

MDPI

Abiotic Stress Tolerance and Genetic Diversity in Plants, 2nd Edition

Abiotic Stress Tolerance and Genetic Diversity in Plants, 2nd Edition

Guest Editor

Andrés J. Cortés

MDPI

Basel • Beijing • Wuhan • Barcelona • Belgrade • Novi Sad • Cluj • Manchester

Guest Editor
Andrés J. Cortés
Facultad de Ciencias Agrarias—
Departamento de Ciencias Forestales
Universidad Nacional de Colombia—
Sede Medellín
Medellín
Colombia

Editorial Office
MDPI AG
Grosspeteranlage 5
4052 Basel, Switzerland

This is a reprint of the Special Issue, published open access by the journal *International Journal of Molecular Sciences* (ISSN 1422-0067), freely accessible at: https://www.mdpi.com/si/ijms/9Y8E57B7V3.

For citation purposes, cite each article independently as indicated on the article page online and as indicated below:

Lastname, A.A.; Lastname, B.B. Article Title. *Journal Name* **Year**, *Volume Number*, Page Range.

ISBN 978-3-7258-8209-0 (Hbk)
ISBN 978-3-7258-8210-6 (PDF)
https://doi.org/10.3390/books978-3-7258-8210-6

© 2026 by the authors. Articles in this reprint are Open Access and distributed under the Creative Commons Attribution (CC BY) license. The reprint as a whole is distributed by MDPI under the terms and conditions of the Creative Commons Attribution-NonCommercial-NoDerivs (CC BY-NC-ND) license (https://creativecommons.org/licenses/by-nc-nd/4.0/).

Contents

About the Editor . . . . . **vii**

Preface . . . . . **ix**

Andrés J. Cortés
Leveraging Genetic Diversity for Abiotic Stress Tolerance
Reprinted from: *Int. J. Mol. Sci.* **2026**, *27*, 4258, https://doi.org/10.3390/ijms27104258 . . . . . **1**

Shahin Imran, Shuntaro Ono, Rie Horie, Maki Katsuhara and Tomoaki Horie
Chloride-Transporting OsHKT1;1 Splice Variants and Their Expression Profiles Under Salinity Stress in Rice
Reprinted from: *Int. J. Mol. Sci.* **2026**, *27*, 1178, https://doi.org/10.3390/ijms27031178 . . . . . **16**

Sebastián Arenas and Andrés J. Cortés
Unveiling the Genomic Architecture of Phenotypic Plasticity Using Multiple GWAS Approaches Under Contrasting Conditions of Water Availability: A Model for Barley
Reprinted from: *Int. J. Mol. Sci.* **2026**, *27*, 652, https://doi.org/10.3390/ijms27020652 . . . . . **37**

Haozhe Li, Zhibin Sun, Weiye Li, Xiaolong Yin, Xian Xu, Xiaolin Zhang, et al.
Research on Cold Resistance of *Kandelia obovata* Transplanted to Zhoushan Area at the mRNA Level
Reprinted from: *Int. J. Mol. Sci.* **2025**, *27*, 429, https://doi.org/10.3390/ijms27010429 . . . . . **61**

Yuwan Zhao, Shunquan Chen, Mao Qin, Kejuan Shui, Riqing Li, Baoli Yang, et al.
Genome-Wide Identification of *FCS-Like Zinc Finger (FLZ)* Family Genes in Three *Brassica* Plant Species and Functional Characterization of *BolFLZ*s in Chinese Kale Under Abiotic Stresses
Reprinted from: *Int. J. Mol. Sci.* **2024**, *25*, 12907, https://doi.org/10.3390/ijms252312907 . . . . . **82**

Jamie A. O'Rourke and Michelle A. Graham
Investigating the Role of Known Arabidopsis Iron Genes in a Stress Resilient Soybean Line
Reprinted from: *Int. J. Mol. Sci.* **2024**, *25*, 11480, https://doi.org/10.3390/ijms252111480 . . . . . **103**

Prasit Khunsanit, Kitiporn Plaimas, Supachitra Chadchawan and Teerapong Buaboocha
Profiling of Key Hub Genes Using a Two-State Weighted Gene Co-Expression Network of 'Jao Khao' Rice under Soil Salinity Stress Based on Time-Series Transcriptome Data
Reprinted from: *Int. J. Mol. Sci.* **2024**, *25*, 11086, https://doi.org/10.3390/ijms252011086 . . . . . **120**

Xiaolin Yin, Qinmei Gao, Feng Wang, Weihao Liu, Yiting Luo, Shuixiu Zhong, et al.
Marker-Assisted Selection of Jacalin-Related Lectin Genes *OsJRL45* and *OsJRL40* Derived from Sea Rice 86 Enhances Salt Tolerance in Rice
Reprinted from: *Int. J. Mol. Sci.* **2024**, *25*, 10912, https://doi.org/10.3390/ijms252010912 . . . . . **142**

Qi Wang, Jianzhong Wu, Guili Di, Qian Zhao, Chao Gao, Dongmei Zhang, et al.
Identification of Cold Tolerance Transcriptional Regulatory Genes in Seedlings of *Medicago sativa* L. and *Medicago falcata* L.
Reprinted from: *Int. J. Mol. Sci.* **2024**, *25*, 10345, https://doi.org/10.3390/ijms251910345 . . . . . **167**

Shugao Fan, Linyan Jia, Jiawei Wu and Ying Zhao
Harnessing the Potential of CRISPR/Cas in Targeted Alfalfa Improvement for Stress Resilience
Reprinted from: *Int. J. Mol. Sci.* **2025**, *26*, 3311, https://doi.org/10.3390/ijms26073311 . . . . . **188**

About the Editor

Andrés J. Cortés

Andrés J. Cortés holds an Associate Professorship in Forest Geneticist at Universidad Nacional de Colombia - Sede Medellin. He graduated as Plant Geneticist (PhD) from Uppsala University (Sweden), and as Biologist (BSc Hons; MSc) from Universidad de los Andes (Colombia). His research experience spans the International Center for Tropical Agriculture (CGIAR–CIAT), the University of Fribourg (Switzerland), the Swiss Federal Institute for Forest, Snow and Landscape Research (WSL–SLF), the Swedish University of Agricultural Sciences (SLU), and the Colombian Agricultural Research Corporation (AGROSAVIA).

Andrés J. Cortés is interested in investigating the genetic adaptive potential in trees and plants of agroecological interest using genomic, evolutionary, and ecological tools. In particular, he has explored rootstock-mediated inheritance in avocado and cacao trees, genetic adaptation to climate change in willow species, abiotic stress tolerance and genetic diversity in beans, and adaptive diversification across various plant lineages at the Páramo—a rapidly-evolving ecosystem that provides water resources to the Neotropics.

Preface

In the imminent fate of climate change, the timing of this Reprint, the second edition of the Special Issue "Abiotic Stress Tolerance and Genetic Diversity in Plants", is pertinent, as it advances our understanding of the genetic bases of tolerance to abiotic stresses, which may be utilized to breed more resilient plant populations. This Reprint would certainly not have been possible without the interest and commitment of all the authors and reviewers.

Andrés J. Cortés
Guest Editor

International Journal of
Molecular Sciences

MDPI

Editorial

Leveraging Genetic Diversity for Abiotic Stress Tolerance

Andrés J. Cortés

Facultad de Ciencias Agrarias—Departamento de Ciencias Forestales, Universidad Nacional de Colombia—Sede Medellín, Medellín 050034, Colombia; ancortesv@unal.edu.co

Climate-change-driven abiotic stresses, once regarded as episodic constraints for major staple crops, are now main selective forces driving the agronomic and evolutionary trajectories of plants [1]. Increasing climatic variability has been manifested in the last decade as recurrent and extreme droughts [2], heatwaves [3], and cold fronts [4–7], which together are pushing crops and natural populations toward the limits of their plastic [8] and adaptive capacity [9]. Plant breeding and management efforts have buffered some of these challenges [10,11], yet they have often relied on relatively narrow genetic bases and a reductionist set of productive [12] and eco-physiological functional traits [13]. Since this standing variation is insufficient to cope with the rapid pace of environmental change [14,15], an urgent expansion in the repertoire of nature-based solutions is demanded. In particular, boosting abiotic stress tolerance would benefit by expanding the classical recurrent trait improvement cycle and germplasm mobilization approaches to encompass a high-throughput exploration and introgression of hidden allelic variation [16], as well as genetic forecasting of the adaptative [17] and conversation potentials [18–21]. For that, modern and more integrated molecular, ecological, computational, and trait discovery and screening approaches must be envisioned [22]. In order to help bridge this gap, this second edition of the Special Issue "Abiotic Stress Tolerance and Genetic Diversity in Plants" has assembled nine contributions, spanning a rich variety of scales, from gene networks to population-level studies. This compilation reinforces the fact that abiotic stress tolerance is a complex, multi-dimensional, polygenic, and environmentally dependent abstractable property [23], rather than a simple predefined phenotype encoded by few deterministic genes with major effects. While abiotic stresses impact plant productivity and survival under climate change, genetic and omic platforms are converging to reshape strategies for breeding more resilient crops and maintaining species ecosystem services.

1. Molecular and Transcriptomic Bases of Abiotic Stress Responses

Understanding how plants perceive, process, and respond to abiotic stress at the molecular level remains a central challenge for advancing climate-resilient agriculture and conservation strategies [24]. Rapid progress in transcriptomics, comparative genomics, and systems biology has enabled a shift from single-gene studies to family- and network-based assessments, revealing the complex regulatory architectures that underlie stress adaptation [9,25]. These approaches are capable of uncovering cryptic functional variation within wild relatives [26], locally adapted germplasm [27,28], and polyploid genomes [29]—sources of innovation that, until very recently, have been systematically deployed into breeding and conservation programs. As discussed below, gene family evolution, functional validation, and temporal expression dynamics help to determine how transcriptional regulation shapes plant responses to environmental pressures [30–32].

As a first case study that goes beyond primary gene pools, the contribution by Wong et al. [33] investigates cold tolerance response mechanisms by comparing cultivated alfalfa (*Medicago sativa*) with its wild relative *Medicago falcata*. The authors expose seedlings of both species to low-temperature treatment (4 °C) as well as to control conditions, and analyze leaf tissues at defined time points using RNA-seq, differential gene expression, and transcription factor enrichment analyses. The results show that *M. falcata* exhibits a broader transcriptional response with significantly more differentially expressed genes (DEGs) and enrichment in key regulatory families such as bHLH, ARR-B, and AP2/ERF [34–39]. The authors conclude that wild germplasm harbors a richer regulatory network for stress response than its cultivated counterparts, suggesting that domestication has eroded the diversity of stress-responsive pathways. It also illustrates how comparative transcriptomics uncover functionally relevant regulatory variation, reinforcing the importance of integrating wild genetic resources aimed at enhancing resilience.

Similarly, but this time looking into locally adapted germplasm, O'Rourke and Graham [40] provide a compelling example of how stress-resilient crop provenances can harbor novel adaptive mechanisms that are not predictable from model species. Focusing on soybean (*Glycine max*), the authors investigate the function of three iron deficiency response genes—FIT, HY5, and PYE—in the iron-deficit-tolerant Swedish line Fiskeby III (PI 438471), using virus-induced gene silencing combined with RNA-seq analyses under iron-sufficient and iron-deficient conditions. Strikingly, while silencing FIT and HY5 alters broader stress-responsive transcriptional networks, it does not compromise iron deficiency tolerance, demonstrating that this genotype relies on alternative, previously uncharacterized, genetic pathways to cope with iron scarcity. These findings challenge the widespread assumption that stress tolerance mechanisms are conserved across species, and highlight the limitations of extrapolating from model organisms such as *Arabidopsis thaliana*. Instead, the study encourages exploring crop-specific and locally adapted germplasm to uncover hidden sources of genetic diversity for stress resilience.

In a more temporal expression context, Khunsanit and collaborators [41] leverage time-series transcriptomics and network-based approaches to dissect the molecular basis of salinity tolerance in rice (*Oryza sativa*), focusing on the salt-tolerant Thai variety 'Jao Khao'. Using 36 RNA-seq libraries sampled across six time points (0–48 h) under 160 mM NaCl, the authors construct a two-state weighted gene co-expression network that enables the identification of 1950 highly variable genes and 111 key hub genes associated with the salt stress response. These hub genes were enriched in pathways related to energy metabolism, photosynthetic light reactions, ATP synthesis, and transport processes, with early upregulation during the initial phases of salt stress, a pattern further validated by qRT-PCR for key genes such as RuBisCo and ATP synthase. The study demonstrates that rapid metabolic reprogramming, particularly the management of cellular energy balance, is transversal to stress adaptation. It also demonstrates how merging integrative transcriptomic and systems biology frameworks across the temporal continuum uncover functionally relevant candidate gene targets to harness abiotic stress responses in crops.

Finally, Zhao and collaborators [42] offer a comprehensive genome-wide characterization of the *FCS-like zinc finger (FLZ)* gene family, implied in stress responses as well as plant development and senescence, across three *Brassica* species, identifying 113 genes and revealing their expansion largely driven by whole-genome duplication events, well-studied events in *Brassica* genome evolution. Through integrative phylogenomic, collinearity, and expression analyses, combined with protein–protein interaction assays, the study demonstrates that a subset of these genes (i.e., seven out of 15 tested) shows significant responsiveness to abiotic stresses, while many FLZ proteins interact with central energy-sensing kinases (SnRK1), highlighting a conserved regulatory module linking stress signaling and metabolic control.

https://doi.org/10.3390/ijms27104258

Overall, these studies offer a genome-wide functional exploration of stress-responsive genetic mechanisms in plants, highlighting how integrated approaches can uncover candidate genes linked to abiotic stress resilience [43,44]. The works combine high-throughput genomic screening and expression profiling under stress conditions, which enables authors to identify key gene families exhibiting differential regulation and potential roles in adaptive responses [45–47], while also revealing patterns of gene duplication and structural diversification responsible for functional innovation [48]. The studies move beyond descriptive genomics after linking molecular signatures and expression profiles to stress-related pathways, thereby contributing to a more mechanistic understanding of how plants perceive and respond to climate pressures, even at local scales [49,50]. They also exemplify how modern bioinformatics and molecular biology tools can reveal previously hidden layers of genetic diversity, both at the population and the polyploid genomic levels, offering promising targets for molecular breeding and the customization of climate-resilient populations [51]. Ultimately, these studies reinforce the value of integrating genomic, functional, and evolutionary analyses to unlock adaptive potential in plants [52].

2. Transitioning from Functional Bases to Targeted Gene Editing

Based on the molecular and transcriptomic understanding outlined above, the natural next step is to functionally validate and bioengineer the causal variants that are responsible for abiotic stress responses [53]. While genome-wide expression and comparative evolutionary analyses of major gene families have been key in identifying candidate genes and regulatory networks [54], they are often limited in terms of determining how specific alleles, isoforms, or regulatory elements translate into phenotypic resilience. Recent advances in functional genomics are beginning to bridge this gap by combining fine-scale molecular characterization with experimental validation across heterologous systems and genome editing platforms. These approaches not only disclose previously overlooked layers of variation—such as alternative splicing or regulatory sequence diversity—but also enable their direct manipulation for plant improvement. That said, the following studies illustrate how moving from gene discovery to mechanistic validation and targeted intervention enable a first approach to utilizing cryptic adaptive potential, accelerating the deployment of stress-resilient traits, and reinforcing the convergence of molecular biology, biotechnology, and breeding in the face of escalating abiotic challenges [55].

Illustrating the first scenario, Imran et al. [56] study functional variation in the sodium transporter *OsHKT1;1* for salt tolerance in rice (*Oryza sativa*). The authors test two splicing variants across three heterologous systems (i.e., plant cells, yeast, and *Xenopus oocytes*) using subcellular localization, ion flux measurements, and gene expression analyses. The team demonstrate that splicing variants differ in ion selectivity and transport efficiency, offering a cryptic source of variation for crop improvement. After all, not only gene presence, but also alternative splicing contributes to plasticity, expanding the functional repertoire of key transporters involved in ion homeostasis.

Meanwhile, at the frontiers of gene editing, Fan and collaborators [57] reviewed CRISPR/Cas-based genome editing [58,59] in alfalfa (*Medicago sativa*), a key forage crop with historically underexploited genomic resources. The work summarizes how merging conventional breeding with emerging genomic, transcriptomic, and functional studies enable identifying candidate genes and pathways associated with traits such as nutrient use efficiency and freezing tolerance, among other abiotic stress responses. The synthesis prospects multiplex gene editing, regulatory region targeting, and trait engineering strategies to boost these candidate targets. The authors claim that while genome editing enables precise manipulation of stress-related genes, challenges remain in transformation efficiency and the complexity of polygenic traits. They conclude that genome editing with a systems-level understanding would enhance abiotic stress tolerance [60–62].

https://doi.org/10.3390/ijms27104258

The convergence of molecular biology, genomics, and biotechnology fast-track plant improvement, particularly under relatively simple Mendelian genetic architectures underlying abiotic stress responses [63,64]. However, these efforts, while useful at identifying and manipulating individual target functional variants [65], demand an understanding of how such molecular bases perform across more complex polygenetic and environmentally conditioned scenarios [66,67]. In other words, while functional validation and genome editing provide unprecedented precision to customize stress-responsive pathways [68], their ultimate impact will depend on integrating these advances within frameworks that explicitly account for genotype-by-environment interactions [69,70] and phenotypic plasticity [71], as discussed in the next section. In this sense, a catalog of functionally characterized and gene-edited alleles represents only one component to achieve resilience in plants, since the former must be contextualized within diverse environmentally conditioned responses [72–75] and broader phylogenetic backgrounds [76–78]. Bridging this gap requires moving beyond controlled model systems toward strategies that harness both bioengineered variation and naturally occurring adaptive diversity for pre-breeding [79] and conservation initiatives [80].

3. Plastic and Adaptive Responses for Climate-Resilient Breeding

The previous works exemplify how the evolutionary diversification across hidden layers of genetic redundancy and functional specialization can harbor adaptive potential to cope with environmental stressors, providing a repertoire of candidate genes for molecular breeding. Additionally, while advances in functional genomics and genome editing are rapidly improving our ability to identify and manipulate some of these variants, their ultimate value depends on how effectively these efforts can be translated into reliable and deployable plant populations under current environmental variability. In this context, phenotypic plasticity forecasting [17,81] and pre-breeding efforts to mobilize alleles from locally adapted germplasm to elite backgrounds [82] are required to handle the intrinsic genotype-by-environment interaction that more deterministic molecular models often overlook. Rather than viewing environmental-dependent responses as a limitation, emerging frameworks now recognize plastic clines as genetically controlled [83], selectable traits that can be harnessed to enhance resilience across heterogeneous and shifting climates [84]. At the same time, stress-adapted populations thriving in extreme or marginal environments provide access to cryptic allelic variation that is largely absent from elite breeding gene pools [85]. The following studies illustrate how integrating genotype-by-environment interactions and pre-breeding-oriented approaches can bridge the gap between functional discovery and application, ultimately enabling the development of plant populations and varieties able to cope with increasing abiotic pressures.

In an first effort to understand the genomic bases of phenotypic plasticity, Arenas and Cortés [86] re-studied drought-induced phenotypic plasticity in barley (*Hordeum vulgare*) using a diversity panel of 1277 genotypes evaluated under contrasting water regimes (i.e., well-watered vs. drought conditions). Using five plasticity indices and four genome-wide association study (GWAS) models, the authors identified 239 significant SNPs, including 27 within coding regions. Notably, many loci exhibited context-dependent antagonistic pleiotropy, where allelic effects differed across environments. Therefore, the study was able to conclude that plasticity is genetically controlled and environment-dependent, challenging traditional breeding strategies that assume stable allele effects. The work moves beyond single-locality mapping to explicitly model genotype-by-environment interactions, offering a conceptual and methodological framework for integrating phenotypic plasticity into genomic prediction and breeding strategies. Once these contrasting genetic responses are understood, they can be utilized to unlock hidden adaptive potential for crop improvement under increasingly variable water availability [87].

Meanwhile, the work by Yin et al. [88] advances the deployment of cryptic genetic diversity within a pre-breeding framework by demonstrating how salt-stress-adapted germplasm can be harnessed for crop improvement through molecular breeding. Focusing on rice, the authors identify and functionally validate two jacalin-related lectin genes—*OsJRL45* and *OsJRL40*—derived from the stress-resilient "Sea Rice 86" genotype, showing that their marker-assisted introgression significantly enhances salt tolerance. Because this study integrates gene expression analyses under salinity stress with breeding-oriented validation, it bridges the gap between gene discovery and downstream applications, highlighting lectin-mediated pathways as key components of stress response networks. Importantly, this work exemplifies how underutilized germplasm pre-adapted to or extreme environments harbors adaptive alleles absent from conventional breeding gene pools and how modern genomic tools can accelerate their deployment. In doing so, the study reinforces the importance of coupling functional genomics with marker-assisted selection to unlock hidden reservoirs of abiotic stress tolerance, providing a practical roadmap for developing resilient crop varieties in the face of increasing soil salinization.

Together, these two studies highlight the fact that climate-resilient breeding not only requires identifying exotic superior genotypes and alleles [89] and reconstructing the molecular mechanism responsible for that superiority [90], but also urge an understanding of how those networks are reshaped across environmental contexts [91,92] and genetic backgrounds [93,94]. Once phenotypic plasticity, genotype-by-environment interactions, and stress-adapted germplasm are explicitly incorporated into breeding pipelines, it would be possible to transcend beyond single-trait plant improvement strategies toward more predictive frameworks of the adaptative potential. These same principles spread beyond crops, as the identification and mobilization of context-dependent adaptive variation help sustain resilience in natural populations under rapid environmental change.

4. Leveraging Abiotic Stress Tolerance in Natural Populations

Moving beyond crop breeding applications, which tend to occupy a major focus in the abiotic stress tolerance literature, the same conceptual and methodological workflows used to study and harness cryptic adaptive variation and its environmental dependency can be extended to natural populations facing rapid environmental change. As climate pressures intensify, conservation [95], restoration [96], and assisted migration [97] and gene flow [98,99] efforts increasingly rely on identifying and mobilizing adaptive variation already present in wild and marginal plant populations. In this context, integrating genomics, transcriptomics, and *in situ* ecological data offers a powerful avenue to uncover how non-model and perennial species respond to abiotic stress across their range.

In a first effort in this line, Li et al. [100] examine cold tolerance in a mangrove species (*Kandelia obovata*) by comparing a reference cold-sensitive population and its transplanted counterpart to higher-latitude environments, revealing adaptive responses in a coastal woody plant under novel climatic conditions. The authors perform RNA-seq, differential expression analysis, SNP identification, and transcription factor prediction to identify DEGs under chilling stress. Their analyses reveal the enrichment of pathways related to phenylpropanoid biosynthesis, carbohydrate metabolism, and plant hormone signaling, alongside the differential regulation of key transcription factor families such as NAC, MYB, WRKY, and ERF [101–104], all of which are central to stress signaling networks. The work highlights that both genetic and post-transcriptional mechanisms underlie cold adaptation. Integrating experimental *in situ* population surveys with transcriptomic and functional analyses enables an understanding of how perennial species rely on regulatory strategies to expand their ecological niche, complementing the genomic basis of stress tolerance in non-model systems and reinforcing the importance of leveraging ecologically relevant germplasm for conservation and restoration under shifting temperature regimes.

Natural populations offer not only reservoirs of biodiversity, but also repositories of adaptive potential shaped by local environmental pressures [55]. Merging multi-omics screenings [105] with ecological and geographic metadata allows for the identification and mobilization of standing adaptive variation as part of conservation, restoration, and assisted adaptation strategies [106]. All compiled efforts (Table 1) deepen our understanding of the evolutionary genomic basis of local adaptation, while providing applied tools for conserving the genetic diversity that underlies abiotic stress tolerance, maintaining ecosystem resilience, and guiding targeted interventions under shifting climatic regimes.

Table 1. Synthesis of the nine contributing studies to the Special Issue "Abiotic Stress Tolerance and Genetic Diversity in Plants" in its second edition. The table is ordered as per the narrative. Abbreviations: DEGs stand for differentially expressed genes, others are already declared within the table.

Species Group	Study Goal	Sampling	Omics Technologies	Key Findings	Reference
Cultivated alfalfa (*Medicago sativa*) & its wild relative (*Medicago falcata*)	Assess cold tolerance mechanisms in cultivated and wild seedlings	Expression screening 24 h and 120 h after low-temperature (4 °C)	RNA-seq	Wild *M. falcata* has broader transcriptional response with more DEGs	Wong et al. [33]
Soybean (*Glycine max*)	Validate three iron deficiency response genes (i.e., FIT, HY5 and PYE)	Iron-deficit-tolerant Swedish line Fiskeby III (PI 438471)	Virus-induced gene silencing and RNA-seq	Silencing FIT and HY5 does not compromise iron deficiency tolerance	O'Rourke and Graham [40]
Rice (*Oryza sativa*)	Dissect the molecular bases of salinity tolerance in rice	Salt-tolerant Thai variety 'Jao Khao'	RNA-seq libraries sampled across six time points (0–48 h)	A total of 1950 variable and 111 hub genes linked with the salt tolerance	Khunsanit et al. [41]
Chinese kale (*Brassica oleracea* L. var. *alboglabra*)	Characterize abiotic stress response of *FCS-like zinc finger (FLZ)* genes	Chinese kale (*B. oleracea*), cabbage (*B. rapa*) and black mustard (*B. nigra*)	Phylogenomic, expression analyses, and protein–protein assays	FLZ proteins interact with central energy-sensing kinases (SnRK1)	Zhao et al. [42]
Rice (*Oryza sativa*)	Study variation in the sodium transporter *OsHKT1;1* for salt tolerance	Two splicing variants across three heterologous systems	Subcellular localization and expression analyses	Splicing variants differ in ion selectivity and transport efficiency	Imran et al. [56]
Alfalfa (*Medicago sativa*)	Review CRISPR/Cas in alfalfa for abiotic stress tolerance	Literature review	Genomics and transcriptomics	Systems-level genome editing benefits abiotic stress tolerance	Fan et al. [57]
Barley (*Hordeum vulgare*)	Reconstruct the genomic bases of plasticity to drought stress	Genotypes (1277) evaluated under well-watered vs. drought conditions	Five plasticity indices and four genome-wide association study (GWAS)	Drought stress plasticity is genetically and environment-dependent	Arenas and Cortés [86]
Rice (*Oryza sativa*)	Validate two genes (*OsJRL45* and *OsJRL40*) for salt stress tolerance	Salt stress-adapted "Sea Rice 86" and recombinant inbred lines (RILs)	RT-qPCR, yeast two-hybrid and bimolecular fluorescence	Marker-assisted introgression in RILs enhances salt tolerance	Yin et al. [88]
Mangrove (*Kandelia obovata*)	Examine cold tolerance in a cold-sensitive mangrove species	Cold-sensitive population transplanted to higher-latitude climates	RNA-seq	Genetic and post-transcriptional mechanisms underlie cold adaptation	Li et al. [100]

5. Perspectives

Taken together, the contributed studies on abiotic stress tolerance in plants reveal that the field is advancing rapidly in technical capacity but still grappling with conceptual, translational [107], and cross-disciplinary challenges [108,109]. A major persistent gap is the scale mismatch between molecular network discovery and ecological deployment. While transcriptomic experimental studies with moderate sample sizes provide high-resolution temporal snapshots of molecular stress responses, they capture only a fraction of the environmental variability experienced in the field. On the other hand, observational population-level analyses on hundreds and thousands of genotypes disclose complex genotype-by-environment interactions that are difficult to reconcile with epigenetic screening under controlled conditions. Bridging these scales together under the same lens would require experimental designs that integrate controlled setups with field-based validation [110] across environmental gradients [111,112] (Figure 1).

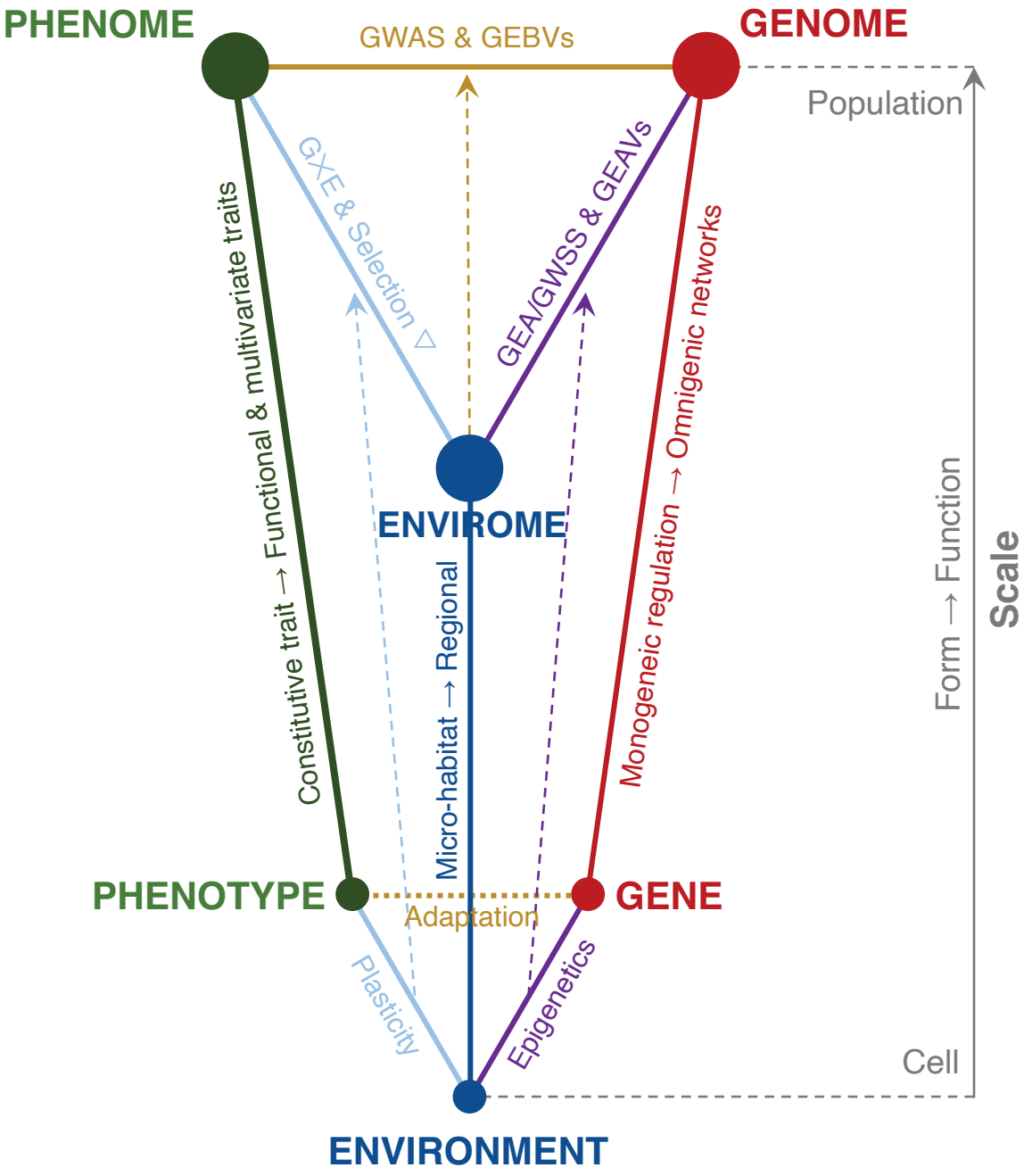


Figure 1. Conceptual framework depicting a tridimensional plant breeding triangle projected across spatial scales to leverage genetic diversity for abiotic stress tolerance under climate change. The diagram

links the environment in which the plant experiences abiotic stress, the phenotypic variation that shapes tolerance, and the corresponding standing genetic variation enabling such plant responses. Together, these axes contextualize how environment–genotype–phenotype relationships interplay across spatial scales. The vertical dimension represents biological spatial organization, spanning from micro-habitats to regional climatic gradients for the environmental axis, from cellular monogenic processes to population-level polygenic dynamics for the genetic axis, and from a single constitutive trait to multivariate functional traits for the phenotypic axis. For instance, *(i)* the abstraction of the environment is no longer a discretization into few localities and climatic variables, but instead is currently acknowledging its continuum nature across space and environmental layers (i.e., envirome) through the enviromics paradigm. Similarly, *(ii)* at the molecular level, the transition from a monogenic understating to omnigenic regulatory networks implies that abiotic stress responses are now being recognized as governed by complex, interconnected gene systems rather than single major-effect loci, yet identifying some of the latter are still necessary for more targeted gene editing and biotechnological applications. The more complex poly/omnigenic level can jointly be attributed to coding variation, regulatory elements, and epigenetic modifications, as well as post-transcriptional processes such as alternative splicing, all of which account for the missing heritability of the more monogenic models. These molecular interactions collectively define the functional genome, which interacts with environmental stresses and the envirome to regulate a cascade of transcriptional and metabolic responses with implications on the tolerant phenotype. Finally, moving upward in scale, *(iii)* the phenomic axis depicts a continuum from constitutive traits to complex multivariate phenotypes that integrate developmental, physiological, and morphological functional responses. Such phenomic responses are shaped by phenotypic plasticity and genotype-by-environment (G $\times$ E) interactions, with the first mediating short-term acclimation through transgenerational epigenic inheritance and the second contributing to long-term adaptive potential, all of which serve as conceptual processes linking phenotype and environment (i.e., plasticity), phenotype and genotype (i.e., adaptation), and genotype and environment (i.e., epigenic responses). The framework also invites incorporating technical approaches and models borrowed from the plant breeding and eco-evolutionary disciplines capable of helping integrate all three axes. Specifically, analytical techniques such as genome-wide association studies (GWASs), genome–environment associations (GEAs), genome-wide selection scans (GWSSs), and genomic prediction and its corresponding genomic estimated breeding (GEBVs) and adaptive (GEAVs) values, enable the genomic architecture of stress tolerance (i.e., GWAS as a bridge between the phenotypic and genomic axes) and polygenic adaptation (i.e., GEA, GWSS and GEAVs as a link between the environmental and genomic axes) to be dissected and utilized to forecast climate change responses (i.e., GEBVs and GEAVs, respectively linking the phenotypic and environmental axes with the genetic axis). The cutting-edge integration of these approaches not only allow allelic variants and genomic regions associated with both functional trait performance and environmental adaptation to be identified, but also facilitate their deployment into pre-breeding and conservation programs. In parallel, the environmental filtering of functional phenotypes through natural and artificial selection can be assessed respectively using selection gradient and G $\times$ E analyses, unifying the phenomic and environmental dimensions. Last, the bidirectional feedback among phenotype, genotype, and environment reinforces the fact that adaptive responses to abiotic stresses are not solely a function of genetic determinants, but also of context-dependent expression and ecological interactions. This reflects the shift to a systems-level multi-dimensional understanding of abiotic stress tolerance, advocating for the integration of multi-omics data (e.g., genomics, transcriptomics, phenomics, and enviromics) with theorical developments from the ecological, evolutionary, and plant breeding fields. More importantly, by bridging scales (from genes to ecosystems) and processes (from molecular function to population adaptation), the roadmap offers a valuable guideline to harness cryptic genetic diversity for abiotic stress tolerance under rapid climate change in both crops and natural plant populations.

A second challenge lies in the fragmentation of multi-omics data. While individual studies employ transcriptomics, GWASs, or functional assays, few integrate these layers into cohesive predictive models. For example, candidate SNPs derived from GWAS models are not always directly linked to expression profiles or metabolic pathways, limiting their interpretability [113,114]. Similarly, so far, efforts to utilize transcriptomic signatures into predictive breeding frameworks are scarce. This dichotomy translates into a conceptual tension between reductionist and systems-level functional studies, which together would provide mechanistic clarity at the level of individual gene families and metabolic pathways, and population genomics assessments, capable of revealing highly polygenic environmental-dependent architectures. Reconciling these paradigms requires moving toward omnigenic reconstructions and network-based functional validation [115], where multiple genes and pathways are accounted for simultaneously. Merging multi-omics [116] and environmental data, across spatial, temporal and evolutionary scales [117,118], is now being assisted by machine learning and systems biology workflows [119–122].

Meanwhile, the compiled studies report a persistent underutilization of secondary gene pools, wild resources, and marginal populations, which are the ones more likely to harbor allelic variation useful for abiotic stress tolerance after thousands of years of co-evolution with local pressures. The richness of adaptive variation outside elite germplasm remains unattractable for most pre-breeding programs, not to mention conservation and reforestation efforts, most likely due to difficulties in assessing and accessing the adapted variants and divergent complex epistatic fitness architectures that preclude their direct trade-off-free use [123]. Therefore, approaches such as genomic-guided introgression and assisted gene flow must be scaled up to fully exploit these resources, together with translational societal efforts to increase adoption [107] and communitarian involvement [124].

Additionally, although genome editing has transformative potential, its scalation to complex traits remains limited. At the moment, while editing single genes is feasible, manipulating entire polygenic architectures is still a bottleneck. Future efforts must therefore focus on multiplex editing and regulatory network bioengineering [125], potentially targeting transcription factor hubs. Last, acknowledging that plasticity is not only environmentally modulated but also genetically controlled [126] is reshaping it as a breeding target, enabling plant improvement to utilize plastic and adaptive responses [87] as part of the nascent enviromics paradigm [127–136], enhancing resilience under variable climates.

6. Conclusions

This Special Issue reinforces the fact that abiotic stress tolerance is governed by complex regulatory networks across highly polygenic and environmentally dependent architectures, which cannot be fully captured through single-layer or reductionist approaches. Instead, boosting plant resilience would require integrating cryptic genetic variation, transcriptional regulation, alternative splicing patterns, and genotype-by-environment interaction across spatial and temporal scales. Moving forward, a key priority would be to integrate multi-omics datasets—including genomics, transcriptomics, phenomics, and environmental covariates—into more unified, predictive frameworks capable of linking causal variants to system-level phenotypes under heterogeneous, and even simultaneous, abiotic stresses. Achieving this integration will require advances in network inference and machine learning, and particularly joint experimental designs that explicitly couple controlled functional assays with population-level validation across environmental gradients. Scaling the utilization of exotic germplasm through genomic-enabled introgression, multi-target genetic editing, and assisted gene flow will help mobilizing standing adaptation from the wild. Abiotic stress resilience can no longer be harnessed through discrete gene targets, but requires rethinking it as interconnected omnigenic regulatory networks embedded within evolving populations and ecosystems.

https://doi.org/10.3390/ijms27104258

Funding: The working time of the Guest Editor for the second edition of the Special Issue "Abiotic Stress Tolerance and Genetic Diversity in Plants" has been kindly sponsored by the Swedish Research Council (VR's grants 2016-00418/2022-04411) and the Royal Swedish Academy of Sciences (KVA's grant BS2017-003).

Institutional Review Board Statement: Not applicable.

Informed Consent Statement: Not applicable.

Data Availability Statement: All contributing articles to the Special Issue "Abiotic Stress Tolerance and Genetic Diversity in Plants", second edition, are available here https://www.mdpi.com/si/ijms/9Y8E57B7V3 as accessed on 24 April 2026.

Acknowledgments: This second edition of the Special Issue on "Abiotic Stress Tolerance and Genetic Diversity in Plants" would not have been possible without the interest and effort of all authors and reviewers.

Conflicts of Interest: The author declare no conflicts of interest.

References

1. Hultgren, A.; Carleton, T.; Delgado, M.; Gergel, D.R.; Greenstone, M.; Houser, T.; Hsiang, S.; Jina, A.; Kopp, R.E.; Malevich, S.B.; et al. Impacts of climate change on global agriculture accounting for adaptation. *Nature* **2025**, *642*, 644–652. [CrossRef]
2. Merchuk-Ovnat, L.; Silberman, R.; Laiba, E.; Maurer, A.; Pillen, K.; Faigenboim, A.; Fridman, E. Genome scan identifies flowering-independent effects of barley HsDry2.2 locus on yield traits under water deficit. *J. Exp. Bot.* **2018**, *69*, 1765–1779. [CrossRef] [PubMed]
3. Leon-Garcia, I.V.; Lasso, E. High heat tolerance in plants from the Andean highlands: Implications for paramos in a warmer world. *PLoS ONE* **2019**, *14*, e0224218. [CrossRef]
4. Gottfried, M.; Pauli, H.; Futschik, A.; Akhalkatsi, M.; Barančok, P.; Benito Alonso, J.L.; Coldea, G.; Dick, J.; Erschbamer, B.; Fernández Calzado, M.a.R.; et al. Continent-wide response of mountain vegetation to climate change. *Nat. Clim. Change* **2012**, *2*, 111–115. [CrossRef]
5. Rumpf, S.B.; Hulber, K.; Klonner, G.; Moser, D.; Schutz, M.; Wessely, J.; Willner, W.; Zimmermann, N.E.; Dullinger, S. Range dynamics of mountain plants decrease with elevation. *Proc. Natl. Acad. Sci. USA* **2018**, *115*, 1848–1853. [CrossRef]
6. Fragata, I.; Lopes-Cunha, M.; Barbaro, M.; Kellen, B.; Lima, M.; Santos, M.A.; Faria, G.S.; Santos, M.; Matos, M.; Simoes, P. How much can history constrain adaptive evolution? A real-time evolutionary approach of inversion polymorphisms in *Drosophila subobscura*. *J. Evol. Biol.* **2014**, *27*, 2727–2738. [CrossRef]
7. Chala, D.; Brochmann, C.; Psomas, A.; Ehrich, D.; Gizaw, A.; Masao, C.A.; Bakkestuen, V.; Zimmermann, N.E. Good-bye to tropical alpine plant giants under warmer climates? Loss of range and genetic diversity in *Lobelia rhynchopetalum*. *Ecol. Evol.* **2016**, *6*, 8931–8941. [CrossRef]
8. Valladares, F.; Matesanz, S.; Guilhaumon, F.; Araujo, M.B.; Balaguer, L.; Benito-Garzon, M.; Cornwell, W.; Gianoli, E.; van Kleunen, M.; Naya, D.E.; et al. The effects of phenotypic plasticity and local adaptation on forecasts of species range shifts under climate change. *Ecol. Lett.* **2014**, *17*, 1351–1364. [CrossRef]
9. Gutaker, R.M.; Purugganan, M.D. Adaptation and the Geographic Spread of Crop Species. *Annu. Rev. Plant Biol.* **2023**, *75*, 679–706. [CrossRef]
10. Varshney, R.K.; Barmukh, R.; Roorkiwal, M.; Qi, Y.; Kholova, J.; Tuberosa, R.; Reynolds, M.P.; Tardieu, F.; Siddique, K.H.M. Breeding custom-designed crops for improved drought adaptation. *Adv. Genet.* **2021**, *2*, e202100017. [CrossRef]
11. Migicovsky, Z. Genomic resources for crop wild relatives are critical for perennial fruit breeding and conservation. *Am. J. Bot.* **2025**, *112*, e70068. [CrossRef]
12. Gomez-Fernandez, A. Reconstructing the evolutionary history of herbaceous crops through trait-based ecology. *Am. J. Bot.* **2025**, *112*, e70107. [CrossRef]
13. Branch, H.A. The sleeping giant needs coffee: Overlooked areas for integrating plant ecophysiology and evolutionary biology. *Am. J. Bot.* **2026**, *113*, e70164. [CrossRef] [PubMed]
14. Cortinovis, G.; Di Vittori, V.; Bellucci, E.; Bitocchi, E.; Papa, R. Adaptation to novel environments during crop diversification. *Curr. Opin. Plant Biol.* **2020**, *56*, 203–217. [CrossRef]
15. Kristensen, T.N.; Ketola, T.; Kronholm, I. Adaptation to environmental stress at different timescales. *Ann. N. Y. Acad. Sci.* **2018**, *1476*, 5–22. [CrossRef]
16. Cortés, A.J. Abiotic Stress Tolerance Boosted by Genetic Diversity in Plants. *Int. J. Mol. Sci.* **2024**, *25*, 5367. [CrossRef]

17. Razgour, O.; Forester, B.; Taggart, J.B.; Bekaert, M.; Juste, J.; Ibanez, C.; Puechmaille, S.J.; Novella-Fernandez, R.; Alberdi, A.; Manel, S. Considering adaptive genetic variation in climate change vulnerability assessment reduces species range loss projections. *Proc. Natl. Acad. Sci. USA* **2019**, *116*, 10418–10423. [CrossRef]
18. Ibáñez, I.; Primack, R.B.; Miller-Rushing, A.J.; Ellwood, E.; Higuchi, H.; Lee, S.D.; Kobori, H.; Silander, J.A. Forecasting phenology under global warming. *Philos. Trans. R. Soc. B Biol. Sci.* **2010**, *365*, 3247–3260.
19. Cotto, O.; Wessely, J.; Georges, D.; Klonner, G.; Schmid, M.; Dullinger, S.; Thuiller, W.; Guillaume, F. A dynamic eco-evolutionary model predicts slow response of alpine plants to climate warming. *Nat. Commun.* **2017**, *8*, 15399. [CrossRef] [PubMed]
20. Jay, F.; Manel, S.; Alvarez, N.; Durand, E.Y.; Thuiller, W.; Holderegger, R.; Taberlet, P.; François, O. Forecasting changes in population genetic structure of alpine plants in response to global warming. *Mol. Ecol.* **2012**, *21*, 2354–2368. [CrossRef] [PubMed]
21. Botkin, D.B.; Saxe, H.; Araújo, M.B.; Betts, R.; Bradshaw, R.H.W.; Cedhagen, T.; Chesson, P.; Dawson, T.P.; Etterson, J.R.; Faith, D.P.; et al. Forecasting the Effects of Global Warming on Biodiversity. *BioScience* **2007**, *57*, 227–236. [CrossRef]
22. Cortés, A.J.; López-Hernández, F.; Blair, M.W. Crop Modeling for Future Climate Change Adaptation. In *Digital Agriculture: A Solution for Sustainable Food and Nutritional Security*; Priyadarshan, P.M., Jain, S.M., Suprasanna, P., Al-Khayri, J.M., Eds.; Springer International Publishing: Cham, Switzerland, 2024; pp. 625–639.
23. Barghi, N.; Hermisson, J.; Schlötterer, C. Polygenic adaptation: A unifying framework to understand positive selection. *Nat. Rev. Genet.* **2020**, *21*, 769–781. [CrossRef]
24. Peng, B.; Guan, K.; Tang, J.; Ainsworth, E.A.; Asseng, S.; Bernacchi, C.J.; Cooper, M.; Delucia, E.H.; Elliott, J.W.; Ewert, F.; et al. Towards a multiscale crop modelling framework for climate change adaptation assessment. *Nat. Plants* **2020**, *6*, 338–348. [CrossRef]
25. Benitez-Alfonso, Y.; Soanes, B.K.; Zimba, S.; Sinanaj, B.; German, L.; Sharma, V.; Bohra, A.; Kolesnikova, A.; Dunn, J.A.; Martin, A.C.; et al. Enhancing climate change resilience in agricultural crops. *Curr. Biol.* **2023**, *33*, R1246–R1261. [CrossRef] [PubMed]
26. Cortés, A.J.; Cornille, A.; Yockteng, R. Evolutionary Genetics of Crop-Wild Complexes. *Genes* **2022**, *13*, 1. [CrossRef]
27. Weigel, D.; Nordborg, M. Population Genomics for Understanding Adaptation in Wild Plant Species. *Annu. Rev. Genet.* **2015**, *49*, 315–338. [CrossRef] [PubMed]
28. Castaneda-Alvarez, N.P.; Khoury, C.K.; Achicanoy, H.A.; Bernau, V.; Dempewolf, H.; Eastwood, R.J.; Guarino, L.; Harker, R.H.; Jarvis, A.; Maxted, N.; et al. Global conservation priorities for crop wild relatives. *Nat. Plants* **2016**, *2*, 16022. [CrossRef]
29. Cortés, A.J.; Barnaby, J.Y. Editorial: Harnessing genebanks: High-throughput phenotyping and genotyping of crop wild relatives and landraces. *Front. Plant Sci.* **2023**, *14*, 1149469. [CrossRef] [PubMed]
30. Parmesan, C.; Hanley, M.E. Plants and climate change: Complexities and surprises. *Ann. Bot.* **2015**, *116*, 849–864. [CrossRef]
31. Alsos, I.G.; Ehrich, D.; Thuiller, W.; Eidesen, P.B.; Tribsch, A.; Schönswetter, P.; Lagaye, C.; Taberlet, P.; Brochmann, C. Genetic consequences of climate change for northern plants. *Proc. R. Soc. B Biol. Sci.* **2012**, *279*, 2042–2051. [CrossRef] [PubMed]
32. Jump, A.S.; Penuelas, J. Running to stand still: Adaptation and the response of plants to rapid climate change. *Ecol. Lett.* **2005**, *8*, 1010–1020. [CrossRef] [PubMed]
33. Wang, Q.; Wu, J.; Di, G.; Zhao, Q.; Gao, C.; Zhang, D.; Wang, J.; Shen, Z.; Han, W. Identification of Cold Tolerance Transcriptional Regulatory Genes in Seedlings of *Medicago sativa* L. and *Medicago falcata* L. *Int. J. Mol. Sci.* **2024**, *25*, 10345. [CrossRef]
34. Mizoia, J.; Shinozakib, K.; Yamaguchi-Shinozaki, K. AP2/ERF family transcription factors in plant abiotic stress responses. *Biochim. Et Biophys. Acta* **2012**, *1819*, 86–96. [CrossRef] [PubMed]
35. Yang, C.-Y.; Hsu, F.-C.; Li, J.-P.; Wang, N.-N.; Shih, M.-C. The AP2/ERF transcription factor AtERF73/HRE1 modulates ethylene responses during hypoxia in *Arabidopsis*. *Plant Physiol.* **2011**, *156*, 202–212. [CrossRef]
36. Qi, W.; Sun, F.; Wang, Q.; Chen, M.; Huang, Y.; Feng, Y.; Luo, X.; Yang, J. Rice ethylene-response AP2/ERF factor OsEATB restricts internode elongation by down-regulating a gibberellin biosynthetic gene. *Plant Physiol.* **2011**, *157*, 216–228. [CrossRef]
37. Yu, Z.X.; Li, J.X.; Yang, C.Q.; Hu, W.L.; Wang, L.J.; Chen, X.Y. The Jasmonate-Responsive *AP2/ERF* Transcription Factors *AaERF1* and *AaERF2* Positively Regulate Artemisinin Biosynthesis in *Artemisia annua* L. *Mol. Plant* **2011**, *5*, 353–365. [CrossRef] [PubMed]
38. Zhuang, J.; Xiong, A.S.; Peng, R.H.; Gao, F.; Zhu, B.; Zhang, J.A.; Fu, X.Y.; Jin, X.F.; Chen, J.M.; Zhang, Z.; et al. Analysis of Brassica rapa ESTs: Gene discovery and expression patterns of AP2/ERF family genes. *Mol. Biol. Rep.* **2010**, *37*, 2485–2492. [CrossRef]
39. Licausi, F.; Giorgi, F.M.; Zenoni, S.; Osti, F.; Pezzotti, M.; Perata, P. Genomic and transcriptomic analysis of the AP2/ERF superfamily in *Vitis vinifera*. *BMC Genom.* **2010**, *11*, 719. [CrossRef]
40. O'Rourke, J.A.; Graham, M.A. Investigating the Role of Known Arabidopsis Iron Genes in a Stress Resilient Soybean Line. *Int. J. Mol. Sci.* **2024**, *25*, 11480. [CrossRef]
41. Khunsanit, P.; Plaimas, K.; Chadchawan, S.; Buaboocha, T. Profiling of Key Hub Genes Using a Two-State Weighted Gene Co-Expression Network of 'Jao Khao' Rice under Soil Salinity Stress Based on Time-Series Transcriptome Data. *Int. J. Mol. Sci.* **2024**, *25*, 11086. [CrossRef] [PubMed]
42. Zhao, Y.; Chen, S.; Qin, M.; Shui, K.; Li, R.; Yang, B.; Liu, J.; Chen, Z. Genome-Wide Identification of *FCS-Like Zinc Finger (FLZ)* Family Genes in Three *Brassica* Plant Species and Functional Characterization of *BolFLZs* in Chinese Kale Under Abiotic Stresses. *Int. J. Mol. Sci.* **2024**, *25*, 12907. [CrossRef]

43. López-Hernández, F.; Roda, F.; Cortés, A.J. Machine Learning and Pangenomics: Revolutionizing Plant Breeding for a Sustainable Future. In *Plant Breeding 2050*; Priyadarshan, P.M., Ortiz, R., Eds.; Springer: Singapore, 2025; pp. 509–523.
44. Reichstein, M.; Bahn, M.; Mahecha, M.D.; Kattge, J.; Baldocchi, D.D. Linking plant and ecosystem functional biogeography. *Proc. Natl. Acad. Sci. USA* **2014**, *111*, 13697–13702. [CrossRef]
45. Zhao, X.; Han, X.; Lu, X.; Yang, H.; Wang, Z.Y.; Chai, M. Genome-Wide Identification and Characterization of the Msr Gene Family in Alfalfa under Abiotic Stress. *Int. J. Mol. Sci.* **2023**, *24*, 9638. [CrossRef]
46. Wang, H.; Yu, J.; Zhu, B.; Gu, L.; Wang, H.; Du, X.; Zeng, T.; Tang, H. The SbbHLH041-*SbEXPA11* Module Enhances Cadmium Accumulation and Rescues Biomass by Increasing Photosynthetic Efficiency in Sorghum. *Int. J. Mol. Sci.* **2023**, *24*, 13061. [CrossRef]
47. Huang, X.; Qiu, X.; Wang, Y.; Abubakar, A.S.; Chen, P.; Chen, J.; Chen, K.; Yu, C.; Wang, X.; Gao, G.; et al. Genome-Wide Investigation of the NAC Transcription Factor Family in *Apocynum venetum* Revealed Their Synergistic Roles in Abiotic Stress Response and Trehalose Metabolism. *Int. J. Mol. Sci.* **2023**, *24*, 4578. [CrossRef]
48. López-Hernández, F.; Cortés, A.J. Transcriptomic Signatures of Somaclonal Variation. In *Plant Transcriptomics and Epitranscriptomics*; Springer: Singapore, 2026; pp. 135–153.
49. Lembrechts, J.J.; Lenoir, J. Microclimatic conditions anywhere at any time! *Glob. Change Biol.* **2020**, *26*, 337–339. [CrossRef] [PubMed]
50. Abdelaziz, M.; Anderson, J.T.; Rochford, M.E.; Bemmels, J.B.; Jameel, M.I.; Denney, D.A. Small spaces, big impacts: Contributions of micro-environmental variation to population persistence under climate change. *AoB Plants* **2020**, *12*, plaa005. [CrossRef]
51. Du, H.; Liang, Z.; Cortés, A.J. Editorial: Evolution of crop genomes and epigenomes, volume II. *Front. Plant Sci.* **2025**, *16*, 1623554. [CrossRef]
52. Cortés, A.J. Unlocking genebanks for climate adaptation. *Nat. Clim. Change* **2025**, *15*, 590–592. [CrossRef]
53. Myburg, A.A.; Hussey, S.G.; Wang, J.P.; Street, N.R.; Mizrachi, E. Systems and Synthetic Biology of Forest Trees: A Bioengineering Paradigm for Woody Biomass Feedstocks. *Front. Plant Sci.* **2019**, *10*, 775. [CrossRef] [PubMed]
54. Ma, Y.; Zhong, M.; Li, J.; Jiang, Y.; Zhou, X.; Justice Ijeoma, C.; Tang, X.; Chen, S.; Cao, S. Genome Identification and Evolutionary Analysis of *LBD* Genes and Response to Environmental Factors in *Phoebe bournei*. *Int. J. Mol. Sci.* **2023**, *24*, 12581. [CrossRef]
55. Bohra, A.; Kilian, B.; Sivasankar, S.; Caccamo, M.; Mba, C.; McCouch, S.R.; Varshney, R.K. Reap the crop wild relatives for breeding future crops. *Trends Biotechnol.* **2021**, *40*, 412–431. [CrossRef]
56. Imran, S.; Ono, S.; Horie, R.; Katsuhara, M.; Horie, T. Chloride-Transporting OsHKT1;1 Splice Variants and Their Expression Profiles Under Salinity Stress in Rice. *Int. J. Mol. Sci.* **2026**, *27*, 1178. [CrossRef]
57. Fan, S.; Jia, L.; Wu, J.; Zhao, Y. Harnessing the Potential of CRISPR/Cas in Targeted Alfalfa Improvement for Stress Resilience. *Int. J. Mol. Sci.* **2025**, *26*, 3311. [CrossRef] [PubMed]
58. Doudna, J.A.; Charpentier, E. Genome editing. The new frontier of genome engineering with CRISPR-Cas9. *Science* **2014**, *346*, 1258096. [CrossRef] [PubMed]
59. Rodríguez-Leal, D.; Lemmon, Z.H.; Man, J.; Bartlett, M.E.; Lippman, Z.B. Engineering Quantitative Trait Variation for Crop Improvement by Genome Editing. *Cell* **2017**, *171*, 470–480.e478. [CrossRef] [PubMed]
60. Barrero, L.S.; Willmann, M.R.; Craft, E.J.; Akther, K.M.; Harrington, S.E.; Garzon-Martinez, G.A.; Glahn, R.P.; Piñeros, M.A.; McCouch, S.R. Identifying genes associated with abiotic stress tolerance suitable for CRISPR/Cas9 editing in upland rice cultivars adapted to acid soils. *Plant Direct* **2022**, *6*, e469. [CrossRef]
61. Li, R.; Liu, C.; Zhao, R.; Wang, L.; Chen, L.; Yu, W.; Zhang, S.; Sheng, J.; Shen, L. CRISPR/Cas9-Mediated *SlNPR1* mutagenesis reduces tomato plant drought tolerance. *BMC Plant Biol.* **2019**, *19*, 38. [CrossRef]
62. Wang, L.; Chen, L.; Li, R.; Zhao, R.; Yang, M.; Sheng, J.; Shen, L. Reduced Drought Tolerance by CRISPR/Cas9-Mediated SlMAPK3 Mutagenesis in Tomato Plants. *J. Agric. Food Chem.* **2017**, *65*, 8674–8682. [CrossRef]
63. Robinson, J.M.; Hodgson, R.; Krauss, S.L.; Liddicoat, C.; Malik, A.A.; Martin, B.C.; Mohr, J.J.; Moreno-Mateos, D.; Munoz-Rojas, M.; Peddle, S.D.; et al. Opportunities and challenges for microbiomics in ecosystem restoration. *Trends Ecol. Evol.* **2023**, *38*, 1189–1202. [CrossRef]
64. Park, D.S.; Willis, C.G.; Xi, Z.; Kartesz, J.T.; Davis, C.C.; Worthington, S. Machine Learning Predicts Large Scale Declines in Native Plant Phylogenetic Diversity. *New Phytol.* **2020**, *227*, 1544–1556. [CrossRef]
65. Guo, H.; Nie, C.Y.; Li, Z.; Kang, J.; Wang, X.L.; Cui, Y.N. Physiological and Transcriptional Analyses Provide Insight into Maintaining Ion Homeostasis of Sweet Sorghum under Salt Stress. *Int. J. Mol. Sci.* **2023**, *24*, 11045. [CrossRef] [PubMed]
66. Wirojsirasak, W.; Songsri, P.; Jongrungklang, N.; Tangphatsornruang, S.; Klomsa-Ard, P.; Ukoskit, K. A Large-Scale Candidate-Gene Association Mapping for Drought Tolerance and Agronomic Traits in Sugarcane. *Int. J. Mol. Sci.* **2023**, *24*, 12801. [CrossRef]
67. Ravelombola, W.; Dong, L.; Barickman, T.C.; Xiong, H.; Manley, A.; Cason, J.; Pham, H.; Zia, B.; Mou, B.; Shi, A. Genetic Architecture of Salt Tolerance in Cowpea (*Vigna unguiculata* (L.) Walp.) at Seedling Stage Using a Whole Genome Resequencing Approach. *Int. J. Mol. Sci.* **2023**, *24*, 15281. [CrossRef]

68. Brautigam, K.; Vining, K.J.; Lafon-Placette, C.; Fossdal, C.G.; Mirouze, M.; Marcos, J.G.; Fluch, S.; Fraga, M.F.; Guevara, M.A.; Abarca, D.; et al. Epigenetic regulation of adaptive responses of forest tree species to the environment. *Ecol. Evol.* **2013**, *3*, 399–415. [CrossRef]
69. Parra-Londono, S.; López-Hernández, F.; Montoya, G.; Henao-Rojas, J.C.; Ossa-Ossa, G.A.; Cortés, A.J. Merging Phenotypic Stability Analysis and Genomic Prediction for Multi-Environment Breeding in *Capsicum* spp. *Agronomy* **2025**, *15*, 2690. [CrossRef]
70. López-Hernández, F.; Burbano-Erazo, E.; León-Pacheco, R.I.; Cordero-Cordero, C.C.; Villanueva-Mejía, D.F.; Tofiño-Rivera, A.P.; Cortés, A.J. Multi-Environment Genome-Wide Association Studies of Yield Traits in Common Bean (*Phaseolus vulgaris* L.) × Tepary Bean (*P. acutifolius* A. Gray) Interspecific Advanced Lines in Humid and Dry Colombian Caribbean Subregions. *Agronomy* **2023**, *13*, 1396. [CrossRef]
71. Arnold, P.A.; Kruuk, L.E.B.; Nicotra, A.B. How to analyse plant phenotypic plasticity in response to a changing climate. *New Phytol.* **2019**, *222*, 1235–1241. [CrossRef]
72. Tognetti, R. Adaptation to climate change of dioecious plants: Does gender balance matter? *Tree Physiol.* **2012**, *32*, 1321–1324. [CrossRef]
73. Chuine, I. Why does phenology drive species distribution? *Philos. Trans. R. Soc. Lond. B Biol. Sci.* **2010**, *365*, 3149–3160. [CrossRef] [PubMed]
74. Valladares, F.; Niinemets, U. Shade Tolerance, a Key Plant Feature of Complex Nature and Consequences. *Annu. Rev. Ecol. Evol. Syst.* **2008**, *39*, 237–257. [CrossRef]
75. Franks, S.J.; Weis, A.E. A change in climate causes rapid evolution of multiple life-history traits and their interactions in an annual plant. *J. Evol. Biol.* **2008**, *21*, 1321–1334. [CrossRef]
76. Bai, X.; Qiao, P.; Liu, H.; Shang, Y.; Guo, J.; Dai, K. Genome-wide identification of the E-class gene family in wheat: Evolution, expression, and interaction. *Front. Plant Sci.* **2024**, *15*, 1419437. [CrossRef]
77. Jezkova, T.; Wiens, J.J. Rates of change in climatic niches in plant and animal populations are much slower than projected climate change. *Proc. Biol. Sci.* **2016**, *283*, 20162104. [CrossRef]
78. Franks, S.J.; Weis, A.E. Climate change alters reproductive isolation and potential gene flow in an annual plant. *Evol. Appl.* **2009**, *2*, 481–488. [CrossRef]
79. Bedoya-Londoño, S.; Cañas-Gutiérrez, G.P.; Cortés, A.J. Breeding Without Breeding: Enabling Indirect Selection Schemes for Tropical Tree Improvement. In *Genomics Based Approaches for Tropical Tree Improvement and Conservation*; Springer: Singapore, 2025; pp. 19–42.
80. Arenas, S.; Cortés, A.J.; Jaramillo-Correa, J.P. Toward a Genomic-Enabled Selection in Natural Tree Populations for Long-Term Management and Conservation. In *Genomics Based Approaches for Tropical Tree Improvement and Conservation*; Springer: Singapore, 2025; pp. 243–278.
81. Lachmuth, S.; Capblancq, T.; Keller, S.; Fitzpatrick, M. Assessing uncertainty in genomic offset forecasts from landscape genomic models (and implications for restoration and assisted migration). *Front. Ecol. Evol.* **2023**, *11*, 1155783. [CrossRef]
82. López-Hernández, F.; Villanueva-Mejía, D.F.; Tofiño-Rivera, A.P.; Cortés, A.J. Genomic prediction of adaptation in common bean (*Phaseolus vulgaris* L.) × Tepary bean (*P. acutifolius* A. Gray) hybrids. *Int. J. Mol. Sci.* **2025**, *26*, 7370. [CrossRef]
83. Arenas, S.; Djabali, Y.; Rincent, R.; Cubry, P.; Martin, M.L.; Blein-Nicolas, M.; Laplaze, L.; Schneider, H.; Grondin, A. Modeling plant phenotypic plasticity and its underlying genetic architecture: A comparative study. *J. Exp. Bot.* **2025**, *76*, 2239–2251. [CrossRef] [PubMed]
84. Reyer, C.P.; Leuzinger, S.; Rammig, A.; Wolf, A.; Bartholomeus, R.P.; Bonfante, A.; de Lorenzi, F.; Dury, M.; Gloning, P.; Abou Jaoude, R.; et al. A plant's perspective of extremes: Terrestrial plant responses to changing climatic variability. *Glob. Change Biol.* **2013**, *19*, 75–89. [CrossRef]
85. Bedoya-Canas, L.E.; López-Hernández, F.; Cortés, A.J. Climate change adaptation of high-elevation *Polylepis* forests. *Forests* **2024**, *15*, 811. [CrossRef]
86. Arenas, S.; Cortés, A.J. Unveiling the Genomic Architecture of Phenotypic Plasticity Using Multiple GWAS Approaches Under Contrasting Conditions of Water Availability: A Model for Barley. *Int. J. Mol. Sci.* **2026**, *27*, 652. [CrossRef]
87. Campbell, Q.; Castañeda-Álvarez, N.; Domingo, R.; Bishop-von Wettberg, E.; Runck, B.; Nandkangré, H.; Halpin-McCormick, A.; Fumia, N.; Neyhart, J.; Kilian, B.; et al. Prioritizing parents from global genebanks to breed climate-resilient crops. *Nat. Clim. Change* **2025**, *15*, 673–681. [CrossRef]
88. Yin, X.; Gao, Q.; Wang, F.; Liu, W.; Luo, Y.; Zhong, S.; Feng, J.; Bai, R.; Chen, L.; Dai, X.; et al. Marker-Assisted Selection of Jacalin-Related Lectin Genes *OsJRL45* and *OsJRL40* Derived from Sea Rice 86 Enhances Salt Tolerance in Rice. *Int. J. Mol. Sci.* **2024**, *25*, 10912. [CrossRef]
89. McCouch, S. Diversifying Selection in Plant Breeding. *PLoS Biol.* **2004**, *2*, 1507–1512. [CrossRef] [PubMed]
90. Lasky, J.R.; Josephs, E.B.; Morris, G.P. Genotype-environment associations to reveal the molecular basis of environmental adaptation. *Plant Cell* **2023**, *35*, 125–138. [CrossRef] [PubMed]

91. López-Hernández, F.; Rosero-Alpala, M.G.; Rosero, A.; Cortés, A.J. Projected Shifts in Colombian Sweet Potato Germplasm Under Climate Change. *Horticulturae* **2025**, *11*, 1080. [CrossRef]
92. Juma, I.; Valencia, J.B.; Cortés, A.J. Predicting Suitable Regions for Avocado (*Persea americana* Mill.) Tree Cultivation in Tanzania. *Horticulturae* **2025**, *12*, 24. [CrossRef]
93. Cañas-Gutierrez, G.P.; López-Hernandez, F.; Cortés, A.J. Whole Genome Resequencing of 205 Avocado Trees Unveils the Genomic Patterns of Racial Divergence in the Americas. *Int. J. Mol. Sci.* **2025**, *26*, 10353. [CrossRef]
94. Cortés, A.J.; Hussein, J.M.; Juma, I. Genomic Diversity of Avocado in the Morogoro Region and Southern Highlands of Tanzania. *Int. J. Mol. Sci.* **2026**, *27*, 3083. [CrossRef] [PubMed]
95. Ramírez-Gil, J.G.; López-Hernandez, F.; Conejo-Rodriguez, D.F.; Henao-Rojas, J.C.; Quiroga-Benavides, K.E.; Cortés, A.J.; Chacón-Sanchez, M.I. GermVersity: A free and user-friendly interface to enhance the visualization and analysis of genebank data. *PLoS ONE* **2026**, *21*, e0340826. [CrossRef]
96. Breed, M.F.; Harrison, P.A.; Blyth, C.; Byrne, M.; Gaget, V.; Gellie, N.J.C.; Groom, S.V.C.; Hodgson, R.; Mills, J.G.; Prowse, T.A.A.; et al. The potential of genomics for restoring ecosystems and biodiversity. *Nat. Rev. Genet.* **2019**, *20*, 615–628. [CrossRef] [PubMed]
97. Aitken, S.N.; Yeaman, S.; Holliday, J.A.; Wang, T.; Curtis-McLane, S. Adaptation, migration or extirpation: Climate change outcomes for tree populations. *Evol. Appl.* **2008**, *1*, 95–111. [CrossRef] [PubMed]
98. Aitken, S.N.; Whitlock, M.C. Assisted Gene Flow to Facilitate Local Adaptation to Climate Change. *Annu. Rev. Ecol. Evol. Syst.* **2013**, *44*, 367–388. [CrossRef]
99. Aitken, S.N.; Bemmels, J.B. Time to get moving: Assisted gene flow of forest trees. *Evol. Appl.* **2016**, *9*, 271–290. [CrossRef]
100. Li, H.; Sun, Z.; Li, W.; Yin, X.; Xu, X.; Zhang, X.; Yan, X.; Wang, X.; Li, Y.; Ma, A. Research on Cold Resistance of *Kandelia obovata* Transplanted to Zhoushan Area at the mRNA Level. *Int. J. Mol. Sci.* **2025**, *27*, 429. [CrossRef]
101. Fick, A.; Swart, V.; Bombarely, A.; van den Berg, N. Comparative transcriptional analysis of *Persea americana MYB*, *WRKY* and *AP2/ERF* transcription factors following Phytophthora cinnamomi infection. *Mol. Plant Pathol.* **2024**, *25*, e13453. [CrossRef]
102. Seo, P.J.; Lee, S.B.; Suh, M.C.; Park, M.-J.; Go, Y.S.; Park, C.-M. The MYB96 Transcription Factor Regulates Cuticular Wax Biosynthesis under Drought Conditions in *Arabidopsis*. *Plant Cell Online* **2011**, *23*, 1138–1152. [CrossRef]
103. Galbiati, M.; Matus, J.; Francia, P.; Rusconi, F.; Cañón, P.; Medina, C.; Conti, L.; Cominelli, E.; Tonelli, C.; Arce-Johnson, P. The grapevine guard cell-related *VvMYB60* transcription factor is involved in the regulation of stomatal activity and is differentially expressed in response to ABA and osmotic stress. *BMC Plant Biol.* **2011**, *11*, 142. [CrossRef] [PubMed]
104. Mellway, R.D.; Tran, L.T.; Prouse, M.B.; Campbell, M.M.; Constabel, C.P. The Wound-, Pathogen-, and Ultraviolet B-Responsive MYB134 Gene Encodes an R2R3 MYB Transcription Factor That Regulates Proanthocyanidin Synthesis in Poplar. *Plant Physiol.* **2009**, *150*, 924–941. [CrossRef]
105. Cortés, A.J. Omics Technologies in Molecular Biology. *Int. J. Mol. Sci.* **2026**, *27*, 3349. [CrossRef]
106. Cortés, A.J.; Castillejo, M.Á.; Yockteng, R. 'Omics' Approaches for Crop Improvement. *Agronomy* **2023**, *13*, 1401. [CrossRef]
107. Kholova, J.; Urban, M.O.; Bavorova, M.; Ceccarelli, S.; Cosmas, L.; Desczka, S.; Grando, S.; Lensink, R.; Nchanji, E.; Pavlik, J.; et al. Promoting new crop cultivars in low-income countries requires a transdisciplinary approach. *Nat. Plants* **2024**, *10*, 1610–1613. [CrossRef]
108. McCouch, S.; Navabi, K.; Abberton, M.; Anglin, N.L.; Barbieri, R.L.; Baum, M.; Bett, K.; Booker, H.; Brown, G.L.; Bryan, G.J.; et al. Mobilizing crop biodiversity. *Mol. Plant* **2020**, *13*, 1341–1344. [CrossRef]
109. Spindel, J.E.; McCouch, S.R. When more is better: How data sharing would accelerate genomic selection of crop plants. *New Phytol.* **2016**, *212*, 814–826. [CrossRef]
110. Khaipho-Burch, M.; Cooper, M.; Crossa, J.; Leon, N.d.; Holland, J.; Lewis, R.; McCouch, S.; Murray, S.C.; Rabbi, I.; Ronald, P.; et al. Scale up trials to validate modified crops' benefits. *Nature* **2023**, *621*, 470–473. [CrossRef] [PubMed]
111. VanWallendael, A.; Lowry, D.B.; Hamilton, J.A. One hundred years into the study of ecotypes, new advances are being made through large-scale field experiments in perennial plant systems. *Curr. Opin. Plant Biol.* **2022**, *66*, 102152. [CrossRef] [PubMed]
112. Barrett, R.D.H.; Hoekstra, H.E. Molecular spandrels: Tests of adaptation at the genetic level. *Nat. Rev. Genet.* **2011**, *12*, 767–780. [CrossRef]
113. Manolio, T.A.; Collins, F.S.; Cox, N.J.; Goldstein, D.B.; Hindorff, L.A.; Hunter, D.J.; McCarthy, M.I.; Ramos, E.M.; Cardon, L.R.; Chakravarti, A.; et al. Finding the missing heritability of complex diseases. *Nature* **2009**, *461*, 747–753. [CrossRef]
114. Maher, B. The case of the missing heritability. *Nature* **2008**, *456*, 18–21. [CrossRef]
115. Boyle, E.A.; Li, Y.I.; Pritchard, J.K. An Expanded View of Complex Traits: From Polygenic to Omnigenic. *Cell* **2017**, *169*, 1177–1186. [CrossRef]
116. Zavafer, A.; Bates, H.; Mancilla, C.; Ralph, P.J. Phenomics: Conceptualization and importance for plant physiology. *Trends Plant Sci.* **2023**, *28*, 1004–1013. [CrossRef] [PubMed]
117. Feng, J.; Dan, X.; Cui, Y.; Gong, Y.; Peng, M.; Sang, Y.; Ingvarsson, P.K.; Wang, J. Integrating evolutionary genomics of forest trees to inform future tree breeding amid rapid climate change. *Plant Commun.* **2024**, *5*, 101044. [CrossRef] [PubMed]
118. Jaramillo, C.; Rueda, M.J.; Mora, G. Cenozoic plant diversity in the neotropics. *Science* **2006**, *311*, 1893–1896. [CrossRef]

119. Varshney, R.K. The Plant Genome special issue: Advances in genomic selection and application of machine learning in genomic prediction for crop improvement. *Plant Genome* **2021**, *14*, e20178. [CrossRef]
120. Schrider, D.R.; Kern, A.D. Supervised Machine Learning for Population Genetics: A New Paradigm. *Trends Genet.* **2018**, *34*, 301–312. [CrossRef]
121. Libbrecht, M.W.; Noble, W.S. Machine learning applications in genetics and genomics. *Nat. Rev. Genet.* **2015**, *16*, 321–332. [CrossRef]
122. Ma, C.; Zhang, H.H.; Wang, X. Machine learning for Big Data analytics in plants. *Trends Plant Sci.* **2014**, *19*, 798–808. [CrossRef]
123. Monyak, T.; Morris, G.P. Epistatic fitness landscapes emerge from parallel adaptive walks in breeding network metapopulations. *bioRxiv* **2026**. [CrossRef]
124. Peláez, D.; Aguilar, P.A.; Mercado, M.; López-Hernández, F.; Guzmán, M.; Burbano-Erazo, E.; Denning-James, K.; Medina, C.I.; Blair, M.W.; De Vega, J.J.; et al. Genotype selection, and seed uniformity and multiplication to ensure common bean (*Phaseolus vulgaris* L.) var. Liborino. *Agronomy* **2022**, *12*, 2285. [CrossRef]
125. Lemmon, Z.H.; Reem, N.T.; Dalrymple, J.; Soyk, S.; Swartwood, K.E.; Rodriguez-Leal, D.; Eck, J.V.; Lippman, Z.B. Rapid improvement of domestication traits in an orphan crop by genome editing. *Nat. Plants* **2018**, *4*, 766–770. [CrossRef]
126. Laitinen, R.A.E. Importance of phenotypic plasticity in crop resilience. *J. Exp. Bot.* **2024**, *75*, 670–673. [CrossRef]
127. Callister, A.N.; Costa-Neto, G.; Bradshaw, B.P.; Elms, S.; Crossa, J.; Brawner, J.T. Enviromic prediction enables the characterization and mapping of *Eucalyptus globulus* Labill breeding zones. *Tree Genet. Genomes* **2024**, *20*, 3. [CrossRef]
128. Heinemann, A.B.; Costa-Neto, G.; Fritsche-Neto, R.; da Matta, D.H.; Fernandes, I.K. Enviromic prediction is useful to define the limits of climate adaptation: A case study of common bean in Brazil. *Field Crops Res.* **2022**, *286*, 108628. [CrossRef]
129. Resende, R.T.; Piepho, H.P.; Rosa, G.J.M.; Silva-Junior, O.B.; Silva, F.F.e.; Resende, M.D.V.d.; Grattapaglia, D. *Enviromics* in breeding: Applications and perspectives on envirotypic-assisted selection. *Theor. Appl. Genet.* **2021**, *134*, 95–112. [CrossRef] [PubMed]
130. Costa-Neto, G.; Fritsche-Neto, R. Enviromics: Bridging different sources of data, building one framework. *Crop Breed. Appl. Biotechnol.* **2021**, *21*, e393521S393512. [CrossRef]
131. Crossa, J.; Fritsche-Neto, R.; Montesinos-Lopez, O.A.; Costa-Neto, G.; Dreisigacker, S.; Montesinos-Lopez, A.; Bentley, A.R. The Modern Plant Breeding Triangle: Optimizing the Use of Genomics, Phenomics, and Enviromics Data. *Front. Plant Sci.* **2021**, *12*, 651480. [CrossRef]
132. Cooper, M.; Messina, C.D. Can We Harness "Enviromics" to Accelerate Crop Improvement by Integrating Breeding and Agronomy? *Front. Plant Sci.* **2021**, *12*, 735143. [CrossRef]
133. Costa-Neto, G.; Crossa, J.; Fritsche-Neto, R. Enviromic assembly increases accuracy and reduces costs of the genomic prediction for yield plasticity. *bioRxiv* **2021**. [CrossRef]
134. Costa-Neto, G.; Crossa, J.; Fritsche-Neto, R. Enviromic Assembly Increases Accuracy and Reduces Costs of the Genomic Prediction for Yield Plasticity in Maize. *Front. Plant Sci.* **2021**, *12*, 717552. [CrossRef]
135. Costa-Neto, G.; Galli, G.; Carvalho, H.F.; Crossa, J.; Fritsche-Neto, R.; de Koning, D.J. *EnvRtype*: A software to interplay enviromics and quantitative genomics in agriculture. *G3* **2021**, *11*, jkab040. [CrossRef] [PubMed]
136. Costa-Neto, G.; Fritsche-Neto, R.; Crossa, J. Nonlinear kernels, dominance, and envirotyping data increase the accuracy of genome-based prediction in multi-environment trials. *Heredity* **2020**, *126*, 92–106. [CrossRef] [PubMed]

Disclaimer/Publisher's Note: The statements, opinions and data contained in all publications are solely those of the individual author(s) and contributor(s) and not of MDPI and/or the editor(s). MDPI and/or the editor(s) disclaim responsibility for any injury to people or property resulting from any ideas, methods, instructions or products referred to in the content.

International Journal of
Molecular Sciences

MDPI

Article

Chloride-Transporting OsHKT1;1 Splice Variants and Their Expression Profiles Under Salinity Stress in Rice

Shahin Imran [1,2], Shuntaro Ono [1,3], Rie Horie [4], Maki Katsuhara [1,*] and Tomoaki Horie [4,*]

[1] Institute of Plant Science and Resources, Okayama University, Kurashiki 710-0046, Okayama, Japan; ptj87a5q@s.okayama-u.ac.jp (S.I.)
[2] Department of Agronomy, Khulna Agricultural University, Khulna 9100, Khulna, Bangladesh
[3] Graduate School of Science and Engineering, Saitama University, Saitama 338-8570, Saitama, Japan
[4] Division of Applied Biology, Faculty of Textile Science and Technology, Shinshu University, Ueda 386-8567, Nagano, Japan
* Correspondence: kmaki@okayama-u.ac.jp (M.K.); horie@shinshu-u.ac.jp (T.H.)

Abstract

OsHKT1;1, a member of the high-affinity K^+ transporter (HKT) family, plays a key role in Na^+ homeostasis and salinity tolerance in rice. In our previous study, multiple potential *OsHKT1;1* splicing variants were identified, as well as the full-length (FL) *OsHKT1;1* transcript from the salt-tolerant rice Pokkali. However, most previous studies focused solely on the full-length protein, leaving the transport functions of splice variants largely unexamined. In this study, we focused on the splice variant OsHKT1;1-V2 and compared its function and gene expression with those of OsHKT1;1-FL. Two-electrode voltage clamp experiments using *Xenopus laevis* oocytes revealed that the 1st start codon of OsHKT1;1-V2 is functional to exhibit bidirectional currents in bath solutions containing NaCl. Unlike the Na^+-selective feature of OsHKT1;1-FL, OsHKT1;1-V2 primarily mediated Cl^- transport with weak Na^+ selectivity, which was supported by the higher Cl^- accumulation in OsHKT1;1-V2–expressing oocytes. Subcellular localization analyses using oocytes and *Arabidopsis* mesophyll cells indicated plasma membrane localization of OsHKT1;1-V2, similar to OsHKT1;1-FL. Functional assays using a yeast mutant further indicated that OsHKT1;1-FL, but not OsHKT1;1-V2, mediates Na^+ uptake. The same *OsHKT1;1* variants were identified in the *japonica* cultivar Nipponbare, and OsHKT1;1-V2 of the cultivar showed Cl^- transport properties similar to the one from Pokkali. Quantitative PCR analyses revealed higher abundance of *OsHKT1;1-FL* transcripts in Nipponbare than in Pokkali with markedly lower *OsHKT1;1-V2* levels in Pokkali under salt stress. This study provides a new insight into HKT-mediated ion homeostasis under salinity stress.

Keywords: HKT; heterologous expression systems; Na^+ selectivity; Cl^- selectivity; rice

1. Introduction

High concentrations of soluble or exchangeable salts (in most cases, the cation is Na^+) inhibit plant growth under salinity stress, which is a globally alarming issue that significantly lowers the yield and development of major crops. Rice (*Oryza sativa*) is the most susceptible to salt stress among cereal crops [1,2]. When toxic Na ions are adequately excluded, redistributed, and compartmentalized in the plant body, the plants are likely to exhibit tolerance to salinity stress.

High-affinity K^+ transporters (HKTs) are known to be involved in the transport of Na^+ and K^+ in plants, and some of them are crucial for maintaining Na^+/K^+ balance

under salinity stress [3,4]. Therefore, HKTs have been widely examined since the first report of the *TaHKT2;1* gene in bread wheat (*Triticum aestivum*) [5]. HKTs are classified into two subfamilies, and transporters belonging to subfamily 1 (HKT1s) have generally been shown to be selective for Na^+ [6–9]. The ability of plants to withstand salt has been demonstrated for both HKT1s and HKT2s.

In monocotyledon rice, the *japonica* cultivar was reported to maintain seven functional *HKT* genes, among which four genes (*OsHKT1;1*, *OsHKT1;3*, *OsHKT1;4*, and *OsHKT1;5*) were grouped in subfamily 1 [10,11]. Heterologous expression studies of OsHKT1;1 from rice using *Xenopus laevis* (*X. laevis*) oocytes showed Na^+-selective transport in an inward-rectifying manner [8,12]. HKT1;1 transporters identified in various plant species exhibit robust Na^+ selectivity when expressed in *Xenopus laevis* oocytes: AtHKT1;1 from *Arabidopsis* [7], HvHKT1;1 from barley [13], CmHKT1;1 from pumpkin [14], SvHKT1;1 from halophytic turf grass (*Sporobolus virginicus*) [15], VviHKT1;1 from grapevine [16], and VcHKT1;1 from blueberry [17]. Some HKT1 transporters interact with other ion homeostasis systems, such as the SOS pathway and K^+ transporters [18,19], forming a coordinated regulatory network that maintains ionic balance and cellular stability under salinity stress [20,21]. OsHKT1;1 has been shown to be involved in limiting Na^+ accumulation in leaves and contributing to salt tolerance based on the analysis of an insertional mutation in the *OsHKT1;1* gene [22]. Recent studies have further demonstrated that natural allelic variations in *OsHKT1;1* contribute significantly to genotypic differences in Na^+ distribution within rice. Genome-wide association analysis using a global diversity panel identified *OsHKT1;1* as the gene underlying a major QTL (RNC4) that regulates root Na^+ content, with indica accessions generally carrying alleles that promote higher root Na^+ accumulation than japonica accessions [23]. Functional assays revealed that three indica-predominant non-synonymous substitutions increased the inward Na^+ transport activity of OsHKT1;1, and introduction of the *indica* allele into a *japonica* background reproduced the high-root-Na^+ phenotype. These results support earlier findings that *OsHKT1;1* limits Na^+ accumulation in shoots and improves salt tolerance [22]. Furthermore, a combination of screening of salt-tolerant rice mutant lines and the MutMap method identified a key transcription factor gene that encodes a B-type response regulator OsRR22, suggesting the involvement of *OsHKT1;1* in rice salt tolerance [24].

In our previous study, an interesting phenomenon was found in the *OsHKT1;1* gene in a salt-tolerant landrace, Pokkali, in which potential alternative splicing variants encoding transporters that show distinct ion selectivity were identified in addition to the full-length *OsHKT1;1* transcript [8]. Alternative splicing (AS) is a post-transcriptional process that fine-tunes gene function. In rice, AS is broadly reprogrammed by salinity and other abiotic stresses, generating isoforms that adjust protein abundance and activity as conditions change [25]. This regulatory flexibility is evident in genes such as *OsDREB2B*, *OsHSFA2d*, and *OsMYB7*, where stress-dependent switching to functional splice variants enhances stress tolerance [25–28]. Similar patterns in other species reinforce the central role of AS in stress adaptation. In foxtail millet, for example, salt stress induces two *SiCYP19* splice variants, and *SiCYP19-b* more effectively improves tolerance by increasing proline and reducing ROS [29]. In *Populus euphratica*, AS of *PeuHKT1;3* generates the isoform *PeuHKT1;3a*, which alters pore-loop structure, enhances K^+ transport, and improves K^+/Na^+ homeostasis [30]. In *Arabidopsis*, *At-SRAS1* produces two splice variants with opposite functions: *At-SRAS1.1* (full-length, active E3 ligase) enhances salt tolerance, while *At-SRAS1.2* (truncated) reduces it [31]. In the halophyte *Thellungiella salsuginea*, salt stress induces multiple splice variants of *TsHKT1;2*, among which the functional isoforms (TsHKT1;2a/2b) interact with other HKT1 proteins to reduce Na^+ uptake and enhance salt tolerance [32]. In rice, *OsHKT1;4* also shows tissue-dependent splice variation that affects Na^+ retrieval and supports ionic

balance under salinity [33]. Despite these findings, AS regulation of HKTs in rice remains largely uncharacterized, and only a few other studies have reported splicing variants of HKTs [9,34].

Although alternative splicing of *OsHKT1;1* has been reported, the functional analyses of these variants, particularly whether they exhibit different transport characteristics from the full-length protein, remain unclear. Therefore, in the present study, we focused on one of the eight variants of the *OsHKT1;1* gene from Pokkali, *OsHKT1;1-V2*, to characterize its expression profile and transport properties. We present the results of heterologous expression analyses, which exhibit Cl^- transport features with far less selectivity for Na^+ of OsHKT1;1-V2 than those of full-length OsHKT1;1. Furthermore, we showed evidence that identical potential splicing variants exist in a salt-sensitive *japonica* cultivar, Nipponbare, and that OsHKT1;1-V2 from Nipponbare also exhibits similar Cl^- transport properties, although the expression levels of the full-length and OsHKT1;1-V2 variant seemed to be differentially regulated between the two varieties. We provide new insights into the mechanisms of ion homeostasis in rice, mediated by the potential alternative splicing of an important salt tolerance gene, *OsHKT1;1*, and discuss questions to be elucidated for pursuing the physiological impacts.

2. Results

2.1. Identification of a Functional Frame in the OsHKT1;1-V2 Variant

In our previous study, two start codons were identified in the *OsHKT1;1-V2* variant (Figure 1A) [8]. We artificially truncated and produced two fragments of *OsHKT1;1-V2* named *OsHKT1;1-V2(1)* and *OsHKT1;1-V2(2)*. *OsHKT1;1-V2(1)* is composed of 519 nucleotides, encoding 172 putative amino acid residues. In contrast, *OsHKT1;1-V2(2)* is composed of 957 nucleotides encoding 318 putative amino acid residues (Figure 1A, Supplementary Figure S1). *X. laevis* oocytes were injected with cRNAs of *OsHKT1;1-V2*, *OsHKT1;1-V2(1)*, and *OsHKT1;1-V2(2)*, and TEVC experiments were performed to identify which fragment induces bidirectional ionic currents like OsHKT1;1-V2 [8]. OsHKT1;1-V2(1) but not OsHKT1;1-V2(2) showed ionic currents in both NaCl and KCl bath solutions as OsHKT1;1-V2 (Figure 1B,C). These results suggest that the start codon of OsHKT1;1-V2 is the 1st methionine. Furthermore, histochemical analysis indicated that FLAG tag-fused OsHKT1;1-FL and OsHKT1;1-V2 proteins were localized in the plasma membrane (PM) of oocytes (Figure 1D,E). In contrast, control oocytes injected with water showed no robust green fluorescence in the PM (Figure 1F).

2.2. Subcellular Localization of GFP-Fused OsHKT1;1-FL and OsHKT1;1-V2 in Plant Cells

To study the subcellular localization in plant cells, green fluorescence protein (GFP) was fused with OsHKT1;1-FL and OsHKT1;1-V2 at the N-terminus. DNA constructs to express either GFP, GFP-OsHKT1;1-FL, or GFP-OsHKT1;1-V2 were introduced into *Arabidopsis* leaf protoplasts [35]. Cells expressing GFP showed strong fluorescence in the cytosol, which did not overlap with the plasma membrane marker FM4-64 (Figure 2A–D). GFP fluorescence from cells expressing GFP-OsHKT1;1-FL was observed at the cell periphery, overlapping with FM4-64 fluorescence (Figure 2F–I). A similar overlap of GFP and FM4-64 fluorescence was observed in cells expressing GFP-OsHKT1;1-V2 (Figure 2K–N). Plot-profile fluorescence intensity analysis of the merged fluorescence images supported the above-mentioned observation (Figure 2E,J,O). Together with the negative control experiments shown in Figure 2P–S, these results suggest the plasma membrane localization of OsHKT1;1-V2 as OsHKT1;1-FL.

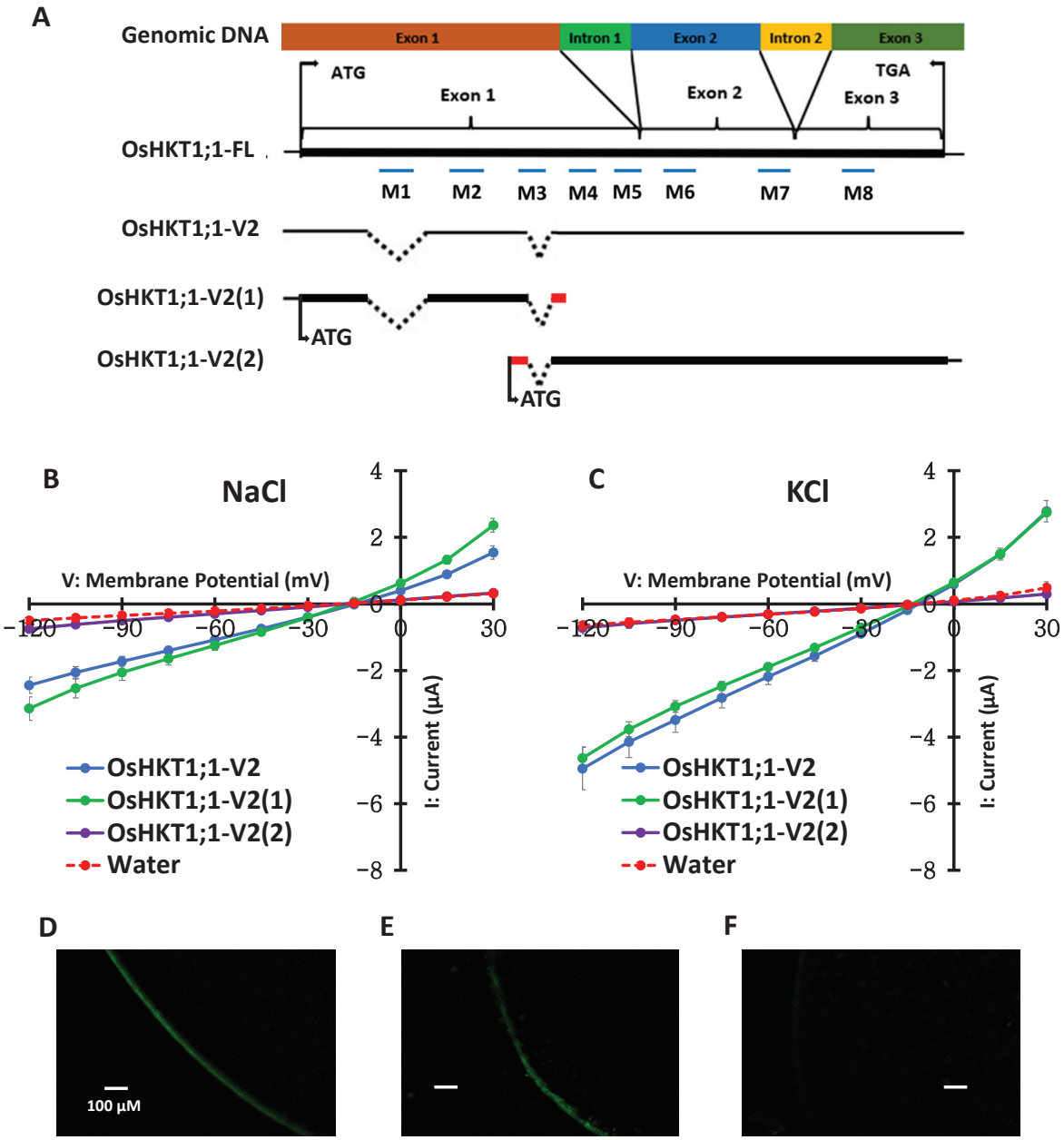


Figure 1. The first methionine functions as a start codon in the *OsHKT1;1-V2* variant. (**A**) Schematic representation of *OsHKT1;1-V2* mRNA, presumably produced by alternative splicing, and its artificially truncated fragments, *OsHKT1;1-V2(1)* and *OsHKT1;1-V2(2)*, each of which contains only one first methionine that could function as a start codon. Boxes indicate amino acid regions that are the same as those in OsHKT1;1-FL (black) or different from those in *OsHKT1;1-FL* (red) because of the frameshift. Dotted lines indicate missing nucleotide regions (gaps compared to the *OsHKT1;1-FL* sequence) due to alternative splicing events. The predicted transmembrane domains (M1–M8) were annotated based on previously curated information in the UniProt database. (**B**,**C**) Transport properties of OsHKT1;1-V2 and its artificial variants, characterized by two-electrode voltage clamp experiments using *X. laevis* oocytes immersed in external solutions containing 96 mM NaCl or 96 mM KCl. Data represent means ± SE, n = 15–18, from three independent experiments performed using different batches of oocytes. (**D**–**F**) Detection of fluorescence derived from the FLAG-tag in oocytes expressing FLAG-OsHKT1;1-FL (**D**) or FLAG-OsHKT1;1-V2 (**E**) or in oocytes injected with water (**F**). All external solutions contained 1.8 mM $CaCl_2$, 1.8 mM $MgCl_2$, 1.8 mM mannitol, and 10 mM HEPES (pH 7.5 with Tris) as background elements. Oocytes were isolated and injected with 50 ng cRNAs/50 nL or 50 nL of nuclease-free water as a negative control, and then incubated for approximately 4 h at 18 °C.

https://doi.org/10.3390/ijms27031178

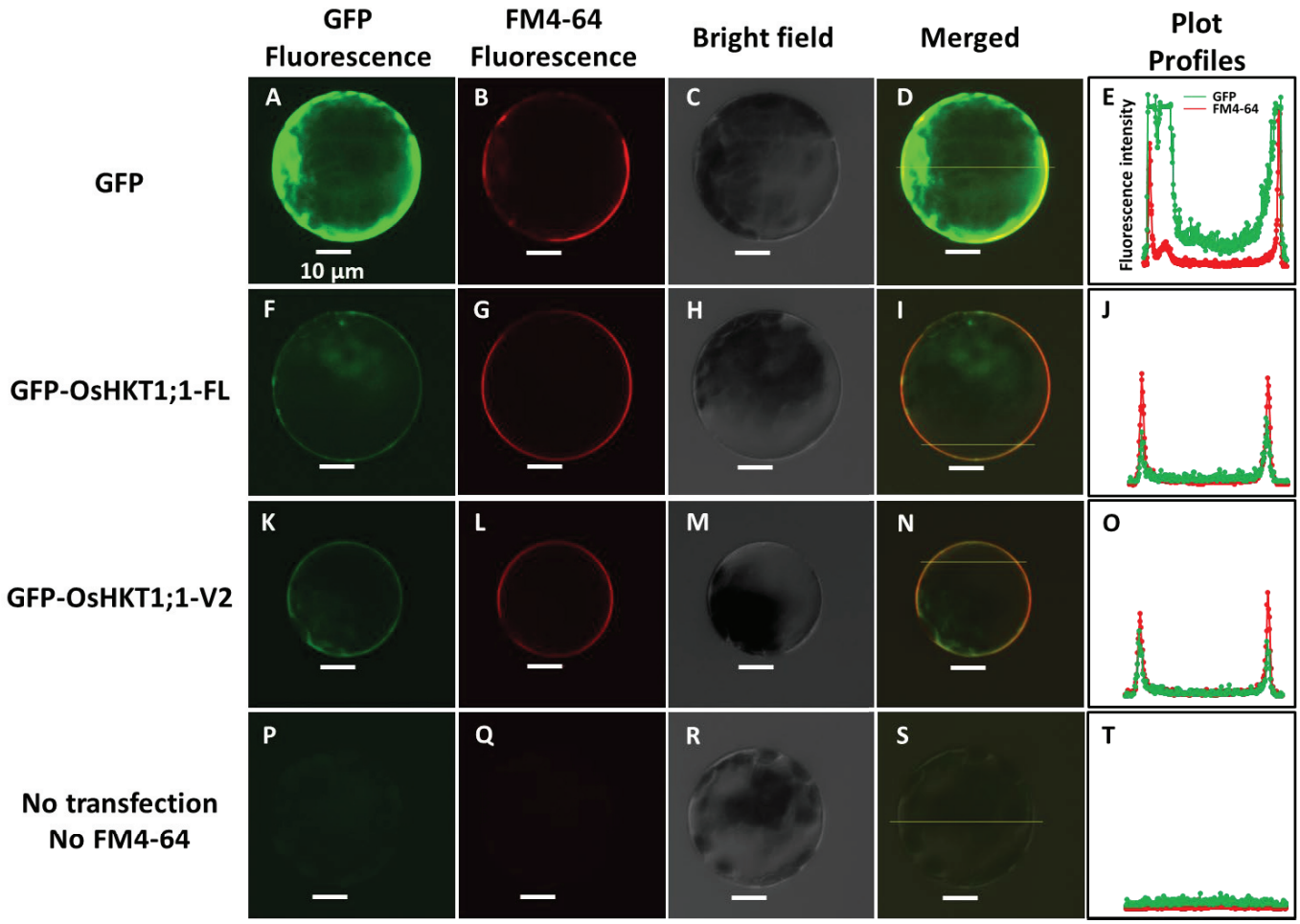


Figure 2. Subcellular localization of GFP-fused OsHKT1;1 transporters in *Arabidopsis* protoplasts. GFP (**A**–**D**), GFP-OsHKT1;1-FL (**F**–**I**), or GFP-OsHKT1;1-V2 (**K**–**N**) was transiently overexpressed in *Arabidopsis* leaf protoplasts. The cells were incubated with FM4-64, which was used as a PM marker. Protoplasts that were not transfected or treated with FM4-64 (**P**–**S**) were used as negative controls. Plot-profile fluorescence intensity analysis of protoplasts expressing different constructs (red and green colors represent fluorescence from FM4-64 and GFP, respectively): GFP (**E**), GFP-OsHKT1;1-FL (**J**), GFP-OsHKT1;1-V2 (**O**), and untransfected and no FM4-64-treated protoplasts (**T**).

2.3. Substrate Selectivity of OsHKT1;1-FL and OsHKT1;1-V2

Current–voltage relationships were obtained in the presence of 96 mM NaCl (96 mM Na^+ and 96 mM Cl^-), 9.6 mM NaCl + 84.6 mM Na gluconate (total 96 mM Na^+ and 9.6 mM Cl^-), and 9.6 mM NaCl + 84.6 mM Choline Cl (9.6 mM Na^+ and total 96 mM Cl^-) by conducting electrophysiological TEVC experiments using *X. laevis* oocytes. As described previously [12], a decrease in Na^+ concentration from 96 mM to 9.6 mM largely reduced the inward currents in OsHKT1;1-FL and showed no tendency to produce robust outward currents (Supplementary Figure S2). In contrast, the same change in solution did not affect OsHKT1;1-V2-mediated currents (Figure 3A). Next, we changed the Cl^- concentration of the bath solution while keeping the Na^+ concentration at 96 mM during TEVC measurements. The 10 times reduction in the Cl^- concentration led to an increase in OsHKT1;1-V2-mediated currents with a positive shift in the reversal potential of 13 mV (Figure 3A, purple and green lines). Note that similar large currents were never observed in water-injected oocytes under any bath condition (Figure 3B).

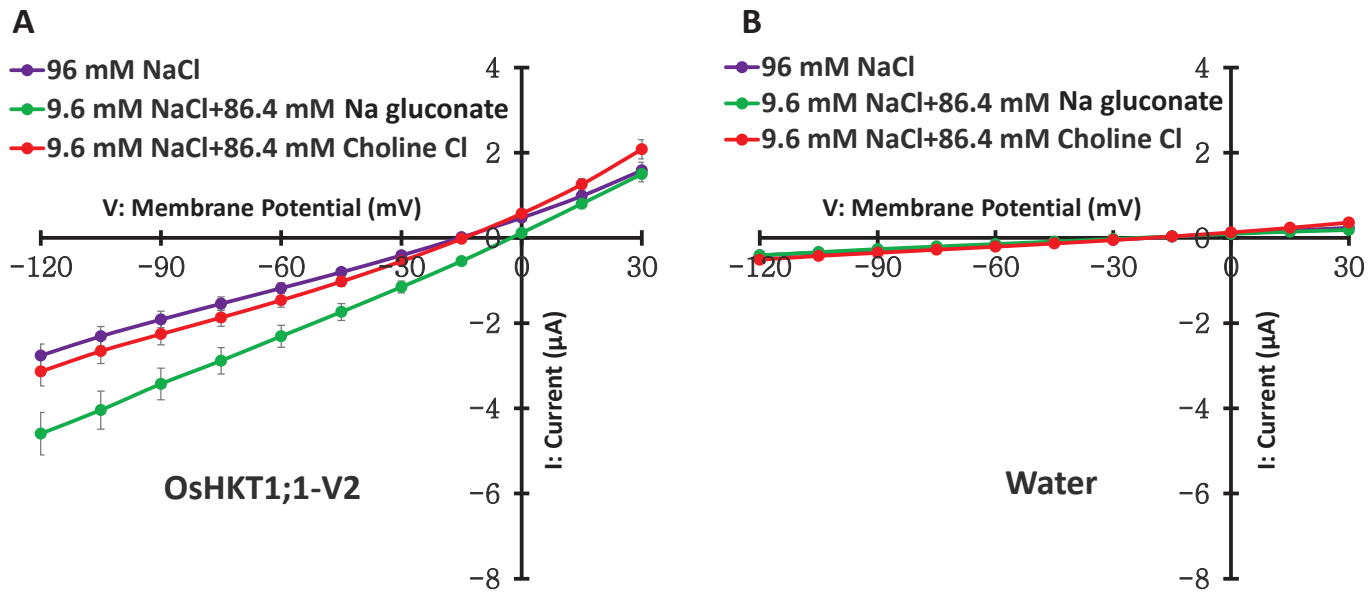


Figure 3. Current–voltage relationships of OsHKT1;1-V2 (**A**) expressed in *X. laevis* oocytes and the oocytes injected with water (**B**). The external solutions used were 96 mM NaCl, 9.6 mM NaCl + 86.4 mM Na gluconate, or 9.6 mM NaCl + 86.4 mM Choline Cl. All external solutions contain, as background elements, 1.8 mM $CaCl_2$, 1.8 mM $MgCl_2$, 1.8 mM mannitol, and 10 mM HEPES (pH 7.5 with Tris). Oocytes were injected with 50 ng cRNAs/50 nL and then incubated for approximately 4 h (OsHKT1;1-V2) or 18 h (water-injected oocytes) at 18 °C before TEVC measurements (note that incubation of OsHKT1;1-V2-expressing oocytes for more than 4 h made it difficult to use them for TEVC experiments due to apparent damage). Data are presented as means ± SE, n = 10–15, from two independent experiments performed with different batches of oocytes.

Next, oocytes expressing OsHKT1;1-V2 were analyzed in 96 mM NaCl (96 mM Na^+ and 96 mM Cl^-), 96 mM Na gluconate (total 96 mM Na^+ and 0 mM Cl^-), and 96 mM Choline Cl (0 mM Na^+ and total 96 mM Cl^-) solutions with voltage steps from +90 to −120 mV in 15 mV decrements to examine outward currents. OsHKT1;1-V2 expressed in oocytes exhibited large outward currents with no reversal potential shift when the solution was changed from 96 mM NaCl to 96 mM Choline Cl, by which Na^+ concentration was decreased from 96 mM to 0 mM (Supplementary Figure S3A, purple and red lines). In contrast, reversal potential shifts occurred according to a change in Cl^- concentration from 96 mM to 0 mM in OsHKT1;1-V2 (Supplementary Figure S3A, purple and red lines vs. green line). Note that endogenous outward currents were also observed in water-injected oocytes, but they were never the same extent as OsHKT1;1-V2-expressing oocytes in every bath condition (Supplementary Figure S3B). These results suggest that the currents induced by OsHKT1;1-V2 largely depend on Cl^-.

2.4. Substrate Concentration Dependency of OsHKT1;1-FL and OsHKT1;1-V2

Further TEVC measurements were performed using oocytes expressing OsHKT1;1-FL or OsHKT1;1-V2 in a series of bath solutions that contained Cl^- as the sole permeable monovalent anion (96, 48, 12, and 6 mM as choline chloride) or Na^+ as the sole permeable monovalent cation (96, 48, 12, and 6 mM as Na gluconate). OsHKT1;1-FL-expressing oocytes showed currents comparable to those of water-injected control oocytes, with no reversal potential shift in a series of changes in Cl^- concentration (Figure 4A,B, Supplementary Figure S4B). However, OsHKT1;1-FL showed large and various currents with reversal potential shifts in a series of changes in the Na^+ concentration (Figure 5A,B). These data suggest that OsHKT1;1-FL mediates the transport of Na^+. In contrast, oocytes

expressing OsHKT1;1-V2 exhibited robust inward and outward currents with reversal potential shifts in a series of changes in the Cl^- concentration (Figure 4C,D). In contrast, OsHKT1;1-V2-expressing oocytes showed larger currents than water-injected control oocytes in accordance with a series change in the Na^+ concentration; however, the reversal potential did not alter as in oocytes expressing OsHKT1;1-FL (Figure 5B–D, Supplementary Figure S4A). These data suggest that, unlike OsHKT1;1-FL, OsHKT1;1-V2 is selective for Cl^- and mediates its transport.

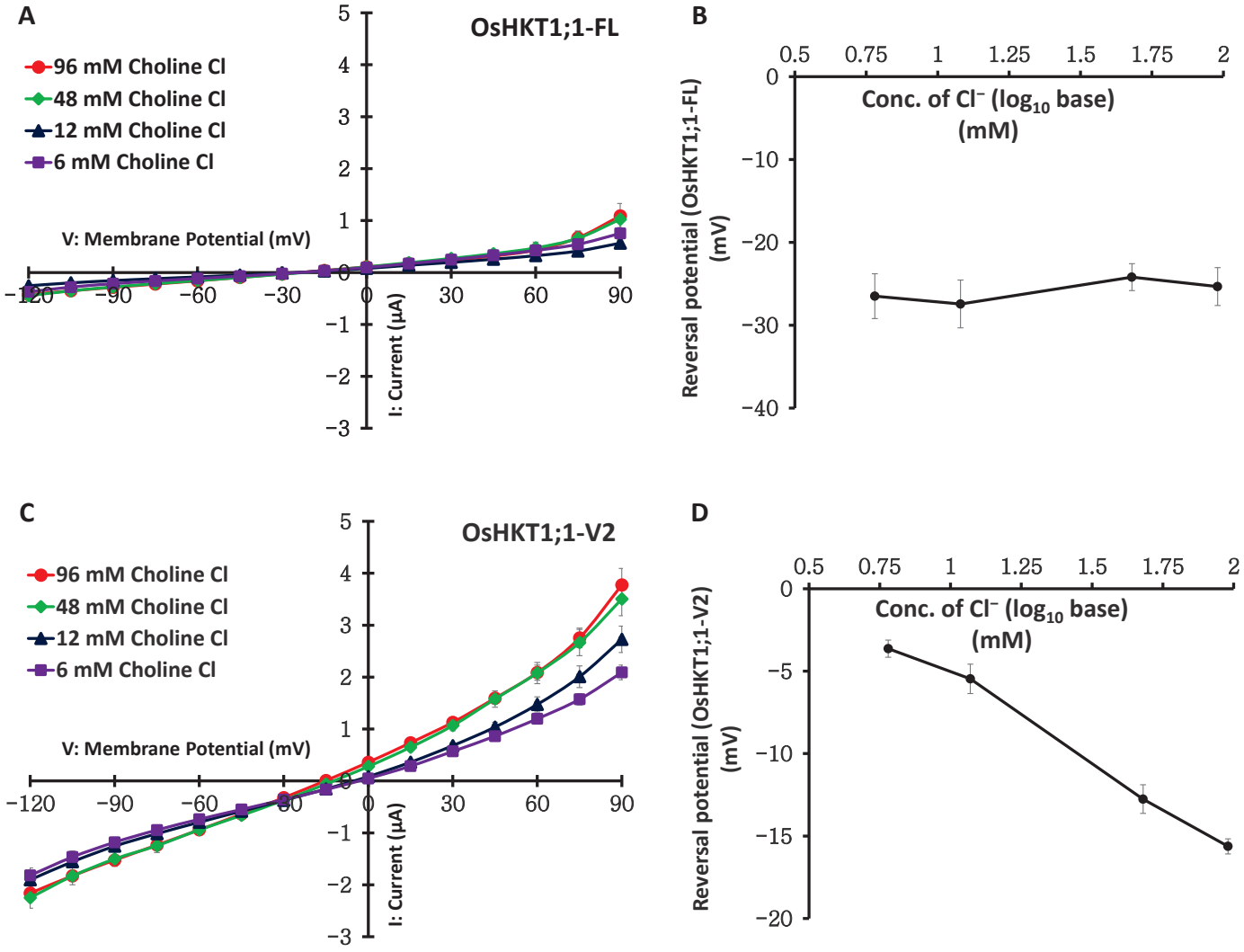


Figure 4. Chloride concentration dependency of OsHKT1;1-FL and OsHKT1;1-V2 expressed in *X. laevis* oocytes. (**A**,**C**) Current–voltage relationships of oocytes expressing OsHKT1;1-FL and OsHKT1;1-V2. (**B**,**D**) Log10 base reversal potential analysis of OsHKT1;1-FL and OsHKT1;1-V2, respectively. A series of choline chloride solutions with concentrations ranging from 96 mM to 6 mM was used as the external bath solution. The basic components of the solutions were 1.8 mM $CaCl_2$, 1.8 mM $MgCl_2$, 1.8 mM mannitol, and 10 mM HEPES, and the pH was adjusted to 7.5 using Tris. The 48, 12, and 6 mM choline chloride solutions contained 38, 63, and 68 mM Mg gluconate, respectively. Oocytes were isolated and injected with 2.5 ng cRNAs/50 nL and then incubated for approximately 18 h for OsHKT1;1-FL or 4 h for OsHKT1;1-V2 at 18 °C. To obtain current–voltage relationships, voltage steps (2 s) were applied from +90 to −120 mV in 15 mV decrements. Data are presented as mean ± SE, n = 16–18, from two independent experiments using different batches of oocytes.

https://doi.org/10.3390/ijms27031178

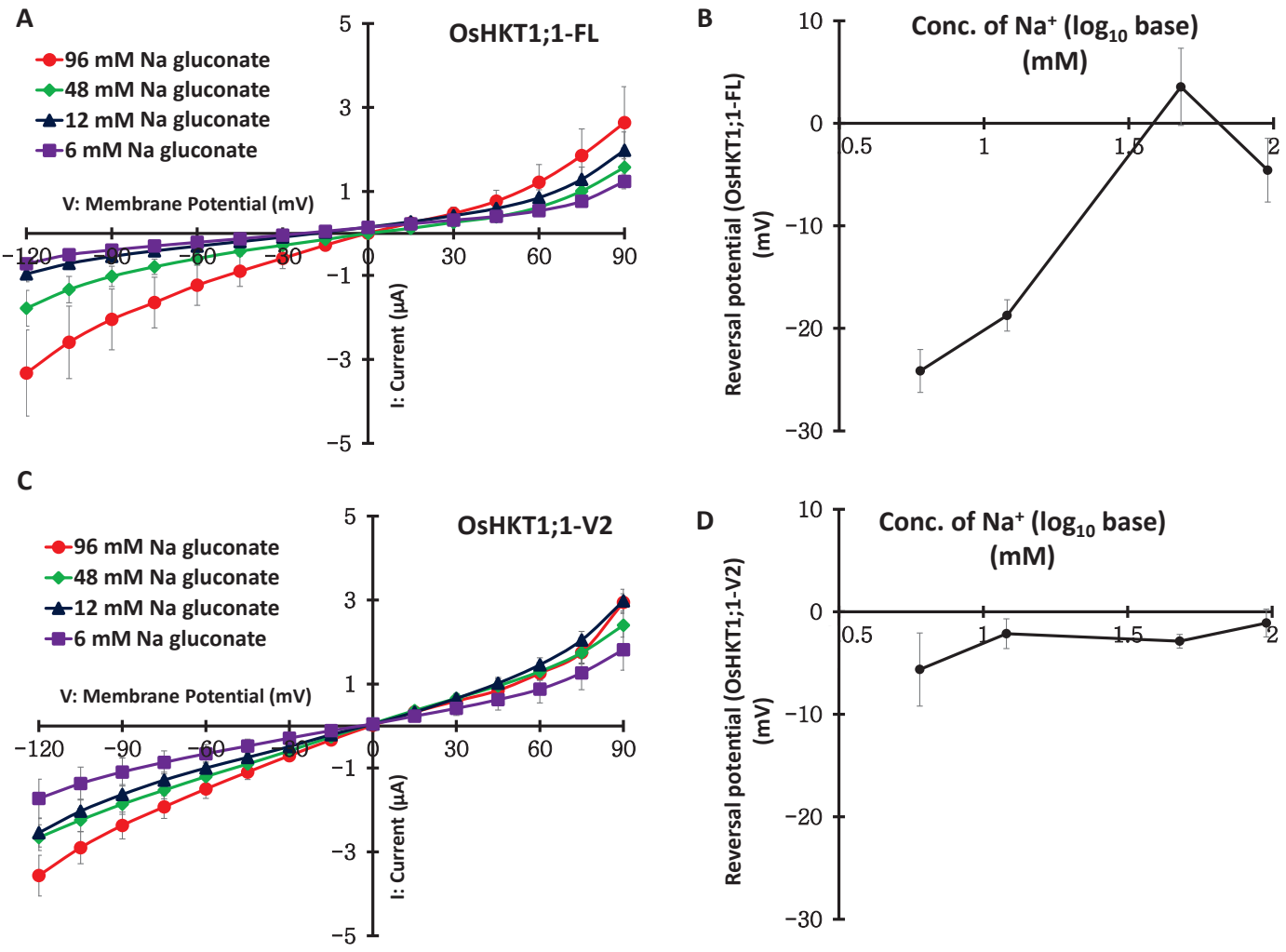


Figure 5. Sodium concentration dependency of OsHKT1;1-FL and OsHKT1;1-V2 expressed in *X. laevis* oocytes. (**A**,**C**) Current–voltage relationships from oocytes expressing OsHKT1;1-FL and OsHKT1;1-V2, respectively. (**B**,**D**) Log10 base reversal potential analysis of OsHKT1;1-FL and OsHKT1;1-V2, respectively. A series of sodium gluconate solutions with concentrations ranging from 96 mM to 6 mM was used as the external bath solution. The basic components of the solutions contained 1.8 mM Ca gluconate, 1.8 mM Mg gluconate, 1.8 mM mannitol, and 10 mM HEPES, and the pH was adjusted to 7.5 using Tris. The 48, 12, and 6 mM sodium gluconate solutions contained 38, 63, and 68 mM Mg gluconate, respectively. Oocytes were isolated and injected with 2.5 ng cRNAs/50 nL and then incubated for about 18 h for OsHKT1;1-FL or 4 h for OsHKT1;1-V2 at 18 °C. To obtain current–voltage relationships, voltage steps (2 s) were applied from +90 to −120 mV in 15 mV decrements. Data are presented as mean ± SE, n = 15–16, from two independent experiments using different batches of oocytes.

2.5. Cl^- Contents in Oocytes

Cl^- accumulation was investigated using oocytes injected with water, *OsHKT1;1-FL* cRNA, or *OsHKT1;1-V2* cRNA, which were incubated in 96 mM choline chloride-containing medium (Figure 6). The total Cl^- content showed that OsHKT1;1-V2-expressing oocytes (2.5 ng cRNA) accumulated significantly more Cl^- than OsHKT1;1-FL-expressing (2.5 ng cRNA) and water-injected oocytes (Figure 6). Furthermore, a 10-fold increase in the injection volume of the *OsHKT1;1-V2* cRNA (25 ng) resulted in the accumulation of approximately 6 times more Cl^- (Figure 6). To verify that the observed Cl^- increase was specifically due to Cl^- influx and not caused by nonspecific anion accumulation, the same experiment was performed in Na-gluconate medium without Cl^-. Under these Cl^--free conditions,

all oocytes, including those expressing OsHKT1;1-V2, showed low Cl^- levels (Figure 6). These results support that OsHKT1;1-V2 mediates Cl^- transport in the PM of oocytes, as suggested by the TEVC experiments shown in Figures 3 and 4.

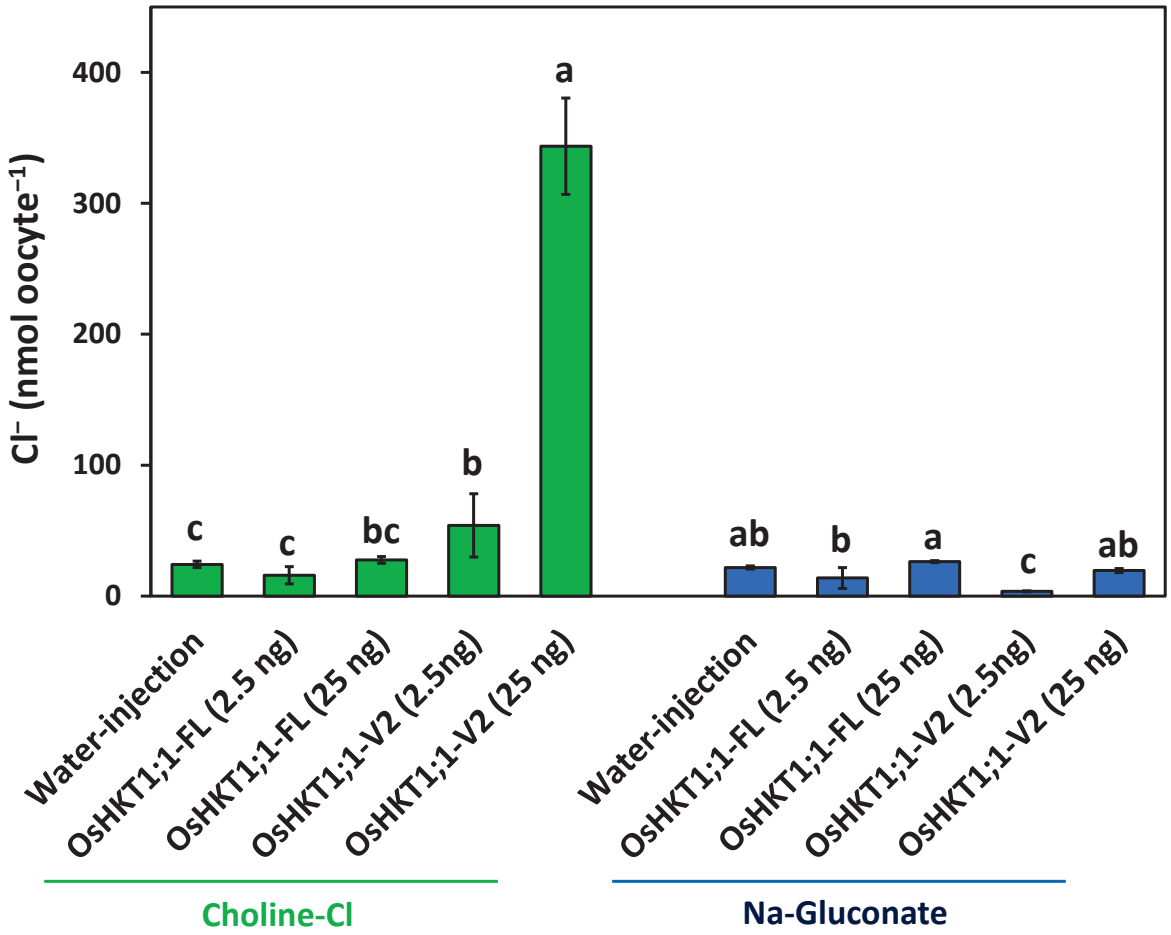


Figure 6. Cl^- contents of oocytes injected with *OsHKT1;1-FL* cRNA, *OsHKT1;1-V2* cRNA, or water. Oocytes were treated with 96 mM Na-gluconate or 96 mM choline-Cl solution for 6 h at room temperature. See Section 4 for details. Data are shown as mean ± SD. 4 to 8 batches of oocytes were used to measure Cl^- contents (note that each batch included 8–10 oocytes): n = 8 batches for OsHKT1;1-FL (2.5 ng), 8 for OsHKT1;1-FL (25 ng), 8 for OsHKT1;1-V2 (2.5 ng), 8 for OsHKT1;1-V2 (25 ng), and 8 for water injection in a choline Cl treatment; and n = 8 batches for OsHKT1;1-FL (2.5 ng), 4 for OsHKT1;1-FL (25 ng), 4 for OsHKT1;1-V2 (2.5 ng), 4 for OsHKT1;1-V2 (25 ng), and 8 for water injection in a Na-gluconate treatment. A one-way ANOVA with Tukey post hoc test was used for the Choline-Cl and Na-Gluconate group separately; different lowercase letters indicate statistically significant differences ($p < 0.05$).

2.6. Functional Characterization of OsHKT1;1 Transporters in Yeast

OsHKT1;1-FL and *OsHKT1;1-V2* were introduced into the Na^+-sensitive mutant yeast strain G19 to further examine the Na^+ transport capacity of *OsHKT1;1-FL* and *OsHKT1;1-V2*. No remarkable difference was found in the growth among *OsHKT1;1-FL*, *OsHKT1;1-V2*, and empty vector-harboring G19 cells under the control condition (Figure 7, left panel). However, the presence of 50 mM NaCl caused severe growth defects in OsHKT1;1-FL-expressing cells. In contrast, cells expressing *OsHKT1;1-V2* grew similarly to the vector-harboring control cells (Figure 7, right panel). These data indicate that *OsHKT1;1-FL*, but not *OsHKT1;1-V2*, possibly accelerated Na^+ uptake in yeast cells, leading to toxicity and growth reduction in the cells under NaCl-added conditions. Thus Na^+ contents of G19 transformants were determined under no or 50 mM NaCl conditions (Figure 7C). After 18

and 21 h incubation, for control and NaCl-added conditions, respectively, in the presence of galactose, G19 cells expressing OsHKT1;1-FL were found to accumulate significantly higher levels of Na^+ than the others in both conditions (Figure 7C). Whereas Na^+ contents of vector control and OsHKT1;1-V2 lines were at similar levels (Figure 7C). These results were consistent with the growth phenotype (50 mM NaCl; Figure 7B).

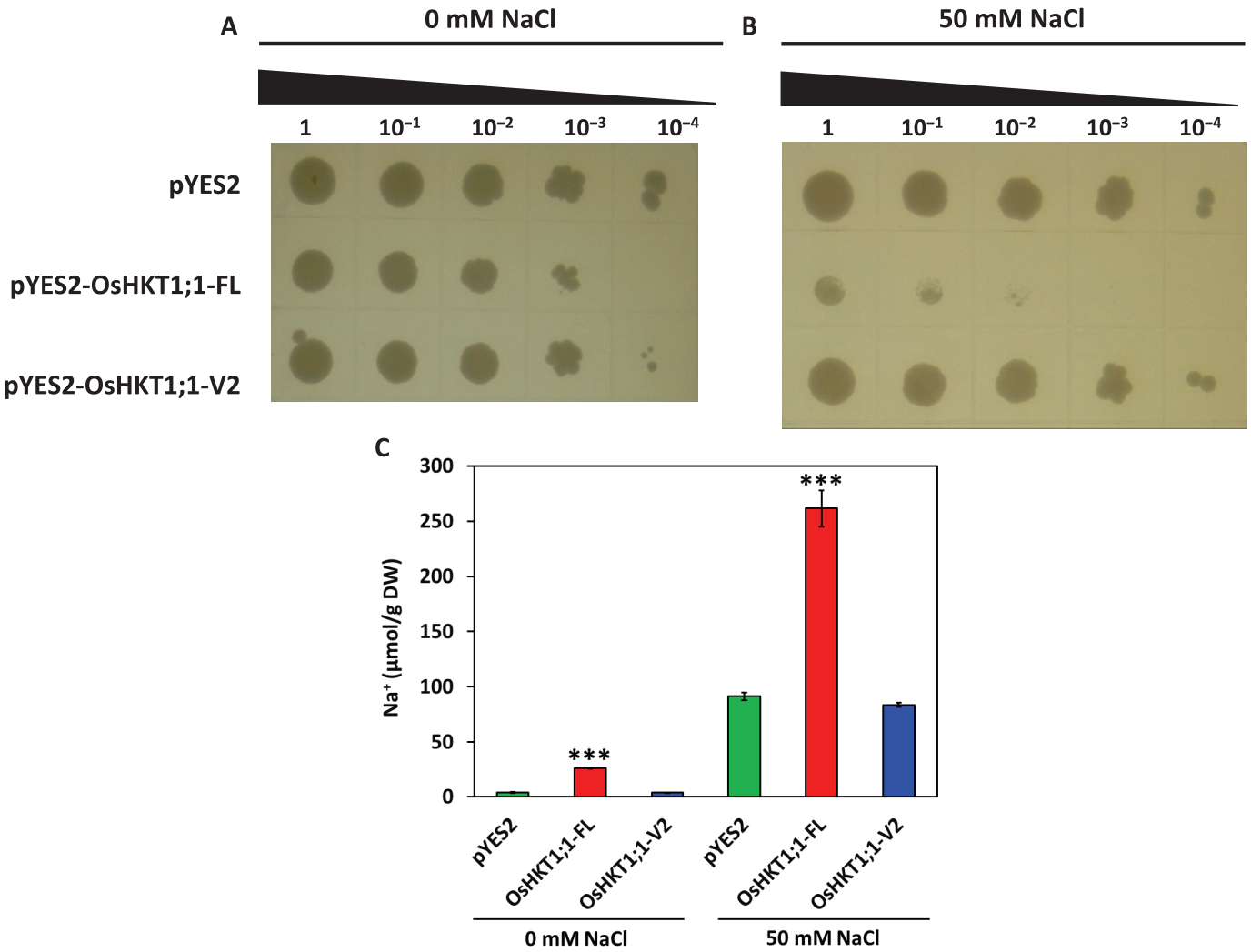


Figure 7. Functional characterizations of *OsHKT1;1-FL* and *OsHKT1;1-V2* in the G19 yeast strain. Growth of G19 cells transformed with empty vector (pYES2), pYES2-*OsHKT1;1-FL*, and pYES2-*OsHKT1;1-V2*. Each G19 transformant was incubated at 30 °C for 4 days on -Ura medium plates [0.67% (*w*/*v*) yeast nitrogen base without amino acids, 0.077% (*w*/*v*) drop out mix-Ura, 2% (*w*/*v*) galactose, 1% (*w*/*v*) raffinose, and 2% agar] containing 0 mM NaCl (**A**) or 50 mM NaCl (**B**). Numbers (1, 10^{-1}, 10^{-2}, 10^{-3}, 10^{-4}) on the top of each panel indicate the serial dilutions (OD_{600}) of yeast cells spotted on the medium. (**C**) Na^+ content of G19 transformants that were incubated in liquid synthetic complete (SC) medium supplemented with or without 50 mM NaCl for 18 (control) and 21 (NaCl-treated) h at 30 °C ($n = 5$, ± SD). Asterisks denote significant differences from control (pYES2 empty vector) (Student's *t*-test: *** $p < 0.001$).

2.7. Transport Properties of OsHKT1;1-FL and Variants from Nipponbare

In a previous study [8] and in Figures 1–7 in the present study, possible *OsHKT1;1* splicing variants, in addition to the full-length cDNA from salt-tolerant *indica* rice, Pokkali, were investigated. Therefore, we attempted to determine whether these *OsHKT1;1* splicing variants could also be found in the salt-sensitive *japonica* rice, Nipponbare, and whether they functioned in a manner similar to those from Pokkali. *OsHKT1;1* cDNAs were isolated

from Nipponbare, and their transport properties were examined by TEVC experiments. Eight possible *OsHKT1;1* variants were detected in addition to the full-length cDNA from Nipponbare as Pokkali [8]. Comparative analysis revealed amino acid substitutions in OsHKT1;1 between the two genotypes (Supplementary Figure S5A–I). However, oocytes expressing Nipponbare (Ni) OsHKT1;1-FL and OsHKT1;1-V6 exhibited inward-rectifying currents in the presence of 96 mM NaCl, with much smaller currents of OsHKT1;1-V6 than OsHKT1;1-FL (Figure 8A). In contrast to Ni-OsHKT1;1-V1 and -V4, whose currents were similar to those from water-injected control oocytes (Figure 8A), Ni-OsHKT1;1-V2, -V3, -V5, -V7, and-V8 mediated ionic currents in a bidirectional manner, depending on the membrane voltage (Figure 8B). There was no remarkable difference in the pattern of elicited currents mediated by these variants between Pokkali and Nipponbare.

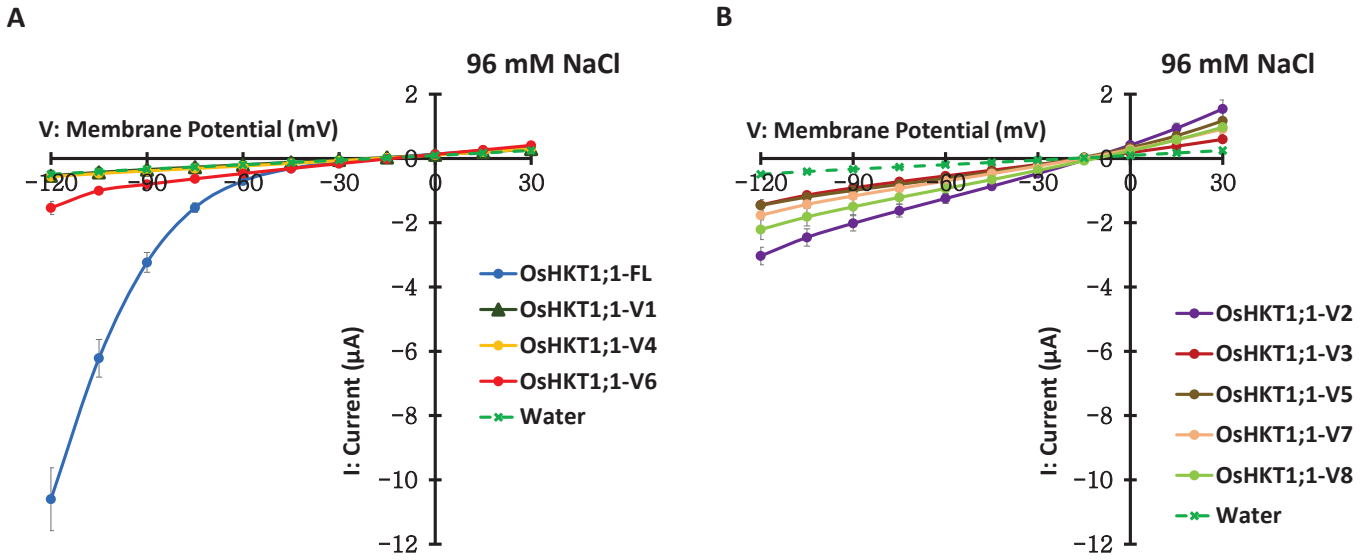


Figure 8. TEVC recordings of oocytes expressing OsHKT1;1-FL and OsHKT1;1 variants derived from cv. Nipponbare. (**A**) Current–voltage relationships from oocytes expressing OsHKT1;1-FL, -V1, -V4, and-V6 and oocytes injected with water. (**B**) Current–voltage relationships from oocytes expressing OsHKT1;1-V2, -V3, -V5, -V7, and-V8 and oocytes injected with water. The external bath solution contained 96 mM NaCl, 1.8 mM $CaCl_2$, 1.8 mM $MgCl_2$, 1.8 mM mannitol, and 10 mM HEPES (pH 7.5, with Tris). Data are presented as mean ± SE, n = 10–18, from two independent experiments using different batches of oocytes.

Next, oocytes expressing Ni-OsHKT1;1-FL and Ni-OsHKT1;1-V2 were examined in Cl^- solutions (96, 48, 12, and 6 mM as choline chloride) (Supplementary Figure S6). Current–voltage relationships obtained from Ni-OsHKT1;1-FL expressed in oocytes showed small or no currents and no reversal potential shift with changes in Cl^- concentrations in the bath solution (Supplementary Figure S6A,B). In contrast, oocytes injected with *OsHKT1;1-V2* cRNA exhibited both inward and outward currents with apparent reversal potential shifts according to the Cl^- concentration (Supplementary Figure S6C,D). These data suggest that Ni-OsHKT1;1-V2, but not Ni-OsHKT1;1-FL, mediates Cl^- transport, as observed in those transporters from Pokkali.

2.8. Expression Analyses of OsHKT1;1-FL and OsHKT1;1-V2 in Shoots and Roots

We next investigated the transcript levels of *OsHKT1;1-FL* and *OsHKT1;1-V2* in Pokkali and Nipponbare by conducting qPCR-based absolute quantification. Without stress, Nipponbare plants accumulated approximately five times more *OsHKT1;1-FL* transcripts than Pokkali in shoots (Figure 9A). However, in the case of *OsHKT1;1-V2*, the transcript level in shoots was approximately six times higher in Pokkali than in Nipponbare (Figure 9A at

time 0; note that the scale for transcript amounts is log-10-based). Interestingly, salt stress (100 mM NaCl) temporally increased both *OsHKT1;1-FL* and *OsHKT1;1-V2* transcripts in Nipponbare, peaking at 12 h, whereas those of Pokkali decreased (Figure 9A). In roots, the *OsHKT1;1-FL* transcript level was much lower in Pokkali than in Nipponbare, and so was the level of the *OsHKT1;1-V2* transcript under control conditions (Figure 9B). The OsHKT1;1-FL transcript level was temporally increased, peaking at 6 h after salt stress in Nipponbare, but this observation was not applied to Pokkali (Figure 9B). The levels of the other transcripts were maintained relatively constant during the periods investigated (Figure 9B). These results indicate a differential regulatory mechanism of *OsHKT1;1* gene expression between rice genotypes.

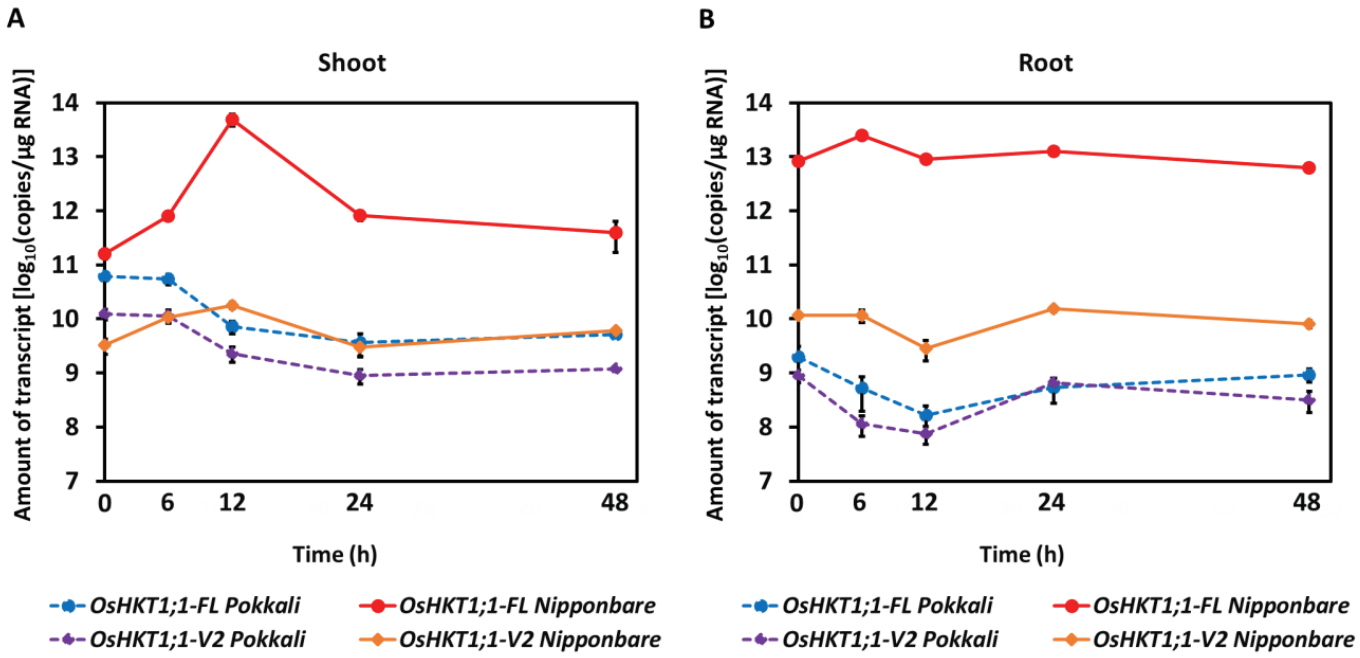


Figure 9. Absolute quantification of *OsHKT1;1-FL* and *OsHKT1;1-V2* transcript levels in Pokkali and Nipponbare plants with or without salt stress. The number of transcripts is displayed in log10 base in shoots (**A**) and roots (**B**). Fourteen-day-old seedlings of both varieties were treated with or without 100 mM NaCl (6–48 h) before total RNA extraction. Data are presented as the mean ± SE (n = 6).

3. Discussion

HKT membrane proteins are known to be relevant to Na^+ homeostasis in plants, including under salinity stress. Na^+ exclusion protects photosynthetic tissues from salt-induced damage [6], and some of the Na^+-selective class I HKT (HKT1) transporters play a key role in excluding Na^+ from leaves, enhancing salinity tolerance [4,22,36–39]. In rice, OsHKT1;1 and OsHKT1;3 exhibit strong and weak inward rectification for Na^+ transport, respectively [8,9,12]. Many other studies on the homologue of HKT1;1 from barley, pumpkin, grapevine, blueberry, and wild turf *Sporobolus virginicus* have also revealed Na^+-selective transport as OsHKT1;1 [13–17]. Campbell et al. [23] showed that natural allelic variants of *OsHKT1;1* underlie the divergence in root Na^+ content between japonica and indica rice cultivars. They reported three non-synonymous mutations associated with higher OsHKT1;1 activity and Na^+ transport efficiency, explaining the genetic basis for the diversity in salt tolerance in rice. This study also provides strong genetic evidence that *OsHKT1;1* plays a central role in Na^+ homeostasis and is an important target for improving salinity tolerance through molecular breeding. Additionally, *OsHKT1;1* interacts with the Salt Overly Sensitive (SOS) pathway and other transporters, implying a complex regulatory network for ion balance and salt stress response [11,18,20,40].

In our previous study, eight *OsHKT1;1* variants (V1-V8) that could be the product of alternative splicing were identified in addition to the full-length *OsHKT1;1-FL* cDNA in the salt-tolerant rice cultivar Pokkali [8]. In this study, we focused on the variant *OsHKT1;1-V2* as the transcript level was significantly higher than that of *OsHKT1;1-FL* in shoots of Pokkali, and *OsHKT1;1-V2* cRNA-injected oocytes exhibited larger inward and outward currents than other variants in both NaCl and KCl bath solutions [8]. Although two start codons are present in *OsHKT1;1-V2* mRNA, the present study demonstrated that the first start codon of *OsHKT1;1-V2* is functional (Figure 1A–C). The plasma membrane localization of FLAG-tagged OsHKT1;1-V2 in oocytes (Figure 1E) indicated that the ionic currents elicited by OsHKT1;1-V2 (Figures 1 and 3–5) were not artifacts or leaks. In the present study, the co-localization of GFP-fused OsHKT1;1-FL or OsHKT1;1-V2 with the dye FM4-64 in the plasma membrane was further demonstrated in *Arabidopsis* protoplasts (Figure 2), supporting the above-mentioned notion.

OsHKT1;1-FL was confirmed to mediate Na^+ transport, as reported previously [8] (Figure 7, Supplementary Figure S2). Interestingly, however, OsHKT1;1-V2 displayed distinct selectivity for Na^+ and Cl^-: the OsHKT1;1-V2 protein expressed in oocytes was responsive to the changes in the Cl^- concentration but not the Na^+ concentration, suggesting a preference for Cl^- transport over Na^+ transport (Figure 3, Supplementary Figure S3). OsHKT1;1-FL showed a concentration-dependent reversal potential shift only in Na^+ bath solutions, whereas OsHKT1;1-V2 showed no concentration-dependent reversal potential shifts in Na^+ solutions (Figure 5, Supplementary Figure S7). In contrast to the lack of reversal potential shifts in OsHKT1;1-V2-expressing oocytes upon Na^+ concentration changes, the observed apparent reversal potential shifts upon Cl^- concentration changes again suggested that OsHKT1;1-V2 is more selective for Cl^- (Figures 4 and 5). This electrophysiological suggestion was further supported by the measurements of Cl^- contents of oocytes expressing OsHKT1;1-V2, which accumulated significantly more Cl^- than the oocytes expressing OsHKT1;1-FL after incubation in the examination solution (Figure 6). In fact, oocytes expressing OsHKT1;1-V2 (2.5 ng cRNA) in the medium exhibited an average reversal potential of −17 mV (Supplementary Figure S3A), while the resting potential of the oocytes was approximately −9 mV, which was +8 mV higher than the reversal potential, indicating that Cl^- influx can be triggered under the tested conditions. The obtained results were consistent with those from the TEVC analysis (Figures 3–5, Supplementary Figure S3). On the other hand, functional assays using the yeast G19 strain supported the notion that OsHKT1;1-FL, but not OsHKT1;1-V2, mediates Na^+ uptake (Figure 7). In addition to the growth phenotype, quantification of Na^+ levels in yeast cells provided evidence that OsHKT1;1-FL but not OsHKT1;1-V2 led to overaccumulation of Na^+ even under a control condition where the existence of 1 mM or less Na^+ is expected (Figure 7C). This result confirms that the growth inhibition observed in OsHKT1;1-FL-expressing G19 strain is attributable to enhanced Na^+ uptake. More importantly, the lack of remarkable Na^+ accumulation in OsHKT1;1-V2-expressing cells is fully consistent with the electrophysiological analyses in *Xenopus* oocytes (Figures 3 and 5).

During salt stress, maintenance of Cl^- homeostasis is crucial because excess cytosolic Cl^- can be toxic [41,42]. Cl^- detoxification involves xylem loading, vacuolar sequestration, and efflux from roots [41,43]. Chloride channels (CLCs) are membrane proteins that mediate Cl^- and NO_3^- transport across plant membranes, contributing to pH regulation and stress tolerance [44,45]. Each CLC monomer contains 16–18 transmembrane α-helices that form a self-contained anion pore and a cytosolic CBS domain that regulates gating through conformational and nucleotide-dependent mechanisms [45,46]. The conserved GxGxPE and GKxGPxxH motifs form part of the selectivity filter, where serine or proline residues determine Cl^- versus NO_3^- specificity [47]. Overexpression of *GmCLC1*,

CsCLC-c, and *ZmCLC-d* has been reported to enhance salt tolerance by promoting vacuolar Cl^- sequestration and reducing cytosolic accumulation [48–50]. The plasma membrane transporters NPF2.4 and SLAH1 are proposed to function in regulating Cl^- loading into the xylem [51,52], whereas tonoplast-localized CLCs mediate Cl^-/H^+ antiport to sequester Cl^- into vacuoles [41,42]. Additionally, *AtCCC1* functions as a Na^+:K^+:Cl^- cotransporter essential for maintaining ion balance and osmotic potential [53]. Loss-of-function mutants of *AtCCC1* and *OsCCC1* exhibit stunted growth and excessive Cl^- accumulation in shoots, indicating that CCC1 participates in Cl^- retrieval and homeostasis [53,54]. Moreover, some ALMT members (*AtALMT9* and *AtALMT12*) facilitate Cl^- transport [55,56].

In the present study, we demonstrated that the OsHKT1;1-V2 splice variant encodes a protein of 172 amino acids with a single predicted transmembrane helix (Supplementary Figure S1A). Despite lacking the canonical pore-forming domains of HKTs, TEVC assays revealed robust inward and outward currents, suggesting that OsHKT1;1-V2 may form a self-associated complex that is permeable to Cl^-. Sequence inspection of OsHKT1;1-V2 revealed a central hydrophobic stretch (residues 96–118; "LWVLILLMLMGGEVFTSMLGLYF") (Supplementary Figure S1A), likely forming the ion-conducting α-helix, surrounded by charged and polar residues that could stabilize Cl^- within the pore. Notably, OsHKT1;1-V2 contains an upstream GKxGPxx pattern (residues 61–67) that resembles part of the conserved GKxGPxxH selectivity motif present in plant CLC proteins (Supplementary Figure S1A). Although this pattern lacks the canonical histidine present in CLC selectivity filters, it may still contribute to local structural flexibility or pore shaping, providing a residual signature of the anion-interacting architecture. Interestingly, the overall minimal architecture of OsHKT1;1-V2 parallels the basic structural layout of inwardly rectifying K^+ (Kir) channels, which are composed of two transmembrane helices (TM1 and TM2) connected by a pore-forming loop and assembled as a tetramer to form a functional channel [57]. Kir channels exhibit inward rectification through pore blockage by intracellular Mg^{2+} and polyamines, allowing greater ion influx than efflux [57]. By analogy, OsHKT1;1-V2 might represent a minimal anion-conducting module, in which its single transmembrane helix or multimeric assembly provides a rudimentary Cl^- pathway.

Although *Xenopus* oocytes have endogenous anion channels, the following facts minimize the possibility that these channels contributed to the OsHKT1;1-V2-associated currents. First, in contrast to the Cl^--dependent reversal potential changes seen in OsHKT1;1-V2-expressing oocytes (Figure 4C,D, Supplementary Figure S6C,D), water-injected controls showed only small inward and outward currents that did not change with external Cl^- concentration (Supplementary Figure S4B). Second, Cl^- accumulation assays demonstrated that water-injected oocytes consistently showed minimal Cl^- accumulation under all tested conditions, and OsHKT1;1-V2-expressing oocytes showed an increase in Cl^- accumulation (Figure 6). Note, however, that we cannot exclude the possibility that the OsHKT1;1-V2 variant interacts with other membrane proteins to form a minimal Cl^--selective channel in oocytes. Thus, further mechanistic research will be needed. Approaches such as expressing dominant-negative OsHKT1;1-V2 mutants, testing OsHKT1;1-V2 multimerization biochemically, and reconstituting purified OsHKT1;1-V2 into liposomes or artificial membranes would clarify whether OsHKT1;1-V2 exhibits an inherently channel-forming feature by itself.

Although some amino acid substitutions were detected in the variants of *OsHKT1;1* between Pokkali and Nipponbare (Supplementary Figure S5), the lineup of *OsHKT1;1* transcripts was identical between the two cultivars [8]. In addition, OsHKT1;1-FL and other OsHKT1;1 variants derived from Nipponbare exhibited transport profiles similar to those of OsHKT1;1 transporters from Pokkali (Figure 8) [8]. Moreover, the similarity in the substrate selectivity of the OsHKT1;1-V2 variants from both rice varieties suggested

that the function of OsHKT1;1-V2 in ion homeostasis might be conserved across different genetic backgrounds (Figures 4 and 5, Supplementary Figure S6).

It has been reported that the transcript levels of *OsHKT1;1* in shoots increased significantly, showing a 3- to 5-fold rise after 12 h of salt treatment, whereas no upregulation was observed in roots [22]. In contrast, *HvHKT1;1* was upregulated in roots under salinity stress, with relatively lower expression levels detected in leaves and sheaths [41]. Similarly, the transcript levels of *HKT1;1* have been analyzed in other plant species, in which the expression level was found to be increased in response to salt stress in both shoots and roots, or only in roots [58–60]. However, previous reports have only quantified full-length mRNA and have not considered variants. Absolute quantification of *OsHKT1;1* transcripts in the present and previous studies demonstrated that the expression levels varied among variants and between the cultivars. Nipponbare exhibited higher and more stable expression of *OsHKT1;1-FL* under salt stress (Figure 9). As *OsHKT1;1* has been proposed to be a salt-tolerant determinant in rice [22–24], it is intriguing that salt-tolerant Pokkali did not increase *OsHKT1;1* transcripts and maintained a lower level of expression during salt stress compared with those in salt-sensitive Nipponbare (Figure 9). These results indicate that *OsHKT1;1* may function to maintain basal ion homeostasis in Pokkali under normal condition and have a limited role in Pokkali under salt stress, although *OsHKT1;1* in a salt-tolerant *indica* rice cultivar Zhenshan 2 was found to play a more essential role in the mechanism of salt tolerance [23]. In Pokkali, other specific transporters/channels, including OsHKT1;5 [2], may have significant functions under salt stress.

Overall, these results highlight the unexpected characteristics of the *OsHKT1;1* splicing variant OsHKT1;1-V2 in rice, which was suggested to encode a possible Cl^- channel. However, the expression of *OsHKT1;1-V2* was lower than that of *OsHKT1;1-FL* in both Pokkali and Nipponbare. However, important questions remain to be elucidated: (i) Does OsHKT1;1-V2 function as a Cl^- channel in rice? If so, (ii) does OsHKT1;1-V2 contribute to Cl^- homeostasis and salt tolerance? (iii) Does the differential regulation in the expression of *OsHKT1;1-FL* and *OsHKT1;1-V2* between Nipponbare and Pokkali reflect the mechanism of salt tolerance in rice? In addition, further studies are needed to explore the regulatory mechanisms behind the splicing of *OsHKT1;1* and to investigate whether some of the variants other than OsHKT1;1-V2 could also contribute to ion homeostasis in rice plants, including upon salt stress.

4. Materials and Methods

4.1. Plant Material and Growth Conditions

Seeds of Nipponbare (*Oryza sativa* L. ssp. *japonica*), a salt-sensitive rice cultivar, were sterilized, germinated, and grown hydroponically as described previously [8]. Total RNA was extracted from 14-day-old plants.

4.2. Extraction of RNA, and cDNA Synthesis

Total RNA was extracted, and its quality and integrity were assessed before synthesizing cDNA, following a previously described protocol [8]. The *OsHKT1;1* cDNAs were then amplified using *OsHKT1;1* cloning primers and subsequently inserted into a pCR4 topo vector (Invitrogen, Carlsbad, CA, USA).

4.3. Preparation of cRNA for X. laevis Oocytes Heterologous Expression

Full-length *OsHKT1:1* (*OsHKT1;1-FL*) and a variant (*OsHKT1;1-V2*) cRNAs from Pokkali (*Oryza sativa* L. ssp. *indica*) have already been prepared [8]. The cDNAs of *OsHKT1;1* from Nipponbare (*Oryza sativa* L. ssp. *japonica*) were cloned into a pXβG vector, and capped RNA (cRNA) synthesis was performed according to the procedure outlined by Imran

et al. [8]. Oocytes were collected and injected with cRNA at concentrations of 50 ng/50 nL or 2.5 ng/50 nL, or with 50 nL of nuclease-free water as a negative control. The oocytes were then incubated at 18 °C, unless otherwise mentioned, in a modified Barth's solution (MBS) until electrophysiological measurements were conducted as described [61].

4.4. Electrophysiology

Oocyte currents were measured using the two-electrode voltage clamp (TEVC) technique, conducted 1 d after cRNA injection, unless otherwise mentioned. TEVC recordings and subsequent data analysis were performed using an Axoclamp 900A amplifier (Molecular Devices, San Jose, CA, USA), Axon Instruments Digidata 1440A (Molecular Devices, San Jose, CA, USA), and pCLAMP 10 software (Molecular Devices, San Jose, CA, USA). The bath solutions were prepared with a baseline concentration of 1.8 mM $MgCl_2$, 1.8 mM $CaCl_2$, and 10 mM HEPES at pH 7.5 with Tris, and chloride salts of the monovalent cations were used. Gluconic acid magnesium (II) salt or D-mannitol was added as needed to maintain the osmolality of the external solutions between 200 and 220 mOsm in all measurements. To obtain current–voltage relationships, voltage steps (2 s) were applied from +30 to −120 mV in 15 mV decrements unless otherwise mentioned.

4.5. Determination of Cl^- Content in X. laevis Oocytes

Oocytes were injected with 50 nL of water or cRNA of *OsHKT1;1-FL* (2.5 ng) and *OsHKT1;1-V2* (2.5 ng and 25 ng), then incubated in 1× MBS medium for 24 h (*OsHKT1;1-FL*) or 4 h (*OsHKT1;1-V2*) at 18 °C. For the measurement of Cl^- accumulation, the oocytes were transferred to 1 mL of Na-gluconate or choline-Cl solutions. The Na-gluconate solution contained 96 mM Na gluconate, 1.8 mM Ca gluconate, 1.8 mM Mg gluconate, 1.8 mM mannitol, and 10 mM HEPES (pH 7.5 with Tris). The choline-Cl solution contained 96 mM choline Cl, 1.8 mM Ca gluconate, 1.8 mM Mg gluconate, 1.8 mM mannitol, and 10 mM HEPES (pH 7.5 with Tris). After a 6 h incubation at room temperature, the oocytes were washed three times with isotonic Ca-gluconate solution and then placed in a 1.5 mL tube to homogenize in Milli-Q water. Cell debris was removed by centrifugation. The supernatant was collected, diluted, and used for ion analysis using an anion chromatography system.

4.6. Subcellular Localization Analysis Using Arabidopsis Protoplasts

Subcellular localization analysis of OsHKT1;1-FL and OsHKT1;1-V2 proteins was conducted in Arabidopsis leaf protoplasts [35], which were transfected with the modified pTH2 vector [62] containing OsHKT1;1-FL or OsHKT1;1-V2 fused with GFP at the N-terminus under the control of the CaMV 35S promoter. Transfection was performed using the polyethylene glycol (PEG 4000) method, as described by Yoo et al. [63] and Sasaki et al. [64]. Protoplasts suspended in the re-suspension solution (0.5 M mannitol, 20 mM KCl, and 4 mM MES, pH 5.7) were incubated in the dark at 24 °C for 16 h [65]. The plasma membrane was visualized using FM4-64 (16 μM, 5 min). Images of the protoplasts were captured using an Olympus FluoView 1000 Confocal Microscope (Olympus Corporation, Hachioji, Tokyo, Japan). GFP was detected using 473 nm excitation with a 490–525 nm bandpass filter, whereas FM4-64 and chlorophyll were observed with 543 nm excitation and a 560–620 nm bandpass filter.

4.7. Subcellular Localization in Oocytes by Immunocytochemistry

Subcellular localization in oocytes was analyzed using OsHKT1;1-FL and OsHKT1;1-V2 with a FLAG tag (DYKDDDDK) at their N-termini. cRNAs were synthesized using an oocyte expression vector, pXβG vector, including O*sHKT1;1-FL* or *OsHKT1;1-V2* with the sequence of FLAG tag, according to the procedure outlined by Imran et al. [8]. Immunohistochemical analysis was performed as described by Shibasaka et al. [66]. A volume of

50 ng/50 nl for OsHKT1;1-FL and 2.5 ng/50 nl for OsHKT1;1-V2 cRNAs or RNase-free water as a negative control was injected into the oocyte and incubated at 18 °C for 24 h (OsHKT1;1-FL) or 4 h (OsHKT1;1-V2). Subsequently, the samples were fixed for 3 h in 4% (*w*/*v*) formaldehyde solution (pH 7.4) and embedded in 5% agarose. Sections of 100 μm thickness were prepared using a micro slicer (Doshin EM, Osaka, Japan) and subjected to blocking in a buffer containing 50 mM Tris (pH 8.0), 150 mM NaCl, 0.1% Tween 20, and 3% BSA for 1 h at 25 °C. Immunolabeling was performed using primary antibodies, including rat anti-FLAG (raised against the synthetic peptide CDYKDDDDK, Invitrogen, Carlsbad, CA, USA), applied overnight at 4 °C. After three washes, the samples were incubated for another hour with a secondary antibody (Alexa Fluor 488-conjugated goat anti-rabbit IgG, Invitrogen, Carlsbad, CA, USA). After two washes with TBS-T (50 mM Tris, pH 8.0, 150 mM NaCl, 0.1% Tween 20) and a final wash with TBS (50 mM Tris, pH 8.0, 150 mM NaCl), fluorescent signals were observed using a fluorescence microscope (BZ-X700, Keyence, Osaka, Japan).

4.8. Functional Characterization of OsHKT1;1-FL and OsHKT1;1-V2 in Yeast

The CDSs of *OsHKT1;1-FL* and *OsHKT1;1-V2* were cloned into the pYES2 vector and transformed into the well-known Na^+-sensitive yeast strain G19, which lacks Na^+ efflux transporters ENA1-4 [67,68]. Positive transformants were selected on Ura-selective medium plates [0.67% (*w*/*v*) yeast nitrogen base without amino acids, 0.077% (*w*/*v*) dropout mix-Ura, 2% (*w*/*v*) glucose, and 2% (*w*/*v*) agar]. For the yeast growth test, all transformed yeasts were cultured overnight at 30 °C in SC-Ura medium until the OD_{600} reached 1.0, and 10-fold serially diluted cultures were incubated on Ura-induced medium [0.67% (*w*/*v*) yeast nitrogen base without amino acids, 0.077% (*w*/*v*) dropout mix-Ura, 2% (*w*/*v*) galactose, 1% (*w*/*v*) raffinose, and 2% (*w*/*v*) agar] plates containing 50 mM NaCl. The plates were incubated at 30 °C for 4 days, and yeast cell growth was recorded.

4.9. Determination of Ion Contents in Yeast Cells

To quantify intracellular Na^+, each transgenic G19 line was grown in liquid synthetic complete (SC) medium supplemented with or without 50 mM NaCl and galactose at 30 °C. Prior to the main culture, each transformant was cultured in a glass test tube filled with 5 mL SC-Ura glucose medium for overnight at 30 °C. 0.1 mL of each full growth-culture solution was inoculated in a 300 mL Erlenmeyer flask filled with 100 mL SC-Ura galactose medium. After incubation for 18 h (control) and 21 h (NaCl) at 30 °C at 130 rpm, each line was collected by swing-bucket centrifugation using 50 mL centrifuge tubes and then washed by 100 mL of sterilized ultrapure water. After 3 time washes, 10 mL of the washed culture solution was devided in a 15 mL centrifuge tube, and then samples were collected by swing-bucket centrifugation. All harvested samples were dried at 60 °C for 2 days. The dried samples were weighed and digested by 1 mL of ultrapure nitric acid for 24 h. Digests were subsequently heated at 95 °C for 15 min, which was repeated two times. Sodium (Na^+) concentrations were quantified by inductively coupled plasma–mass spectrometry (ICP-MS).

4.10. Expression Analysis

Total RNA extraction, first-strand cDNA synthesis, and absolute quantification of gene expression using specific cDNAs standards were performed as previously described [8]. Total RNA was treated with DNase to remove contaminating genomic DNA (gDNA).

4.11. Statistical Analyses

Statistical analyses were performed using IBM SPSS Statistics (version 25). Significant differences were identified using a *t*-test (*** $p < 0.001$) for Figure 7 and a one-way ANOVA, and Tukey's HSD test ($p < 0.05$) for Figure 6.

https://doi.org/10.3390/ijms27031178

Supplementary Materials: The following supporting information can be downloaded at: https://www.mdpi.com/article/10.3390/ijms27031178/s1.

Author Contributions: Conceptualization, T.H. and M.K.; methodology, T.H. and M.K.; formal analysis, S.I. and T.H.; investigation, S.I., S.O. and R.H.; writing—original draft preparation, S.I.; writing—review and editing, T.H. and M.K.; supervision, M.K.; project administration, M.K.; funding acquisition, M.K. All authors have read and agreed to the published version of the manuscript.

Funding: This research was supported by JSPS KAKENHI Grant Number JP20K06708 to M.K. and T.M., and an OU fellowship to S.I.

Institutional Review Board Statement: The amphibian animal experiment protocols have been allowed without a review by the Animal Care and Use Committee, Okayama University according to relevant national guidelines.

Informed Consent Statement: Not applicable.

Data Availability Statement: The data supporting the findings of this study are available from the corresponding authors upon reasonable request.

Acknowledgments: We thank Takayuki Sasaki, IPSR, Okayama University, for assisting with subcellular localization studies. We also thank Yoshiyuki Tsuchiya for isolating the oocytes. This work was supported by JSPS Program for Forming Japan's Peak Research Universities (J-PEAKS) Grant Number JPJS00420230010.

Conflicts of Interest: The authors declare no conflicts of interest.

Abbreviations

The following abbreviations are used in this manuscript:

cDNA	Complementary DNA
cRNA	Capped RNA
gDNA	Genomic DNA
GFP	Green fluorescence protein
HKT	High-Affinity Potassium Transporter
mRNA	Messenger RNA
SOS	Salt Overly Sensitive
TEVC	Two-electrode voltage clamp

References

1. Munns, R.; Tester, M. Mechanisms of salinity tolerance. *Annu. Rev. Plant Biol.* **2008**, *59*, 651–681. [CrossRef] [PubMed]
2. Singh, R.K.; Redoña, E.; Refuerzo, L. Varietal Improvement for Abiotic Stress Tolerance in Crop Plants: Special Reference to Salinity in Rice. In *Abiotic Stress Adaptation in Plants*; Pareek, A., Sopory, S., Bohnert, H., Eds.; Springer: Dordrecht, Germany, 2009; pp. 387–415. [CrossRef]
3. Rus, A.; Yokoi, S.; Sharkhuu, A.; Reddy, M.; Lee, B.H.; Matsumoto, T.K.; Koiwa, H.; Zhu, J.K.; Bressan, R.A.; Hasegawa, P.M. AtHKT1 is a salt tolerance determinant that controls Na^+ entry into plant roots. *Proc. Natl. Acad. Sci. USA* **2001**, *98*, 14150–14155. [CrossRef] [PubMed]
4. Mäser, P.; Eckelman, B.; Vaidyanathan, R.; Horie, T.; Fairbairn, D.J.; Kubo, M.; Yamagami, M.; Yamaguchi, K.; Nishimura, M.; Uozumi, N.; et al. Altered shoot/root Na^+ distribution and bifurcating salt sensitivity in *Arabidopsis* by genetic disruption of the Na^+ transporter *AtHKT1*. *FEBS Lett.* **2002**, *531*, 157–161. [CrossRef] [PubMed]
5. Rubio, F.; Gassmann, W.; Schroeder, J.I. Sodium-driven potassium uptake by the plant potassium transporter HKT1 and mutations conferring salt tolerance. *Science* **1995**, *270*, 1660–1663. [CrossRef]
6. Hauser, F.; Horie, T. A conserved primary salt tolerance mechanism mediated by HKT transporters: A mechanism for sodium exclusion and maintenance of high K^+/Na^+ ratio in leaves during salinity stress. *Plant Cell Environ.* **2010**, *33*, 552–565. [CrossRef]
7. Xue, S.; Yao, X.; Luo, W.; Jha, D.; Tester, M.; Horie, T.; Schroeder, J.I. AtHKT1;1 Mediates Nernstian Sodium Channel Transport Properties in *Arabidopsis* Root Stellar Cells. *PLoS ONE* **2011**, *6*, e24725. [CrossRef]
8. Imran, S.; Horie, T.; Katsuhara, M. Expression and ion transport activity of rice *OsHKT1;1* variants. *Plants* **2020**, *9*, 16. [CrossRef]

9. Imran, S.; Tsuchiya, Y.; Tran, S.T.H.; Katsuhara, M. Identification and characterization of rice *OsHKT1;3* variants. *Plants* **2021**, *10*, 2006. [CrossRef]
10. Garciadeblás, B.; Senn, M.E.; Bañuelos, M.A.; Rodríguez-Navarro, A. Sodium transport and HKT transporters: The rice model. *Plant J.* **2003**, *34*, 788–801. [CrossRef]
11. Horie, T.; Hauser, F.; Schroeder, J.I. HKT transporter-mediated salinity resistance mechanisms in *Arabidopsis* and monocot crop plants. *Trends Plant Sci.* **2009**, *14*, 660–668. [CrossRef]
12. Jabnoune, M.; Espeout, S.; Mieulet, D.; Fizames, C.; Verdeil, J.L.; Conéjéro, G.; Rodríguez-Navarro, A.; Sentenac, H.; Guiderdoni, E.; Abdelly, C.; et al. Diversity in expression patterns and functional properties in the rice HKT transporter family. *Plant Physiol.* **2009**, *150*, 1955–1971. [CrossRef]
13. Han, Y.; Yin, S.; Huang, L.; Wu, X.; Zeng, J.; Liu, X.; Qiu, L.; Munns, R.; Chen, Z.H.; Zhang, G. A sodium transporter HvHKT1;1 confers salt tolerance in barley via regulating tissue and cell ion homeostasis. *Plant Cell Physiol.* **2018**, *59*, 1976–1989. [CrossRef] [PubMed]
14. Wei, L.; Liu, L.; Chen, Z.; Huang, Y.; Yang, L.; Wang, P.; Xue, S.; Bie, Z. CmCNIH1 improves salt tolerance by influencing the trafficking of CmHKT1;1 in pumpkin. *Plant J.* **2023**, *114*, 1353–1368. [CrossRef] [PubMed]
15. Kawakami, Y.; Imran, S.; Katsuhara, M.; Tada, Y. Na^+ transporter SvHKT1; 1 from a halophytic turf grass is specifically upregulated by high Na+ concentration and regulates shoot Na^+ concentration. *Int. J. Mol. Sci.* **2020**, *21*, 6100. [CrossRef] [PubMed]
16. Henderson, S.W.; Dunlevy, J.D.; Wu, Y.; Blackmore, D.H.; Walker, R.R.; Edwards, E.J.; Gilliham, M.; Walker, A.R. Functional differences in transport properties of natural HKT1;1 variants influence shoot Na^+ exclusion in grapevine rootstocks. *New Phytol.* **2018**, *217*, 1113–1127. [CrossRef]
17. Song, H.; Cao, Y.; Zhao, X.; Zhang, L. Na^+-preferential ion transporter HKT1;1 mediates salt tolerance in blueberry. *Plant Physiol.* **2023**, *194*, 511–529. [CrossRef]
18. Shi, H.; Ishitani, M.; Kim, C.; Zhu, J.K. The *Arabidopsis thaliana* salt tolerance gene *SOS1* encodes a putative Na^+/H^+ antiporter. *Proc. Natl. Acad. Sci. USA* **2000**, *97*, 6896–6901. [CrossRef]
19. Zhu, J.K. Salt and drought stress signal transduction in plants. *Annu. Rev. Plant Biol.* **2002**, *53*, 247–273. [CrossRef]
20. Hasegawa, P.M. Sodium (Na^+) homeostasis and salt tolerance of plants. *Environ. Exp. Bot.* **2013**, *92*, 19–31. [CrossRef]
21. Shabala, S.; Cuin, T.A. Potassium transport and plant salt tolerance. *Physiol. Plant.* **2008**, *133*, 651–669. [CrossRef]
22. Wang, R.; Jing, W.; Xiao, L.; Jin, Y.; Shen, L.; Zhang, W. The rice high-affinity potassium transporter1;1 is involved in salt tolerance and regulated by an MYB-type transcription factor. *Plant Physiol.* **2015**, *168*, 1076–1090. [CrossRef] [PubMed]
23. Campbell, M.T.; Bandillo, N.; Al Shiblawi, F.R.A.; Sharma, S.; Liu, K.; Du, Q.; Schmitz, A.J.; Zhang, C.; Véry, A.A.; Lorenz, A.J.; et al. Allelic variants of *OsHKT1;1* underlie the divergence between *indica* and *japonica* subspecies of rice (*Oryza sativa*) for root sodium content. *PLoS Genet.* **2017**, *13*, e1006823. [CrossRef] [PubMed]
24. Takagi, H.; Tamiru, M.; Abe, A.; Yoshida, K.; Uemura, A.; Yaegashi, H.; Obara, T.; Oikawa, K.; Utsushi, H.; Kanzaki, E.; et al. MutMap accelerates breeding of a salt-tolerant rice cultivar. *Nat. Biotechnol.* **2015**, *33*, 445–449. [CrossRef] [PubMed]
25. Ganie, S.A.; Reddy, A.S.N. Stress-induced changes in alternative splicing landscape in rice: Functional significance of splice isoforms in stress tolerance. *Biology* **2021**, *10*, 309. [CrossRef]
26. Matsukura, S.; Mizoi, J.; Yoshida, T.; Todaka, D.; Ito, Y.; Maruyama, K.; Shinozaki, K.; Yamaguchi-Shinozaki, K. Comprehensive analysis of rice *DREB2*-type genes that encode transcription factors involved in the expression of abiotic stress-responsive genes. *Mol. Genet. Genom.* **2010**, *283*, 185–196. [CrossRef]
27. Cheng, Q.; Zhou, Y.; Liu, Z.; Zhang, L.; Song, G.; Guo, Z.; Wang, W.; Qu, X.; Zhu, Y.; Yang, D. An alternatively spliced heat shock transcription factor, *OsHSFA2dI*, functions in the heat stress-induced unfolded protein response in rice. *Plant Biol.* **2015**, *17*, 419–429. [CrossRef]
28. Magaraggia, F.; Solinas, G.; Valle, G.; Giovinazzo, G.; Coraggio, I. Maturation and translation mechanisms involved in the expression of a myb gene of rice. *Plant Mol. Biol.* **1997**, *35*, 1003–1008. [CrossRef]
29. Zhang, Y.; Chen, Z.; Tian, H.; Wu, Y.; Kong, Y.; Wang, X.; Sui, N. Alternative splicing plays a crucial role in the salt tolerance of foxtail millet. *J. Agric. Food Chem.* **2024**, *72*, 10814–10827. [CrossRef]
30. Lv, J.; Zhou, F.; Wei, Q.; Long, X.; Tian, W.; Zhai, J.; Wang, J.; Zhang, Q.; Wan, D. An alternative 3′ splice site of *PeuHKT1;3* improves the response to salt stress through enhancing affinity to K^+ in *Populus*. *Plant Physiol. Biochem.* **2024**, *212*, 108776. [CrossRef]
31. Zhou, Y.; Li, X.H.; Guo, Q.H.; Liu, P.; Li, Y.; Wu, C.A.; Yang, G.D.; Huang, J.G.; Zhang, S.Z.; Zheng, C.C.; et al. Salt responsive alternative splicing of a RING finger E3 ligase modulates the salt stress tolerance by fine-tuning the balance of COP9 signalosome subunit 5A. *PLoS Genet.* **2021**, *17*, e1009898. [CrossRef]
32. Lv, M.; Xiong, Y.; Yang, H.; Wang, J.; Zhang, L.; Zuo, K. The interaction complexes of TsHKT1 splicing variants enhance salt tolerance of *Thellungiella salsuginea* by decreasing Na^+ uptake. *Plant Sci.* **2025**, *23*, 112678. [CrossRef] [PubMed]

33. Cotsaftis, O.; Plett, D.; Shirley, N.; Tester, M.; Hrmova, M. A Two-Staged model of Na^+ exclusion in rice explained by 3D modeling of HKT transporters and alternative splicing. *PLoS ONE* **2012**, *7*, e39865. [CrossRef] [PubMed]
34. Ren, Z.; Liu, Y.; Kang, D.; Fan, K.; Wang, C.; Wang, G.; Liu, Y. Two alternative splicing variants of maize *HKT1;1* confer salt tolerance in transgenic tobacco plants. *Plant Cell Tissue Organ Cult.* **2015**, *123*, 569–578. [CrossRef]
35. Wu, F.H.; Shen, S.C.; Lee, L.Y.; Lee, S.H.; Chan, M.T.; Lin, C.S. Tape-*Arabidopsis* Sandwich-a simpler Arabidopsis protoplast isolation method. *Plant Methods* **2009**, *5*, 16. [CrossRef]
36. Ren, Z.H.; Gao, J.P.; Li, L.G.; Cai, X.L.; Huang, W.; Chao, D.Y.; Zhu, M.Z.; Wang, Z.Y.; Luan, S.; Lin, H.X. A rice quantitative trait locus for salt tolerance encodes a sodium transporter. *Nat. Genet.* **2005**, *37*, 1141–1146. [CrossRef]
37. Sunarpi, X.; Horie, T.; Motoda, J.; Kubo, M.; Yang, H.; Yoda, K.; Horie, R.; Chan, W.Y.; Leung, H.Y.; Hattori, K.; et al. Enhanced salt tolerance mediated by AtHKT1 transporter-induced Na^+ unloading from xylem vessels to xylem parenchyma cells. *Plant J.* **2005**, *44*, 928–938. [CrossRef]
38. Byrt, C.S.; Platten, J.D.; Spielmeyer, W.; James, R.A.; Lagudah, E.S.; Dennis, E.S.; Tester, M.; Munns, R. HKT1;5-like cation transporters linked to Na^+ exclusion loci in wheat, Nax2 and Kna1. *Plant Physiol.* **2007**, *143*, 1918–1928. [CrossRef]
39. Munns, R.; James, R.A.; Xu, B.; Athman, A.; Conn, S.J.; Jordans, C.; Byrt, C.S.; Hare, R.A.; Tyerman, S.D.; Tester, M.; et al. Wheat grain yield on saline soils is improved by an ancestral Na^+ transporter gene. *Nat. Biotech.* **2012**, *30*, 360–364. [CrossRef]
40. Plett, D.; Safwat, G.; Gilliham, M.; Skrumsager Møller, I.; Roy, S.; Shirley, N.; Jacobs, A.; Johnson, A.; Tester, M. Improved salinity tolerance of rice through cell type-specific expression of *AtHKT1;1*. *PLoS ONE* **2010**, *5*, e12571. [CrossRef]
41. Ismail, A.M.; Horie, T. Genomics, physiology, and molecular breeding approaches for improving salt tolerance. *Annu. Rev. Plant Biol.* **2017**, *68*, 405–434. [CrossRef]
42. Liu, L.; Li, X.; Wang, C.; Ni, Y.; Liu, X. The role of chloride channels in plant responses to NaCl. *Int. J. Mol. Sci.* **2023**, *25*, 19. [CrossRef] [PubMed]
43. Wu, H.; Li, Z. The importance of Cl^- exclusion and vacuolar Cl^- sequestration: Revisiting the role of Cl^- transport in plant salt tolerance. *Front. Plant Sci.* **2019**, *10*, 1418. [CrossRef] [PubMed]
44. Nedelyaeva, O.I.; Shuvalov, A.V.; Balnokin, Y.V. Chloride channels and transporters of the CLC family in plants. *Russ. J. Plant Physiol.* **2020**, *67*, 767–784. [CrossRef]
45. Subba, A.; Tomar, S.; Pareek, A.; Singla-Pareek, S.L. The chloride channels: Silently serving the plants. *Physiol. Plant.* **2021**, *171*, 688–702. [CrossRef]
46. Feng, L.; Campbell, E.B.; Hsiung, Y.; MacKinnon, R. Structure of a eukaryotic CLC transporter defines an intermediate state in the trans port cycle. *Science* **2010**, *330*, 635–641. [CrossRef]
47. Wege, S.; Jossier, M.; Filleur, S.; Thomine, S.; Barbier-Brygoo, H.; Gambale, F.; De Angeli, A. The proline 160 in the selectivity filter of the Arabidopsis NO_3^-/H^+ exchanger AtCLCa is essential for nitrate accumulation in *planta*. *Plant J.* **2010**, *63*, 861–869. [CrossRef]
48. Wei, P.; Wang, L.; Liu, A.; Yu, B.; Lam, H.M. *GmCLC1* confers enhanced salt tolerance through regulating chloride accumulation in soybean. *Front. Plant Sci.* **2016**, *7*, 1082. [CrossRef]
49. Wei, Q.; Liu, Y.; Zhou, G.; Li, Q.; Yang, C.; Peng, S.A. Overexpression of *CsCLCc*, a chloride channel gene from Poncirus trifoliata, enhances salt tolerance in *Arabidopsis*. *Plant Mol. Biol. Rep.* **2013**, *31*, 1548–1557. [CrossRef]
50. Wang, S.; Su, S.Z.; Wu, Y.; Li, S.P.; Shan, X.H.; Liu, H.K.; Wang, S.; Yuan, Y.P. Overexpression of maize chloride channel gene *ZmCLC-d* in *Arabidopsis thaliana* improved its stress resistance. *Biol. Plant.* **2015**, *59*, 55–64. [CrossRef]
51. Colmenero-Flores, J.M.; Franco-Navarro, J.D.; Cubero-Font, P.; Peinado-Torrubia, P.; Rosales, M.A. Chloride as a beneficial macronutrient in higher plants: New roles and regulation. *Int. J. Mol. Sci.* **2019**, *20*, 4686. [CrossRef]
52. Zhang, H.; Yu, C.; Zhang, Q.; Qiu, Z.; Zhang, X.; Hou, Y.; Zang, J. Salinity survival: Molecular mechanisms and adaptive strategies in plants. *Front. Plant Sci.* **2025**, *16*, 1527952. [CrossRef] [PubMed]
53. Colmenero-Flores, J.M.; Martínez, G.; Gamba, G.; Vázquez, N.; Iglesias, D.J.; Brumós, J.; Talón, M. Identification and functional characterization of cation–chloride cotransporters in plants. *Plant J.* **2007**, *50*, 278–292. [CrossRef] [PubMed]
54. Chen, Z.C.; Yamaji, N.; Fujii-Kashino, M.; Ma, J.F. A cation-chloride cotransporter gene is required for cell elongation and osmoregulation in rice. *Plant Physiol.* **2016**, *171*, 494–507. [CrossRef] [PubMed]
55. Sasaki, T.; Mori, I.C.; Furuichi, T.; Munemasa, S.; Toyooka, K.; Matsuoka, K.; Murata, Y.; Yamamoto, Y. Closing plant stomata requires a homolog of an aluminum-activated malate transporter. *Plant Cell Physiol.* **2010**, *51*, 354–365. [CrossRef]
56. Baetz, U.; Eisenach, C.; Tohge, T.; Martinoia, E.; De Angeli, A. Vacuolar chloride fluxes impact ion content and distribution during early salinity stress. *Plant Physiol.* **2016**, *172*, 1167–1181. [CrossRef]
57. Hibino, H.; Inanobe, A.; Furutani, K.; Murakami, S.; Findlay, I.A.; Kurachi, Y. Inwardly rectifying potassium channels: Their structure, function, and physiological roles. *Physiol. Rev.* **2010**, *90*, 291–366. [CrossRef]
58. Fu, S.; Chen, X.; Jiang, Y.; Dai, S.; Zhang, H.; Feng, S.; Zhou, A. Characterization of the Na^+-preferential transporter HKT1.1 from halophyte shrub *Salix linearistipularis*. *Physiol. Mol. Biol. Plants* **2025**, *31*, 823–833. [CrossRef]

59. Sun JingYu, S.J.; Cao HaiShun, C.H.; Cheng JinTao, C.J.; He XiaoMeng, H.X.; Sohail, H.; Niu MengLiang, N.M.; Huang Yuan, H.Y.; Bie ZhiLong, B.Z. Pumpkin CmHKT1;1 controls shoot Na^+ accumulation via limiting Na^+ transport from rootstock to scion in grafted cucumber. *Int. J. Mol. Sci.* **2018**, *19*, 2648. [CrossRef]
60. Zhu, Z.; Liu, X.; Meng, F.; Jiang, A.; Zhou, Y.; Yuan, F.; Chen, M. *LbHKT1;1* negatively regulates salt tolerance of *Limonium bicolor* by decreasing salt secretion rate of salt glands. *Plant Cell Environ.* **2025**, *48*, 3544–3558. [CrossRef]
61. Katsuhara, M.; Akiyama, Y.; Koshio, K.; Shibasaka, M.; Kasamo, K. Functional analysis of water channels in barley roots. *Plant Cell Physiol.* **2002**, *43*, 885–893. [CrossRef]
62. Chiu, W.L.; Niwa, Y.; Zeng, W.; Hirano, T.; Kobayashi, H.; Sheen, J. Engineered GFP as a vital reporter in plants. *Curr. Biol.* **1996**, *6*, 325–330. [CrossRef]
63. Yoo, S.D.; Cho, Y.H.; Sheen, J. *Arabidopsis* mesophyll protoplasts: A versatile cell system for transient gene expression analysis. *Nat. Protoc.* **2007**, *2*, 1565–1572. [CrossRef] [PubMed]
64. Sasaki, T.; Tsuchiya, Y.; Ariyoshi, M.; Nakano, R.; Ushijima, K.; Kubo, Y.; Mori, I.C.; Higashiizumi, E.; Galis, I.; Yamamoto, Y. Two members of the aluminum-activated malate transporter family, SlALMT4 and SlALMT5, are expressed during fruit development, and the overexpression of SlALMT5 alters organic acid contents in seeds in tomato (*Solanum lycopersicum*). *Plant Cell Physiol.* **2016**, *57*, 2367–2379. [CrossRef] [PubMed]
65. Zhang, Y.; Su, J.; Duan, S.; Ao, Y.; Dai, J.; Liu, J.; Wang, P.; Li, Y.; Liu, B.; Feng, D.; et al. A highly efficient rice green tissue protoplast system for transient gene expression and studying light/chloroplast-related processes. *Plant Methods* **2011**, *7*, 30. [CrossRef] [PubMed]
66. Shibasaka, M.; Horie, T.; Katsuhara, M. Mechanisms activating latent functions of PIP aquaporin water channels via the interaction between PIP1 and PIP2 proteins. *Plant Cell Physiol.* **2021**, *62*, 92–99. [CrossRef]
67. Quintero, F.J.; Garciadeblás, B.; Rodríguez-Navarro, A. The *SAL1* gene of Arabidopsis, encoding an enzyme with 3′(2′), 5′-bisphosphate nucleotidase and inositol polyphosphate 1-phosphatase activities, increases salt tolerance in yeast. *Plant Cell* **1996**, *8*, 529–537. [CrossRef]
68. Haxim, Y.; Wang, L.; Pan, Z.; Fan, X.; Ma, J. A novel high-affinity potassium transporter SeHKT1;2 from halophyte *Salicornia europaea* shows strong selectivity for Na^+ rather than K^+. *Front. Plant Sci.* **2023**, *14*, 1104070. [CrossRef]

Disclaimer/Publisher's Note: The statements, opinions and data contained in all publications are solely those of the individual author(s) and contributor(s) and not of MDPI and/or the editor(s). MDPI and/or the editor(s) disclaim responsibility for any injury to people or property resulting from any ideas, methods, instructions or products referred to in the content.

International Journal of
Molecular Sciences

MDPI

Article

Unveiling the Genomic Architecture of Phenotypic Plasticity Using Multiple GWAS Approaches Under Contrasting Conditions of Water Availability: A Model for Barley

Sebastián Arenas [1,*] and Andrés J. Cortés [2,*]

[1] Department of Plant Protection Biology, Swedish University of Agricultural Sciences, 23422 Lomma, Sweden
[2] Facultad de Ciencias Agrarias—Departamento de Ciencias Forestales, Universidad Nacional de Colombia—Sede Medellín, Medellín 050034, Colombia
* Correspondence: sebastian.arenas@slu.se (S.A.); ancortesv@unal.edu.co (A.J.C.)

Abstract

Phenotypic plasticity is a key mechanism by which crops adjust to fluctuating environmental conditions, yet its genetic basis under drought remains poorly characterized in barley (*Hordeum vulgare*). We hypothesized that phenotypic plasticity under drought is controlled by a distinct, trait-specific genetic architecture that can be detected using complementary plasticity metrics and genome-wide association studies (GWAS). Here, we examined data from 1277 spring barley genotypes grown under well-watered and water-limited conditions to quantify plastic responses across two developmental traits (i.e., heading time, and maturity) and seven productivity-related traits (i.e., total dry matter, plant grain yield, grain number, grain weight, harvest index, vegetative dry weight, and grain-filling period). The experimental design, based on contrasting water regimes across a large diversity panel, allowed robust assessment of genotype-by-environment interactions. We combined five complementary plasticity estimators with four independent GWAS approaches to resolve the genomic architecture underlying trait-specific plasticity. Environmental effects dominated variation in yield-related traits, whereas developmental traits remained more genetically determined. The different plasticity metrics captured distinct but partially overlapping response dimensions, and their integration greatly increased the robustness of association signals. A total of 239 high-confidence SNPs obtained for top traits, those associated across metrics and methods, were enriched in coding regions and mapped to genes involved in osmoregulation, carbohydrate metabolism, hormonal pathways, and ion transport. A total of 27 high-confidence SNPs were located in coding regions, showing genotype-specific differences in the magnitude and even direction of phenotypic plasticity. These loci exhibited opposite allelic effects across water regimes, consistent with context-dependent antagonistic pleiotropy. The fact that candidate alleles for the plastic response modulate environmental sensitivity differently highlights that drought resilience arises from environment-contingent genetic architectures. Overall, these results provide a comprehensive framework for dissecting plasticity and identify concrete genomic targets for indirect selection targeting crop resilience with improved performance under increasingly variable water availability.

Keywords: abiotic stress tolerance; drought stress; genomic bases of plasticity; genetic mapping; GWAS; antagonistic pleiotropy; *Hordeum vulgare*

1. Introduction

Water availability is one of the major environmental constraints limiting agricultural productivity worldwide [1]. Increasingly frequent and intense drought events, driven by ongoing climate change, substantially reduce crop performance and yield stability, especially in semi-arid regions where water scarcity strongly restricts plant growth, reproduction, and survival [2]. Therefore, understanding the underlying mechanisms on how plants perceive, respond, and adapt to fluctuating water conditions is therefore essential for maintaining crop resilience and ensuring future food security [3–5].

Barley (*Hordeum vulgare* L.) is a globally important cereal cultivated across a broad range of agro-ecological zones, from temperate to dryland environments [6]. Its wide environmental breadth and agronomic relevance make it an excellent model for dissecting the mechanisms responsible for plant plasticity and adaptation to abiotic stress, including drought and water limitation [7]. Despite this, our understanding of the physiological and genetic processes governing barley's responses to contrasting water regimes remains incomplete, particularly regarding the genetic determinants of phenotypic plasticity [8].

Plant responses to water limitation arise from a suite of avoidance, tolerance, and resilience mechanisms that operate across biological scales [9], from gene expression and metabolic adjustments to morphological changes and final yield components [10]. Many of these responses are mediated by phenotypic plasticity, classically defined as the capacity of a genotype to alter its phenotype in response to environmental variation [11,12]. Plasticity, together with genetic adaptation, are widely recognized as key drivers of plant responses to heterogeneous environments [13]. Yet, although the ecological relevance of plastic responses is well established, its genetic architecture remains poorly characterized, often assuming that it is merely a secondary consequence of stress tolerance. Instead, plasticity is starting to be recognized as a genetically regulated trait that varies among genotypes within the same species [14,15]. Accurately quantifying plasticity is therefore essential for identifying genes and pathways that control plastic plant responses under climate change.

A variety of methodological approaches have been proposed to quantify plasticity and genotype-by-environment interactions (G×E) [14,16]. Simple indices, such as trait ratios, absolute differences, or covariances between environments, capture broad phenotypic shifts, while more integrative estimators such as the Relative Distance Plasticity Index (RDPI), reaction-norm slopes derived from linear models, and multivariate approaches capture distinct dimensions of plastic behavior, including magnitude, direction, and stability. Because these estimators are not equivalent and emphasize different biological interpretations, combining them provides a more complete picture of the plastic response [17].

Meanwhile, genome-wide association studies (GWAS) offer a powerful framework for identifying loci underlying plasticity (as per a specific estimator) [18–21]. However, classical GWAS models face well-known limitations [22–24], including reduced power for complex traits [20,25], sensitivity to population structure [15,26,27], and difficulty capturing non-additive or interactive genetic effects [28–30]. This being said, merging multiple GWAS approaches has emerged as an effective strategy for detecting robust and reproducible associations [18,19]. Mixed-model approaches (e.g., rrBLUP, BLINK) provide statistical rigor and account for population stratification and kinship, whereas machine learning methods (e.g., Random Forest, XGBoost) capture non-linear patterns and higher-order interactions often missed by linear models. Overlapping signals across methods would substantially increase confidence in candidate loci and reduce model-specific false positives. Applying integrative GWAS framework to phenotypic plasticity [20,31] under contrasting water regimes offers a unique opportunity to uncover the genetic basis of drought-related plastic responses [32,33]. Genomic regions consistent across plasticity metrics and methodological

approaches are likely to represent key components of drought response pathways that modulate performance and stability in variable environments [34–37].

Therefore, the main objective of this study was to dissect the genomic architecture of phenotypic plasticity in a diverse panel of 1277 barley genotypes grown under well-watered and water-limited conditions [8]. After integrating multiple plasticity estimators with complementary GWAS methodologies, we aim to: (i) identify loci and candidate genes associated with plastic responses to drought, (ii) explore whether they differ in direction and magnitude, (iii) characterize the biological processes underlying adaptive phenotypic shifts, and (iv) demonstrate the value of utilizing a diversity of plasticity estimators and GWAS methods in resolving complex genetic architectures.

We hypothesize that alleles that enhance barley performance under drought impose a trade-off on fitness cost under well-watered conditions due to antagonistic pleiotropy acting on shared metabolic and developmental pathways [16,38]. This work provides an integrative framework for linking plasticity metrics, genomic variation, and functional annotation, ultimately contributing to a deeper understanding of how barley, and potentially other cereals, modulates its phenotype under fluctuating water environments. Our findings offer insights relevant for breeding programs focused on enhancing drought resilience through a more comprehensive understanding of phenotypic plasticity.

2. Results

2.1. Phenotypic Responses to Water Availability

Phenotypic summary statistics analyses confirmed that the contrast between well-watered (WW) and water-limited (WL) treatments produced significant differences for six evaluated traits (Table 1), which were retain herein after.

Table 1. Summary statistics of traits differing under contrasting water regimes. Descriptive statistics (mean, standard deviation, and standard error) of GFP values across environments (WW and WL). Values highlight reduced trait means under stress and increased variance across genotypes, consistent with differential plastic responses.

Trait	Trait Description	n	Well-Watered (WW)			Water-Limited (WL)		
			Mean	±	SE	Mean	±	SE
GFP	Grain-filling period	1279	36.01	±	0.16	30.09	±	0.14
GY	Grain yield	1279	18.33	±	0.11	7.63	±	0.14
TDM	Total dry matter	1279	59.93	±	0.31	42.17	±	0.26
MAT	Maturity	1279	136.8	±	0.16	132.3	±	0.16
GN	Grain number	1279	300.3	±	2.2	207.8	±	2.73
HI	Harvest index	1279	31.6	±	0.19	22.18	±	0.39

Genotypes presented consistently higher values under WW conditions, a pattern corroborated by highly significant Wilcoxon tests (Figure 1). Marked reductions were observed under WL in productive variables, especially in GY, GN, DM, and HI. In contrast, developmental traits such as HEA and MAT showed more stable responses, with less variation between treatments. Line plots showed slight heterogeneity in response: while most showed a decrease in yield and biomass under WL, a subset of lines showed opposite patterns, with increases in value under stress conditions. This divergent behavior was evident in the reaction norms (Figure S1), where genotype–environment trajectories revealed that phenotypic plasticity varies not only in magnitude but also in direction.

https://doi.org/10.3390/ijms27020652

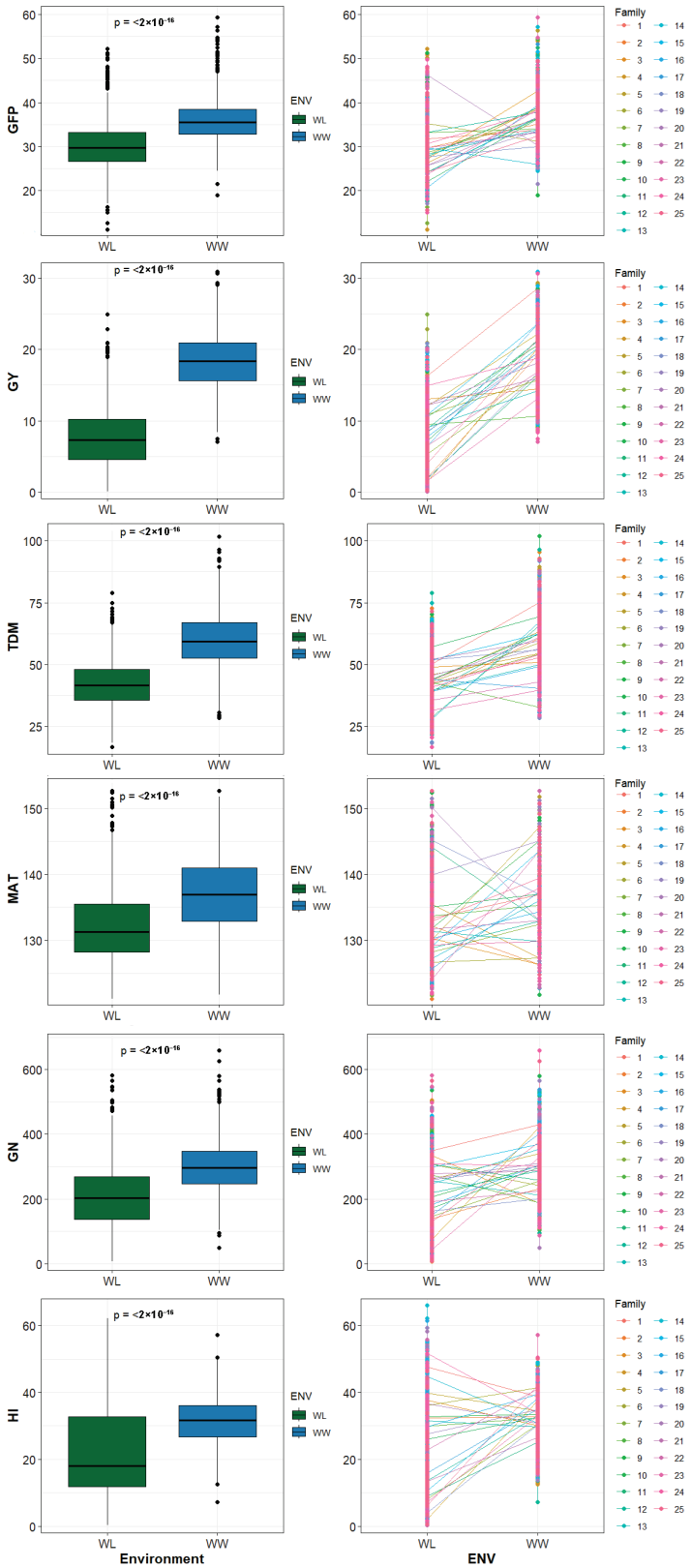


Figure 1. Phenotypic variation across water regimes. Boxplots (**left**) and line plots (**right**) show the distribution of traits in barley grown under well-watered (WW) and water-limited (WL) conditions. Each point represents an individual genotype. Wilcoxon rank-sum tests reveal significant differences between environments ($p < 0.001$). Trait abbreviations are detailed in Table 1.

https://doi.org/10.3390/ijms27020652

2.2. Variance Partitioning and G×E Interactions

The variance decomposition (Table 2) revealed that the relative importance of genetic (G) and environmental (E) components varied considerably between traits. The results showed a dependence on the environmental context. In the case of GY, the environment explained around 80% of the variation, while the VG contributed only 7%, indicating a strong dependence of performance on water availability. In contrast, in HEA traits, the genetic component accounted for more than 70% of the variance, with a reduced environmental effect, reflecting stricter and more stable genetic control under stress conditions. Other traits such as GFP, GN, HI, TDM, and MAT showed intermediate proportions, suggesting a complex interaction between genotype and environment (G×E). The GW trait was discarded because the proportion of VG explained was not significant, while HEA was excluded due to the absence of a relevant VE effect on water limitation. Likewise, VDW was discarded because it was the trait with the highest proportion of variation explained by residual variance. These variance patterns highlight the diversity of mechanisms underlying different types of traits, from those strongly determined by genetics to those more modulated by the environment. Thus, six traits were retained for further analysis (GFP, GN, GY, TDM, MAT, and HI, as abbreviated in Table 1).

Table 2. Genetic (G), and water treatment (ENV) random effects within the trait variance.

Trait	Var. G	Prop. G	*p*-Value G	Var. ENV	Prop. ENV	*p*-Value ENV	Var. Residual	Prop. Residual
GFP	6.41	17.59	1.6×10^{-35}	17.51	48.01	2.1×10^{-259}	12.55	34.40
GN	2140.39	19.39	6.0×10^{-30}	4254.48	38.53	1.5×10^{-197}	4645.76	42.08
GW	0.00	0.82	0.25	0.00	75.48	0	0.00	23.70
GY	5.30	7.37	9.6×10^{-41}	57.24	79.63	0	9.35	13.00
HEA	18.13	77.61	7×10^{-289}	0.78	3.32	4.6×10^{-52}	4.45	19.06
HI	19.00	13.78	2.9×10^{-12}	43.54	31.59	2.7×10^{-135}	75.29	54.62
MAT	8.99	29.22	2.7×10^{-60}	10.14	32.95	1.3×10^{-195}	11.64	37.83
TDM	30.89	12.86	2.0×10^{-43}	158.72	66.09	0	50.55	21.05
VDW	21.22	28.36	2.1×10^{-33}	12.94	12.29	3.0×10^{-81}	40.68	59.35

The comparison of phenotypic means under contrasting irrigation conditions for the six selected traits (Table 1) showed significant reductions in most of the traits under WL. GY decreased from 18.33 g in WW to 7.63 g in WL, representing a reduction of nearly 60%. Similarly, GN decreased from 300.3 to 207.8, demonstrating the direct influence of water availability on reproductive capacity. TDM also decreased from 59.93 g in WW to 42.17 g in WL, reflecting a generalized physiological impact. These decreases were accompanied by an increase in variability between genotypes, suggesting genetic differences in response to water deficit. HI and GFP showed intermediate responses. HI decreased from 31.6% in WW to 22.2% in WL, indicating lower efficiency in converting biomass to grain under water limitation, and GFP decreased from 36.01 to 30.09 days.

The PP estimators (Figure S2) unveiled positive correlations with each other, validating that they capture related, although not identical, facets of the response. CV was discarded due to its high correlation with other variables, leaving WW, WL, Ratio, RDPI, and Linear as the central metrics, which were used to structure the association analyses.

2.3. Population Structure and Linkage Disequilibrium

Population structure analysis (Figure 2A) showed that the SNPs in the study are distributed randomly across barley chromosomes. It was also observed that the 1277 genotypes were distributed in undifferentiated groups, without drastic genetic barriers, and

therefore the genetic structure was very weak (Figure 2B). This aligns with the neutral hypothesis of random mating and population panmixia.

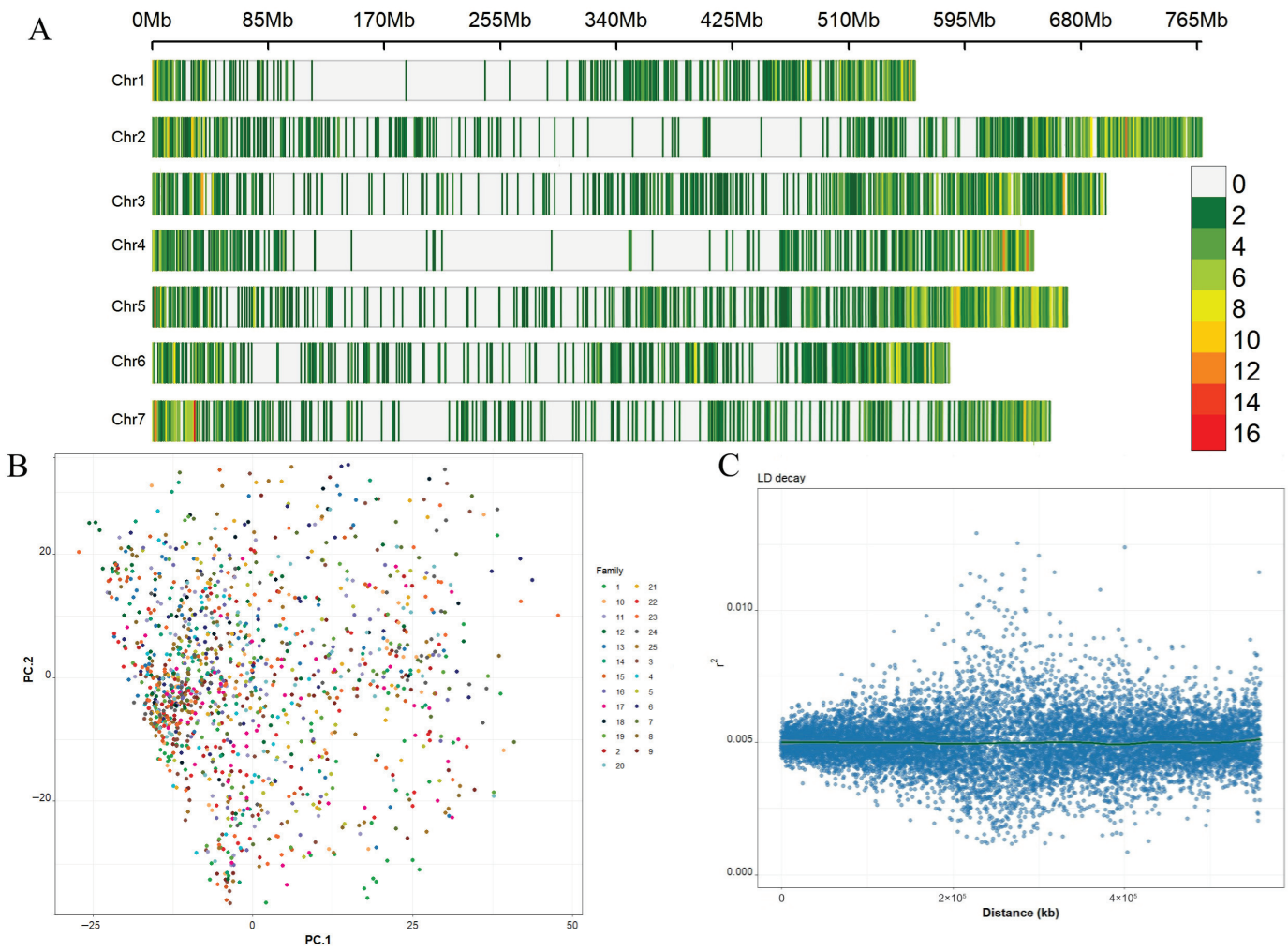


Figure 2. Population structure and linkage disequilibrium in the HEB population. (**A**) Genome-wide marker distribution across the seven barley chromosomes. (**B**) Principal component analysis (PCA) of 1277 barley genotypes based on genome-wide SNP data. The first two components explain major axes of population structure and separate families within the population. (**C**) Genome-wide LD decay estimated by r^2 as a function of physical distance. The observed rapid LD decay indicates high mapping resolution, supporting the power of subsequent GWAS analyses.

Additionally, the estimation of linkage disequilibrium (LD decay) indicated a rapid loss of correlation with physical distance, ensuring high resolution power for the detection of associations at the SNP level (Figure 2C). Low genetic structure allowed effective exploration of genetic variation and the genomic architecture responsible for trait variation without compromising the statistical power of the associations.

2.4. Genotype–Phenotype Association (GWAS)

2.4.1. Overlap Between GWAS Methods

The association analyses (GWAS) performed using the four approaches (BLINK, rrBLUP, RF, and XGBoost) detected a considerable number of SNPs associated with the traits and with the different PP estimators (Figure 3).

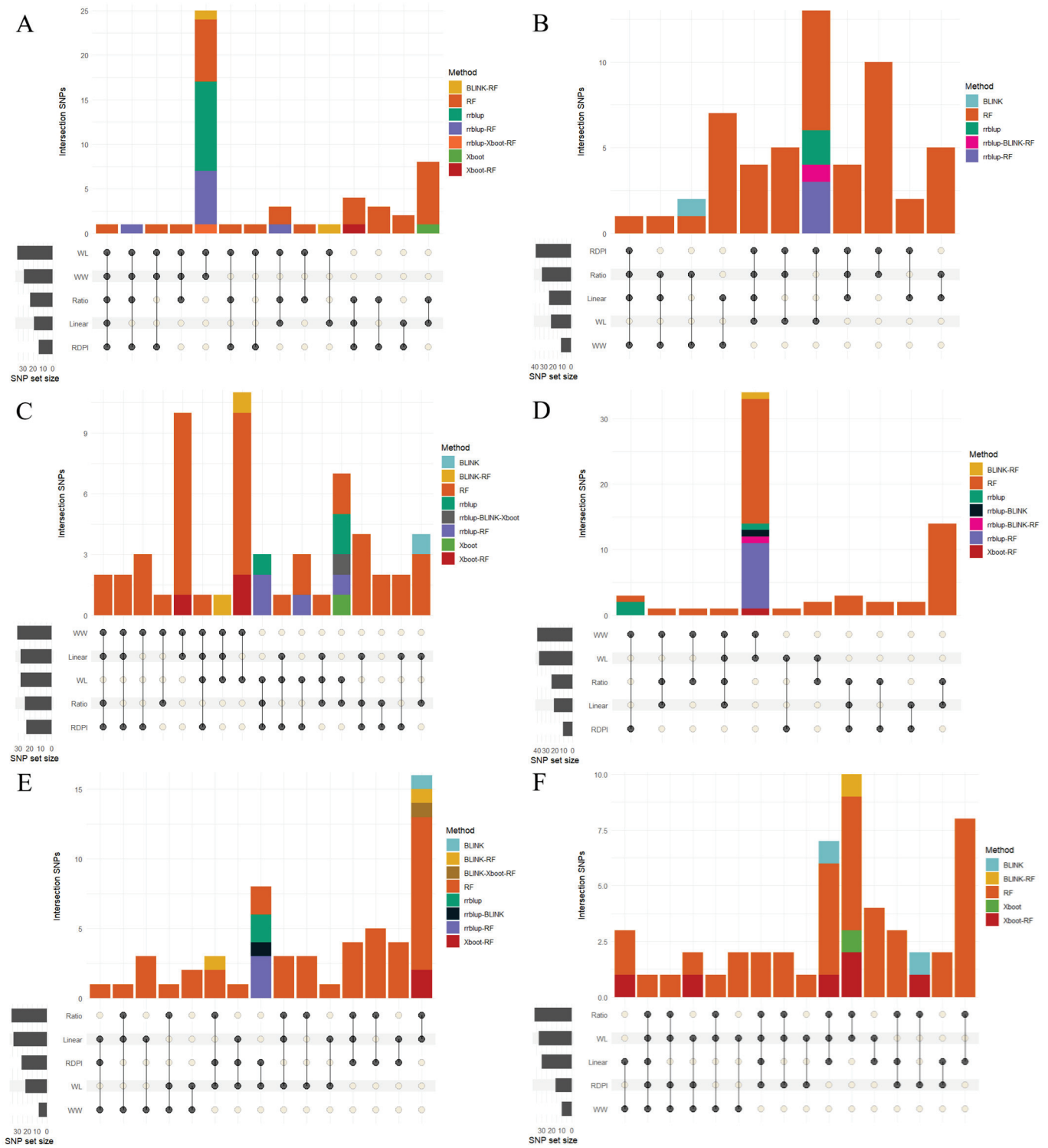


Figure 3. Summary of GWAS results obtained using four approaches: BLINK, rrBLUP, Random Forest (RF), and XGBoost (colored barplots) across different plasticity components (horizontal grey bars at the bottom of each subpannel). Results are presented for the traits GFP (**A**), GY (**B**), TDM (**C**), MAT (**D**), GN (**E**), and HI (**F**). Several markers were consistently detected across multiple methods, strengthening the confidence in associations. Identified loci underlying phenotypic plasticity to water stress in barley compare consistently across methodologies.

The QTLs identified by two or more plant status estimators were considered high-priority candidates, which substantially reduced the initial list of markers and increased confidence in the retained associations, as they represented consistent and robust signals

https://doi.org/10.3390/ijms27020652

in the face of methodological differences. Overall, the bar graphs in Figure 3 summarized the distribution of significant QTLs obtained by different methods and metrics. In each panel, corresponding to the GFP, MAT, GY, GN, TDM, and HI traits, the colored bars reflected the frequency of association detection by method, while the lower dots indicate the intersections between the absolute values (WW, WL) and the plasticity metrics (Ratio, Linear, and RDPI).

Comparative analysis between traits showed notable variations in the consistency and overlap of associations between methods. The GFP and MAT traits showed the greatest overlap of SNPs, with several markers detected consistently by three or more approaches. In contrast, GY and GN showed more dispersed associations with less overlap between methods, while TDM recorded a limited number of signals without consistent overlaps. The HI trait exhibited a more defined pattern, with a recurring group of SNPs detected by rrBLUP, RF, and XGBoost.

Overall, the bar plots reflect heterogeneity in the density and overlap of associations between traits, highlighting the ability of different GWAS approaches to capture the genetic complexity underlying phenotypic plasticity under contrasting water availability conditions. It was observed that a machine learning-based method (RF) tended to identify a greater number of unique associations, while BLINK and rrBLUP concentrated on more conservative signals but coincided with other approaches. BLINK and Xboot were the most stringent methods and generated the fewest individual associations. HI was the only one that presented common associations for three different methodologies. The highest intersection sets corresponded to combinations of rrBLUP-RF and BLINK–rrBLUP, which reinforces the complementarity of statistical in the detection of relevant loci.

2.4.2. Trait-Specific Patterns of Association

PP estimators showed variable patterns between traits and methods, revealing both common and specific metrics. In general, the WW and WL indices concentrated the highest number of associations, followed by derived estimators such as Ratio and Linear, while RDPI showed a lower detection frequency. In the GFP and MAT traits, repeated associations were observed between multiple metrics, indicating a broad coincidence of SNPs detected under different plasticity approaches. In contrast, the GY, GN, and TDM traits showed more dispersed sets, with little overlap between metrics and a predominance of associations specific to a single estimator. HI showed an intermediate pattern, where the Ratio and Linear metrics coincided with those derived from WW and WL, forming the group with the highest number of intersections between estimators. Overall, the plasticity methods revealed a heterogeneous distribution of signals, with a predominance of coincidences in developmental traits and less convergence in yield traits.

2.4.3. Effect Sizes and Polygenic Architecture

The values obtained showed that, although the magnitude of the effects varied between plasticity metrics, in all cases the QTLs explained a small fraction of the total variance, generally below 10% (Table 3). This reflects the highly polygenic nature of the traits evaluated. It was observed that for GFP, MAT, and HI, the genetic proportion was higher than the environmental components, indicating greater genetic control in these traits. This pattern was repeated across the different plasticity metrics, especially in the phenotypic means, where VG values reached 8.4% for GFP, 10.4% for MAT, and 11.8% for HI, contrasting with VE, which were close to zero in most cases. In contrast, GY and GN showed a high contribution of residual error, suggesting a predominant influence of external factors and interactions not captured by the models. These results are consistent with high environmental sensitivity to water stress. For TDM, the different models did

https://doi.org/10.3390/ijms27020652

not detect consistent QTLs, confirming the weak genetic signal in this trait or a much more polygenic structure. In contrast, HI showed the highest VG values, especially in the phenotypic means (G = 11.78%) and in the Ratio (8.31%). Overall, comparisons between metrics showed that phenotypic means explained a greater proportion of the variance than phenotypic plasticity (RDPI, Ratio, and Linear; explanatory values below 10%). Likewise, in very few cases was the environmental component significant, suggesting that differences between genotypes and genotype × environment interaction dominate.

Table 3. Genetic (G) and water treatment (ENV) random effects on trait variance. Proportion of variation captured by QTLs (%) from SNPs obtained across the four GWAS methods. Only SNPs present in at least two categories (WW, WL, Linear, Ratio, or RDPI) were retained. QTLs detected across multiple methodologies were compared for consistency. See trait abbreviation as in Table 1.

Trait	Plasticity Measure	G	E	Res. Error
GFP	Phenotypic means	8.41	4.63	1.92
	RDPI	2.84	0.02	2.65
	Ratio	1.75	0	5.23
	Linear	2.94	0	5.84
GY	Phenotypic means	5.41	0	2.07
	RDPI	1.05	0.01	2.57
	Ratio	0	0	2.95
	Linear	0	0	2.1
TDM	Phenotypic means	0	0	1.85
	RDPI	0	0	3.83
	Ratio	0	0	4.57
	Linear	0	0	3.45
MAT	Phenotypic means	10.4	0.056	0.34
	RDPI	0	0.07	2.32
	Ratio	0.83	0.06	4.55
	Linear	1.12	0.05	3.97
GN	Phenotypic means	2.52	0	2.63
	RDPI	0	0	2.11
	Ratio	0	0	3.61
	Linear	0	0	4.48
HI	Phenotypic means	11.78	0	4.06
	RDPI	1.28	0.003	1.97
	Ratio	8.31	0	5.67
	Linear	1.24	0.06	4.88

2.5. Functional Annotation and GO Enrichment and Genomic Distribution of Significant SNPs

2.5.1. Genomic Distribution of Significant SNPs

Functional annotation of the retained SNPs showed that a significant proportion were located in coding regions of the genome, indicating that several of the detected markers could have direct effects on functional genes or gene regions. GO term enrichment analyses identified a prominent representation of metabolic process, catalytic activity, and ion binding. These categories group genes associated with primary metabolic processes, enzymatic activity, and cellular regulation, consistent with the plant's response to water deficit conditions. Most of the annotated genes were concentrated in cellular and metabolic processes (Figure 4), including biosynthetic process, binding, and macromolecule metabolic process, which had the highest number of genes and moderate statistical significance values. The presence of terms such as organelle and intracellular membrane-bound organelle indicates that some of the associated genes participate in cell organization and organelle

structure, while others that are less represented are associated with cation and metal ion bindings and even with developmental processes. Overall, the enrichment results suggest that the genomic regions detected are linked to basic cellular functions and metabolic maintenance during exposure to water stress.

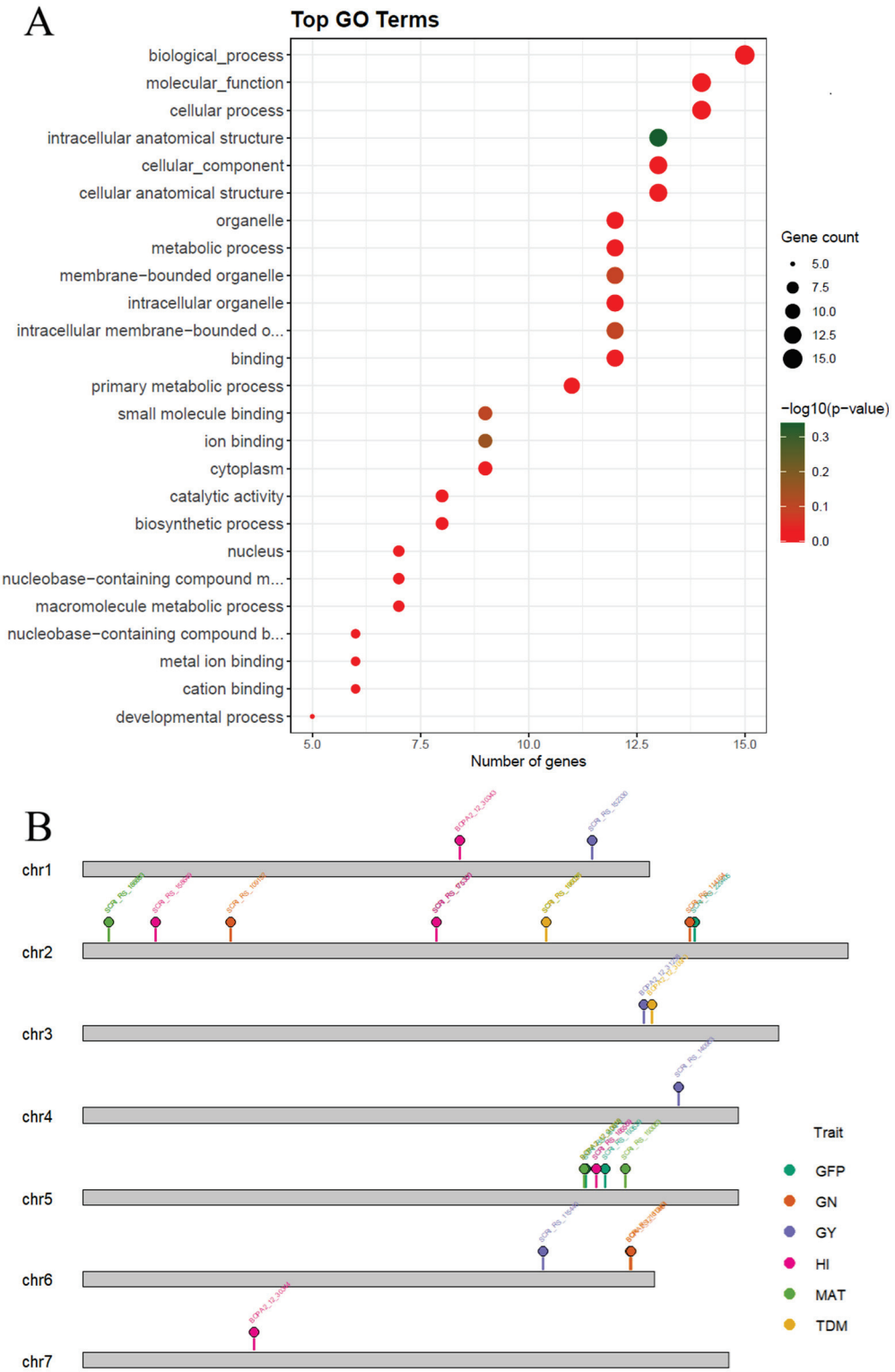


Figure 4. Functional characterization of significant markers located in coding regions detected in the GWAS for water tolerance in barley. (**A**) Associated genes were annotated, GO terms identified, and pathway enrichment visualized. (**B**) Although the reduced number of markers limited resolution for genetic mapping, several significant terms were identified, supporting biological relevance.

The candidate gene annotation (Table 4) efficiently complemented this analysis by identifying SNPs located in genes with known functions in signaling, metabolism, and growth regulation. Among them were proteins with HEAT repeats, hyperosmolarity-dependent calcium channels, serine/threonine kinases, sucrose phosphate synthase, gibberellin receptors, sucrose phosphate synthases, and enzymes involved in energy metabolism. These genes were mainly associated with the GFP, GY, HI, GN, and MAT traits, and several of them were present for the plasticity metrics and in more than one GWAS methodology. The chromosomes with the most relevant associations were 2H, 3H, 4H, 6H, and 7H. Together, functional annotation and GO enrichment confirm that the identified SNPs are grouped into relevant metabolic and structural pathways linked to the response to contrasting water availability conditions.

Table 4. Top candidate gene annotation identified by multiple GWAS approaches under water stress conditions in barley include loci involved in calcium signaling, stress response regulation, redox homeostasis, growth regulation, and carbohydrate metabolism, stressing key pathways underlying phenotypic plasticity.

Trait	Marker	Chr	Position	Gene_ID	Description
GFP	SCRI_RS_188893	2H	26,375,085	HORVU.MOR.9832	HEAT repeat-containing protein
GFP	SCRI_RS_175300	2H	3.56×10^8	HORVU.MOR.4842	Hyperosmolality-gated Ca^{2+} permeable channel 3.1
GFP	SCRI_RS_196026	2H	4.66×10^8	HORVU.MOR.1167	Similarly to H062205.9 protein (*Oryza sativa*)
GFP	SCRI_RS_190690	2H	5.26×10^8	HORVU.MOR.9742	EDAT1-like protein (*Arabidopsis thaliana*)
GN	BOPA2_12_3061	5H	5.05×10^8	HORVU.MOR.6703	Synaptotagmin-2 (*Arabidopsis thaliana*)
GN	SCRI_RS_161043	6H	5.51×10^8	HORVU.MOR.3705	Nicotinate mononucleotide adenyltransferase
GN	SCRI_RS_163143	6H	5.51×10^8	HORVU.MOR.8951	S-(hydroxymethyl)glutathione dehydrogenase
GY	SCRI_RS_175440	2H	3.56×10^8	HORVU.MOR.4842	Hyperosmolality-gated Ca^{2+} permeable channel 3.1
HI	SCRI_RS_186949	4H	35937077	HORVU.MOR.3335	Serine/threonine-protein kinase homolog
HI	BOPA2_12_3034	7H	1.72×10^8	HORVU.MOR.1424	Gibberellin receptor GID1L2
HI	BOPA2_12_3097	3H	5.72×10^8	HORVU.MOR.5994	Sucrose phosphate synthase
MAT	SCRI_RS_188893	2H	26,375,085	HORVU.MOR.9832	HEAT repeat-containing protein

The candidate genes listed in Table 4 represent loci prioritized based on consistent detection across multiple GWAS methodologies and plasticity estimators. While experimental validation of gene expression or function was beyond the scope of this study, the integration of genomic position, functional annotation, and pathway-level enrichment provides a robust framework for biological interpretation of plasticity-associated loci to the water stress.

The chromosomal distribution of significant coding SNPs is illustrated in the kayogram (Figure 4B). This visualization showed the physical positions of the associated loci on the seven barley chromosomes, with color codes distinguishing the implicated traits. A non-random distribution of SNPs was observed, with clear clustering in certain chromosomal regions, particularly on chromosomes 2H and 5H, suggesting potential hotspots of trait-associated variation. Some markers shared across traits were observed on the same chromosomes. These localized concentrations of markers could indicate linkage disequilibrium with functional genes or regulatory regions involved in stress tolerance and metabolic regulation. SNP positions and gene annotations were defined based on the *Hordeum vulgare* cv. Morex reference genome (Ensembl Plants, assembly IBSC v2), using the corresponding annotation release.

https://doi.org/10.3390/ijms27020652

2.5.2. Allele-Specific Plasticity Patterns

SNPs located in coding regions were plotted together with the phenotypic plasticity values corresponding to their genotypes (Figure 5). A recurring pattern was observed, where the direction of the response varied between alleles of the same marker. Some genotypes carrying a certain allele showed increases under WL conditions, while others showed reductions in the same trait. This variation in response between alleles within the same locus demonstrates genetic heterogeneity in the expression of plasticity and reflects that the effects associated with each marker can manifest in opposite ways depending on the genetic and environmental context.

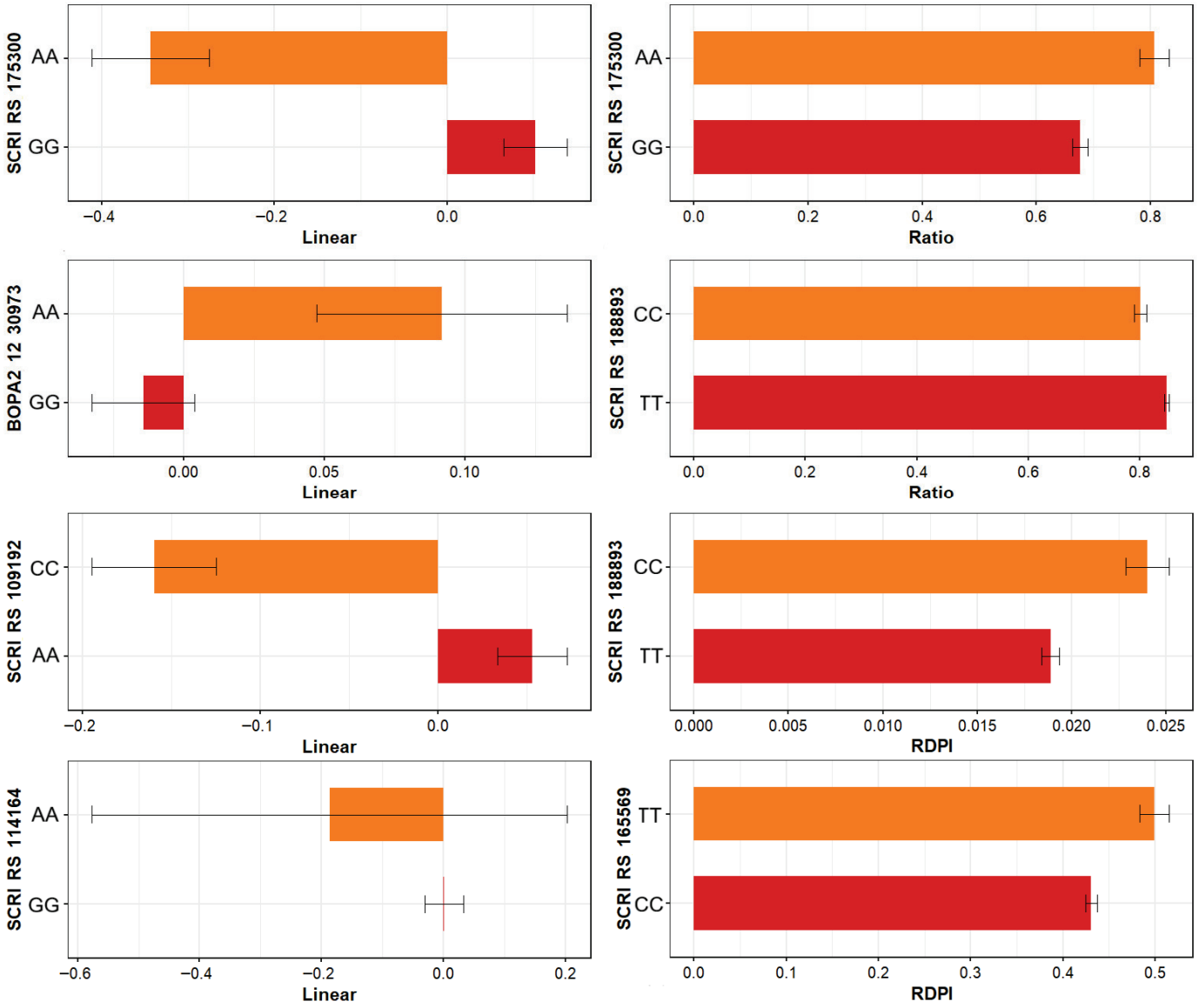


Figure 5. Representative examples of eight SNPs (each subpanel) located in coding regions associated with plasticity indices (i.e., linear and RDPI, respectively, in the left and right column of subpanels). For these markers, phenotypic plasticity varied between genotypes (*y* axes) in opposite directions (*x* axes) suggesting antagonistic pleiotropy, highlighting the complex interaction between genetic variants, metabolic pathways, and trait responses under water-limited condition.

3. Discussion

Water limitation remains one of the most critical constraints on barley productivity worldwide [39–42], and understanding the genetic mechanisms that shape plant responses

to fluctuating hydrological conditions is essential for climate-resilient agriculture [4,10]. Here we used a large and genetically diverse barley panel [8] to explore the genomic architecture of phenotypic plasticity under contrasting water regimes [20]. After integrating multiple plasticity estimators and four complementary GWAS approaches, we were able to provide one of the most comprehensive assessments to date of the loci and biological pathways underlying plastic responses to drought, and test its context-dependent effects.

3.1. Plasticity Is Trait-Dependent and Genotype-Specific

Phenotypic analyses revealed that water limitation caused substantial reductions in yield and biomass traits, whereas phenological traits were comparatively stable. These contrasting patterns reflect differences in the sensitivity of developmental versus reproductive processes to drought [33], consistent with previous reports in barley and other cereals [15,39,42]. Importantly, reaction norm analyses showed that plasticity varied not only in magnitude but also in direction [43], some genotypes exhibited increases in certain traits under water stress.

This opposing behavior demonstrates that plasticity is not uniform [13], reinforcing that it constitutes a genetically regulated trait rather than a simple by-product of stress exposure [44]. The identification of genotypes showing improved performance under WL conditions suggests that different allelic polygenic combinations modulate growth-stress trade-offs [17,45], generating a spectrum of strategies ranging from conservative to opportunistic responses in the face of water scarcity [19,46]. Overall, these observations reinforce the conclusions of theoretical frameworks proposing that plasticity is multidimensional, genotype-dependent, and shaped by both environmental and genetic effects [17,18,47]. The variation observed here highlights the value of treating plasticity as an environment-dependent discrete phenotype that can be quantified and genetically dissected [19,48].

Variance decomposition revealed trait-specific contrasts in the relative importance of genetic, environmental, and residual components [31]. Plant developmental traits HEA and MAT displayed strong genetic control and relatively low environmental sensitivity, whereas yield-related traits were dominated by environmental effects, particularly water availability. The reduction in GW, TDM, and GY under drought, with increases in between-genotype variability, suggests that these traits depend more heavily on context-specific interactions and may be governed by many small-effect loci [8,49], consistent with their highly polygenic nature [18,50]. While residual variance was large for yield traits, genetic components were still detectable in several other traits (i.e., GFP, MAT, HI), enabling successful association mapping. The exclusion of traits dominated by residual noise (e.g., VDW, GW) improved the resolution of genomic and biological interpretations.

3.2. Combining Multiple Plasticity Estimators and GWAS Models Increases Detection Robustness

A key contribution of this study is the integration of diverse plasticity estimators [12], absolute values (WW and WL), Ratio, RDPI, and Linear slopes, to capture distinct facets of environmental sensitivity [11]. Although these metrics were positively correlated, each retained unique information, supporting the use of multiple estimators to avoid over-simplifying the plastic response [20,51]. Applying four GWAS methodologies spanning statistical (rrBLUP, BLINK) and machine learning approaches (RF, XGBoost) revealed both complementary and method-specific associations. Machine learning models identified a broader set of associations [52,53], likely capturing non-linear and interactive effects, while BLINK and XGBoost prioritized highly conservative signals. Importantly, SNPs were retained only when detected by at least two plasticity estimators, and methodological convergence (e.g., rrBLUP–RF or BLINK–rrBLUP intersections) further strengthened confidence in the identified loci. This consensus-based strategy reduces false positives

inherent to single-method GWAS and enhances the reproducibility of detected QTLs, a major drawback of single-context GWAS mapping efforts [32,54,55].

The heterogeneity in overlap across traits is biologically informative [56]. Developmental traits (i.e., GFP and MAT) displayed high concordance among metrics and methods, reflecting more stable, genetically determined responses. In contrast, yield-related traits showed lower overlap, reinforcing their complex and environmentally sensitive nature. These patterns mirror observations from GWAS of drought plasticity in maize and barley [15,57], where developmental traits tend to be governed by more consistent genomic regions [16], while yield traits depend on diffuse, context-dependent genomic architectures.

3.3. Plasticity QTLs Are Polygenic, with Small-Effects, and Enriched in Coding Regions

Across traits and plasticity metrics, most QTLs explained small fractions of phenotypic variance (<10%), consistent with a highly polygenic architecture. This finding reinforces polygenic models of plasticity proposed in theoretical studies [45,58] and empirical results in crops such as maize, rice, and wheat [16,20]. The predominance of small-effect loci suggests that plasticity emerges from the cumulative action of many genes rather than a few major-effect regulators [15,59].

A notable outcome is the substantial proportion of significant SNPs located in coding regions [60]. This pattern suggests that putative functional variants within proteins, rather than only regulatory or intergenic polymorphisms [61,62], may play a prominent role in mediating responses to water availability [49]. Functional annotation and GO enrichment analyses support this interpretation. Enriched terms were dominated by categories related to primary metabolism, catalytic activity, intracellular processes, and ion binding. These functions align well with known drought-response pathways, including osmotic adjustment [63,64], ROS detoxification [65], carbohydrate remobilization, and cell homeostasis.

Candidate genes identified near significant SNPs further reinforce this biological context. We detected genes involved in signaling (e.g., serine/threonine kinases, calcium channels), metabolic reprogramming (e.g., sucrose phosphate synthase), growth regulation (e.g., gibberellin receptors), and structural processes (e.g., organelle organization). Many of these gene families have been implicated in drought tolerance and plastic developmental adjustments in other crops [40,42,66–93]. Their recurrence across traits and plasticity metrics highlights them as promising targets for functional validation.

Furthermore, chromosomal patterns reveal potential hotspots of plasticity regulation. The karyogram revealed clusters of significant SNPs on chromosomes 2H, 5H, 6H, and 7H. Some of these regions coincide with previously reported loci associated with drought tolerance, yield stability, and phenology, including the HsDry2.2 locus. These recurrent clusters may represent pleiotropy hotspots for plasticity regulation where multiple physiological pathways converge [94].

3.4. Opposite Allelic Responses Suggest Antagonistic Pleiotropy

The presence of shared loci across multiple traits and plasticity metrics suggests pleiotropy or tight linkage, reflecting the interconnected nature of physiological and metabolic adjustments under drought [95]. Plots linking allelic variants to plasticity metrics highlight another central finding, which is that alleles at the same locus can drive opposite phenotypic responses depending on the environment [32,47]. Some alleles increased trait values under drought, while others reduced them, supporting the hypothesis that plasticity arises from a complex interplay of additive, interactive, and potentially epistatic effects under an antagonistic pleiotropy framework [96]. This may suggest that drought-beneficial alleles may increase osmotic adjustment, reduce growth rate, or shift resource allocation, traits that are advantageous under stress but reduce yield or biomass under optimal con-

ditions [15,18,97]. Substitution of the stress-beneficial alleles, in near-isogenic lines for instance [98,99], will cause a measurable performance penalty in non-stress conditions.

This allelic heterogeneity has relevant implications for plant breeding. For instance, it demonstrates that (i) plasticity cannot be treated as uniformly beneficial, (ii) loci underlying plasticity need to be evaluated for both direction and magnitude of response across contrasting contexts, and (iii) breeding for plasticity requires careful definition of desirable response trajectories, as different genotypes could converge to similar performance.

3.5. Perspectives

Our results reinforce the value of integrating multiple plasticity metrics and diverse GWAS methodologies to dissect the genetic basis of complex adaptive traits. Coding-region variants and metabolic regulators suggest that plasticity may be improved through targeted recurrent introgression or genomic selection strategies focused on alleles that optimize physiological flexibility under drought. Key implications for breeding pipelines include (i) the necessity to incorporate plasticity into selection frameworks (not only absolute trait values), (ii) QTLs with consistent signals across multiple plasticity estimators represent robust candidates for marker-assisted selection, and (iii) developmental plasticity (MAT, GFP) appears more genetically tractable via an assortment of GWAS methods and may serve as a stable predictor of adaptive responses to heterogeneous environments [93].

Additionally, yield plasticity is highly polygenic [48], suggesting genomic selection may be more effective than single-locus approaches [100]. Future work should envision functional validation of candidate genes, assessment of epistatic interactions, and analyses across broader environmental gradients trying to achieve the enviromics spectrum [57,101]. Integrating transcriptomic [102], metabolomic data [103] and pangenomic [104,105] would also help clarifying how these loci mechanistically modulate physiological pathways in response to stress [106–108].

4. Materials and Methods

4.1. Experimental Design

The experimental material consisted of a large collection of approximately 1277 barley genotypes (*Hordeum vulgare* L.), representing lines and families (25) covering a highly diverse range of genetic and geographical variation previously described in studies of genome-wide scan for the identification of flowering-independent effects [8].

Specifically, the panel corresponds to the HEB-25 population, a wild barley-derived nested association mapping population developed to capture broad genetic diversity relevant to drought adaptation and yield stability. This population was selected because it segregates for drought-responsive loci independently of flowering time and has been extensively validated for the study of genotype-by-environment interactions under water deficit conditions [8].

This diversity provided the appropriate basis for a detailed analysis of the genetic architecture of phenotypic plasticity, following the conceptual framework established by Valladares et al. [109,110] and Arenas et al. [111–113], who emphasized that plasticity is not a uniform trait, but rather a specific attribute of genotypes, dependent on genetic, environmental, and random factors [109,112].

The trials were conducted in two completely contrasting environments in terms of water availability, which has already been described in detail [8]. The well-watered (WW) environment represented an optimal growing scenario without water limitations. On the other hand, the water-limited (WL) environment was designed to induce water stress during critical stages of the cycle, particularly heading and grain filling.

Field trials were conducted over two consecutive growing seasons (2014–2015 and 2015–2016) under controlled conditions an insect-proof net house at the experimental farm of The Hebrew University of Jerusalem (Rehovot, Israel). Plants were grown in canals that allowed for differentiated irrigation between adjacent experimental units. To replicate the natural rainfall pattern of the eastern Mediterranean region, irrigation was applied in winter and gradually reduced until early spring. Water limitation was imposed quantitatively by reducing seasonal irrigation volumes (WW: 25–34 m^3; WL: 13–26 m^3, depending on the season). Drought stress intensity was monitored physiologically by measuring stomatal conductance at multiple developmental stages using a porometer, ensuring an approximate 30% reduction in conductance under WL compared to WW conditions [8].

The experimental design included completely randomized blocks with replicates in both environments, ensuring comparability and control of environmental variability. Throughout the cycle, highly relevant agronomic and developmental traits were measured: number of grains (GN), grain weight (GW), grain yield (GY), total biomass (TDM), harvest index (HI), days to heading (HEA), days to maturity (MAT), green biomass (GFP), and dry weight of stems (VDW). Phenological traits were recorded through field observations, while yield and biomass traits were quantified after harvest and drying in the laboratory. Genotypes were not classified a priori as drought-tolerant or drought-susceptible. Instead, tolerance-related responses were inferred a posteriori based on observed phenotypic measures and plasticity across contrasting water regimes, allowing an unbiased assessment of genotype-specific environmental response.

4.2. Calculation of Plasticity Metrics

Several complementary approaches were used to characterize phenotypes, each reflecting different dimensions of the response to the environment. First, we worked with absolute values under WW and WL, which represent the extremes of the response range. Additionally, we calculated metrics derived from phenotypic plasticity: the WW/WL ratio, which provides a simple relative measure of change, and the relative plasticity index (RDPI) [114,115], calculated as the absolute difference (or distance) between conditions divided by the sum of both, as follows (Equation (1)):

$$RDPI = \mid X_{WW} - X_{WL} \mid / X_{WW} + X_{WL} \quad (1)$$

We also considered the coefficient of variation (CV) as a proxy for intra-genotype variability across environments and thus serve as an alternative indicator of plasticity, particularly when differences in scale or baseline values challenged ratio-based metrics [116]. However, due to its strong correlation with other estimators in our data (Figure S2) and to avoid redundancy, CV was excluded from the final association analyses.

Meanwhile, the linear estimator was obtained from the classic model of Finlay and Wilkinson (1963) [117]. The latter is based on the regression of the yield of each genotype against a gradient of environments, expressed as follows (Equation (2)):

$$y_{ij} = \mu_i + b_i + E_j + \varepsilon_{ij} \quad (2)$$

where y_{ij} corresponds to the phenotype of genotype i in environment j, μ_i is the average of the genotype, b_i is the slope that reflects its environmental sensitivity, and ε_{ij} is the residual error. Genotypes with slopes close to one are interpreted as stable, while higher or lower values denote relative sensitivity or insensitivity, and it is the value of this slope that will represent linear plasticity [112,116]. Thus, the GWAS analysis was based on five main estimators: WW, WL, Ratio, RDPI, and Linear.

https://doi.org/10.3390/ijms27020652

The differences between environments were evaluated using the nonparametric Wilcoxon signed-rank test, statistically confirming that the WL condition induced significant phenotypic variations. To decompose the variance of each trait, linear mixed models were used, in which the phenotype was expressed as follows (Equation (3)):

$$y_{ij} = \mu_i + G_i + E_j + (GE)_{ij} + \varepsilon_{ijk} \quad (3)$$

where G_i represented the genotypic effect, E_j the environmental effect, $(GE)_{ij}$ the genotype-by-environment interaction, and ε_{ijk} the residual error, as reported in Djabali et al. (2023) [118]. Using this framework, the proportions of variance attributable to genetics, environment, and residuals were estimated, quantifying the relative importance of each.

4.3. Genetic Mapping of Plastic Responses

Genomic analysis included genotyping using a dense panel of SNPs distributed across the seven chromosomes of barley. These were genotyped using the Infinium iSelect 9K barley chip [119], which consists of 7864 SNPs [120]. The inclusion of SNPs that were polymorphic in at least one HEB family and that met the predefined quality criteria [<10% missing data and no complete linkage disequilibrium with another SNP in the set] resulted in 5709 informative loci. Using these data, linkage disequilibrium decay (LD decay) was estimated, which will give us adequate resolution for genome-wide association mapping. Subsequently, the population structure was evaluated using principal component analysis (PCA), allowing us to detect and correct for the presence of substructures. In addition, a rapid reduction in association was observed as a function of physical distance.

All statistical analyses were performed using the R software environment (R version 4.4.2; [121]). Descriptive statistics, variance partitioning, and nonparametric tests were implemented using base R functions. Principal component analysis (PCA) was conducted using the prcomp() function. Genome-wide association analyses were performed using the corresponding software and packages associated with each method, while downstream data handling and integration were carried out in R. Data visualization and figure generation were performed using the ggplot2 package [122], ensuring consistent graphical representation across traits and plasticity estimators.

The GWAS was carried out using four independent methodologies representing two different paradigms. From the classical statistical approach, rrBLUP and BLINK were used. The rrBLUP analyses were performed in R using the rrBLUP package [123], which implements ridge regression best linear unbiased prediction models for genome-wide association studies. BLINK analyses were conducted using the GAPIT [124] framework. Default parameters were applied unless otherwise specified. The former is a ridge regression model that allows thousands of markers to be handled simultaneously, modeling the random effect of SNPs as $u \sim N\left(0, \sigma^2 K\right)$, where K is the kinship matrix (or the already defined genetic structure). BLINK, on the other hand, is an extension of the classic FarmCPU model, incorporating linkage disequilibrium information and Bayesian selection criteria, increasing power and reducing false positives. In parallel, two machine learning methodologies were used: Random Forest (RF), which constructs multiple decision trees and combines their results, and XGBoost, a gradient-based boosting algorithm that optimizes a regularized loss function. To define reliable associations, SNPs were first identified independently within each GWAS method by trait and plasticity estimator. Only SNPs detected by at least two plasticity estimators were retained, and among these, loci identified by more than one GWAS methodology were prioritized as high-confidence associations. This conservative strategy was adopted to reduce false positives and ensure robustness across analytical frameworks.

https://doi.org/10.3390/ijms27020652

4.4. Estimating the Relevance of Plasticity QTLs

The filtered SNPs were subjected to functional annotation using the barley reference genome in Ensembl Plants. Their location in coding, intronic, or intergenic regions was identified, and those in coding regions were selected for GO term enrichment analysis. The procedure included the construction of sets of genes associated with significant SNPs, the definition of a genome-wide reference set, and the application of overrepresentation tests (Fisher's exact test) with false discovery rate (FDR) correction. Significantly enriched terms were organized into categories of biological processes, molecular functions, and cellular components. This annotation-based enrichment framework was specifically employed to provide a systematic, biologically grounded interpretation of the genetic signals derived from the GWAS, rather than to establish direct causal validation of individual loci. By assessing the collective functional patterns of SNP-linked genes, GO analysis enabled the identification of coherent biological pathways underlying phenotypic plasticity responses to drought, thereby reducing reliance on single-gene interpretations. Finally, associations between SNPs located in coding regions and plasticity values were plotted, visualizing how alternative alleles generated divergent phenotypic trajectories in different environments. Within the framework of this study, this integrative annotation-enrichment approach provides sufficient functional context to support the interpretation of plasticity-related QTLs without requiring further experimental validation.

5. Conclusions

This study demonstrates that drought-related phenotypic plasticity in barley is a genetically regulated and strongly trait-dependent phenomenon. Across a diverse panel of 1277 genotypes, we show that yield-related traits are predominantly shaped by environmental variation, while developmental traits maintain stronger genetic control. Integrating five complementary plasticity estimators with four GWAS methodologies enabled us to identify a robust set of loci consistently associated with plastic responses. These associated SNPs were enriched in coding regions and linked to pathways including osmotic regulation, carbohydrate metabolism, hormonal signaling, and ion transport, offering concrete genomic targets for improving drought resilience. Many alleles showed opposite effects across environments, suggesting that due to antagonistic pleiotropy plasticity cannot be captured by evaluating performance under a single condition. Instead, the identified loci highlight the need to breed for context-dependent responsiveness.

The strength of this study lies in the integration of multiple plasticity metrics with independent GWAS approaches, which increased robustness and reproducibility of genetic associations. By focusing on pathway-level functional enrichment rather than single-locus validation, the results provide a biologically coherent interpretation of plasticity-related loci. Overall, this framework supports the use of phenotypic plasticity as an explicit target in breeding strategies aimed at improving crop performance under variable water availability, although laboratory validation is still important.

Supplementary Materials: The following supporting information can be downloaded at https://www.mdpi.com/article/10.3390/ijms27020652/s1.

Author Contributions: Conceptualization, S.A. and A.J.C.; data curation, S.A.; methodology, S.A.; validation, S.A. and A.J.C.; visualization, S.A.; writing—original draft preparation, S.A. and A.J.C.; writing—review and editing, S.A. and A.J.C.; project administration, A.J.C. All authors have read and agreed to the published version of the manuscript.

Funding: A.J.C. acknowledged funding from rom Vetenskapsrådet (VR) through grant 2022-04411, which made possible a synergistic meeting between the authors in Alnarp, Sweden, during the summer of 2025.

Institutional Review Board Statement: Not applicable.

Informed Consent Statement: Not applicable.

Data Availability Statement: The phenotypic plasticity metrics and all analysis scripts generated in this study will be made publicly available upon acceptance of the manuscript. The raw genomic data and the original phenotypic measurements used here are openly available from the publication "Genome scan identifies flowering-independent effects of barley HsDry2.2 locus on yield traits under water deficit" (Merchuk-Ovnat et al., 2018, *Journal of Experimental Botany*), https://doi.org/10.1093/jxb/ery016 [8].

Acknowledgments: A.J.C. thanks Vetenskapsrådet (VR) for their academic support. S.A. To UIS and UNAM, my alma maters.

Conflicts of Interest: The authors declare no conflicts of interest.

References

1. Kallis, G. Droughts. *Annu. Rev. Environ. Resour.* **2008**, *33*, 85–118. [CrossRef]
2. Cortés, A.J.; Monserrate, F.; Ramírez-Villegas, J.; Madriñán, S.; Blair, M.W. Drought Tolerance in Wild Plant Populations: The Case of Common Beans (*Phaseolus vulgaris* L.). *PLoS ONE* **2013**, *8*, e62898. [CrossRef]
3. Martignago, D.; Rico-Medina, A.; Blasco-Escamez, D.; Fontanet-Manzaneque, J.B.; Cano-Delgado, A.I. Drought Resistance by Engineering Plant Tissue-Specific Responses. *Front. Plant Sci.* **2019**, *10*, 1676. [CrossRef] [PubMed]
4. Varshney, R.K.; Barmukh, R.; Roorkiwal, M.; Qi, Y.; Kholova, J.; Tuberosa, R.; Reynolds, M.P.; Tardieu, F.; Siddique, K.H.M. Breeding custom-designed crops for improved drought adaptation. *Adv. Genet.* **2021**, *2*, e202100017. [CrossRef]
5. Cortés, A.J. Unlocking genebanks for climate adaptation. *Nat. Clim. Change* **2025**, *15*, 590–592. [CrossRef]
6. Russell, J.; Mascher, M.; Dawson, I.K.; Kyriakidis, S.; Calixto, C.; Freund, F.; Bayer, M.; Milne, I.; Marshall-Griffiths, T.; Heinen, S.; et al. Exome sequencing of geographically diverse barley landraces and wild relatives gives insights into environmental adaptation. *Nat. Genet.* **2016**, *48*, 1024–1030. [CrossRef]
7. Abebe, T.D.; Naz, A.A.; Leon, J. Landscape genomics reveal signatures of local adaptation in barley (*Hordeum vulgare* L.). *Front. Plant Sci.* **2015**, *6*, 813. [CrossRef]
8. Merchuk-Ovnat, L.; Silberman, R.; Laiba, E.; Maurer, A.; Pillen, K.; Faigenboim, A.; Fridman, E. Genome scan identifies flowering-independent effects of barley HsDry2.2 locus on yield traits under water deficit. *J. Exp. Bot.* **2018**, *69*, 1765–1779. [CrossRef]
9. Logan, M.L.; Cox, C.L. Genetic Constraints, Transcriptome Plasticity, and the Evolutionary Response to Climate Change. *Front. Genet.* **2020**, *11*, 538226. [CrossRef]
10. Bartels, D.; Sunkar, R. Drought and salt tolerance in plants. *Crit. Rev. Plant Sci.* **2005**, *24*, 23–58. [CrossRef]
11. Arnold, P.A.; Kruuk, L.E.B.; Nicotra, A.B. How to analyse plant phenotypic plasticity in response to a changing climate. *New Phytol.* **2019**, *222*, 1235–1241. [CrossRef]
12. Fox, R.J.; Donelson, J.M.; Schunter, C.; Ravasi, T.; Gaitan-Espitia, J.D. Beyond buying time: The role of plasticity in phenotypic adaptation to rapid environmental change. *Philos. Trans. R. Soc. B Biol. Sci.* **2019**, *374*, 20180174. [CrossRef] [PubMed]
13. Kelly, M. Adaptation to climate change through genetic accommodation and assimilation of plastic phenotypes. *Philos. Trans. R. Soc. B Biol. Sci.* **2019**, *374*, 20180176. [CrossRef] [PubMed]
14. Crossa, J.; Perez-Rodriguez, P.; Cuevas, J.; Montesinos-Lopez, O.; Jarquin, D.; de Los Campos, G.; Burgueno, J.; Gonzalez-Camacho, J.M.; Perez-Elizalde, S.; Beyene, Y.; et al. Genomic selection in plant breeding: Methods, models, and perspectives. *Trends Plant Sci.* **2017**, *22*, 961–975. [CrossRef]
15. Li, X.; Guo, T.; Wang, J.; Bekele, W.A.; Sukumaran, S.; Vanous, A.E.; McNellie, J.P.; Tibbs-Cortes, L.E.; Lopes, M.S.; Lamkey, K.R.; et al. An integrated framework reinstating the environmental dimension for GWAS and genomic selection in crops. *Mol. Plant* **2021**, *14*, 874–887. [CrossRef]
16. Wei, J.; Guo, T.; Mu, Q.; Alladassi, B.M.E.; Mural, R.V.; Boyles, R.E.; Hoffmann, L.; Hayes, C.M.; Sigmon, B.; Thompson, A.M.; et al. Genetic and Environmental Patterns Underlying Phenotypic Plasticity in Flowering Time and Plant Height in Sorghum. *Plant Cell Environ.* **2025**, *48*, 2727–2738. [CrossRef]
17. Kikuchi, S.; Bheemanahalli, R.; Jagadish, K.S.V.; Kumagai, E.; Masuya, Y.; Kuroda, E.; Raghavan, C.; Dingkuhn, M.; Abe, A.; Shimono, H. Genome-wide association mapping for phenotypic plasticity in rice. *Plant Cell Environ.* **2017**, *40*, 1565–1575. [CrossRef]
18. Huang, Y.; Qi, Z.; Li, J.; You, J.; Zhang, X.; Wang, M. Genetic interrogation of phenotypic plasticity informs genome-enabled breeding in cotton. *J. Genet. Genom.* **2023**, *50*, 971–982. [CrossRef] [PubMed]

19. Guo, W.; Wang, F.; Lv, J.; Yu, J.; Wu, Y.; Wuriyanghan, H.; Le, L.; Pu, L. Phenotyping, genome-wide dissection, and prediction of maize root architecture for temperate adaptability. *iMeta* **2025**, *4*, e70015. [CrossRef]
20. Schneider, H.M.; Lynch, J.P. Should Root Plasticity Be a Crop Breeding Target? *Front. Plant Sci.* **2020**, *11*, 546. [CrossRef]
21. Hirschhorn, J.N.; Daly, M.J. Genome-wide association studies for common diseases and complex traits. *Nat. Rev. Genet.* **2005**, *6*, 95–108. [CrossRef]
22. Lambert, C.G.; Black, L.J. Learning from our GWAS mistakes: From experimental design to scientific method. *Biostatistics* **2012**, *13*, 195–203. [CrossRef]
23. Tam, V.; Patel, N.; Turcotte, M.; Bossé, Y.; Paré, G.; Meyre, D. Benefits and limitations of genome-wide association studies. *Nat. Rev. Genet.* **2019**, *20*, 467–484. [CrossRef]
24. Korte, A.; Farlow, A. The advantages and limitations of trait analysis with GWAS: A review. *Plant Methods* **2013**, *9*, 29. [CrossRef] [PubMed]
25. Wray, N.R.; Yang, J.; Hayes, B.J.; Price, A.L.; Goddard, M.E.; Visscher, P.M. Pitfalls of predicting complex traits from SNPs. *Nat. Rev. Genet.* **2013**, *14*, 507–515. [CrossRef] [PubMed]
26. Barton, N.; Hermisson, J.; Nordborg, M. Why structure matters. *eLife* **2019**, *8*, 45380. [CrossRef]
27. Denning-James, K.E.; Chater, C.; Cortes, A.J.; Blair, M.W.; Pelaez, D.; Hall, A.; De Vega, J.J. Genome-wide association mapping dissects the selective breeding of determinacy and photoperiod sensitivity in common bean (*Phaseolus vulgaris* L.). *G3* **2025**, *15*, jkaf090. https://doi.org/10.1093/g3journal/jkaf090. Erratum in *G3* **2025**, *15*, jkaf141. [CrossRef]
28. Brachi, B.; Morris, G.P.; Borevitz, J.O. Genome-wide association studies in plants: The missing heritability is in the field. *Genome Biol.* **2011**, *12*, 232. [CrossRef] [PubMed]
29. Gibson, G. Hints of hidden heritability in GWAS. *Nat. Genet.* **2010**, *42*, 558–560. [CrossRef]
30. Manolio, T.A.; Collins, F.S.; Cox, N.J.; Goldstein, D.B.; Hindorff, L.A.; Hunter, D.J.; McCarthy, M.I.; Ramos, E.M.; Cardon, L.R.; Chakravarti, A.; et al. Finding the missing heritability of complex diseases. *Nature* **2009**, *461*, 747–753. [CrossRef]
31. Brachi, B.; Faure, N.; Bergelson, J.; Cuguen, J.; Roux, F. Genome-wide association mapping of flowering time in Arabidopsis thaliana in nature: Genetics for underlying components and reaction norms across two successive years. *Acta Bot. Gall.* **2013**, *160*, 205–219. [CrossRef] [PubMed]
32. López-Hernández, F.; Burbano-Erazo, E.; León-Pacheco, R.I.; Cordero-Cordero, C.C.; Villanueva-Mejía, D.F.; Tofiño-Rivera, A.P.; Cortés, A.J. Multi-Environment Genome-Wide Association Studies of Yield Traits in Common Bean (*Phaseolus vulgaris* L.) × Tepary Bean (*P. acutifolius* A. Gray) Interspecific Advanced Lines in Humid and Dry Colombian Caribbean Subregions. *Agronomy* **2023**, *13*, 1396. [CrossRef]
33. Cortés, A.J.; Blair, M.W. Genotyping by Sequencing and Genome—Environment Associations in Wild Common Bean Predict Widespread Divergent Adaptation to Drought. *Front. Plant Sci.* **2018**, *9*, 128. [CrossRef]
34. Labastida, D.; Ingvarsson, P.K.; Rendón-Anaya, M. Dissecting the genetic basis of drought responses in common bean using natural variation. *Front. Plant Sci.* **2023**, *14*, 1143873. [CrossRef]
35. Wirojsirasak, W.; Songsri, P.; Jongrungklang, N.; Tangphatsornruang, S.; Klomsa-Ard, P.; Ukoskit, K. A Large-Scale Candidate-Gene Association Mapping for Drought Tolerance and Agronomic Traits in Sugarcane. *Int. J. Mol. Sci.* **2023**, *24*, 12801. [CrossRef] [PubMed]
36. Guerrero-Sánchez, V.M.; López-Hidalgo, C.; Rey, M.-D.; Castillejo, M.Á.; Jorrín-Novo, J.V.; Escandón, M. Multiomic Data Integration in the Analysis of Drought-Responsive Mechanisms in *Quercus ilex* Seedlings. *Plants* **2022**, *11*, 3067. [CrossRef]
37. Burbano-Erazo, E.; León-Pacheco, R.; Cordero-Cordero, C.; López-Hernández, F.; Cortés, A.; Tofiño-Rivera, A. Multi-Environment Yield Components in Advanced Common Bean (*Phaseolus vulgaris* L.) × Tepary Bean (*P. acutifolius* A. Gray) Interspecific Lines for Heat and Drought Tolerance. *Agronomy* **2021**, *11*, 1978. [CrossRef]
38. Etterson, J.R.; Shaw, R.G. Constraint to Adaptive Evolution in Response to Global Warming. *Science* **2001**, *294*, 151–154. [CrossRef] [PubMed]
39. Worch, S.; Kalladan, R.; Harshavardhan, V.T.; Pietsch, C.; Korzun, V.; Kuntze, L.; Borner, A.; Wobus, U.; Roder, M.S.; Sreenivasulu, N. Haplotyping, linkage mapping and expression analysis of barley genes regulated by terminal drought stress influencing seed quality. *BMC Plant Biol.* **2011**, *11*, 1. [CrossRef]
40. Seiler, C.; Harshavardhan, V.T.; Rajesh, K.; Reddy, P.S.; Strickert, M.; Rolletschek, H.; Scholz, U.; Wobus, U.; Sreenivasulu, N. ABA biosynthesis and degradation contributing to ABA homeostasis during barley seed development under control and terminal drought-stress conditions. *J. Exp. Bot.* **2011**, *62*, 2615–2632. [CrossRef]
41. Chloupek, O.; Dostal, V.; Streda, T.; Psota, V.; Dvorackova, O. Drought tolerance of barley varieties in relation to their root system size. *Plant Breed.* **2010**, *129*, 630–636. [CrossRef]
42. Nayak, S.N.; Balaji, J.; Upadhyaya, H.D.; Hash, C.T.; Kishor, P.B.K.; Chattopadhyay, D.; Rodriquez, L.M.; Blair, M.W.; Baum, M.; McNally, K.; et al. Isolation and sequence analysis of DREB2A homologues in three cereal and two legume species. *Plant Sci.* **2009**, *177*, 460–467. [CrossRef]

43. Franks, S.J.; Weber, J.J.; Aitken, S.N. Evolutionary and plastic responses to climate change in terrestrial plant populations. *Evol. Appl.* **2014**, *7*, 123–139. [CrossRef]
44. Nicotra, A.B.; Segal, D.L.; Hoyle, G.L.; Schrey, A.W.; Verhoeven, K.J.; Richards, C.L. Adaptive plasticity and epigenetic variation in response to warming in an Alpine plant. *Ecol. Evol.* **2015**, *5*, 634–647. [CrossRef] [PubMed]
45. Barghi, N.; Hermisson, J.; Schlötterer, C. Polygenic adaptation: A unifying framework to understand positive selection. *Nat. Rev. Genet.* **2020**, *21*, 769–781. https://doi.org/10.1038/s41576-020-0250-z. Erratum in *Rev. Genet.* **2020**, *21*, 782. [CrossRef] [PubMed]
46. Csillery, K.; Rodriguez-Verdugo, A.; Rellstab, C.; Guillaume, F. Detecting the genomic signal of polygenic adaptation and the role of epistasis in evolution. *Mol. Ecol.* **2018**, *27*, 606–612. [CrossRef] [PubMed]
47. López-Hernández, F.; Villanueva-Mejía, D.F.; Tofiño-Rivera, A.P.; Cortés, A.J. Genomic prediction of adaptation in common bean (*Phaseolus vulgaris* L.) × Tepary bean (*P. acutifolius* A. Gray) hybrids. *Int. J. Mol. Sci.* **2025**, *26*, 7370. [CrossRef]
48. Alam, O.; Purugganan, M.D. Domestication and the evolution of crops: Variable syndromes, complex genetic architectures, and ecological entanglements. *Plant Cell* **2024**, *36*, 1227–1241. [CrossRef]
49. Stephan, W. Signatures of positive selection: From selective sweeps at individual loci to subtle allele frequency changes in polygenic adaptation. *Mol. Ecol.* **2016**, *25*, 79–88. [CrossRef]
50. Pritchard, J.K.; Pickrell, J.K.; Coop, G. The Genetics of Human Adaptation: Hard Sweeps, Soft Sweeps, and Polygenic Adaptation. *Curr. Biol.* **2010**, *20*, R208–R215. [CrossRef]
51. Lecheta, M.C.; Awde, D.N.; O'Leary, T.S.; Unfried, L.N.; Jacobs, N.A.; Whitlock, M.H.; McCabe, E.; Powers, B.; Bora, K.; Waters, J.S.; et al. Integrating GWAS and Transcriptomics to Identify the Molecular Underpinnings of Thermal Stress Responses in *Drosophila melanogaster*. *Front. Genet.* **2020**, *11*, 658. [CrossRef]
52. Schrider, D.R.; Kern, A.D. Supervised Machine Learning for Population Genetics: A New Paradigm. *Trends Genet.* **2018**, *34*, 301–312. [CrossRef]
53. Libbrecht, M.W.; Noble, W.S. Machine learning applications in genetics and genomics. *Nat. Rev. Genet.* **2015**, *16*, 321–332. [CrossRef]
54. McLeod, L.; Barchi, L.; Tumino, G.; Tripodi, P.; Salinier, J.; Gros, C.; Boyaci, H.F.; Ozalp, R.; Borovsky, Y.; Schafleitner, R.; et al. Multi-environment association study highlights candidate genes for robust agronomic quantitative trait loci in a novel worldwide *Capsicum* core collection. *Plant J.* **2023**, *116*, 1508–1528. [CrossRef] [PubMed]
55. Garreta, L.; Cerón-Souza, I.; Palacio, M.R.; Reyes-Herrera, P.H. MultiGWAS: An integrative tool for Genome Wide Association Studies (GWAS) in tetraploid organisms. *Ecol. Evol.* **2021**, *11*, 7411–7426. [CrossRef] [PubMed]
56. Nakombo-Gbassault, P.; Arenas, S.; Affortit, P.; Faye, A.; Flis, P.; Sine, B.; Moukouanga, D.; Gantet, P.; Komba, E.K.; Kane, N.; et al. Genetic control of the leaf ionome in pearl millet and correlation with root and agromorphological traits. *PLoS ONE* **2025**, *20*, e0319140. [CrossRef] [PubMed]
57. Costa-Neto, G.; Crossa, J.; Fritsche-Neto, R. Enviromic Assembly Increases Accuracy and Reduces Costs of the Genomic Prediction for Yield Plasticity in Maize. *Front. Plant Sci.* **2021**, *12*, 717552. [CrossRef]
58. Boyle, E.A.; Li, Y.I.; Pritchard, J.K. An Expanded View of Complex Traits: From Polygenic to Omnigenic. *Cell* **2017**, *169*, 1177–1186. [CrossRef] [PubMed]
59. Huang, R.; Jiang, L.; Zheng, J.; Wang, T.; Wang, H.; Huang, Y.; Hong, Z. Genetic bases of rice grain shape: So many genes, so little known. *TRENDS Plant Sci.* **2013**, *18*, 218–226. [CrossRef]
60. Joly-Lopez, Z.; Flowers, J.M.; Purugganan, M.D. Developing maps of fitness consequences for plant genomes. *Curr. Opin. Plant Biol.* **2016**, *30*, 101–107. [CrossRef]
61. Haegeman, B.; Weitz, J.S. A neutral theory of genome evolution and the frequency distribution of genes. *BMC Genom.* **2012**, *13*, 196. [CrossRef]
62. Nei, M. The Neutral Theory of Molecular Evolution in the Genomic Era. *Annu. Rev. Genom. Hum. Genet.* **2010**, *11*, 265–289. [CrossRef]
63. Chinnusamy, V.; Jagendorf, A.; Zhu, J.K. Understanding and improving salt tolerance in plants. *Crop Sci.* **2005**, *45*, 437–448. [CrossRef]
64. Tyerman, S.D.; Niemietz, C.M.; Bramley, H. Plant aquaporins: Multifunctional water and solute channels with expanding roles. *Plant Cell Environ.* **2002**, *25*, 173–194. [CrossRef]
65. Turner, T.L.; Bourne, E.C.; Von Wettberg, E.J.; Hu, T.T.; Nuzhdin, S.V. Population resequencing reveals local adaptation of Arabidopsis lyrata to serpentine soils. *Nat. Genet.* **2010**, *42*, 260–263. [CrossRef] [PubMed]
66. Wu, N.; Jiang, T.; Feng, Y.; Yuan, M. Genome-wide identification and expression analysis of soybean bHLH transcription factor and its molecular mechanism on grain protein synthesis. *Front. Plant Sci.* **2025**, *16*, 1481565. [CrossRef] [PubMed]
67. Ouyang, W.; Chen, L.; Ma, J.; Liu, X.; Chen, H.; Yang, H.; Guo, W.; Shan, Z.; Yang, Z.; Chen, S.; et al. Identification of Quantitative Trait Locus and Candidate Genes for Drought Tolerance in a Soybean Recombinant Inbred Line Population. *Int. J. Mol. Sci.* **2022**, *23*, 10828. [CrossRef]

68. Sachdeva, S.; Bharadwaj, C.; Singh, R.K.; Jain, P.K.; Patil, B.S.; Roorkiwal, M.; Varshney, R. Characterization of ASR gene and its role in drought tolerance in chickpea (*Cicer arietinum* L.). *PLoS ONE* **2020**, *15*, e0234550. [CrossRef]
69. Li, R.; Liu, C.; Zhao, R.; Wang, L.; Chen, L.; Yu, W.; Zhang, S.; Sheng, J.; Shen, L. CRISPR/Cas9-Mediated *SlNPR1* mutagenesis reduces tomato plant drought tolerance. *BMC Plant Biol.* **2019**, *19*, 38. [CrossRef]
70. Wang, L.; Chen, L.; Li, R.; Zhao, R.; Yang, M.; Sheng, J.; Shen, L. Reduced Drought Tolerance by CRISPR/Cas9-Mediated SlMAPK3 Mutagenesis in Tomato Plants. *J. Agric. Food Chem.* **2017**, *65*, 8674–8682. [CrossRef]
71. Blair, M.W.; Cortés, A.J.; This, D. Identification of an *ERECTA* gene and its drought adaptation associations with wild and cultivated common bean. *Plant Sci.* **2016**, *242*, 250–259. [CrossRef]
72. Sadhukhan, A.; Kobayashi, Y.; Kobayashi, Y.; Tokizawa, M.; Yamamoto, Y.Y.; Iuchi, S.; Koyama, H.; Panda, S.K.; Sahoo, L. VuDREB2A, a novel DREB2-type transcription factor in the drought-tolerant legume cowpea, mediates DRE-dependent expression of stress-responsive genes and confers enhanced drought resistance in transgenic *Arabidopsis*. *Planta* **2014**, *240*, 645–664. [CrossRef]
73. Uga, Y.; Sugimoto, K.; Ogawa, S.; Rane, J.; Ishitani, M.; Hara, N.; Kitomi, Y.; Inukai, Y.; Ono, K.; Kanno, N.; et al. Control of root system architecture by DEEPER ROOTING 1 increases rice yield under drought conditions. *Nat. Genet.* **2013**, *45*, 1097–1102. [CrossRef] [PubMed]
74. Cortés, A.J.; Chavarro, M.C.; Madriñán, S.; This, D.; Blair, M.W. Molecular ecology and selection in the drought-related *Asr* gene polymorphisms in wild and cultivated common bean (*Phaseolus vulgaris* L.). *BMC Genet.* **2012**, *13*, 58. [CrossRef]
75. Cortés, A.J.; This, D.; Chavarro, C.; Madriñán, S.; Blair, M.W. Nucleotide diversity patterns at the drought-related *DREB2* encoding genes in wild and cultivated common bean (*Phaseolus vulgaris* L.). *Theor. Appl. Genet.* **2012**, *125*, 1069–1085. [CrossRef]
76. Kim, J.-S.; Mizoi, J.; Yoshida, T.; Fujita, Y.; Nakajima, J.; Ohori, T.; Todaka, D.; Nakashima, K.; Hirayama, T.; Shinozaki, K.; et al. An ABRE promoter sequence is involved in osmotic stress-responsive expression of the *DREB2A* gene, which encodes a transcription factor regulating drought-inducible genes in *Arabidopsis*. *Plant Cell Physiol.* **2011**, *52*, 2136–2146. [CrossRef]
77. Yao, X.; Xiong, W.; Ye, T.; Wu, Y. Overexpression of the aspartic protease ASPG1 gene confers drought avoidance in Arabidopsis. *J. Exp. Bot.* **2012**, *63*, 2579–2593. [CrossRef]
78. Wei, A.; He, C.; Li, B.; Li, N.; Zhang, J. The pyramid of transgenes *TsVP* and *BetA* effectively enhances the drought tolerance of maize plants. *Plant Biotechnol. J.* **2011**, *9*, 216–229. https://doi.org/10.1111/j.1467-7652.2010.00548.x. Correction in *Plant Biotechnol. J.* **2011**, *9*, 418. [CrossRef] [PubMed]
79. Fukao, T.; Yeung, E.; Bailey-Serres, J. The Submergence Tolerance Regulator SUB1A Mediates Crosstalk between Submergence and Drought Tolerance in Rice. *Plant Cell* **2011**, *23*, 412–427. [CrossRef] [PubMed]
80. Su, Z.; Li, X.; Hao, Z.; Xie, C.; Li, M.; Weng, J.; Zhang, D.; Liang, X.; Wang, Z.; Gao, J.; et al. Association Analysis of the *nced* and *rab28* Genes with Phenotypic Traits Under Water Stress in Maize. *Plant Mol. Biol. Report.* **2011**, *29*, 714–722. [CrossRef]
81. Guo, M.; Rupe, M.; Simmons, C.; Sivasankar, S. The Maize ERECTA Genes for Improving Plant Growth, Transpiration, Efficiency and Drought Tolerance in Crop Plants. U.S. Patent 7847158B2, 7 December 2010.
82. Seo, J.-S.; Joo, J.; Kim, M.-J.; Kim, Y.-K.; Nahm, B.H.; Song, S.I.; Cheong, J.-J.; Lee, J.S.; Kim, J.-K.; Choi, Y.D. OsbHLH148, a basic helix-loop-helix protein, interacts with OsJAZ proteins in a jasmonate signaling pathway leading to drought tolerance in rice. *Plant J.* **2011**, *65*, 907–921. [CrossRef]
83. Lata, C.; Bhutty, S.; Bahadur, R.P.; Majee, M.; Prasad, M. Association of an SNP in a novel DREB2-like gene SiDREB2 with stress tolerance in foxtail millet [*Setaria italica* (L.)]. *J. Exp. Bot.* **2011**, *62*, 3387–3401. [CrossRef] [PubMed]
84. Li, H.; Jiang, H.; Bu, Q.; Zhao, Q.; Sun, J.; Xie, Q.; Li, C. The Arabidopsis RING Finger E3 Ligase RHA2b Acts Additively with RHA2a in Regulating ABA Signaling and Drought Response. *Plant Physiol.* **2011**, *156*, 550–563. [CrossRef]
85. Ye, N.; Zhu, G.; Liu, Y.; Li, Y.; Zhang, J. ABA Controls H_2O_2 Accumulation Through the Induction of OsCATB in Rice Leaves Under Water Stress. *Plant Cell Physiol.* **2011**, *52*, 689–698.
86. Campo, S.; Peris-Peris, C.; Montesinos, L.; Penas, G.; Messeguer, J.; San Segundo, B. Expression of the maize *ZmGF14-6* gene in rice confers tolerance to drought stress while enhancing susceptibility to pathogen infection. *J. Exp. Bot.* **2011**, *63*, 983–999. [CrossRef]
87. Sun, L.; Wang, Y.P.; Chen, P.; Ren, J.; Ji, K.; Li, Q.; Li, P.; Dai, S.J.; Leng, P. Transcriptional regulation of *SlPYL*, *SlPP2C*, and *SlSnRK2* gene families encoding ABA signal core components during tomato fruit development and drought stress. *J. Exp. Bot.* **2011**, *62*, 5659–5669. [CrossRef] [PubMed]
88. Chen, J.B.; Zhang, X.Y.; Jing, R.L.; Blair, M.W.; Mao, X.G.; Wang, S.M. Cloning and genetic diversity analysis of a new P5CS gene from common bean (*Phaseolus vulgaris* L.). *Theor. Appl. Genet.* **2010**, *120*, 1393–1404. [CrossRef] [PubMed]
89. Giombini, M.I.; Frankel, N.; Lusem, N.D.; Hasson, E. Nucleotide polymorphism in the drought responsive gene *Asr2* in wild populations of tomato. *Genetica* **2009**, *136*, 13–25. [CrossRef]
90. Bahrndorff, S.; Tunnacliffe, A.; Wise, M.J.; McGee, B.; Holmstrup, M.; Loeschcke, V. Bioinformatics and protein expression analyses implicate LEA proteins in the drought response of *Collembola*. *J. Insect Physiol.* **2009**, *55*, 210–217. [CrossRef]

91. Gao, S.; Zhang, H.; Tian, Y.; Li, F.; Zhang, Z.; Lu, X.; Chen, X.; Huang, R. Expression of TERF1 in rice regulates expression of stress-responsive genes and enhances tolerance to drought and high-salinity. *Plant Cell Rep.* **2008**, *27*, 1787–1795. [CrossRef]
92. Chen, J.Q.; Meng, X.P.; Zhang, Y.; Xia, M.; Wang, X.P. Over-expression of *OsDREB* genes lead to enhanced drought tolerance in rice. *Biotechnol. Lett.* **2008**, *30*, 2191–2198. [CrossRef]
93. Wang, Q.; Guan, Y.; Wu, Y.; Chen, H.; Chen, F.; Chu, C. Overexpression of a rice *OsDREB1F* gene increases salt, drought, and low temperature tolerance in both *Arabidopsis* and rice. *Plant Mol. Biol.* **2008**, *67*, 589–602. [CrossRef]
94. Rashotte, A.M.; Mason, M.G.; Hutchison, C.E.; Ferreira, F.J.; Schaller, G.E.; Kieber, J.J. A subset of *Arabidopsis* AP2 transcription factors mediates cytokinin responses in concert with a two-component pathway. *Proc. Natl. Acad. Sci. USA* **2006**, *103*, 11081–11085. [CrossRef]
95. Messina, C.D.; Podlich, D.; Dong, Z.; Samples, M.; Cooper, M. Yield-trait performance landscapes: From theory to application in breeding maize for drought tolerance. *J. Exp. Bot.* **2011**, *62*, 855–868. [CrossRef] [PubMed]
96. López-Hernández, F.; Cortés, A.J. Last-generation genome–environment associations reveal the genetic basis of heat tolerance in common bean (*Phaseolus vulgaris* L.). *Front. Genet.* **2019**, *10*, 22. [CrossRef] [PubMed]
97. Beebe, S.E.; Rao, I.M.; Blair, M.W.; Acosta-Gallegos, J.A. Phenotyping common beans for adaptation to drought. *Front. Physiol.* **2013**, *4*, 35. [CrossRef] [PubMed]
98. Gregorio, G.B.; Senadhira, D.; Mendoza, R.D.; Manigbas, N.L.; Roxas, J.P.; Guerta, C.Q. Progress in breeding for salinity tolerance and associated abiotic stresses in rice. *Field Crops Res.* **2002**, *76*, 91–101. [CrossRef]
99. Laitinen, R.A.E. Importance of phenotypic plasticity in crop resilience. *J. Exp. Bot.* **2024**, *75*, 670–673. [CrossRef]
100. Westbrook, J.W.; Zhang, Q.; Mandal, M.K.; Jenkins, E.V.; Barth, L.E.; Jenkins, J.W.; Grimwood, J.; Schmutz, J.; Holliday, J.A. Optimizing genomic selection for blight resistance in American chestnut backcross populations: A trade-off with American chestnut ancestry implies resistance is polygenic. *Evol. Appl.* **2020**, *13*, 31–47. [CrossRef]
101. Costa-Neto, G.; Fritsche-Neto, R. Enviromics: Bridging different sources of data, building one framework. *Crop Breed. Appl. Biotechnol.* **2021**, *21*, e393521S393512. [CrossRef]
102. López-Hernández, F.; Cortés, A.J. Whole Transcriptome Sequencing Unveils the Genomic Determinants of Putative Somaclonal Variation in Mint (*Mentha* L.). *Int. J. Mol. Sci.* **2022**, *23*, 5291. [CrossRef]
103. Parra-Londono, S.; López-Hernández, F.; Montoya, G.; Henao-Rojas, J.C.; Ossa-Ossa, G.A.; Cortés, A.J. Merging Phenotypic Stability Analysis and Genomic Prediction for Multi-Environment Breeding in *Capsicum* spp. *Agronomy* **2025**, *15*, 2690. [CrossRef]
104. López-Hernández, F.; Roda, F.; Cortés, A.J. Machine Learning and Pangenomics: Revolutionizing Plant Breeding for a Sustainable Future. In *Plant Breeding 2050*; Priyadarshan, P.M., Ortiz, R., Eds.; Springer: Berlin/Heidelberg, Germany, 2025; pp. 509–523.
105. Cortés, A.J.; Castillejo, M.Á.; Yockteng, R. 'Omics' Approaches for Crop Improvement. *Agronomy* **2023**, *13*, 1401. [CrossRef]
106. Cortés, A.J.; López-Hernández, F. Harnessing Crop Wild Diversity for Climate Change Adaptation. *Genes* **2021**, *12*, 783. [CrossRef] [PubMed]
107. Cortés, A.J.; López-Hernández, F.; Osorio-Rodriguez, D. Predicting thermal adaptation by looking into populations' genomic past. *Front. Genet.* **2020**, *11*, 564515. [CrossRef] [PubMed]
108. Cortés, A.J.; Restrepo-Montoya, M.; Bedoya-Canas, L.E. Modern Strategies to Assess and Breed Forest Tree Adaptation to Changing Climate. *Front. Plant Sci.* **2020**, *11*, 583323. [CrossRef]
109. Valladares, F.; Matesanz, S.; Guilhaumon, F.; Araujo, M.B.; Balaguer, L.; Benito-Garzon, M.; Cornwell, W.; Gianoli, E.; van Kleunen, M.; Naya, D.E.; et al. The effects of phenotypic plasticity and local adaptation on forecasts of species range shifts under climate change. *Ecol. Lett.* **2014**, *17*, 1351–1364. [CrossRef]
110. Valladares, F.; Niinemets, U. Shade Tolerance, a Key Plant Feature of Complex Nature and Consequences. *Annu. Rev. Ecol. Evol. Syst.* **2008**, *39*, 237–257. [CrossRef]
111. Arenas, S.; Cortés, A.J.; Jaramillo-Correa, J.P. Toward a Genomic-Enabled Selection in Natural Tree Populations for Long-Term Management and Conservation. In *Genomics Based Approaches for Tropical Tree Improvement and Conservation*; Springer: Singapore, 2025; pp. 243–278.
112. Arenas, S.; Djabali, Y.; Rincent, R.; Cubry, P.; Martin, M.L.; Blein-Nicolas, M.; Laplaze, L.; Schneider, H.; Grondin, A. Modeling plant phenotypic plasticity and its underlying genetic architecture: A comparative study. *J. Exp. Bot.* **2025**, *76*, 2239–2251. [CrossRef]
113. Arenas, S.; Cortés, A.J.; Mastretta-Yanes, A.; Jaramillo-Correa, J.P. Evaluating the accuracy of genomic prediction for the management and conservation of relictual natural tree populations. *Tree Genet. Genomes* **2021**, *17*, 12. [CrossRef]
114. Valladares, F.; Sanchez-Gomez, D.; Zavala, M.A. Quantitative estimation of phenotypic plasticity: Bridging the gap between the evolutionary concept and its ecological applications. *J. Ecol.* **2006**, *94*, 1103–1116. [CrossRef]
115. Alvarez, J.A.; Cortizo, S.C.; Gyenge, J.E. Yield stability and phenotypic plasticity of *Populus* spp. clones growing in environmental gradients: I-yield stability under field conditions. *For. Ecol. Manag.* **2020**, *463*, 117995. [CrossRef]
116. Kusmec, A.; Srinivasan, S.; Nettleton, D.; Schnable, P.S. Distinct genetic architectures for phenotype means and plasticities in Zea mays. *Nat. Plants* **2017**, *3*, 715–723. [CrossRef]

117. Finlay, K.W.; Wilkinson, G.N. The analysis of adaptation in a plant-breeding programme. *Aust. J. Agric. Res.* **1963**, *14*, 742–754. [CrossRef]
118. Djabali, Y.; Rincent, R.; Martin, M.L.; Blein-Nicolas, M. Plasticity QTLs specifically contribute to the genotype × water availability interaction in maize. *Theor. Appl. Genet.* **2023**, *136*, 228. [CrossRef]
119. Maurer, A.; Draba, V.; Jiang, Y.; Schnaithmann, F.; Sharma, R.; Schumann, E.; Kilian, B.; Reif, J.C.; Pillen, K. Modelling the genetic architecture of flowering time control in barley through nested association mapping. *BMC Genom.* **2015**, *16*, 290. [CrossRef]
120. Comadran, J.; Kilian, B.; Russell, J.; Ramsay, L.; Stein, N.; Ganal, M.; Shaw, P.; Bayer, M.; Thomas, W.; Marshall, D.; et al. Natural variation in a homolog of *Antirrhinum CENTRORADIALIS* contributed to spring growth habit and environmental adaptation in cultivated barley. *Nat. Genet.* **2012**, *44*, 1388–1392. [CrossRef]
121. R Core Team. *R: A Language and Environment for Statistical Computing*; R Foundation for Statistical Computing: Vienna, Austria, 2024. Available online: https://www.R-project.org/ (accessed on 1 January 2026).
122. Wickham, H. *ggplot2: Elegant Graphics for Data Analysis*; Springer: New York, NY, USA, 2016. [CrossRef]
123. Endelman, J.B. Ridge regression and other kernels for genomic selection with R package rrBLUP. *Plant Genome* **2011**, *4*, 250–255. [CrossRef]
124. Tang, Y.; Liu, X.; Wang, J.; Li, M.; Wang, Q.; Tian, F.; Su, Z.; Zhang, Z. GAPIT Version 2: An enhanced integrated tool for genomic association and prediction. *Plant Genome* **2016**, *9*, plantgenome2015.11.0120. [CrossRef]

Disclaimer/Publisher's Note: The statements, opinions and data contained in all publications are solely those of the individual author(s) and contributor(s) and not of MDPI and/or the editor(s). MDPI and/or the editor(s) disclaim responsibility for any injury to people or property resulting from any ideas, methods, instructions or products referred to in the content.

International Journal of
Molecular Sciences

MDPI

Article

Research on Cold Resistance of *Kandelia obovata* Transplanted to Zhoushan Area at the mRNA Level

Haozhe Li [1,2,3], Zhibin Sun [2,3,*], Weiye Li [4], Xiaolong Yin [4], Xian Xu [4], Xiaolin Zhang [1], Xiaojun Yan [1], Xinan Wang [2,3], Yuanyuan Li [5] and Aijun Ma [2,3,*]

1 Laboratory of Marine Biology Protein Engineering, Marine Science and Technical College, Zhejiang Ocean University, Zhoushan 316022, China; lihaozhe0601@163.com (H.L.); zhangxiaolin@zjou.edu.cn (X.Z.); yanxj@zjou.edu.cn (X.Y.)
2 State Key Laboratory of Mariculture Biobreeding and Sustainable Goods, Qingdao Key Laboratory for Marine Fish Breeding and Biotechnology, Yellow Sea Fisheries Research Institute, Chinese Academy of Fishery Sciences, China-ASEAN Belt and Road Joint Laboratory on Mariculture Technology (Qingdao), Qingdao 266071, China; wangxa@ysfri.ac.cn
3 Laboratory for Marine Biology and Biotechnology, Qingdao Marine Science and Technology Center, Qingdao 266237, China
4 Zhoushan Fisheries Research Institute, Zhoushan 316000, China; liweiye2000@126.com (W.L.); xlyhndx@163.com (X.Y.); 17805806502@163.com (X.X.)
5 CAS Center for Excellence in Molecular Plant Sciences, Chinese Academy of Sciences, Shanghai 200032, China; yyli@cemps.ac.cn
* Correspondence: sunzb@ysfri.ac.cn (Z.S.); maaj@ysfri.ac.cn (A.M.)

Abstract

To elucidate the physiological and molecular mechanisms underlying cold tolerance in the mangrove species *Kandelia obovata* Sheue & al, this study measured the antioxidant enzyme activities and photosynthetic pigment contents of two populations—cold-tolerant and -sensitive—under natural overwintering conditions. In addition, transcriptome sequencing was performed to analyze differentially expressed genes (DEGs), transcription factor families, single nucleotide polymorphisms (SNPs), and alternative splicing events. The results showed that catalase activity was significantly elevated in the cold-tolerant population, which enhanced the efficiency of hydrogen peroxide scavenging. In contrast, although the superoxide dismutase activity was relatively high in the cold-sensitive population, its downstream scavenging capacity was insufficient, resulting in an overall lower antioxidant efficiency. The KEGG enrichment analysis indicated that pathways such as phenylpropanoid biosynthesis, amino sugar metabolism, and plant hormone signal transduction might be involved in the response to low-temperature stress. Further analysis revealed that transcription factors such as WRKY, NAC, MYB, and ERF were differentially expressed at significant levels in the cold-tolerant population, suggesting that they may play important roles in low-temperature adaptation. In addition, the diversity of SNPs and alternative splicing events may enhance protein function and contribute to improved cold tolerance. In summary, the cold-tolerant *K. obovata* population achieves low-temperature tolerance through multiple mechanisms, including antioxidant defense, metabolic regulation, and transcriptional as well as post-transcriptional regulation. This study provides a theoretical basis for elucidating the molecular foundations of cold tolerance in *K. obovata*.

Keywords: *Kandelia obovata*; low-temperature stress; physiological mechanisms; transcriptome; SNP

1. Introduction

Mangroves, tropical or subtropical intertidal plants, are primarily distributed along coastal shallows or estuarine mudflats at the interface between land and sea, forming evergreen woody plant communities dominated by mangrove species [1]. In China, mangroves are mainly found along the southern coastal provinces, including Hainan, Guangdong, Guangxi, Fujian, and Zhejiang [2], exhibiting characteristics of both terrestrial and marine plant communities. Mangrove species are light-demanding [3], salt- and alkali-tolerant [4,5], but sensitive to low temperatures [6]. They can purify water [7], filter organic matter and pollutants, promote sediment deposition [8], and play important roles in coastal protection as well as in resisting tides and wave action [9]. Mangroves also play a critical role in ecosystems, earning the reputation of "coastal guardians and green lungs of the ocean." They provide important habitats for rare and endangered waterfowl, as well as breeding grounds for fish, shrimp, crabs, and shellfish [10], offering both significant economic value and ecological benefits.

Kandelia obovata, of the family Rhizophoraceae, is the most widely distributed and cold-tolerant mangrove species in China, occurring at the highest latitudes among mangroves [11]. However, its distribution is still limited by low temperatures. It is excellent material for studies on high-latitude introduction and cultivation. However, due to global warming and anthropogenic disturbances [12], natural mangroves are facing the risk of decline or even disappearance [13]. Temperature can influence the distribution of temperature-sensitive plants such as *K. obovata* [14]. Extreme low-temperature events during winter in Zhejiang can cause frost damage to *K. obovata*, affecting its overwintering ability. Historical records indicate that multiple extreme cold wave events in southern China in 2008 had severe negative impacts on local mangroves [11]. Even more seriously, in 2010, an extremely low-temperature cold wave in the Ximen Island area of Wenzhou caused severe frost damage to introduced *K. obovata* plants, resulting in inhibited photosynthetic pigment synthesis, disrupted antioxidant systems, and ionic imbalances in trees of different ages [15]. Therefore, to achieve successful introduction of *K. obovata* in northern Zhejiang, it is particularly urgent and critical to investigate its cold tolerance.

Previous studies have examined the effects of low temperatures on photosynthesis and antioxidant enzyme activities in mangrove species such as *Bruguiera gymnorrhiza*, *K. obovata*, and *Rhizophora stylosa* [16]. The results indicate that severe low-temperature stress can significantly reduce leaf net photosynthetic rates and stomatal conductance in mangroves. Meanwhile, the activities of enzymes superoxide dismutase (SOD) and peroxidase (POD) decrease significantly, and malondialdehyde (MDA) content increases markedly. Under low-temperature stress, chlorophyll content in mangrove leaves also declines, thereby affecting normal photosynthetic processes. Current studies on *K. obovata* have focused on seedling propagation [17], carbon sequestration [18], and physiological mechanisms, with limited investigations into the molecular mechanisms underlying cold tolerance. High-throughput sequencing combined with physiological analyses can provide a better understanding of the cold tolerance mechanisms in *K. obovata*.

In this study, researchers conducted long-term observations of *K. obovata* seedlings in Zhoushan, Zhejiang Province, including propagation and introduction. Based on data analysis, post-winter individuals were broadly classified into two groups: those that survived the winter, designated as the cold-tolerant group, and those that died after winter, designated as the cold-sensitive group. Although both groups originated from the same batch of *K. obovata* seedlings, they may derive from different mother plants and possess genetic differences, which could lead to distinct cold tolerance during winter [19]. In the cold-tolerant group, leaves remained healthy and gradually recovered after winter, allowing the plants to survive; in contrast, individuals in the cold-sensitive group either

https://doi.org/10.3390/ijms27010429

withered and died directly or exhibited slight leaf yellowing and failed to recover from cold-induced damage, ultimately leading to death. In this study, leaves from both cold-tolerant and -sensitive *K. obovata* groups were selected for physiological measurements and transcriptome sequencing. By assessing differences in enzyme activities and photosynthetic pigment contents between individuals with distinct cold tolerance, we aimed to investigate the functional roles of enzymes critical in the cold response of *K. obovata*. At the same time, key differentially expressed genes (DEGs) were identified, and the metabolic pathways and transcription factor (TF) families they regulate were explored to uncover potential genetic differences. This study combines physiological assessments and transcriptome profiling of *K. obovata* under natural overwintering conditions. Comparative analyses of antioxidant enzyme activities and mRNA-level gene expression between cold-tolerant and -sensitive plants provide preliminary insights into the molecular mechanisms underlying cold resistance. Furthermore, the exploration of potential SNPs and AS events may provide a theoretical foundation for the introduction of *K. obovata* to higher-latitude regions and for future selective breeding efforts.

2. Results

2.1. Comparison of the Survival Rate of Kandelia obovata After Overwintering

During the entire overwintering period, survival and mortality rates of *K. obovata* in Groups A and B were recorded and analyzed (Table 1). The cold-tolerant subgroup A1 had 1339 surviving individuals, comparable to the 1351 survivors in group B. The total number of deaths in group B was 1649, which was 74 higher than the total deaths in group A; these individuals likely died immediately during the cold wave and thus did not possess cold tolerance. Comparison of the survival rates between subgroup A1 and the entire group B demonstrates the feasibility of manually classifying *K. obovata* seedlings into cold-tolerant and -sensitive groups during the overwintering period.

Table 1. Survival rate of *K obovata* during natural overwintering.

Group	Number Planted (Plants)	Number Survived (Plants)	Survival Rate (%)	Number Dead (Plants)	Mortality Rate (%)
A1 (cold-tolerant)	1500	1339	89.3	161	10.7
A2 (cold-sensitive)	1500	86	5.72	1414	94.28
B (control)	3000	1351	45.03	1649	54.97

2.2. Physiological Differences Between K. obovata Populations Under Low-Temperature Stress After Overwintering

To verify the physiological differences between the cold-tolerant and -sensitive *K. obovata* populations in response to low-temperature stress, the photosynthetic pigments and antioxidant systems in their leaves were analyzed. No significant differences were observed in chlorophyll contents between the two groups (Table 2). The levels of chlorophyll a, chlorophyll b, and total chlorophyll were statistically comparable ($p > 0.05$), suggesting that photosynthetic pigments were not the main factors contributing to the difference in cold tolerance between the two populations during the early overwintering stage. However, significant differences were observed between the antioxidant systems of the two groups. The CAT activity in the cold-tolerant group was 14.72 ± 0.19 U/g, significantly higher than in the cold-sensitive group ($p < 0.05$). As a key enzyme responsible for removal of hydrogen peroxide (H_2O_2), the higher activity of CAT indicates that the cold-tolerant population possesses a stronger reactive oxygen species (ROS) scavenging capacity under low-temperature stress, thereby reducing lipid peroxidation damage to cell membranes. In contrast, the SOD activity in the cold-sensitive group was 1435.10 ± 23.89 U/g, signifi-

https://doi.org/10.3390/ijms27010429

cantly higher than in the cold-tolerant group ($p < 0.05$), indicating a stronger capacity for scavenging superoxide anions (O_2^-). This difference may be associated with an immature cold-resistance mechanism in the cold-sensitive population, which tends to rely more on the early-stage removal of ROS but lacks an efficient pathway for subsequent of H_2O_2 decomposition. The POD activity was non-significantly lower in the cold-tolerant than the cold-sensitive group. Similarly, the MDA content was higher in the cold-sensitive group but showed no significant difference between the two populations. These results suggest that the degree of lipid peroxidation and certain antioxidant pathways did not differ substantially between the groups.

Table 2. Enzyme activities in different experimental groups.

Detection Type	Cold-Tolerant Group	Cold-Sensitive Group
Chlorophyll a (mg/g)	0.28 ± 0.05^{a}	0.32 ± 0.02^{a}
Chlorophyll b (mg/g)	0.68 ± 0.09^{a}	0.70 ± 0.03^{a}
Total chlorophyll content (mg/g)	0.96 ± 0.06^{a}	1.01 ± 0.01^{a}
CAT (U/g)	14.72 ± 0.19^{a}	4.01 ± 0.89^{b}
SOD (U/g)	1213.76 ± 66.24^{a}	1435.10 ± 23.89^{b}
POD (U/g)	52.63 ± 6.11^{a}	61.89 ± 0.97^{a}
MDA (nmol/g)	18.40 ± 0.83^{a}	19.37 ± 0.81^{a}

Note: different superscript letters in the same row indicate significant differences ($p < 0.05$).

2.3. Quality Control Analysis of Raw Sequencing Data

Transcriptome sequencing was performed on a total of six samples, including both the experimental and control groups, generating 42.02 Gb of raw data. After removing low-quality reads and adapter sequences, the range of clean reads per sample was 42,780,366–50,516,336 (Table 3), with an error rate of approximately 0.01%. The Q20 values all exceeded 98.9%, Q30 values exceeded 96.45%, and the GC content was 45.45–45.93%. The clean reads of each sample were aligned to the *K. obovata* reference genome (version: GWHACBH00000000.1; source: https://ngdc.cncb.ac.cn/gwh/Assembly/20708/show (accessed on 4 December 2025)), and the mapping results are summarized in Table 4. The range of the total mapping rate was 97.79–98.12%, of the multiple-mapped rate was 3.16–3.96%, and of the uniquely mapped rate was 93.83–94.97%. These results indicate that the transcriptome sequencing data are of high quality and reliable for subsequent analyses.

Table 3. Quality assessment of transcriptome sequencing data.

Sample	Clean Reads	Clean Bases	Error Rate (%)	Q20 (%)	Q30 (%)	GC Content (%)
AL1	42,780,366	6,437,354,464	0.0118	98.90	96.45	45.93
AL2	46,537,646	6,992,527,814	0.0117	98.96	96.63	45.71
AL3	49,719,668	7,469,910,026	0.0116	99.00	96.77	45.84
BL1	44,857,924	6,742,092,163	0.0116	98.98	96.73	45.45
BL2	50,516,336	7,585,021,404	0.0115	99.02	96.86	45.60
BL3	45,178,010	6,789,571,579	0.0116	98.99	96.74	45.64

Table 4. Mapping statistics of transcriptome sequencing reads to the reference genome.

Sample	Clean Reads	Total Mapped (%)	Multiple Mapped (%)	Uniquely Mapped (%)
AL1	42,780,366	97.95	3.39	94.56
AL2	46,537,646	97.89	3.67	94.22
AL3	49,719,668	97.88	3.73	94.15
BL1	44,857,924	97.79	3.96	93.83
BL2	50,516,336	97.93	3.39	94.54
BL3	45,178,010	98.12	3.16	94.97

2.4. Differential Gene Expression Analysis

A total of 19,197 expressed genes were detected: 17,264 known and 1933 novel genes. Principal component analysis (PCA) of the six samples from the cold-tolerant and -sensitive groups (Figure 1) clustered the three samples from the cold-tolerant group together, whereas the cold-sensitive samples displayed a more dispersed pattern. This may be because all samples originated from the same batch of naturally overwintered plants, and leaf selection did not specifically target visibly green or nearly senescent leaves. Since the cold stress response is not equivalent to senescence, PCA cannot perfectly separate the two groups. Nevertheless, this does not compromise the reliability of the results.

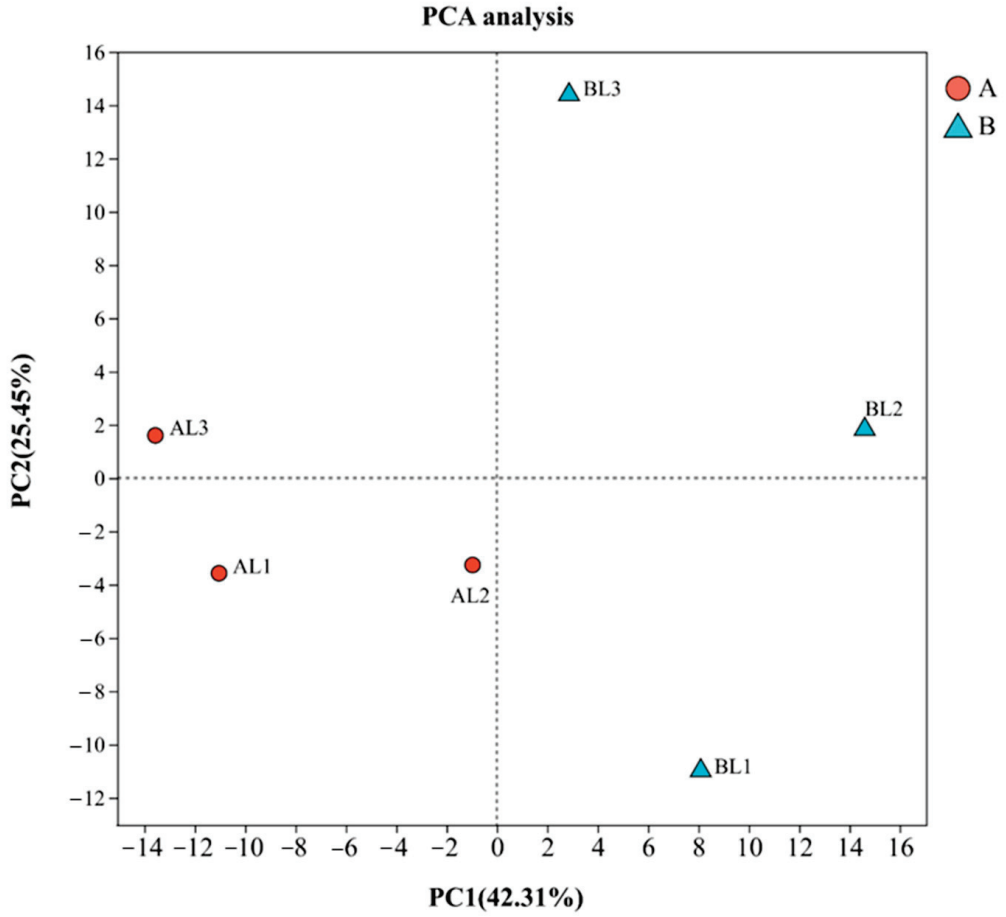


Figure 1. PCA of samples. PCA was performed on normalized expression data to evaluate the overall similarity and differences among samples from groups A and B. Each point represents a biological replicate ($n = 3$).

Based on the quantified gene expression levels, DEG analysis between the two groups was performed using DESeq2. Genes with $|\log2 \text{ fold change (FC)}| \geq 1$ and p-value < 0.05 were considered to be DEGs. The volcano plot (Figure 2) showed a total of 246 identified DEGs, including 224 significantly downregulated and 22 significantly upregulated genes.

2.5. GO and KEGG Annotation and Enrichment Analysis of Differentially Expressed Genes

The purpose of Gene Ontology (GO) annotation is to classify the functions of target genes or transcripts. Using the GO database, genes and their products are functionally categorized. Results of enrichment and annotation analysis of the DEGs are shown in Figure 3, with the y-axis representing the second-level GO terms, the x-axis indicating the number of genes mapped to each term, and the colors denoting the three main GO categories. At the second-level classification, the DEGs were mainly annotated to cellu-

https://doi.org/10.3390/ijms27010429

lar anatomical entity, catalytic activity, cellular process, binding, and metabolic process (Figure 3A). At the third-level classification, DEGs were predominantly associated with intrinsic component of membrane, organic substance metabolic process, and ion binding (Figure 3B). At the fourth-level classification, DEGs were mainly annotated to integral component of membrane, cation binding, and intracellular organelle (Figure 3C).

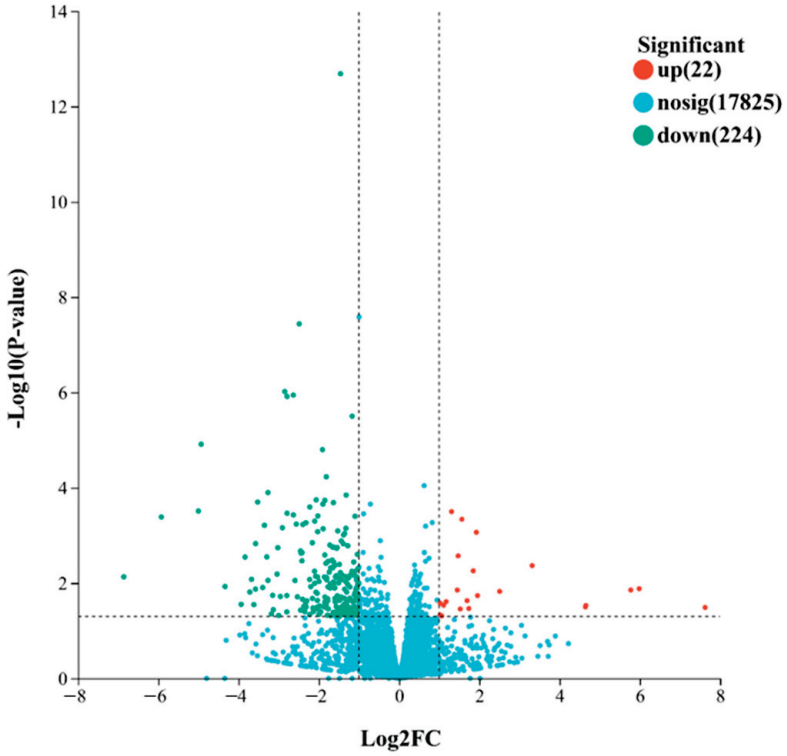


Figure 2. Volcano plot of DEGs between groups A and B. DEGs were defined as genes with $|\log_2$ fold change$| \geq 1$ and adjusted p-value < 0.05. Dashed lines indicate thresholds for statistical significance and fold change: the horizontal dashed line corresponds to Padjust = 0.05, and the vertical dashed lines correspond to log2 fold change = ± 1. Upregulated and downregulated genes are indicated in red and cyan, respectively.

The GO enrichment analysis of the DEGs was performed using GOATOOLS, and significance was assessed with Fisher's exact test. The GO terms with Padjust < 0.05 were considered significantly enriched. In Figure 3D, the y-axis represents the GO terms, while the x-axis indicates the Rich Factor, defined as the ratio of the number of DEGs mapped to a GO term to the total number of annotated genes. A higher Rich Factor indicates greater enrichment. The size of the bubbles corresponds to the number of DEGs in each GO term, and the color represents different Padjust ranges. The most significantly enriched terms included xyloglucan metabolic process, apoplast, and iron ion binding, while terms with the largest number of DEGs include oxidoreductase activity and extracellular region (Figure 3D).

Using the KEGG database, DEGs were classified according to the pathways they participate in or the functions they perform. The DEGs were mainly annotated to pathways related to metabolism and plant hormone signal transduction (Figure 4 and Table 5). In terms of gene number, the highest enrichment was in phenylpropanoid biosynthesis, followed by plant hormone signal transduction, and then amino sugar and nucleotide sugar metabolism. Regarding significance, DEGs in *K. obovata* leaves under low-temperature stress were most significantly enriched in phenylpropanoid biosynthesis, followed by amino sugar and nucleotide sugar metabolism, with plant hormone signal transduction ranking third.

https://doi.org/10.3390/ijms27010429

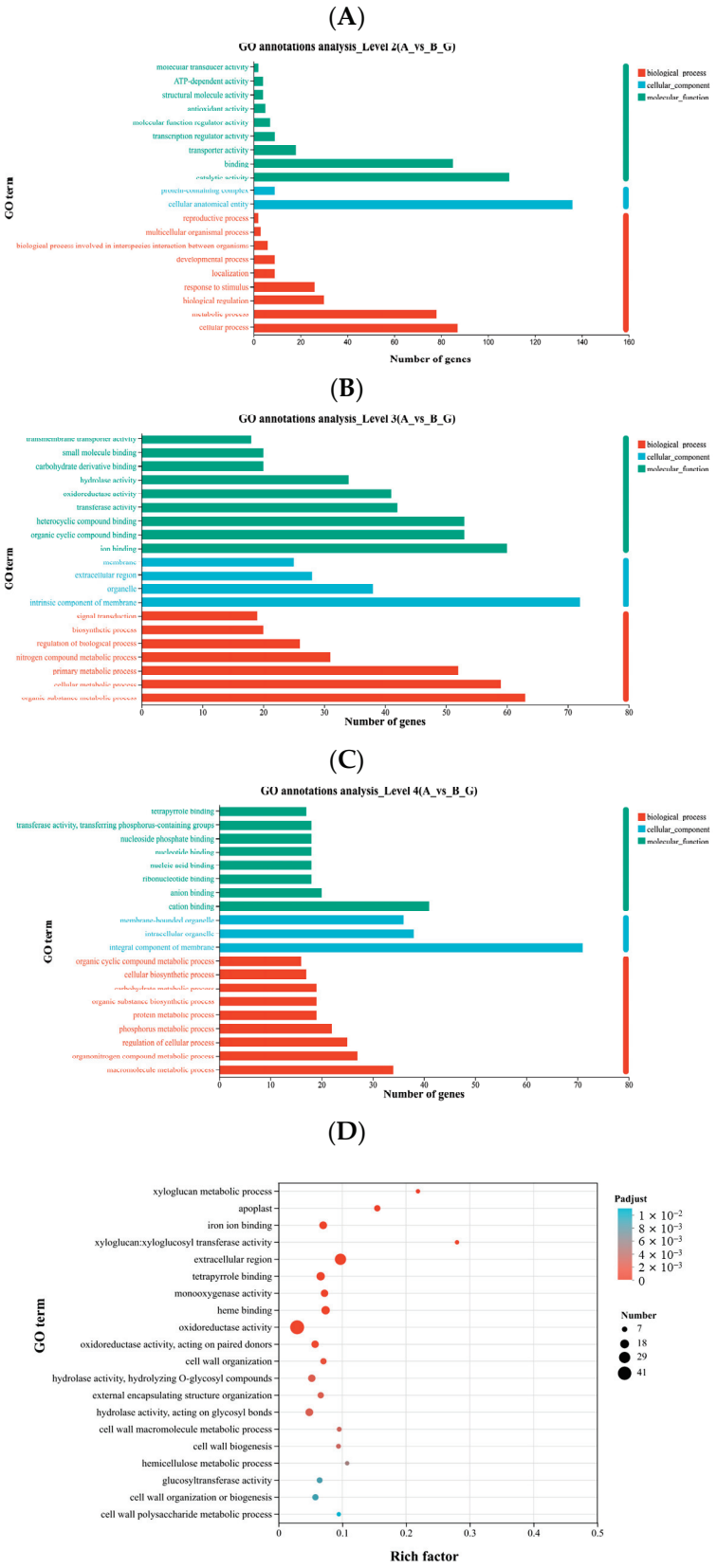


Figure 3. GO term annotation of DEGs between groups A and B at levels (**A**) 2, (**B**) 3 and (**C**) 4; (**D**) GO enrichment analysis of DEGs. Panels (**A**–**C**) show GO annotation: the y-axis represents GO terms, and the x-axis indicates the number of genes mapped to each term. Colors distinguish different gene sets. Panel (**D**) shows GO enrichment results. GO terms with an adjusted Padjust < 0.05 are considered significantly enriched. Bubble size represents the number of genes in each term, and color indicates the enrichment significance.

https://doi.org/10.3390/ijms27010429

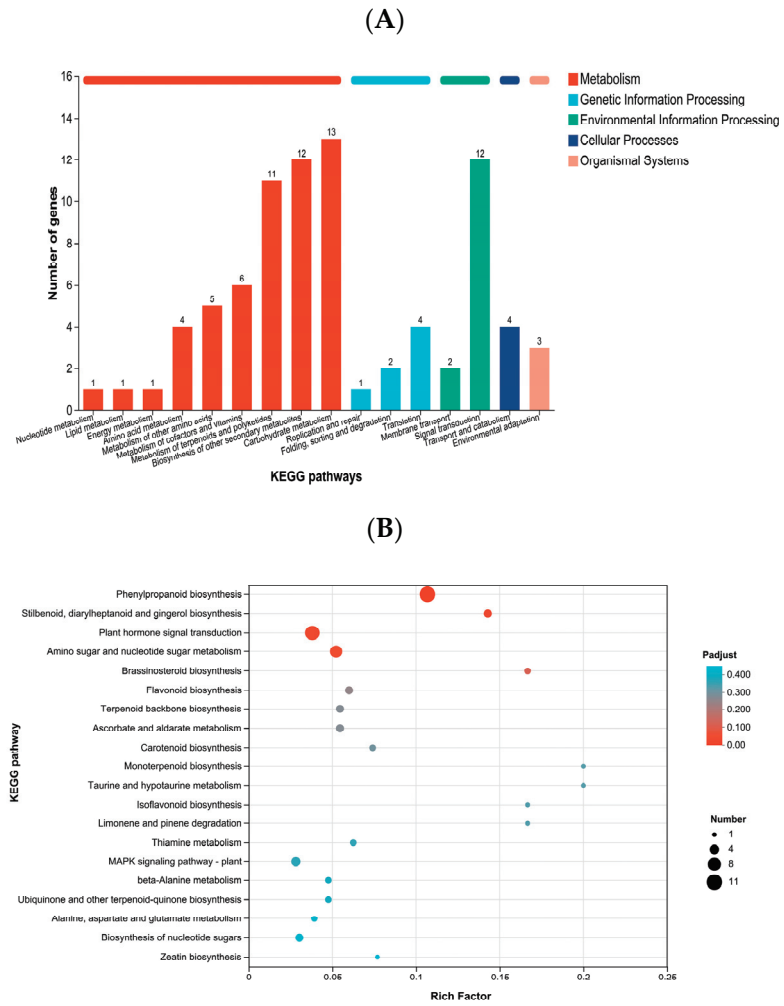


Figure 4. (**A**) KEGG annotation of DEGs and (**B**) KEGG enrichment analysis of DEGs between groups A and B. Panel (**A**) shows KEGG pathway annotation, with the x-axis representing pathway names and the y-axis indicating the number of genes mapped to each pathway. Panel (**B**) shows KEGG enrichment results, with pathways having an adjusted Padjust < 0.05 considered significantly enriched. Bubble size represents the number of genes in each pathway, and color indicates enrichment significance.

Table 5. Top five KEGG pathways with significant enrichment in DEGs of *K. obovata*.

KEGG Pathway	Pathway ID	Number of DEGs	*p*-Value	Padjust	First Category	Second Category
Phenylpropanoid biosynthesis	map00940	11	5.98×10^{-8}	3.23×10^{-6}	Metabolism	Biosynthesis of other secondary metabolites
Amino sugar and nucleotide sugar metabolism	map00520	7	1.50×10^{-3}	0.0404	Metabolism	Carbohydrate metabolism
Plant hormone signal transduction	map04075	10	1.76×10^{-3}	0.0317	Environmental Information Processing	Signal transduction
Stilbenoid, diarylheptanoid and gingerol biosynthesis	map00945	3	2.21×10^{-3}	0.0299	Metabolism	Biosynthesis of other secondary metabolites
Brassinosteroid biosynthesis	map00905	2	9.62×10^{-3}	0.104	Metabolism	Metabolism of terpenoids and polyketides

2.6. Transcription Factor Prediction and qRT-PCR Validation

A total of 38,624 transcripts were detected in the transcriptome sequencing: 16,018 known and 22,606 novel transcripts. Prediction of TFs, using the Plant Transcription Factor Database (PlantTFDB), revealed that 2519 genes encode putative TFs, which were annotated into 1314 TFs belonging to 47 TF families (Figure 5). The 10 TF families with the largest number of genes were MYB-related, MYB, bHLH, ERF, HB-other, NAC, WRKY, bZIP, B3, and GRAS. Among these, the first eight families have been reported to play important roles in plant cold tolerance.

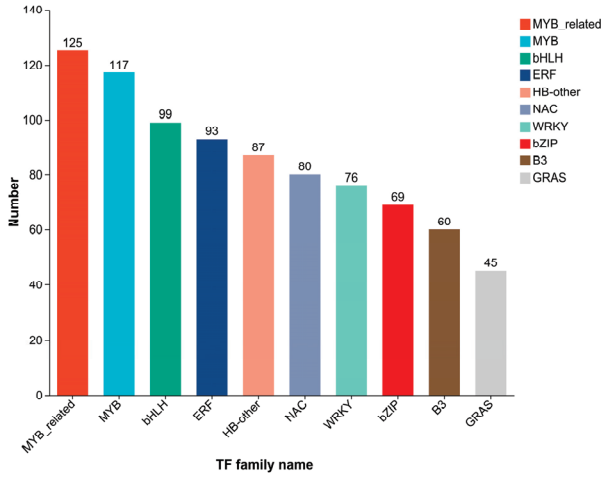


Figure 5. Distribution of transcription factor families in the samples. The y-axis represents the number of genes, and the x-axis indicates different TF families. Different colors are used to distinguish different TF families.

Based on the DEGs identified in the volcano plot (Figure 2), a total of 246 genes were differentially expressed between the cold-tolerant and -sensitive groups. Among them, 20 DEGs belong to 10 different TF families (Figure 6), with MYB, WRKY, ERF, NAC, and MYB-related previously demonstrated to be associated with cold tolerance.

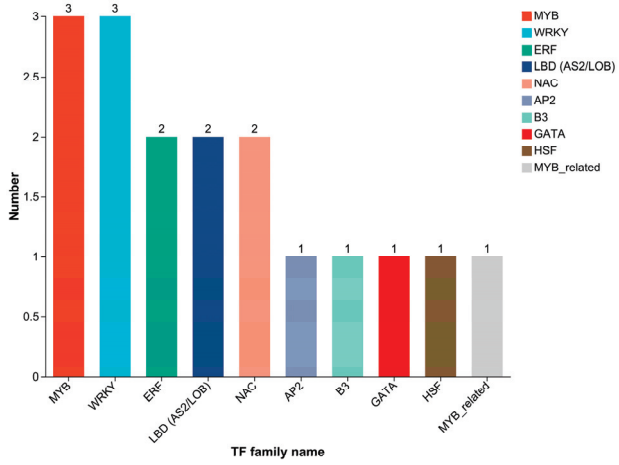


Figure 6. Distribution of transcription factor families among DEGs between groups A and B. The y-axis represents the number of genes, and the x-axis indicates different TF families. Different colors are used to distinguish different TF families.

To validate the reliability of the transcriptome data, seven DEGs (*geneMaker00014971*, *geneMaker00007720*, *geneMaker00006849*, *geneMaker00008016*, *geneMaker00000397*, *geneMaker00004010*, and *geneMaker00008573)* were randomly selected for qRT-PCR verification: three upregulated and four downregulated genes. The relative expression patterns of these

genes were consistent with the transcriptome sequencing results (Figure 7), indicating that the transcriptome data generated in this study are accurate and reliable.

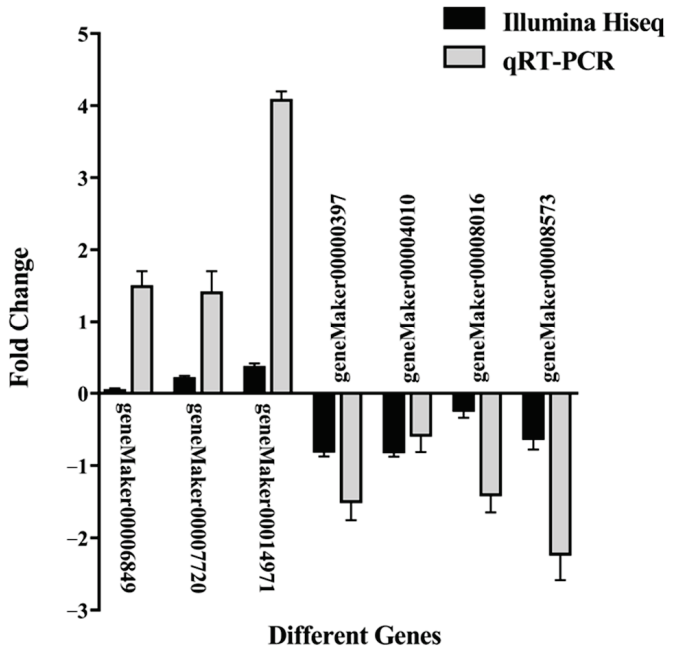


Figure 7. qRT-PCR validation of relative expression of selected DEGs between groups A and B. The x-axis represents different genes, and the y-axis shows log2 fold change, allowing negative values to indicate downregulation. For each gene, two bars are shown: black one for RNA-seq and gray one for qRT-PCR. Bar heights represent the mean of three biological replicates, and error bars indicate ± standard deviation (SD).

2.7. Alternative Splicing and SNP Analysis

From the transcriptome sequencing results of the cold-tolerant and -sensitive groups, five types of differential alternative splicing (AS) events were identified (Figure 8). Among them, skipped exon (SE) was the most prevalent, with a total of 385 events, accounting for 50.79%, followed by alternative 5′ splice site (A5SS, 17.15%), alternative 3′ splice site (A3SS, 17.02%), and retained intron (RI, 10.42%), while mutually exclusive exons (MXE) were the least frequent, representing only 4.62%. The SE was the most significant AS pattern in terms of differential expression, comprising 172 significant exclusion events and 213 significant inclusion events (Figure 9). The A5SS and A3SS events also exhibited inclusion/exclusion differences between the two groups, whereas the numbers of RI and MXE events were comparatively lower.

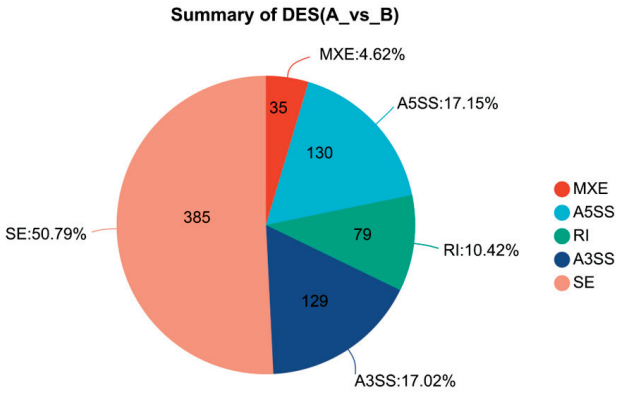


Figure 8. Distribution of AS events between groups A and B. The pie chart shows the proportions of five AS types: SE, MXE, A5SS, RI, and A3SS.

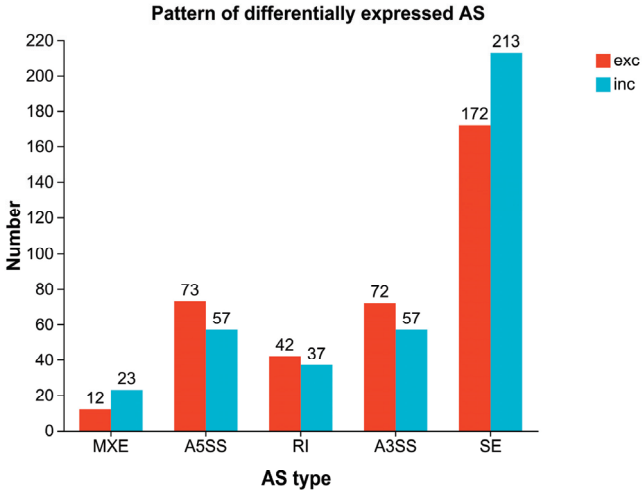


Figure 9. Differential AS patterns between cold-tolerant and -sensitive groups. Comparison of alternative splicing events between groups A and B. The bar chart shows the number of five AS event types (SE, MXE, A5SS, RI, and A3SS) in each group. For each AS type, two bars are shown: red one for exon exclusion (exc) and blue one for inclusion (inc).

Single nucleotide polymorphisms (SNPs) refer to variations at a single nucleotide position in a DNA sequence, including transitions and transversions. In this study, transcriptome sequencing was performed on three samples each from the cold-tolerant and -sensitive *K. obovata* groups to analyze gene expression differences. The sequencing results were aligned to the reference genome, and are presented in Figure 10 and Table 6. The SNP type distribution patterns were largely consistent between the cold-tolerant and -sensitive groups. A total of 11,495–12,982 SNP sites were identified. The number of transition mutations (Ti; A/G, C/T, G/A, and T/C) was significantly higher than that of transversion mutations (Tv; A/C, G/C, C/A, A/T, C/G, G/T, T/A, and T/G), with Ti/Tv ratios ranging within 1.24–1.30. Further comparison showed that C/T and G/A transitions were the most abundant, with each sample containing over 1800–2000 sites, whereas transversions were less frequent, with range 428–971. Overall, the total number of SNPs was slightly higher in the cold-tolerant than the cold-sensitive group.

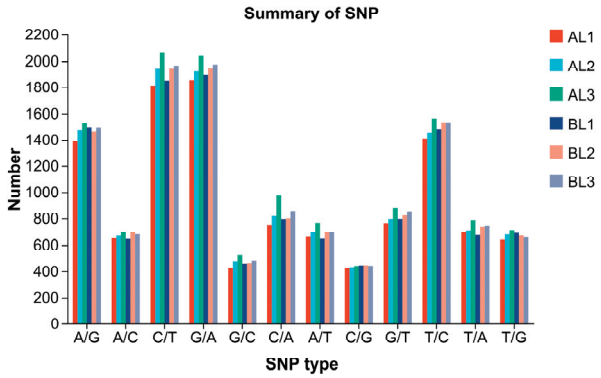


Figure 10. Distribution of single nucleotide polymorphism types in *K. obovata* samples from groups A and B. The x-axis represents SNP types and the y-axis represents the number of SNPs. SNPs are categorized as transitions (A↔G, C↔T) or transversions (A↔C, A↔T, G↔C, G↔T).

By comparing the SNP sites between the cold-tolerant and -sensitive groups, a total of 35 genes with significant SNP differences were identified. Integrating the transcriptome expression data revealed significant differences in KEGG metabolic pathways for *geneMaker00005577* and *geneMaker00013925*. The former is primarily involved in Phenylpropanoid biosynthesis, flavonoid biosynthesis, and stilbenoid, diarylheptanoid and gin-

gerol biosynthesis, catalyzing the conversion of caffeoyl-CoA to feruloyl-CoA, representing a key node for lignin, flavonoid, and gingerol synthesis. This gene harbors a G → A mutation in the 5′ UTR and is significantly downregulated. The latter is mainly involved in the Monoterpenoid biosynthesis pathway, catalyzing the reversible conversion between menthone and neomenthol. This gene carries a nonsynonymous mutation in the exon region, causing the amino acid property to change from hydrophobic to polar, and is also downregulated. The mutations and altered expression of these two genes may reduce the flux of defense-related metabolic pathways, thereby affect the synthesis of antioxidants and signal molecules and regulate the physiological and metabolic adaptation of *K. obovata* under low-temperature stress.

Table 6. Summary of single nucleotide polymorphism types across experimental samples.

Type		AL1	AL2	AL3	BL1	BL2	BL3
Transition (Ti)	A/G	1388	1474	1529	1493	1464	1492
	C/T	1814	1936	2060	1852	1936	1967
	G/A	1856	1919	2038	1892	1937	1974
	T/C	1411	1454	1563	1480	1534	1534
Total		6469	6783	7189	6717	6871	6967
Transversion (Tv)	A/C	650	667	703	645	694	678
	G/C	429	479	525	460	464	482
	C/A	754	818	971	794	800	862
	A/T	661	694	766	646	700	700
	C/G	428	432	442	447	448	443
	G/T	764	795	885	795	823	859
	T/A	700	713	785	672	741	748
	T/G	640	677	715	689	668	657
Total		5026	5275	5793	5148	5338	5429
Ti/Tv		1.29	1.29	1.24	1.30	1.29	1.28
Total		11,495	12,058	12,982	11,865	12,209	12,396

3. Discussion

3.1. Physiological Differences Between Groups

When plants are exposed to low-temperature conditions, membrane lipid fluidity and metabolic rates decrease, leading to impaired electron transport and excessive production of ROS, including O_2^-, H_2O_2, and hydroxyl radical (·OH). The accumulation of ROS can damage membrane lipids, proteins, and pigments, resulting in the formation of the lipid peroxidation product MDA. Simultaneously, the photosynthetic system is compromised, chloroplast membrane structures are disrupted, and chlorophyll degradation occurs. Under low-temperature stress, mangrove plants maintain photosynthesis through photosynthetic pigments [20] and simultaneously rely on the antioxidant enzyme system to scavenge ROS, thereby coping with environmental stress [21]. Chlorophyll a and chlorophyll b are the primary pigments in photosynthesis, and are directly involved in light absorption and electron transport, while total chlorophyll content provides an overall measure of the photosynthetic pigment level.

The results of this study showed no significant differences between the two groups of *K. obovata* in chlorophyll a, chlorophyll b, or total chlorophyll content ($p > 0.05$). This is mainly related to the sampling criteria of the experiment: the cold-tolerant and -sensitive groups exhibited only minor differences in leaf status at the early stage. After overwintering, as ambient temperatures gradually increased, the cold-tolerant *K. obovata* plants progressively resumed growth, whereas the cold-sensitive group failed to recover due to severe damage. Consequently, the physiological differences between the two groups

https://doi.org/10.3390/ijms27010429

increased over time. This divergence may not only result from differential responses to low temperature stress, but also reflect differences in survival status. Therefore, sampling was conducted during the early recovery stage after overwintering in this study.

Under low-temperature stress, plants rapidly activate the antioxidant defense system to scavenge ROS through various enzymatic reactions [22] (Figure 11). The first antioxidant enzyme to act within the ROS scavenging system is SOD, catalyzing the dismutation of O_2^- into H_2O_2 thereby reducing oxidative damage to cells [23]. Enzyme CAT is key in removing H_2O_2 and preventing its accumulation from damaging cell membranes. Previous studies have shown that CAT activity in mangroves increases under cold conditions [14], which facilitates H_2O_2 scavenging and helps maintain membrane stability. Another important enzyme in the plant antioxidant system is POD, capable of eliminating excess ROS, and plays a crucial role in maintaining normal physiological functions and enhancing tolerance to low-temperature stress [21]. The final product of membrane lipid peroxidation, MDA, reflects the extent of cellular membrane damage and serves as an important indicator of plant cold tolerance [24]. The accumulation of MDA in plants is closely correlated with their cold tolerance: higher MDA levels indicate more severe oxidative damage to cell membranes and, consequently, lower cold tolerance [25].

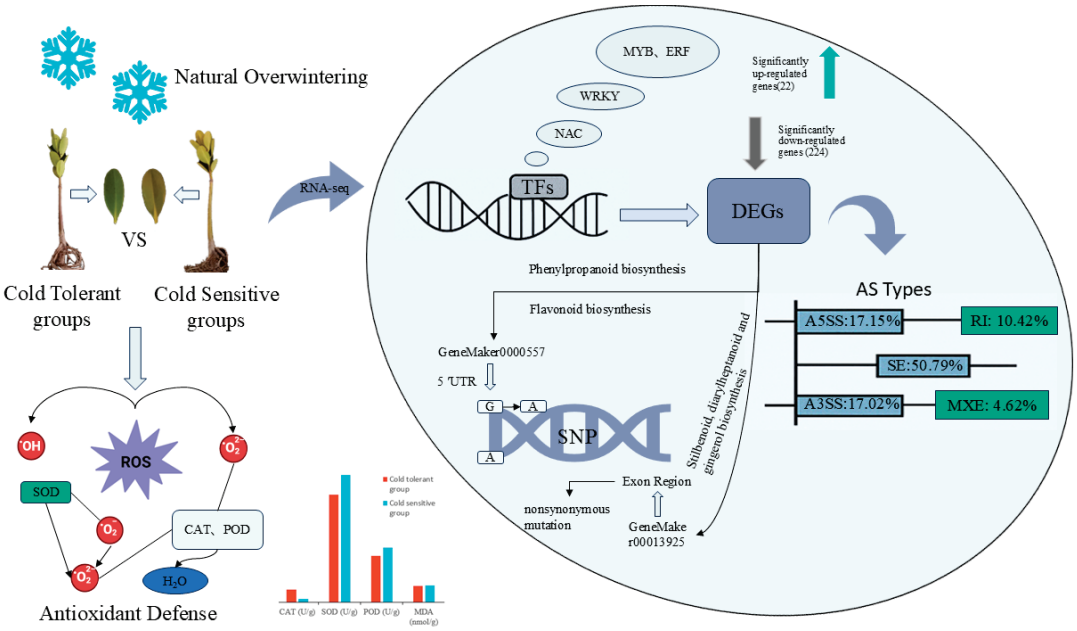


Figure 11. Proposed antioxidant and transcriptional regulatory mechanisms of *K. obovata* under natural overwintering conditions. The model integrates all data from this study, including sample information, measured enzyme activities and antioxidant defense indicators, and transcriptomic data such as TFs, DEGs, AS, and SNPs. Specific data sources are detailed in the Results and Discussion sections.

The results of this study indicate that during the initial phase of antioxidant defense, SOD activity was significantly higher in the cold-sensitive than the cold-tolerant group, suggesting that the cold-sensitive population primarily relies on early-stage O_2^- scavenging under low-temperature conditions, while downstream H_2O_2 decomposition may be insufficient, limiting overall antioxidant efficiency. These findings are consistent with previous studies [26]. During the adaptation phase to low-temperature stress, CAT activity was significantly higher in the cold-tolerant than the cold-sensitive group, indicating that the cold-tolerant group can decompose H_2O_2 more efficiently, thereby enhancing antioxidant defense under low temperatures. In contrast, POD activity did not differ significantly between the two groups ($p > 0.05$), possibly because this enzyme plays a limited role in the low-temperature response or functions more in a synergistic manner. Although MDA

content did not differ significantly between groups, the cold-tolerant group exhibited lower MDA levels, indirectly reflecting stronger leaf antioxidant capacity and higher cold tolerance, consistent with the above results.

In summary, cold-tolerant *K. obovata* populations may enhance overall antioxidant defense under low temperatures primarily by increasing CAT activity and thereby improving H_2O_2 scavenging capacity. In contrast, although SOD activity is higher in cold-sensitive populations, their downstream H_2O_2 decomposition may be insufficient, resulting in lower overall antioxidant efficiency and contributing to interpopulation differences in cold tolerance. Differences in POD activity and MDA content were not significant, possibly because certain antioxidant pathways and levels of lipid peroxidation contribute only minimally to the observed variation in cold tolerance between populations. Another possible reason for this non-significant difference was the relatively limited sample size (n = 3) inherent to the experimental design.

3.2. Differential Expression Between Groups

The DEGs in *K. obovata* leaves under low-temperature stress exhibited distinct distribution patterns across various levels of GO annotation (Figure 3A–C). The GO enrichment analysis (Padjust < 0.05) revealed that the most significantly enriched functions were xyloglucan metabolic process, apoplast, and iron ion binding, while the functions with the highest number of DEGs were oxidoreductase activity and extracellular region (Figure 3D). These findings suggest that *K. obovata* may maintain cellular structure by regulating cell wall polysaccharide metabolism [27], modulate stress signaling through extracellular region-associated genes, and regulate ROS and ion homeostasis via oxidoreductase and metal ion-binding genes.

The KEGG annotation results indicated that DEGs were primarily enriched in metabolic pathways and hormone signal transduction-related pathways (Figure 4A). Significance analysis revealed that the phenylpropanoid biosynthesis pathway was the most significantly enriched, followed by amino sugar and nucleotide sugar metabolism and plant hormone signal transduction (Figure 4B). Previous studies have shown that pathways such as phenylpropanoid and jasmonic acid biosynthesis [28] are more readily activated under severe stress. During stress, the activation of starch and sucrose metabolism, the TCA cycle, glycolysis, and the pentose phosphate pathway can provide carbon sources and ATP for the synthesis of amino acids such as phenylalanine, valine, and threonine, thereby maintaining normal metabolic processes [25], which is consistent with our findings.

The GO and KEGG analyses indicate that under low-temperature stress, *K. obovata* leaves employ a multilayered response mechanism involving membrane protection, regulation of cell wall metabolism, ROS scavenging, maintenance of ion homeostasis, and hormone signal transduction. The significant enrichment of xyloglucan and amino sugar metabolic pathways suggests that *K. obovata* may enhance membrane and wall stability by regulating cell wall polysaccharides, thereby maintaining cellular structure under low-temperature stress. Genes related to iron and cation binding indicate that ion homeostasis plays a role in signal transduction and defense mechanisms. Furthermore, the enrichment of phenylpropanoid biosynthesis and plant hormone signaling pathways implies that *K. obovata* may coordinate the expression of defense genes through secondary metabolite production and hormone regulation, enabling metabolic adjustment and cold tolerance under low-temperature conditions.

Overall, the molecular response of *K. obovata* under low-temperature stress exhibits a multilayered, coordinated regulation, in which structural maintenance, redox regulation, and signaling pathways act synergistically to enhance cold tolerance. These findings

provide a molecular basis for a deeper understanding of the low-temperature adaptation mechanisms in *K. obovata*.

3.3. Differential Transcription Factor Expression Between Groups

Gene expression regulation has a central role for TFs, and they participate in various physiological and biochemical processes and modulate plant responses to environmental stresses. In-depth investigation of TFs allows a more comprehensive understanding of the physiological responses and adaptive mechanisms employed by individual plants and their populations in response to environmental changes. Through transcriptome sequencing of annual *K. obovata* leaves, this study identified significant differences in gene expression between cold-tolerant and -sensitive groups. Such TFs as WRKY, NAC, MYB, bHLH, and ERF exhibited marked differential expression between the two groups, consistent with their established roles in plant cold tolerance [29]. Previous studies have shown that the TF WRKY40 can enhance cold tolerance in transgenic *Arabidopsis thaliana* [26]. The NAC family TFs have also been confirmed to participate in regulating plant low-temperature tolerance. For example, the *AmNAC11* gene from *Ammopiptanthus mongolicus* is induced by drought, cold, and high-salinity stress, and its expression in *Arabidopsis thaliana* via Agrobacterium-mediated transformation significantly improves tolerance to freezing and drought stress [30]. The bHLH TFs make a significant contribution to *K. obovata* cold tolerance, and the expression of *kobHLH* genes is associated with responses to cold stress [31]. Additionally, MYB [32] and ERF [33] TFs similarly promote physiological adaptation to low-temperature conditions by regulating the expression of cold-responsive genes.

The results of this study indicate that the high expression of certain TFs in the cold-tolerant *K. obovata* may activate a series of downstream defense responses, such as enhanced antioxidant enzyme activity and accumulation of osmolytes, thereby improving plant adaptation to cold environments (Figure 11). In the cold-sensitive group, reduced expression of these TFs may limit downstream defense responses, rendering the plants more susceptible to low-temperature stress. In summary, our transcriptome analysis and qRT-PCR validation demonstrates that differences in cold tolerance in *K. obovata* are closely associated with the expression of specific TF families, providing important insights into the molecular mechanisms underlying cold resistance.

3.4. Genetic Variation Between Groups

Both SNPs and AS play key roles in plant responses to abiotic stress, serving as important mechanisms for environmental adaptation and regulation of gene expression. Previous genome-wide association studies in rice have identified genes involved in responses to low-temperature stress and chilling accumulation, and screened for significantly associated SNPs [34]. In this study, SNPs at the transcriptome level were analyzed, revealing that cold-tolerant and sensitive *K. obovata* groups exhibited largely similar mutation types. Mutations in coding regions and transcriptionally active regions were predominantly transitions, with a Ti/Tv ratio stable around 1.3. This feature is consistent with SNP patterns reported in most plant transcriptomes or genomes. Further analysis indicated that C/T and G/A transitions were dominant, suggesting involvement of processes such as cytosine methylation deamination and RNA editing [35]. As a mangrove species evolved in coastal environments, *K. obovata* is frequently exposed to high salinity, hypoxia, and dramatic temperature fluctuations, which may promote the accumulation of C/T and G/A mutations through DNA methylation [36] and post-transcriptional regulatory mechanisms.

Combined analysis of SNP variation and transcriptome expression revealed that two genes in the cold-tolerant and -sensitive *K. obovata* groups harbored a 5′ UTR mutation

and a nonsynonymous mutation in the exon region, respectively, and exhibited significant enrichment in KEGG metabolic pathways (Figure 11). A 5′ UTR mutation may weaken TF binding or alter mRNA secondary structure stability, leading to gene downregulation. This change could reduce lignin and flavonoid biosynthesis, thereby decreasing the accumulation of antioxidants and structural defense metabolites, ultimately affecting cold tolerance. Previous studies have also shown that the biosynthesis of phenylpropanoids and flavonoids contributes to enhancing cold tolerance in mangrove species [37], consistent with our findings. Alternatively, it may represent a regulatory strategy of "energy redistribution," whereby structural metabolism is temporarily suppressed under low-temperature conditions to maintain a stable energy supply for critical cold-responsive metabolic processes. The nonsynonymous mutation in the exon region alters the amino acid property (hydrophobic → polar), which is predicted to affect the enzyme's substrate-binding site or stability, thereby influencing catalytic efficiency and reducing the biosynthesis rate of monoterpenes. For example, the production of monoterpene defense compounds, such as volatile monoterpenes, may be suppressed, subsequently weakening signal transduction and the intensity of defense responses. Taken together, the combined analysis of SNP variation and transcriptome expression suggests that mutations in *geneMaker00005577* and *geneMaker00013925* may influence physiological metabolism and cold tolerance in *K. obovata* under low-temperature stress by modulating defense-related metabolic fluxes, the antioxidant system, and signaling processes.

Statistical analysis of the number and types of AS events between the two groups revealed substantial differences in AS patterns between cold-tolerant and sensitive *K. obovata* populations, with SE events being predominant (Figure 11), consistent with previous studies. Exon skipping can directly alter coding region length or cause loss of protein domains, representing one of the most functionally impactful splicing types, suggesting a potential key role in the formation of cold tolerance in *K. obovata*. Further integration of the results from Figures 8 and 9 indicated that SE, A5SS, and A3SS events exhibited significant differences in both inclusion and exclusion counts, implying not only quantitative differences in AS events between the two groups but also a trend toward pattern conversion. These findings suggest that certain genes in the cold-tolerant population may preferentially undergo SE, and such differential splicing patterns could serve as molecular markers for cold tolerance.

Taken together, AS events in the *K. obovata* transcriptome provide an additional layer of regulatory mechanisms for low-temperature adaptation during its northward migration. Consistent with the SNP results, transcript-level variation not only manifests as nucleotide substitutions but also affects protein structure and function through altered splicing patterns, offering important insights into the molecular mechanisms underlying cold tolerance in *K. obovata*.

4. Materials and Methods

4.1. Experimental Materials

The experimental materials were collected from the research base of the Zhoushan Fisheries Research Institute, Zhejiang Province. Using the nursery seedling transplantation method, 6000 *K. obovata* seedlings were randomly divided into groups A and B and transplanted into circular plastic pots filled with sediment. Seedlings were cultivated in a nursery at a density of 12 plants/m^2, with tidal conditions simulated. Seawater was applied twice daily, and the seedlings underwent one natural overwintering. Survival was recorded daily. The plastic pots used had an upper diameter of 25.0 cm, height of 13.0 cm, and bottom diameter of 20.0 cm, with a small circular hole at the base to prevent water accumulation.

Based on previous observations, *K. obovata* seedlings during the overwintering period were broadly classified into two groups. The first group exhibited greenish leaves and remained healthy after winter, surviving throughout the observation period; this group was defined as the cold-tolerant group. The second group showed yellowing leaves without leaf drop or withering initially, but failed to recover from overwintering damage and eventually withered; this group was defined as the cold-sensitive group. During the overwintering period, based on previous observations and the phenotypic characteristics and overall condition of the seedlings, the 3000 *K. obovata* seedlings in Group A were further classified into a cold-tolerant subgroup (A1) and -sensitive subgroup (A2), while Group B, serving as a natural population without classification, was retained as a control for Group A (Figure 12). Survival and mortality rates were calculated and the comparative results between Groups A and B are summarized in Table 1.

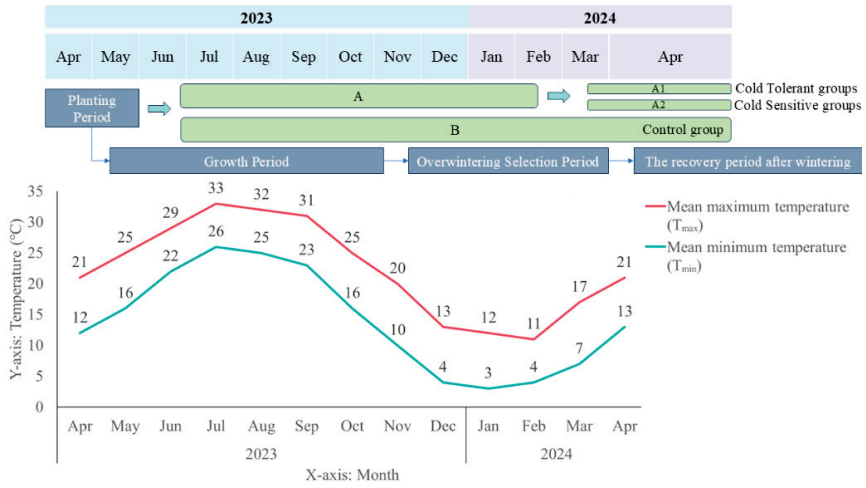


Figure 12. Schematic diagram of *K.obovata* planting period and key time points. The diagram indicates sample groups, sampling time points, and the overall temperature changes during the overwintering period. Temperature data were obtained from publicly available meteorological records (https://www.tianqi24.com/zhoushan/history2023.html (accessed on 4 December 2025)).

4.2. Experimental Methods

In this experiment, three ten-leaf-stage seedlings were randomly selected from each of the cold-tolerant and -sensitive groups. Surface soil and dust were gently washed off with deionized water, and the leaves were dried using paper towels. The second pair of leaves from ten-leaf-stage seedlings (consisting of five leaf pairs) was selected as the experimental material. The samples were carefully placed on a laboratory bench, photographed for comparison, and retained for records. (Figure 13). Leaf sampling was performed using scissors and forceps sterilized with 75% ethanol. Each sample was placed into pre-labeled, pre-cooled RNase-free cryotubes, immediately frozen in liquid nitrogen for 30 min, and subsequently stored at −80 °C. After collecting samples from three cold-tolerant and three cold-sensitive plants, they were designated as AL1, AL2, AL3, and BL1, BL2, BL3, respectively, serving as three biological replicates for each group.

After confirming through subsequent observations that the selected seedlings met expected phenotypic criteria, three replicates from each group were submitted for transcriptome sequencing.

Subsequently, RNA extraction and transcriptome sequencing were outsourced to Shanghai Meiji Biomedical Technology Co., Ltd. (Shanghai, China). Enzyme activities of superoxide dismutase (SOD), catalase (CAT), and peroxidase (POD) and malondialdehyde (MDA) content were measured for the cold-tolerant and -sensitive groups using commercial assay kits (Nanjing Jiancheng Bioengineering Institute (Nanjing, China)) according to

https://doi.org/10.3390/ijms27010429

the manufacturer's protocols. All measurements were performed using fresh leaf tissue, homogenized in normal saline (NaCl 0.9%), and strictly following the instructions provided with the assay kits. Enzyme activities were expressed as units per gram of fresh tissue ($U \cdot g^{-1}$ FW). Chlorophyll a, chlorophyll b, and total chlorophyll contents were determined using a chlorophyll content assay kit (Suzhou Grace Biotech Co., Ltd. (Suzhou, China)).

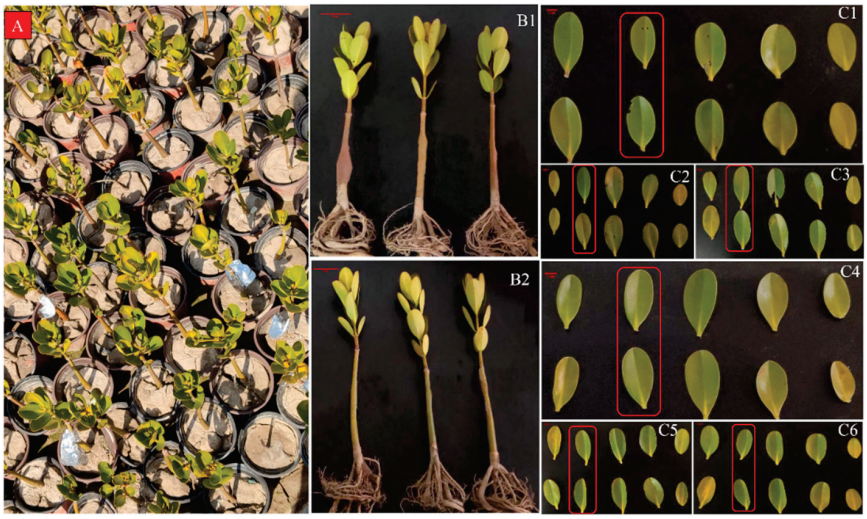


Figure 13. Sampling schematic of cold-tolerant and -sensitive *K. obovata* plants. (**A**) Distribution and marking of seedlings. (**B1**) Cold-tolerant and (**B2**) -sensitive *K. obovata* individuals, each group comprising three biological replicates. (**C1**–**C3**) Leaves collected from seedlings shown in (**B1**), and (**C4**–**C6**) leaves collected from seedlings shown in (**B2**). For all samples, half of the second pair of leaves was used for RNA-seq and the other half for physiological measurements.

To validate the reliability of the transcriptome sequencing results, seven DEGs were selected for quantitative real-time PCR (qRT-PCR) verification. Primers were designed for the selected genes using Primer Premier 5 software (Premier Biosoft, Palo Alto, CA, USA), with *KoACT2* [38] serving as the internal reference gene. Primer sequences are listed in Table 7. The qRT-PCR reactions were performed using the TB Green® Premix Ex Taq™ II FAST qPCR Kit (TAKARA Bio Inc. (Nara, Japan)) on a CFX Duet Real-Time PCR System (Bio-Rad Laboratories, Inc. (Hercules, CA, USA)). Each 10 µL reaction contained 5 µL TB Green Premix Ex Taq II, 0.4 µL of each forward and reverse primer, 3.95 µL RNase-free water, and 0.25 µL cDNA template. The thermal cycling program consisted of an initial denaturation at 95 °C for 30 s, followed by 39 cycles of 95 °C for 5 s and 60 °C for 30 s for annealing and extension. The relative expression levels of DEGs were calculated using the $2^{-\Delta\Delta CT}$ method. Statistical analyses, including analysis of variance and Pearson correlation analysis, were performed using IBM SPSS Statistics 26 (IBM Corp., Armonk, NY, USA), and graphs were generated with GraphPad Prism 8 (GraphPad Software, San Diego, CA, USA).

Table 7. Primers sequences used in the qRT-PCR.

Gene ID	Forward Primer (5′→3′)	Reverse Primer (5′→3′)
MYB-related-14971	GCAGGTTCGGAGCAGCAATTATC	ACATCTGATTTAGTGCGTTCGTTGG
MYB-7720	TTCAGACCTTCTACCGACAACCATC	GAGTGGCTGCTGAGTTTGTTTGG
LBD (AS2/LOB)-6849	GCTGTGGTGGATGGCGAGAG	TGTTGGCATCACGGACTCCTTG
LBD (AS2/LOB)-8016	TTTCCTCCTTGAACCCTCACATCTC	CCCAGGTCACACTAGCACACTATTC
GATA-397	CGACCACATTGACGACCTCCTC	ACTCGGACTCAGCAGACCAAATG
ERF-4010	CCATCGGGACCACCAACTAAAGG	AGGCGACCACGTATCCAATGC
ERF-8573	TGGATCGAAGACATGGCAAGAGG	GTTGAGATGGAGCGGAGTAGATGG
KoACT2 (internal reference)	ACCGAGGCTCCTCTTAATCC	AGCTGGCACATTGAAGGTCT

5. Conclusions

This study demonstrates that *K. obovata* exhibits multilayered physiological and molecular response mechanisms under low-temperature stress. There was significantly higher CAT activity in the cold-tolerant than the cold-sensitive group, enhancing H_2O_2 scavenging efficiency, whereas the cold-sensitive group exhibited higher SOD activity but insufficient downstream H_2O_2 clearance, resulting in lower overall antioxidant efficiency. The DEGs were primarily associated with maintenance of cellular structure, metabolic activities, redox regulation, and ion homeostasis. Significant enrichment was observed in xyloglucan metabolism, extracellular region functions, and iron ion binding. Additionally, phenylpropanoid biosynthesis, amino sugar metabolism, and plant hormone signal transduction pathways were involved in the low-temperature response. In the cold-tolerant population, TFs such as WRKY, NAC, MYB, and ERF exhibited significant differential expression, potentially activating downstream antioxidant and osmotic adjustment responses, thereby enhancing cold tolerance. The SNP and AS analyses indicated that gene mutations and splicing pattern diversity may enhance protein function and low-temperature adaptability. Overall, *K. obovata* enhances cold tolerance under low-temperature stress through multilayered mechanisms, including cellular structure protection, antioxidant regulation, maintenance of ion homeostasis, and regulation by TFs and AS. This study provides a theoretical basis for elucidating the molecular foundations of low-temperature adaptation in *K. obovata*.

In addition, the phenotypic differences observed in this study, such as leaf coloration, may provide a reference for early selection of cold-tolerant plants. The cold related differential gene markers or exploration of transcription factors obtained in this study could provide theoretical basis for selecting parental plants from the source population and further screening of cold-tolerant *K. obovata* varieties in introduced regions.

Author Contributions: H.L. participated in the methodology, writing—original draft, data curation, software, formal analysis. Z.S. participated in the data curation, software, writing—review and editing. W.L. participated in the software, formal analysis. X.Y. (Xiaolong Yin) participated in the investigation, methodology, and validation. X.X. participated in the software, formal analysis. X.Z. participated in the data curation. X.Y. (Xiaojun Yan) participated in the data curation. X.W. participated in the software, formal analysis, writing—review and editing. Y.L. participated in the data curation and formal analysis. A.M. participated in the funding acquisition, supervision, project administration, resources. All authors have read and agreed to the published version of the manuscript.

Funding: This work was supported by grants from the National Key R & D Program of China (grant numbers 2022YFE0203900); Guangdong S & T programme (grant numbers 2022B1212050002).

Institutional Review Board Statement: Not applicable.

Informed Consent Statement: Not applicable.

Data Availability Statement: The data presented in this study are available on request from the corresponding author.

Acknowledgments: We thank all the authors for their contributions to this article.

Conflicts of Interest: We confirm that the manuscript and all its contents have not been published previously and are not under consideration by any other journal. All authors have reviewed and approved the final version of the manuscript, declare no conflicts of interest, and consent to its submission to *IJMS*.

References

1. Yang, X.; Dai, Z.; Yuan, R.; Guo, Z.; Xi, H.; He, Z.; Wei, M. Effects of salinity on assembly characteristics and function of microbial communities in the phyllosphere and rhizosphere of salt-tolerant Avicennia marina mangrove species. *Microbiol. Spectr.* **2023**, *11*, e0300022. [CrossRef] [PubMed]
2. Wang, F.; Liu, J.; Qin, G.; Zhang, J.; Zhou, J.; Wu, J.; Zhang, L.; Thapa, P.; Sanders, C.J.; Santos, I.R.; et al. Coastal blue carbon in China as a nature-based solution toward carbon neutrality. *Innovation* **2023**, *4*, 100481. [CrossRef] [PubMed]
3. Kitao, M.; Utsugi, H.; Kuramoto, S.; Tabuchi, R.; Fujimoto, K.; Lihpai, S. Light-dependent photosynthetic characteristics indicated by chlorophyll fluorescence in five mangrove species native to Pohnpei Island, Micronesia. *Physiol. Plant.* **2003**, *117*, 376–382. [CrossRef] [PubMed]
4. Shen, Z.-J.; Chen, J.; Ghoto, K.; Hu, W.-J.; Gao, G.-F.; Luo, M.-R.; Li, Z.; Simon, M.; Zhu, X.-Y.; Zheng, H.-L. Proteomic analysis on mangrove plant Avicennia marina leaves reveals nitric oxide enhances the salt tolerance by up-regulating photosynthetic and energy metabolic protein expression. *Tree Physiol.* **2018**, *38*, 1605–1622. [CrossRef]
5. Liu, H.; An, X.; Liu, X.; Yang, S.; Liu, Y.; Wei, X.; Li, X.; Chen, Q.; Wang, J. Molecular mechanism of salinity and waterlogging tolerance in mangrove Kandelia obovata. *Front. Plant Sci.* **2024**, *15*, 1354249. [CrossRef]
6. Du, Z.; You, S.; Zhao, X.; Xiong, L.; Li, J. Genome-wide identification of WRKY genes and their responses to chilling stress in Kandelia obovata. *Front. Genet.* **2022**, *13*, 875316. [CrossRef]
7. Zhou, Y.-Y.; Wang, Y.-S.; Sun, C.-C. Molecular Cloning and Expression Analysis of the Typical class III chitinase genes from three mangrove species under heavy metal stress. *Plants* **2023**, *12*, 1681. [CrossRef]
8. Britto Martins de Oliveira, J.; Corrêa Junior, D.; Parente, C.E.T.; Frases, S. Fungi in Mangrove: Ecological Importance, Climate Change Impacts, and the Role in Environmental Remediation. *Microorganisms* **2025**, *13*, 878. [CrossRef]
9. Mossa, M.; De Padova, D. Interaction between waves and vegetation. *Sci. Rep.* **2025**, *15*, 6157. [CrossRef]
10. Zhao, J.; Li, C.; Wang, T.; Li, C.; Shen, J.; Liu, Y.; Wu, P. Distribution pattern of mangrove fish communities in China. *Biology* **2022**, *11*, 1696. [CrossRef]
11. Chen, L.; Wang, W.; Li, Q.Q.; Zhang, Y.; Yang, S.; Osland, M.J.; Huang, J.; Peng, C. Mangrove species' responses to winter air temperature extremes in China. *Ecosphere* **2017**, *8*, e01865. [CrossRef]
12. Yang, J.; Wu, A.; Li, J.; Wei, H.; Qin, J.; Tian, H.; Fan, D.; Wu, W.; Chen, S.; Tong, X.; et al. Structured and unstructured intraspecific propagule trait variation across environmental gradients in a widespread mangrove. *Ecol. Evol.* **2024**, *14*, e10835. [CrossRef] [PubMed]
13. Liao, J.; Li, G.; Zhang, S.; Yang, Y.; Li, Y.; Dong, Z.; Guo, Y.; Wang, Z. Global warming exacerbates the risk of habitat loss for regional mangrove species. *Sci. Rep.* **2025**, *15*, 19710. [CrossRef] [PubMed]
14. Liu, X.; Lu, X.; Yang, S.; Liu, Y.; Wang, W.; Wei, X.; Ji, H.; Zhang, B.; Xin, W.; Wen, J.; et al. Role of exogenous abscisic acid in freezing tolerance of mangrove Kandelia obovata under natural frost condition at near 32° N. *BMC Plant Biol.* **2022**, *22*, 593. [CrossRef]
15. Zheng, C.; Liu, W.; Qiu, J.; Huang, L.; Huang, X.; Chen, S. Comparison of physiological characteristics of Kandelia obovata at different ages in winter in the northernmost mangrove transplanted area of China. *Acta Ecol. Sin.* **2013**, *33*, 132–138. [CrossRef]
16. Inoue, T.; Akaji, Y.; Baba, S.; Noguchi, K. Temperature dependence of O2 respiration in mangrove leaves and roots: Implications for seedling dispersal phenology. *New Phytol.* **2023**, *237*, 100–112. [CrossRef]
17. Zhang, J.; Ouyang, S.; Cai, X.; Yang, S.; Chen, Q.; Yang, J.; Song, Z.; Zhang, W.; Wang, Y.; Zhu, Y.; et al. Phenotypic adaptation and genomic variation of Kandelia obovata associated with its northern introduction along southeastern coast of China. *Front. Plant Sci.* **2025**, *16*, 1512620. [CrossRef]
18. He, Z.; Sun, H.; Peng, Y.; Hu, Z.; Cao, Y.; Lee, S.Y. Colonization by native species enhances the carbon storage capacity of exotic mangrove monocultures. *Carbon Balance Manag.* **2020**, *15*, 28. [CrossRef]
19. Lu, W.-X.; Zhang, B.-H.; Zhang, Y.-Y.; Yang, S.-C. Differentiation of cold tolerance in an artificial population of a mangrove species, Kandelia obovata, is associated with geographic origins. *Front. Plant Sci.* **2022**, *12*, 695746. [CrossRef]
20. Liu, W.; Zheng, C.; Chen, J.; Qiu, J.; Huang, Z.; Wang, Q.; Ye, Y. Cold acclimation improves photosynthesis by regulating the ascorbate–glutathione cycle in chloroplasts of Kandelia obovata. *J. For. Res.* **2019**, *30*, 755–765. [CrossRef]
21. Peng, Y.-L.; Wang, Y.-S.; Fei, J.; Sun, C.-C.; Cheng, H. Ecophysiological differences between three mangrove seedlings (Kandelia obovata, Aegiceras corniculatum, and Avicennia marina) exposed to chilling stress. *Ecotoxicology* **2015**, *24*, 1722–1732. [CrossRef]
22. Feng, Y.; Li, Z.; Kong, X.; Khan, A.; Ullah, N.; Zhang, X. Plant coping with cold stress: Molecular and physiological adaptive mechanisms with future perspectives. *Cells* **2025**, *14*, 110. [CrossRef] [PubMed]
23. Li, C.; Mur, L.A.; Wang, Q.; Hou, X.; Zhao, C.; Chen, Z.; Wu, J.; Guo, Q. ROS scavenging and ion homeostasis is required for the adaptation of halophyte Karelinia caspia to high salinity. *Front. Plant Sci.* **2022**, *13*, 979956. [CrossRef] [PubMed]
24. Qi, C.; Zhang, H.; Liu, Y.; Wang, X.; Dong, D.; Yuan, X.; Li, X.; Zhang, X.; Li, X.; Zhang, N.; et al. CsSNAT positively regulates salt tolerance and growth of cucumber by promoting melatonin biosynthesis. *Environ. Exp. Bot.* **2020**, *175*, 104036. [CrossRef]

25. Guan, Y.; Hu, W.; Xu, Y.; Sarengaowa; Ji, Y.; Yang, X.; Feng, K. Proteomic analysis validates previous findings on wounding-responsive plant hormone signaling and primary metabolism contributing to the biosynthesis of secondary metabolites based on metabolomic analysis in harvested broccoli (*Brassica oleracea* L. var. italica). *Food Res. Int.* **2021**, *145*, 110388. [CrossRef]
26. Fei, J.; Wang, Y.-S.; Cheng, H.; Su, Y.-B.; Zhong, Y.-J.; Zheng, L. The Kandelia obovata transcription factor KoWRKY40 enhances cold tolerance in transgenic Arabidopsis. *BMC Plant Biol.* **2022**, *22*, 274. [CrossRef]
27. Zhang, B.; Gao, Y.; Zhang, L.; Zhou, Y. The plant cell wall: Biosynthesis, construction, and functions. *J. Integr. Plant Biol.* **2021**, *63*, 251–272. [CrossRef]
28. Zhang, J.; Fan, T.; Cai, X.; Ouyang, S.; Yang, J.; Song, Z.; Zhang, W.; Wang, Y.; Zhu, Y.; Nan, P. Comparative transcriptomic and metabolomic analysis of two related Kandelia obovata populations in response to cold wave. *Phenomics* **2025**, 1–17. [CrossRef]
29. Du, Z.; You, S.; Yang, D.; Tao, Y.; Zhu, Y.; Sun, W.; Chen, Z.; Li, J. Comprehensive analysis of the NAC transcription factor gene family in Kandelia obovata reveals potential members related to chilling tolerance. *Front. Plant Sci.* **2022**, *13*, 1048822. [CrossRef]
30. Pang, X.; Xue, M.; Ren, M.; Nan, D.; Wu, Y.; Guo, H. Ammopiptanthus mongolicus stress-responsive NAC gene enhances the tolerance of transgenic Arabidopsis thaliana to drought and cold stresses. *Genet. Mol. Biol.* **2019**, *42*, 624–634. [CrossRef]
31. Li, J.; Chen, S.; Yin, Y.; Shan, Q.; Zheng, C.; Chen, Y. Genome-Wide Analysis of bHLH family genes and identification of members associated with cold/drought-induced photoinhibition in Kandelia obovata. *Int. J. Mol. Sci.* **2023**, *24*, 15942. [CrossRef] [PubMed]
32. An, J.-P.; Wang, X.-F.; Zhang, X.-W.; Xu, H.-F.; Bi, S.-Q.; You, C.-X.; Hao, Y.-J. An apple MYB transcription factor regulates cold tolerance and anthocyanin accumulation and undergoes MIEL1-mediated degradation. *Plant Biotechnol. J.* **2020**, *18*, 337–353. [CrossRef] [PubMed]
33. Illgen, S.; Zintl, S.; Zuther, E.; Hincha, D.K.; Schmülling, T. Characterisation of the *ERF102* to *ERF105* genes of Arabidopsis thaliana and their role in the response to cold stress. *Plant Mol. Biol.* **2020**, *103*, 303–320. [CrossRef] [PubMed]
34. Li, J.; Khatab, A.A.; Hu, L.; Zhao, L.; Yang, J.; Wang, L.; Xie, G. Genome-wide association mapping identifies new candidate genes for cold stress and chilling acclimation at seedling stage in rice (*Oryza sativa* L.). *Int. J. Mol. Sci.* **2022**, *23*, 13208. [CrossRef]
35. Rahman, A.; Yadav, N.S.; Byeon, B.; Ilnytskyy, Y.; Kovalchuk, I. Genomic and epigenomic changes in the progeny of cold-stressed Arabidopsis thaliana plants. *Int. J. Mol. Sci.* **2024**, *25*, 2795. [CrossRef]
36. Zhao, Y.; Zhong, Y.; Ye, C.; Liang, P.; Pan, X.; Zhang, Y.Y.; Zhang, Y.; Shen, Y. Multi-omics analyses on Kandelia obovata reveal its response to transplanting and genetic differentiation among populations. *BMC Plant Biol.* **2021**, *21*, 341. [CrossRef]
37. Wang, S.-M.; Wang, Y.-S.; Cheng, H. Comparative transcriptomics and metabolomics analyses of Avicennia marina and Kandelia obovata under chilling stress during seedling stage. *Int. J. Mol. Sci.* **2023**, *24*, 16989. [CrossRef]
38. Hong, L.; Su, W.; Zhang, Y.; Ye, C.; Shen, Y.; Li, Q.Q. Transcriptome profiling during mangrove viviparity in response to abscisic acid. *Sci. Rep.* **2018**, *8*, 770. [CrossRef]

Disclaimer/Publisher's Note: The statements, opinions and data contained in all publications are solely those of the individual author(s) and contributor(s) and not of MDPI and/or the editor(s). MDPI and/or the editor(s) disclaim responsibility for any injury to people or property resulting from any ideas, methods, instructions or products referred to in the content.

International Journal of
Molecular Sciences

MDPI

Article

Genome-Wide Identification of *FCS-Like Zinc Finger (FLZ)* Family Genes in Three *Brassica* Plant Species and Functional Characterization of *BolFLZ*s in Chinese Kale Under Abiotic Stresses

Yuwan Zhao [1,†], Shunquan Chen [2,†], Mao Qin [2], Kejuan Shui [3], Riqing Li [2], Baoli Yang [2], Jin Liu [2] and Zhufeng Chen [1,*]

[1] Center for Biological Science and Technology, Key Laboratory of Cell Proliferation and Regulation Biology of Ministry of Education, Zhuhai Macao Biotechnology Joint Laboratory, Faculty of Arts and Sciences, Beijing Normal University, Zhuhai 519087, China; ywanzhao@163.com
[2] Shenzhen Inspection and Testing Center of Agricultural Product Quality and Safety, Shenzhen 518071, China; 2018010158@m.scnu.edu.cn (S.C.); mqin@outlook.com (M.Q.); liriqing246@163.com (R.L.); ybl0212@163.com (B.Y.); ahappyheart@126.com (J.L.)
[3] Technical Center of Gongbei Customs, Zhuhai 519087, China; yishuhuaiciwater@163.com
* Correspondence: zfchen@bnu.edu.cn
† These authors contribute equally to this work.

Abstract: FCS-like zinc finger (FLZ) proteins are plant-specific regulatory proteins, which contain a highly conserved FLZ domain, and they play critical roles in plant growth and stress responses. Although the *FLZ* family has been systematically characterized in certain plants, it remains underexplored in *Brassica* species, which are vital sources of vegetables, edible oils, and condiments for human consumption and are highly sensitive to various abiotic stresses. Following the whole-genome triplication events (WGT) in *Brassica*, elucidating how the *FLZ* genes have expanded, differentiated, and responded to abiotic stresses is valuable for uncovering the genetic basis and functionality of these genes. In this study, we identified a total of 113 *FLZ* genes from three diploid *Brassica* species and classified them into four groups on the basis of their amino acid sequences. Additionally, we identified 109 collinear gene pairs across these *Brassica* species, which are dispersed among different chromosomes, suggesting that whole-genome duplication (WGD) has significantly contributed to the expansion of the *FLZ* family. Subcellular localization revealed that six representative BolFLZ proteins are located in the nucleus and cytoplasm. Yeast two-hybrid assays revealed that 13 selected BolFLZs interact with BolSnRK1α1 and BolSnRK1α2, confirming the conservation of the SnRK1α-FLZ module in *Brassica* species. Expression profile analysis revealed differential expression patterns of *BolFLZ* across various tissues. Notably, the expression levels of seven *BolFLZ* genes out of the fifteen genes analyzed changed significantly following treatment with various abiotic stressors, indicating that the *BolFLZ* genes play distinct physiological roles and respond uniquely to abiotic stresses in *Brassica* species. Together, our results provide a comprehensive overview of the *FLZ* gene family in *Brassica* species and insights into their potential applications for enhancing stress tolerance and growth in Chinese kale.

Keywords: abiotic stresses; *Brassica*; Chinese kale; expression analysis; *FLZ* gene family

1. Introduction

FCS-like zinc finger (FLZ) proteins represent a class of plant-specific regulatory proteins characterized by a conserved FLZ domain, also known as domain of unknown function 581 (DUF581) [1]. The FLZ domain comprises an assembly of 70 amino acid residues possessing a conserved CX2CX17–19FCSX2C motif [2]. The first protein harboring the FLZ domain was identified through aging-associated enhancer capture experiments [3]. This protein can be induced by senescence and is crucial in abscisic

acid (ABA)-mediated seed dormancy, which is a desirable trait in agricultural production because it inhibits the preharvest sprouting of many grains and seeds [4]. Since the importance of FLZ proteins in plant stress resistance and developmental growth has been progressively revealed, plant scientists have increasingly focused their attention on extensive investigations of the *FLZ* gene family, aiming to increase crop resilience and yield under various environmental conditions.

To date, members of the *FLZ* gene family have been shown to be essential for various biological processes, including plant development, senescence, stress responses, and sugar signaling [4–7]. Recent research has indicated that the *FLZ* gene is a critical component of the gene regulatory network involved in controlling flowering time in plants. In Arabidopsis, AtFLZ13 negatively regulates flowering time by promoting FLOWERING LOCUS C (FLC) transcription with ABI5 and interacting with FLC to inhibit FLOWERING LOCUS T (FT) and SUPPRESSOR OF OVEREXPRESSION OF CONSTANS 1 (SOC1) [8]. Additionally, OsFLZ2 interacts with OsMADS51, a rice orthologue of Arabidopsis FLC, to finely tune flowering time under short-day conditions [9,10]. These findings suggest that FLZ proteins could function as transcription factors to regulate gene expression. In addition to those in rice and Arabidopsis, several studies across diverse plant species, including maize (*Zea mays*), wheat (*Triticum aestivum*), tomato *(Solanum lycopersicum)*, cotton (*Gossypium hirsutum*), and liquorice (*Glycyrrhiza inflata*), have revealed that FLZ proteins play significant roles in mediating responses to various stress conditions [5–7,11,12]. For example, *ZmFLZ14* negatively regulates a plant's response to carbon starvation [13], whereas certain *GhFLZ* genes serve as key regulatory factors in the response of *G. hirsutum* to cold stress [12].

Most notably, FLZ proteins serve as scaffolding proteins for sucrose nonfermenting related kinase 1 (SnRK1), interacting with its kinase subunits to assist SnRK1 in sensing energy deficits caused by adverse conditions and coordinating cellular responses for adaptation in plants [1,14–16]. SnRK1 acts as a central integrator of energy metabolism, stress, and developmental signals [14,17]. SnRK1 promotes catabolism while minimizing anabolism by reprogramming the transcriptional machinery, thus enabling plants to survive under low-energy conditions and increasing tolerance to various biotic and abiotic stresses by regulating the transcription of genes associated with stress tolerance [17–19]. In Arabidopsis, AtFLZ3 (DUF581-9) functions as a novel negative regulator of the key energy sensor SnRK1 by inhibiting its activity through the physical blockade of the phosphorylation of its catalytic subunit KIN10 under energy-sufficient conditions. Under low-energy conditions, AtFLZ3 undergoes partial degradation by the proteasome, alleviating its inhibition and allowing the plant to perform essential low-energy responses [20,21]. In rice, a yeast two-hybrid assay revealed strong interactions between eight OsFLZ proteins and SnRK1A, with OsFLZ18 negatively regulating SnRK1 activity to suppress αAmy3 expression, which subsequently modulates rice seed germination and coleoptile growth under submerged conditions [22]. Given the profound impact of *FLZ*s on plant development regulation and their critical role in coordinating responses to biotic and abiotic stress signals, identification and functional studies of plant *FLZ* family genes have attracted increasing attention. However, the genome-wide identification and annotation of *FLZ* genes have yet to be reported in *Brassica* species. Novel insights into FLZ proteins from a diverse array of plant species, particularly those within horticultural crops, are essential.

Brassica species, which are rich in vitamins, minerals, and phytochemicals that offer numerous health benefits, serve as a global source of essential nutrients and edible vegetable oils for human consumption [23,24]. A significant whole-genome triplication (WGT) event occurred in almost all commercially important *Brassica* species approximately 22.5 million years ago, resulting in three diploid species (*Brassica rapa*, AA, 2n = 20; *B. nigra*, BB, 2n = 16; and *B. oleracea*, CC, 2n = 18) and three allotetraploid species (*B. juncea*, AABB, 2n = 36; *B. napus*, AACC, 2n = 38; and *B. carinata*, BBCC, 2n = 34) [25,26]. The evolutionary relationships among the six crop species are depicted by U's triangle, wherein the three key diploids form the vertices, whereas the three allotetraploids originated from interspecific hybridization between the diploids [27]. Whole-genome sequencing of *Brassica* species

has demonstrated that whole-genome triplication (WGT) not only plays an important role in the speciation and morphotype diversification of these plants but also contributes to the diversification of stress-related genes in *Brassica* crop species [26,28]. In *Brassica rapa*, genes that respond to environmental stresses were preferentially retained after WGT, which is regarded as a mechanism for protecting plants from harmful stresses [29]. As a result of WGD, WGT, and tandem and segmental duplications, the number of members within numerous multigene families has expanded across various *Brassica* crop species, exhibiting responsiveness to a range of diverse stresses [28]. Approximately 3% and 4% of tandemly duplicated genes are responsive to abiotic stresses in *B. rapa* and *B. oleracea*, respectively [30]. Moreover, because of WGD, numerous genes have been identified in *Brassica* species in response to salt stress [31]. Given the considerable variability in stress sensitivity among *Brassica* species and varieties [28,32], studying stress-regulated genes in *Brassica* provides insights into gene function and evolution while also expanding opportunities for genetic engineering of crops resistant to diverse stresses.

In this study, we hypothesize that if the *FLZ* gene family in *Brassica* species has expanded through WGT events, there will be an increased number of genes and gene differentiation, which may lead to each exhibiting unique responses to abiotic stresses within these species. To test this hypothesis, we performed a comprehensive genome-wide analysis of the *FLZ* gene family across three *Brassica* plant species, examining chromosomal distribution, conserved amino acid residues in the FLZ-type domain, phylogenetic relationships, synteny analysis, gene structure, conserved motifs, and potential cis-acting elements in the promoter. Additionally, we investigated the subcellular localization and spatiotemporal expression patterns of BolFLZ proteins from Chinese kale (*Brassica oleracea* L. var. *alboglabra*), an original Chinese *Brassica* vegetable known for its high nutritional value [33]. We also examined the potential protein–protein interactions between BolFLZs and BolSnRK1α, as they form a complex associated with diverse functions. Finally, we conducted a detailed analysis of the responsiveness of the *BolFLZ* gene family to various stresses in Chinese kale via quantitative real-time PCR (qRT–PCR). This research provides new insights into FLZ proteins across *Brassica* species, highlighting their potential role in the response to abiotic stress. The findings of this study provide valuable reference data and a theoretical foundation for future research on the biological functions of the *FLZ* gene family in *Brassica*.

2. Results

2.1. Identification and Classification of FLZ Genes in the Three Brassica Plant Species

In this study, BLAST was initially carried out to search for *FLZ* genes in the genomes of three *Brassica* species. The obtained sequences were further verified through a hidden Markov model via previously described methods. Finally, we identified 36, 41, and 36 *FLZ* genes in Chinese cabbage (*Brassica rapa*; Bca), black mustard (*Brassica nigra*; Bni), and Chinese kale (*Brassica oleracea*; Bol), respectively. These genes were designated *BcaFLZ1-BcaFLZ36*, *BniFLZ1-BniFLZ41*, and *BolFLZ1-BolFLZ36* on the basis of their chromosomal locations (Table S1). These findings revealed that the number of *FLZs* slightly varied between species, which could be attributed to the loss or duplication of genes throughout the evolutionary history of *Brassica*.

Detailed information for each *FLZ* gene, including the gene name, locus ID, chromosome location, open reading frame (ORF), protein length, predicted molecular weight (MW), isoelectric point (pI), and subcellular localization, is presented in Table S1. Among the 113 putative FLZ proteins, the lengths of the protein sequences encoded by the FLZ genes vary from 69 amino acids in BniFLZ19 to 335 amino acids in BcaFLZ14, and the relative molecular weights range from 8.018 to 37.322 kDa. The theoretical pI values range from 4.56 for BcaFLZ35 to 10.03 for BolFLZ5, with 80 proteins having a pI value greater than 7 and the remaining proteins having a pI value less than 7, suggesting that this gene family is biased towards basic amino acids. The aliphatic indices of these 113 putative FLZ proteins ranged from 38.57 to 90.48. The grand average of hydropathicity (GRAVY) scores,

which are all less than zero, range from −1.458 for BniFLZ25 to −0.245 for BcaFLZ14, suggesting that these proteins are hydrophilic. Considering that proteins with an instability index less than 40 are classified as stable, all FLZ proteins in the three *Brassica* species are predicted to exhibit instability coefficients exceeding 40, which indicates significant instability. These results confirm that the 113 putative FLZ proteins across the three *Brassica* plant species exhibit significant variation in their protein characteristics.

2.2. Phylogenetic Analysis of FLZ Proteins

To investigate the phylogenetic relationships among FLZ proteins, the amino acid sequences of FLZs from three *Brassica* species (*Brassica rapa*, *Brassica nigra*, and *Brassica oleracea*), rice (*O. sativa*), and Arabidopsis (*A. thaliana*) were utilized to construct an unrooted phylogenetic tree via the neighbor-joining method (Figure 1). The analysis categorized these proteins into four monophyletic clades on the basis of sequence identity. Clade I, the largest, comprises 71 FLZ members, followed by Clade II, with 41 members, and Clade III, the smallest, with 16 FLZs. Notably, the distribution trends for BcaFLZs, BniFLZs, and BolFLZs were similar, with a significant presence in Clade I, which included 17 BcaFLZs, 23 BniFLZs, and 17 BolFLZs. Each of the other three clades contained approximately equal numbers of the three *Brassica* FLZ types. Additionally, Clade II had the greatest number of OsFLZs, with 15 members, whereas Clade I contained 9 AtFLZ genes, more than the other subfamilies did. Notably, only one *AtFLZ* gene was placed into Clade III (Figure 1). All FLZs shared a common ancestor in each clade, suggesting that the diversity of plant FLZ proteins developed before the evolutionary split between monocots and dicots (Figure 1).

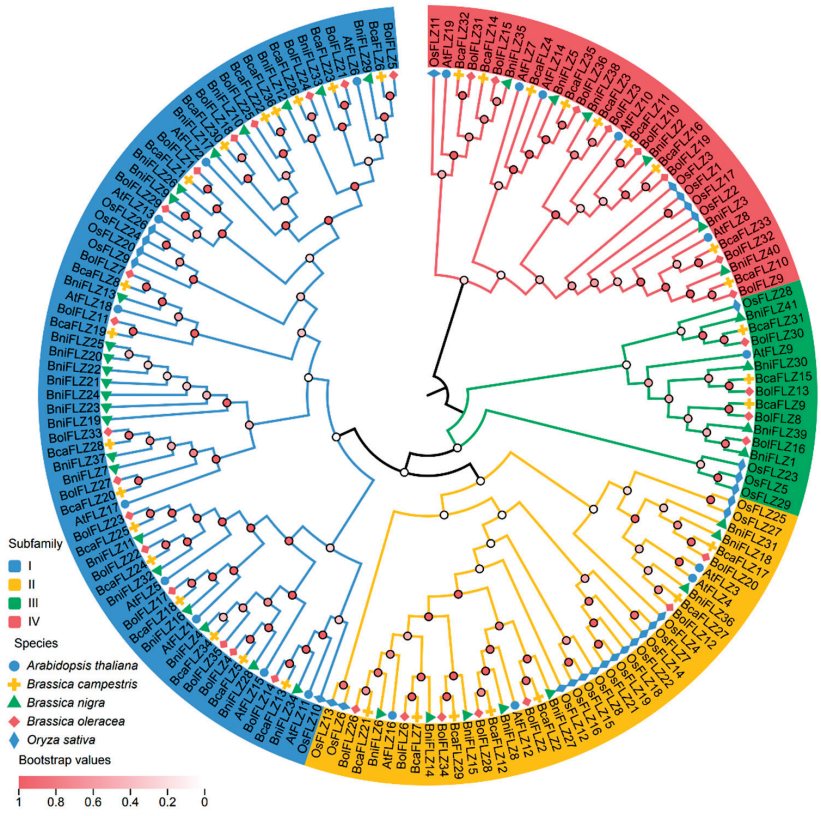


Figure 1. Phylogenetic tree of the FLZs in the three *Brassica* species, Arabidopsis, and rice. The phylogenetic tree was generated via the neighbor-joining (NJ) method implemented in MEGA X software (version 11.0) with the JTT model and pairwise gap deletion option. Bootstrap analysis was conducted with 1000 iterations, and the bootstrap values are represented by the color intensity of the circles at each node in the phylogenetic tree. The phylogenetic tree is divided into four subgroups, represented by blue, yellow, red, and green. The FLZ proteins from the five species are denoted with distinct shapes and colors in the phylogenetic analysis.

2.3. Analysis of Gene Structure and Identification of Conserved Motifs

To better elucidate the diversification of the *FLZ* genes in the three *Brassica* species, the exon/intron organization and conserved motifs of *FLZs* were analyzed. The exon/intron organization of the coding sequences of individual *FLZ* genes, including the number and length of exons/introns, is shown in Figure S1. The results indicate that all *FLZ* genes harbored only one intron except for *BcaFLZ14*, which consisted of five introns (Figure S1).

To further examine the structural diversity of *FLZ* in the three *Brassica* species, the conserved motifs of the 113 FLZ proteins were analyzed via MEME online software, and 15 different conserved motifs (motifs 1–15) were identified (Figure S2). The motif analysis revealed that nearly all of the FLZ proteins contained two motifs (motif 1 and motif 2), with the exception of BcaFLZ13, which contained only motif 2. Together with the results of the conserved structural domain analysis, we found that 101 FLZ proteins contained the zf-FLZ domain, whereas 12 FLZ proteins contained the zf-FLZ superfamily domain (Figure 2). The results of both analyses revealed that motifs 1 and 2 may represent the FCS-like zinc-finger domain. Furthermore, phylogenetic tree analysis revealed that genes within each subgroup presented unique gene structures and conserved motifs (Figure 2). Related genes in subgroups have similar motifs, indicating similar functions in the FLZ family.

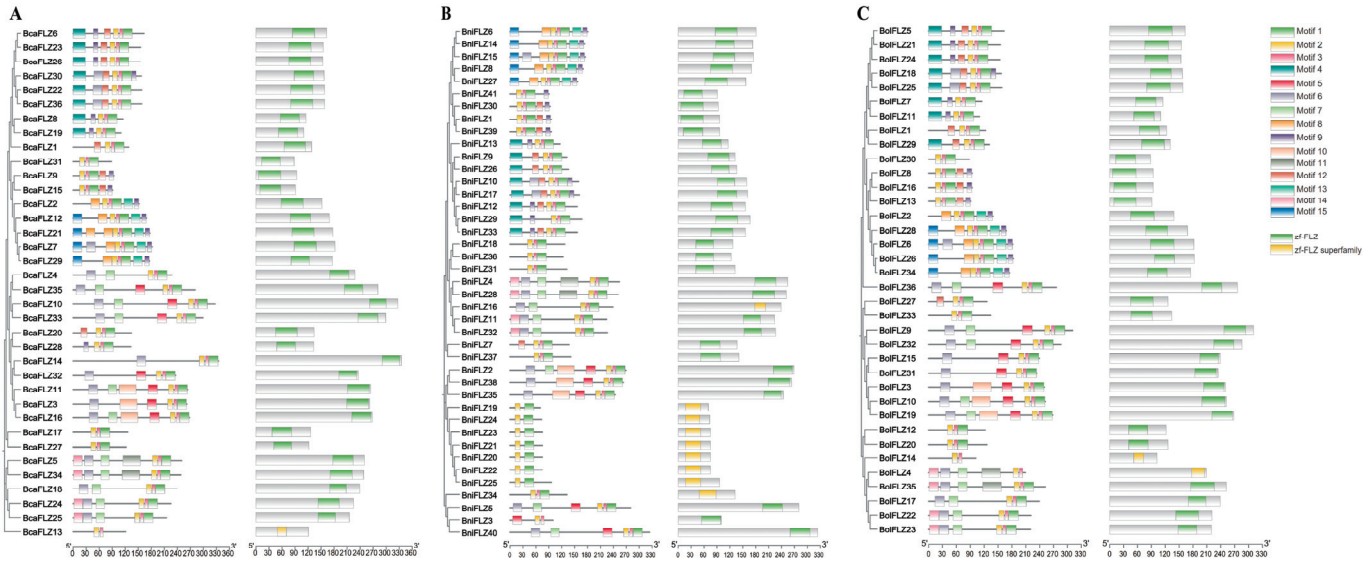


Figure 2. Conserved motif and domain analyses of the FLZs of the three *Brassica* species. (**A**) *Brassica rapa*; (**B**) *Brassica nigra*; and (**C**) *Brassica oleracea*. Fifteen conserved motifs of FLZ proteins were identified, and the size of each motif was proportional to the scale. The conserved domains of the FLZ proteins were examined via NCBI conserved domain search and SMART. The FCS-like zinc-finger domain (zf-FLZ) is represented by green boxes, and the zf-FLZ superfamily is represented by yellow boxes.

Furthermore, recent research has shown that some FLZ proteins possess a conserved ATG8 (autophagy-related 8)-interacting motif (AIM) (EDYTLV) on the first β-sheet, which is highly conserved across plant species and plays a crucial role in autophagy and energy balance regulation [13]. Therefore, we used the FIMO-Motif search tool (https://meme-suite.org/meme/tools/fimo; accessed on 17 August 2024) to identify which FLZ proteins also contained AIM motifs in the three *Brassica* species [34]. Finally, we identified 13, 11, and 13 FLZ proteins containing AIM motifs in *Brassica rapa*, *Brassica nigra*, and *Brassica oleracea*, respectively (Table S2). The results indicated that the core AIM sequences and their surrounding residues were highly conserved across the three *Brassica* species (Figure S3).

2.4. Chromosome Distribution, Gene Duplication, and Collinearity Analysis of FLZ Genes

Gene localization helps in elucidating the function and role of genes and their interactions with each other. There are 10 chromosomes (2n = 2X = 20) in the *Brassica rapa* genome (Figure S4A), 8 chromosomes (2n = 2X = 16) in the *Brassica nigra* genome (Figure S4B), and 9 chromosomes (2n = 2X = 18) in the *Brassica oleracea* genome (Figure S4C). This study analyzed the genomic distribution of 113 *FLZs* across the three *Brassica* species via data from the *Brassica* genome database, which revealed that the *FLZ* genes are located on multiple chromosomes. Moreover, the *FLZ* genes were unevenly distributed across the chromosomes in *Brassica rapa* and *Brassica nigra*, including one gene, designated *BcaFLZ36*, located on contig00301 in *Brassica rapa* (Figure S4A,B). However, the 36 *FLZ* genes in *Brassica oleracea* were relatively evenly distributed across the nine chromosomes (Figure S4C, Table S3).

During evolution, chromosomes are amplified in different genomic regions through fragment duplication, tandem duplication, and genome-wide duplication (WGD), which help expand gene families [35]. In this study, we analyzed gene duplication within the *FLZ* gene family via TBtools II software (https://github.com/CJ-Chen/TBtools; accessed on 20 April 2024) [36]. As depicted in Figure 3A–C, a total of 109 gene pairs across the three *Brassica* species presented signs of duplication events, with these gene pairs located on different chromosomes. Specifically, 36, 36, and 37 duplication events were identified in *Brassica rapa*, *Brassica nigra*, and *Brassica oleracea*, respectively (Table S4). *Brassica* species have undergone WGT events during their evolution [26], suggesting that these pairs of *FLZ* genes likely originated from WGD. Moreover, high-density *FLZ* gene clusters have been identified in certain chromosomal regions, such as chromosome 4 of *Brassica nigra*, which includes seven *BniFLZ* genes, *BniFLZ19–BniFLZ25*, spanning positions 48,783 kb to 48,891 kb. A chromosomal segment of no more than 200 kb that includes two or more genes is classified as a tandem duplication [37], which suggests that these *FLZ* genes may have originated from tandem duplication. In addition, we observed five additional tandem duplication events involving ten *FLZ* genes in the three *Brassica* species: *BcaFLZ13* and *BcaFLZ14*; *BcaFLZ32* and *BcaFLZ33*; *BniFLZ34* and *BcaFLZ35*; *BolFLZ14* and *BolFLZ15*; and *BolFLZ31* and *BolFLZ32* (Figure S4). Previous studies have indicated that WGD and tandem duplication exhibit a compensatory relationship in gene expansion, wherein WGD simultaneously increases the dosage of all genes, whereas tandem duplication promotes the formation of gene clusters on chromosomes [29]. Following WGD, the redundancy introduced by duplication may diminish the necessity for additional gene expansion via tandem duplication, resulting in a reduction in tandem gene arrays [29], which is consistent with the findings presented in this study. Taken together, these results suggest that the expansion of the *FLZ* gene family in *Brassica* species mainly originated from WGD, followed by tandem duplication.

We subsequently calculated the Ka/Ks ratio to gain a deeper understanding of the selective pressures on the *FLZ* genes of the three *Brassica* species. Generally, a Ka/Ks ratio greater than 1 indicates adaptive evolution under positive selection, a ratio of 1 indicates neutral selection, and a ratio less than 1 indicates negative or purifying selection [38]. In our study, the Ka/Ks ratios for the duplicated gene pairs were all less than 1 (Table S4), suggesting that the *FLZ* gene family has undergone purifying selection and maintained a high degree of conservation throughout its evolutionary history. This finding is consistent with earlier results from Ka/Ks analyses of *FLZ* genes in various plant species, including *Arabidopsis*, rice, potato, eggplant, and pepper [7,39].

To further investigate the evolutionary relationships among the three *Brassica* species, the genomes of *Brassica rapa* (Bca) and *Brassica nigra* (Bni) were analyzed alongside the *Brassica oleracea* (Bol) genome to examine the collinearity relationships within the *FLZ* gene family. Among the three *Brassica* species, a total of 316 collinear gene pairs were identified (Figure 3D, Table S5), which included 108 pairs between *Brassica rapa* and *Brassica oleracea*, 105 pairs between *Brassica oleracea* and *Brassica nigra*, and 103 pairs between *Brassica rapa* and *Brassica nigra*. Additionally, we examined the genomic collinearity between *Brassica oleracea* and *Arabidopsis thaliana* and identified 40 pairs (Table S5).

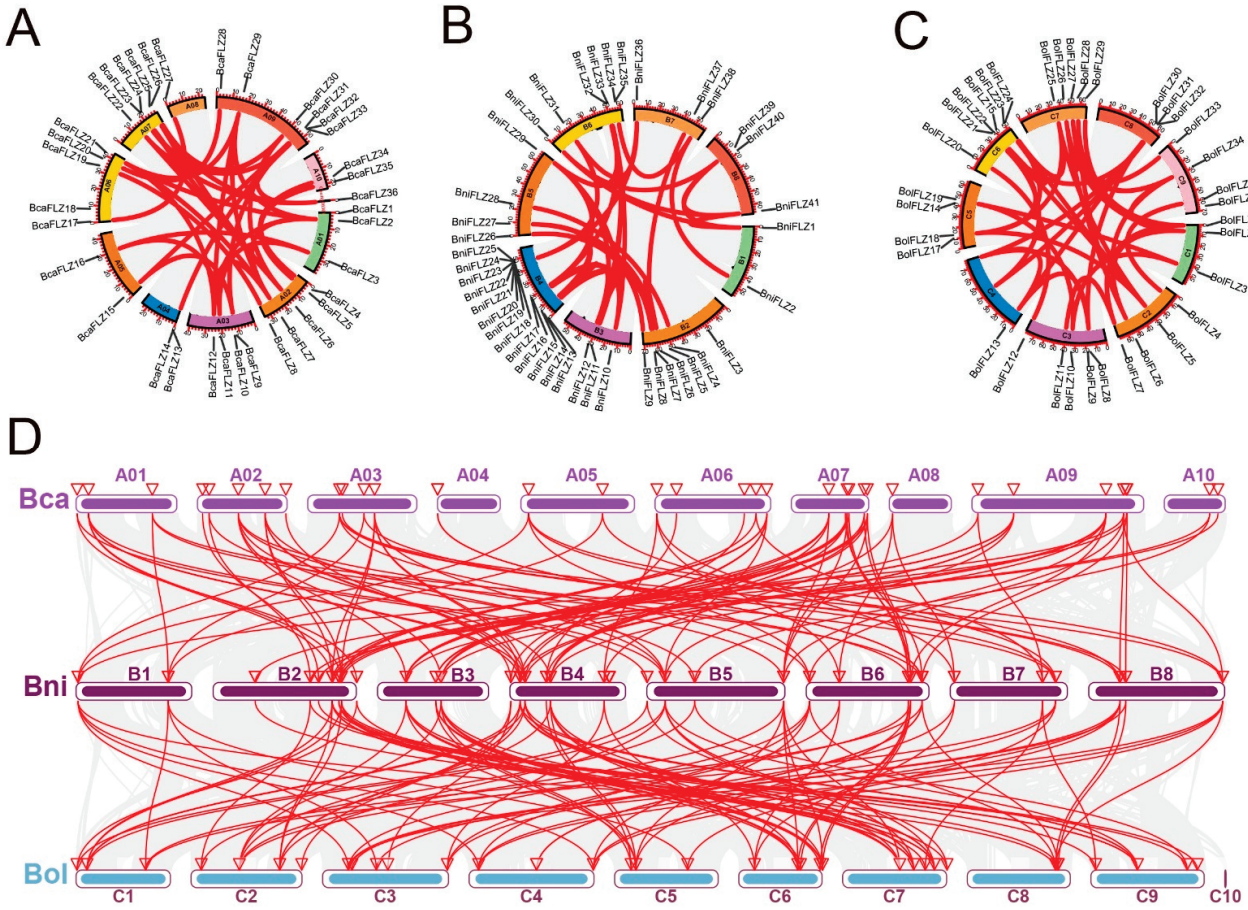


Figure 3. Gene position and collinearity analysis of the *FLZ* genes. Gene position and duplicated gene pairs in (**A**) *Brassica rapa*; (**B**) *Brassica nigra*; and (**C**) *Brassica oleracea*. Duplicated gene pairs are linked by red lines. (**D**) Synteny analyses of the *FLZ* genes between the three *Brassica* species. The gray lines indicate the synteny blocks between the genomes of the two species, whereas the red lines represent the syntenic pairs of the *FLZ* gene family between the genomes of the two species. A01–A10, B1–B8, and C1–C10 represent the chromosomes of the three species.

2.5. Cis-Acting Regulatory Elements in the Promoters of BolFLZ Genes

Chinese kale, which is native to southern China, is a significant vegetable among the *Brassica oleracea* species and is classified as part of the CC genome type [33,40]. In this study, our detailed research focused on the *BolFLZ* genes of Chinese kale among the three *Brassica* species analyzed herein.

Gene expression in distinct biological processes is regulated by upstream transcription factors that bind to specific promoter-associated cis-acting elements. Cis-acting elements play pivotal roles in gene expression regulation, and their identification is crucial for understanding the direct or indirect regulatory influences of specific factors. This process will deepen our understanding of the complexities of gene expression divergence, overlap, and redundancy within the *FLZ* gene family. Therefore, to explore the biological function of the *BolFLZ* genes, the 2000 bp upstream sequences of 36 *BolFLZ* genes were extracted via TBtools II software (https://github.com/CJ-Chen/TBtools; accessed on 20 April 2024) and then submitted to the PlantCARE platform for cis-acting regulatory element prediction. As shown in Figure 4 and Table S6, 36 *BolFLZ* genes were found to contain a total of 42 different cis-acting elements, which included the following: (1) hormone response elements sensitive to ABA, methyl jasmonate (MeJA), gibberellic acid (GA), and auxin; (2) stress-related elements associated with conditions such as drought, cold, and anaerobic induction; (3) cis-acting elements involved in plant growth and development; and (4) cis-acting elements related to light responsiveness. Taken together, the diversity of

these regulatory elements suggests that the *BolFLZ* gene family is closely associated with a wide range of biological activities and may act as key regulators, linking various hormone signaling pathways with other important biological functions.

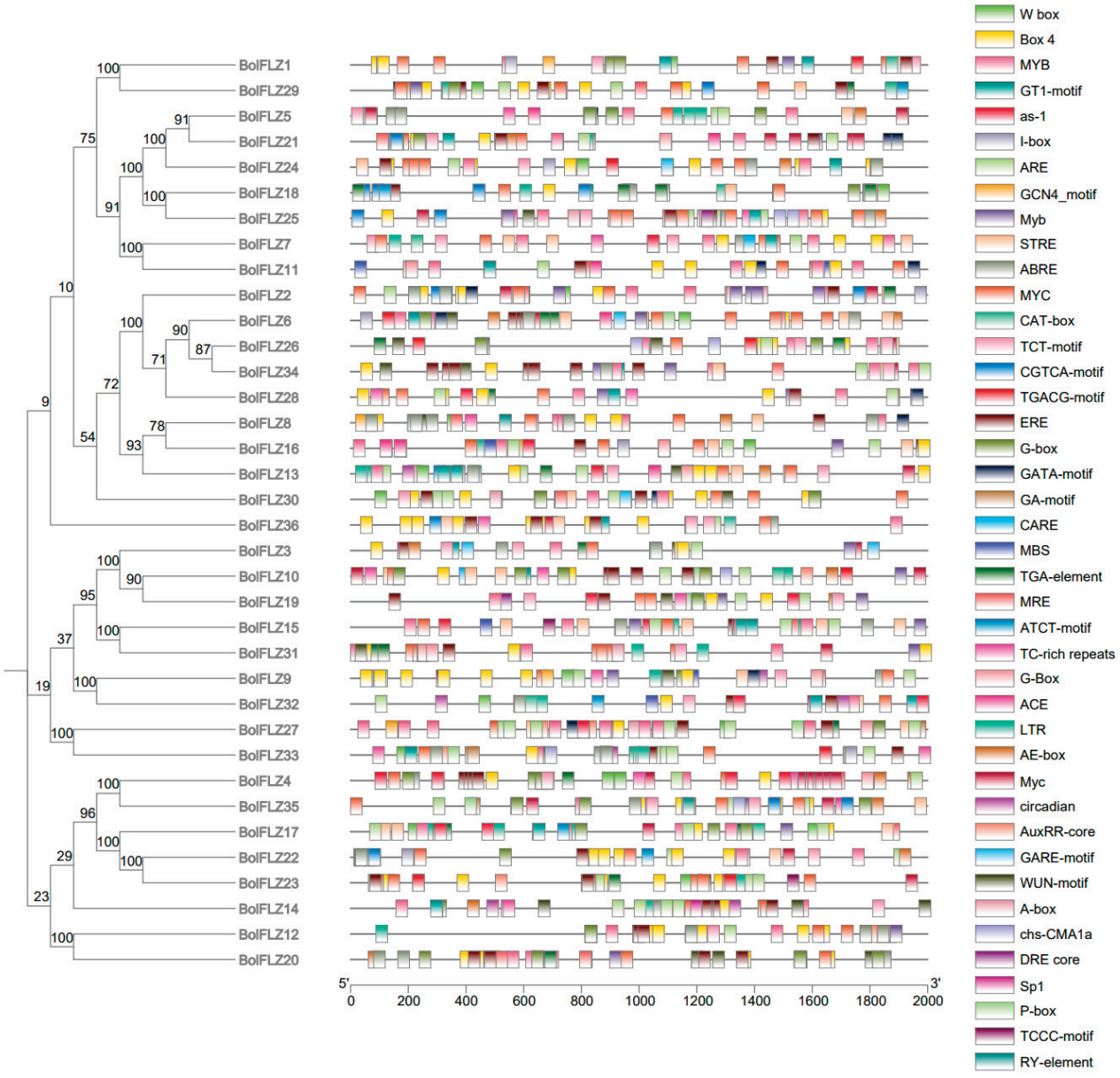


Figure 4. Analysis of cis-acting elements in the promoter regions of *BolFLZ*. The 2000 bp promoter region (upstream of the 5′UTR) of each *BolFLZ* gene was analyzed for cis-acting elements. Different cis-acting elements are indicated by different colors.

2.6. Expression Patterns of the BolFLZ Genes in Various Chinese Kale Tissues

The spatial expression pattern of a gene provides critical insights into its possible functions and regulatory roles within an organism. To elucidate the tissue-specific expression patterns of the *BolFLZ* genes in Chinese kale, we conducted qRT–PCR analysis to assess their relative expression levels across various tissues. We analyzed the tissue-specific expression profiles of the *BolFLZ* genes in various organs of Chinese kale, including the roots, leaves, and stems of 12-day-old plants; the floral buds of 12-week-old plants; the siliques of 18-week-old plants; and dry seeds, providing a broad representation of the plant's tissue types (Figure 5). Notably, most *BolFLZ* genes presented elevated expression levels in floral buds, roots, and siliques, whereas their expression was relatively low in leaves and dry seeds. Certain *BolFLZ* genes presented

pronounced tissue-specific expression. For example, *BolFLZ01*, *BolFLZ08*, and *BolFLZ29* were specifically and highly expressed in the roots of 15-day-old seedlings, with expression levels ranging from 3~100-fold higher than those in other tissues. In contrast, *BolFLZ03*, *BolFLZ14*, *BolFLZ18*, *BolFLZ26*, and *BolFLZ27* were preferentially expressed in floral buds, where their expression levels were 2~110-fold greater than those in the other tissues. Furthermore, *BolFLZ34* exhibited high and specific expression in dry seeds, with levels 3~30-fold higher than those in other tissues (Figure 5). qRT–PCR analysis revealed these differential expression patterns, suggesting diverse roles for *BolFLZ* genes in tissue-specific developmental processes and physiological functions within Chinese kale.

2.7. Subcellular Localization of Six Typical BolFLZ Proteins

The subcellular localization of a protein is essential for comprehending its function and significantly contributes to functional gene studies. Bioinformatics analyses indicated that BolFLZ proteins may localize in various cellular compartments, including the nucleus, cytoplasm, chloroplasts, and mitochondria (Table S1). To validate this prediction, we selected six representative BolFLZ proteins across four distinct clades (Figure 1): three proteins from clade I, the largest, and one protein from each of the remaining clades. NLS-mCherry served as a control for the nuclear localization signal, and six-week-old *Nicotiana benthamiana* leaf epidermal cells were employed to ascertain the subcellular localization of these proteins. Additionally, 35S-GFP was separately transformed as an additional control to verify that the detected subcellular localization patterns were not due to artifacts from the transformation process or the GFP tag. Confocal laser scanning microscopy revealed that the green fluorescent protein (GFP) fusion protein signals for BolFLZ1, 13, 26, 33, and 36 were present in both the nucleus and cytoplasm, resembling the distribution pattern of GFP alone (Figure 6). Notably, the BolFLZ18-GFP signals were exclusively localized to the nucleus (Figure 6). These findings are generally consistent with prior bioinformatics predictions, indicating that these proteins predominantly operate within the nucleus and cytoplasm, in line with observations in other species [7,11].

2.8. Interactions of BolFLZ Proteins with BolSnRK1 Proteins

Previous studies have shown that FLZ proteins can interact with the catalytic α subunits of SnRK1 in Arabidopsis, maize, and rice [5,15,16,22]. In this study, we performed a BLASTP search of the Chinese kale genome using the protein sequence of AtSnRK1.1 (AT3G01090.1) as a query and successfully identified two genes encoding the catalytic α subunit of SnRK1, hereafter referred to as BolSnRK1α1 and BolSnRK1α2. To explore the potential interactions between the BolFLZ proteins and the BolSnRK1α1 and BolSnRK1α2 proteins, a yeast two-hybrid assay was conducted. Thirteen BolFLZs from four distinct groups were chosen for this study. The selected proteins included BolFLZ01, BolFLZ17, BolFLZ18, BolFLZ23, BolFLZ29, BolFLZ33, and BolFLZ35 from Group I; BolFLZ02 and BolFLZ26 from Group II; BolFLZ13 from Group III; and BolFLZ19, BolFLZ31, and BolFLZ36 from Group IV (Figure 1). Furthermore, these proteins display a range of physicochemical properties and predicted subcellular localizations (Table S1), ensuring that the selected FLZ proteins accurately represent the broader FLZ gene family in Chinese kale. To this end, the full-length BolFLZs were fused to the GAL4 activation domain (AD), and BolSnRK1α1 and BolSnRK1α2 were fused to the DNA-binding domain (BD), resulting in the AD-BolFLZs and BD-BolSnRK1α1/α2 vectors, respectively. As anticipated, all thirteen AD-BolFLZs interacted with BD-BolSnRK1α1 and BD-BolSnRK1α2 but not with the empty BD vector (Figure 7). As shown in Figure 7, most of the BolFLZ proteins presented more robust growth in yeast cells cotransformed with BolSnRK1α2 than in those cotransformed with BolSnRK1α1 on high-strength selective media (SD–Trp/–Leu/–His/–Ade, SD-4), suggesting a potentially stronger binding affinity between the BolFLZ proteins and the BolSnRK1α2 protein. In contrast, BolFLZ26 displayed a weaker interaction with BolSnRK1α2 than with BolSnRK1α1, as indicated by the reduced growth of yeast transformants on SD-4 medium plates (Figure 7), highlighting the variability in protein–protein interaction strengths within the BolFLZ family.

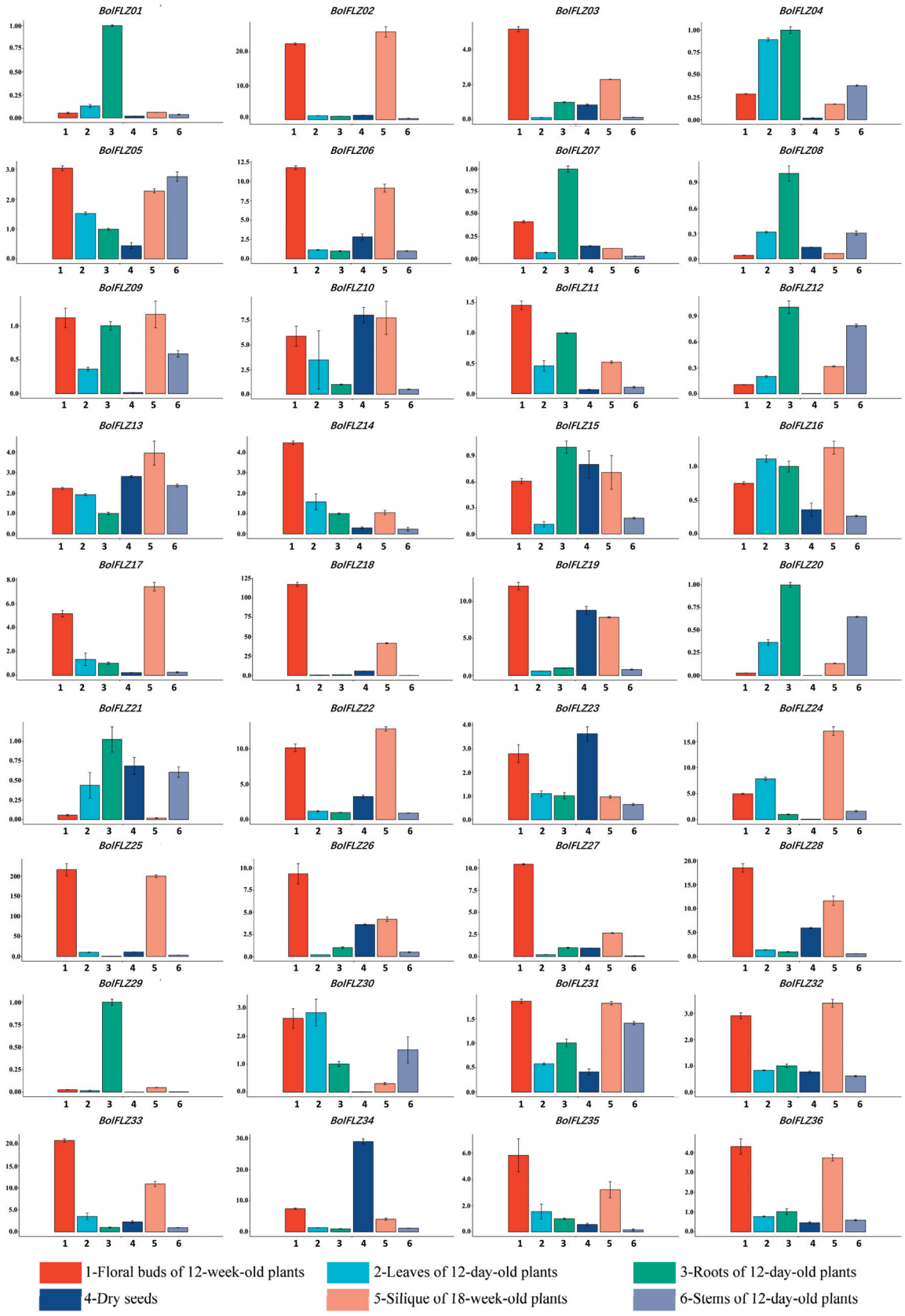


Figure 5. Expression profiles of the *BolFLZ* genes in different tissues. The expression profile data for the *BolFLZ* genes in various Chinese kale tissues were obtained through qRT–PCR. All analyses used *BolTubulin8* as an internal reference gene. The data shown are the means ± SDs of three biological replicates.

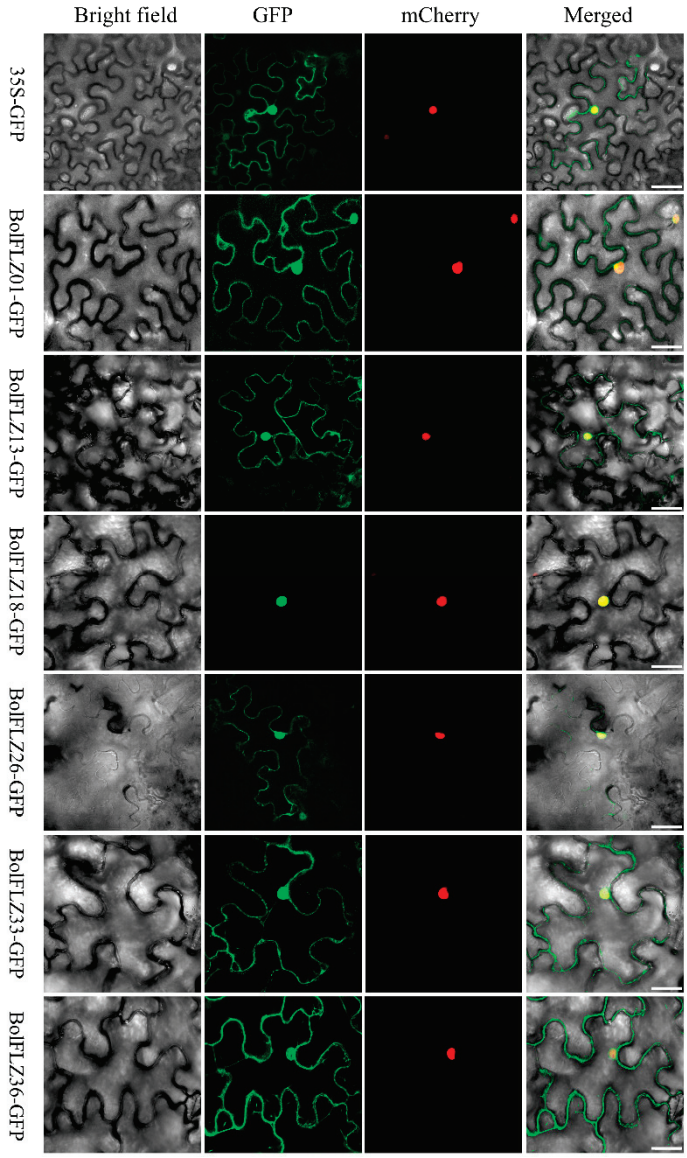


Figure 6. Subcellular localization of the six selected BolFLZ proteins. The BolFLZ-GFP fusion proteins, which were transiently expressed in tobacco (*Nicotiana benthamiana*) leaves, were observed via laser scanning confocal microscopy. The *35S-BolFLZ-GFP* constructs and *NLS-mCherry* (a nuclear marker) were cotransformed into the epidermal cells of tobacco. The *35S-GFP* construct served as a control. Scale bars represent 50 μm.

2.9. Expression Patterns of the BolFLZs in Response to Abiotic Stresses

Chinese kale is classified as an environmentally sensitive leafy vegetable and is particularly susceptible to abiotic stresses [40,41]. In the Arabidopsis genome, a total of 19 *FLZ* genes have been identified, the majority of which exhibit active responses to various stress treatments [17]. Previous studies have reported that *FLZ* genes in other plant species are also closely associated with stress responses [5,11,22]. According to cis-acting element analysis, all the *BolFLZ* promoters contained cis-acting elements associated with stress responsiveness (Figure 4). To elucidate the potential functions of the *BolFLZ* gene family, we analyzed the expression patterns of 15 selected *BolFLZ* genes from four distinct subfamilies under different abiotic stresses, including heat, cold, drought, and salt, via qRT–PCR. Given that ABA is the most critical stress phytohormone [42], we also examined the responsiveness of the *BolFLZ* genes to ABA treatment.

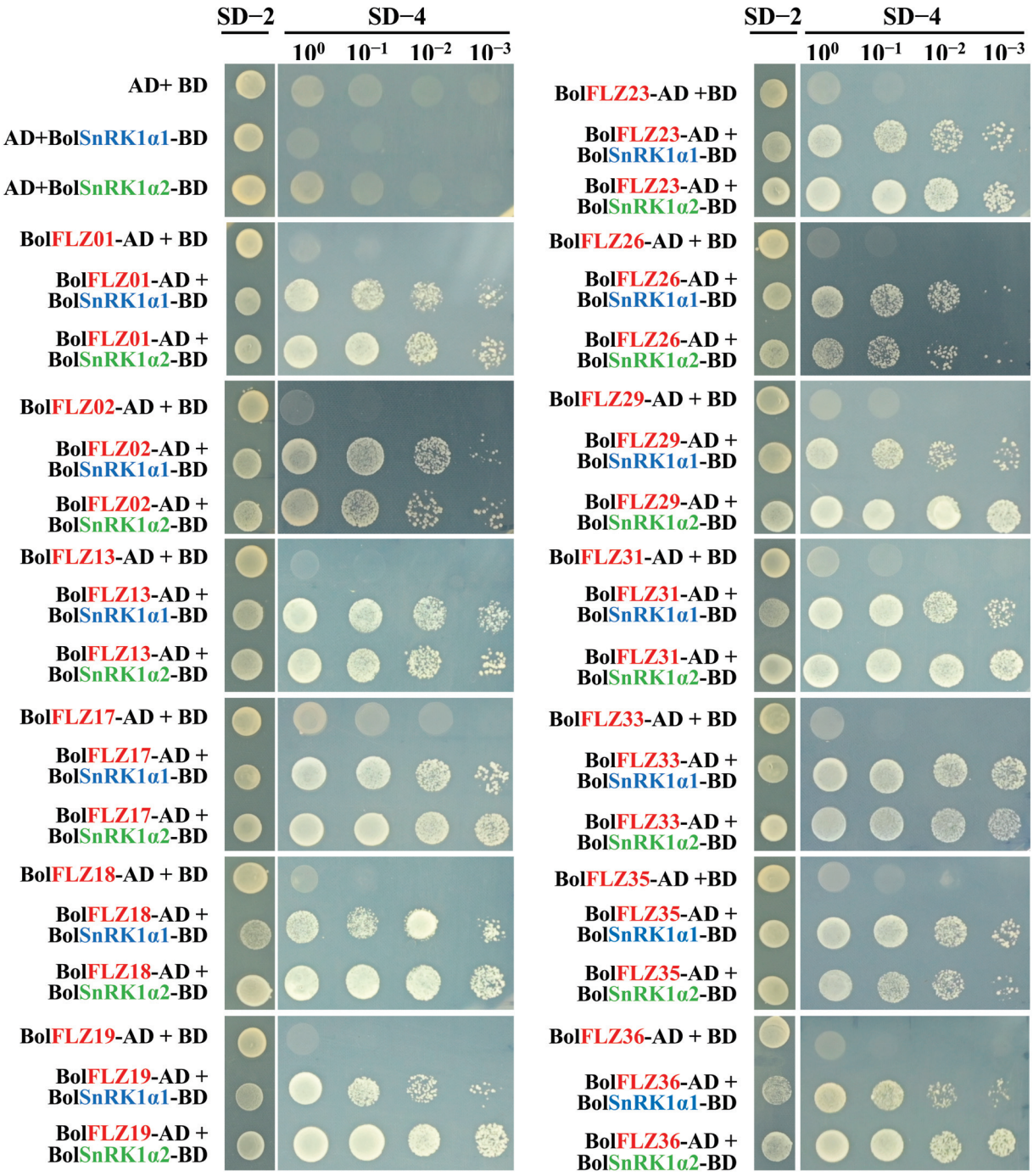


Figure 7. Thirteen selected BolFLZs interact with BolSnRK1α1 and BolSnRK1α2 in yeast cells. BolSnRK1α1 and BolSnRK1α2 were fused to the activation domain (AD), and the full-length BolFLZ protein was fused to the DNA-binding domain (BD). Cotransformed yeast clones were drip-inoculated onto SD/-Leu-Trp (SD-2) and SD/-Leu-Trp-His-Ade (SD-4) plates to test the interaction and subsequently cultured in a growth chamber.

The results indicated that the expression levels of the *BolFLZ* genes could be influenced by various stress treatments, and these genes appeared to respond relatively consistently to different stress treatments, with 10 genes upregulated and 5 genes downregulated (Figure 8). Under heat treatment, the expression levels of 6 genes—*BolFLZ09*, *BolFLZ18*, *BolFLZ20*, *BolFLZ25*, *BolFLZ27*, and *BolFLZ33*—increased 3- to 20-fold, whereas the expression levels of *BolFLZ01*, *BolFLZ23*, and *BolFLZ31* significantly decreased. In contrast, the expression of

BolFLZ19 initially decreased before increasing, whereas the expression of *BolFLZ30* initially increased before decreasing. Cold stress also had a strong effect on the expression of these 15 *BolFLZ* genes, with most being significantly upregulated, including *BolFLZ02*, *BolFLZ09*, *BolFLZ16*, *BolFLZ18*, *BolFLZ20*, *BolFLZ25*, *BolFLZ27*, *BolFLZ33*, and *BolFLZ36*, among which *BolFLZ09* and *BolFLZ30* presented the most significant increases. In contrast, the expression levels of *BolFLZ13* and *BolFLZ31* significantly decreased. Additionally, the expression levels of *BolFLZ01* and *BolFLZ23* were downregulated during the initial phase of cold treatment and subsequently upregulated after 12 h. Under salt treatment, the expression levels of *BolFLZ09*, *BolFLZ18*, *BolFLZ20*, *BolFLZ27*, and *BolFLZ33* were elevated at nearly all the analyzed time points. The expression levels of *BolFLZ19*, *BolFLZ23*, and *BolFLZ31* significantly decreased following salt treatment. PEG-simulated drought stress (20% PEG 4000) resulted in increased expression levels of *BolFLZ09*, *BolFLZ18*, *BolFLZ25*, and *BolFLZ27* at most analyzed time points. The expression levels of *BolFLZ01*, *BolFLZ23*, and *BolFLZ31* were inhibited by PEG. Interestingly, the expression levels of *BolFLZ20*, *BolFLZ33*, and *BolFLZ36* decreased after 2 h of PEG4000 treatment but subsequently increased at the other analyzed time points.

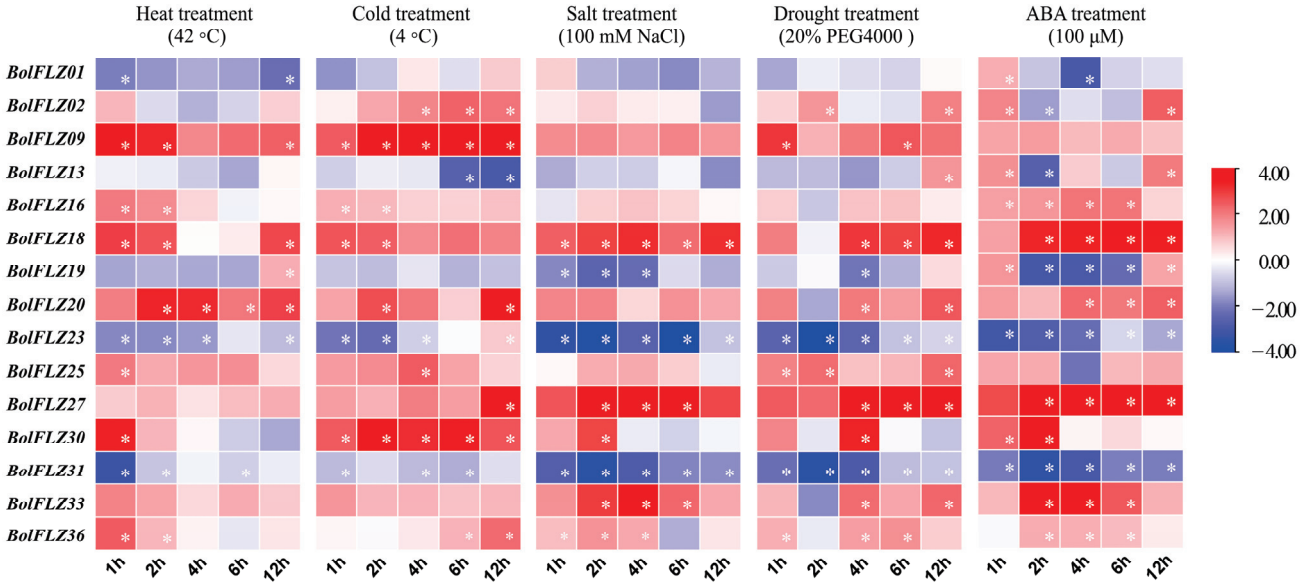


Figure 8. Analysis of *BolFLZ* gene expression under abiotic stress conditions via qRT–PCR. Heat (42 °C), cold (4 °C), salt (NaCl), drought (PEG4000), and hormone (ABA) stresses were applied to 12-day-old Chinese kale plants to analyze the responsiveness of the *BolFLZ* genes. Samples collected from well-watered Chinese kale plants served as controls. The relative expression levels of the *BolFLZ* genes were determined via qRT–PCR following treatment durations of 1 h, 2 h, 4 h, 6 h, and 12 h. The expression levels of related genes were calculated via the $2^{-\Delta\Delta Ct}$ method, with 0 h used as a control. The data were subsequently converted to log2FC values and visualized via TBtools II. The values for each time point represent the means of three biological replicates. The red and blue colors indicate increased and decreased expression levels, respectively, relative to those in the control. * refers to significant differences with $p < 0.05$ compared with the corresponding 0 h controls.

Finally, we assessed the response of these 15 *BolFLZ* genes to ABA. The results demonstrated that the expression levels of *BolFLZ16*, *BolFLZ18*, *BolFLZ20*, *BolFLZ27*, *BolFLZ33*, and *BolFLZ36* were significantly upregulated following ABA treatment, whereas the expression levels of *BolFLZ23* and *BolFLZ31* were significantly inhibited by ABA treatment. The expression level of *BolFLZ01* increased during the first hour of ABA treatment but subsequently decreased. The expression levels of *BolFLZ02*, *BolFLZ13*, *BolFLZ19*, and *BolFLZ25* decreased at specific time points but increased at 1 h and 12 h after ABA treatment. These results suggest that different *BolFLZ* genes may play distinct roles in the stress response to various environmental stresses.

As described above, most *BolFLZ* genes tended to be upregulated in response to all abiotic stresses in this study (Figure 8), suggesting that the *BolFLZ* gene family may play a positive role in stress tolerance in Chinese kale. Notably, five members (*BolFLZ09*, *BolFLZ18*, *BolFLZ20*, *BolFLZ27*, and *BolFLZ30*) were significantly upregulated in response to all the treatments. Among them, *BolFLZ30* stands out for its robust induction, ranging from 10- to 40-fold greater than that of the control samples under the various stress treatments, suggesting a significant role in mediating stress responses in Chinese kale. In contrast, the expression levels of two members (*BolFLZ23* and *BolFLZ31*) were significantly inhibited under various stress conditions, suggesting that these genes may be negatively regulated in such scenarios. However, only a few genes, such as *BolFLZ02*, exhibit disordered expression patterns under abiotic stress.

Furthermore, the expression levels of the *BolFLZ* genes appear to be more sensitive to ABA treatment than to other stress treatments (Figure 8). This heightened sensitivity suggests that the *BolFLZ* genes may play a pivotal role in the ABA signaling pathway in plants, which is essential for adapting to environmental stresses such as drought, cold, and high salinity. The ABA-induced changes in the expression of the *BolFLZ* genes may represent a key mechanism through which plants fine-tune their stress responses, potentially leading to more efficient adaptation and survival strategies under adverse conditions. However, further research is necessary to validate these findings and explore this hypothesis in future studies.

Taken together, the varied expression patterns of *BolFLZ* genes under different abiotic stresses suggest the complex involvement of this gene family in stress responses, highlighting the need for further investigation into their role in plant abiotic stress.

3. Discussion

3.1. Conservation and Evolution of the FLZ Gene Family in Brassica Species

The FLZ genes constitute a poorly studied gene family that is widely present in plants, and their biological functions are only just beginning to be explored [2,13]. Molecular function studies on the *FLZ* genes of Arabidopsis and rice have revealed the crucial role of this gene family in regulating plant growth and development as well as stress responses [8,9,13,22]; however, this gene family has not been examined in *Brassica* species, which are classical model organisms for investigating polyploid evolution [30]. These species have gained increasing attention because of their significant economic value. Previous studies have shown that Arabidopsis and the *Brassica* lineage diverged ~24 million years ago [25]. *Brassica* subsequently underwent a unique WGT, followed by extensive gene loss, gene acquisition, and chromosomal rearrangements involving partial duplications and deletions [26]. Although complete genome sequences are available, the *FLZ* genes in *Brassica* species have yet to be identified and comprehensively analyzed. To further our understanding of the *FLZ* gene family, we systematically analyzed *FLZ* family genes in three diploid *Brassica* species (*Brassica rapa*, *Brassica nigra*, and *Brassica oleracea*) and discovered potential candidate genes for further functional analysis.

The number of *FLZ* genes varies significantly among species, with 19 identified in Arabidopsis [1], 37 in maize [5], 29 in rice [22], 19 in tomato [7], and 21 in liquorice [11]. In this study, a total of 113 *FLZ* genes were identified across the three *Brassica* species, including 36 each in *Brassica rapa* and *Brassica oleracea* and 41 in *Brassica nigra* (Figure 1 and Table S2). These *Brassica* species have a similar number of *FLZ* genes as maize but significantly more than most other plants. The variations in the number of *FLZ* genes among species may arise from the evolutionary and domestication processes of these species. Furthermore, structural characterization revealed that these *FLZ* genes had highly conserved structural domains; however, the protein length, number of motifs, and composition of each family varied significantly (Figure 2). Notably, excluding *BcaFLZ14*, which contains five introns, the 112 *FLZ* genes possess only one intron (Figure S1), indicating that *FLZ*s are associated with the response to both biotic and abiotic stress since genes responsive to stress exhibit

fewer introns [43]. In this study, the FLZ proteins in the *Brassica* species were grouped into four monophyletic branches on the basis of protein sequence identity (Figure 1), which is consistent with previous findings in four *Solanaceae* species [7]. In addition, different subgroups may be responsible for varying functions.

Gene duplication not only expands the genome content but also diversifies gene function to ensure the optimal adaptability and evolution of plants [35,44]. In this study, 109 gene pairs were found to be collinear and dispersed across different chromosomes (Figure 4), suggesting that WGD significantly contributed to the expansion of the *FLZ* family in the three *Brassica* species. Moreover, the greater number of *FLZ* paralogues in *Brassica* is consistent with the extensive history of gene/genome duplication events in this species [26]. Theoretically, the number of *FLZ* genes in *Brassica* species is expected to be three- to six-fold greater than that in Arabidopsis because of WGT events. However, the reduced copy number of FLZ proteins in the three diploid *Brassica* species suggests that certain members of the *FLZ* family may have been lost or undergone genetic alterations during evolution, as previously mentioned [45,46]. This loss or alteration may be due to the fact that, during the prolonged course of natural selection, the number of *FLZ* genes was likely sufficient for *Brassica*, resulting in the nonretention of some duplicated *FLZ* genes within the *Brassica* genome. The duplicates retained in the genome primarily provided adaptive advantages, including enhanced stress tolerance and reproductive benefits under challenging conditions [28].

3.2. FLZ Proteins Mediate Protein Interactions

The FLZ domain is regarded as the canonical protein–protein interaction module of FLZ proteins, enabling these proteins to serve as molecular scaffolds that promote extensive interactions with diverse proteins, such as kinases and transcription factors, thereby contributing significantly to numerous cellular processes [39,47]. Among these proteins, SnRK1 is recognized as the first protein identified to interact with FLZ domain-containing proteins, resulting in the formation of a complex that plays a critical role in regulating glucose homeostasis, developmental transitions, and stress signaling through its interaction with the SnRK1α subunit [1,5,15]. For example, OsFLZ18 specifically binds to SnRK1A, thereby suppressing the expression of the αAmy3 gene, a crucial positive regulator of rice flooding tolerance [22]. In Arabidopsis, FLZ6 and FLZ10 form a complex with SnRK1 near the endoplasmic reticulum (ER) while modulating the levels of SnRK1α in response to energy availability [16]. In this study, we identified BolSnRK1α1 and BolSnRK1α2, two genes that encode the SnRK1 catalytic α subunits in Chinese kale, and demonstrated their significant interaction with BolFLZs through yeast two-hybrid analysis (Figure 8), which is consistent with previous reports in maize, tomato, and liquorice [5,7,11]. However, the underlying molecular mechanism remains elusive in these plants. Overall, these findings indicate that the SnRK1α-FLZ regulatory module is conserved in Chinese kale, highlighting its potential as a fundamental component in the plant stress response and developmental mechanisms.

Recently, Yang et al. (2023) identified seven FLZ proteins in Arabidopsis as previously uncharacterized ATG8-interacting partners that function as repressors of SnRK1 signaling, negatively modulating autophagy and plant tolerance to carbon starvation. In addition to those in Arabidopsis, the ATG8-FLZ-SnRK1 regulatory modules in maize have been confirmed to regulate plant tolerance to energy starvation and appear to be highly conserved in seed plants [13]. Protein sequence analysis revealed that the canonical EDYTLV sequence within the FLZ domain, referred to as the AIM, is crucial for determining whether FLZ binds to ATG8 [13]. In this study, we identified 37 FLZ proteins containing AIM motifs (EDYTLV) in the three *Brassica* species (Table S2) that exhibit a highly conserved AIM (Figure S3). Considering the conservation of the ATG8-FLZ-SnRK1 regulatory axis throughout the evolutionary history of seed plants, we suspect that AIM-containing FLZs might interact with ATG8 in *Brassica* species. However, this hypothesis requires future experimental validation.

Furthermore, research indicates that the FLZ proteins exhibit homo- and heterodimerization properties. In Arabidopsis, a yeast two-hybrid assay demonstrated that FLZ7, FLZ10, FLZ12, and FLZ15 exhibit homologous dimerization and strong heterodimerization with other FLZ proteins, whereas FLZ1, FLZ6, and FLZ11 interact specifically with only one or two FLZ proteins [15]. These multiprotein complexes may possess promiscuous interaction properties that facilitate the recruitment of additional subunits to the complex [15]. In plants, including *Brassica* species, we hypothesize that there is a high probability of selective interactions among FLZ proteins, potentially leading to the assembly of homo- and heterodimers. However, to our knowledge, similar reports have not been published in species besides Arabidopsis.

3.3. Potential Roles of BolFLZ Family Genes in Abiotic Stress Responses

Chinese kale (*Brassica oleracea* var. *alboglabra*), which is native to China and cultivated primarily in South China and Southeast Asia, is valued for its flavor and nutritional benefits, including its ability to produce vitamin C, carotenoids, phenolics, and glucosinolates [33,48]. However, similar to other *Brassica* vegetables, Chinese kale is highly sensitive to abiotic stress, such as extreme temperatures, drought, and altered salinity, which frequently results in reduced yield and quality [40]. Hence, identifying genes that respond to abiotic stress is a critical initial step towards breeding cultivars with improved stress tolerance.

The available evidence indicates a significant role for the *FLZ* gene family in plant stress tolerance and adaptive growth [17]. For example, TaFLZ2D functions as a positive regulator of salt stress tolerance by enhancing ion stress tolerance and reactive oxygen species (ROS) detoxification capabilities in wheat [6]. OsFLZ18 negatively regulates flood tolerance in rice by interacting with SnRK1A and suppressing its transcriptional activation of the αAmy3 gene [22]. Virus-induced gene silencing (VIGS) experiments indicated that both SlFLZ2 and SlFLZ18 play positive roles in heat tolerance in tomato [7]. Despite these findings, the precise roles of the FLZ proteins in the growth and development of *Brassica* species, particularly in response to abiotic stress, remain to be fully characterized.

Bioinformatic analysis revealed that the promoters of the *BolFLZ* genes contain various cis-regulatory elements involved in regulating plant growth and development, hormone signal transduction, and stress responses. This finding is supported by qRT–PCR evidence that the expression of the *BolFLZ* genes fluctuates significantly under various abiotic stresses (Figure 8). The majority of these genes are positively regulated by stress, whereas a minority, such as *BolFLZ23* and *BolFLZ31*, exhibit downregulated expression. However, how these genes are involved in regulating stress responses in Chinese kale requires further research and deserves further study in our future work, particularly the role of the FLZ proteins in heat tolerance, which is crucial because the sensitivity of Chinese kale to heat limits its distribution and production [40].

4. Materials and Methods

4.1. Plant Materials and Growth Conditions

Chinese kale (*Brassica oleracea* L. var. *alboglabra*) for tissue-specific expression analysis was cultivated in a glasshouse at 25 °C under a 16 h/8 h light/dark photoperiod. For the abiotic stress treatments, the seeds were surface sterilized in 75% (*v*/*v*) ethanol for 15 s, followed by 0.6% (*v*/*v*) sodium hypochlorite solution for 15 min, and then rinsed three times with sterile water. These sterilized seeds were cultured on 1/2 MS media for 7 days at 25 °C and then transferred to a simple hydroponic culture system utilizing 1/2 Hoagland nutrient solution (pH 5.8–6.0). After 5 days of growth, the seedlings were subjected to various treatments, including heat stress (42 °C), cold stress (4 °C), 100 mM NaCl (at 25 °C), 100 μM ABA (at 25 °C), and 20% PEG4000 (at 25 °C). Following treatments lasting 0 h, 1 h, 2 h, 4 h, 6 h, and 12 h, the leaves of three seedlings were pooled to form one sample, harvested, and frozen in liquid nitrogen for RNA isolation. All the experiments were conducted with three independent biological replicates.

4.2. Database Searches and Sequence Retrieval

The genomic data for Chinese cabbage (*Brassica rapa*; Bca), black mustard (*Brassica nigra*; Bni), and Chinese kale (*Brassica oleracea*; Bol) are sourced from the following links: http://tbir.njau.edu.cn/NhCCDbHubs/downloadFile_fileShow.action (accessed on 23 March 2024) [49], https://cruciferseq.ca/Bnigra_download (accessed on 23 March 2024) [27], and https://ngdc.cncb.ac.cn/gwh/Assembly/83516/show (accessed on 23 March 2024) [50]. *AtFLZ* and *AtSnRK1α* data were downloaded from the TAIR database (https://www.arabidopsis.org/; accessed on 20 March 2024). *OsFLZ* data were downloaded from the RGAP database (http://rice.plantbiology.msu.edu/; accessed on 20 March 2024).

To identify *FLZ* gene family members in the three *Brassica* species, we employed a multistep approach. Initially, we conducted a BLASTP search using previously reported Arabidopsis *FLZ* gene family protein sequences. Concurrently, we utilized the hidden Markov model (HMM) of the FLZ family protein structure obtained from the Pfam database (http://pfam.sanger.ac.uk; accessed on 28 March 2024) to search for protein sequences containing the characteristic domain (PF04570). Candidate genes were selected by intersecting the results from these two methods. We subsequently verified the structural domains of the candidate proteins via online analysis tools from Pfam (http://pfam.xfam.org/; accessed on 6 April 2024), NCBI Batch CD Search (https://www.ncbi.nlm.nih.gov/Structure/bwrpsb/bwrpsb.cgi; accessed on 6 April 2024), and SMART (http://smart.embl-heidelberg.de/; accessed on 6 April 2024). Finally, we manually screened nonredundant putative FLZ sequences, removing those lacking the complete FLZ domain or containing incomplete FLZ domains.

The physicochemical properties of the deduced FLZ protein sequences, including pI, MW, GRAVY, and hydrophilicity, were estimated via the ProtParam tool (https://web.ExPASy.org/protparam/; accessed on 10 April 2024). The subcellular localization of FLZ proteins in the three *Brassica* species was predicted via the WoLF PSORT web server (https://wolfpsort.hgc.jp/; accessed on 10 April 2024).

4.3. Sequence Alignment and Phylogenetic Analysis of the FLZ Proteins

The full-length sequences of FLZ proteins from three *Brassica* species, Chinese cabbage, black mustard, and Chinese kale, as well as Arabidopsis and rice, were used to construct phylogenetic trees via the MUSCLE method in the software MEGA X (version 11.0). Multiple sequence alignments were performed via the default parameters of ClustalW within the MEGA X program. The phylogenetic trees were constructed via the neighbor–joining (NJ) method on the basis of the p-distance model. Bootstrap analysis with 1000 replications was performed to validate the trees. The trees were then visualized via the online tool iTOL (https://itol.embl.de/upload.cgi; accessed on 15 November 2024).

4.4. Genomic Structure, Motif, and Domain Analyses of FLZ Members in the Three Brassica Species

To illustrate the exon/intron profiles of *FLZ* genes in the three *Brassica* species, the Gene Structure Display Server program (GSDS, http://gsds.gao-lab.org/; accessed on 20 April 2024) was used on the basis of a comparison between CDS and genomic DNA sequences. To better illustrate the structural relationships of the *FLZ* genes in the three *Brassica* species, the gene structures of the three *Brassica* species were visualized via TBtools II software (https://github.com/CJ-Chen/TBtools; accessed on 20 April 2024) [36].

For the identification of conserved motifs, the FLZ protein sequences from the three *Brassica* species were uploaded to the MEME program (http://meme-suite.org/tools/meme; accessed on 21 April 2024), setting the number of motifs to identify as 15, with other parameters remaining at their default values [51]. The results were visualized via TBtools II software (https://github.com/CJ-Chen/TBtools; accessed on 20 April 2024).

4.5. Analysis of the Cis-Regulatory Elements in the Promoters of FLZ Genes

TBtools II software (https://github.com/CJ-Chen/TBtools; accessed on 20 April 2024) was used to extract the promoter regions 2000 bp upstream of the translation start codons (ATG) in the three *Brassica* species [36]. The sequences were submitted to the online database PlantCARE (http://bioinformatics.psb.ugent.be/webtools/plantcare/html/; accessed on 22 April 2024) for analysis of cis-acting elements [52]. Gene information and cis-acting element information were submitted to the GSDS (http://gsds.gao-lab.org/; accessed on 22 April 2024) website to obtain a map of the cis-acting elements for visualization [53].

4.6. Subcellular Localization Assays in Nicotiana benthamiana Leaves

We assessed the subcellular localization of the BolFLZs through transient expression assays in the leaf epidermal cells of 6-week-old *Nicotiana benthamiana*. The full-length coding sequences (CDSs) of the *BolFLZs* were subsequently cloned and inserted into the binary vector pCambia1300-UBQ-GFP in frame with a GFP tag at the C-terminus; the primers used are listed in Table S7. The fusion constructs were cotransfected into tobacco leaves along with a nuclear localization marker (NLS-mCherry) via an agroinoculation assay. A Zeiss LSM 800 confocal laser scanning microscope (Germany) was used to determine the localization of the target proteins three days postinoculation.

4.7. RNA Isolation and Quantitative Real-Time PCR Analysis

Total RNA was extracted from multiple tissues of *Brassica* plants at different developmental stages via the Eastep™ Universal RNA Extraction Kit (Promega, Shanghai, China). Samples were collected from the roots, leaves, and stems of 12-day-old plants; the floral buds of 12-week-old plants; the siliques of 18-week-old plants; and dry seeds. The quality and concentration of the extracted RNA were assessed via a NanoDrop 2000 spectrophotometer (Thermo Fisher Scientific, Waltham, MA, USA). cDNA synthesis was performed using 2 μg of total RNA from each sample via the TransScript All-in-One First-Strand cDNA Synthesis Kit (Vazyme, Nanjing, China) following the manufacturer's protocol. The synthesized cDNA was diluted and used as a template for quantitative real-time PCR (qRT–PCR). Specific primers for qRT–PCR were designed via the PrimerQuest Tool (https://sg.idtdna.com/PrimerQuest/Home/Index; accessed on 28 April 2024) and subsequently validated for specificity via TBtools II software (https://github.com/CJ-Chen/TBtools; accessed on 20 April 2024) (Table S7). The *BolTubulin8* housekeeping gene served as an internal control to normalize expression data and account for variations in sample loading and amplification efficiency [41]. Ct values for *BolTubulin8* ranging from 20 to 25 are considered effective. Reactions were conducted in a 10 μL volume containing diluted cDNA, specific primers, and SYBR Green PCR Master Mix (Vazyme, Nanjing, China). Amplification and detection were performed on a CFX96 real-time system (Bio-Rad, California, USA). The thermal cycling conditions were as follows: initial denaturation at 95 °C for 1 min, followed by 45 cycles of denaturation at 95 °C for 10 s, and annealing/extension at 60 °C for 15 s. The melting curve program consisted of a continuous increase in temperature from 60 °C to 95 °C, with continuous fluorescence measurements. The relative expression levels of the target genes were calculated via the comparative CT ($2^{-\Delta\Delta CT}$) method. The specific primers used for each gene are detailed in Table S7.

4.8. Yeast Two-Hybrid Assay

The yeast two-hybrid assay was conducted according to the manufacturer's protocols (Clontech, Mountain View, CA, USA). The cDNAs encoding the BolSnRK1α1 and BolSnRK1α2 proteins were subsequently cloned and inserted into the pGBKT7 vector to serve as bait constructs, and the cDNAs of the BolFLZ family members were subsequently cloned and inserted into the pGADT7 vector to serve as prey constructs. The specific primers used in these cloning procedures are detailed in Table S7. The yeast strain AH109 was cotransformed with different combinations of these vectors. Protein–protein

interactions were assessed by cultivating the yeast transformants on synthetic dropout (SD/-His/-Trp) and synthetic quadruple dropout (SD/-His/-Trp/-Leu/-Ade) solid media and incubating them at 30 °C for 3–5 days to assess the growth of colonies. To assess the strength of these interactions, a serial dilution of the yeast suspension was conducted to establish a 10-fold concentration gradient, and yeast growth was monitored across varying dilution levels. Standardized photography was employed to maintain consistency in evaluating colony growth. All experiments were conducted with three biological replicates to ensure the reproducibility of the interaction strengths observed.

4.9. Statistical Analysis

Microsoft Excel 2021 was used for data entry and statistical analysis, and GraphPad Prism 9.5 (GraphPad Software, LLC, San Diego, CA, USA) was used to generate the bar graphs.

5. Conclusions

In this study, a total of 113 *FLZ* genes were identified in the three *Brassica* species and classified into four groups. Chromosomal mapping and synteny analysis revealed that the 113 *FLZ* genes were distributed across all chromosomes, with some gene clustering. WGD and tandem duplication were identified as the main causes of FLZ gene expansion in the three *Brassica* species. The *FLZ* genes all contain the zf-FLZ domain and have few introns, suggesting that they function as stress response factors. A total of 13 representative BolFLZ proteins from distinct groups interact with BolSnRK1α1 and BolSnRK1α2. Furthermore, qRT–PCR analysis revealed that the expression levels of the *BolFLZ* genes varied across different tissues and were significantly altered in response to heat, cold, drought, salt, or ABA stresses, highlighting their potential roles in environmental adaptation in Chinese kale. This study enhances our understanding of the *FLZ* genes in *Brassica* species and paves the way for further exploration of the functions of the *BolFLZ* genes in Chinese kale. Future studies should focus on elucidating the underlying mechanisms to investigate their potential roles in stress signaling pathways. Furthermore, investigating the interactions between the BolFLZ proteins and other key regulatory proteins may reveal novel mechanisms of stress response and adaptation in *Brassica* species.

Supplementary Materials: The following supporting information can be downloaded at: https://www.mdpi.com/article/10.3390/ijms252312907/s1.

Author Contributions: Z.C., S.C., M.Q., and R.L. conceived and designed this research; Z.C., Y.Z., S.C., K.S., and B.Y. performed the experiments; Z.C., Y.Z., and M.Q. analyzed the data; S.C., and J.L. provided suggestions for the experiments. Z.C. wrote the manuscript. Z.C. and Y.Z. revised the manuscript. All authors have read and agreed to the published version of the manuscript.

Funding: This work was supported by the Guangdong Basic and Applied Basic Research Foundation (2024A1515010688, 2023B1515120050, and 2021A1515012523).

Institutional Review Board Statement: Not applicable.

Informed Consent Statement: Not applicable.

Data Availability Statement: Data will be made available upon request.

Acknowledgments: The authors thank Lubin Zhang for providing valuable suggestions for the experiments.

Conflicts of Interest: The authors declare no conflicts of interest.

References

1. Nietzsche, M.; Schießl, I.; Börnke, F. The Complex Becomes More Complex: Protein-Protein Interactions of SnRK1 with DUF581 Family Proteins Provide a Framework for Cell- and Stimulus Type-Specific SnRK1 Signaling in Plants. *Front. Plant Sci.* **2014**, *5*, 54. [CrossRef] [PubMed]
2. Jamsheer K, M.; Laxmi, A. DUF581 Is Plant Specific FCS-Like Zinc Finger Involved in Protein-Protein Interaction. *PLoS ONE* **2014**, *9*, e99074. [CrossRef]

3. He, Y.; Tang, W.; Swain, J.D.; Green, A.L.; Jack, T.P.; Gan, S. Networking Senescence-Regulating Pathways by Using Arabidopsis Enhancer Trap Lines. *Plant Physiol.* **2001**, *126*, 707–716. [CrossRef]
4. He, Y.; Gan, S. A Novel Zinc-Finger Protein with a Proline-Rich Domain Mediates ABA-Regulated Seed Dormancy in Arabidopsis. *Plant Mol. Biol.* **2004**, *54*, 1–9. [CrossRef]
5. Chen, S.; Li, X.; Yang, C.; Yan, W.; Liu, C.; Tang, X.; Gao, C. Genome-Wide Identification and Characterization of FCS-Like Zinc Finger (FLZ) Family Genes in Maize (*Zea mays*) and Functional Analysis of *ZmFLZ25* in Plant Abscisic Acid Response. *Int. J. Mol. Sci.* **2021**, *22*, 3529. [CrossRef]
6. Qin, Y.; Cui, S.; Cui, P.; Zhang, B.; Quan, X. TaFLZ2D Enhances Salinity Stress Tolerance via Superior Ability for Ionic Stress Tolerance and ROS Detoxification. *Plant Physiol. Biochem.* **2021**, *168*, 516–525. [CrossRef]
7. Ma, F.; Liang, Y.; Wang, Q.; Li, W.; Khan, A.; Li, B.; Wang, Y.; Su, H.; Zhang, R.; Guo, C.; et al. Genome-Wide Identification of FCS-Like Zinc Finger (FLZ) Genes in Four Solanaceae Plant Species and Functional Characterization of SlFLZ2 and SlFLZ18 in Tomato under Heat Stress. *Sci. Hortic.* **2023**, *317*, 112015. [CrossRef]
8. Li, X.; Lai, M.; Li, K.; Yang, L.; Liao, J.; Gao, Y.; Wang, Y.; Gao, C.; Shen, W.; Luo, M.; et al. FLZ13 Interacts with FLC and ABI5 to Negatively Regulate Flowering Time in Arabidopsis. *New Phytol.* **2024**, *241*, 1334–1347. [CrossRef]
9. Ma, Y.; Dong, J.; Yang, W.; Chen, L.; Wu, W.; Li, W.; Zhou, L.; Wang, J.; Chen, J.; Yang, T.; et al. OsFLZ2 Interacts with OsMADS51 to Fine-Tune Rice Flowering Time. *Development* **2022**, *149*, dev200862. [CrossRef]
10. Kim, S.L.; Lee, S.; Kim, H.J.; Nam, H.G.; An, G. OsMADS51 Is a Short-Day Flowering Promoter That Functions Upstream of Ehd1, OsMADS14, and Hd3a. *Plant Physiol.* **2007**, *145*, 1484–1494. [CrossRef]
11. Yang, C.; Shi, G.; Li, Y.; Luo, M.; Wang, H.; Wang, J.; Yuan, L.; Wang, Y.; Li, Y. Genome-Wide Identification of SnRK1 Catalytic α Subunit and FLZ Proteins in Glycyrrhiza Inflata Bat. Highlights Their Potential Roles in Licorice Growth and Abiotic Stress Responses. *Int. J. Mol. Sci.* **2022**, *24*, 121. [CrossRef] [PubMed]
12. Wang, J.; Li, Z.; Liang, Y.; Zheng, J.; Gong, Z.; Zhou, G.; Xu, Y.; Li, X. Genome-Wide Identification and Expression Reveal the Involvement of the FCS-like Zinc Finger (FLZ) Gene Family in *Gossypium hirsutum* at Low Temperature. *PeerJ* **2023**, *11*, e14690. [CrossRef] [PubMed]
13. Yang, C.; Li, X.; Yang, L.; Chen, S.; Liao, J.; Li, K.; Zhou, J.; Shen, W.; Zhuang, X.; Bai, M.; et al. A Positive Feedback Regulation of SnRK1 Signaling by Autophagy in Plants. *Mol. Plant* **2023**, *16*, 1192–1211. [CrossRef] [PubMed]
14. Baena-González, E.; Rolland, F.; Thevelein, J.M.; Sheen, J. A Central Integrator of Transcription Networks in Plant Stress and Energy Signalling. *Nature* **2007**, *448*, 938–942. [CrossRef] [PubMed]
15. Jamsheer K, M.; Shukla, B.N.; Jindal, S.; Gopan, N.; Mannully, C.T.; Laxmi, A. The FCS-like Zinc Finger Scaffold of the Kinase SnRK1 Is Formed by the Coordinated Actions of the FLZ Domain and Intrinsically Disordered Regions. *J. Biol. Chem.* **2018**, *293*, 13134–13150. [CrossRef]
16. Jamsheer K, M.; Sharma, M.; Singh, D.; Mannully, C.T.; Jindal, S.; Shukla, B.N.; Laxmi, A. FCS-like Zinc Finger 6 and 10 Repress SnRK1 Signalling in Arabidopsis. *Plant J.* **2018**, *94*, 232–245. [CrossRef]
17. Jamsheer K, M.; Laxmi, A. Expression of Arabidopsis FCS-Like Zinc Finger Genes Is Differentially Regulated by Sugars, Cellular Energy Level, and Abiotic Stress. *Front. Plant Sci.* **2015**, *6*, 746. [CrossRef]
18. Jossier, M.; Bouly, J.; Meimoun, P.; Arjmand, A.; Lessard, P.; Hawley, S.; Grahame Hardie, D.; Thomas, M. SnRK1 (SNF1-related Kinase 1) Has a Central Role in Sugar and ABA Signalling in *Arabidopsis Thaliana*. *Plant J.* **2009**, *59*, 316–328. [CrossRef]
19. Cho, Y.-H.; Hong, J.-W.; Kim, E.-C.; Yoo, S.-D. Regulatory Functions of SnRK1 in Stress-Responsive Gene Expression and in Plant Growth and Development. *Plant Physiol.* **2012**, *158*, 1955–1964. [CrossRef]
20. Bortlik, J.; Lühle, J.; Alseekh, S.; Weiste, C.; Fernie, A.R.; Dröge-Laser, W.; Börnke, F. DOMAIN OF UNKNOWN FUNCTION581-9 Negatively Regulates SnRK1 Kinase Activity. *Plant Physiol.* **2024**, *194*, 1853–1869. [CrossRef] [PubMed]
21. González-Fuente, M. DUFfers Can Be Useful—Some Even Save Energy! DUF581-9 Negatively Regulates the Key Energy Sensor SnRK1. *Plant Physiol.* **2024**, *194*, 1273–1275. [CrossRef] [PubMed]
22. Ma, Y.; Zhao, J.; Fu, H.; Yang, T.; Dong, J.; Yang, W.; Chen, L.; Zhou, L.; Wang, J.; Liu, B.; et al. Genome-Wide Identification, Expression and Functional Analysis Reveal the Involvement of FCS-Like Zinc Finger Gene Family in Submergence Response in Rice. *Rice* **2021**, *14*, 76. [CrossRef] [PubMed]
23. Lu, K.; Wei, L.; Li, X.; Wang, Y.; Wu, J.; Liu, M.; Zhang, C.; Chen, Z.; Xiao, Z.; Jian, H.; et al. Whole-Genome Resequencing Reveals Brassica Napus Origin and Genetic Loci Involved in Its Improvement. *Nat. Commun.* **2019**, *10*, 1154. [CrossRef] [PubMed]
24. Li, J.; Yu, X.; Zhang, C.; Li, N.; Zhao, J. The Application of CRISPR/Cas Technologies to Brassica Crops: Current Progress and Future Perspectives. *aBIOTECH* **2022**, *3*, 146–161. [CrossRef] [PubMed]
25. Lysak, M.A.; Koch, M.A.; Pecinka, A.; Schubert, I. Chromosome Triplication Found across the Tribe Brassiceae. *Genome Res.* **2005**, *15*, 516–525. [CrossRef] [PubMed]
26. Cheng, F.; Wu, J.; Wang, X. Genome Triplication Drove the Diversification of Brassica Plants. *Hortic. Res.* **2014**, *1*, 14024. [CrossRef]
27. Perumal, S.; Koh, C.S.; Jin, L.; Buchwaldt, M.; Higgins, E.E.; Zheng, C.; Sankoff, D.; Robinson, S.J.; Kagale, S.; Navabi, Z.-K.; et al. A High-Contiguity Brassica Nigra Genome Localizes Active Centromeres and Defines the Ancestral Brassica Genome. *Nat. Plants* **2020**, *6*, 929–941. [CrossRef] [PubMed]
28. Das Laha, S.; Dutta, S.; Schäffner, A.R.; Das, M. Gene Duplication and Stress Genomics in *Brassica*s: Current Understanding and Future Prospects. *J. Plant Physiol.* **2020**, *255*, 153293. [CrossRef] [PubMed]

29. Fang, L.; Cheng, F.; Wu, J.; Wang, X. The Impact of Genome Triplication on Tandem Gene Evolution in Brassica Rapa. *Front. Plant Sci.* **2012**, *3*, 261. [CrossRef]
30. Liu, S.; Liu, Y.; Yang, X.; Tong, C.; Edwards, D.; Parkin, I.A.P.; Zhao, M.; Ma, J.; Yu, J.; Huang, S.; et al. The Brassica Oleracea Genome Reveals the Asymmetrical Evolution of Polyploid Genomes. *Nat. Commun.* **2014**, *5*, 3930. [CrossRef]
31. Shahzad, B.; Rehman, A.; Tanveer, M.; Wang, L.; Park, S.K.; Ali, A. Salt Stress in Brassica: Effects, Tolerance Mechanisms, and Management. *J. Plant Growth Regul.* **2022**, *41*, 781–795. [CrossRef]
32. Raza, M.A.; Sohail, H.; Hassan, M.A.; Sajad, S.; Xing, Y.; Song, J. Cold Stress in *Brassica* Vegetables: Morpho-Physiological and Molecular Responses Underlying Adaptive Mechanism. *Sci. Hortic.* **2024**, *329*, 113002. [CrossRef]
33. Lei, J.; Chen, G.; Chen, C.; Cao, B. Germplasm Diversity of Chinese Kale in China. *Hortic. Plant J.* **2017**, *3*, 101–104. [CrossRef]
34. Grant, C.E.; Bailey, T.L.; Noble, W.S. FIMO: Scanning for Occurrences of a given Motif. *Bioinformatics* **2011**, *27*, 1017–1018. [CrossRef] [PubMed]
35. Xu, G.; Guo, C.; Shan, H.; Kong, H. Divergence of Duplicate Genes in Exon-Intron Structure. *Proc. Natl. Acad. Sci. USA* **2012**, *109*, 1187–1192. [CrossRef] [PubMed]
36. Chen, C.; Wu, Y.; Li, J.; Wang, X.; Zeng, Z.; Xu, J.; Liu, Y.; Feng, J.; Chen, H.; He, Y.; et al. TBtools-II: A "One for All, All for One" Bioinformatics Platform for Biological Big-Data Mining. *Mol. Plant* **2023**, *16*, 1733–1742. [CrossRef] [PubMed]
37. Holub, E.B. The Arms Race Is Ancient History in Arabidopsis, the Wildflower. *Nat. Rev. Genet.* **2001**, *2*, 516–527. [CrossRef]
38. Hurst, L.D. The Ka/Ks Ratio: Diagnosing the Form of Sequence Evolution. *Trends Genet.* **2002**, *18*, 486. [CrossRef]
39. Jamsheer K, M.; Mannully, C.T.; Gopan, N.; Laxmi, A. Comprehensive Evolutionary and Expression Analysis of FCS-Like Zinc Finger Gene Family Yields Insights into Their Origin, Expansion and Divergence. *PLoS ONE* **2015**, *10*, e0134328. [CrossRef]
40. Zou, L.; Yu, B.; Ma, X.-L.; Cao, B.; Chen, G.; Chen, C.; Lei, J. Cloning and Expression Analysis of the BocMBF1c Gene Involved in Heat Tolerance in Chinese Kale. *Int. J. Mol. Sci.* **2019**, *20*, 5637. [CrossRef]
41. Zhu, Z.; Sun, B.; Xu, X.; Chen, H.; Zou, L.; Chen, G.; Cao, B.; Chen, C.; Lei, J. Overexpression of AtEDT1/HDG11 in Chinese Kale (Brassica Oleracea Var. Alboglabra) Enhances Drought and Osmotic Stress Tolerance. *Front. Plant Sci.* **2016**, *7*, 1285. [CrossRef] [PubMed]
42. Sah, S.K.; Reddy, K.R.; Li, J. Abscisic Acid and Abiotic Stress Tolerance in Crop Plants. *Front. Plant Sci.* **2016**, *7*, 571. [CrossRef] [PubMed]
43. Liu, H.; Lyu, H.; Zhu, K.; Van De Peer, Y.; Cheng, Z.M. The Emergence and Evolution of Intron-poor and Intronless Genes in Intron-rich Plant Gene Families. *Plant J.* **2021**, *105*, 1072–1082. [CrossRef] [PubMed]
44. Liang, Y.; Xiong, Z.; Zheng, J.; Xu, D.; Zhu, Z.; Xiang, J.; Gan, J.; Raboanatahiry, N.; Yin, Y.; Li, M. Genome-Wide Identification, Structural Analysis and New Insights into Late Embryogenesis Abundant (LEA) Gene Family Formation Pattern in Brassica Napus. *Sci. Rep.* **2016**, *6*, 24265. [CrossRef] [PubMed]
45. Lagercrantz, U. Comparative Mapping Between Arabidopsis Thaliana and Brassica Nigra Indicates That Brassica Genomes Have Evolved Through Extensive Genome Replication Accompanied by Chromosome Fusions and Frequent Rearrangements. *Genetics* **1998**, *150*, 1217–1228. [CrossRef]
46. Whittle, C.A.; Krochko, J.E. Transcript Profiling Provides Evidence of Functional Divergence and Expression Networks among Ribosomal Protein Gene Paralogs in Brassica Napus. *Plant Cell* **2009**, *21*, 2203–2219. [CrossRef]
47. Nietzsche, M.; Landgraf, R.; Tohge, T.; Börnke, F. A Protein–Protein Interaction Network Linking the Energy-Sensor Kinase SnRK1 to Multiple Signaling Pathways in Arabidopsis Thaliana. *Curr. Plant Biol.* **2016**, *5*, 36–44. [CrossRef]
48. Sun, B. CRISPR/Cas9-Mediated Mutagenesis of Homologous Genes in Chinese Kale. *Sci. Rep.* **2018**, *8*, 16786. [CrossRef]
49. Li, Y.; Liu, G.-F.; Ma, L.-M.; Liu, T.-K.; Zhang, C.-W.; Xiao, D.; Zheng, H.-K.; Chen, F.; Hou, X.-L. A Chromosome-Level Reference Genome of Non-Heading Chinese Cabbage [*Brassica campestris* (Syn. *Brassica rapa*) Ssp. Chinensis]. *Hortic. Res.* **2020**, *7*, 212. [CrossRef]
50. Guo, N.; Wang, S.; Wang, T.; Duan, M.; Zong, M.; Miao, L.; Han, S.; Wang, G.; Liu, X.; Zhang, D.; et al. Graph-Based Pan-Genome of Brassica Oleracea Provides New Insights into Its Domestication and Morphotype Diversification. *Plant Commun.* **2024**, *5*, 100791. [CrossRef]
51. Bailey, T.L.; Johnson, J.; Grant, C.E.; Noble, W.S. The MEME Suite. *Nucleic Acids Res.* **2015**, *43*, W39–W49. [CrossRef] [PubMed]
52. Lescot, M. PlantCARE, a Database of Plant Cis-Acting Regulatory Elements and a Portal to Tools for in Silico Analysis of Promoter Sequences. *Nucleic Acids Res.* **2002**, *30*, 325–327. [CrossRef] [PubMed]
53. Hu, B.; Jin, J.; Guo, A.-Y.; Zhang, H.; Luo, J.; Gao, G. GSDS 2.0: An Upgraded Gene Feature Visualization Server. *Bioinformatics* **2015**, *31*, 1296–1297. [CrossRef] [PubMed]

Disclaimer/Publisher's Note: The statements, opinions and data contained in all publications are solely those of the individual author(s) and contributor(s) and not of MDPI and/or the editor(s). MDPI and/or the editor(s) disclaim responsibility for any injury to people or property resulting from any ideas, methods, instructions or products referred to in the content.

International Journal of
Molecular Sciences

MDPI

Article

Investigating the Role of Known Arabidopsis Iron Genes in a Stress Resilient Soybean Line

Jamie A. O'Rourke * and Michelle A. Graham

Agricultural Research Service, Corn Insects, and Crop Genetics Research Unit, United States Department of Agriculture, Ames, IA 50010, USA; michelle.graham@usda.gov
* Correspondence: jamie.orourke@usda.gov; Tel.: +1-515-294-7824

Abstract: Genes involved in iron deficiency responses have been well characterized in *Arabidopsis thaliana*, but their roles in crop species have not been well explored. Reliance on model species may fail to identify novel iron stress mechanisms present within crop species, likely selected by hundreds of years of selection. Fiskeby III (PI 438471) is a soybean line from Sweden that demonstrates high levels of resilience to numerous stresses. Earlier Fiskeby III studies have identified a suite of genes responding to iron deficiency stress in Fiskeby III that are also associated with Arabidopsis iron deficiency responses. We were interested in determining how canonical iron genes function in Fiskeby III under normal and iron stress conditions. To investigate this, we used virus-induced gene silencing to knock down gene expression of three iron deficiency response genes (FER-like iron deficiency induced transcription factor (FIT), elongated hypocotyl 5 (HY5) and popeye (PYE)) in Fiskeby III. Analyses of RNAseq data generated from silenced plants in iron-sufficient and -deficient conditions found silencing FIT and HY5 altered general stress responses but did not impact iron deficiency tolerance, confirming Fiskeby III utilizes novel mechanisms to tolerate iron deficiency stress.

Keywords: soybean; iron deficiency; RNAseq; Fiskeby III

1. Introduction

Iron (Fe) is the fourth most abundant mineral in the earth's crust. However, the majority of iron is present as Fe^{3+}, which is not biologically available to plants. Plants can only directly utilize iron in the Fe^{2+} form, which is much less prevalent in the soil than Fe^{3+}. Many environmental factors including weather conditions and soil properties can shift the balance of Fe^{3+} to Fe^{2+}. Plants have evolved two strategies to handle low iron conditions, strategy I and strategy II [1]. Strategy I is a reduction-based approach. Plants excrete protons via Arabidopsis H^+ ATPase2 (AHA2) to acidify the rhizosphere. Next, a root membrane bound reductase ferric reduction oxidase 2 (FRO2) reduces Fe^{3+} to Fe^{2+}. This usable iron is then transported into the root of the plant by iron-regulated transporter 1 (IRT1). Strategy II is chelation-based. Strategy II plants release phytosiderophores, members of the mugineic acid family, from the roots to solubilize and bind Fe^{3+} and the entire complex is then transported into the roots. It was originally proposed that monocot species use strategy II, while dicot species use strategy I. However, recent findings have demonstrated that dicots can induce some aspects of the strategy II response [2,3]. Current evidence suggests soybean utilizes the strategy I response.

The research in our labs has focused on the soybean line Clark (PI548533), an iron efficient line. In our studies we have found Clark has a unique response to iron deficiency (−Fe) stress, inducing genes associated with stress, defense, and iron uptake and transport genes while repressing genes associated with DNA replication, methylation, and photosynthesis [4–10]. The iron efficiency of Clark is conferred by a quantitative trait loci (QTL) on GmChr03 [11–13], while the Fiskeby III efficiency is conferred by a QTL on GmChr05 [14]. Given the high resilience of Fiskeby III to multiple stresses and the different sources of

the iron stress tolerance, we were interested in determining how Fiskeby III iron stress tolerance would be impacted by silencing major genes involved in the iron stress response.

Most knowledge of strategy I responses comes from studies in *Arabidopsis thaliana*. However, the findings from Arabidopsis have not directly translated to soybean. In this study, we utilized virus-induced gene silencing (VIGS) to down-regulate three of the key genes in the Arabidopsis −Fe response pathway: FER-like iron deficiency-induced transcription factor (FIT), elongated hypocotyl 5 (HY5), and popeye (PYE) in the Fiskeby III soybean line. These genes were chosen because they are either differentially expressed in Fiskeby III due to iron deficiency stress (PYE, [15]), or are believed to regulate (based on Arabidopsis) DEGs identified in earlier Fiskeby III studies (FIT and HY5, [15,16]). Understanding if and how these genes function in soybean, particularly a line that is so stress resilient, will help us understand how soybean modifies gene expression profiles to address nutrient deficiencies.

Basic-helix-loop-helix (bHLH) transcription factors (TFs) regulate many facets of strategy I iron deficiency response. One of the major bHLH TFs associated with −Fe is FIT (*At2g28160*) [17,18]. In Arabidopsis, FIT is a key regulator of Fe acquisition, serving as a central hub to integrate signals from developmental and environmental pathways to maintain Fe homeostasis [19]. In *fit* knockout mutants, plants are iron deficient, even when grown on iron replete media [20]. FIT regulates the expression of the main strategy I genes including *AHA2*, *FRO2*, and *IRT1* [21]. Under −Fe conditions, a suite of bHLH TFs including bHLH038, bHLH039, bHLH100, and bHLH101 directly interact with FIT to activate FIT [18,22]. In earlier Fiskeby III studies, *bHLH038* was differentially expressed in response to iron [16]. As these data were collected after 16 days in hydroponics, we hypothesize that FIT may be associated with the regulation of *bHLH038* in Fiskeby III.

A second important bHLH TF is POPEYE (PYE, *At3g947640*). PYE regulates Arabidopsis growth and development during −Fe stress [23]. Originally, PYE was thought to regulate Fe homeostasis independently of FIT. However, it has since been found that PYE directly interacts with bHLH TFs, including bHLH038/039/100/101/104/105/115. It is well known that bHLH038 and bHLH039 interact with FIT [18]. As PYE represses bHLH38/39 transcription, PYE is not acting completely independently of FIT [24]. In Arabidopsis, PYE expression is induced by −Fe and is required to inhibit the excessive induction of Fe homeostasis-associated genes [23]. PYE also serves to protect plants from light damage, including reactive oxygen species and the destruction of photosynthetic machinery. Specifically, under −Fe, the grana in Arabidopsis thylakoids de-stack, but in PYE mutants the grana remain stacked [25]. Previous experiments silencing a candidate gene associated with the GmChr05 QTL found PYE was up-regulated in leaves compared to EV in both +Fe and −Fe conditions [15].

Elongated Hypocotyl 5 (HY5, *At5g11260*) is a bZIP TF that was originally identified as an important component of light responses and the regulation of seedling development [26]. Further studies revealed HY5 plays multiple roles in plant development, signaling, and stress responses [27]. HY5 is unique in that it is a shoot-to-root mobile signal that coordinates plant carbon and nitrogen uptake [28]. HY5 is also involved in multiple hormone signaling pathways including gibberellic acid, brassinosteroids, ethylene, auxin, and abscisic acid, all of which have been implicated in −Fe responses in multiple species [27,29]. In Arabidopsis, HY5 is known to be involved in regulating −Fe responses, regulating the expression of multiple genes involved in iron uptake and homeostasis [30], and was recently shown to directly interact with both FIT and PYE [31,32] to regulate iron homeostasis. This is reaffirmed in Arabidopsis HY5 knockout plants, which are stunted with chlorotic leaves under −Fe conditions. In previous work by our lab, the HY5 transcription factor binding site was over-represented amongst the promoters of differentially expressed genes, indicating a role for HY5 in soybean −Fe responses as well [5,15,16]. Together, these three genes control a large swath of genes associated with the strategy I −Fe responses in Arabidopsis. However, an improved understanding of these genes in soybean, an agronomically important crop, is important to developing more resilient plants. Fiskeby III is the

most abiotic stress-resilient soybean line we have identified. An improved understanding of how these genes function in Fiskeby III could help us translate the stress tolerance of Fiskeby III into elite breeding lines.

2. Results

Viral constructs were tested in both Williams 82 and Fiskeby III soil-grown plants. Williams 82 was utilized since it carries the historical IDC QTL from Gm03. Comparing the VIGS constructs in soil-grown Williams 82 plants to EV-infected plants found significantly higher SPAD levels for VIGS_FIT plants and significantly lower SPAD levels for VIGS_HY5 plants. VIGS_HY5 plants also showed significantly reduced height and weight (Figure S1). There were no statistically significant changes in VIGS_PYE plants for any of the phenotypic measurements used. In soil-grown Fiskeby III plants, there were no statistical differences among any of the phenotypic measurements for any of the silenced plants Because these genes are important in iron-stress responses, we were most interested in whether these genes showed a phenotype in iron-stressed plants, which we generated using hydroponics. Like the soil-grown plants, there were no statistically significant changes in phenotypic measurements for any of the silenced plants grown in +Fe and −Fe hydroponics. Given the high resilience of Fiskeby III to multiple abiotic stresses, including iron deficiency, the lack of phenotypic changes was not surprising. If the candidate genes identified from Arabidopsis play a role in the Fiskeby III iron-stress response, we expect to see transcriptional changes in response to silencing, and a sub-set of these changes should be unique to each of the constructs, despite a lack of phenotypic change. Based on our previous research, we know iron stress-tolerant soybean (genotype, Clark) exhibits strong gene expression changes within one hour of iron stress exposure [6,7]. Therefore, we used RNA-seq to characterize Fiskeby III responses to HY5, FIT, and PYE silencing one hour after iron-stress exposure. These transcriptional changes should provide insight into the iron-stress tolerance of Fiskeby III.

2.1. Analyses of RNAseq Data

2.1.1. Silencing Effect

The design of the RNAseq experiment allowed us to make two different types of comparison, silencing effect and iron treatment effect (described below). The silencing effect contrasted VIGS_HY5, VIGS_FIT, or VIGS_PYE to EV, examining +Fe and −Fe separately. The silencing effect would identify genes differentially expressed, directly or indirectly, in response to the silencing of HY5, FIT, or PYE in the different conditions (Tables S1 and S2). The total number of identified DEGs for both comparisons are listed in Table 1. The distribution of the DEGs identified is also visualized by Venn diagrams in Figure 1A,C.

Contrary to our expectations, there were fewer DEGs identified in EV vs. VIGS plants in −Fe conditions than in +Fe conditions. VIGS_HY5 vs. EV in both +Fe and −Fe conditions identified the most DEGs in the silencing effect analyses. Further analysis of the RNA-seq data from the silenced plants should identify novel strategies utilized by Fiskeby III to counter iron stress. We used the GO tool (version 4) on soybase.org (accessed on 3 March 2023) to identify over-represented (corrected $p < 0.05$) GO terms for all DEGs within a VIGS construct of interest (Table S3). Within a DEG list, DEGs were divided into those induced or repressed by silencing. The 637 DEGs induced when comparing VIGS_FIT to EV plants in +Fe conditions were largely associated with photosynthesis (15 GO terms) including GO terms photosynthesis, thylakoid membrane organization, light reaction, chlorophyll biosynthesis, carotenoid biosynthesis, and response to light. This likely reflects the importance of iron ions in the electron transport chain. Other induced GO terms included those associated with fatty acid biosynthesis, response to hormones (auxin and jasmonic acid stimulus), divalent metal ion transport, defense response-incompatible reaction, cellular cation homeostasis, ammonia assimilation cycle, and iron-sulfur cluster assembly. The 324 DEGs repressed by FIT silencing in +Fe conditions included 15 GO

terms associated with DNA replication, DNA methylation, cell cycle regulation, and gene silencing. Given the few DEGs identified for the same comparison under −Fe conditions, it is not surprising there are no statistically significant GO terms identified. However, by comparing DEGs directly, we identified 17 DEGs common to FIT-silenced plants in −Fe and +Fe, many with Arabidopsis homologs with functions related to stress tolerance, immunity, and/or abscisic acid signaling. AtPYL4 (Glyma.01g124700, Glyma.06g039000, and Glyma.07g155500) is involved in ABA signaling and drought-resistance [33]. AtATL6 (Glyma.09g140700) and AtNDL1 (Glyma.20g223800) regulate responses to salt stress [34,35]. AtLYK3 (Glyma.08g200800) regulates plant immunity [36] and abscisic acid signaling.

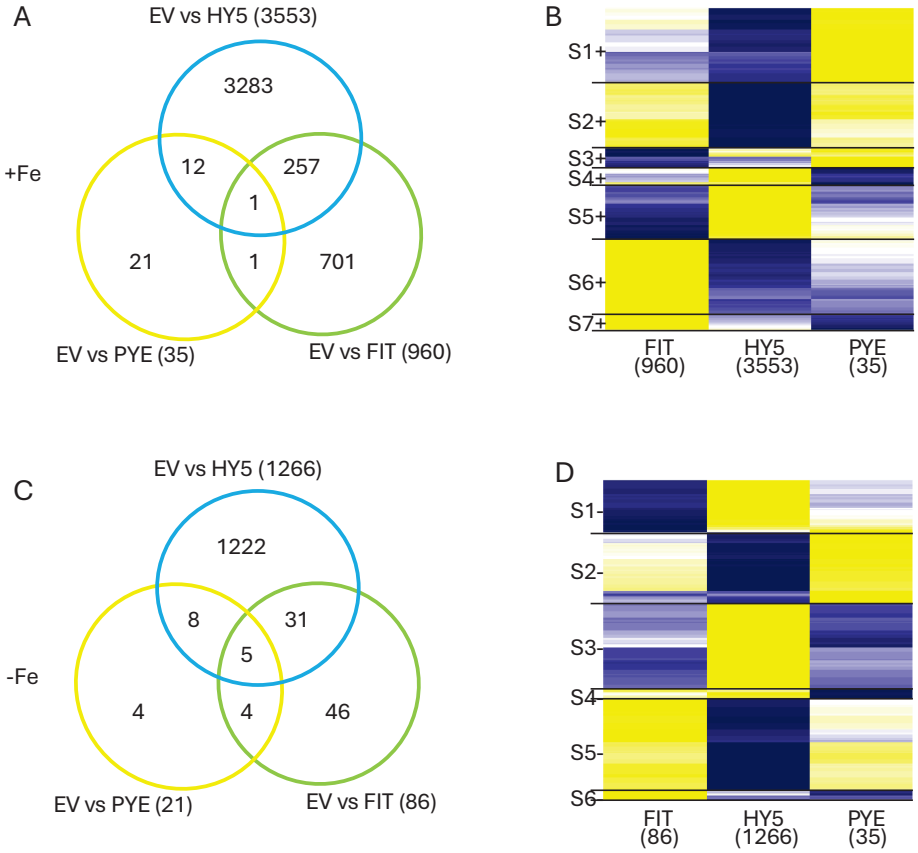


Figure 1. Intersection of DEGs from the silencing effect analyses. Venn diagrams and corresponding heatmaps represent EV vs. VIGs silenced plants in either +Fe conditions (**A**,**B**) or –Fe conditions (**C**,**D**). DEGs were identified as those with an FDR < 0.05. The Venn diagrams (**A**,**C**) identify genes unique to an analysis or genes differentially expressed in multiple analyses. The cluster analyses to generate heatmaps (**B**,**D**) were performed in R to group genes by similar expression patterns. Genes in yellow are induced while those in blue are repressed. These groupings are delineated by the horizontal black lines, and each cluster is assigned a unique designation to the left of the heatmap; S1+–7+ represent silencing effect analyses in +Fe conditions, S1–6—represent genotype analyses in –Fe conditions. The total number of DEGs identified by each analysis is provided outside the circles of interest (**A**,**C**) in the Venn diagrams and below the column of interest in the heatmaps (**B**,**D**).

For DEGs responding to silencing in VIGS_HY5 vs. EV under +Fe conditions, we identified 2612 repressed DEGs corresponding to 70 statistically significant GO terms. A large number of GO terms (20) were associated with DNA replication, DNA methylation, cell cycle regulation, and gene silencing. We also identified significant GO terms associated with fatty acid, sterol, flavonoid, flavanol, phenylpropanoid, anthocyanin, polysaccharide, jasmonic acid and lipid biosynthesis, lipid oxidation, and response to UV, sucrose stimulus, wounding, cadmium, Karrikin, and cylopentenone. The 941 DEGs induced by HY5 silenc-

ing in +Fe were associated with two significant GO terms: production of siRNA involved in RNA interference and autophagy.

Table 1. The nine comparisons made in the RNAseq analyses are listed in the column Comparison. These comparisons are divided by silencing effect (VIGS vs. EV in either +Fe or −Fe) or iron stress treatment (VIGS −Fe vs. +Fe) analyses. For each comparison, the total number of differentially expressed genes (DEGs Total) identified is provided, the number of DEGs that are induced (DEGs Induced) and down-regulated (DEGs Repressed), and the number of GO terms associated with the total number of DEGs (GO Terms).

Analysis	Comparison	DEGs Total	DEGs Induced	DEGs Repressed	GO Terms
Silencing Effect	VIGS_FIT −Fe vs. EV	86	51	35	0
	VIGS_FIT +Fe vs. EV	960	637	323	52
	VIGS_HY5 −Fe vs. EV	1266	582	684	17
	VIGS_HY5 +Fe vs. EV	3553	941	2612	57
	VIGS_PYE −Fe vs. EV	21	11	10	0
	VIGS_PYE +Fe vs. EV	35	31	4	0
Trt Effect	EV: −Fe vs. +Fe	0	0	0	0
	VIGS_FIT: −Fe vs. +Fe	655	538	117	41
	VIGS_HY5: −Fe vs. +Fe	111	2	109	9
	VIGS_PYE: −Fe vs. +Fe	11	0	11	0

Under −Fe conditions, we identified 684 DEGs repressed by HY5 silencing corresponding to 28 statistically significant GO terms. Of these, 14 GO terms associated with DNA replication/methylation/cell cycle and photosynthesis were also significant among HY5 silencing repressed genes in +Fe conditions. The 582 DEGs induced in −Fe conditions were associated with silencing (post-transcriptional and virus-induced gene silencing). It is worth noting that 704 DEGs were shared by HY5 silencing in −Fe and +Fe conditions. Unique to the −Fe analyses is the GO term 'divalent metal transport', which is associated with 21 DEGs. Examining the annotation of these genes indicates these genes are associated with photosynthesis, likely due to the high iron requirement of the electron transport chain and chlorophyll formation.

No significant GO terms were identified for any VIGS_PYE analyses, likely due to the small number of DEGs identified. This suggests silencing PYE had little impact on Fiskeby III gene expression. This could mean that PYE does not have a role in iron stress responses in leaves or, alternatively, due to the polyploid nature of the soybean genome, gene redundancy could mask the impact of silencing.

To visualize the expression patterns of the genotype analyses, we used RStudio (version 4.3.2) to conduct hierarchical clustering and build heatmaps (Figure 1B,D). For each heatmap, we created a nonredundant list of all DEGs identified when comparing VIGS_FIT, VIGS_HY5, and VIGS_PYE to EV in +Fe conditions or −Fe conditions. In +Fe conditions, clusters S2+ (882 DEGS), S4+ (247 DEGs), and S5+ (705 DEGs) were made up of DEGs significant only in VIGS_HY5 plants (>94.7%). Cluster S2+ was associated with a broad range of GO terms including the biosynthesis of fatty acid, sterol, brassinosteroid, flavonoid, coumarin, anthocyanin, and polysaccharide. Cluster S4+ had no significant GO terms, while cluster S5+ was associated with gene silencing (Table S5). Cluster S1+ (973) was also largely composed of VIGS_HY5 DEGs, however, 106 were also significant in VIGS_FIT, with expression patterns conserved across constructs. This cluster was associated with GO terms related to DNA replication/methylation and the cell cycle. Clusters S3+, S6+, and S7+ were composed with DEGs from both VIGS_HY5 and VIGS_FIT. In cluster S3+, 70 DEGs were common to VIGS_HY5 and VIGS_FIT plants, and expressed similarly. The 1004 DEGs in cluster S6+ was composed of 467 DEGs from VIGS_FIT, and 581 DEGs from VIGS_HY5. Similarly, of the 213 DEGs in cluster S7+, 128 came from VIGS_FIT and 93

came from VIGS_HY5. In Fe- conditions, more than 90% of DEGs within a cluster were only significant in VIGS_HY5, highlighting what little impact the VIGS_FIT and VIGS_PYE constructs had in −Fe conditions.

2.1.2. Treatment Effect

The treatment effect contrasted −Fe vs. +Fe for EV, VIGS_FIT, VIGS_HY5, and VIGS_PYE plants separately. This would identify genes differentially expressed in response to iron availability in specific VIGS backgrounds. If silencing had no effect on iron responsiveness, we would expect the VIGS_FIT, VIGS_HY5, and VIGS_PYE constructs would have the same DEGs as the EV construct. However, if silencing impacted iron stress responsiveness, different DEGs could be identified when comparing EV DEGs to the other VIGS constructs. Not surprisingly, given the high stress tolerance of Fiskeby III, no DEGs were identified in EV −Fe vs. +Fe (Table 1). Therefore, the 11, 111, and 655 DEGs identified in PYE, HY5, and FIT plants, respectively, became iron-responsive as a result of silencing. This suggests all three genes regulate, directly or indirectly, iron-responsive genes in Fiskeby III. Overall, the treatment effect analyses identified fewer genes than silencing effect analyses (Tables 1 and S6 and Figure 2). Of the 655 DEGs responding to iron treatment in FIT-silenced plants, 379 were unique to the iron treatment response, confirming FIT-silencing altered the iron responsiveness of these genes. Comparing DEGs responding to HY5-silencing relative to EV in +Fe and −Fe conditions to DEGs responding to iron treatment, we identified only 13 unique DEGs. This suggests HY5 function is important in both +Fe and −Fe conditions. As in the silencing effect analyses, the treatment analyses for VIGS_PYE failed to identify any over-represented GO terms.

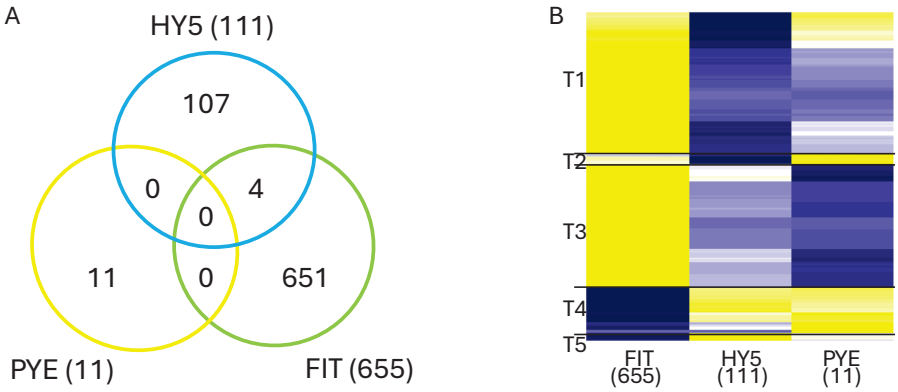


Figure 2. Intersection of DEGs from the treatment effect analyses. Venn diagrams and corresponding heatmaps represent DEGs identified from comparing VIG-silenced plants grown in −Fe vs. +Fe. DEGs were identified as those with an FDR < 0.05. Venn diagram (**A**) identifies genes unique to a single candidate gene analysis or genes differentially expressed by silencing multiple candidate genes. The cluster analyses to generate the heatmap (**B**) were performed in R to group genes by similar expression patterns. Genes in yellow are induced, while those in blue are repressed. These groupings are delineated by the horizontal black lines, and each cluster is assigned a unique designation to the left of the heatmap (T1–5). The total number of DEGs identified by each analysis is provided outside the circle of interest (**A**) in the Venn diagram, and below the column of interest in the heatmap (**B**).

Mirroring our analyses of the silencing effect, each of the three treatment gene lists was divided by induced or repressed. The induced and repressed gene lists were then used with the GO tool on SoyBase to identify over-represented (Corrected $p < 0.05$) GO terms. The 538 induced genes from the VIGS_FIT analyses were mainly associated with photosynthesis (15 GO terms) including photosynthesis, response to light, and chloroplast organization. Again, reflecting the importance of iron in photosynthetic processes. There were no GO terms associated with the 117 repressed genes in VIGS_FIT. The VIGS_HY5 analysis is unique in that, of the 111 DEGs identified, 109 were repressed. Five of the eight GO terms identified from the 109 repressed genes are associated with fatty acids and wax,

including lipid biosynthesis, cuticle development, fatty acid metabolism, cutin biosynthesis, and lipid metabolism. Finally, the PYE analyses identified 11 DEGs, all induced. Five of the 11 genes are associated with nucleosome assembly processes.

As with the DEGs identified from the silencing effect analyses, we used a non-redundant list of treatment DEGs to build a heatmap using RStudio (version 4.3.2) (Figure 2B). This heatmap showed that, like the silencing effect heatmaps, the expression pattern of genes in FIT-silenced plants are dramatically different from those in HY5. Cluster T1 is composed of genes from both FIT (249 DEGs) and HY5 (85 DEGs) with four overlapping genes, but expressed in the opposite direction. These 330 DEGs are associated with 31 GO terms, 13 of which are associated with photosynthetic processes including chlorophyll biosynthesis, response to light, and thylakoid organization. Genes in cluster T2 are unique to HY5, while genes in clusters T3 and T4 are unique to FIT. There are no statistically significant GO terms associated with T2, likely due to the few genes in the cluster. Cluster T3 (289 DEGs) is, again, associated with photosynthesis (six GO terms) but also DNA replication/methylation (four GO terms). The only statistically significant GO term associated with T4 is nucleosome assembly. Finally, T5 (20 DEGs, 18 from FIT and 2 from HY5) are associated with reciprocal DNA recombination. Notably absent were any GO categories related to iron uptake, transport, or metabolism.

2.1.3. Known Iron Genes

Given the lack of GO categories involved with iron uptake/transport, we examined the annotations associated with the Arabidopsis homologs of each of the DEGs in all nine (silencing effect and treatment) comparisons. In the silencing effect −Fe analyses (Table S2), only two classic iron genes were identified. The first was *Glyma.15G274600*, a homolog of *FRD3* (*At3G08040*), which is a plasma membrane transporter that is important for iron distribution and homeostasis [37]. In our experiment, *FRD3* expression is induced in VIGS_HY5 plants compared to the EV plants under both −Fe and +Fe conditions. The second, a homolog of *HY5* (*Glyma.04G225300*, which shares <80% of the sequence identity with the VIGS construct sequence), was repressed. The lack of additional iron-specific genes, either induced or repressed, under −Fe conditions may indicate that the timing of the sampling was such that we failed to capture the expression of these genes in leaves or possibly that the resilience of Fiskeby III means 60 min of −Fe stress is not enough to induce the canonical genes.

In contrast to the two iron-specific DEGs identified under −Fe conditions, in +Fe conditions, silencing effect analyses identified 28 homologs of genes known to be involved in the iron stress-response (Table S1). All 28 DEGs were identified in the VIGS_HY5 vs. EV +Fe comparison. These genes include homologs of *BRUTUS (BTS*, *Glyma.07G093700* and *Glyma.09G182600*), *FIT* (*Glyma.12G178500*), *bHLH038* (*Glyma.03G130400* and *Glyma.03G130600*), *bHLH121* (*Glyma.08G148500*), *ORG1* (*Glyma.04G236600*), *OPT3* (*Glyma.17G006100*), *IREG1* (*Glyma.01G128300*), *HY5* (*Glyma.08G302500*), *FRD3* (*Glyma.15G274600*), and *NRAMP3* (*Glyma.05G101700* and *Glyma.17G165200*). The homologs of *bHLH121*, *IREG1*, *HY5*, and *FRD3* are all induced in HY5-silenced plants compared to EV. Conversely, the homologs of *BTS*, *FIT*, *bHLH038*, *ORG1*, *OPT3*, and *NRAMP3* are all repressed in VIGS_HY5 plants. Three additional iron-associated genes were identified, one, a homolog of *PYE* (*Glyma.17G098900*), is induced in VIGS_PYE vs. EV +Fe analyses, possibly an artifact of the silencing process since this gene shares >80% nucleotide identity to the silenced PYE gene. The two remaining genes of interest are heavy metal transporters (*Glyma.19G012900* and *Glyma.19G209500*), induced and repressed, respectively, in VIGS_FIT vs. EV +Fe comparisons.

The treatment analyses (Table S6) only identified four iron-specific genes, all four of which are induced in the FIT analysis. Two of the genes are generic iron genes: a vacuolar iron transporter (VIT) responsible for transporting excess iron in and out of the vacuole (*Glyma.04G225300*), and a cation transporter, which could transport a wide range of cations beyond iron (*Glyma.15G262300*). Glyma.10G146600 encodes IREG3, an iron transporter

important in maintaining cellular ion homeostasis [38]. Finally, Glyma.09G018600 encodes a homolog of Arabidopsis ferric reduction oxidase 6 (FRO6). In tobacco, overexpressing FRO6 increases iron deficiency tolerance [39].

In addition to looking for iron genes identified from Arabidopsis, we compared the DEGs identified in this study to the DEGs identified from eight previous studies by our group using multiple genotypes and multiple timepoints (30 min, 60 min, 120 min, 1 day, 2 days, 7 days, 10 days, 16 days) [5,7–10,15,16,40]. Comparing the DEGs in this study to these publications identified 54 DEGs from the silencing +Fe analyses, 27 DEGs from the silencing −Fe analyses, and 20 DEGs from the treatment analyses that were also differentially expressed in an earlier study (Table S7). Overwhelmingly (>80%), the DEGs were identified from a previous study using Fiskeby III where plants were subjected to 16 days of −Fe stress. The lack of overlap with other studies confirms the Fiskeby III utilizes novel stress response pathways.

Studies have shown that iron-deficient plants produce high levels of reactive oxygen species (ROS), which may serve as an iron-deficient signal or serve as part of ROS-scavenging enzymes [41–45]. No GO terms associated with ROS or oxidation stress were over-represented in any of our analyses. However, querying individual lists for genes associated with ROS oxidative stress (catalases, superoxide dismutases, ascorbate peroxidases, glutathione, and peroxiredoxins) identified 79 DEGs in silencing +Fe, 30 DEGs in silencing −Fe, and 11 DEGs in the treatment analyses (Table S8). In both silencing analyses, the majority of the oxidative stress genes are associated with glutathione. Glutathione, with ascorbic acid, acts to maintain redox balance through scavenging and removal of hydrogen peroxide. Under −Fe conditions, increased glutathione and ascorbic acid protect against −Fe by preserving chlorophyll [46] and allow plants to grow as if in +Fe conditions. In our data, most glutathione-associated genes were identified in the VIGS_HY5 plants under +Fe and −Fe conditions, and are repressed in the VIGS_HY5 plant compared to VIGS_EV. The repression of these genes in silenced plants under both +Fe and −Fe conditions indicate they are not unique to iron stress and may play a role in general stress responses.

2.1.4. Potential Regulation of Fiskeby III Responses

To understand the regulation of the DEGs identified in this study, we used CLOVER [47] to identify any over-represented transcription factor binding sites (TFBS) in the 1000 bp promoters of the DEGs (Table 2). To maximize both computational resources and biological insights, we analyzed induced and repressed genes of each list separately (Table S4). For VIGS_FIT vs. EV in +Fe we identified 64 TFBS motifs over-represented in the promoters of induced genes and 27 TFBS motifs in the promoters of repressed genes. The motifs are associated with 617 induced genes and 319 repressed genes, which is nearly all the DEGs for the FIT gene silencing analyses. The induced genes are largely associated with photosynthetic processes, while the repressed genes are associated with DNA replication and methylation processes. For VIGS_FIT vs. EV in −Fe we identified three over-represented TFBS associated with induced genes and three different TFBS associated with the repressed genes. The motifs are associated with 31 repressed genes and 36 induced genes. The VIGS_FIT treatment comparison identified 44 TFBS over-represented in the promoters of the 518 induced genes and two motifs over-represented in the promoters of 117 genes. Comparing the silencing effect to the treatment effect found 40 of the 44 TFBS were conserved between treatment and VIGS_FIT +Fe comparisons among the induced genes, representing 246 of the 262 genes conserved between the two comparisons.

For VIGS_HY5 vs. EV in +Fe, we identified 144 TFBS motifs identified in promoters of the repressed genes (2612), 35 of which were MYB TFBS (Tables 2 and S4). The 144 statistically significant TFBS identified correspond to 2210 DEGs, nearly all of the 2612 DEGs. The 35 MYB TFBS were identified in the promoter regions of 1293 of the DEGs. These 1293 DEGs are associated with DNA replication/methylation, growth, and defense. These results suggest HY5 is involved in regulating MYB TFs associated with repressing the expression of these genes. The CLOVER results of VIGS_HY5 vs. EV in −Fe conditions identified

15 TFBS in down-regulated genes and 58 TFBS in up-regulated genes. Two TFBS were conserved between up- and down-regulated genes: an ABA-insensitive 5/Dc3 promoter binding factor 3 (DPBF3) binding site (MA1338.2) and a HY5 binding site (MA0551.1). DPBF3 TF is associated with abscisic acid (ABA), including regulating interactions between ABA and sugar signaling and regulating response to ABA and drought stress [48,49]. The HY5 TFBS was identified in the promoter of 50 down-regulated and 43 up-regulated genes. Not surprisingly, given the role HY5 plays in light reactions [29,31,50], the promoters with the HY5 TFBS are associated with genes involved in photosynthesis. Identifying the HY5 TFBS in the promoter of DEGs from VIGS_HY5 plants confirms that the DEGs are associated with HY5.

Table 2. Six of the nine comparisons (silencing effect +Fe, silencing effect −Fe, and treatment) divided into induced and repressed genes. The number of identified transcription factor binding sites (TFBS) identified by CLOVER are denoted in the TFBS column. The specific motifs can be found in Table S4. No statistically significant TFBS were identified for any of the PYE analyses due to the small number of DEGs.

Analysis	Comparison	TFBS
Silencing Effect	VIGS_HY5 vs. EV +Fe Induced	9
	VIGS_HY5 vs. EV +Fe Repressed	144
	VIGS_HY5 vs. EV −Fe Induced	58
	VIGS_HY5 vs. EV −Fe Repressed	15
Treatment Effect	VIGS_PYE −Fe vs. EV	0
	VIGS_PYE +Fe vs. EV	17
Silencing Effect	VIGS_FIT vs. EV +Fe Induced	64
	VIGS_FIT vs. EV +Fe Repressed	27
	VIGS_FIT vs. EV −Fe Induced	3
	VIGS_FIT vs. EV −Fe Repressed	3
Treatment Effect	VIGS_FIT +Fe vs. −Fe Induced	44
	VIGS_FIT +Fe vs. −Fe Repressed	2

The treatment (−Fe vs. +Fe) analyses of VIGS_HY5 plants identified 111 DEGs (Table 1). CLOVER analyses identified 17 over-represented TFBS (Table 2), including eight MYB TFBS in the 109 promoters of repressed genes. The MYB TFBS are identified in 101 of the 109 down-regulated genes. The majority of these genes (87) were also repressed in VIGS plants compared to EV. These genes are associated with lipid and flavonoid biosynthesis. The only differentially expressed MYB in the treatment comparison is MYB94, which is associated with inducing cuticular wax. It has been well documented that HY5 directly regulates MYB TFs in response to light. However, this is the first evidence that HY5 is regulating MYBs in response to iron deficiency.

3. Discussion

The iron uptake system has been well characterized in model species. However, translating the findings from model species to crop species has proven inefficient. This knowledge gap means iron deficiency is still a major issue for soybean growers, as increasing iron deficiency correlates with increasing yield loss [51,52]. The soybean genotype Fiskeby III is unique in its tolerance to multiple abiotic stresses. Previous studies have identified multiple iron tolerance QTL, including the canonical soybean iron QTL on GmChr03 and a novel QTL on GmChr05. While improved iron tolerance has been mapped to these regions, how plants achieve improved tolerance is still not understood. In comparing DEGs from this study to previous publications that focused on the GmChr03 QTL, there was little overlap of specific DEGs, though the same GO categories were identified. We believe the GmChr03 QTL in Fiskeby III serves as a secondary iron homeostasis system, and that Fiskeby III overwhelmingly utilizes the GmChr05 mechanisms. While breeders can integrate the QTLs, more targeted selection is desirable. Therefore, identifying specific

genes of interest will help breeders select lines with improved tolerance and associated yield. Given the increased tolerance of Fiskeby III to multiple abiotic stresses, we were interested in seeing whether the canonical genes identified from Arabidopsis for iron deficiency tolerance would impact the iron tolerance of Fiskeby III. Accordingly, we used VIGS to silence the homologs of three canonical genes associated with iron deficiency stress in Arabidopsis (PYE, HY5, and FIT) in Fiskeby III grown in soil and in iron-sufficient and -deficient hydroponics. In addition, we conducted RNAseq analyses to determine how silencing these genes impacted gene expression in Fiskeby III.

Silencing FIT in Williams 82 soil-grown plants resulted in significant differences in SPAD values. In previous soybean research, SPAD values have been successfully used to map quantitative trait loci for iron deficiency chlorosis. In this study, VIGS_FIT plants had significantly higher SPAD levels than the EV control plants, suggesting silencing FIT improved plant health. In Arabidopsis, *fit*1 seedlings were chlorotic and died two to three weeks after germination [21] Silencing FIT in Fiskeby III had no significant phenotype in soil or hydroponic conditions. Interestingly, silencing FIT identified many of the same genes that have been previously shown to respond to iron stress in the IDC-tolerant line Clark. The repression of genes involved in DNA replication/methylation and photosynthesis and induction of genes associated with iron uptake and homeostasis, defense, and stress are hallmarks of the Clark iron stress response. In this study, the silencing of FIT in iron-sufficient conditions repressed genes associated with DNA replication/methylation, and induced genes associated with photosynthesis and defense. Interestingly, we failed to identify genes responding to FIT silencing that were associated with iron uptake and homeostasis. To confirm this response, we used the best Arabidopsis homologs of DEGs responding to FIT silencing to cross-reference the 34 robustly FIT-regulated genes identified by Mai et al. [46]. None of the FIT-regulated genes identified by Mai et al. [46] was identified in our analyses. This suggests that, in soybean, FIT is a negative regulator of iron stress responses. This is supported by the 655 DEGs that became iron-responsive in FIT-silenced plants. In particular, FIT appears to regulate the iron responsiveness of photosynthetic genes.

Silencing HY5 in Williams 82 plants grown in soil resulted in significantly lower SPAD levels, reduced plant height, and reduced plant weight. This is consistent with findings by Mankotia et al. [30] who reported HY5 mutants had reduced chlorophyll content and growth under iron stress conditions. This would suggest that HY5 is a positive regulator of iron stress responses in Williams 82. However, the silencing of HY5 in Fiskeby III had no significant phenotype in soil or in iron-sufficient or -deficient hydroponics. As above, RNAseq analysis revealed HY5 silencing resulted in the repression of DEGS associated with DNA replication/methylation and photosynthesis in iron-sufficient and -deficient conditions. This mirrors expression patterns observed by Atwood et al. [4], who used the silencing of the DNA replication gene *GmRPA3c* to relieve iron stress symptoms in the iron stress susceptible line IsoClark. This suggests that HY5 is a negative regulator of iron stress responses in Fiskeby III. In particular, 105 DEGS associated with the biosynthesis of lipids, long-chain fatty acids, cutin, and flavonoids were repressed by iron stress due to HY5 silencing.

In contrast to silencing HY5 and FIT, silencing PYE had no phenotype in either Williams 82 or Fiskeby III. In Arabidopsis, the leaves of *pye-1* plants became chlorotic when seeds were germinated on iron-deficient media [23]. When transferred from sufficient to deficient conditions, *pye-1* plants had reduced chlorophyll content relative to wild type plants. In Arabidopsis, PYE represses the transcription of *bHLH38*, *bHLH39*, *bHLH100*, and *bHLH101* which interact with FIT to induce iron stress-responses [24]. While the redundant functions of *bHLH38*, *bHLH39*, *bHLH100*, and *bHLH101* have long been recognized, refs. [40,53] recently demonstrated the four genes lie in three syntenic blocks, helping to explain their co-regulation by PYE. Interestingly, only two homeologous genes with significant sequence homology and synteny to *bHLH38*, *bHLH39*, *bHLH100*, and *bHLH101* are present in the soybean genome. Silencing both homologs (syntenic to bHLH28) via

VIGS resulted in no phenotype in iron-sufficient conditions. Combined with our results, this suggests this complex of genes does not function in soybean as predicted by reviewing the Arabidopsis literature.

Fiskeby III's ability to tolerate iron stress is confirmed by the fact that no DEGs responding to iron stress were identified from EV plants. While silencing FIT, HY5, and PYE had no phenotypic impact on Fiskeby III, they did help identify genes and pathways that could be contributing to Fiskeby III's iron stress-tolerance. In our study, the treatment analyses of HY5 identified 109 repressed genes largely associated with fatty acid and wax biosynthesis, including cuticle development and cutin biosynthesis. Whaley et al. [54] hypothesized that abiotic stress tolerance of Fiskeby III was associated with the altered leaf physiology, providing passive resistance to ozone stress exposure. They found increased levels of wax and cutin biosynthetic genes in Mandarin (Ottawa) leaves compared to Fiskeby III, hypothesizing that increased expression in Mandarin (Ottawa) was an effort by the plant to increase the physical barrier to ozone penetration of the leaves. Our findings suggest these pathways are turned on very early in response to iron stress in Fiskeby III. In pear (*Pyrus communis*) and peach (*Prunus persica*), −Fe conditions reduce cuticular wax in leaves, thus altering water relations, and pest and disease resistance [55].

Given the large number of DEGs identified in many of our comparisons, we compared the gene lists to see if the response of Fiskeby III to the silencing of each of the three genes was conserved (Figures 1 and 2). In the silencing effect comparisons (VIGS vs. EV), only a small number of the genes are differentially expressed in multiple gene lists (Figure 1). Under +Fe conditions, only a single gene is differentially expressed in all three comparisons. This gene (*Glyma.09G172500*) corresponds to Arabidopsis map kinase kinase 9 (*At1g73500*), which positively regulates salt tolerance in Arabidopsis [56,57]. Under −Fe conditions, there are five genes differentially expressed in all three comparisons, and four of the Arabidopsis homologs are closely involved in defense/stress responses. These four genes include homologs of KTI1 (*Glyma.08G235400*, *At1g73260*), which modulates programmed cell death in plant/pathogen interactions; RIC1 (*Glyma.10G251400*, *At2g33460*), which interacts with ROP2 to fine-tune microtubule dynamics in response to salt stress; a serine proteinase inhibitor (*Glyma.20G205800*, *At2g38870*), which is involved in plant defense by encoding pathogenesis related proteins; and HKL1 (*Glyma.11G15800*, *At1G50460*), which is a negative regulator of plant growth and a positive regulator of immune responses [58–62]. None of these four genes is known to interact with each other in Arabidopsis (String-db). Despite the few genes differentially expressed in all three comparisons in both +Fe and −Fe analyses, there were a significant number of DEGs shared between HY5 vs. EV, and FIT vs. EV, comparisons in both +Fe and −Fe conditions. That silencing HY5 and FIT would affect the same genes is possible as HY5 was recently shown to positively regulate FIT in roots [31].

GO analysis allows us to determine the biological processes in plants affected by either the genotype or treatment comparisons being made. This is particularly powerful when coupled with heatmaps developed for each of the three comparisons (Figures 1 and 2). Given the role of iron in photosynthesis, it is not surprising that many of the identified GO terms are associated with photosynthesis. GO terms associated with DNA replication and methylation were over-represented in both genotype and treatment analyses. The GO term with the largest number of genes associated with it was identified in cluster S6+. GO term GO:0019288, isopentenyl diphosphate biosynthesis, mevalonate-independent pathway (MEP) was associated with 102 genes. Five of the seven genes in the MEP pathway (DXS, DXR, CMK, HDS, and HDR) are easily identified in our dataset and all are down-regulated in HY5-silenced plants. Isopentenyl diphosphate is a precursor for isoprenoid compounds. Isoprenoids are very diverse and very prevalent, anywhere from 20,000 to 35,000 different isoprenoids have been identified in different species [63]. The MEP pathway is functional in the chloroplast, so the down-regulation of these genes often results in reduced chloroplast and carotenoid development [63]. The MEP pathway is also used to synthesize phytohormones including gibberellins, abscisic acid, and cytokinins [64]. The repression of genes

associated with the MEP pathway may reflect the reduced photosynthesis of HY5-silenced Fiskeby III plants, even in +Fe conditions. Among the 71 over-represented GO categories identified from genes in cluster S6+, 17 are associated with photosynthesis. Two GO categories (GO:0009072 and GO0009073) are associated with aromatic amino acid (tryptophan, phenylalanine, and tyrosine) biosynthesis. Increased aromatic amino acid levels have been associated with improved abiotic stress tolerance [65,66]. Of the 35 genes associated with tyrosine, tryptophan, and phenylalanine, 32 are repressed in HY5-silenced plants under +Fe conditions compared to EV. It is possible that silencing HY5 reduces the abiotic stress tolerance through the repression of these genes. The remaining GO categories in all other clusters reflect diverse cellular processes.

4. Materials and Methods

4.1. Construct Development

Virus-induced gene silencing (VIGS) constructs were developed to knock down the expression of either GmFIT (*Glyma.13G322100*), GmHY5 (*Glyma.18G117100*), or GmPYE (*Glyma.05G027600*). These candidate genes were identified through previous experiments [5,15,16]. Reciprocal BLASTN was used to ensure these genes were the closest homolog to the Arabidopsis gene of interest. A fourth construct with no target gene insert, empty vector (EV), was used to control for viral symptoms. Silenced plants will be referred to as VIGS_FIT, VIGS_HY5, and VIGS_PYE. VIGS vectors were designed by cloning ~300 bp of the target gene of interest into the RNA2 of the bean pod mottle virus (BPMV) vector in the antisense orientation according to the protocol by Whitham et al. [67] using the following primers: GmFIT_F *GCTGTACGACTTTGTTGC*, GmFIT_R *ACTGAATGTGGAGCTTGG*, GmHY5_F *AGAGGGAGCAATAGTGG*, GmHY5_R *CGATTAATCAACCACACC*, GmPYE_F *AGATACAGGCAAGACTGG*, and GmPYE_R *TCCAAGCAGTTGTGATGG*. Due to the duplicated nature of the soybean genome, it is probable that the constructs silenced homoeologous genes within the genome. Previous studies have shown genes with >80% nucleotide identity will be silenced by a construct of interest [68]. Using BLASTN (version 2.2.29), we identified the homologs with >80% identity that are likely silenced by our constructs. Specifically, the FIT construct may also silence *Glyma.13G175200*, *Glyma.12G178500*, *Glyma.12G081200*, *Glyma.10G080900*, and *Glyma.04G034500*, while the HY5 construct might also silence *Glyma.08G302500*, and the PYE construct might also silence *Glyma.17G098900.* The two viral RNAs (RNA1 and RNA2) were used together in particle bombardment of the unifoliate Williams 82 soybean plants. VIGS infection was confirmed using a BPMV ELISA antibody assay (Agdia, Elkhart, IN, USA). Tissue from positive plants was collected, freeze-dried, and stored at −20. For this study, 150 mg of stored tissue was added to 150 mLs of PBS buffer. The tissue was disrupted in a TissueLyser II (Qiagen®, Germantown, MD, USA) at 80 rpm for 30 s.

4.2. Phenotyping VIGS Plants

For soil tests with Williams 82, seeds were germinated in Metro-Mix 900 potting soil (Sun Grow Horticulture, Agawam, MA, USA). For soil tests with Fiskeby III, seeds were germinated in grade 2 vermiculite (U-line vermiculite, Pleasant Prairie, WI, USA) for 6 days, then transferred to pots with the same soil mixture. Plants were infected with VIGS constructs when the unifoliates were fully expanded. To infect plants, carborundum was dusted over the leaves and 20 µL of the slurry was pipetted onto each of the first true leaves and manually rubbed. Plants were maintained in soil for 14 days before phenotyping. Phenotypic measurements included: SPAD readings, shoot height (from cotyledons), and shoot weight. For phenotyping in hydroponics, Fiskeby III seeds were started in vermiculite as described above. Seven days after planting (DAP), seedlings were removed from the vermiculite, triple rinsed in double distilled water, and placed into iron-sufficient (+Fe) hydroponic solutions (100 µM $Fe(NO_3)_3$) as described previously [69]. After 24 h in hydroponics, unifoliate leaves were infected with unique VIGS constructs as described above. Plants in hydroponics were maintained in +Fe solutions for 14 days after

VIGS infection. On day 14, plants were rinsed in new +Fe hydroponic solution, and then half the plants were moved into new +Fe hydroponic solutions and half the plants were moved into −Fe (50 μM $Fe(NO_3)_3$) hydroponic solutions. Plants were left in their new hydroponic solutions for 21 days, at which point the phenotypic measurements described above were taken.

4.3. Collecting Tissue for RNAseq Analyses

For RNA-seq analyses of plants grown in hydroponics, plants were treated exactly as described for plants used for VIGS phenotyping in hydroponics, but plants were only placed in +Fe or −Fe hydroponic solutions for 60 min. After 60 min, plants were removed from hydroponics, and the third trifoliate was collected, immediately flash frozen in liquid nitrogen, and moved to −80 storage. All hydroponics plants (phenotyping and RNAseq) were maintained in the same growth chamber.

4.4. RNAseq Library Preparation and Transcriptomic Analyses

Total RNA was extracted using the Qiagen RNeasy Plant Mini kits (Qiagen®, Germantown, MD, USA). After RNA extraction, the remaining DNA was removed using the Ambion Turbo DNAse Free kit (Ambion®, Austin, TX, USA). The resulting RNA was further purified using the Qiagen MinElute RNA cleanup kits (Qiagen®, Germantown, MD, USA). Sample integrity and purity were confirmed using an Implen NanoPhotometer N60 (Implen, Munich, Germany). Samples were submitted to the Iowa State University DNA facility for sequencing. mRNA-Seq libraries were generated, and Illumina adapter sequences were added to 32 multiplex samples per lane. All samples were sequenced on the NovaSeq 6000 (Illumina®, San Diego, CA, USA), generating 100 bp paired-end reads. Samples were distributed across three sequencing lanes. In total, 1,095,391,734 reads were generated. The quality of these reads was confirmed using FastQC (version 0.11.9) [70]. Illumina adaptor sequences and reads <50 bp, with leading or trailing quality below 3, and when a sliding window (4 bp) average quality score <15, they were removed using Trimmomatic (version 0.39) [71]. The remaining reads were aligned to the soybean genome sequence (Gmax_508_v4.0.fa, downloaded from phytozome.net accessed on 2 March 2023) using HiSat2 (version 2.2.1) [72] and default parameters. Read counts per gene were examined to make sure the silenced gene for that sample had the highest number of reads; this is a result of viral reads with the target gene of interest and confirms VIGS infection and gene silencing. Additionally, samples were screened using FASTQ Screen (version 0.14.1) [73] to confirm viral infection. These two approaches led to the removal of a single sample EV + Fe4, as VIGS infection (and thus gene silencing ability) could not be confirmed. All remaining samples were realigned to a modified.gff file where GmFIT, GmPYE, and GmHY5 were removed (Glyma.13G322100, Glyma.05G027600, and Glyma.18G117100, respectively). This modification ensured the viral reads mapping to the target gene of interest (FIT, PYE, and HY5) were not included in the alignments because they would skew normalization and downstream statistical analyses. Each sample was aligned individually, and the output was written to SAM files. SAM files were converted to BAM files, sorted, and indexed using samtools (version 1.16) [74]. Normalized reads are available at the NCBI SRA database PRJNA1164167.

Sorted and indexed BAM files were merged and loaded into RStudio [75] for differential gene expression analysis using edgeR (version 3.18.1) [76,77]. Samples were normalized using the trimmed mean of M to account for variations in library sizes. Subsequent visualizations of biological replicates revealed two samples with altered expression patterns compared to the other three replicates. Accordingly, one VIGS_FIT and one VIGS_PYE sample (both from +Fe-grown plants) were removed. Samples were re-normalized, and differentially expressed genes were identified by comparing each target gene's samples to the EV control samples (Tables S1, S2 and S6). An FDR of 0.05 was used to identify significantly differentially expressed genes.

Annotations were assigned to each significantly differentially expressed gene using the Gene Annotation Lookup tool at soybase.org (version 4). Significantly over-represented gene ontology (GO) terms (Corrected $p < 0.05$) associated with each of the DEG lists were identified using the GO Term Enrichment tool (version 4) at soybase.org. CLOVER [47] was used to examine the 1000 bp promoter region of each DEG for significantly over-represented (p-value = 0) transcription factor binding sites (TFBS) from the JASPAR 2022 plant non-redundant TFBS database [78]. Identified TFBS are provided in Table S4.

5. Conclusions

Based on the available literature, we believed GmFIT and GmHy5 would operate in iron-deficient conditions to induce iron stress-responses. While silencing GmFIT had no observable phenotype in Fiskeby III, our analyses demonstrate that GmFIT is a negative regulator of iron stress-responses in Fiskeby III. While silencing GmFIT did impact the expression of canonical iron uptake and homeostasis genes, it also restored the iron responsiveness of a suite of genes associated with photosynthesis and the chloroplast. Similarly, silencing the negative regulator GmHY5 resulted in the differential expression of DEGs associated with the Clark iron stress response: DNA replication/methylation, photosynthesis, stress, and defense. However, canonical iron uptake and homeostasis genes are still missing from the Fiskeby III iron stress toolbox. This suggests there must be an alternative pathway for iron uptake and utilization in Fiskeby III. We recently identified a MATE transporter that was located with an IDC QTL on chromosome 5, and was differentially expressed in response to iron stress, and when silenced in Fiskeby III resulted in chlorosis symptoms in iron-sufficient conditions [14–16]. Surprisingly, the. RNA-seq of VIGS plants identified only 150 DEGs. However, RNA-seq analyses across multiple timepoints and tissues confirms that Fiskeby III invokes most aspects of the Clark iron stress-responses. This suggests Fiskeby III does not induce stress-specific responses, but instead induces more general stress responses to all stresses.

Supplementary Materials: The following supporting information can be downloaded at: https://www.mdpi.com/article/10.3390/ijms252111480/s1.

Author Contributions: Conceptualization, J.A.O. and M.A.G.; methodology, J.A.O. and M.A.G.; formal analysis, J.A.O.; writing—original draft preparation, J.A.O.; writing—review and editing, M.A.G. All authors have read and agreed to the published version of the manuscript.

Funding: This research was funded by USDA-ARS project 5030-21220-007-000D and used resources provided by the SCINet project of the USDA-ARS project number 0500-00093-001-00-D.

Data Availability Statement: The original data presented in the study are openly available in the NCBI SRA database at https://www.ncbi.nlm.nih.gov/sra/ (accessed on 24 September 2024) using the reference PRJNA1164167.

Conflicts of Interest: The authors declare no conflicts of interest. The mention of trade names or commercial products in this publication is solely for the purpose of providing specific information and does not imply recommendation or endorsement by the U.S. Department of Agriculture. USDA-ARS is an equal opportunity employer and provider.

References

1. Marschner, H. *Mineral Nutrition of Higher Plants*; Academic Press Limited: San Diego, CA, USA, 1995. [CrossRef]
2. Grillet, L.; Schmidt, W. Iron acquisition strategies in land plants: Not so different after all. *New Phytol.* **2019**, *224*, 11–18. [CrossRef] [PubMed]
3. Li, M.; Watanabe, S.; Gao, F.; Dubos, C. Iron nutrition in plants: Towards a new paradigm. *Plants* **2023**, *12*, 384. [CrossRef] [PubMed]
4. Atwood, S.E.; O'Rourke, J.A.; Peiffer, G.A.; Yin, T.; Majumder, M.; Zhang, C.; Cianzio, S.R.; Hill, J.H.; Cook, D.; Whitham, S.A.; et al. Replication protein A subunit 3 and the iron efficiency response in soybean. *Plant Cell Environ.* **2014**, *37*, 213–234. [CrossRef] [PubMed]
5. Atencio, L.; Salazar, J.; Lauter, A.N.M.; Gonzales, M.D.; O'Rourke, J.A.; Graham, M.A. Characterizing short and long term iron stress responses in iron deficiency tolerant and susceptible soybean (*Glycine max* L. Merr). *Plant Stress* **2021**, *2*, 100012. [CrossRef]

6. Moran Lauter, A.N.; Peiffer, G.A.; Yin, T.; Whitham, S.A.; Cook, D.; Shoemaker, R.C.; Graham, M.A. Identification of candidate genes involved in early iron deficiency chlorosis signaling in soybean (*Glycine max*) roots and leaves. *BMC Genom.* **2014**, *15*, 1. [CrossRef]
7. Moran Lauter, A.N.; Rutter, L.; Cook, D.; O'Rourke, J.A.; Graham, M.A. Examining short-term responses to a long-term problem: RNA-seq analyses of iron deficiency chlorosis tolerant soybean. *Int. J. Mol. Sci.* **2020**, *21*, 3591. [CrossRef]
8. Kohlhase, D.R.; McCabe, C.E.; Singh, A.K.; O'Rourke, J.A.; Graham, M.A. Comparing Early Transcriptomic Responses of 18 Soybean (Glycine max) Genotypes to Iron Stress. *Int. J. Mol. Sci.* **2021**, *22*, 11643. [CrossRef]
9. O'Rourke, J.; Graham, M.A. Gene expression responses to sequential nutrient deficiency stresses in soybean. *Int. J. Mol. Sci.* **2021**, *22*, 1252. [CrossRef]
10. O'Rourke, J.A.; McCabe, C.E.; Graham, M.A. Dynamic gene expression changes in response to micronutrient, macronutrient, and multiple stress exposure in soybean. *Funct. Integr. Genom.* **2020**, *20*, 321–341. [CrossRef]
11. Assefa, T.; Zhang, J.; Chowda-Reddy, R.V.; Lauter, A.N.M.; Singh, A.; O'Rourke, J.A.; Graham, M.A.; Singh, A.K. Deconstrcting the genetic architecture of iron deficiency chlorosis in soybean using genome-wide approaches. *BMC Plant Biol.* **2020**, *20*, 42. [CrossRef]
12. Lin, S.-F.; Baumer, J.S.; Ivers, D.; de Cianzo, S.R.; Shoemaker, R.C. Field and nutrient solution tests measure similar mechanisms controlling iron deficiency chlorosis in soybean. *Crop Sci.* **1998**, *38*, 254–259. [CrossRef]
13. Lin, S.; Cianzio, S.; Shoemaker, R. Mapping genetic loci for iron deficiency chlorosis in soybean. *Mol. Breed.* **1997**, *3*, 219–229. [CrossRef]
14. Merry, R.; Butenhoff, K.; Campbell, B.W.; Michno, J.-M.; Wang, D.; Orf, J.H.; Lorenz, A.J.; Stupar, R.M. Identification and fine-mapping of a soybean quantitative trait locus on chromosome 5 confering tolerance to iron deficiency chlorosis. *Plant Genome* **2019**, *12*, 190007. [CrossRef] [PubMed]
15. O'Rourke, J.A.; Graham, M.A. Coupling VIGS with short and long-term stress exposure to understand the Fiskeby III iron deficiency stress response. *Int. J. Mol. Sci.* **2022**, *24*, 647. [CrossRef] [PubMed]
16. O'Rourke, J.A.; Morrisey, M.J.; Merry, R.; Espina, M.J.; Lorenz, A.J.; Stupar, R.M.; Graham, M.A. Mining Fiskeby III and Mandarin (Ottawa) Expression Profiles to Understand Iron Stress Tolerant Responses in Soybean. *Int. J. Mol. Sci.* **2021**, *22*, 11032. [CrossRef]
17. Bauer, P.; Ling, H.-Q.; Guerinot, M.L. FIT, the FER-like iron deficiency induced transcription factor in Arabidopsis. *Plant Physiol. Biochem.* **2007**, *45*, 260–261. [CrossRef]
18. Yuan, Y.; Wu, H.; Wang, N.; Li, J.; Zhao, W.; Du, J.; Wang, D.; Ling, H.-Q. FIT interacts with AtbHLH38 and AtbHLH39 in regulating iron uptake gene expression for iron homeostasis in Arabidopsis. *Cell Res.* **2008**, *18*, 385–397. [CrossRef]
19. Schwartz, B.; Bauer, P. FIT, a regulatory hub for iron deficiency and stress signaling in roots, and FIT-dependent and independent gene signatures. *J. Exp. Bot.* **2020**, *71*, 1694–1705. [CrossRef]
20. Chen, C.-L.; Cui, Y.; Cui, M.; Zhou, W.-J.; Wu, H.-L.; Ling, H.-Q. A FIT binding protein is involved in modulating iron and zinc homeostasis in Arabidopsis. *Plant Cell Environ.* **2018**, *41*, 1698–1714. [CrossRef]
21. Colangelo, E.P.; Guerinot, M.L. The essential basic helix-loop-helix protein FIT1 is required for the iron deficiency response. *Plant Cell* **2004**, *16*, 3400–3412. [CrossRef]
22. Sivitz, A.B.; Hermand, V.; Curie, C.; Vert, G. Arabidopsis bHLH100 and bHLH101 control iron homeostasis via a FIT-independent pathway. *PLoS ONE* **2012**, *7*, e44843. [CrossRef] [PubMed]
23. Long, T.A.; Tsukagoshi, H.; Busch, W.; Lahner, B.; Salt, D.E.; Benfey, P.N. The bHLH transcription factor POPEYE regulates response to iron deficiency in Arabidopsis roots. *Plant Cell* **2010**, *22*, 2219–2236. [CrossRef] [PubMed]
24. Na Pu, M.; Liang, G. The transcription factor POPEYE negatively regulates the expression of bHLH 1b genes to maintain iron homeostasis. *J. Exp. Bot.* **2023**, *74*, 2754–2767. [CrossRef]
25. Akmakjian, G.Z.; Riaz, N.; Guerinot, M.L. Photoprotection during iron deficiency is mediated by the bHLH transcription factors PYE and ILR3. *Proc. Natl. Acad. Sci. USA* **2021**, *118*, e2024918118. [CrossRef]
26. Jiao, Y.; Lau, O.S.; Deng, X.W. Light regulated transcriptional networks in higher plants. *Nat. Rev. Genet.* **2007**, *8*, 217–230. [CrossRef]
27. Gangappa, S.N.; Botto, J.F. The multifacetted roles of HY5 in plant growth and development. *Mol. Plant* **2016**, *9*, 1353–1365. [CrossRef]
28. Chen, X.; Yao, Q.; Gao, X.; Jiang, C.; Harberd, N.P.; Fu, X. Shoot-to-root mobile transcription factor HY5 coordinates plant carbon and nitrogen acquisition. *Curr. Biol.* **2016**, *26*, 640–646. [CrossRef]
29. Cluis, C.P.; Mouchel, C.F.; Hardtke, C.S. The Arabidopsis transcription factor HY5 integrates light and hormone signaling pathways. *Plant J.* **2004**, *38*, 332–347. [CrossRef]
30. Mankotia, S.; Singh, D.; Monika, K.; Kalra, M.; Meena, H.; Meena, V.; Yadav, R.K.; Pandey, A.K.; Satbhai, S.B. Elongated Hypocotyl 5 regulates BRUTUS and affects iron acquisition and homeostasis in *Arabidopsis thaliana*. *Plant J.* **2023**, *114*, 1267–1284. [CrossRef]
31. Mankotia, S.; Jakhar, P.; Satbhai, S.B. HY5: A key regulator for light mediated nutrient uptake and utilization by plants. *New Phytol.* **2024**, *241*, 1929–1935. [CrossRef]
32. Mankotia, S.; Dubey, A.; Jakhar, P.; Shikha, D.; Koolath, V.; Kumar, A.; Satbhai, S.B. Elongated Hypocotyl 5 (HY5) and Popeye (PYE) regulate intercellular iron transport in plants. *Plant Cell Environ.* **2024**. [CrossRef] [PubMed]

33. Pizzio, G.A.; Rodriguez, L.; Antoni, R.; Gonzalez-Guzman, M.; Yunta, C.; Merilo, E.; Kollist, H.; Albert, A.; Rodriguez, P.L. The PYL4 A194T mutant uncovers a key role of PYR1-LIKE4/PROTEIN PHOSPHATASE 2CA interaction for abscisic acid signaling and plant drought resistance. *Plant Physiol* **2013**, *163*, 441–455. [CrossRef] [PubMed]
34. Du, M.; Lu, D.; Liu, X. The Arabidopsis ubiquitin ligases ATL32 and ATL6 regulate plant response to salt stress in an ABA-independent manner. *Biochem. Biophys. Res. Commun.* **2023**, *685*, 149156. [CrossRef] [PubMed]
35. Gupta, N.; Kanojia, A.; Katiyar, A.; Mudgil, Y. Molecular characterization of NDL1-AGB1 mediated salt stress signaling: Further exploration of the role of *NDL1* interacting partners. *Cells* **2021**, *10*, 2261. [CrossRef] [PubMed]
36. Hu, S.-P.; Li, J.-J.; Dhar, N.; Li, J.-P.; Chen, J.-Y.; Jian, W.; Dai, X.-F.; Yang, X.-Y. Lysin motif (LysM) proteins: Interlinking manipulation of plant immunity and fungi. *Int. J. Mol. Sci.* **2021**, *22*, 3114. [CrossRef]
37. Scheepers, M.; Spielmann, J.; Boulanger, M.; Carnol, M.; Bosman, B.; De Pauw, E.; Goormaghtigh, E.; Motte, P.; Hanikenne, M. Intertwined metal homeostasis, oxidative and biotic stress responses in the Arabidopsis frd3 mutant. *Plant J.* **2019**, *102*, 34–52. [CrossRef]
38. Kim, L.J.; Tsuyuki, K.M.; Hu, F.; Park, E.Y.; Zhang, J.; Iraheta, J.G.; Chia, J.; Huang, R.; Tucker, A.E.; Clyne, M.; et al. Ferroportin 3 is a dual-targeted mitochondrial/chloroplast iron exporter necessary for iron homeostasis in Arabidopsis. *Plant J.* **2021**, *107*, 215–236. [CrossRef]
39. Li, L.-Y.; Cai, Q.-Y.; Yu, D.-S.; Guo, C.-H. Overexpression of AtFRO6 in transgenic tobacco enhances ferric chelate reductase activity in leaves and increases tolerance to iron-deficiency chlorosis. *Mol. Biol. Rep.* **2010**, *38*, 3605–3613. [CrossRef]
40. Kohlhase, D.R.; O'rourke, J.A.; Graham, M.A. GmGLU1 and GmRR4 contribute to iron deficiency tolerance in soybean. *Front. Plant Sci.* **2024**, *15*, 1295952. [CrossRef]
41. Santos, C.S.; Ozgur, R.; Uzilday, B.; Turkan, I.; Roriz, M.; Rangel, A.O.; Carvalho, S.M.; Vasconcelos, M.W. Understanding the role of the antioxidant system and the tetrapyrrole cycle in iron deficiency chlorosis. *Plants* **2019**, *8*, 348. [CrossRef]
42. Singh, N.; Bhatla, S.C. Heme oxygenase-nitric oxide cross-talk-mediated iron homeostasis in plants under oxidative stress. *Free Radic. Biol. Med.* **2022**, *182*, 192–205. [CrossRef] [PubMed]
43. Sun, C.; Wu, T.; Zhai, L.; Li, D.; Zhang, X.; Xu, X.; Ma, H.; Wang, Y.; Han, Z. Reactive oxygen species function to mediate the Fe deficiency response in an Fe-efficient apple genotype: An early response mechanism for enhancing reactive oxygen prodyction. *Front. Plant Sci.* **2016**, *7*, 1726. [CrossRef] [PubMed]
44. Garcia-Caparros, P.; De Filippis, L.; Gul, A.; Hasanuzzaman, M.; Ozturk, M.; Altay, V.; Lao, M.T. Oxidative stress and antioxidant metabolism under adverse environmental conditions: A review. *Bot. Rev.* **2021**, *87*, 421–466. [CrossRef]
45. Santos, C.S.; Sousa, C.; Bagheri, M.; Pinho, S.; Vasconcelos, M.W. Predicting iron deficiency and oxidative stress in Glycine max through Fourier transform infrared spectroscopy in a time-course experiment. *Plant Soil* **2024**, *496*, 161–177. [CrossRef]
46. Ramírez, L.; Bartoli, C.G.; Lamattina, L. Glutathione and ascorbic acid protect Arabidopsis plants against detrimental effects of iron deficiency. *J. Exp. Bot.* **2013**, *64*, 3169–3178. [CrossRef]
47. Frith, M.C.; Fu, Y.; Yu, L.; Chen, J.F.; Hansen, U.; Weng, Z. Detection of functional DNA motifs via statistical over-representation. *Nucleic Acids Res.* **2004**, *32*, 1372–1381. [CrossRef]
48. Qian, D.; Zhang, Z.; He, J.; Zhang, P.; Ou, X.; Li, T.; Niu, L.; Nan, Q.; Niu, Y.; He, W.; et al. Arabidopsis ADF5 promotes stomatal closure by regulating actin cytoskeleton remodeling in response to ABA and drought stress. *J. Exp. Bot.* **2018**, *70*, 435–446. [CrossRef]
49. Zhang, Y.; Chen, X.; Feng, J.; Shen, Y.; Huang, Y. The proteome and phosphoproteome uncovers candidate proteins associated with vacuolar phosphate signal multiplied by vacuolar phosphate transporter 1 (VPT1) in Arabidopsis. *Mol. Cell. Proteom.* **2023**, *22*, 100549. [CrossRef]
50. He, Z.; Zhao, X.; Kong, F.; Zuo, Z.; Liu, X. TCP2 positively regulates HY5/HYH and photomorphogenesis in Arabidopsis. *J. Exp. Bot.* **2016**, *67*, 775–785. [CrossRef]
51. Hansen, N.; Jolley, V.; Naeve, S.; Goos, R. Iron deficiency of soybean in the north central U.S. and associated soil properties. *Soil Sci. Plant Nutr.* **2004**, *50*, 983–987. [CrossRef]
52. Merry, R.; Dobbels, A.A.; Sadok, W.; Naeve, S.; Stupar, R.M.; Lorenz, A.J. Iron deficiency in soybean. *Crop Sci.* **2021**, *62*, 36–52. [CrossRef]
53. Wang, N.; Cui, Y.; Liu, Y.; Fan, H.; Du, J.; Huang, Z.; Yuan, Y.; Wu, H.; Ling, H.-Q. Requirement and functional redundancy of Ib subgroup bHLH proteins for iron deficiency responses and uptake in *Arabidopsis thaliana*. *Mol. Plant* **2013**, *6*, 503–513. [CrossRef] [PubMed]
54. Whaley, A.; Sheridan, J.; Safari, S.; Burton, A.; Burkey, K.; Schlueter, J. RNA-seq analysis reveals genetic response and tolerance mechanisms to ozone exposure in soybean. *BMC Genom.* **2015**, *16*, 426. [CrossRef] [PubMed]
55. Fernández, V.; Eichert, T.; Del Río, V.; López-Casado, G.; Heredia-Guerrero, J.A.; Abadía, A.; Heredia, A.; Abadía, J. Leaf structural changes associated iwth iron deficiency chlorosis in field grown pear and peach: Physiological implications. *Plant Soil* **2008**, *311*, 161. [CrossRef]
56. Liu, J.; Wang, X.; Yang, L.; Nan, W.; Ruan, M.; Bi, Y. Involvement of active MKK9-MAPK3/MAPK6 in increasing respiration in salt treated *Arabidopsis callus*. *Protoplasma* **2020**, *257*, 965–977. [CrossRef]
57. Shen, L.; Zhuang, B.; Wu, Q.; Zhang, H.; Nie, J.; Jing, W.; Yang, L.; Zhang, W. Phosphatidic acid promotes the activation and plasma membrane localization of MKK7 and MKK9 in response to salt stress. *Plant Sci.* **2019**, *287*, 110190. [CrossRef]

58. Zhang, M.; Koh, J.; Liu, L.; Shao, Z.; Liu, H.; Hu, S.; Zhu, N.; Dufresne, C.P.; Chen, S.; Wang, Q. Critical role of COI1-dependent jasmonate pathway in AAL toxin induced PCD in tomato revealed by comparative proteomics. *Sci. Rep.* **2016**, *6*, 28451. [CrossRef]
59. Li, J.; Brader, G.; Palva, E.T. Kunitz trypsin inhibitor: An antagonisti of cell death triggered by photpathogens and fumonisin B1 in Arabidopsis. *Mol. Plant* **2008**, *1*, 482–495. [CrossRef]
60. Li, C.; Lu, H.; Li, W.; Yuan, M.; Fu, Y. A ROP2-RIC1 pathway fine-tunes microtubule reorganization for salt tolerance in Arabidopsis. *Plant Cell Environ.* **2018**, *40*, 1127–1142. [CrossRef]
61. Sels, J.; Mathys, J.; De Coninck, B.M.; Cammue, B.P.; De Bolle, M.F. Plant pathogenesis-related (PR) proteins: A focus on PR peptides. *Plant Physiol. Biochem.* **2008**, *46*, 941–950. [CrossRef]
62. Jing, W.; Uddin, S.; Chakraborty, R.; Van Anh, D.T.; Macoy, D.M.; Park, S.O.; Ryu, G.R.; Kim, Y.H.; Cha, J.; Kim, W.-Y.; et al. Molecular characterization of HEXOKINASE1 in plant innate immunity. *Appl. Biol. Chem.* **2020**, *63*, 76. [CrossRef]
63. Cordoba, E.; Salmi, M.; León, P. Unravelling the regulatory mechanisms that modulate the MEP pathway in higher plants. *J. Exp. Bot.* **2009**, *60*, 2933–2943. [CrossRef] [PubMed]
64. Suzuki, M.; Nakagawa, S.; Kamide, Y.; Kobayashi, K.; Ohyama, K.; Hashinokuchi, H.; Kiuchi, R.; Saito, K.; Muranaka, T.; Nagata, N. Complete blockage of the mevalonate pathway results in male gametophyte lethality. *J. Exp. Bot.* **2009**, *60*, 2055–2064. [CrossRef] [PubMed]
65. Oliva, M.; Guy, A.; Galili, G.; Dor, E.; Schweitzer, R.; Amir, R.; Hacham, Y. Enhanced production of aromatic amino acids in tobacco plants leads to increased phenylpropanoid metabolites and tolerance to stresses. *Front. Plant Sci.* **2021**, *11*, 604349. [CrossRef]
66. Batista-Silva, W.; Heinemann, B.; Rugen, N.; Nunes-Nesi, A.; Araújo, W.L.; Braun, H.-P.; Hildebrandt, T.M. The role of amino acid metabolism during abiotic stress release. *Plant Cell Environ.* **2019**, *42*, 1630–1644. [CrossRef]
67. Whitham, S.A.; Lincoln, L.M.; Chowda-Reddy, R.V.; Dittman, J.D.; O'Rourke, J.A.; Graham, M.A. Virus-Induced Gene Silencing and Transient Gene Expression in Soybean (*Glycine max*) Using Bean Pod Mottle Virus Infectious Clones. *Curr. Protoc. Plant Biol.* **2016**, *1*, 263–283. [CrossRef]
68. Pandey, A.K.; Yang, C.; Zhang, C.; Graham, M.A.; Horstman, H.D.; Lee, Y.; Zabotina, O.A.; Hill, J.H.; Pedley, K.F.; Whitham, S.A. Functional analysis of the Asian soybean rust resistance pathway mediated by Rpp2. *Mol. Plant-Microbe Interact.* **2011**, *24*, 194–206. [CrossRef]
69. Chaney, R.L.; Coulombe, B.A.; Bell, P.F.; Angle, J.S. Detailed method to screen dicot cultivars for resistance to Fe-chlorosis using FeDTPA and bicarbonate in nutrient solutions. *J. Plant Nutr.* **1992**, *15*, 2063–2083. [CrossRef]
70. Andrews, S. *FastQC: A Quality Control Tool for High Throughput Sequence Data*; Babraham Bioinformatics: Cambridge, UK, 2010.
71. Bolger, A.M.; Lohse, M.; Usadel, B. Trimmomatic: A flexible trimmer for Illunina sequence data. *Bioinformatics* **2014**, *30*, 2114–2120. [CrossRef]
72. Kim, D.; Langmead, B.; Salzberg, S.L. HISAT: A fast spliced aligner with low memory requirements. *Nat. Methods* **2015**, *12*, 357–360. [CrossRef]
73. Wingett, S.W.; Andrews, S. FastQ Screen: A tool for multi-genome mapping nd quality control (version 0.14.1). *F1000Research* **2018**, *7*, 1338. [CrossRef] [PubMed]
74. Li, H.; Handsaker, B.; Wysoker, A.; Fennell, T.; Ruan, J.; Homer, N.; Marth, G.; Abecasis, G.; Durbin, R. The sequence alignment/map format and SAMtools. *Bioinformatics* **2009**, *25*, 2078–2079. [CrossRef] [PubMed]
75. RStudio Team. *RStudio: Integrated Development for R*; RStudio Inc.: Boston, MA, USA, 2015.
76. Chen, Y.; Lun, A.T.L.; Smyth, G.K. From reads to genes to pathways: Differential expression analysis of RNA-seq experiments using Rsubread and the edgeR quasi-likelihood pipeline. *F1000Research* **2016**, *5*, 1438. [CrossRef] [PubMed]
77. Robinson, M.D.; McCarthy, D.J.; Smyth, G.K. edgeR: A Bioconductor package for differential expression analysis of digital gene expression data. *Bioinformatics* **2010**, *26*, 139–140. [CrossRef]
78. Castro-Mondragon, J.A.; Riudavets-Puig, R.; Rauluseviciute, I.; Berhanu Lemma, R.; Turchi, L.; Blanc-Mathieu, R.; Lucas, J.; Boddie, P.; Khan, A.; Manosalva Pérez, N.; et al. JASPAR 2022: The 9th release of the open-access database of transcription factor binding profiles. *Nucleic Acids Res.* **2022**, *50*, D165–D173. [CrossRef]

Disclaimer/Publisher's Note: The statements, opinions and data contained in all publications are solely those of the individual author(s) and contributor(s) and not of MDPI and/or the editor(s). MDPI and/or the editor(s) disclaim responsibility for any injury to people or property resulting from any ideas, methods, instructions or products referred to in the content.

International Journal of
Molecular Sciences

MDPI

Article

Profiling of Key Hub Genes Using a Two-State Weighted Gene Co-Expression Network of 'Jao Khao' Rice under Soil Salinity Stress Based on Time-Series Transcriptome Data

Prasit Khunsanit [1,2], Kitiporn Plaimas [3], Supachitra Chadchawan [4,5] and Teerapong Buaboocha [2,5,*]

[1] Program in Biotechnology, Faculty of Science, Chulalongkorn University, Bangkok 10330, Thailand; khunsanit.prasit@gmail.com
[2] Center of Excellence in Molecular Crop, Department of Biochemistry, Faculty of Science, Chulalongkorn University, Bangkok 10330, Thailand
[3] Department of Mathematics and Computer Science, Faculty of Science, Chulalongkorn University, Bangkok 10330, Thailand; kitiporn.p@chula.ac.th
[4] Center of Excellence in Environment and Plant Physiology, Department of Botany, Faculty of Science, Chulalongkorn University, Bangkok 10330, Thailand; supachitra.c@chula.ac.th
[5] Omics Sciences and Bioinformatics Center, Faculty of Science, Chulalongkorn University, Bangkok 10330, Thailand
* Correspondence: teerapong.b@chula.ac.th; Tel.: +66-2-218-5419

Abstract: RNA-sequencing enables the comprehensive detection of gene expression levels at specific time points and facilitates the identification of stress-related genes through co-expression network analysis. Understanding the molecular mechanisms and identifying key genes associated with salt tolerance is crucial for developing rice varieties that can thrive in saline environments, particularly in regions affected by soil salinization. In this study, we conducted an RNA-sequencing-based time-course transcriptome analysis of 'Jao Khao', a salt-tolerant Thai rice variety, grown under normal or saline (160 mM NaCl) soil conditions. Leaf samples were collected at 0, 3, 6, 12, 24, and 48 h. In total, 36 RNA libraries were sequenced. 'Jao Khao' was found to be highly salt-tolerant, as indicated by the non-significant differences in relative water content, cell membrane stability, leaf greenness, and chlorophyll fluorescence over a 9-day period under saline conditions. Plant growth was slightly retarded during days 3–6 but recovered by day 9. Based on time-series transcriptome data, we conducted differential gene expression and weighted gene co-expression network analyses. Through centrality change from normal to salinity network, 111 key hub genes were identified among 1,950 highly variable genes. Enriched genes were involved in ATP-driven transport, light reactions and response to light, ATP synthesis and carbon fixation, disease resistance and proteinase inhibitor activity. These genes were upregulated early during salt stress and RT-qPCR showed that 'Jao Khao' exhibited an early upregulation trend of two important genes in energy metabolism: RuBisCo (*LOC_Os10g21268*) and ATP synthase (*LOC_Os10g21264*). Our findings highlight the importance of managing energy requirements in the initial phase of the plant salt-stress response. Therefore, manipulation of the energy metabolism should be the focus in plant resistance breeding and the genes identified in this work can serve as potentially effective candidates.

Keywords: network-based analysis; rice; RNA-sequencing; salt tolerance; transcriptomic; two-state co-expression network; weighted co-expression network

1. Introduction

High soil salinity significantly affects rice cultivation by impeding root water absorption, leading to osmotic stress in plant cells. Moreover, an excessive influx of NaCl can exacerbate ionic and oxidative stress [1]. Understanding the molecular mechanisms underlying salt tolerance is essential for enhancing the resilience of rice varieties to salinity,

particularly in areas affected by soil salinization. Salt tolerance is governed by numerous genes or quantitative trait loci (QTLs), which collaborate via co-regulation and/or co-expression to alleviate salinity-induced stress via intricate molecular mechanisms.

Transcript–transcript association network analysis plays a crucial role in the elucidation of the molecular mechanisms of a biological system in systems biology studies [2]. With the progression of deep genome sequencing, RNA-sequencing has been used to investigate gene expression in rice under particular abiotic stimuli, such as salinity [3]. Weighted gene co-expression network analysis (WGCNA), a molecular biological correlation network analysis method, uses transcriptome data to analyze intricate gene-regulatory networks by grouping co-expressed genes into adjacency modules and classifying them based on functional and pathway enrichment. This approach relies on a strong pairwise correlation of transcript levels between specific time points. WGCNA was initially developed by Langfelder and Horvath [4]. WGCNA has proven to be effective in identifying hub genes associated with both biotic and abiotic stresses. For example, in Arabidopsis, network centrality analyses for identifying key transcription factors crucial in drought stress conditions revealed 117 transcription factors with hub-like properties [5]. Similarly, in rice seedlings, 17 potential candidates associated with drought, salinity, and heat stress were identified by analyzing centrality properties and densely interconnected interactions [6].

Two-state GCNA was adopted to identify key genes in the global (encompassing transcriptome data from two conditions), the normal-state (containing transcriptome data from seedlings grown under normal conditions), and the stress-state (containing transcriptome data from stress conditions) networks. The global network served as an overarching network. The two-state networks facilitated analysis of the centrality changes from the normal to the saline conditions. Using two-state WGCNA, Sonsungsan, et al. [7] identified key salt tolerance genes in 'Luang Pratahn', a Thai rice variety, and reported that more than 44% of the key genes were related to salt stress and various stress responses. Chutimanukul, et al. [8] performed WGCNA to detect potential salt-tolerance genes in chromosome segment substitution lines of 'Khao Dawk Mali 105'. *OsBTBZ1* (LOC_Os01g66890), initially identified as a potential salt-tolerance gene, was further characterized and found to function as a salt-tolerance gene operating via abscisic acid (ABA)-dependent pathways [9].

Since salt tolerance is a multigene trait involving several cellular processes and dependent on the plant genetic background, comprehensive identification of key genes involved and their variations among different varieties will lead to complete understandings on the mechanisms of salinity tolerance. The Thai rice variety 'Jao Khao' is salt-tolerant during both the seedling and flowering stages and maintains high yields under saline conditions [10,11]. In the present study, we conducted two-state WGCNA of 'Jao Khao' rice at the seedling stage using transcriptomic time-series data to compare responses under normal and saline conditions. The aim of this study was to identify major cellular processes and crucial hub genes implicated in salt stress.

2. Results

2.1. Salt-Stress Related Phenotypes of 'Jao Khao' under Saline Soil Conditions

We determined the tiller number, plant weight, salt injury evaluation system (SES), cell membrane stability (CMS), and relative water content (RWC) at days 0, 3, 6, and 9 under normal and saline (160 mM NaCl) soil conditions. All phenotypic data are presented in Figure 1 and Supplementary Table S1 and Figure S1. In response to salt stress, the tiller number tended to increase from day 0 to day 9, and the SES score significantly increased from day 0 to day 6 but decreased on day 9 (Figure 1A,B). Shoot and root fresh weights and dry weights were lower in the saline treatment group on days 3 and 6 but did not significantly differ on day 9 (Figure 1C–F). The percentages of dry/fresh weight, which represent the proportions of dry mass and water content, indicated that the shoots of plants under normal conditions contained slightly more water (lower mass percentage) than those of plants under saline conditions during days 6–9, whereas the roots did not significantly differ in terms of water content between the two conditions (Figure 1G,H). Unlike 'Pokkali'

and 'IR29' (Supplementary Figure S2), the CMS and RWC of 'Jao Khao' did not change under saline conditions during the 9-day treatment (Figure 1I,J).

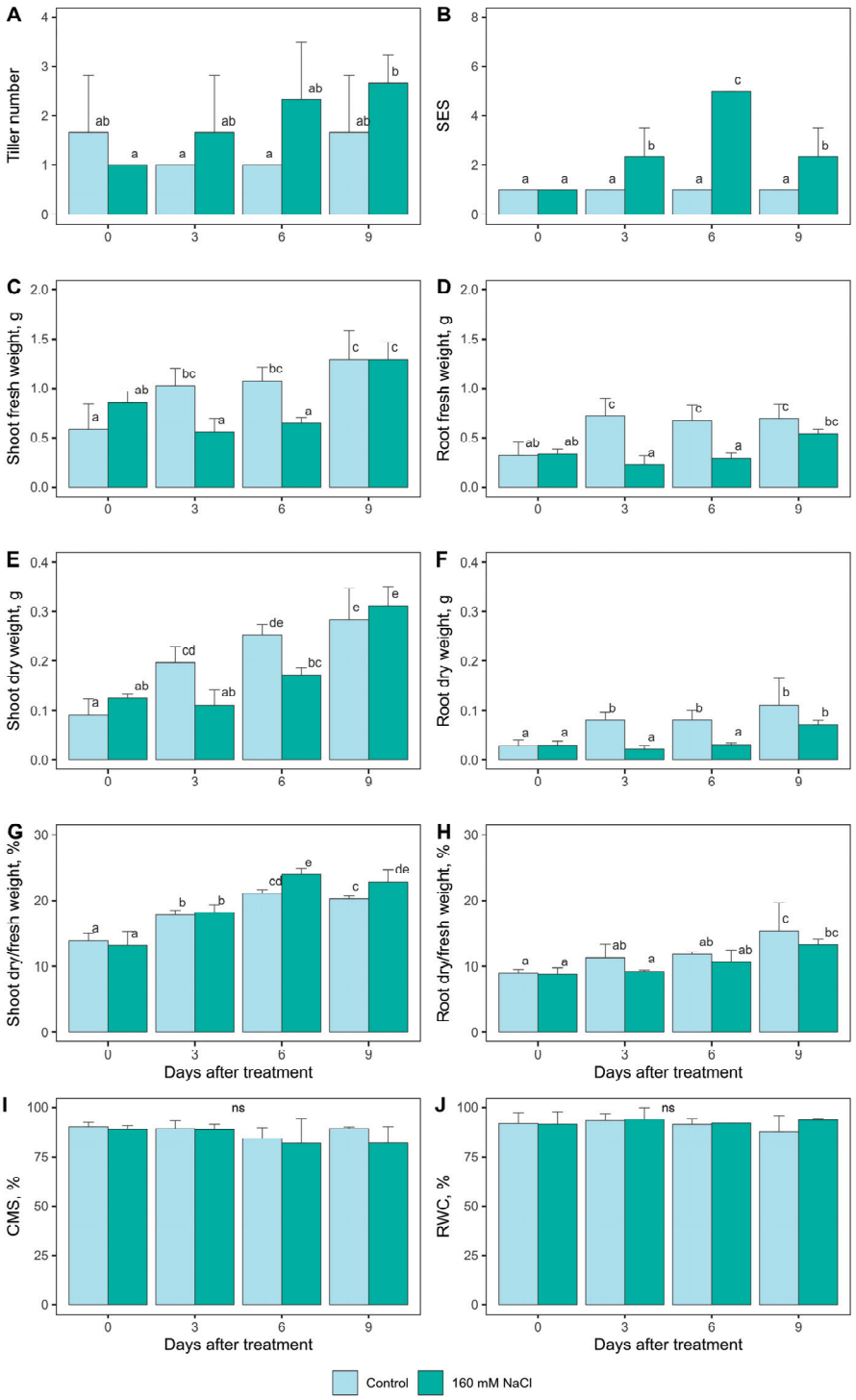


Figure 1. Comparison of phenotypic traits between normal and saline conditions of 'Jao Khao'. (**A**) tiller number, (**B**) SES, (**C**) shoot fresh weight, (**D**) root fresh weight, (**E**) shoot dry weight, (**F**) root dry weight, (**G**) shoot dry-to-fresh weight ratio, (**H**) root dry-to-fresh weight ratio, (**I**) CMS, and (**J**) RWC. Data are presented as means ± SD (n = 3). Statistical significance was determined using the Duncan multiple range test. Significant differences ($p \leq 0.05$) are indicated by different letters. ns: not significant.

2.2. Leaf Greenness and Chlorophyll Fluorescence of 'Jao Khao' under Saline Soil Conditions

According to the SPAD index, which represents leaf greenness, 'Jao Khao' can maintain the leaf greenness during the 9-day salt stress (Figure 2A), while the indices of 'IR29' and 'Pokkali' markedly decreased in days 6 and 9, respectively, under salt stress (Supplementary Figure S3A,B). Similarly, 'Jao Khao' seedlings were able to maintain a high maximum quantum yield of PSII (Fv/Fm), compared to that of normal conditions throughout the 9-day period of salt stress (Figure 2B), and significantly higher than those of 'IR29' and 'Pokkali', which markedly decreased on days 6 and 9, respectively (Supplementary Figure S3C,D). Consistently, the Performance index (Pi), which indicates alterations in the photosynthetic apparatus of plants under stress, based on light energy absorption [8,12,13] of 'Jao Khao' was maintained until day 9 (Figure 2C), which was also higher than those of 'IR29' and 'Pokkali' (Supplementary Figure S3E,F).

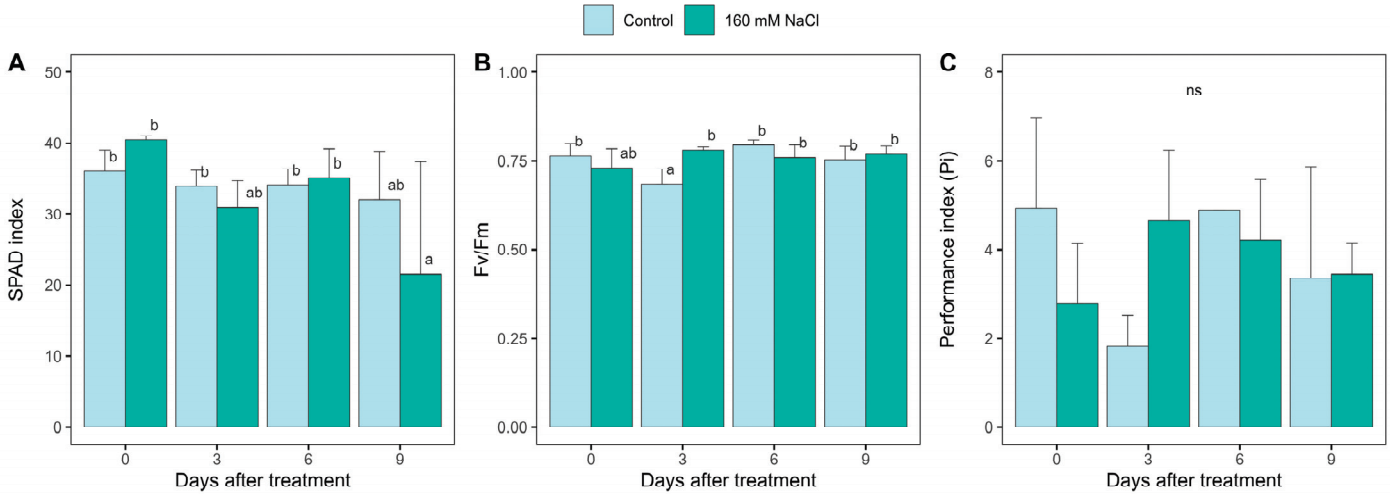


Figure 2. Leaf greenness and chlorophyll fluorescence of 'Jao Khao' compared between that of control and salt conditions. (**A**) SPAD index, (**B**) Maximum PSII efficiency (Fv/Fm), and (**C**) Performance index (Pi). Data are presented as means ± SD (n = 3). Statistical significance was determined using the Duncan multiple range test. Significant differences ($p \leq 0.05$) are indicated by different letters. ns: not significant.

2.3. Overview of Two-State Network Analysis

We constructed three networks: a global network encompassing all data, covering both the normal and salinity states, and separate networks for the normal and saline states. First, all genes were normalized and qualified, after which WGCNA was used to create the networks. The global network served as an overview of the network analysis, including module detection. For the normal- and saline-state networks, genes were not clustered into modules; rather, node centralities (DG, BW, CN, and CC) were calculated. To identify key genes in each module, changes in the centrality values from the normal- to the saline-state network were assessed. In total, 27,106,303 read counts and 38,993 genes were obtained from the 36 libraries. The raw read counts (Figure 3A) were normalized using DESeq2, (version 1.44.0) and after filtering out genes with low variation across all conditions, 1950 genes that passed the 95th percentile threshold were retained. In WGCNA, the soft threshold was determined based on a power of 10 (Figure 3B) selected for calculating the adjacency matrix. The heatmap of topological overlapping matrix plot (Figure 3C) shows the clustering of genes with similar expression patterns into modules. In this context, modules and clusters represent the same concept, that is, genes grouped together based on shared expression profiles. The minimum number of genes per module was set to 35, resulting in seven modules: grey (362 genes), green (59 genes), turquoise (610 genes), yellow (113 genes), red (48 genes), blue (567 genes), and brown (191 genes) (Table 1 and Figure 3C).

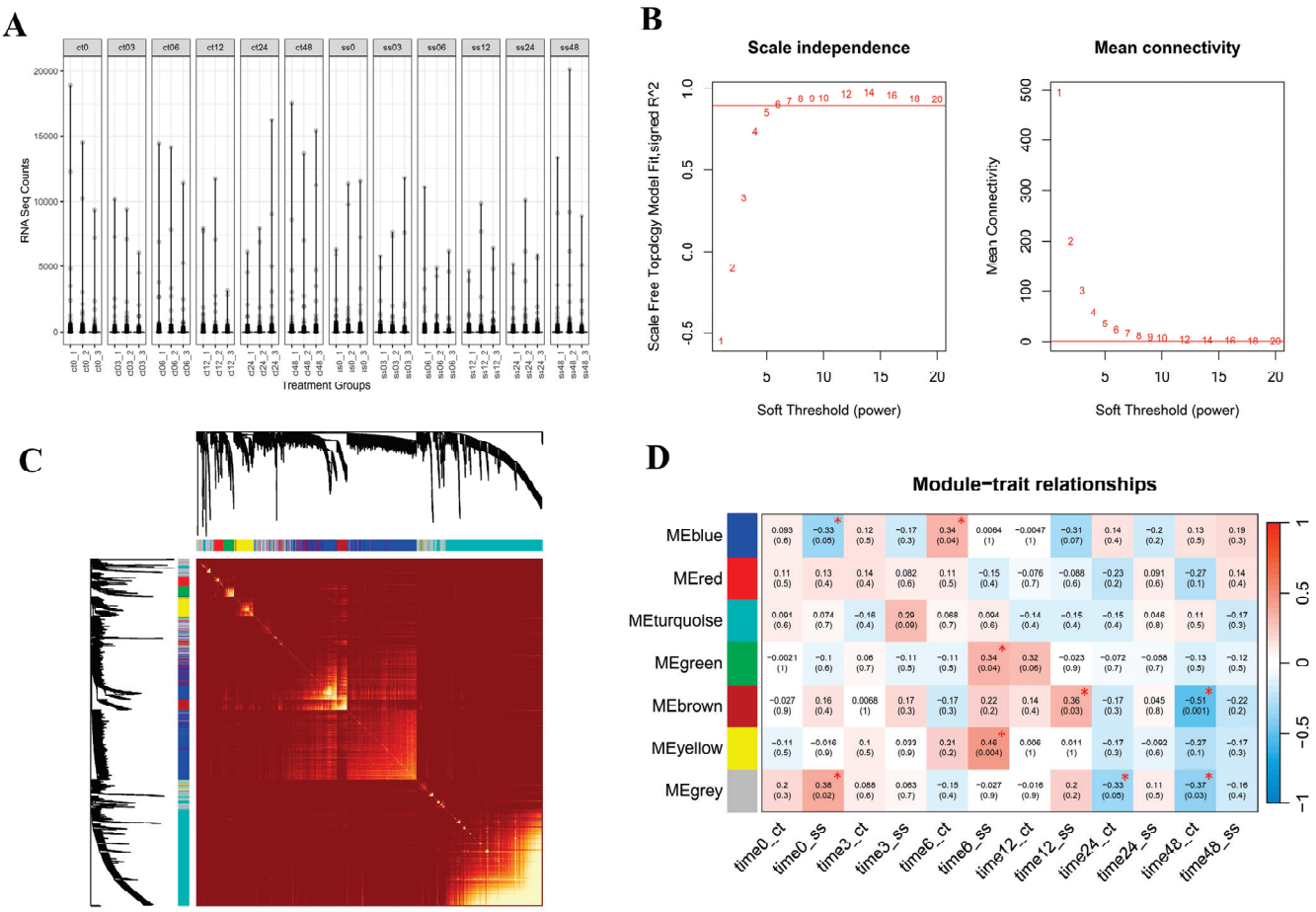


Figure 3. Normalized read counts of 36 RNA-sequencing library (**A**), scale-free topology and mean connectivity (the horizontal red line was at R^2 = 0.9) (**B**), the heatmap of topological overlapping matrix (TOM) plot visualizing the strength of the connections (similarity) between genes with the bright yellow color indicating genes with more connections or shared neighbors in the network and the colors representing modules displayed on both axes (**C**), and module–trait relationships (MTR) (**D**). The colors of modules include blue, red, turquoise, green, brown, yellow and grey. The letters ct and ss indicate control conditions and salt stress conditions, respectively. ME: Module Eigengene, a representative of gene expression levels in a cluster of co-expressed genes. Significant differences ($p \leq 0.05$) are indicated by *.

Table 1. Modules and key genes.

Module	Grey	Green	Turquoise	Yellow	Red	Blue	Brown	Sum
Total genes	362	59	610	113	48	567	191	1950
Key genes	14	5	59	13	1	18	1	111
Percentage	3.9	8.5	9.7	11.5	2.1	3.2	0.5	5.7

2.4. Determination of Node Centralities

The network properties of the three networks were calculated based on the WGCNA results and a summary of the network statistics is provided in Table 2. To include all connections, edge weights were set to 0.1 or higher [7]. The saline-state network had a higher number of nodes (1351 nodes) than the normal-state network (1204 nodes), whereas the global network had an even lower number of nodes (909 nodes). The normal-state network had 59,749 edges, an average degree of 206.420, and 52 connections per node. In contrast, the salinity-state network had 54,090 edges, a lower average degree of 120.038,

and only 21 connections per node. The diameter was the largest in the saline-state network (16) and the smallest in the global network (7). These findings suggested that during salt stress, 'Jao Khao' rice exhibited altered expression of genes (nodes), but the genes were less connected as indicated by the decreased number of edges, which led to an increased network diameter. A smaller diameter typically indicates a more compact and closely connected network, whereas a larger diameter suggests a more dispersed or loosely connected network.

Table 2. Network properties of the three co-expression networks.

Network Properties	Global Network	Normal-State Network	Salinity-State Network
Number of nodes	909	1204	1351
Number of edges	42,543	59,749	54,090
Average degree	157.002	206.420	120.038
Diameter	7	9	16
Average clustering coefficient	0.845	0.831	0.806
Number of connections per node	28	52	21

A comparison of the centrality distribution between the normal- and saline-state networks is shown in Figure 4. The density of degree values increased during salt exposure in the range of 0–70 (genes with low connections) but decreased in the range of 200–400 (genes with high connections) (Figure 4A). Similarly, the density of closeness increased in the range of 0–0.5 but decreased in the range of 0.5–1 (Figure 4B). The densities of betweenness clearly decreased under salt stress (Figure 4C) and clustering coefficients exhibited left-skewed distribution in both networks (Figure 4D).

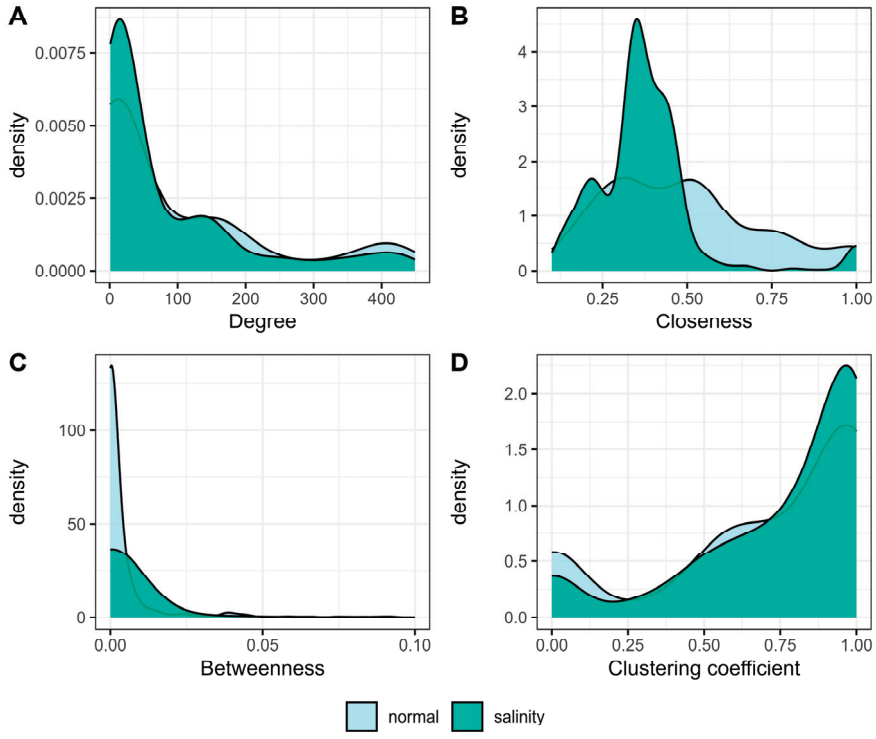


Figure 4. Comparison of the distribution of centrality between the normal-state and saline-state networks for (**A**) degree, (**B**) closeness, (**C**) betweenness, and (**D**) the clustering coefficient.

2.5. Module Relationships with Multiple Time Points

The module–trait relationships (MTRs) were used to explain the correlation between genes in each module and time points. MTRs were established for the global network, as depicted in Figure 3D. 'Jao Khao' rice, which is highly resistant to salinity and, under saline conditions, has a similar phenotype to that under normal growth conditions (Figure 1), exhibited a few significant correlations between module genes and time points. However, we observed a significant upregulation of genes in three modules related to saline treatment at specific time points. Genes in the yellow module were upregulated at 6 h (MTRs = 0.46, $p = 0.004$), as were those in the green module (MTRs = 0.34, $p = 0.04$), whereas those in the brown module were upregulated at 12 h (MTRs = 0.36, $p = 0.03$). These results suggest that the expression of genes in these modules was upregulated early. Details of the relationship between genes in this module and salt stress are provided in Section 3. This observation correlates with the summarized network properties presented in Table 2, which indicate that salt stress in 'Jao Khao' rice initiates an alteration in gene expression as suggested by the increase in the number of nodes, but with fewer connections among them.

2.6. Functional and Pathway Enrichment Analyses

To elucidate the biological relevance of the gene expression data, gene enrichment analysis was conducted using genes from each module by mapping them to the rice annotation database using the clusterProfiler function in R (version 4.4.1) [14]. GO terms were used to categorize the genes into BP, CC, and MF categories. GO terms were identified for genes within all modules except the grey module (Figure 5 and Supplementary Table S3). The green module was largely associated with BP (100%), including response to light intensity. The turquoise module was mainly involved in MF (100%), including serine-type endopeptidase inhibitor activity, *O*-acyltransferase activity, and ADP-binding. The yellow module was correlated with CC (62%), including photosystems and chloroplast thylakoid membrane; BP (29%), including photosynthesis and response to light stimulus; and MF (9%), i.e., chlorophyll binding. The red module was exclusively associated with BP (100%), including microsporogenesis, carotenoid biosynthetic process, and glycosyl-phosphatidylinositol (GPI) anchor biosynthetic process. The blue module was associated with MF (65%), including hexosyltransferase activity, RuBisCo activity, and ATP synthase activity; BP (24%), including ATP synthesis and carbon fixation; and CC (12%), including ATPase complex. Finally, the brown module was related to MF (44%), including RuBisCo activity, ATP hydrolysis activity, and antioxidant activity; CC (33%), including thylakoid lumen, vacuole membrane, and ribosome; and BP (22%), including the response to blue light.

The results of KEGG pathway enrichment analysis of the genes each module are provided in Figure 6 and Supplementary Table S4. The yellow and blue modules exhibited related pathways including glyoxylate and dicarboxylate metabolism, carbon fixation in photosynthetic organisms, oxidative phosphorylation, photosynthesis, and carbon metabolism with some of them overlapped. The yellow module was also enriched in glycine, serine and threonine metabolism, and thiamine metabolism. The red and grey modules shared the carotenoid biosynthesis pathway. Additionally, the red module exhibited several terms related to fatty acids. These findings suggest that the significant genes within these modules are primarily involved in photosynthesis-related pathways and carbon metabolism.

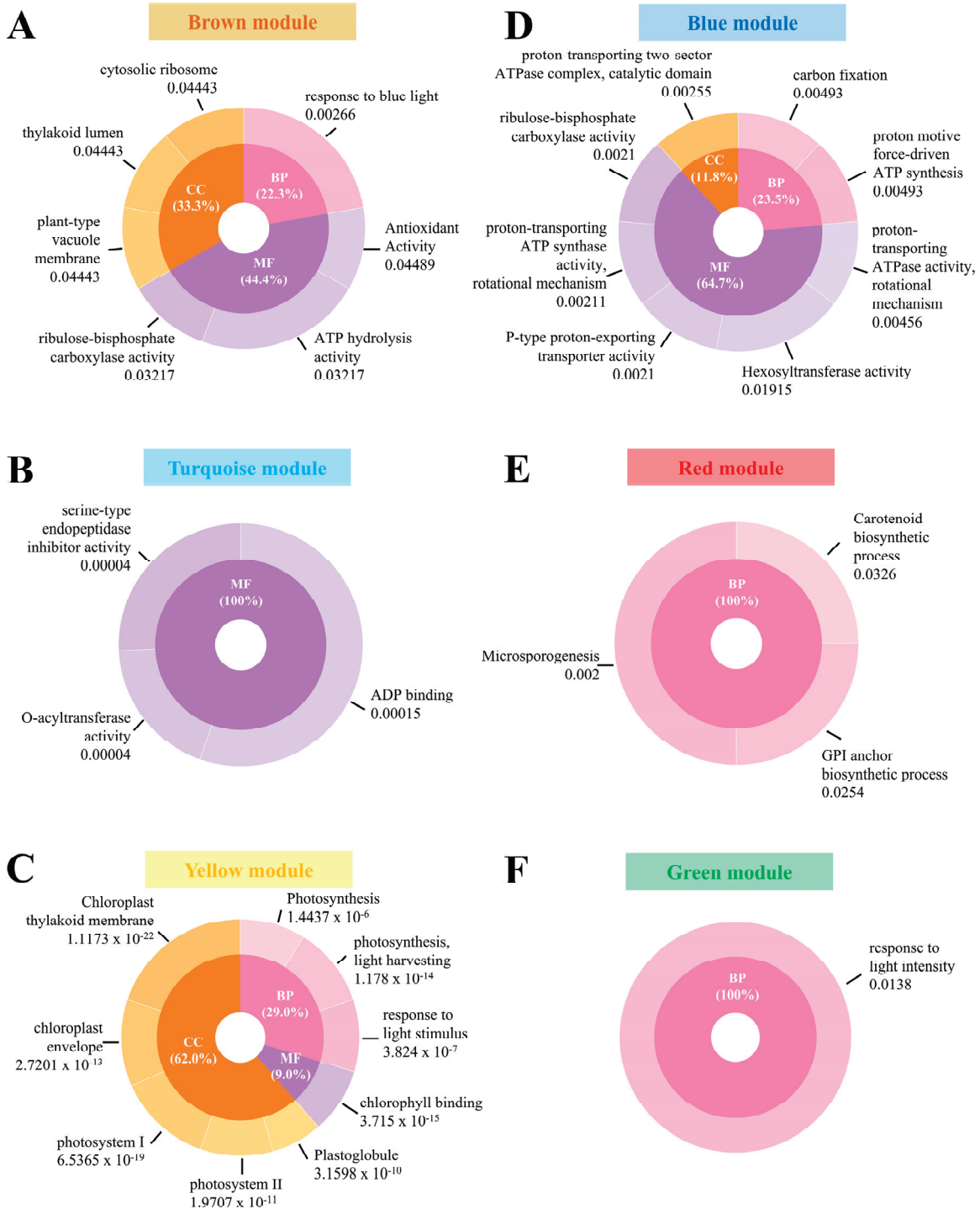


Figure 5. Gene Ontology (GO) enrichment analysis results for each module. *p*-values were adjusted using the Benjamini–Hochberg correction. (**A**) Brown module, (**B**) turquoise module, (**C**) yellow module, (**D**) blue module, (**E**) red module, and (**F**) green module. GO terms include biological process (BP), cellular component (CC), and molecular function (MF).

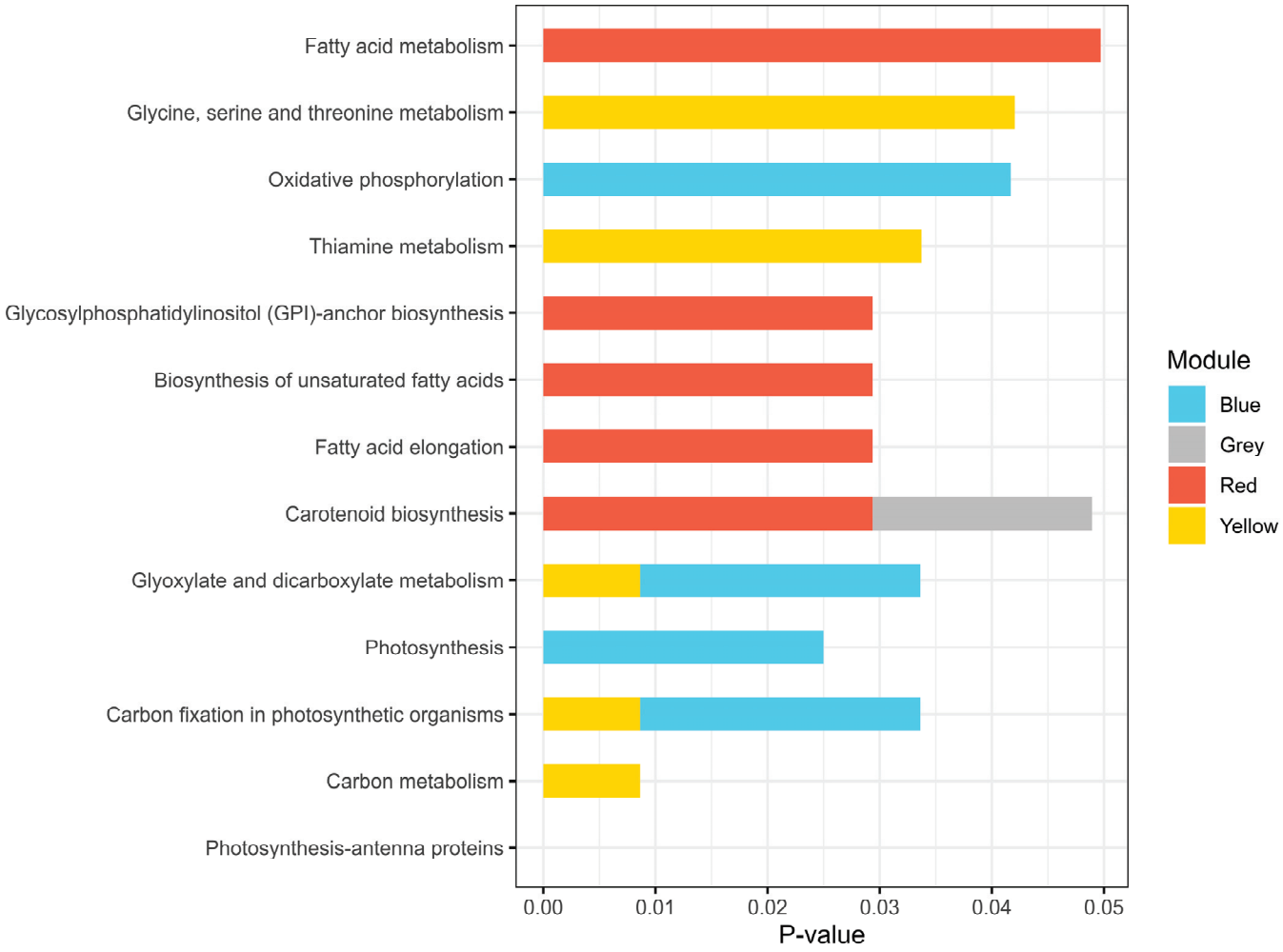


Figure 6. Kyoto Encyclopedia of Genes and Genomes (KEGG) pathway enrichment results for each module. *p*-values were adjusted using the Benjamini–Hochberg correction.

2.7. Investigation of Modular Hub Genes

Analysis focusing on the differences in node centrality between the normal- and saline-state networks identified 111 key genes, which were mapped onto the global network. The genes were distributed across the grey (14 genes), green (5 genes), turquoise (59 genes), yellow (13 genes), red (1 gene), blue (18 genes), and brown (1 gene) modules as indicated in Table 2 and Supplementary Table S2, and across the 12 chromosomes of the rice genome as illustrated in Supplementary Figure S4. Notably, key hub genes were found on all chromosomes. Genes within the same module were often located in close proximity on a chromosome. Chromosomes 11, 1, and 4 contained the highest numbers of key genes (23, 19, and 11 genes, respectively), whereas chromosome 5 had only one key gene. Key genes were mapped to the global state network as shown in Figure 7.

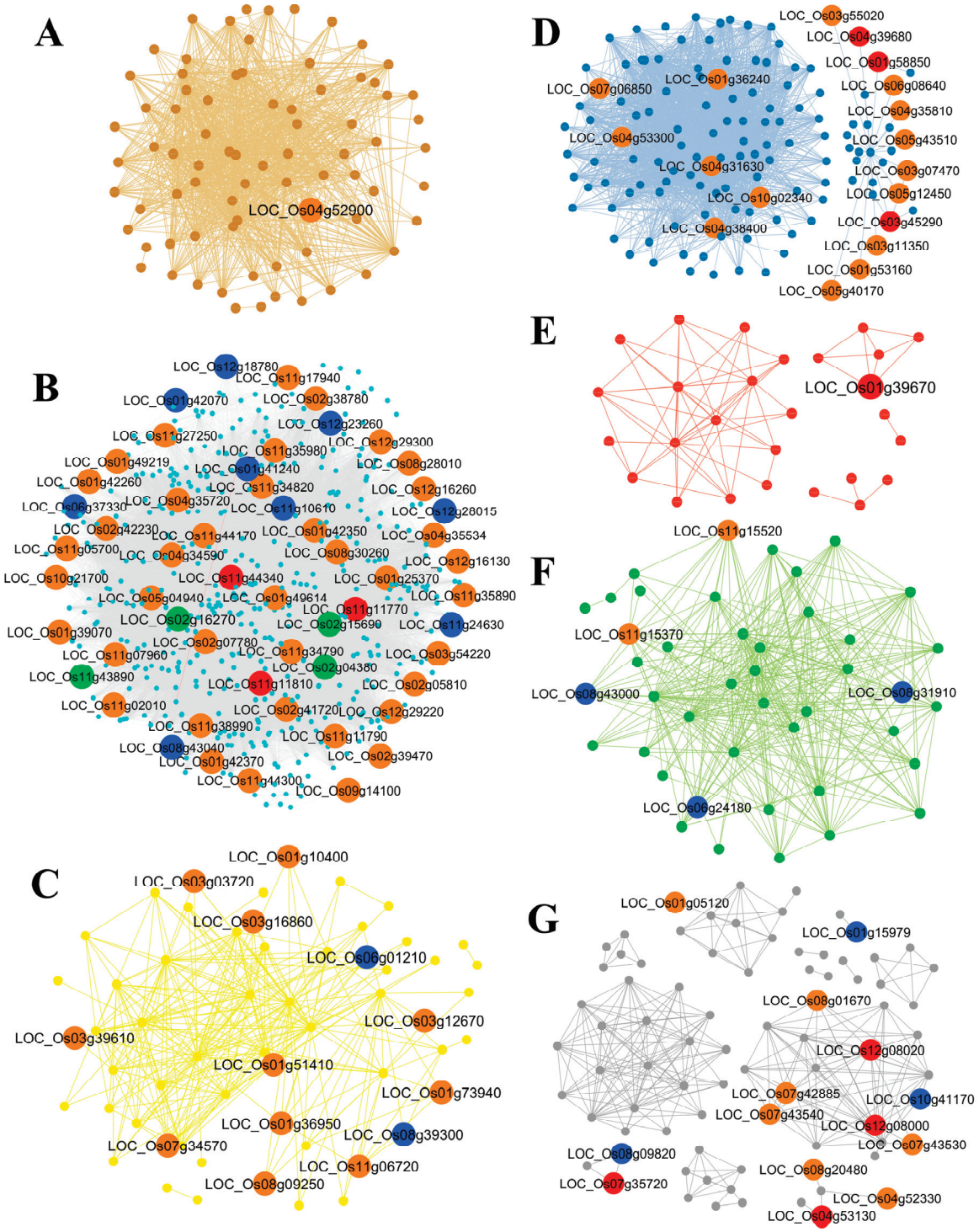


Figure 7. Gene networks and key genes were identified based on the centrality change between the two states (normal and saline) and mapped to the global state network. (**A**) Brown module, (**B**) turquoise module, (**C**) yellow module, (**D**) blue module, (**E**) red module, (**F**) green module, and (**G**) grey module. Small nodes and edges are colored according to the module they belong to. Large nodes represent key genes detected based on DG, BW, CN, and CC centrality, with combinations of 1, 2, 3, and 4 centrality measures, which are indicated in bright colors: green, blue, orange, and red, respectively.

2.8. 'Jao Khao' Exhibits Early Upregulation of Genes Involved in Energy Metabolism

As the significant genes within these modules are primarily involved in energy metabolism processes, such as light reactions, carbon fixation, and ATP synthesis, two genes involved in these processes were selected for expression analysis via RT-qPCR. They included genes encoding RuBisCo (*LOC_Os10g21268*) and ATP synthase (*LOC_Os10g21264*) from the blue module. Their relative expression levels after salt stress treatment for 3, 6, 12, 24, and 48 h were examined in 'Jao Khao' and were compared with those of the salt-tolerant (Pokkali) and salt-sensitive (IR29) standard varieties, respectively (Figure 8). Under salt stress conditions, 'Jao Khao' exhibited an early upregulation trend of *LOC_Os10g21268* expression at 3 and 6 h after treatment, while 'Pokkali' exhibited a delayed upregulation trend at 12 h, followed by 'IR29' at 24 and 48 h (Figure 8A–C). For *LOC_Os10g21264*, all three rice varieties significantly exhibited upregulation. 'Jao Khao' showed the earliest upregulation at 3 h after treatment, 'Pokkali' showed increased expression levels at 12 h, and 'IR29' exhibited upregulation at 24 h after treatment (Figure 8D–F).

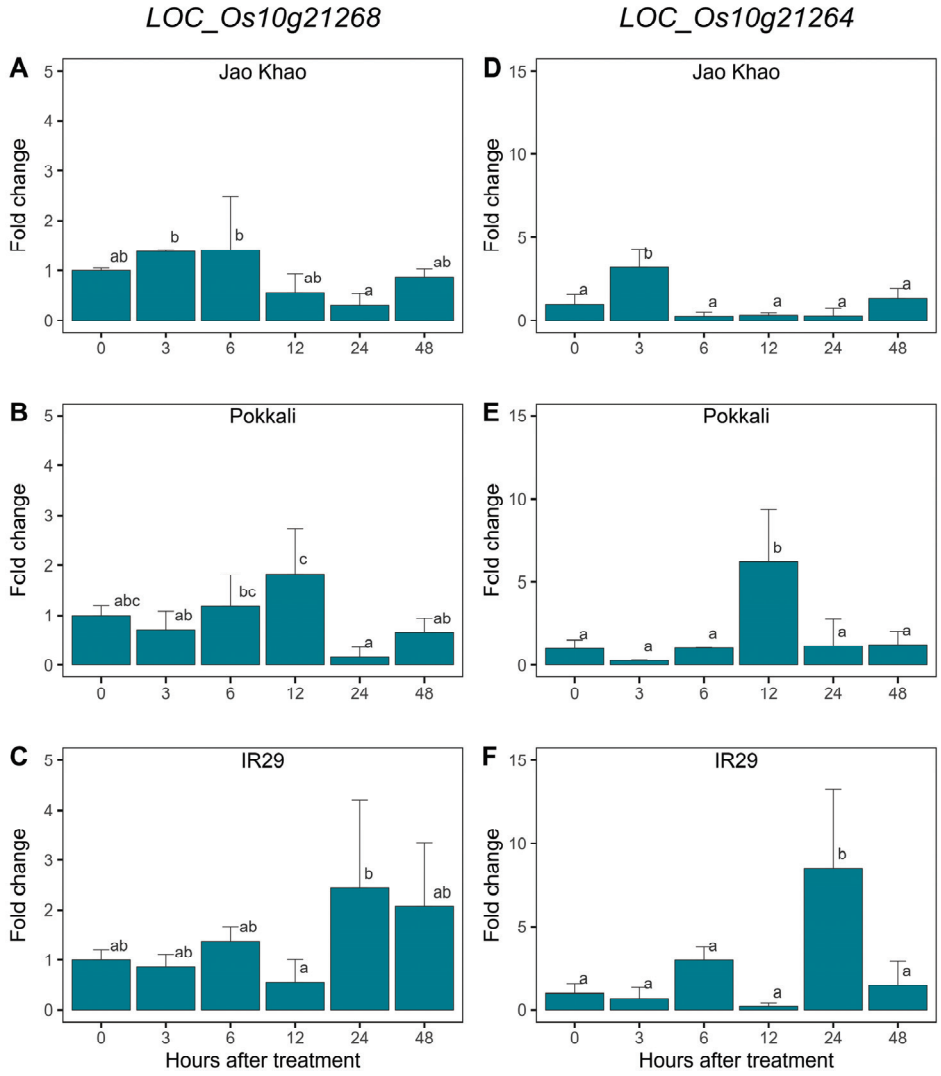


Figure 8. Relative expression levels (fold change) of two genes involved in energy metabolism: *LOC_Os10g21268* and *LOC_Os10g21264* in three varieties: 'Jao Khao' (**A**,**D**), 'Pokkali' (**B**,**E**), and 'IR29' (**C**,**F**) grown under salt stress conditions relative to those under control conditions by RT-qPCR. Data are presented as means ± SD (n = 3). Statistical significance was determined using the Duncan multiple range test. Significant differences ($p \leq 0.05$) are indicated by different letters.

3. Discussion

The salt-tolerant phenotype of the 'Jao Khao' Thai rice variety has been extensively documented, with studies demonstrating its ability to maintain high yields even under saline conditions [11,12]. To investigate the molecular mechanisms underlying its salt tolerance, we conducted a comprehensive gene co-expression analysis based on multi-series transcriptome data. 'Jao Khao' exhibited remarkable salt-tolerance as evidenced by the nonsignificant changes in CMS, RWC, SPAD index, Fv/Fm, and Pi under saline soil conditions for 9 days. RWC can indicate the water status in plant cells, and salt-tolerant genotypes showed a smaller decrease in RWC compared to the sensitive ones [15]. In Arabidopsis, a higher salt tolerance phenotype is evidenced by an improved capacity to maintain RWC and CMS [16].

Measures of centrality, including DG, CN, BW, and the CC, are used to assess the significance of genes within specific modules. Degree centrality conformed to a power-law distribution, in which genes with fewer connections (low centrality values) outnumbered those with more connections (high centrality values). The power value holds significance because it determines the scale-free topology of the resulting network. A scale-free network is defined by a small number of highly connected nodes (hubs) and numerous nodes with few connections, a structure commonly observed in biological systems [8]. In this work, the distribution of degree centrality (Figure 4A) suggested a decrease in highly connected nodes (approximately connected to 150–450 genes) in the saline-state network, potentially indicating the disruption of connections among genes normally interact under control conditions. Although this resulted in an increase in the number of less connected genes (approximately connected to 1–70 genes), many of them were new connections created under salt stress conditions as detected in all modules except the turquoise module, in which most genes became highly connected under salt stress. Genes deemed less important under normal conditions may play pivotal roles under saline conditions [8].

We compared percentage changes in centrality and genes exhibiting a high percentage change in centrality were identified as key genes, resulting in the clustering of seven modules and the identification of 111 key genes (Table 1). The key genes identified in the modules were validated using publicly available data (Supplementary Table S5) and gene enrichment data (Figure 5 and Supplementary Table S3). Upon examining the validated gene annotations, several key genes potentially involved in the salt-response mechanisms specific to each module were identified (Figure 9). The proposed potential mechanism for each module is described below.

3.1. Brown Module

In the brown module, only one key gene, *LOC_Os04g52900*, was identified by DG centrality change, with three combinations of centrality measures (DG, CN, and CC) (Figure 7A). *LOC_Os04g52900* encodes a C-type ATP-binding cassette (ABC) transporter, ABCC1, and was upregulated under salt stress (Figure 9). ABCC1, a member of the ABCC family, participates in the detoxification and reduction of arsenic in rice grains [17]. Another ABCC transporter, OsABCC7, is involved in the root-to-shoot translocation of As(III) [18]. Plant ABCCs can carry out ATP-powered transport of modified toxic compounds (e.g., by conjugation to glutathione or glucose) into the vacuole during the detoxification process [19]. In Arabidopsis, two vacuolar ABCC-type ABC transporters transport ABA glucosyl ester, which is an ABA conjugate that accumulates in the vacuole [20]. In the halotolerant yeast *Debaryomyces hansenii*, vacuolar membrane transporters play major roles in the sequestration of metal ions and some ABCC subfamily members may contribute to salt tolerance [21]. GO enrichment analysis of the brown module identified another ABC transporter gene, *LOC_Os06g51460*, which encodes a G-type ABC transporter (ABCG16). Matsuda et al. [22] reported that RCN1/OsABCG5 functions as a salt-tolerance factor by affecting the balance of sodium and potassium, possibly via the control of SKC1/OsHKT1;5 in the shoots.

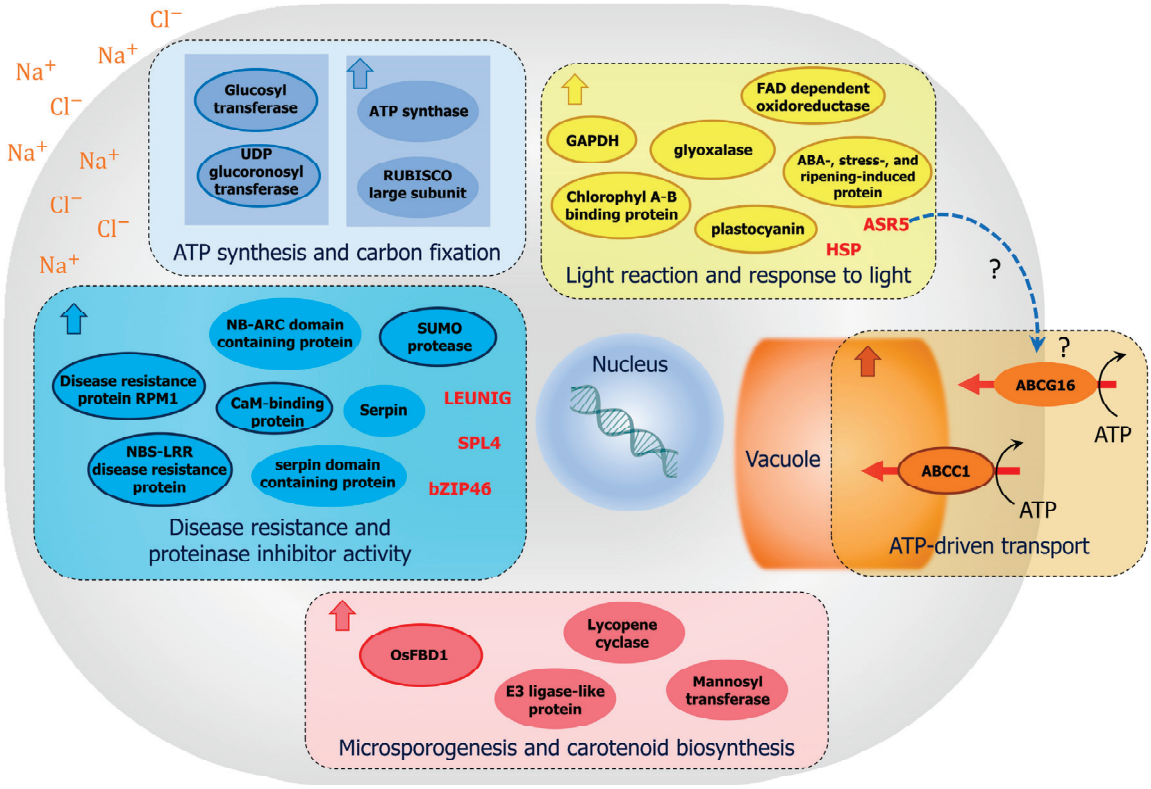


Figure 9. Proposed mechanism of salt stress responses in 'Jao Khao' rice as inferred from a comprehensive analysis of time-course transcriptome data. Names bordered by colored lines are key genes. Transcription factors are shown in red letters. GO enrichment analysis revealed several GO terms related to key plant energy metabolism processes, such as light reactions, carbon fixation, and ATP synthesis. Many genes associated with these GO terms exhibited increased expression under salt stress. These enriched processes indicate the importance of maintaining energy production early during salt stress to regulate ion and water uptake and transport. Other enriched GO terms suggested the involvement of ATP-driven transport and the ubiquitination-proteasome pathway in responses to salt stress. Several candidate transcription factors, including *bZIP46*, *SPL4*, *ASR5*, and the transcriptional corepressor LEUNIG, may coordinate these processes. Dash-arrows and question marks suggest potential regulatory relationships.

3.2. Turquoise Module

The turquoise module contained numerous genes, including 59 key genes that exhibited high centrality (Figure 7B). Among these, 43 genes were detected only in the saline-state network. The genes primarily enriched in this module were associated with GO terms related to disease resistance and serine-type endopeptidase inhibitor activity and were upregulated early during salt stress (Figure 9). One of the enriched GO terms was ADP binding, which included *LOC_Os09g14100* (NB-LRR, disease resistance protein RPS2), *LOC_Os11g10610* (NBS-LRR disease resistance protein), *LOC_Os11g11790* (NBS-LRR type disease resistance protein), *LOC_Os11g11810* (NBS-LRR disease resistance protein), and *LOC_Os11g11770* (disease resistance protein RPM1, similar to the NBS-LRR protein fragment), all of which were key genes. The NBS-LRR family, which is characterized by the presence of a nucleotide-binding site (NBS) and leucine-rich repeat (LRR) domains and may act as receptors in immune and non-immune responses to biotic and abiotic stresses (drought and salt stresses), was prevalent in the turquoise module, suggesting potential signaling overlap between these responses [23]. The genes in this module associated with the enriched GO term proteinase inhibitor activity included *LOC_Os11g11760* (OsSRP-PSG, serpin domain-containing protein), *LOC_Os11g12410* (OsSRP-GAA, serpin domain-containing protein), *LOC_Os11g12420* (serpin-Z6B), *LOC_Os11g13530* (serpin-Z2A),

and *LOC_Os11g13540* (serpin-Z2B), all of which were serine protease inhibitors in the serpin superfamily.

Additional key genes in this module included *LOC_Os11g44340* and *LOC_Os11g44170*, which encode calmodulin-binding proteins. In eukaryotes, calmodulin is an intracellular Ca^{2+}-binding protein that interacts with more than 300 target proteins and peptides [24]. In rice, it plays various roles as a signal transducer in the response to salt stress [25,26]. Other key genes were *LOC_Os01g25370* (SUMO protease), which is involved in SUMOylation, resulting in early flowering and decreased plant height in rice [27], and *LOC_Os01g42350*, *LOC_Os11g05700*, and *LOC_Os01g42370*, encoding transporters including pleiotropic drug resistance proteins and ABC transporter family proteins, which are involved in abiotic and biotic stresses, such as iron deficiency stress [28].

Key genes encoding transcription factors in this module included *LOC_Os02g07780* (SPL4-SBP-box gene family member), which encodes the SQUAMOSA promoter-binding protein domain, a transcription factor that regulates grain size [29], *LOC_Os01g42260* (LUGL, transcriptional corepressor LEUNIG), which influences floral development by modulating auxin levels [30], and *LOC_Os06g10880* (bZIP46 transcription factor), which is positively regulated by ABA signaling and drought stress in rice [31].

3.3. Yellow Module

In the yellow module, 13 key genes were identified (Figure 7C). Among them, eight genes were specific to the saline-state network. Genes in this module were enriched in the GO terms light reactions and response to light. The key genes associated with the enriched GO terms included *LOC_Os03g39610* (LHCB, chlorophyll A-B binding protein), which is involved in photosynthesis, light harvesting, and the response to light [32] The expression of *LOC_Os03g39610* and several other enriched genes associated with photosynthesis and light harvesting initially decreased, but later increased (Figure 9). A similar expression pattern was also observed for *LOC_Os03g03720* (glyceraldehyde-3-phosphate dehydrogenase, GAPDH), which is a potential candidate gene involved in rice tolerance to low light stress and is related to aromatic traits.

Another key gene in this module was *LOC_Os11g06720* gene (ASR5, abscisic acid-, stress-, and ripening-induced protein), which encodes a transcription factor that plays a role in aluminum tolerance by binding STAR1, which encodes an ABC transporter [33]. ASR5 also plays an important role in the drought stress response by regulating ABA biosynthesis, facilitating stomatal closure, and acts as chaperone-like protein to prevent the inactivation of drought stress-related proteins [33,34].

Other key genes were *LOC_Os07g34570* (DR8, FAD-dependent oxidoreductase domain containing protein), which is involved in disease resistance [35,36], *LOC_Os06g01210* (PC, plastocyanin, chloroplast precursor), which functions in electron transport [37], *LOC_Os01g10400* (MT-3a, metallothionein-like protein), which provides tolerance to salinity, drought, and heavy metal stress in rice [38], *LOC_Os08g09250* (GLYI11.2, glyoxalase family protein), which is related to plant stress adaptation [39], and *LOC_Os08g39300* (SGAT, serine:glyoxylate aminotransferase), which controls crucial photorespiratory enzymes in rice at both the transcriptional and post-translational (phosphorylation) levels [40].

3.4. Blue Module

Seventeen of the 18 key genes in the blue module were present only in the saline-state network (Figure 7D). The main GO terms enriched in this module were hexosyltransferase activity, ATP synthase activity, and carbon fixation. The genes associated with hexosyltransferase activity were all key genes whose expression did not significantly change under salt stress (Figure 9), including *LOC_Os05g12450* (UGT, hydroquinone glucosyltransferase), which is triggered by both biotic and abiotic stresses [41], *LOC_Os03g11350* (UDP-glucoronosyl and UDP-glucosyl transferase), and *LOC_Os03g55020* (UDP-glucoronosyl and UDP-glucosyl transferase domain containing protein), which participates in pathogen defense responses [42].

The genes associated with ATP synthase activity and carbon fixation were upregulated under salt stress, unlike the key genes in this module. These genes included *LOC_Os12g10570* (ATP synthase subunit beta), which is involved in carbon and nitrogen metabolism and upregulated under salt stress, *LOC_Os10g21264* (ATP synthase epsilon chain), which was identified by genome-wide association in rice exposed to short-term exposure to salt stress [43], and *LOC_Os10g21268* and *Os01g0791033*, which encode the large subunits of RuBisCo, the key enzyme in carbon fixation and photorespiration. No other genes encoding other subunits ATP synthase or RubisCo were identified.

3.5. Red Module

In the red module (Figure 7E), only one key gene was identified, *LOC_Os01g39670* (FBD1), with two combinations of centrality measures (DG and CC). Genes associated with the enriched GO term microsporogenesis included the key gene FBD1 and *LOC_Os01g39680* (small ubiquitin-like modifier (SUMO) E3 ligase-like protein) (Figure 9). FBD1, an F-box and fibrin-binding domain (FBD) protein involved in floral transition, panicle development, and seed formation [44]. The F-box protein is part of two-gene male sterility systems involved in male fertility in indica–japonica hybrids [45,46]. *LOC_Os01g39960* (lycopene epsilon cyclase, chloroplast precursor) and *LOC_Os01g39810* (Alg9-like mannosyltransferase protein) were associated with the carotenoid biosynthetic process and GPI anchor biosynthetic process, respectively.

Expression of the two genes involved in energy metabolism, RuBisCo and ATP synthase, in 'Jao Khao' was early upregulated under salt stress conditions. ATP synthase is the enzyme that utilizes electrochemical energy to power the synthesis of ATP, a key process involved in active ion transport. In plants, it has been reported that ATP synthase is overexpressed in response to abiotic stresses [47,48]. Wei et al. [49] suggested that increased ATP production in cells could improve plant tolerance to salt stress. Wang et al. [50] reported that *LOC_Os10g21264* was one of the most downregulated DEGs in the *bglu6* mutant, which is involved in ABA recycling in rice under drought conditions. In this study, two ATP synthase genes were co-expressed in the same module. ATP synthase typically consists of two main parts (F_o and F_1) that work together. LOC_Os10g21264 (epsilon subunit), containing a GO term enriched in this study, was selected for validation using RT-qPCR, and the results showed that it was upregulation early. Together with LOC_Os12g10570 (beta subunit), they were the only two ATP synthase genes that showed upregulation in 'Jao Khao' during salt stress. This is similar to a previous study on salt-stress response in *Triticum aestivum*, in which few genes encoding ATP synthase F_1 subunits (beta and delta) were upregulated during salt stress; however, genes encoding other F_1 subunits did not show upregulation [51]. Based on both studies, other regulatory mechanisms of gene expression, that is, translational and posttranslational regulation for genes that encode other subunits of ATP synthases may play a role in response to salt stress without altering the transcript levels. Even with an upregulation of transcript levels of only few genes encoding F_1 subunits, these mechanisms may result in better maintenance of photosynthetic activity and energy production during salt stress as observed in 'Jao Khao' variety in this study. Additionally, in a previous study, the overexpression of a gene encoding a component of the F_o part of the rice mitochondrial ATP synthase was shown to increase salt tolerance; however, the transcript levels of the genes encoding the other mitochondrial F_1F_o-ATPase subunits were mostly not affected by salt stress. This study showed that an increase in the expression of one gene encoding a single component of the ATP synthase could lead to the difference in salt tolerance ability [48]. In this study, the early upregulation of ATP synthase (*LOC_Os10g21264*) in 'Jao Khao' aligns well with its ability to maintain light energy absorption, as indicated by maximum PSII efficiency (Fv/Fm), Performance index (Pi), and survival under saline stress.

Based on our data of gene co-expression network, LOC_Os10g21268 (RuBisCo large subunit) was detected and matched with enriched GO terms; therefore, we selected this gene for validation. RuBisCo is a multi-subunit enzyme that functions as a complex. It

consists of eight large (RbcL) and eight small (RbcS) subunits, which come together to form a functional enzyme. There are multiple annotated RuBisCo large chain and small chain precursor genes in the rice genome with LOC_Os10g21268 that exhibit very high expression levels in leaf (based on RNA-Seq data in the Rice Genome Annotation Project database). The small subunit gene, LOC_Os12g19381, which also exhibited high expression levels in leaf, showed a trend of upregulation under salt stress in this study; however, the difference was not statistically significant, and it was not picked up by the gene co-expression network analysis. For Rubisco to work effectively in catalyzing CO_2-fixing reaction during photosynthesis, all subunits must be correctly assembled and function together. However, in a previous study in rice, overexpression of a RuBisCo large subunit gene alone was found to improve drought tolerance [52].

While these findings underscore the significance of these two genes in energy production under salinity stress, it is important to note that this discovery is based on a single rice variety. This genetic feature might be specific to certain genotypes and not necessarily present in all rice varieties. In addition, salt tolerance is a complex trait regulated by multiple genes and various cellular processes. The identified genes likely contribute to a portion of this trait, interacting with other genes within the plant's genetic backgrounds. The interplay between these genes, each with its own variations, contributes to the diverse salt tolerance observed across different rice varieties.

Overall, GO enrichment analysis revealed gene enrichment in several GO terms involved in central plant energy metabolism, including light reactions, carbon fixation, and ATP synthesis, under saline conditions, which are in agreement with the ability of 'Jao Khao' in maintaining the SPAD index, Fv/Fm, and Pi during the 9-day of salt stress. Most of the genes associated with these GO terms were upregulated under saline conditions. These enriched processes suggest the importance of maintaining energy production early during salt stress for the regulation of ion and water uptake and transport [53]. Further, the results suggested the involvement of ATP-driven transport and the ubiquitination-proteasome pathway in the response of 'Jao Khao' to salt stress. Several candidate transcription factors may coordinate these processes, including *bZIP46*, *SPL4*, *ASR5*, and the transcriptional corepressor LEUNIG. Our findings suggest that these genes may play crucial roles in the response of rice to salt stress.

4. Materials and Methods

4.1. Phenotyping of Rice under Soil-Salt Treatment

'Jao Khao' seeds were germinated in water for 10 days, then transplanted into clay soil with one seedling in a 40 cm^3 pot, supplemented with 16-16-16 fertilizer, for two weeks in a greenhouse under ambient conditions. Two growth conditions were separately established in each tray by soaking in 15 L tap water: normal conditions, in which no salt was applied, and saline conditions, in which the soil was treated with 160 mM NaCl, in a complete randomized design (CRD) with three replicates. This procedure was used for phenotyping, RNA sequencing, and RT-qPCR of separate individual plants after treatment with salt stress at indicated timepoints. At 0, 3, 6, and 9 days after stress exposure, phenotypic characteristics, including shoot and root fresh and dry weights, tiller number, the standard salt injury evaluation system (SES) score, cell membrane stability (CMS), and relative water content (RWC). We conducted additional experiments using the same protocol as described earlier by growing 'Jao Khao' and comparing it with that of 'Pokkali' (a standard salt-tolerant variety) and 'IR29' (a standard salt-sensitive variety) in a CRD with three replications for each time point to determine CMS, RWC, SPAD index, and chlorophyll fluorescence (Fv/Fm and performance index). The experimental methodologies followed the procedures outlined by Kojonna, et al. [16], and Punchkhon, et al. [54]. Statistical significance was assessed using the Duncan multiple range test, with significance defined as $p \leq 0.05$.

4.2. RNA Extraction, Library Preparation, and Sequencing

Fully expanded leaves were collected from three replicates under normal and saline (160 mM NaCl) soil conditions at 0, 3, 6, 12, 24, and 48 h following salt treatment. The leaves were immediately frozen in liquid nitrogen and stored at −80 °C. Total RNA was extracted from the leaves using PureLink™ Plant RNA Purification Reagent (Thermo Fisher Scientific, Waltham, MA, USA), and genomic DNA was removed using DNase I (RNase-free; New England Biolabs, Ipswich, MA, USA). The RNA quality was assessed using an Agilent 2100 bioanalyzer (Agilent, Santa Clara, CA, USA) and RNA concentration was determined using a DeNovix fluorometer (DeNovix, Wilmington, DE, USA). Individually indexed strand-specific RNA-sequencing libraries of all samples were prepared using QIAseq FastSelect–rRNA Plant and QIAseq Stranded mRNA Library kits (Qiagen, Hilden, Germany). The indexed libraries were pooled in equimolar quantities and subjected to cluster generation and 150-nucleotide paired-end sequencing on an Illumina HiSeq sequencer (Illumina, San Diego, CA, USA). In total, 36 cDNA libraries were sequenced.

4.3. Quantification of Gene Expression by RT-qPCR

The youngest fully expanded leaves of 'Jao Khao', 'Pokkali', and 'IR29' were collected at different time points as previously described. RT-qPCR was conducted following the methodology described by Chinpongpanich et al. [25], using three technical replications and at least two biological replicates to assess the gene expression levels of *LOC_Os10g21268* and *LOC_Os10g21264*. The oligonucleotide primers used were as follows: *LOC_Os10g21268*: forward primer—5′ TTCCGAGTAACTCCTCAGCC and reverse primer—5′ GATTATCCTCCCCAACAACGG; and *LOC_Os10g21264*: forward primer—5′ GCCCGCCTTTATCGAGTTAG and reverse primer—5′ TCCCCTACTCCGCCAAATAC. EF-1-α (*LOC_Os03g08010*) was used as internal control with the following primers: forward—5′ ATGGTTGTGGAGACCTTC and reverse—5′ TCACCTTGGCACCGGTTG.

4.4. Data Preprocessing and Screening

The raw reads were subjected to quality control assessment using the FASTQC software (version 0.12.0) and trimmed using Trimmometic-0.39 (https://github.com/usadellab/Trimmomatic/ (accessed on 26 February 2024)). Then, the reads were aligned to the rice reference genome IRGSP-1.0 obtained from the EnsemblPlants database (https://plants.ensembl.org/index.html (accessed on 26 February 2024)) using HISAT2 (https://daehwankimlab.github.io/hisat2/ (accessed on 26 February 2024)). The alignment results in SAM format were converted to the BAM format and indexed using SAMtools (version 1.17) [55]. The aligned reads were quantified using HTSeq-count (https://htseq.readthedocs.io/en/release_0.11.1/count.html (accessed on 26 February 2024)), with the genomic features provided in a GTF file (https://plants.ensembl.org/index.html (accessed on 26 February 2024)). The 36 raw read count datasets were normalized by division by the size factors. To this end, we calculated the variance stabilizing transformation of the read counts of each gene using the 'varianceStabilizingTransformation' function in DESeq2 [56]. Genes with low variation were filtered out using the 'genefilter' package [57]. Genes passing the 95th percentile threshold were used in the WGCNA pipeline (Figure 10).

4.5. WGCNA

We used WGCNA to construct global, normal-state, and saline-state networks to compare the co-functional genes under normal and saline conditions, following the pipeline outlined in Sonsungsan et al. [8] and Suratanee et al. [58] (Figure 10). The transcriptome data were normalized using DESeq2 [56], and genes with high variation were selected. Next, we constructed three WGCNs: one for the global state (using all 36 libraries), one for the normal state (using 18 libraries), and one for the saline state (using 18 libraries). The scale-free topology was assessed to determine the optimal soft threshold (power, β) for calculating the adjacency matrix based on the Pearson correlation of pairwise genes. A power of 10 was selected as the minimum power at which the scale-free topology fit

index curve flattens, achieving a high value (R^2 = 0.974). The normal- and saline-state networks obtained were used to qualify the level of importance of the genes based on various centrality measures.

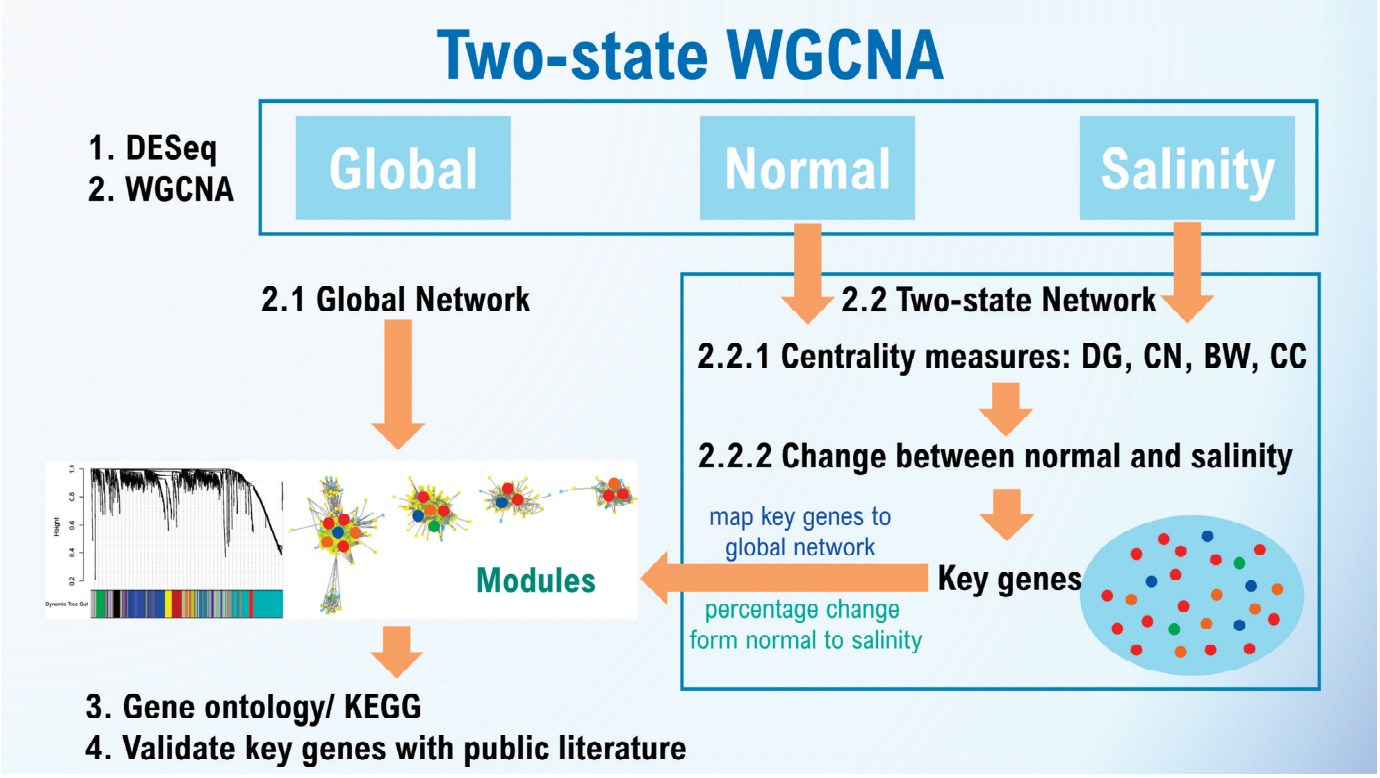


Figure 10. Diagram illustrating the co-expression network analysis pipeline used in the present study.

4.6. Centrality Measurement and Identification of Key Hub Genes

In biological systems, genes exert distinct functions while intricately interacting with each other [59]. A GCN represents connections among entities [60], in which each node represents a gene and the edges represent connections between genes. We analyzed biological networks focusing on key centrality measures such as degree, betweenness, closeness, and the clustering coefficient. Genes exhibiting high centrality properties were denoted as 'hub genes' [61]. The centrality measures, as described by Sonsungsan et al. [7], can be summarized as follows (for details, refer to Supplementary Figures S5–S7).

The degree (DG) of a node is determined by counting the edges connected to it [62]. A high DG indicates significant centrality, implying that the corresponding gene has numerous interactions. Closeness centrality (CN) reflects the average distance of the shortest path from a node to all others in the network, with higher values indicating greater centrality [63]. CN values range from 0 to 1. Betweenness centrality (BW) quantifies the proportion of shortest paths that pass through the node, with a higher BW facilitating network-wide communication. BW helps identify pivotal 'bridge-spanning' nodes that serve as key connectors within the network [64]. The BW of each node ranges from 0 to 1 [7]. The clustering coefficient (CC) measures the proportion of neighbors that are also neighbors of each other. It provides insight into the local network structure, revealing how densely interconnected the immediate neighbors of a node are [7,58,60].

To prepare the data for calculating centrality, the three networks were exported from WGCNA (version 1.73) using the 'exportNetworkToCytoscape' function, and the threshold for the lowest possible correlation was set to 0.1. Subsequently, the 'Analyze Network' function in Cytoscape (version 3.10.0) [65] was used to calculate centralities including DG, BW, CN, and CC. The network property was generated using the same function, which included number of nodes, number of edges, average degree, diameter, average clustering

coefficient and number of connections per node. All four centrality measures were used to assess the changes from the normal-state network to the saline-state network. Two criteria were employed to identify key hub genes: first, only genes loaded into the global network, and second, the percentage of centrality changes from less important genes (low scores) in the normal state to genes with high importance (high scores) in the saline state [7]. The key genes were selected from those exhibiting the percentage change in DG centrality that surpassed 80%.

4.7. Module Detection and Functional and Pathway Enrichment Analyses

Modules in the global co-expression network were detected using WGCNA [4] by calculating the dissimilarity of the topological overlap matrix. The relationship between the modules and the time-course of gene expression was analyzed via WGCNA. Next, the modules were examined for related functions or pathways. We used public annotation data from the Rice Annotation Project Database (IRGSP-1.0-2024-01-11) and OryzaBase (https://shigen.nig.ac.jp/rice/oryzabase/ (accessed on 26 February 2024)) to conduct a Gene Ontology (GO) enrichment analysis, classifying the genes in each global network module based on their function into biological process (BP), cellular component (CC), and molecular function (MF) categories, using the clusterProfiler R function [14]. Additionally, we performed a pathway enrichment analysis by downloading gene annotations from the Kyoto Encyclopedia of Genes and Genomes (KEGG) (https://www.kegg.jp/ (accessed on 26 February 2024)).

5. Conclusions

We compared transcriptome data from 'Jao Khao' rice seedlings grown under normal and saline conditions at multiple time points to identify key hub genes associated with salt tolerance. From the 111 genes selected based on centrality measures from a pool of 1950 highly variable genes by two-state WGCN and GO enrichment analysis, the identified genes involved in ATP-driven transport, light reactions and response to light, ATP synthesis, carbon fixation, disease resistance, and proteinase inhibitor activity were identified as important components of the salt-stress response in rice. Early upregulation of these genes suggests their importance in response to this stressor. Expression of two genes involved in energy metabolism (RuBisCo and ATP synthase) was upregulated early in the salt-tolerant variety, 'Jao Khao.' This indicates that it is important for the plant to manage energy for their survival in the initial phase of salt stress and the processes and key genes identified in this study potentially play important roles. These findings suggest that manipulation of the energy metabolism should be the focus in plant resistance breeding effort.

Supplementary Materials: The following supporting information can be downloaded at: https://www.mdpi.com/article/10.3390/ijms252011086/s1.

Author Contributions: T.B. and S.C. conceptualized the study; P.K. conducted the experiments and drafted the manuscript; P.K., K.P. and T.B. participated in the data analyses; K.P., S.C. and T.B. revised the manuscript. All authors have read and agreed to the published version of the manuscript.

Funding: This research was funded by the NSRF through the Program Management Unit for Human Resources & Institutional Development, Research and Innovation [grant number B05F640097]. P.K. was supported by the Program in Biotechnology Faculty of Science and Graduate School, Chulalongkorn University.

Institutional Review Board Statement: Not applicable.

Informed Consent Statement: Not applicable.

Data Availability Statement: The authors confirm that data supporting the findings of this study are available in the article and its Supplementary Materials (Supplementary Tables S1–S5, Supplementary Figures S1–S7). The exome sequence raw data is available through direct contact with the corresponding author.

Acknowledgments: We are thankful to the Omics Sciences and Bioinformatics Center, Faculty of Science, for their assistance with RNA-sequencing. Special thanks to Bagus Herwibawa, Navarit Jitsamai, and the laboratory members of the Center of Excellence in Molecular Crop, Department of Biochemistry, Faculty of Science, Chulalongkorn University, for their valuable technical support. We thank Susinya Habila and Thammaporn Kojonna from the CEEPP laboratory for providing seeds. Further, we extend our gratitude to Chutarat Punchkhon for the chlorophyll fluorescence technique and Pajaree Sonsungsan from the AVIC Center, Department of Mathematics and Computer Science, for guiding us through the two-state WGCNA procedure.

Conflicts of Interest: The authors declare no conflicts of interest.

References

1. Bundó, M.; Martín-Cardoso, H.; Pesenti, M.; Gómez-Ariza, J.; Castillo, L.; Frouin, J.; Serrat, X.; Nogués, S.; Courtois, B.; Grenier, C.; et al. Integrative approach for precise genotyping and transcriptomics of salt tolerant introgression rice lines. *Front. Plant Sci.* **2022**, *12*, 797141. [CrossRef] [PubMed]
2. Tieri, P.; Farina, L.; Petti, M.; Astolfi, L.; Paci, P.; Castiglione, F. Network inference and reconstruction in bioinformatics. In *Encyclopedia of Bioinformatics and Computational Biology*; Elsevier: Amsterdam, The Netherlands, 2019; pp. 805–813.
3. Zhu, M.; Xie, H.; Wei, X.; Dossa, K.; Yu, Y.; Hui, S.; Tang, G.; Zeng, X.; Yu, Y.; Hu, P. WGCNA analysis of salt-responsive core transcriptome identifies novel hub genes in rice. *Genes* **2019**, *10*, 719. [CrossRef] [PubMed]
4. Langfelder, P.; Horvath, S. WGCNA: An R package for weighted correlation network analysis. *BMC Bioinform.* **2008**, *9*, 559. [CrossRef] [PubMed]
5. Kumar, N.; Mishra, B.K.; Liu, J.; Mohan, B.; Thingujam, D.; Pajerowska-Mukhtar, K.M.; Mukhtar, M.S. Network Biology Analyses and Dynamic Modeling of Gene Regulatory Networks under Drought Stress Reveal Major Transcriptional Regulators in Arabidopsis. *Int. J. Mol. Sci.* **2023**, *24*, 7349. [CrossRef] [PubMed]
6. Ramkumar, M.K.; Mulani, E.; Jadon, V.; Sureshkumar, V.; Krishnan, S.G.; Senthil Kumar, S.; Raveendran, M.; Singh, A.; Solanke, A.U.; Singh, N.K.; et al. Identification of major candidate genes for multiple abiotic stress tolerance at seedling stage by network analysis and their validation by expression profiling in rice (*Oryza sativa* L.). *3 Biotech* **2022**, *12*, 127. [CrossRef]
7. Sonsungsan, P.; Chantanakool, P.; Suratanee, A.; Buaboocha, T.; Comai, L.; Chadchawan, S.; Plaimas, K. Identification of key genes in 'Luang Pratahn', thai salt-tolerant rice, based on time-course data and weighted co-expression networks. *Front. Plant Sci.* **2021**, *12*, 744654. [CrossRef]
8. Chutimanukul, P.; Saputro, T.B.; Mahaprom, P.; Plaimas, K.; Comai, L.; Buaboocha, T.; Siangliw, M.; Toojinda, T.; Chadchawan, S. Combining genome and gene co-expression network analyses for the identification of genes potentially regulating salt tolerance in rice. *Front. Plant Sci.* **2021**, *12*, 704549. [CrossRef]
9. Saputro, T.B.; Jakada, B.H.; Chutimanukul, P.; Comai, L.; Buaboocha, T.; Chadchawan, S. OsBTBZ1 Confers Salt Stress Tolerance in *Arabidopsis thaliana*. *Int. J. Mol. Sci.* **2023**, *24*, 14483. [CrossRef]
10. Habila, S.; Khunpolwattana, N.; Chantarachot, T.; Buaboocha, T.; Comai, L.; Chadchawan, S.; Pongpanich, M. Salt stress responses and SNP-based phylogenetic analysis of Thai rice cultivars. *Plant Genome* **2022**, *15*, e20189. [CrossRef]
11. Lekklar, C.; Suriya-Arunroj, D.; Pongpanich, M.; Comai, L.; Kositsup, B.; Chadchawan, S.; Buaboocha, T. Comparative genomic analysis of rice with contrasting photosynthesis and grain production under salt stress. *Genes* **2019**, *10*, 562. [CrossRef]
12. Ran, X.; Wang, X.; Gao, X.; Liang, H.; Liu, B.; Huang, X. Effects of salt stress on the photosynthetic physiology and mineral ion absorption and distribution in white willow (*Salix alba* L.). *PLoS ONE* **2021**, *16*, e0260086. [CrossRef] [PubMed]
13. Jakada, B.H.; Punchkhon, C.; Syarifudin, A.; Saputro, T.B.; Buaboocha, T.; Chadchawan, S. Rice OBF binding protein 4 (OsOBP4) participates in flowering and regulates salt stress tolerance in *Arabidopsis*. *Environ. Exp. Bot.* **2024**, *221*, 105748. [CrossRef]
14. Yu, G.; Wang, L.-G.; Han, Y.; He, Q.-Y. clusterProfiler: An R package for comparing biological themes among gene clusters. *Omics A J. Integr. Biol.* **2012**, *16*, 284–287. [CrossRef] [PubMed]
15. Nounjan, N.; Chansongkrow, P.; Charoensawan, V.; Siangliw, J.L.; Toojinda, T.; Chadchawan, S.; Theerakulpisut, P. High performance of photosynthesis and osmotic adjustment are associated with salt tolerance ability in rice carrying drought tolerance QTL: Physiological and co-expression network analysis. *Front. Plant Sci.* **2018**, *9*, 1135. [CrossRef] [PubMed]
16. Kojonna, T.; Suttiyut, T.; Khunpolwattana, N.; Pongpanich, M.; Suriya-Arunroj, D.; Comai, L.; Buaboocha, T.; Chadchawan, S. Identification of a negative regulator for salt tolerance at seedling stage via a genome-wide association study of thai rice populations. *Int. J. Mol. Sci.* **2022**, *23*, 1842. [CrossRef] [PubMed]
17. Song, W.-Y.; Yamaki, T.; Yamaji, N.; Ko, D.; Jung, K.-H.; Fujii-Kashino, M.; An, G.; Martinoia, E.; Lee, Y.; Ma, J.F. A rice ABC transporter, OsABCC1, reduces arsenic accumulation in the grain. *Proc. Natl. Acad. Sci. USA* **2014**, *111*, 15699–15704. [CrossRef]
18. Tang, Z.; Chen, Y.; Miller, A.J.; Zhao, F-J. The C-type ATP-binding cassette transporter OsABCC7 is involved in the root-to-shoot translocation of arsenic in rice. *Plant Cell Physiol.* **2019**, *60*, 1525–1535. [CrossRef]
19. Jasinski, M.; Ducos, E.; Martinoia, E.; Boutry, M. The ATP-binding cassette transporters: Structure, function, and gene family comparison between rice and *Arabidopsis*. *Plant Physiol.* **2003**, *131*, 1169–1177. [CrossRef]
20. Burla, B.; Pfrunder, S.; Nagy, R.; Francisco, R.M.; Lee, Y.; Martinoia, E. Vacuolar transport of abscisic acid glucosyl ester is mediated by ATP-binding cassette and proton-antiport mechanisms in *Arabidopsis*. *Plant Physiol.* **2013**, *163*, 1446–1458. [CrossRef]

21. Wasi, M.; Khandelwal, N.K.; Vishwakarma, P.; Lynn, A.M.; Mondal, A.K.; Prasad, R. Inventory of ABC proteins and their putative role in salt and drug tolerance in *Debaryomyces hansenii*. *Gene* **2018**, *676*, 227–242. [CrossRef]
22. Matsuda, S.; Nagasawa, H.; Yamashiro, N.; Yasuno, N.; Watanabe, T.; Kitazawa, H.; Takano, S.; Tokuji, Y.; Tani, M.; Takamure, I.; et al. Rice RCN1/OsABCG5 mutation alters accumulation of essential and nonessential minerals and causes a high Na/K ratio, resulting in a salt-sensitive phenotype. *Plant Sci.* **2014**, *224*, 103–111. [CrossRef] [PubMed]
23. Li, X.; Zhang, Y.; Yin, L.; Lu, J. Overexpression of pathogen-induced grapevine TIR-NB-LRR gene *VaRGA1* enhances disease resistance and drought and salt tolerance in *Nicotiana benthamiana*. *Protoplasma* **2017**, *254*, 957–969. [CrossRef] [PubMed]
24. Andrews, C.; Xu, Y.; Kirberger, M.; Yang, J.J. Structural aspects and prediction of calmodulin-binding proteins. *Int. J. Mol. Sci.* **2020**, *22*, 308. [CrossRef] [PubMed]
25. Chinpongpanich, A.; Limruengroj, K.; Phean-O-Pas, S.; Limpaseni, T.; Buaboocha, T. Expression analysis of calmodulin and calmodulin-like genes from rice, *Oryza sativa* L. *BMC Res. Notes* **2012**, *5*, 625. [CrossRef] [PubMed]
26. Yuenyong, W.; Chinpongpanich, A.; Comai, L.; Chadchawan, S.; Buaboocha, T. Downstream components of the calmodulin signaling pathway in the rice salt stress response revealed by transcriptome profiling and target identification. *BMC Plant Biol.* **2018**, *18*, 335. [CrossRef] [PubMed]
27. Rosa, M.T.; Almeida, D.M.; Pires, I.S.; da Rosa Farias, D.; Martins, A.G.; da Maia, L.C.; de Oliveira, A.C.; Saibo, N.J.; Oliveira, M.M.; Abreu, I.A. Insights into the transcriptional and post-transcriptional regulation of the rice SUMOylation machinery and into the role of two rice SUMO proteases. *BMC Plant Biol.* **2018**, *18*, 349. [CrossRef]
28. Crouzet, J.; Trombik, T.; Fraysse, A.S.; Boutry, M. Organization and function of the plant pleiotropic drug resistance ABC transporter family. *FEBS Lett.* **2006**, *580*, 1123–1130. [CrossRef] [PubMed]
29. Hu, J.; Huang, L.; Chen, G.; Liu, H.; Zhang, Y.; Zhang, R.; Zhang, S.; Liu, J.; Hu, Q.; Hu, F.; et al. The elite alleles of OsSPL4 regulate grain size and increase grain yield in rice. *Rice* **2021**, *14*, 1–18. [CrossRef] [PubMed]
30. Yang, C.; Liu, X.; Li, D.; Zhu, X.; Wei, Z.; Feng, Z.; Zhang, L.; He, J.; Mou, C.; Jiang, L.; et al. OsLUGL is involved in the regulating auxin level and OsARFs expression in rice (*Oryza sativa* L.). *Plant Sci.* **2019**, *288*, 110239. [CrossRef]
31. Tang, N.; Zhang, H.; Li, X.; Xiao, J.; Xiong, L. Constitutive activation of transcription factor OsbZIP46 improves drought tolerance in rice. *Plant Physiol.* **2012**, *158*, 1755–1768. [CrossRef]
32. Chen, H.; Wang, Q.; Fan, M.; Zhang, X.; Feng, P.; Zhu, L.; Wu, J.; Cheng, X.; Wang, J. A Single Nucleotide Variation of CRS2 Affected the Establishment of Photosynthetic System in Rice. *Int. J. Mol. Sci.* **2023**, *24*, 5796. [CrossRef] [PubMed]
33. Arenhart, R.A.; Bai, Y.; de Oliveira, L.F.V.; Neto, L.B.; Schunemann, M.; dos Santos Maraschin, F.; Mariath, J.; Silverio, A.; Sachetto-Martins, G.; Margis, R.; et al. New insights into aluminum tolerance in rice: The ASR5 protein binds the STAR1 promoter and other aluminum-responsive genes. *Mol. Plant* **2014**, *7*, 709–721. [CrossRef] [PubMed]
34. Li, J.; Li, Y.; Yin, Z.; Jiang, J.; Zhang, M.; Guo, X.; Ye, Z.; Zhao, Y.; Xiong, H.; Zhang, Z.; et al. Os ASR 5 enhances drought tolerance through a stomatal closure pathway associated with ABA and H_2O_2 signalling in rice. *Plant Biotechnol. J.* **2017**, *15*, 183–196. [CrossRef] [PubMed]
35. Cheong, H.; Kim, C.-Y.; Jeon, J.-S.; Lee, B.-M.; Sun Moon, J.; Hwang, I. Xanthomonas oryzae pv. oryzae type III effector XopN targets OsVOZ2 and a putative thiamine synthase as a virulence factor in rice. *PLoS ONE* **2013**, *8*, e73346. [CrossRef] [PubMed]
36. Wang, G.; Ding, X.; Yuan, M.; Qiu, D.; Li, X.; Xu, C.; Wang, S. Dual function of rice OsDR8 gene in disease resistance and thiamine accumulation. *Plant Mol. Biol.* **2006**, *60*, 437–449. [CrossRef] [PubMed]
37. Ma, H.; Zhao, H.; Liu, Z.; Zhao, J. The phytocyanin gene family in rice (*Oryza sativa* L.): Genome-wide identification, classification and transcriptional analysis. *PLoS ONE* **2011**, *6*, e25184. [CrossRef] [PubMed]
38. Mekawy, A.M.M.; Assaha, D.V.; Ueda, A. Constitutive overexpression of rice metallothionein-like gene OsMT-3a enhances growth and tolerance of Arabidopsis plants to a combination of various abiotic stresses. *J. Plant Res.* **2020**, *133*, 429–440. [CrossRef] [PubMed]
39. Ananda Mustafiz, A.M.; Ajit Ghosh, A.G.; Tripathi, A.; Charanpreet Kaur, C.K.; Ganguly, A.; Bhavesh, N.; Tripathi, J.; Ashwani Pareek, A.P.; Sopory, S.; Singla-Pareek, S. A unique Ni^{2+}-dependent and methylglyoxal-inducible rice glyoxalase I possesses a single active site and functions in abiotic stress response. *Plant J.* **2014**, *78*, 951–963. [CrossRef] [PubMed]
40. Xu, Z.; Guo, W.; Mo, B.; Pan, Q.; Lu, J.; Wang, Z.; Peng, X.; Zhang, Z. Mitogen-activated protein kinase 2 specifically regulates photorespiration in rice. *Plant Physiol.* **2023**, *193*, 1381–1394. [CrossRef]
41. Brazier-Hicks, M.; Gershater, M.; Dixon, D.; Edwards, R. Substrate specificity and safener inducibility of the plant UDP-glucose-dependent family 1 glycosyltransferase super-family. *Plant Biotechnol. J.* **2018**, *16*, 337–348. [CrossRef]
42. Qiu, D.; Xiao, J.; Xie, W.; Liu, H.; Li, X.; Xiong, L.; Wang, S. Rice gene network inferred from expression profiling of plants overexpressing OsWRKY13, a positive regulator of disease resistance. *Mol. Plant* **2008**, *1*, 538–551. [PubMed]
43. Patishtan Perez, J. Genome Wide Association and Forward Genetic Studies to Identify Genes Involved in Salt Tolerance. University of York. Ph.D. Thesis, The University of York, York, UK, 2016.
44. Jain, M.; Nijhawan, A.; Arora, R.; Agarwal, P.; Ray, S.; Sharma, P.; Kapoor, S.; Tyagi, A.K.; Khurana, J.P. F-box proteins in rice. Genome-wide analysis, classification, temporal and spatial gene expression during panicle and seed development, and regulation by light and abiotic stress. *Plant Physiol.* **2007**, *143*, 1467–1483. [CrossRef] [PubMed]
45. Xie, Y.; Niu, B.; Long, Y.; Li, G.; Tang, J.; Zhang, Y.; Ren, D.; Liu, Y.G.; Chen, L. Suppression or knockout of SaF/SaM overcomes the Sa-mediated hybrid male sterility in rice. *J. Integr. Plant Biol.* **2017**, *59*, 669–679. [CrossRef] [PubMed]

46. Long, Y.; Zhao, L.; Niu, B.; Su, J.; Wu, H.; Chen, Y.; Zhang, Q.; Guo, J.; Zhuang, C.; Mei, M.; et al. Hybrid male sterility in rice controlled by interaction between divergent alleles of two adjacent genes. *Proc. Natl. Acad. Sci. USA* **2008**, *105*, 18871–18876. [CrossRef] [PubMed]
47. Masood, N.I.A.; Hira Mubeen, F.D.; Waheed, R.; Noreen, I.; Zafar, A.; Khanum, P. ATP synthase subunits: Structure and role in plants under stress conditions. *Pak. J. Bot.* **2023**, *55*, 1661–1668.
48. Zhang, X.; Takano, T.; Liu, S. Identification of a mitochondrial ATP synthase small subunit gene (RMtATP6) expressed in response to salts and osmotic stresses in rice (*Oryza sativa* L.). *J. Exp. Bot.* **2006**, *57*, 193–200. [CrossRef]
49. Wei, M.-Y.; Liu, J.-Y.; Li, H.; Hu, W.-J.; Shen, Z.-J.; Qiao, F.; Zhu, C.-Q.; Chen, J.; Liu, X.; Zheng, H.-L. Proteomic analysis reveals the protective role of exogenous hydrogen sulfide against salt stress in rice seedlings. *Nitric Oxide* **2021**, *111*, 14–30. [CrossRef]
50. Wang, C.; Chen, S.; Dong, Y.; Ren, R.; Chen, D.; Chen, X. Chloroplastic Os3BGlu6 contributes significantly to cellular ABA pools and impacts drought tolerance and photosynthesis in rice. *New Phytol.* **2020**, *226*, 1042–1054. [CrossRef]
51. Goyal, E.; Amit, S.K.; Singh, R.S.; Mahato, A.K.; Chand, S.; Kanika, K. Transcriptome profiling of the salt-stress response in *Triticum aestivum* cv. Kharchia Local. *Sci. Rep.* **2016**, *6*, 27752. [CrossRef]
52. Oliveira, J.A.V.D.; Vianello, R.P.; Lanna, A.C.; Dedicova, B.; Rocha, D.C.; Brondani, C. Drought tolerance induced by the overexpression of the nuclear rbcL gene in rice. *Braz. J. Agric. Res.* **2023**, *58*, e03181. [CrossRef]
53. Munns, R.; Day, D.A.; Fricke, W.; Watt, M.; Arsova, B.; Barkla, B.J.; Bose, J.; Byrt, C.S.; Chen, Z.H.; Foster, K.J.; et al. Energy costs of salt tolerance in crop plants. *New Phytol.* **2020**, *225*, 1072–1090. [CrossRef] [PubMed]
54. Punchkhon, C.; Chutimanukul, P.; Chokwiwatkul, R.; Saputro, T.B.; Grennan, A.K.; Diego, N.D.; Spíchal, L.; Chadchawan, S. Role of *LOC_Os01g68450*, containing DUF2358, in salt tolerance is mediated via adaptation of absorbed light energy dissipation. *Plants* **2022**, *11*, 1233. [CrossRef] [PubMed]
55. Li, H.; Handsaker, B.; Wysoker, A.; Fennell, T.; Ruan, J.; Homer, N.; Marth, G.; Abecasis, G.; Durbin, R.; 1000 Genome Project Data Processing Subgroup. The sequence alignment/map format and SAMtools. *Bioinformatics* **2009**, *25*, 2078–2079. [CrossRef] [PubMed]
56. Love, M.I.; Huber, W.; Anders, S. Moderated estimation of fold change and dispersion for RNA-seq data with DESeq2. *Genome Biol.* **2014**, *15*, 1–21. [CrossRef] [PubMed]
57. Gentleman, R.; Carey, V.; Huber, W.; Hahne, F. genefilter: Methods for Filtering Genes from High-Throughput Experiments. Version 1.87.0. 2023. Available online: https://bioconductor.org/packages/devel/bioc/manuals/genefilter/man/genefilter.pdf (accessed on 26 February 2024).
58. Suratanee, A.; Chokrathok, C.; Chutimanukul, P.; Khrueasan, N.; Buaboocha, T.; Chadchawan, S.; Plaimas, K. Two-state co-expression network analysis to identify genes related to salt tolerance in Thai rice. *Genes* **2018**, *9*, 594. [CrossRef]
59. Aoki, K.; Ogata, Y.; Shibata, D. Approaches for extracting practical information from gene co-expression networks in plant biology. *Plant Cell Physiol.* **2007**, *48*, 381–390. [CrossRef]
60. Koschützki, D.; Schreiber, F. Centrality analysis methods for biological networks and their application to gene regulatory networks. *Gene Regul. Syst. Biol.* **2008**, *2*, GRSB-S702. [CrossRef]
61. Plaimas, K.; Eils, R.; König, R. Identifying essential genes in bacterial metabolic networks with machine learning methods. *BMC Syst. Biol.* **2010**, *4*, 56. [CrossRef]
62. Huber, W.; Carey, V.J.; Long, L.; Falcon, S.; Gentleman, R. Graphs in molecular biology. *BMC Bioinform.* **2007**, *8*, S8. [CrossRef]
63. Li, G.; Li, M.; Wang, J.; Li, Y.; Pan, Y. United neighborhood closeness centrality and orthology for predicting essential proteins. In *IEEE/ACM Transactions on Computational Biology and Bioinformatics*; IEEE: New York, NY, USA, 2018; Volume 17, pp. 1451–1458.
64. Hansen, D.L.; Shneiderman, B.; Smith, M.A.; Himelboim, I. Calculating and visualizing network metrics. In *Analyzing Social Media Networks with NodeXL*; Morgan-Kaufmann: Burlington, MA, USA, 2020; pp. 79–94.
65. Shannon, P.; Markiel, A.; Ozier, O.; Baliga, N.S.; Wang, J.T.; Ramage, D.; Amin, N.; Schwikowski, B.; Ideker, T. Cytoscape: A software environment for integrated models of biomolecular interaction networks. *Genome Res.* **2003**, *13*, 2498–2504. [CrossRef]

Disclaimer/Publisher's Note: The statements, opinions and data contained in all publications are solely those of the individual author(s) and contributor(s) and not of MDPI and/or the editor(s). MDPI and/or the editor(s) disclaim responsibility for any injury to people or property resulting from any ideas, methods, instructions or products referred to in the content.

International Journal of
Molecular Sciences

MDPI

Article

Marker-Assisted Selection of Jacalin-Related Lectin Genes *OsJRL45* and *OsJRL40* Derived from Sea Rice 86 Enhances Salt Tolerance in Rice

Xiaolin Yin, Qinmei Gao, Feng Wang, Weihao Liu, Yiting Luo, Shuixiu Zhong, Jiahui Feng, Rui Bai, Liangbi Chen, Xiaojun Dai * and Manzhong Liang *

Hunan Province Key Laboratory of Crop Sterile Germplasm Resource Innovation and Application, College of Life Science, Hunan Normal University, Changsha 410081, China; yinxleffort@163.com (X.Y.); 15802620355@163.com (Q.G.); 13975877142@163.com (F.W.); 18749958161@163.com (W.L.); luoyiting2023@163.com (Y.L.); zsx13207975104@163.com (S.Z.); jiahuifeng@hunnu.edu.cn (J.F.); bairui0511@163.com (R.B.); chenliangbi@126.com (L.C.)
* Correspondence: hnsfdxj0309@hunnu.edu.cn (X.D.); 11062@hunnu.edu.cn (M.L.)

Abstract: Soil salinization limits rice growth and is an important restriction on grain yield. Jacalin-related lectins are involved in multiple stress responses, but their role in salt stress responses and use as molecular markers for salt tolerance remain poorly understood. Salt stress treatments and RT-qPCR analyses of Sea Rice 86 (SR86), 9311, and Nipponbare (Nip) showed that *OsJRL45* and *OsJRL40* enhanced tolerance of salt stress in SR86. Molecular markers based on sequence differences in SR86 and the salt-sensitive variety, 9311, in the intergenic region between *OsJRL45* and *OsJRL40* were validated in recombinant inbred lines derived from SR86 and 9311, hybrid populations, and common rice varieties. Yeast two-hybrid and bimolecular fluorescence complementation demonstrated that OsJRL45 and OsJRL40 interacted. Co-transformation of Nip with *OsJRL45* and *OsJRL40* derived from SR86 had no effect on the mature phenotype in T_2 plants; however, salt stress at the three-leaf stage led to significant increases in CAT, POD, SOD, and Pro contents, but reduced MDA content in transgenic plants. Transcriptomic analysis identified 834 differentially expressed genes in transgenic plants under salt stress. GO and KEGG enrichment analyses indicated that metabolic pathways related to antioxidant responses and osmotic balance were crucial for salt-stress tolerance. Thus, molecular markers based on nucleotide differences in *OsJRL45* and *OsJRL40* provide a novel method for identifying salt-tolerant rice varieties.

Keywords: rice (*Oryza sativa* L.); *OsJRL45*/*OsJRL40*; recombinant inbred lines (RILs); transcriptome

1. Introduction

Rice (*Oryza sativa* L.) is one of the most important food crops globally, with over half of the world's population relying on it as a staple food [1]. The demand for food consumption is rising due to the rapid increase in the global population, although the area of land suitable for arable production decreases year by year due to the increase in salinized land [2]. Addressing the gap between this increased demand due to population growth and the reduction in arable land presents a significant challenge for grain production in China [3,4]. Rice is a salt-sensitive crop that, when subjected to salt stress, responds at the morphological, cellular, and molecular levels [5] in ways that affect essential processes, including photosynthesis and metabolism, leading to growth inhibition or even death [6,7]. At the molecular level, salt stress leads to ion toxicity, osmotic stress, and oxidative stress [8]. Ion toxicity under salt stress is usually due to the excessive accumulation of Na^+ and Cl^-, which causes Na^+ to accumulate in the cytoplasm. This leads to membrane depolarization and K^+ leakage from the cell, ultimately resulting in plant death [9]. OsHAK1, a potassium transporter, promotes K^+ uptake under salt stress and increases the K^+/Na^+

ratio, making this protein crucial for enhanced salt tolerance in rice [10–12]. Many other genes related to ion transport and the regulation of salt tolerance have been identified, including *OsHKT1;5* [13] and *OsAKT2* [14]. To cope with the osmotic stress caused by salt stress, plants produce large amounts of osmotic regulators, including proline, glycerol, sugars, and their derivatives [15]. Salt stress-induced oxidative stress increases the activity of antioxidant enzymes such as catalase (CAT), peroxidase (POD), and superoxide dismutase (SOD), as well as the synthesis of some non-enzymatic antioxidants [16]. The salt tolerance mechanism is thus a complex regulatory network composed of multiple metabolic pathways.

Increased soil salinity necessitates the development of novel methods for improving the tolerance of existing rice varieties to salt stress, as well as the use of conventional breeding techniques, such as backcrossing, recurrent selection, and use of mutations, to develop new varieties. Such approaches have their limitations, as, in addition to the desired genes, unwanted genes may also be passed on to future generations [17]. As genetic diversity serves as the raw material for breeding programs, the generation of segregating populations (F_2 progeny or recombinant inbred lines (RILs)) followed by genetic analysis using a conventional genetic mapping approach can identify important agronomic traits and genes under controlled conditions [18–20]. Such populations contain a large number of genetic variants, enabling advances in crop improvement and the genetic analysis of complex traits, as well as the development of genetic markers to detect quantitative trait loci and isolate the genes responsible [21]. Marker-assisted selection (MAS) is an important molecular tool for rice breeding that minimizes the number of backcross generations required [22]. Markers are used to select indirectly the genetic determinant or determinants of a trait of interest, such as abiotic stress tolerance [23]. The development and availability of markers for use with plant lines carrying genomic regions known to participate in the expression of target traits has made it possible to use MAS to identify major genes controlling such traits [24].

Lectins are proteins that are found in a wide variety of species, including microorganisms, plants, and animals [25]. In plants, lectins are found in vegetative organs such as roots, stems, and leaves [26]. *HvHorcH* is a member of the jacalin-related lectin (JRL) family that is involved in the physiological response of barley (*Hordeum vulgare*) roots to salt stress and also enhances salt tolerance [27]. Abscisic acid (ABA) biosynthesis is inhibited in transgenic Arabidopsis (*Arabidopsis thaliana*) plants expressing *PeJRL* (*Populus euphratica*), thereby reducing the production of ABA-induced ROS and oxidative damage during salt stress [28]. OsJRL, a rice protein, is a JRL belonging to the mannose-binding lectin superfamily. It is up-regulated by *OsJRL* overexpression and increases the expression of stress-related genes under salt stress, enhancing salt tolerance [29]. Lectins are indirectly involved in regulating chlorophyll content and also reduce membrane damage and electrolyte leakage, thus mitigating the effects of salt stress [30]. The expression of *SIT1*, a lectin-encoding gene in rice, is up-regulated under salt stress; SIT1 participates in the MPK3/MPK6 pathway, which increases ethylene synthesis and ROS accumulation [31], and also plays a role in Na^+ efflux by regulating the salt overly sensitive (SOS) pathway [32]. Under salt stress, rice plants overexpressing *OsSalT*, which encodes a mannose-binding protein, have significantly lower Na^+ content than wild-type plants, indicating that this gene plays an important part in the response to salt stress [33]. *OsJRL45* enhances the antioxidant capacity of rice plants and promotes the maintenance of Na^+-K^+ homeostasis under salt stress; *OsJRL45*-overexpression lines show higher salt tolerance, as well as significantly increased grain-filling rates and thousand-grain weights [34]. *OsJRL40* enhances antioxidant enzyme activity and maintains Na^+-K^+ homeostasis under salt stress, as well as regulating salt tolerance in rice by controlling the expression of Na^+-K^+ transporters, salt-response transcription factors, and other salt response-related proteins [35]. Lectins thus play key roles in regulating stress response pathways during salt stress; however, their specific mode of action in response to salt stress requires further study.

The Sea Rice 86 (SR86) cultivar was developed over years of selection and offers many advantages, including high salt tolerance [36]. The identification of OsNACL35, a NAC (NAM, ATAF1/2, and CUC2) transcription factor, in SR86 suggests that salt tolerance may result from an enhanced H_2S yield [37]. Microbial metabolomic analysis of rhizosphere bacteria associated with SR86 seedlings cultivated under different levels of salinity revealed that salt stress significantly alters the diversity of rhizosphere bacteria and rhizosphere metabolites, thereby improving salt tolerance [38]. The *OsJRL45* and *OsJRL40* genes from SR86 enhance the antioxidant capacity of rice plants and promote the maintenance of Na^+-K^+ homeostasis under salt stress [34,35,39]. Not all of the genes related to salt tolerance in SR86 have been identified to date, and most of those that have need to be expressed under stress induction. The use of molecular markers, linkage analysis, and mapping techniques will enable the identification of more genes involved in salt tolerance in this cultivar.

Our previous study hybridized the salt-tolerant rice variety SR86 with a standard cultivar Nip and used bulked segregant analysis (BSA) and genetic mapping to identify salt-tolerant and salt-sensitive populations in the segregating hybrids. We then screened these populations for genes related to salt stress and identified two JRL genes, *OsJRL45* and *OsJRL40* [39]. We also verified the physiological and biochemical functions of *OsJRL45* and *OsJRL40* in salt tolerance in rice [34,35]. In the current study, to better understand the roles played by *OsJRL45* and *OsJRL40* in salt tolerance, and to develop a novel method for mapping salt tolerance in rice, we co-transformed the Nip cultivar with *OsJRL45* and *OsJRL40* from SR86, and also constructed a segregating population derived from SR86 and 9311, a salt-sensitive variety. We screened the hybrid population for salt-tolerant plants by examining the phenotype under salt stress. We identified nucleotide differences associated with salt tolerance in the segregating population and used these to develop molecular markers for salt tolerance. This method improved the efficiency of screening for salt tolerance and shortened the breeding process of salt-tolerant rice, promoting the rapid development of new salt-tolerant rice varieties.

2. Results

2.1. Analysis of OsJRL45 and OsJRL40 Expression under Salt Stress

To analyze the expression of *OsJRL45* and *OsJRL40* in SR86, 9311, and Nip under salt stress, seedlings at the three-leaf stage were treated with 9‰ NaCl for 4 days, followed by a 4-day recovery period (Figure 1A–C). The survival rates of 9311 and Nip were around 20%, while the survival rate of SR86 was 80%, indicating that this variety had significantly higher salt tolerance than either 9311 or Nip (Figure 1D). RT-qPCR analysis of *OsJRL45* and *OsJRL40* expression in SR86, 9311, and Nip after 6, 8, 24, and 48 h of salt stress revealed that both genes were expressed at significantly higher levels in SR86 than in 9311 and Nip (Figure 1E,F). These results suggested that *OsJRL45* and *OsJRL40* enhanced salt stress tolerance in SR86.

2.2. Analysis of Sequence Variation in OsJRL45 and OsJRL40

OsJRL45 and *OsJRL40* are located on rice chromosome 4 and are thus likely to interact with each other (Figure 2A,B). An analysis of sequence variation between SR86 and other rice cultivars revealed a correlation with salt tolerance. The *OsJRL45* and *OsJRL40* sequences from Shuhui 498 (R498) were obtained from the NCBI (https://www.ncbi.nlm.nih.gov/, accessed on 29 June 2022). Both genes contained two exons and one intron (Figure 2). Primers were designed to amplify the *OsJRL45* and *OsJRL40* sequences from the rice cultivars SR86, 9311, L623, R498, Minghui63, Zhenshan97, Yu Chi, Nantehao, Qingzhen, and Meizhan, using NCBI R498 as the reference sequence.

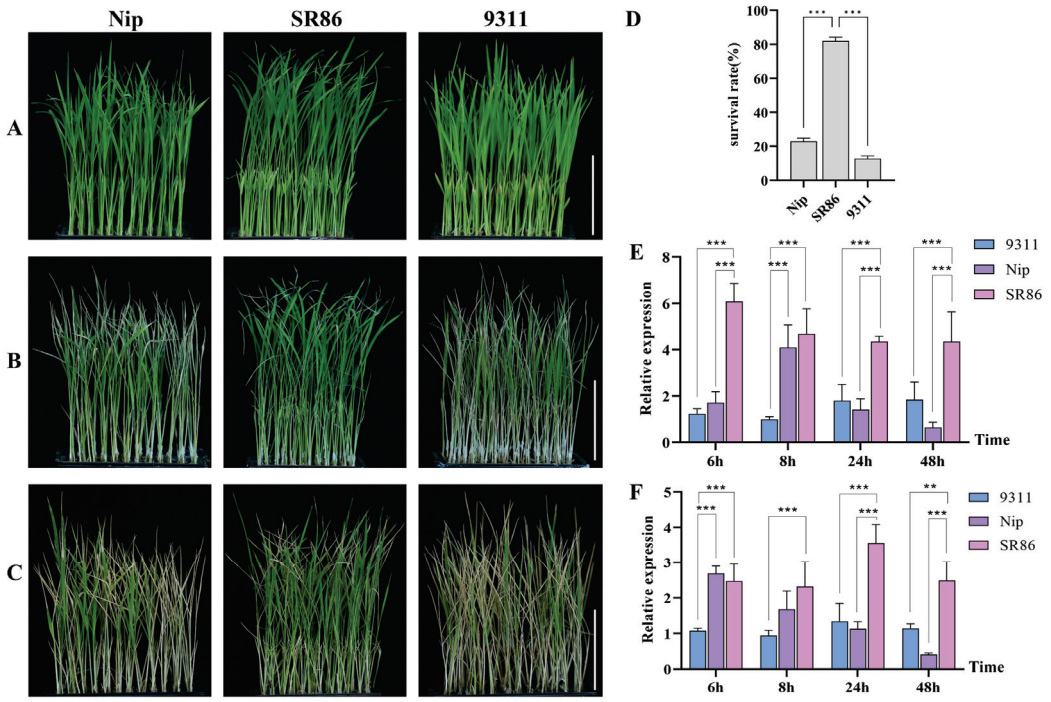


Figure 1. Plant phenotypes and analysis of *OsJRL45* and *OsJRL40* expression at the three-leaf stage under 9‰ NaCl salt stress. (**A**) Appearance of plants at the three-leaf stage before salt stress treatment. (**B**) Appearance of plants after 4 days of treatment with 9‰ NaCl. (**C**) Appearance of plants after recovery for 4 days. (**D**) Survival rates after recovery from salt stress treatment. (**E**) Quantification of RT-qPCR analysis of *OsJRL45* expression. (**F**) Quantification of RT-qPCR analysis of *OsJRL40* expression. Data represent the mean ± SD of three independent replicates; asterisks indicate statistically significant differences (**: $p < 0.01$; ***: $p < 0.001$). Scale bars on (**A**–**C**): 5 cm.

Sequence alignment showed that exon 1 of *OsJRL45* contained eight single nucleotide polymorphisms (SNPs). Amino acid alignment revealed that three SNPs (located 63 base-pairs (bp), 72 bp, and 123 bp after the start codon) were synonymous mutations but that the SNPs located 209 bp, 224 bp, 245 bp, 263 bp, and 268 bp from the start codon led to amino acid changes (Figure 2B). Exon 2 of *OsJRL45* contained one SNP in which adenine (A) in the SR86 and Nantehao sequences was substituted with cytosine (C) in the other cultivars, leading to a change from Glu to Asp in the amino acid sequence (Figure 2B). An SNP in exon 1 of *OsJRL40* was found in a single cultivar, Meizhan. Exon 2 of *OsJRL40* contained one SNP; an adenine (A) in the SR86 sequence was substituted with guanine (G) in other cultivars, resulting in an amino acid change from Ser in SR86 to Gly in the other cultivars (Figure 2B). Genomic sequencing of *OsJRL45* and *OsJRL40* from SR86, R498, Minghui63, and Zhenshan97 revealed that the two genes were only 2605 bp apart. In SR86, the intergenic region contained a 25-bp deletion (GCGCACGACGCG-GCCGCCAGCGTTC); this deletion was located 204 bp downstream from the end of the *OsJRL45* coding sequence and 2401 bp upstream of *OsJRL40*. We therefore designed and validated molecular markers based on the variation in the *OsJRL45* and *OsJRL40* sequences in the different rice varieties.

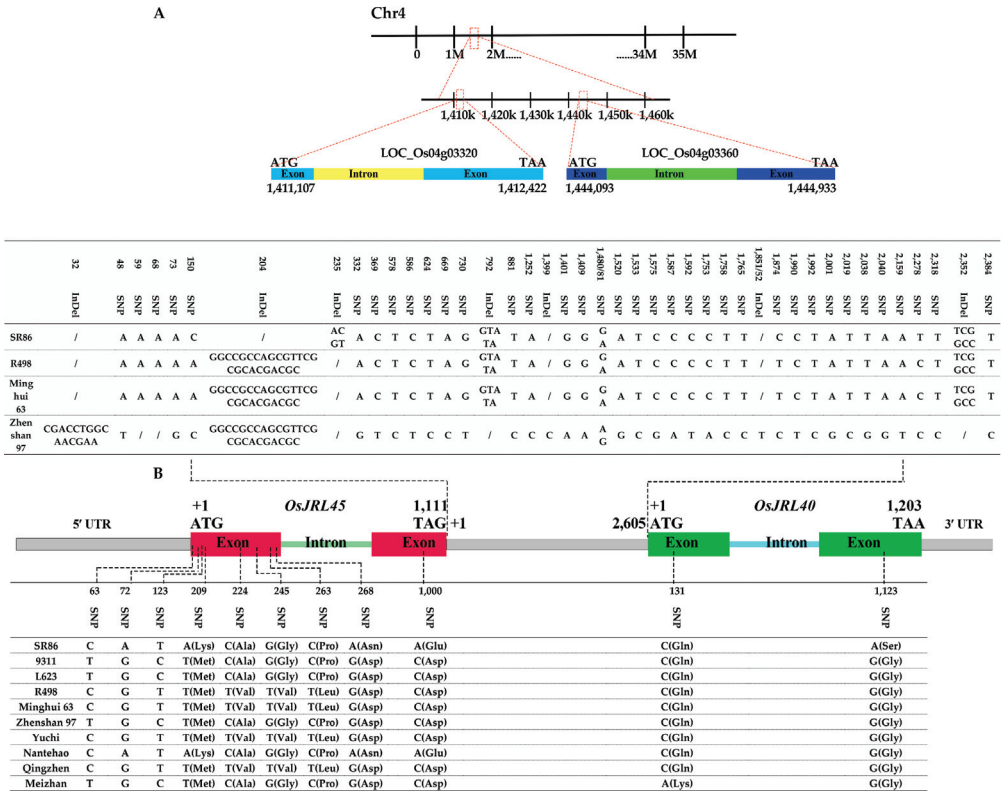


Figure 2. Location and structure of *OsJRL45* and *OsJRL40*. (**A**) Structure of *OsJRL45* and *OsJRL40* in Nip. ATG indicates the start codon. (**B**) Positions of single nucleotide polymorphisms (SNPs) in the exons of *OsJRL45* and *OsJRL40* and the resulting changes in amino acid sequences.

2.3. Validation of Molecular Markers in Populations

An F_1 generation of hybrid progeny was produced by crossing SR86 and 9311. Individual F_1 plants were selected and self-pollinated to produce an F_2 population. We selected 3000 F_2 seeds, which were germinated and the resulting seedlings subjected to 9‰ NaCl salt stress at the three-leaf stage. The surviving salt-tolerant plants were allowed to grow until seed-set and harvest. We then selected 320 individual F_3 seedlings, which were grown to the three-leaf stage under hydroponic conditions, treated with 6‰ NaCl for 5 days to induce salt stress, and then allowed to recover for 5 days (Figure 3). DNA was extracted and analyzed by PCR using the molecular marker primers developed in this study. The PCR products were separated using 2% agarose gel electrophoresis (Figure S1), and a statistical analysis was performed to compare individual plants in the population. Of the F_3 plants tested, 228 plants produced an agarose gel electrophoresis result that closely resembled that of the SR86 parent, 54 plants produced a result that resembled that of the 9311 parent, 36 plants were heterozygous, and the remaining 2 plants did not produce any PCR product (Table 1). These results indicated that molecular marker primers based on nucleotide differences between *OsJRL45* and *OsJRL40* could be used to screen salt-tolerant plants.

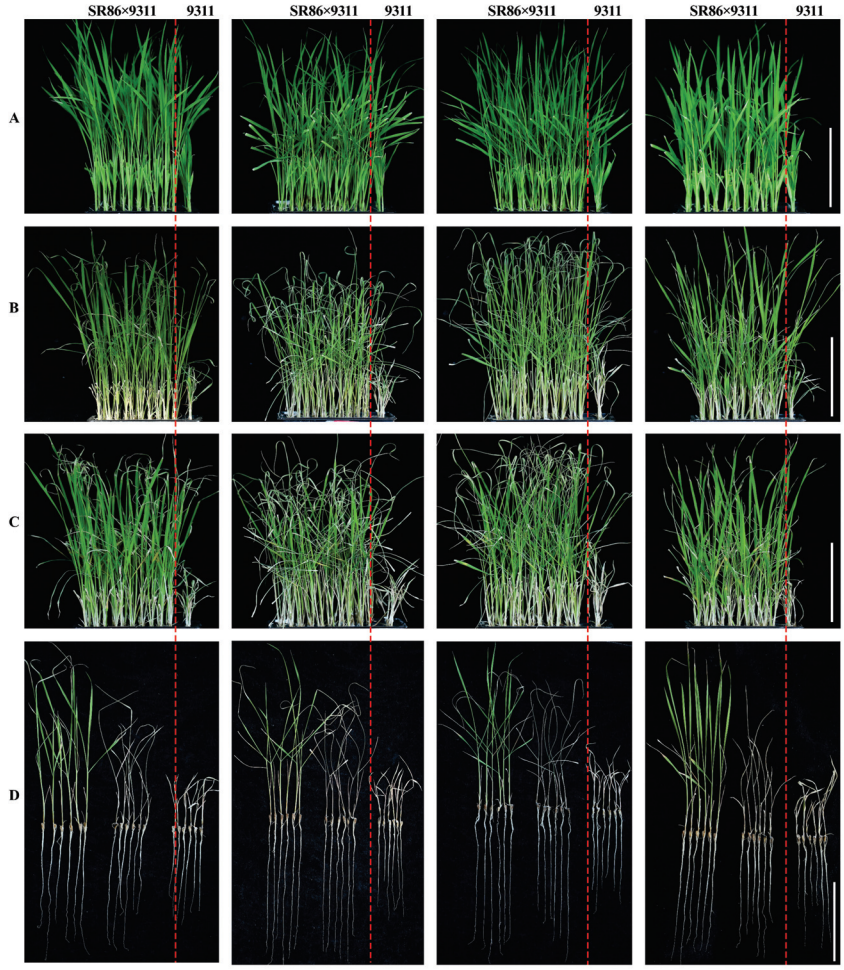


Figure 3. Effect of salt stress on plants from a hybrid population derived from the cross SR86 × 9311. (**A**) Appearance of plants at the three-leaf stage before salt stress treatment. (**B**) Appearance of plants after 5 days of 6‰ NaCl salt stress treatment. (**C**) Appearance of plants after 5 days of recovery. (**D**) Appearance of individual plants after recovery. SR86 × 9311 indicates plants from the hybrid population; plants from the parental line 9311 are shown to the right of the red dotted line. Scale bars on (**A**–**D**): 5 cm.

Table 1. Validation of MAS of salt stress in 320 SR86 × 9311 RILs.

	Number of SR86 × 9311 RILs
SR86	228
9311	54
Heterozygous	36
No product	2
Total	320

2.4. Validation of Molecular Markers for Salt Tolerance

To validate the accuracy of the molecular markers developed in this study to screen for salt-tolerant rice, the markers were verified in a number of rice varieties. DNA was extracted, amplified by PCR, and the PCR products separated using 2% agarose gel electrophoresis. The rice varieties that showed higher salt tolerance (Foer B, Chaimi, Yuejing, Xiangzao 32, Nantehao, R288, Shuhui 527, Aizinuo, and Xiang 628S) produced gel electrophoresis results that closely resembled that of SR86, while salt-intolerant plants produced similar results to 9311 (Figure 4). This indicated that the novel molecular markers designed

to identify salt tolerance were accurate for more than 90% of plants, suggesting that they had high specificity when used for screening.

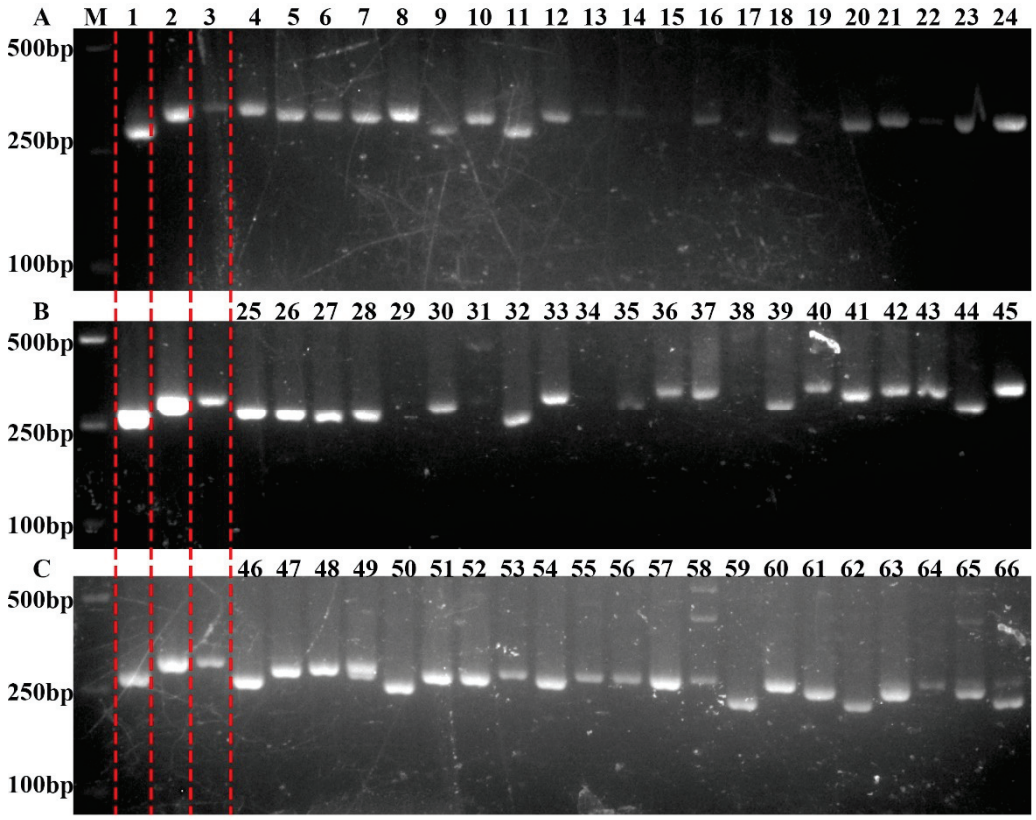


Figure 4. Validation of marker-assisted selection in different rice varieties. Lanes 1, 2 and 3 (indicated by the red dotted lines) represent SR86, 9311, and Nip, respectively. (**A**) From left to right (lanes 4–24): Mei Zhan, Yu Chi, Ming Hui, Zhan F2, Feng Hua Zhan, Fu Yi B, IR64, Chai Mi, Zi 100, B213, Zhu 1S, Guangxiang 24S, Hua 451, Xiang Wan Indica, Yuejing, Xianhui, bolon, Zm273 Bairizao, Zhen Indica 97A, Guangzhan 63S. (**B**) From left to right (lanes 25–45): TTP, Qingzhen, TB, Lemont, Wanhui 110, PA64S, ZhongjiuA, Xiangzao 32, Gang 46B, 7001S2, CHEN 28, Sanyingzhan, Yongping, Qingzhen, Guangsi, IR36, 9311, Nan 11, Xiangzao Indica, IR24. (**C**) From left to right (lanes 46–66): Nantehao, Ludao 2318, R402, R16, R288, Minghui 63, P002, Qiuguang, Shuhui 527, Yujing 1, Zhengxuan 3, Xiaozinuo, D16, Xiangzi 3150, Xiangxiang 628S, Huaihui 210, Yixiang A, Duozi 1, Lila 2, Yuehui A, 750S. M: DNA size marker.

2.5. Validation of MAS for Salt Tolerance in RILs Derived from SR86 × 9311

Salt-tolerant plants were randomly selected from sixth generation RILs derived from SR86 and 9311 hybrids, treated with 9‰ NaCl for 4 days at the three-leaf stage, and then allowed to recover for 4 days (Figure 5A–C). The survival rates after recovery from salt stress treatment were determined. The survival rate of the parental line 9311 was approximately 10%, and that of SR86, the other parental line, was more than 80%. The survival rates of the salt-tolerant hybrids were between 60–70% (Figure 5D). The genotypes of the RILs were verified using specific marker primers based on differences between the SR86 and 9311 sequences. Agarose gel electrophoresis showed that plants with higher salt tolerance were genetically more similar to SR86, while individuals with poorer salt tolerance resembled 9311 genetically (Figure 5E). These results confirmed that the molecular markers developed in this study to identify salt tolerance had high specificity.

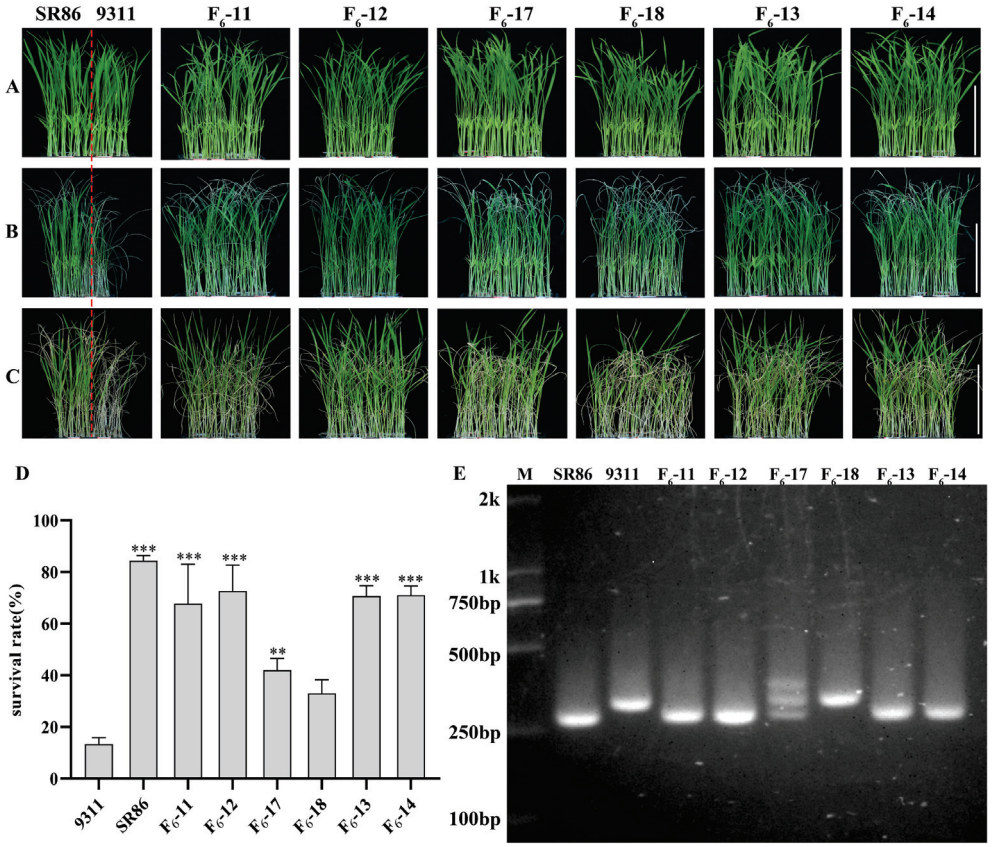


Figure 5. Screening of RILs derived from SR86 × 9311 for salt tolerance. (**A**) Appearance of plants at the three-leaf stage before salt stress treatment. (**B**) Appearance of plants after 4 days of treatment with 9‰ NaCl. (**C**) Appearance of plants after 4 days of recovery from salt stress. F_6 indicates the sixth generation of RILs derived from the cross SR86 × 9311. (**D**) Survival rate statistics: data represent the mean ± SD of three independent replicates; asterisks indicate statistically significant differences (**: $p < 0.01$; ***: $p < 0.001$). (**E**) Genotyping of hybrid plants using specific molecular markers. (**A**–**C**) On the left side of the red dotted line is SR86 and on the right is 9311. M: DNA size marker. Scale bars on (**A**–**C**): 5 cm.

2.6. Analysis of the Interaction between OsJRL45 and OsJRL40

Structural analysis of *OsJRL45* and *OsJRL40* revealed that both genes were located on chromosome 4 (Figure 2A). To determine whether the OsJRL45 and OsJRL40 proteins interacted, OsJRL45 was used as bait in yeast two-hybrid (Y2H) experiments. The yeast strain Y2HGold was co-transformed with the vectors *AD-OsJRL45* and *BD-OsJRL40*. Co-transformed yeast grew normally on SD/-Trp/-Leu/-His/-Ade + X-α-Gal medium (Figure 6A), indicating an interaction between OsJRL45 and OsJRL40.

To verify this Y2H result, bimolecular fluorescence complementation (BiFC) assays were conducted in tobacco leaves. Previous studies showed that OsJRL45 and OsJRL40 are located in the endoplasmic reticulum and cytoplasm, respectively [33,34]. Following co-expression of OsJRL40-YFP^N/OsJRL45-YFP^C, fluorescent signals were detected in the nucleus and cytoplasm (Figure 6B). Taken together, the Y2H and BiFC results indicated that there was an interaction between OsJRL45 and OsJRL40; we therefore speculated that co-expression of *OsJRL45* and *OsJRL40* in rice might enhance their function.

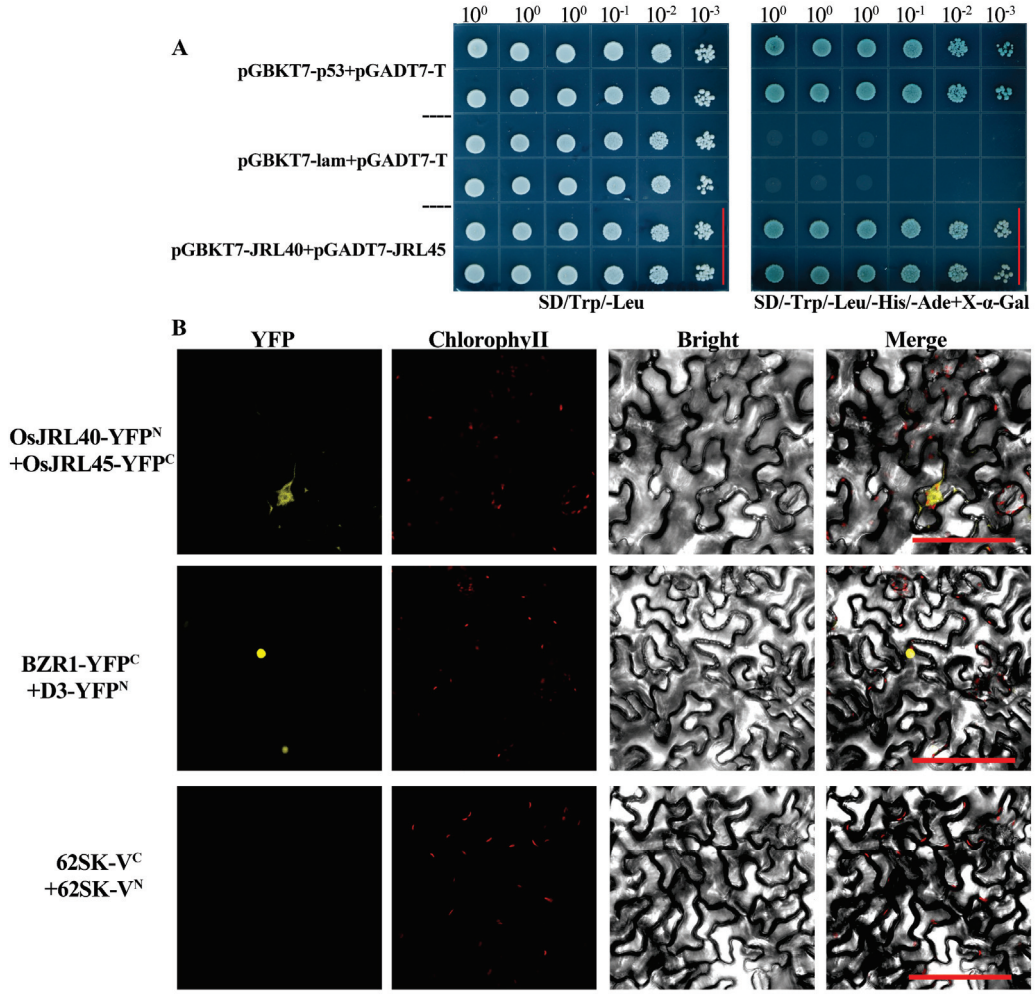


Figure 6. Interaction between OsJRL45 and OsJRL40. (**A**) Yeast two-hybrid (Y2H) assays showing the in vivo interaction between OsJRL45 and OsJRL40. The recombinant plasmids pGBKT7-53/pGADT7-T and pGBKT7-Lam/pGADT7-T were used as positive and negative controls, respectively. SD/-Trp/-Leu medium lacks tryptophan and leucine; SD/-Trp/-Leu/-His/-Ade + X-α-Gal medium lacks adenine, tryptophan, leucine, and histidine. (**B**) Bimolecular fluorescence complementation (BiFC) assay confirming the interaction between OsJRL45 and OsJRL40. Yellow indicates yellow protein fluorescence and red indicates chloroplast channels. BZR1-CYFP/D3-NYFP and 62SK-VC/62SK-VN were used as positive and negative controls, respectively. (**A**) Scale bars: 2 cm, (**B**) Scale bars: 20 μm.

2.7. Analysis of Agronomic Traits in Mature Transgenic Plants Harboring OsJRL45/40 from SR86

To determine whether the phenotype and agronomic traits associated with SR86 could be observed in transgenic Nip plants harboring *OsJRL45* and *OsJRL40* (*OsJRL45/40*) from SR86, the T_2 generation of transgenic plants was observed at maturity to compare their traits and phenotype with wild-type (WT) Nip (Figure 7). The single spike structure and overall phenotype of transgenic plants did not differ significantly from that of WT (Figure 7A,B); in addition, there were no significant differences in grain length, grain width, plant height, effective panicle, and seed-setting rate between transgenic plants and WT plants (Figure 7C–F). There were, however, significant differences between transgenic and WT plants in thousand-grain weight, spike length, and the number of grains per spike (Figure 7G–I). These results indicated that, although co-transformation of Nip with *OsJRL45/40* from SR86 enhanced yield, it did not affect the general phenotype of the plant.

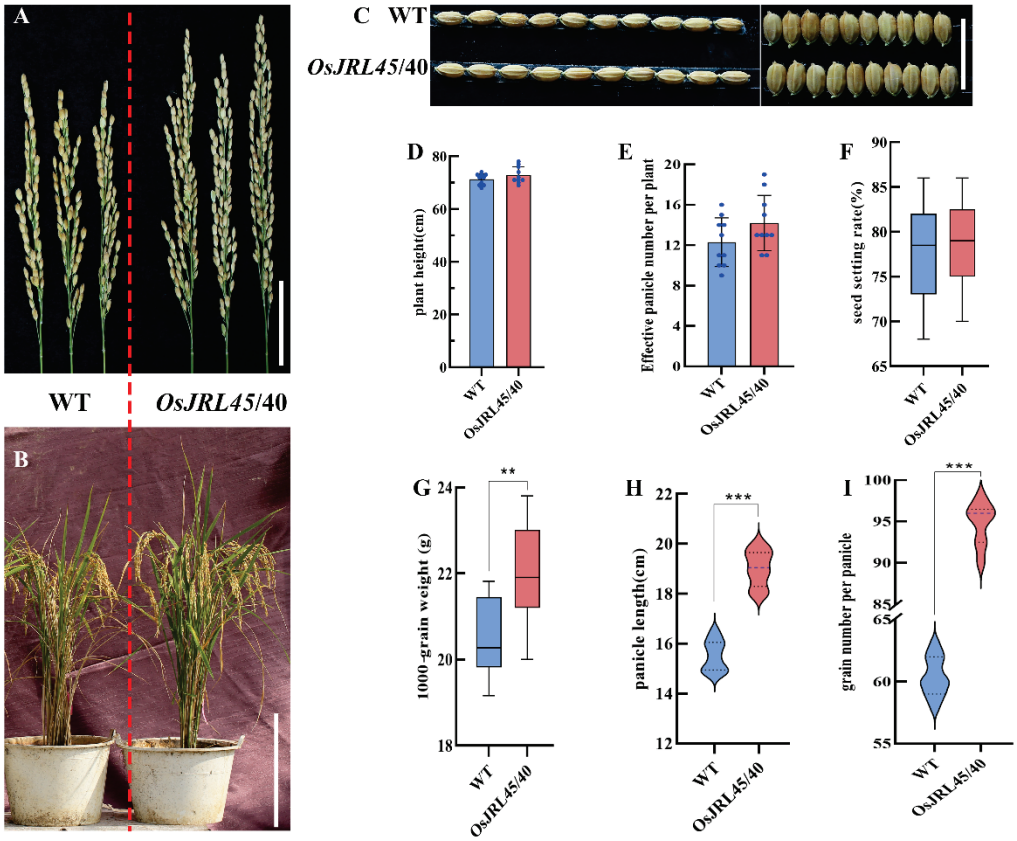


Figure 7. Analysis of agronomic traits in transgenic plants harboring *OsJRL45/40* and Nip wild-type (WT) rice. (**A**) Single spike phenotype. (**B**) Mature plant phenotype. (**C**) Grain length and width phenotypes. (**D**) Plant height. (**E**) Effective panicle. (**F**) Seed-setting rate. (**G**) Thousand-grain weight. (**H**) Spike length. (**I**) Number of grains per spike. Data represent the mean ± SD of three independent replicates; asterisks indicate statistically significant differences (**: $p < 0.01$; ***: $p < 0.001$). (**A**,**B**) On the left side of the red dotted line is WT and on the right is *OsJRL45/40*. Scale bars on (**A**–**C**): 5 cm.

2.8. Co-Transformation with OsJRL45/40 from SR86 Enhances Tolerance of Salt Stress at the Three-Leaf Stage

To further verify whether co-transforming Nip with *OsJRL45* and *OsJRL40* from SR86 enhanced tolerance of salt stress, WT and transgenic plants at the three-leaf stage were subjected to 9‰ NaCl salt stress treatment for 4 days and allowed to recover for 4 days before their phenotypes were observed (Figure 8A–C). The survival rate of the transgenic plants was significantly higher than that of WT (Figure 8D), indicating that salt tolerance was enhanced by transformation with *OsJRL45/40*. Next, the expression of *OsJRL45* and *OsJRL40* in plants exposed to salt stress for 3, 6, 9, or 12 h was quantified using RT-qPCR. This analysis found that expression levels of these genes were significantly higher in the transgenic plants than in the WT (Figure 8E,F). These results confirmed that, at the three-leaf stage, co-transformation with *OsJRL45* and *OsJRL40* from SR86 enhanced tolerance to salt stress.

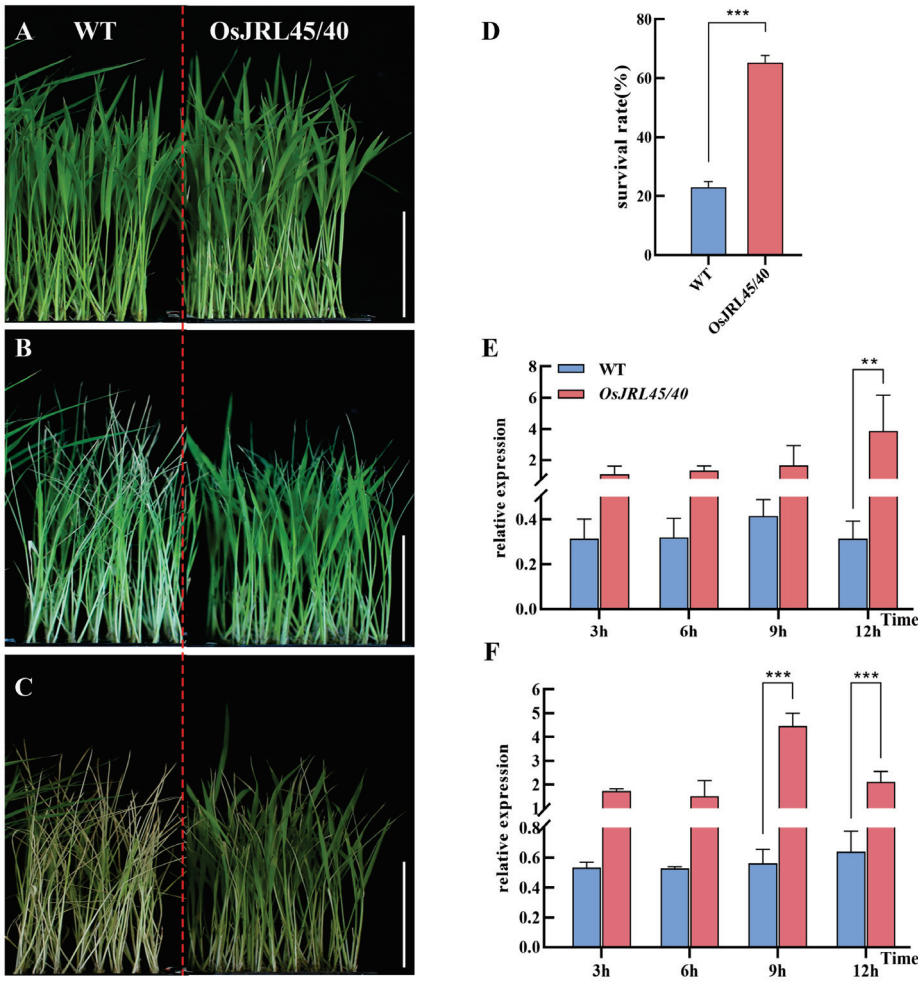


Figure 8. Phenotypic analysis of plants at the three-leaf stage exposed to salt stress by treatment with 9‰ NaCl. (**A**) Appearance of plants at the three-leaf stage before salt stress treatment. (**B**) Appearance of plants after 4 days of treatment with 9‰ NaCl. (**C**) Appearance of plants after 4 days of recovery from salt stress. (**D**) Survival rates after recovery from salt stress. (**E**) Quantification of *OsJRL45* expression by RT-qPCR. (**F**) Quantification of *OsJRL40* expression by RT-qPCR. WT: wild-type Nip; *OsJRL45/40*: transgenic plants. Data represent the means ± SD of three independent replicates; asterisks indicate statistically significant differences (**: $p < 0.01$; ***: $p < 0.001$). (**A**–**C**) On the left side of the red dotted line is WT and on the right is *OsJRL45/40*. Scale bars on (**A**–**C**): 5 cm.

2.9. Co-Transformation with OsJRL45/40 Derived from SR86 Enhances Antioxidant Enzyme Activities under Salt Stress

To analyze the effects of co-transforming Nip WT with *OsJRL45* and *OsJRL40* from SR86 on physiological parameters related to ROS under salt stress, plants at the three-leaf stage were treated with 9‰ NaCl for 24 h. The enzymatic activities of CAT, POD, and SOD were measured in WT and *OsJRL45/40* transgenic plants before and after salt stress treatment, as were the levels of malondialdehyde (MDA) and proline (Pro). The activities of CAT, POD, and SOD, as well as Pro content, were significantly higher in *OsJRL45/40* transgenic plants than in WT, while the MDA content showed the opposite result (Figure 9A–E). This showed that co-transforming Nip with *OsJRL45/40* from SR86 enhanced salt stress tolerance, and improved the homeostasis of related physiological parameters, including enzyme activities.

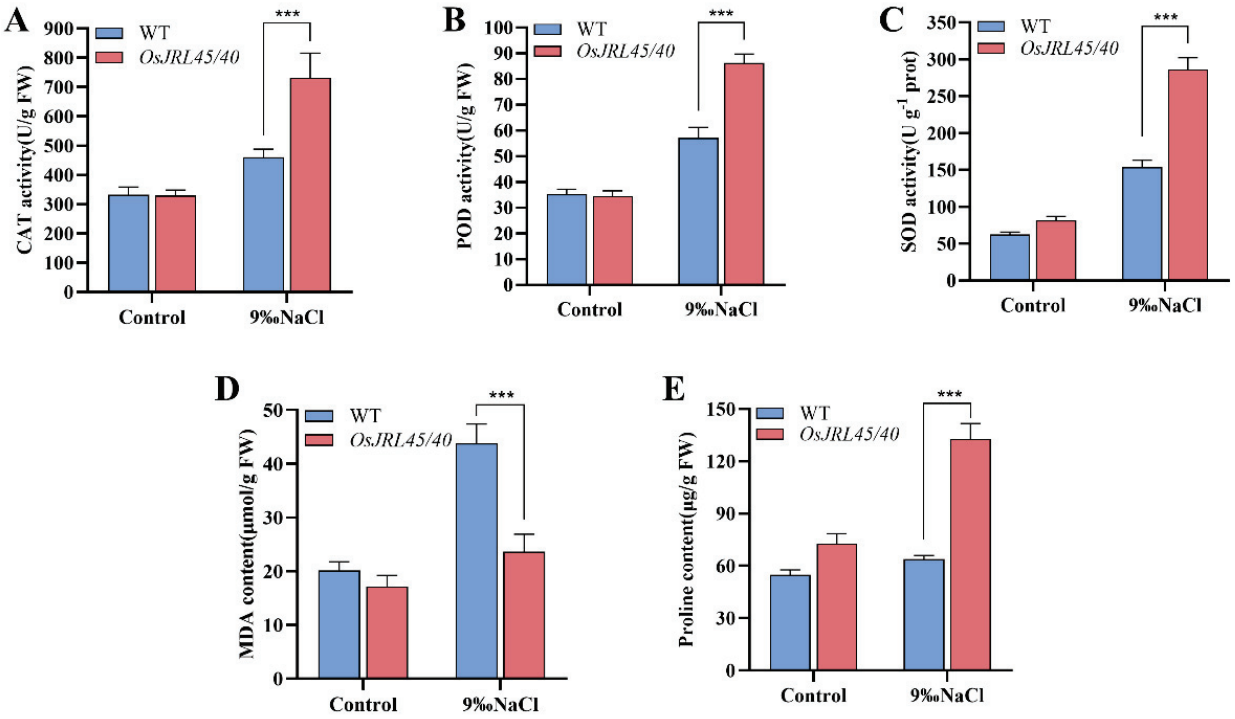


Figure 9. Changes in physiological indicators of plants at the three-leaf stage treated with 9‰ NaCl for 24 h. (**A**) Catalase (CAT) activity. (**B**) Peroxidase (POD) activity. (**C**) Superoxide dismutase (SOD) activity. (**D**) Malondialdehyde (MDA) content. (**E**) Proline (Pro) content. WT: wild-type Nip; *OsJRL45/40*: transgenic plants. Data represent the mean ± SD of three independent replicates; asterisks indicate statistically significant differences (***: $p < 0.001$).

2.10. Analysis of Differentially Expressed Genes

To investigate the salt tolerance of transgenic Nip plants harboring *OsJRL45* and *OsJRL40* from SR86 further, we analyzed differential gene expression before and after salt stress treatment, using Fold Change ≥ 2 and q-value < 0.05 as criteria for determining differentially expressed genes (DEGs). The overlaps between groups of DEGs identified in transgenic and WT plants before and after salt stress treatment are shown in Figure 10A. We identified 1044 DEGs (638 up-regulated and 406 down-regulated) in OsJRL45/40-vs-WT before salt stress treatment and identified 834 DEGs (631 up-regulated and 203 down-regulated) in OsJRL45/40-vs-WT after salt treatment (Figure 10A); this group may contain key genes governing the response to salt stress. Kyoto Encyclopedia of Genes and Genomes (KEGG) enrichment analysis showed that genes that were differentially expressed between WT and transgenic plants before salt stress treatment were involved in "mitogen-activated protein kinase (MAPK) signaling pathway", "plant hormone signal transduction", and "phenylpropanoid biosynthesis" (Figure 10B). Gene ontology (GO) enrichment analysis showed that the DEGs were mainly involved in "metabolic process", "response to stress", "catalytic activity", and "response to abiotic stimulus" (Figure 10C).

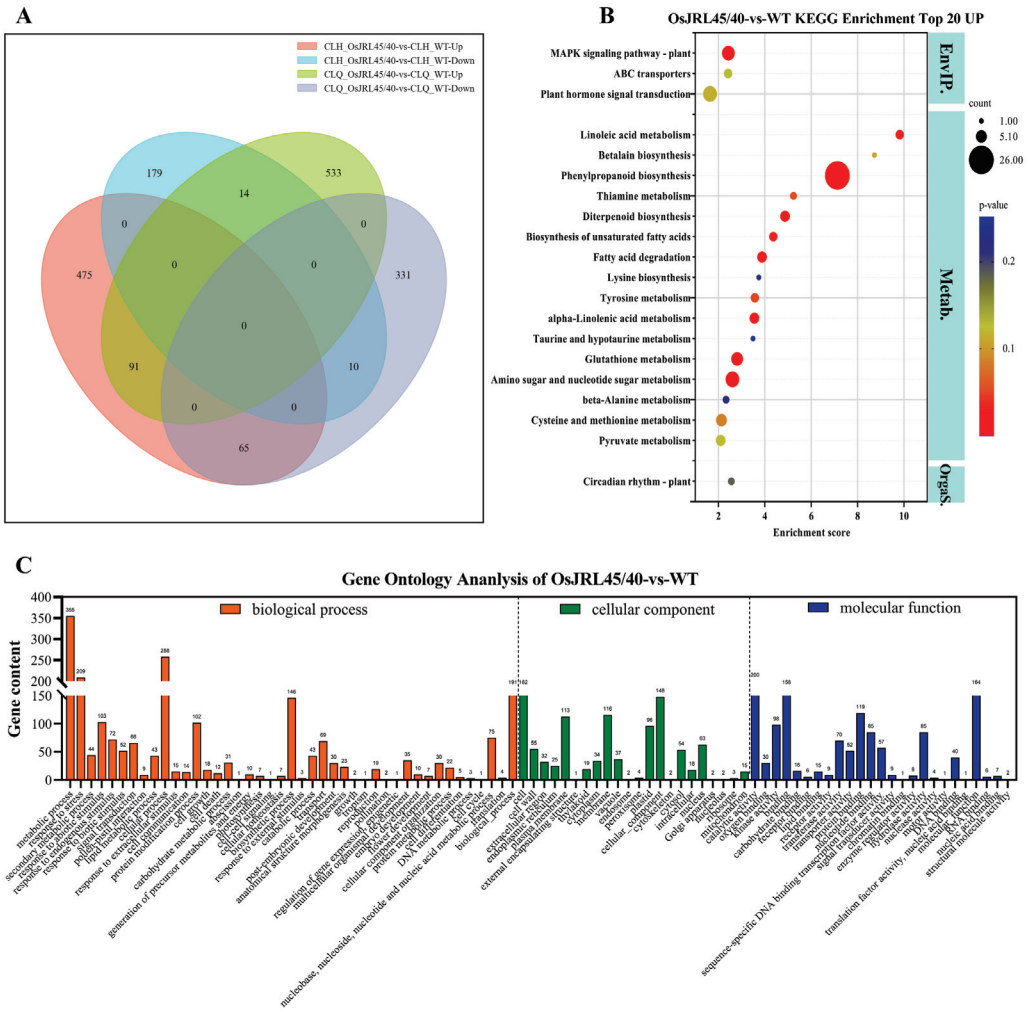


Figure 10. GO and KEGG enrichment analyses of differential gene expression before and after salt stress treatment. (**A**) Venn diagram showing the overlap of differentially expressed genes (DEGs) identified in WT and transgenic seedlings harboring *OsJRL45/40* from SR86 before and after salt stress treatment. CLQ-OsJRL45/40-vs-CLQ-WT-Up/Down: genes that were up-regulated and down-regulated in transgenic plants, relative to their expression in WT plants, under normal conditions; CLH-OsJRL45/40-vs-CLH-WT-Up/Down: genes that were up-regulated and down-regulated in transgenic plants, relative to their expression in WT plants, under salt stress conditions. (**B**) KEGG enrichment analysis of genes differentially expressed in WT and transgenic plants before salt stress treatment. (**C**) Functional annotation of genes differentially expressed in WT and transgenic plants before salt stress treatment.

Volcano plot analysis found that 631 genes were significantly up-regulated and 203 genes significantly down-regulated in transgenic plants, relative to WT, after salt stress treatment (Figure 11A,B). KEGG enrichment analysis showed these DEGs were involved in "linoleic acid metabolism", "photosynthesis", "alpha-linolenic acid metabolism", "2glyoxylate and dicarboxylate metabolism", "carbon fixation in photosynthetic organisms", and "alanine, aspartate, and glutamate metabolism" pathways (Figure 11C). GO enrichment analysis revealed that most of these DEGs were involved in "metabolic process", "response to stress", and "response to abiotic stimulus" (Figure 11D). That a large number of genes were differentially expressed in a short period soon after salt stress treatment indicated that the response to salt stress occurred more rapidly in transgenic plants harboring *OsJRL45/40* from SR86 than in WT plants.

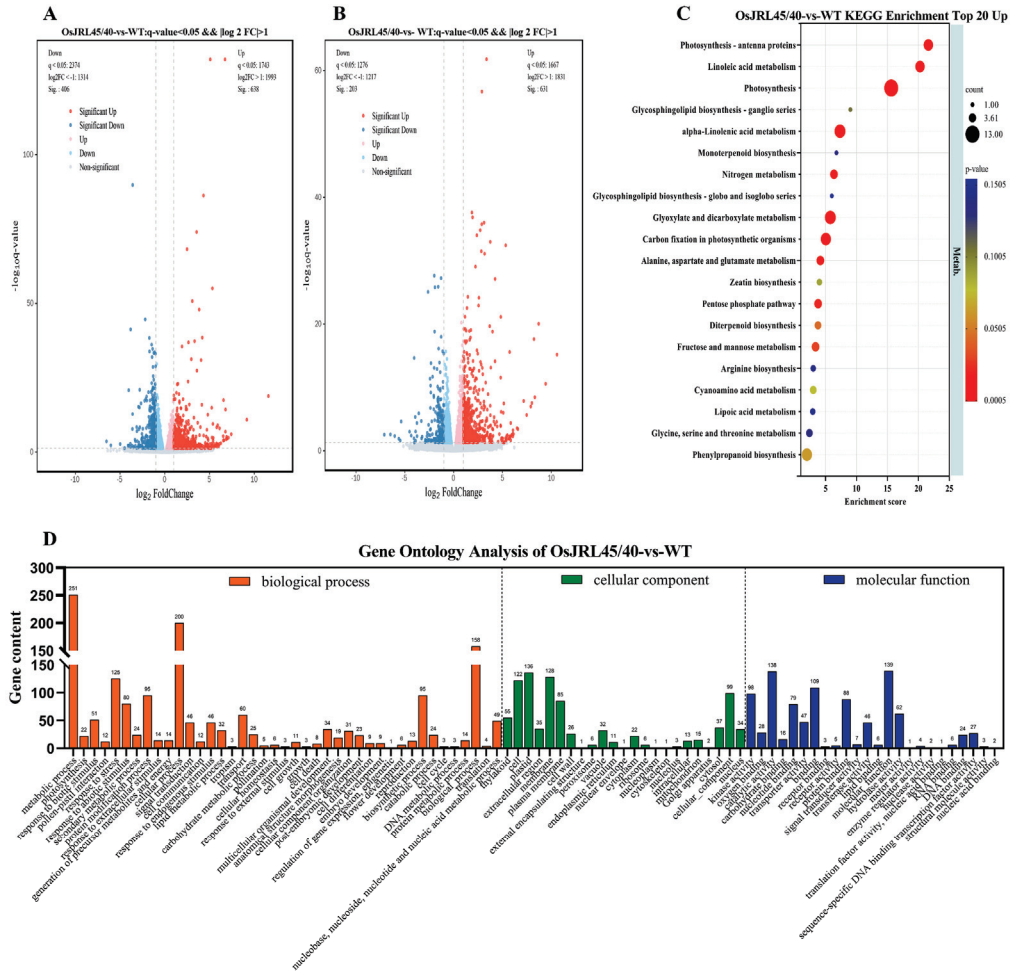


Figure 11. GO and KEGG enrichment analyses of DEGs detected in WT and transgenic plants harboring *OsJRL45/40* from SR86 after salt stress treatment. Volcano plot of DEGs detected (**A**) before and (**B**) after salt stress treatment. (**C**) KEGG enrichment analysis of DEGs detected after salt stress treatment. (**D**) Classification and functional annotation of DEGs between WT and transgenic plants after salt stress treatment.

2.11. Gene Set Enrichment Analysis (GSEA) of the Response to Salt Stress

Further analysis of the Biological Process (BP) using GSEA revealed 104 DEGs were in the process "response to stress", and 65 DEGs were in the process "response to abiotic stimulus" (Figures 12 and 13). Both of these processes include Na^+ transport proteins (Figures 10 and 11), such as sodium transport protein (*OsHKT1;5*), low-affinity sodium transport protein (*OsHKT1;3*), and high-affinity sodium transport protein (*OsHKT2;1*). When rice plants are under salt stress, these transport proteins transport excess Na^+ from the shoots to the roots, preventing excessive Na^+ accumulation in the shoots, thereby reducing Na^+ toxicity and enhancing salt tolerance. These processes also include lipoxygenase genes (*OsLOX1*, *OsHI-LOX*, *OsLOX8*, and *OsLOX11*; Figures 12 and 13). Additionally, two key enzymes in the jasmonic acid (JA) biosynthesis pathway, lipoxygenase (*OsLOX2*) and allene oxide synthase (*OsAOS2*), are in the "response to stress" process (Figure 12). The JA biosynthesis pathway is involved in various signal transduction pathways and regulates physiological and molecular processes in plants; it plays an important signaling role in plant stress responses and thereby in protecting plants from salt stress. Finally, these processes both include E3 ubiquitin ligase (*OsBTBZ1*), galactinol synthase (*OsGolS1/2*), and stress membrane protein (*OsSMP1*), which are all involved in the regulating of the abscisic acid signaling pathway in response to salt stress. Glutamine synthetase (*OsGS2*) is involved in regulating the response to non-ionic osmotic stress, improving salt stress

tolerance. Disease resistance protein (*OsRSR1*) is involved in ROS metabolism and plays an important role in maintaining the integrity of the biological membrane system and in defense against membrane lipid peroxidation under salt stress.

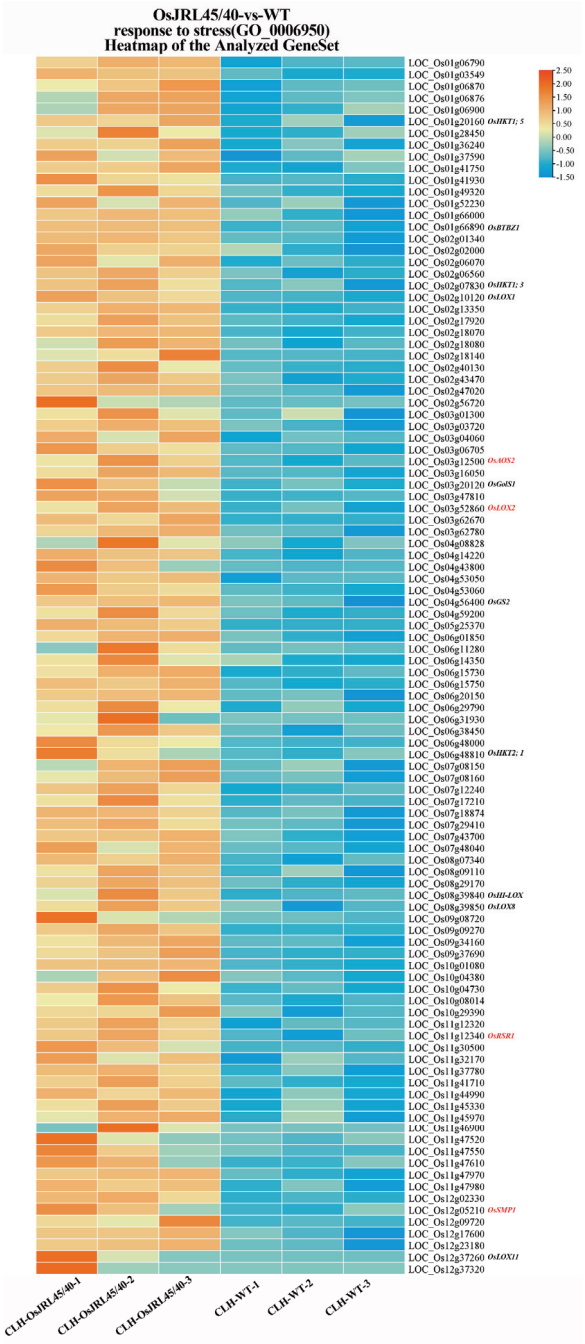


Figure 12. DEGs enriched in "response to stress" GO pathways after salt stress treatment, identified by GSEA. Genes that also appear in Figure 13 are shown in black; genes shown in red are unique to this process.

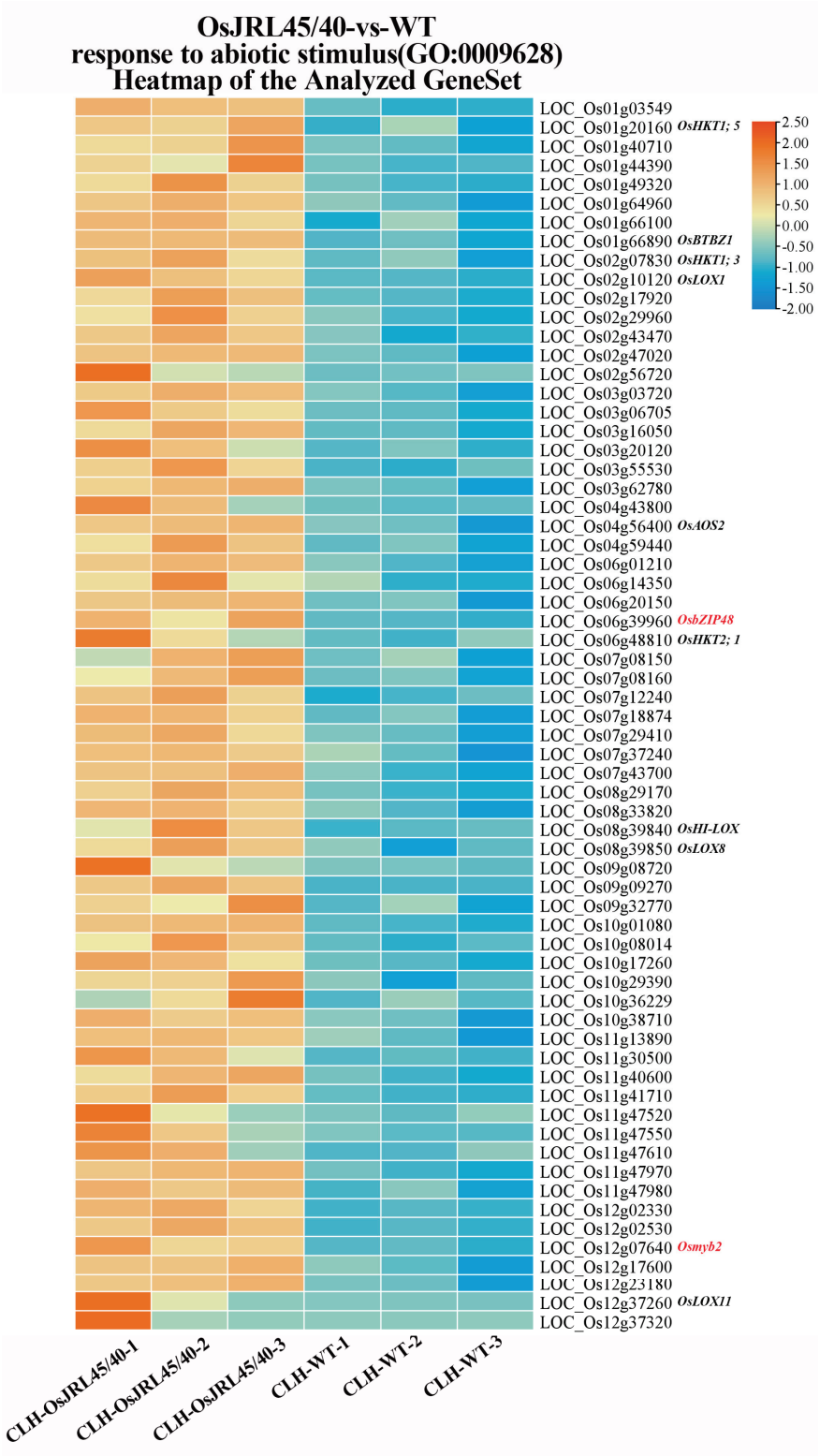


Figure 13. DEGs enriched in "response to abiotic stimulus" GO pathways after salt stress treatment, identified by GSEA. Genes that also appear in Figure 12 are shown in black; genes shown in red are unique to this process.

A bZIP transcription factor (*OsbZIP48*) and an MYB transcription factor (*Osmyb2*) were found in the "response to abiotic stimulus" process (Figure 13). bZIP transcription factors are involved in the biosynthesis of hormones such as gibberellin, JA, and auxin, while MYB transcription factors regulate gene expression, including of their own genes, by directly

binding DNA. All of these results indicated that *OsJRL45/40* co-transgenic plants could respond more quickly to salt stress through a variety of biological processes, including "Na^+ transport protein", "plant hormone regulation pathways", "non-ionic osmotic stress", "reactive oxygen species metabolism", and "DNA transcription factors".

3. Discussion

3.1. OsJRL45 and OsJRL40 Interact Together to Enhance the Salt Tolerance of Plants

Salt stress has a significant impact on plant growth and development, inhibiting seed germination, root and shoot growth, and plant morphology [40]. Many rice varieties are salt-sensitive and severely affected by salt stress. Lectins have been identified in various plant species [41–45], but their roles in responses to stress stimuli are not yet fully understood. We previously demonstrated that two genes encoding lectins, *OsJRL45* and *OsJRL40*, regulate and enhance tolerance to salt stress in rice [34,35]. Since these genes are located close together on chromosome 4, understanding whether they interact and jointly enhance salt tolerance is of great significance.

Salt stress is a common abiotic stress that adversely affects plant development, growth, and production [33,46]. The responses of three rice cultivars, SR86, 9311, and Nip, to salt stress treatment indicated that *OsJRL45* and *OsJRL40* were associated with enhanced tolerance of salt stress in SR86 (Figure 1). Yeast two-hybrid and BiFC assays showed that the OsJRL45 and OsJRL40 proteins interacted (Figure 6). Transforming Nip with *OsJRL45* and *OsJRL40* (*OsJRL45/40*) genes from SR86 did not affect the plant phenotype (Figure 7), although salt tolerance was enhanced in transgenic plants at the three-leaf stage (Figure 8). In rice, salt stress disrupts the balance between reactive oxygen species (ROS) production and scavenging, leading to excessive ROS accumulation, which disrupts plant physiological functions and impedes normal growth and development [47,48]. CAT, POD, and SOD activities increased significantly in the transgenic plants, and their MDA content was significantly lower than that of the WT (Figure 9). Previous studies showed that *OsJRL45* and *OsJRL40* enhance the antioxidant capacity of cells and prevent excessive ROS accumulation [34,35]. The results of transformation with *OsJRL45/40* from SR86 were consistent with these observations, indicating that *OsJRL45* and *OsJRL40* interacted and enhanced salt stress tolerance. High salt concentrations damage rice root development, accelerate leaf curling and yellowing, reduce the number of grains per panicle, and decrease the thousand-grain weight, resulting in yield reduction [49,50]. Therefore, understanding the molecular mechanisms underlying salt tolerance and screening for this trait are key steps for the development of salt-tolerant rice varieties.

3.2. Transcriptome Analysis of OsJRL45 and OsJRL40 Transgenic Seedlings under Salt Stress

Transgenic rice plants harboring *OsJRL45/40* from SR86 exhibited positive physiological responses under salt stress. Key salt-responsive metabolic pathways and DEGs were explored and analyzed using transcriptomic data. RNA-seq analysis identified 1044 DEGs (638 up-regulated and 406 down-regulated) in OsJRL45/40-vs-WT before salt stress treatment and identified 834 DEGs in OsJRL45/40-vs-WT after salt stress treatment; 631 genes were up-regulated and 203 down-regulated, compared with WT plants (Figure 10A). The results of Volcano plot analyses were consistent (Figure 11A,B). Before salt stress treatment, KEGG enrichment analysis showed that the differentially expressed genes between WT and transgenic plants were involved in the "mitogen-activated protein kinase (MAPK) signaling pathway", "plant hormone signaling", and "phenylpropanoid biosynthesis" (Figure 10B). GO enrichment analysis showed that DEGs were mainly involved in "metabolic processes", "responses to stress", "catalytic activity", and "responses to abiotic stimulus" (Figure 10C). KEGG enrichment analysis after salt stress treatment revealed that these DEGs were involved in "linoleic acid metabolism", "photosynthesis", "alpha-linolenic acid metabolism", "2-glyoxylate and dicarboxylate metabolism", "carbon fixation in photosynthetic organisms", and "alanine, aspartic acid, and glutamate metabolism" pathways (Figure 11C). GO enrichment analysis revealed that most of these DEGs were involved in "metabolic pro-

cesses", "responses to stress", and "responses to abiotic stimulus" (Figure 11D). Soon after salt stress treatment, a large number of genes were differentially expressed in a short period of time, indicating that the transgenic plants of *OsJRL45/40* of SR86 could respond more quickly to salt stress than WT plants. GO functional analysis indicated that most DEGs were involved in the pathways "response to stress" and "response to abiotic stimulus" (Figures 10C and 11D).

GSEA of GO enrichment analysis in the biological process (BP) categories "response to stress" and "response to abiotic stimulus" (Figures 12 and 13) identified the Na^+ transporter genes *OsHKT1;5*, *OsHKT1;3*, and *OsHKT2;1*. These transporters transfer excess Na^+ from the shoots, thus reducing Na^+ toxicity and enhancing salt tolerance in rice under salt stress [51–53]. The analysis also identified four lipoxygenase genes, *OsLOX1*, *OsHI-LOX*, *OsLOX8*, and *OsLOX11*. Two key enzymes lipoxygenase (OsLOX2) and allene oxide synthase (OsAOS2), which encode key enzymes in the JA synthesis pathway, which is involved in various signaling pathways and regulates many physiological and molecular processes in plants [54–57], thus protecting plants from salt stress. Additionally, the analysis identified genes involved in regulating the ABA signaling pathway, including E3 ubiquitin ligase (*OsBTBZ1*), galactinol synthase (*OsGolS1/2*), and stress membrane protein (*OsSMP1*); such genes respond to salt stress via ABA-dependent pathways, enhancing tolerance of abiotic stress [58–60]. Glutamine synthetase (*OsGS2*), which is involved in regulating the response to non-ionic osmotic stress, enhances rice tolerance to salt stress. The disease resistance protein (*OsRSR1*), which is involved in the regulation of reactive oxygen metabolism, can defend against lipid peroxidation under salt stress [61], and thus plays an important role in protecting the integrity of the biological membrane structure. The analysis also identified genes involved in the "response to abiotic stimulus" pathway, including a bZIP transcription factor (*OsbZIP48*), which is involved in biosynthesis of the plant hormones gibberellin, JA, and auxin [62], and an MYB transcription factor (*Osmyb2*) that positively regulates *OsHKT1;5* to control its transcription [63]. Consistent with our previous study, co-transformation with *OsJRL45/40* enhanced antioxidant enzyme activity under salt stress through non-ionic osmotic stress and reactive oxygen metabolism processes and regulated Na^+-K^+ homeostasis through Na^+ transport proteins [34,35].

3.3. Sequence Differences between OsJRL45 and OsJRL40: Marker-Assisted Selection (MAS) Analysis for the Selection of Salt-Tolerant Rice

The development of molecular markers that can be used to screen for salt-tolerant rice varieties is crucial for selecting plants with high salt tolerance, as salt stress significantly affects rice yield and quality [64]. Molecular marker-assisted identification and selection of genes that control resistance to these factors have been used for rice improvement [22]. Previous studies showed that *OsJRL45* and *OsJRL40* are located on chromosome 4 [34,35,39]. The *OsJRL45* and *OsJRL40* gene sequences of SR86, 9311, L623, R498, Minghui63, Zhenshan97, Yu Chi, Nantehao, Qingzhen, and Meizhan were amplified by sequencing and aligned, which revealed eight single base differences in exon 1 in the *OsJRL45* gene between these cultivars. The differences at positions 63 (base-pairs (bp)), 72 bp, and 123 bp corresponded to synonymous mutations after the initial ATG, while those at 209 bp, 224 bp, 245 bp, 263 bp, and 268 bp in exon 1 would result in amino acids changes (Figure 2). The single base change in exon 2 at position 1000 bp in the cultivars SR86 and Nantehao are A, resulting in a change to the amino acid Glu, whereas those in remaining cultivars are C, resulting in a change to amino acid Asp (Figure 2). In exon 1 of the *OsJRL40* gene (position 131 bp), only Meizhan showed a single base change to A, and the nucleotides in the remaining cultivars were C. In exon 2 (position 1123 bp), only SR86 had a single base change to A, resulting in a change to the amino acid Ser, whereas in the remainder, the nucleotide was G, resulting in the amino acid Gly (Figure 2). However, sequencing analysis of the sequences between the *OsJRL45* and *OsJRL40* genes of SR86, R498, Minghui63, and Zhenshan97 showed that the distance between the two genes was only 2605 bp, and at 204 bp downstream of *OsJRL45*, the SR86 sequence was missing the 25 bp sequence

GCGCACGACGCGGCCGCCAGCGTTC, which was located 2401 bp upstream of *OsJRL40*. Based on the differences between the genes and the binding of *OsJRL45* and *OsJRL40*, molecular marker primers were designed for use as molecular markers and for validation.

The analyses of the recombinant inbred lines constructed by the hybridization of SR86 and 9311 under salt stress and the molecular marker primers developed in this study showed that the molecular-tagged primers based on the nucleotide differences between *OsJRL45* and *OsJRL40* could be used to screen salt-tolerant plants (Figures 2, 3 and S1 and Table 1). In order to further verify the accuracy of the molecular markers developed in this study for screening salt-tolerant rice, some rice plants commonly used in production were used for analysis. Rice varieties with higher salt tolerance (Foer B, Chaimi, Yuejing, Xiangzao 32, Nantehao, R288, Shuhui 527, Aizinuo, and Xiang 628S) produced gel electrophoresis results that were very similar to those of SR86, while those of salt-intolerant plants were similar to those of 9311 (Figure 4). This suggests that the novel molecular markers designed to identify salt-tolerant plants in this study identified more than 90% of the plants with salt tolerance, indicating that they would have high specificity for the screening of salt-tolerant plants. Salt-tolerant plants were randomly selected in the sixth generation of RILs derived from the R86 and 9311 hybrids, and the genotypes of the RILs were verified using specific marker primers based on differences between SR86 and 9311 sequences. Agarose gel electrophoresis showed that plants with higher salt tolerance were more genetically similar to SR86, while individuals with less salt tolerance were genetically more similar to 9311 (Figure 5E). These results confirm the high specificity of the molecular markers developed in this study for the identification of salt-tolerant rice cultivars. This targeted screening approach minimized the number of undesired traits and reduced the risk of linkage drag while maintaining the desirable genetic background of the parent varieties. This study demonstrated the effectiveness of these novel molecular markers in screens to identify salt-tolerant rice plants, showing that molecular markers based on differences in intergenic nucleotide sequences can facilitate the process of selective breeding.

4. Materials and Methods

4.1. Experimental Plants

The WT rice varieties SR86, Nip, and 9311 used in this study were provided by the rice germplasm resource platform of the Hunan Rice Research Institute [34,35,39,65]. All rice varieties were grown in the field at the Hunan Normal University in Changsha, Hunan Province. All of the experiments reported in this paper comply with the institutional, national, and international guidelines concerning plant genetic resources.

To construct the population of SR86/9311 RILs, SR86 and 9311 plants were crossed. Self-pollinated F_1 plants were used to produce F_2 seeds; after harvest, isolated F_2 progeny were self-pollinated, and individual salt-tolerant and salt-intolerant plants were selected for further inbreeding under salt stress treatment. The RIL population was constructed by continuous inbreeding under salt stress treatment for five generations.

The *OsJRL45* and *OsJRL40* genes from SR86 were amplified by PCR and inserted into the vector pCAMBIA1300 using the gene recombination method. The relevant constructed vector primers are listed in Supplementary Table S1. Nip plants were transformed using *Agrobacterium tumefaciens*-mediated transformation to obtain *OsJRL45/40* transgenic plants. The phenotype and agronomic traits of the transgenic plants were analyzed in the T_2 generation. In addition, a hybrid population was constructed using SR86 and 9311 as parents, from which salt-tolerant plants were screened for subsequent research.

4.2. Construction of Segregating Populations

SR86 and 9311 were crossed in the field at Hunan Normal University. The F_1 generation was self-pollinated to obtain F_2 seeds. F_2 plants were treated with 9‰ salt stress at the seedling stage.

4.3. Marker-Assisted Selection

Total genomic DNA was extracted from rice leaves using the cetyltrimethylammonium bromide (CTAB) method [66]. DNA was analyzed by PCR with a total reaction volume of 10 μL in a PCR instrument (Bio-Rad, T100™ Thermal Cycler, Foster City, CA, USA). The primers are listed in Supplementary Table S3. The PCR amplification regime was as follows: initial denaturation at 94 °C for 5 min, followed by 35 cycles of 94 °C for 30 s, 58 °C for 30 s, and 72 °C for 45 s, with a final extension at 72 °C for 5 min. The PCR products were separated by electrophoresis on 2% agarose gels and visualized under UV light.

4.4. Salt Stress Treatment of Transgenic Plants

Uniform, plump rice seeds were selected and surface-sterilized in 0.3% sodium hypochlorite for 20 min. Seeds were rinsed three times in distilled water, evenly spread across two layers of moist filter paper in a Petri dish, and incubated at 37 °C. After germination, seedlings were transplanted into a 96-well tray containing culture solution. The nutrient solution was changed every 4 days. Rice seedlings were grown under conventional hydroponic conditions until the three-leaf stage (approximately 14 days), then transferred to a hydroponic solution containing 9‰ NaCl for 4 days, and finally moved to a conventional hydroponic solution for recovery for 4 days.

4.5. Measurement of Physiological Parameters

Superoxide dismutase (SOD), peroxidase (POD), catalase (CAT), malondialdehyde (MDA), and proline contents were measured according to the kit manufacturer's instructions (Jiancheng Bioengineering Institute, Nanjing, China) [34,35,39]. Measurements were made before treatment and 24 h after salt stress treatment. All experiments involved three independent biological replicates; data are reported as the mean ± standard deviation (SD).

4.6. RNA Extraction and Quantitative Real-Time PCR (qRT-PCR)

Rice seedlings at the three-leaf stage from the WT and *OsJRL45/40* transgenic lines were treated with 9‰ NaCl. Total RNA was extracted using the TRIzol Reagent (Invitrogen, Waltham, MA, USA) and reverse transcribed using the HiScript II Q RT SuperMix for qPCR (+gDNA wiper) (Vazyme, R223-01, Nanjing, China). qRT-PCR was performed using the ChamQ Universal SYBR qPCR Master Mix (Vazyme, Q711-02, Nanjing, China), with rice *Osactin* as the internal reference gene. Relative gene expression was calculated using the $2^{-\Delta\Delta Ct}$ method and expressed as the mean ± SD [67]. All primers used in the RT-qPCR analysis are listed in the Supplementary Table S2.

4.7. Transcriptomic Data Analysis

Whole WT and *OsJRL45/40* transgenic plants were sampled at the three-leaf stage, before treatment, and 24 h after 9‰ NaCl stress treatment. Three biological replicates were collected for each plant. Samples were frozen in liquid nitrogen and sent on dry ice to OE Biotech Co. Ltd., Shanghai, China for transcriptomic analysis. The RNA-seq data were analyzed as described previously [34,35,68]. The bioinformatics analysis and graphical plotting were performed using the OE Biotech cloud platform. Bioinformatic analysis was performed using the OE Cloud tools at https://cloud.oebiotech.com/task/ accessed on 21 December 2023. The volcano map and other graphics were drawn using R (https://www.r-project.org/, accessed on 25 December 2023) on the OE Cloud platform (https://cloud.oebiotech.com/task/, accessed on 25 December 2023).

4.8. Yeast Two-Hybrid (Y2H) Assays

Yeast two-hybrid assays were performed using the GAL4 yeast two-hybrid system. The coding sequence (CDS) of *OsJRL45* was cloned into the pGADT7 vector to generate *AD-OsJRL45*. The CDS of *OsJRL40* was cloned into the pGBKT7 vector to generate *BD-OsJRL40*. The relevant primers are listed in the Supplementary Table S1. The Y2HGold yeast strain was co-transformed with the *AD-OsJRL45* and *BD-OsJRL40* constructs and grown on the

selection media SD/-Trp/-Leu (lacking tryptophan and leucine) and SD/-Trp/-Leu/-His/-Ade + X-α-Gal (lacking adenine, tryptophan, leucine, and histidine) [69].

4.9. Bimolecular Fluorescence Complementation (BiFC) Assay

The CDS of *OsJRL45* was fused to the C-terminus of yellow fluorescent protein (YFP), and the CDS of *OsJRL40* was fused to the N-terminus of YFP to construct the co-expression vectors OsJRL40-YFP^N and OsJRL45-YFP^C. The specific primers used are listed in the Supplementary Table S1. The plasmids were introduced into *Agrobacterium tumefaciens* (GV3101) by electroporation, and the bacterial suspension was adjusted to an OD 600 of approximately 0.6. Tobacco plants (*Nicotiana benthamiana*) with good growth were selected. The lower epidermis of their leaves was injected with the bacterial suspension and labeled [70]. Tobacco plants were cultured under low light for 2 days following injection. The injected leaves were sampled, mounted on slides, and observed under a confocal laser scanning microscope (Nikon C2-ER) for image capture and recording.

4.10. Statistical Analysis

Data are presented as the mean ± SD of three or more independent replicates. The mean of the replicates for each experiment was calculated using PASW Statistics 18 software. Statistical significance was determined using one-way ANOVA and Student's *t*-test with $p < 0.05$. Bar charts were created using GraphPad Prism 9. Heat maps were constructed and drawn using TBtools-II v.2.119 software [71].

5. Conclusions

Based on the results of the treatments and RT-qPCR analysis of salt-tolerant cultivars SR86, 9311, and Nip under salt stress, we speculated that *OsJRL45* and *OsJRL40* genes contributed to the stronger salt tolerance of SR86. To further validate this hypothesis, we analyzed the sequence differences between the *OsJRL45* and *OsJRL40* genes in SR86 and 9311 using sequencing technology, and developed molecular markers for salt-tolerant screening based on these differences. Subsequently, we constructed a recombinant inbred line population using salt-tolerant SR86 and conventional variety 9311 as parental varieties and verified the effectiveness of the developed molecular markers using rice varieties commonly used for rice production.

Yeast two-hybrid and bimolecular fluorescence complementation further demonstrated the interaction between OsJRL45 and OsJRL40 proteins. In addition, *OsJRL45/40* co-transgenic plants were created by genetic recombination technology, and salt stress treatment and physiological parameters were measured. The results showed that compared with the wild type, the antioxidant enzyme activities (including CAT, POD, SOD) and proline (Pro) content of *OsJRL45/40* co-transgenic rice were significantly increased, while their malondialdehyde (MDA) content was significantly reduced, suggesting that synergy between *OsJRL45* and *OsJRL40* increased salt tolerance.

In addition, transcriptome analysis revealed 834 differentially expressed genes (DEGs) in the *OsJRL45/40* co-transgenic plants under salt stress conditions. GO and KEGG enrichment analysis showed that these differential genes were mainly involved in metabolic pathways related to antioxidant response and osmotic homeostasis, which are known to play a key role in salt stress tolerance.

In summary, synergy between the activities of *OsJRL45* and *OsJRL40* not only increased salt tolerance in rice, but the development of molecular markers based on differences in the sequences of *OsJRL45* and *OsJRL40* between the salt-tolerant variety SR86 and the salt-sensitive variety 9311 was successful in identifying salt-tolerant rice varieties.

Supplementary Materials: The supporting information can be downloaded at: https://www.mdpi.com/article/10.3390/ijms252010912/s1.

Author Contributions: X.Y., M.L. and X.D. designed the experiments, analyzed the data, and revised the manuscript. X.Y. performed the experiments and wrote the manuscript. Q.G., Y.L., R.B., S.Z. and J.F. helped organize the experimental data. X.Y., M.L. and X.D. analyzed the data and revised the manuscript. F.W., W.L., Y.L., R.B., S.Z., J.F. and L.C. provided assistance during the experiments. All authors have read and agreed to the published version of the manuscript.

Funding: This research was funded by the National Key Research and Development Program of China (grant numbers 2016YFD0101107 and 2018YFD0100902), the Hunan Province Key Research and Development Plan (grant number 2016JC2023), and Natural Science Foundation of Hunan Province in China (2022JJ30377).

Institutional Review Board Statement: Not applicable.

Informed Consent Statement: Not applicable.

Data Availability Statement: All of the data supporting the conclusions of this article are provided within the article and in Supplementary Materials. All of the data and materials are available upon reasonable request from the corresponding author.

Conflicts of Interest: The authors declare that the research was conducted in the absence of any commercial or financial relationships that could be construed as potential conflicts of interest.

References

1. Wing, R.A.; Purugganan, M.D.; Zhang, Q. The rice genome revolution: From an ancient grain to Green Super Rice. *Nat. Rev. Genet.* **2018**, *19*, 505–517. [CrossRef] [PubMed]
2. Butcher, K.; Wick, A.F.; DeSutter, T.; Chatterjee, A.; Harmon, J. Soil Salinity: A Threat to Global Food Security. *Agron. J.* **2016**, *108*, 2189–2200. [CrossRef]
3. Godoy, F.; Olivos-Hernandez, K.; Stange, C.; Handford, M. Abiotic Stress in Crop Species: Improving Tolerance by Applying Plant Metabolites. *Plants* **2021**, *10*, 186. [CrossRef]
4. van Dijk, M.; Morley, T.; Rau, M.L.; Saghai, Y. A meta-analysis of projected global food demand and population at risk of hunger for the period 2010–2050. *Nat. Food* **2021**, *2*, 494–501. [CrossRef]
5. Ashraf, M.; Akram, N.A. Improving salinity tolerance of plants through conventional breeding and genetic engineering: An analytical comparison. *Biotechnol. Adv.* **2009**, *27*, 744–752. [CrossRef]
6. Rasheed, A.; Li, H.; Nawaz, M.; Mahmood, A.; Hassan, M.U.; Shah, A.N.; Hussain, F.; Azmat, S.; Gillani, S.F.A.; Majeed, Y.; et al. Molecular tools, potential frontiers for enhancing salinity tolerance in rice: A critical review and future prospective. *Front. Plant Sci.* **2022**, *13*, 966749. [CrossRef]
7. Bhatt, T.; Sharma, A.; Puri, S.; Minha, A.P. Salt Tolerance Mechanisms and Approaches: Future Scope of Halotolerant Genes and Rice Landraces. *Rice Sci.* **2020**, *27*, 368–383. [CrossRef]
8. Hussain, S.; Zhang, J.H.; Zhong, C.; Zhu, L.F.; Cao, X.C.; Yu, S.M.; James, A.B.; Hu, J.J.; Jin, Q.Y. Effects of salt stress on rice growth, development characteristics, and the regulating ways: A review. *J. Integr. Agric.* **2017**, *16*, 2357–2374. [CrossRef]
9. Wu, H.H. Plant salt tolerance and Na^+ sensing and transport. *Crop J.* **2018**, *6*, 215–225. [CrossRef]
10. Chen, G.; Liu, C.; Gao, Z.; Zhang, Y.; Zhang, A.; Zhu, L.; Hu, J.; Ren, D.; Yu, L.; Xu, G.; et al. Variation in the Abundance of *OsHAK1* Transcript Underlies the Differential Salinity Tolerance of an *indica* and a *japonica* Rice Cultivar. *Front. Plant Sci.* **2017**, *8*, 2216. [CrossRef]
11. Chen, G.; Hu, Q.; Luo, L.; Yang, T.; Zhang, S.; Hu, Y.; Yu, L.; Xu, G. Rice potassium transporter OsHAK1 is essential for maintaining potassium-mediated growth and functions in salt tolerance over low and high potassium concentration ranges. *Plant Cell Environ.* **2015**, *38*, 2747–2765. [CrossRef] [PubMed]
12. Rai, H.; Yokoyama, S.; Satoh-Nagasawa, N.; Furukawa, J.; Nomi, T.; Ito, Y.; Fujimura, S.; Takahashi, H.; Suzuki, R.; Yousra, E.; et al. Cesium Uptake by Rice Roots Largely Depends Upon a Single Gene, *HAK1*, Which Encodes a Potassium Transporter. *Plant Cell Physiol.* **2017**, *58*, 1486–1493. [CrossRef]
13. Wang, J.; Nan, N.; Li, N.; Liu, Y.; Wang, T.J.; Hwang, I.; Liu, B.; Xu, Z.Y. A DNA Methylation Reader-Chaperone Regulator-Transcription Factor Complex Activates *OsHKT1;5* Expression during Salinity Stress. *Plant Cell* **2020**, *32*, 3535–3558. [CrossRef]
14. Tian, Q.; Shen, L.; Luan, J.; Zhou, Z.; Guo, D.; Shen, Y.; Jing, W.; Zhang, B.; Zhang, Q.; Zhang, W. Rice shaker potassium channel OsAKT2 positively regulates salt tolerance and grain yield by mediating K^+ redistribution. *Plant Cell Environ.* **2021**, *44*, 2951–2965. [CrossRef]
15. Hao, S.H.; Wang, Y.R.; Yan, Y.X.; Liu, Y.H.; Wang, J.Y.; Chen, S. A Review on Plant Responses to Salt Stress and Their Mechanisms of Salt Resistance. *Horticulturae* **2021**, *7*, 132. [CrossRef]
16. Liu, C.T.; Mao, B.G.; Yuan, D.Y.; Chu, C.C.; Duan, M.J. Salt tolerance in rice: Physiological responses and molecular mechanisms. *Crop J.* **2022**, *10*, 13–25. [CrossRef]
17. Das, G.; Patra, J.K.; Baek, K.H. Insight into MAS: A Molecular Tool for Development of Stress Resistant and Quality of Rice through Gene Stacking. *Front. Plant Sci.* **2017**, *8*, 985.

18. Tamiru, M.; Takagi, H.; Abe, A.; Yokota, T.; Kanzaki, H.; Okamoto, H.; Saitoh, H.; Takahashi, H.; Fujisaki, K.; Oikawa, K.; et al. A chloroplast-localized protein LESION AND LAMINA BENDING affects defence and growth responses in rice. *New Phytol.* **2016**, *210*, 1282–1297. [CrossRef]
19. Nagata, K.; Ando, T.; Nonoue, Y.; Mizubayashi, T.; Kitazawa, N.; Shomura, A.; Matsubara, K.; Ono, N.; Mizobuchi, R.; Shibaya, T.; et al. Advanced backcross QTL analysis reveals complicated genetic control of rice grain shape in a *japonica* x indica cross. *Breed. Sci.* **2015**, *65*, 308–318. [CrossRef]
20. Fekih, R.; Tamiru, M.; Kanzaki, H.; Abe, A.; Yoshida, K.; Kanzaki, E.; Saitoh, H.; Takagi, H.; Natsume, S.; Undan, J.R.; et al. The rice (*Oryza sativa* L.) LESION MIMIC RESEMBLING, which encodes an AAA-type ATPase, is implicated in defense response. *Mol. Genet. Genom.* **2015**, *290*, 611–622. [CrossRef]
21. Fekih, R.; Ishimaru, Y.; Okada, S.; Maeda, M.; Miyagi, R.; Obana, T.; Suzuki, K.; Inamori, M.; Enoki, H.; Yamasaki, M. High-Density Linkage Maps from Japanese Rice *japonica* Recombinant Inbred Lines Using Genotyping by Random Amplicon Sequencing-Direct (GRAS-Di). *Plants* **2023**, *12*, 929. [CrossRef] [PubMed]
22. Hasan, M.M.; Rafii, M.Y.; Ismail, M.R.; Mahmood, M.; Rahim, H.A.; Alam, M.A.; Ashkani, S.; Malek, M.A.; Latif, M.A. Marker-assisted backcrossing: A useful method for rice improvement. *Biotechnol. Biotechnol. Equip.* **2015**, *29*, 237–254. [CrossRef]
23. Prabhu, A.S.; Filippi, M.C.; Silva, G.B.; Silva Lobo, V.L.; Morais, O.P. An Unprecedented Outbreak of Rice Blast on a Newly Released Cultivar BRS Colosso in Brazil. In *Advances in Genetics, Genomics and Control of Rice Blast Disease*; Springer: Dordrecht, The Netherlands, 2009.
24. Collard, B.C.; Mackill, D.J. Marker-assisted selection: An approach for precision plant breeding in the twenty-first century. *Philos. Trans. R. Soc. Lond. B Biol. Sci.* **2008**, *363*, 557–572. [CrossRef]
25. Li, Y.; Zhang, J.; Hu, F.; Adolf, A.; Ackah, M.; Justice, A.A.; Lin, Q.; Li, L.; Zhao, W.G. Cloning and abiotic stress expression analysis of galactose-binding lectin (*GBL*) gene from mulberry and its prokaryotic expression in *E. coli*. *J. Hortic. Sci. Biotechnol.* **2021**, *96*, 24–33. [CrossRef]
26. Tsaneva, M.; Van Damme, E.J.M. 130 years of Plant Lectin Research. *Glycoconj. J.* **2020**, *37*, 533–551. [CrossRef]
27. Witzel, K.; Matros, A.; Bertsch, U.; Aftab, T.; Rutten, T.; Ramireddy, E.; Melzer, M.; Kunze, G.; Mock, H.P. The Jacalin-Related Lectin HvHorcH Is Involved in the Physiological Response of Barley Roots to Salt Stress. *Int. J. Mol. Sci.* **2021**, *22*, 10248. [CrossRef]
28. Zhang, H.; Deng, C.; Yao, J.; Zhang, Y.L.; Zhang, Y.N.; Deng, S.; Zhao, N.; Sa, G.; Zhou, X.; Lu, C.; et al. Populus *euphratica* JRL Mediates ABA Response, Ionic and ROS Homeostasis in Arabidopsis under Salt Stress. *Int. J. Mol. Sci.* **2019**, *20*, 815. [CrossRef]
29. He, X.; Li, L.; Xu, H.; Xi, J.; Cao, X.; Xu, H.; Rong, S.; Dong, Y.; Wang, C.; Chen, R.; et al. A rice jacalin-related mannose-binding lectin gene, *OsJRL*, enhances Escherichia coli viability under high salinity stress and improves salinity tolerance of rice. *Plant Biol. (Stuttg.)* **2017**, *19*, 257–267. [CrossRef]
30. Shekha, S.; Kuma, D. Ectopic Overexpression of Lectin in Transgenic *Brassica juncea* Plants Exhibit Resistance to Fungal Phytopathogen and Showed Alleviation to Salt and Drought Stress. *J. Bioeng. Biomed. Sci.* **2015**, *5*, 147. [CrossRef]
31. Sun, Y.; Qiao, Z.; Muchero, W.; Chen, J.G. Lectin Receptor-Like Kinases: The Sensor and Mediator at the Plant Cell Surface. *Front. Plant Sci.* **2020**, *11*, 596301. [CrossRef]
32. Passricha, N.; Saifi, S.K.; Kharb, P.; Tuteja, N. Rice lectin receptor-like kinase provides salinity tolerance by ion homeostasis. *Biotechnol. Bioeng.* **2020**, *117*, 498–510. [CrossRef] [PubMed]
33. Kaur, N.; Prashanth, K.H.; Bhatti, M.S.; Pati, P.K. *OsSalT* gene cloned from rice provides evidence of its role in salinity and drought stress tolerance. *Plant Sci.* **2022**, *320*, 111306. [CrossRef] [PubMed]
34. Gao, Q.M.; Yin, X.L.; Wang, F.; Zhang, C.Z.; Xiao, F.C.; Wang, H.Y.; Hu, S.C.; Liu, W.H.; Zhou, S.Q.; Chen, L.B.; et al. *Jacalin-related lectin 45* (*OsJRL45*) isolated from 'sea rice 86' enhances rice salt tolerance at the seedling and reproductive stages. *BMC Plant Biol.* **2023**, *23*, 553. [CrossRef] [PubMed]
35. Gao, Q.M.; Yin, X.L.; Wang, F.; Hu, S.C.; Liu, W.H.; Chen, L.B.; Dai, X.J.; Liang, M.Z. *OsJRL40*, a Jacalin-Related Lectin Gene, Promotes Salt Stress Tolerance in Rice. *Int. J. Mol. Sci.* **2023**, *24*, 7441. [CrossRef]
36. Chen, R.S.; Cheng, Y.F.; Han, S.Y.; Van Handel, B.; Dong, L.; Li, X.M.; Xie, X.Q. Whole genome sequencing and comparative transcriptome analysis of a novel seawater adapted, salt-resistant rice cultivar—Sea rice 86. *BMC Genom.* **2017**, *18*, 655. [CrossRef]
37. Sun, Y.; Song, K.; Guo, M.; Wu, H.; Ji, X.; Hou, L.; Liu, X.; Lu, S. A NAC Transcription Factor from 'Sea Rice 86' Enhances Salt Tolerance by Promoting Hydrogen Sulfide Production in Rice Seedlings. *Int. J. Mol. Sci.* **2022**, *23*, 6435. [CrossRef]
38. Wang, G.; Weng, L.; Huang, Y.; Ling, Y.; Zhen, Z.; Lin, Z.; Hu, H.; Li, C.; Guo, J.; Zhou, J.L.; et al. Microbiome-metabolome analysis directed isolation of rhizobacteria capable of enhancing salt tolerance of Sea Rice 86. *Sci. Total Environ.* **2022**, *843*, 156817. [CrossRef]
39. Gao, Q.M.; Wang, H.Y.; Yin, X.L.; Wang, F.; Hu, S.C.; Liu, W.H.; Chen, L.B.; Dai, X.J.; Liang, M.Z. Identification of Salt Tolerance Related Candidate Genes in 'Sea Rice 86' at the Seedling and Reproductive Stages Using QTL-Seq and BSA-Seq. *Genes* **2023**, *14*, 458. [CrossRef]
40. Liang, W.; Ma, X.; Wan, P.; Liu, L. Plant salt-tolerance mechanism: A review. *Biochem. Biophys. Res. Commun.* **2018**, *495*, 286–291. [CrossRef]
41. Quan, X.Y.; Meng, C.; Xie, C.J.; Sun, H.F.; Xu, B.Y.; Bermudez, R.S.; He, W.X. Genome-Wide and Transcriptome Analysis of Jacalin-Related Lectin Genes in Barley and the Functional Characterization of *HvHorcH* in Low-Nitrogen Tolerance in Arabidopsis. *Int. J. Mol. Sci.* **2023**, *24*, 16641. [CrossRef]

42. Zhang, Z.; Huang, B.; Chen, J.; Jiao, Y.; Guo, H.; Liu, S.; Ramakrishnan, M.; Qi, G. Genome-Wide Identification of *JRL* Genes in Moso Bamboo and Their Expression Profiles in Response to Multiple Hormones and Abiotic Stresses. *Front. Plant Sci.* **2021**, *12*, 809666. [CrossRef] [PubMed]
43. Han, Y.J.; Zhong, Z.H.; Song, L.L.; Stefan, O.; Wang, Z.H.; Lu, G.L. Evolutionary analysis of plant jacalin-related lectins (JRLs) family and expression of rice JRLs in response to *Magnaporthe oryzae*. *J. Integr. Agric.* **2018**, *17*, 1252–1266. [CrossRef]
44. Song, M.; Xu, W.; Xiang, Y.; Jia, H.; Zhang, L.; Ma, Z. Association of jacalin-related lectins with wheat responses to stresses revealed by transcriptional profiling. *Plant Mol. Biol.* **2014**, *84*, 95–110. [CrossRef] [PubMed]
45. Nagano, A.J.; Fukao, Y.; Fujiwara, M.; Nishimura, M.; Hara-Nishimura, I. Antagonistic jacalin-related lectins regulate the size of ER body-type beta-glucosidase complexes in *Arabidopsis thaliana*. *Plant Cell Physiol.* **2008**, *49*, 969–980. [CrossRef]
46. Kaur, N.; Sagar, A.; Sharma, P.; Ashish; Pati, P.K. Structural insights into rice *SalTol* QTL located SALT protein. *Sci. Rep.* **2020**, *10*, 16589. [CrossRef]
47. Akladious, S.A.; Mohamed, H.I. Ameliorative effects of calcium nitrate and humic acid on the growth, yield component and biochemical attribute of pepper (*Capsicum annuum*) plants grown under salt stress. *Sci. Hortic.* **2018**, *236*, 244–250. [CrossRef]
48. Kohli, S.K.; Khanna, K.; Bhardwaj, R.; Abd Allah, E.F.; Ahmad, P.; Corpas, F.J. Assessment of Subcellular ROS and NO Metabolism in Higher Plants: Multifunctional Signaling Molecules. *Antioxidants* **2019**, *8*, 641. [CrossRef]
49. Razzaq, A.; Ali, A.; Safdar, L.B.; Zafar, M.M.; Rui, Y.; Shakeel, A.; Shaukat, A.; Ashraf, M.; Gong, W.; Yuan, Y. Salt stress induces physiochemical alterations in rice grain composition and quality. *J. Food Sci.* **2020**, *85*, 14–20. [CrossRef] [PubMed]
50. van Zelm, E.; Zhang, Y.; Testerink, C. Salt Tolerance Mechanisms of Plants. *Annu. Rev. Plant Biol.* **2020**, *71*, 403–433. [CrossRef]
51. Gao, R.; Jia, Y.; Xu, X.; Fu, P.; Zhou, J.; Yang, G. Structural insights into the *Oryza sativa* cation transporters HKTs in salt tolerance. *J. Integr. Plant Biol.* **2024**, *66*, 700–708. [CrossRef]
52. Yu, J.; Zhu, C.; Xuan, W.; An, H.; Tian, Y.; Wang, B.; Chi, W.; Chen, G.; Ge, Y.; Li, J.; et al. Genome-wide association studies identify OsWRKY53 as a key regulator of salt tolerance in rice. *Nat. Commun.* **2023**, *14*, 3550. [CrossRef] [PubMed]
53. Song, J.; Yang, H.; Qiao, C.; Zhu, C.; Bai, T.; Du, H.; Ma, S.; Wang, N.; Luo, C.; Zhang, Y.; et al. Natural variations of chlorophyll fluorescence and ion transporter genes influenced the differential response of *japonica* rice germplasm with different salt tolerances. *Front. Plant Sci.* **2023**, *14*, 1095929. [CrossRef]
54. Muzaffar, A.; Chen, Y.S.; Lee, H.T.; Wu, C.C.; Le, T.T.; Liang, J.Z.; Lu, C.H.; Balasubramaniam, H.; Lo, S.F.; Yu, L.C.; et al. A newly evolved rice-specific gene *JAUP1* regulates jasmonate biosynthesis and signalling to promote root development and multi-stress tolerance. *Plant Biotechnol. J.* **2024**, *22*, 1417–1432. [CrossRef]
55. Shikha, D.; Jakhar, P.; Satbhai, S.B. Role of jasmonate signaling in the regulation of plant responses to nutrient deficiency. *J. Exp. Bot.* **2023**, *74*, 1221–1243. [CrossRef]
56. Ndecky, S.; Nguyen, T.H.; Eiche, E.; Cognat, V.; Pflieger, D.; Pawar, N.; Betting, F.; Saha, S.; Champion, A.; Riemann, M.; et al. Jasmonate signaling controls negative and positive effectors of salt stress tolerance in rice. *J. Exp. Bot.* **2023**, *74*, 3220–3239. [CrossRef]
57. Asif, S.; Jan, R.; Kim, N.; Asaf, S.; Lubna; Khan, M.A.; Kim, E.G.; Jang, Y.H.; Bhatta, D.; Lee, I.J.; et al. Halotolerant endophytic bacteria alleviate salinity stress in rice (*Oryza sativa* L.) by modulating ion content, endogenous hormones, the antioxidant system and gene expression. *BMC Plant Biol.* **2023**, *23*, 494. [CrossRef]
58. Feng, Z.; Xu, Y.; Xie, Z.; Yang, Y.; Lu, G.; Jin, Y.; Wang, M.; Liu, M.; Yang, H.; Li, W.; et al. Overexpression of Abscisic Acid Biosynthesis Gene *OsNCED3* Enhances Survival Rate and Tolerance to Alkaline Stress in Rice Seedlings. *Plants* **2024**, *13*, 1713. [CrossRef]
59. Jin, X.; Li, X.; Xie, Z.; Sun, Y.; Jin, L.; Hu, T.; Huang, J. Nuclear factor OsNF-YC5 modulates rice seed germination by regulating synergistic hormone signaling. *Plant Physiol.* **2023**, *193*, 2825–2847. [CrossRef] [PubMed]
60. Zheng, S.W.; Liu, S.B.; Feng, J.H.; Wang, W.; Wang, Y.W.; Yu, Q.; Liao, Y.R.; Mo, Y.H.; Xu, Z.J.; Li, L.H.; et al. Overexpression of a stress response membrane protein gene *OsSMP1* enhances rice tolerance to salt, cold and heavy metal stress. *Environ. Exp. Bot.* **2021**, *182*, 104327. [CrossRef]
61. Wang, A.; Shu, X.; Jing, X.; Jiao, C.; Chen, L.; Zhang, J.; Ma, L.; Jiang, Y.; Yamamoto, N.; Li, S.; et al. Identification of rice (*Oryza sativa* L.) genes involved in sheath blight resistance via a genome-wide association study. *Plant Biotechnol. J.* **2021**, *19*, 1553–1566. [CrossRef]
62. Zhang, F.; Huang, J.; Guo, H.; Yang, C.; Li, Y.; Shen, S.; Zhan, C.; Qu, L.; Liu, X.; Wang, S.; et al. *OsRLCK160* contributes to flavonoid accumulation and UV-B tolerance by regulating *OsbZIP48* in rice. *Sci. China Life Sci.* **2022**, *65*, 1380–1394. [CrossRef]
63. Liu, Y.; Li, M.; Yu, J.; Ma, A.; Wang, J.; Yun, D.J.; Xu, Z.Y. Plasma membrane-localized Hsp40/DNAJ chaperone protein facilitates OsSUVH7-OsBAG4-OsMYB106 transcriptional complex formation for *OsHKT1;5* activation. *J. Integr. Plant Biol.* **2023**, *65*, 265–279. [CrossRef]
64. Krishnamurthy, S.L.; Sharma, S.K.; Kumar, V.; Tiwari, S.; Singh, N.K. Analysis of genomic region spanning *Saltol* using SSR markers in rice genotypes showing differential seedlings stage salt tolerance. *J. Plant Biochem. Biotechnol.* **2015**, *25*, 331–336. [CrossRef]
65. Dai, X.J.; He, C.; Zhou, L.; Liang, M.Z.; Fu, X.C.; Qin, P.; Yang, Y.Z.; Chen, L.B. Identification of a specific molecular marker for the rice blast-resistant gene *Pigm* and molecular breeding of thermo-sensitive genic male sterile leaf-color marker lines. *Mol. Breed.* **2018**, *38*, 72. [CrossRef]

66. Doyle, J. DNA Protocols for Plants. In *Molecular Techniques in Taxonomy*; Hewitt Godfrey, M., Johnston Andrew, W.B., Young, J., Peter, W., Eds.; Springer: Berlin/Heidelberg, Germany, 1991; pp. 283–293.
67. Livak, K.J.; Schmittgen, T.D. Analysis of relative gene expression data using real-time quantitative PCR and the $2^{-\Delta\Delta C}{}_t$ Method. *Methods* **2001**, *25*, 402–408. [CrossRef]
68. Zhang, K.; Su, J.; Xu, M.; Zhou, Z.; Zhu, X.; Ma, X.; Hou, J.; Tan, L.; Zhu, Z.; Cai, H.; et al. A common wild rice-derived *BOC1* allele reduces callus browning in *indica* rice transformation. *Nat. Commun.* **2020**, *11*, 443. [CrossRef]
69. Wang, J.; Nan, N.; Shi, L.; Li, N.; Huang, S.; Zhang, A.; Liu, Y.; Guo, P.; Liu, B.; Xu, Z.Y. Arabidopsis BRCA1 represses RRTF1-mediated ROS production and ROS-responsive gene expression under dehydration stress. *New Phytol.* **2020**, *228*, 1591–1610. [CrossRef]
70. Ruan, W.; Guo, M.; Wang, X.; Guo, Z.; Xu, Z.; Xu, L.; Zhao, H.; Sun, H.; Yan, C.; Yi, K. Two RING-Finger Ubiquitin E3 Ligases Regulate the Degradation of SPX4, An Internal Phosphate Sensor, for Phosphate Homeostasis and Signaling in Rice. *Mol. Plant* **2019**, *12*, 1060–1074. [CrossRef]
71. Chen, C.; Wu, Y.; Li, J.; Wang, X.; Zeng, Z.; Xu, J.; Liu, Y.; Feng, J.; Chen, H.; He, Y.; et al. TBtools-II: A "one for all, all for one" bioinformatics platform for biological big-data mining. *Mol. Plant* **2023**, *16*, 1733–1742. [CrossRef]

Disclaimer/Publisher's Note: The statements, opinions and data contained in all publications are solely those of the individual author(s) and contributor(s) and not of MDPI and/or the editor(s). MDPI and/or the editor(s) disclaim responsibility for any injury to people or property resulting from any ideas, methods, instructions or products referred to in the content.

International Journal of
Molecular Sciences

MDPI

Article

Identification of Cold Tolerance Transcriptional Regulatory Genes in Seedlings of *Medicago sativa* L. and *Medicago falcata* L.

Qi Wang [1,2,†], Jianzhong Wu [1,†], Guili Di [3], Qian Zhao [4], Chao Gao [1], Dongmei Zhang [1], Jianli Wang [1], Zhongbao Shen [1] and Weibo Han [1,*]

[1] Institute of Forage and Grassland Sciences, Heilongjiang Academy of Agricultural Sciences, Harbin 150086, China; m18846603788@163.com (Q.W.); wujianzhong@haas.cn (J.W.); gaochaopdf2000@163.com (C.G.); zhd_mei@163.com (D.Z.); wangjianlivip@126.com (J.W.); shzhb1973@126.com (Z.S.)
[2] College of Life Science and Technology, Harbin Normal University, Harbin 150025, China
[3] Institute of Industrial Crops, Heilongjiang Academy of Agricultural Sciences, Harbin 150086, China; diguili59@163.com
[4] Cultivation and Farming Research Institute, Heilongjiang Academy of Agricultural Sciences, Harbin 150086, China; zhaoqian0401@sina.com
* Correspondence: alclever@163.com
† These authors contributed equally to this work.

Abstract: Alfalfa species *Medicago sativa* L. (MS) and *Medicago falcata* L. (MF), globally prominent perennial leguminous forages, hold substantial economic value. However, our comprehension of the molecular mechanisms governing their resistance to cold stress remains limited. To address this knowledge gap, we scrutinized and compared MS and MF cold-stress responses at the molecular level following 24 h and 120 h low-temperature exposure (4 °C). Our study revealed that MF had superior physiological resilience to cold stress compared with MS, and its morphology was healthier under cold stress, and its malondialdehyde content and superoxide dismutase activity increased, first, and then decreased, while the soluble sugar content continued to accumulate. Transcriptome analysis showed that after 120 h of exposure, there were different gene-expression patterns between MS and MF, including 1274 and 2983 genes that were continuously up-regulated, respectively, and a total of 923 genes were included, including star cold-resistant genes such as *ICE1* and *SIP1*. Gene ontology (GO) enrichment and Kyoto Encyclopedia of Genes and Genomes (KEGG) pathway analyses revealed numerous inter-species differences in sustained cold-stress responses. Notably, MS-exclusive genes included a single transcription factor (TF) gene and several genes associated with a single DNA repair-related pathway, whereas MF-exclusive genes comprised nine TF genes and genes associated with 14 pathways. Both species exhibited high-level expression of genes encoding TFs belonging to AP2-EREBP, ARR-B, and bHLH TF families, indicating their potential roles in sustaining cold resistance in alfalfa-related species. These findings provide insights into the molecular mechanisms governing cold-stress responses in MS and MF, which could inform breeding programs aimed at enhancing cold-stress resistance in alfalfa cultivars.

Keywords: DEGs; cold tolerance; transcriptome; *Medicago sativa* L.; *Medicago falcata* L.

1. Introduction

Medicago sativa L. (MS), commonly known as alfalfa, is a perennial herbaceous plant belonging to the pea family (Fabaceae) within the order Fabales (legumes). Alfalfa, renowned for its exceptional nutrient content, is the most extensively cultivated legume forage globally. However, its wild relative, *Medicago falcata* L. (MF), exhibits superior resistance to drought, cold, and infertile soil conditions [1], making MF a valuable parent material in breeding programs aimed at enhancing MS resilience to harsh growing environments [2]. In China, alfalfa cultivation primarily occurs in North China, where recurring frost damage of

seedlings or plants following low-temperature exposure presents significant challenges to alfalfa production and dissemination, impacting animal husbandry [3]. This vulnerability results in substantial economic losses, necessitating a deeper understanding of the impact of low-temperature stress on alfalfa and the molecular mechanisms governing its response to cold stress.

Cold stress induces various overt detrimental effects, including surface lesions, discoloration, tissue destruction, and accelerated aging [4,5], while at the cellular level, it disrupts the cell membrane, leading to electrolyte leakage and malondialdehyde (MDA) production [6], as well as to changes in gene transcription and protein synthesis [7]. Ultimately, these changes hinder plant growth, with the degree of impact varying depending on a plant's genetic composition and stress tolerance.

Current studies have shown that alfalfa can scavenge toxic free radicals and reactive oxygen species (ROS) by activating the antioxidant defense system in response to cold stress [8], or alleviate oxidative stress by enhancing the level of autophagy, such as Zhao et al. [9] found that *MsATG13* overexpression can increase the level of autophagy, increase the content of proline and antioxidant enzymes, and enhance the antioxidant defense capacity under cold-stress conditions. Meanwhile, alfalfa utilizes osmotic regulatory substances to enhance cell fluid content and reduce cell osmotic potential, consequently lowering the cellular freezing point; additionally, they bolster the protoplasm's capability to alleviate cell damage [10,11]. In addition, plant hormones emerge as crucial modulators in the regulation of cold-stress signal transduction. For instance, abscisic acid (ABA) controls the expression of COR genes by modulating C-repeat binding factor (CBF) transcription [12], and it has been speculated that C-repeat binding factor-like (CBFl) may play the same role in alfalfa [13]. Furthermore, several differentially expressed genes (DEGs) potentially related to autumn dormancy have been identified using the synthetic backcrossing strategy (SBS). This strategy utilizes crown buds and whole alfalfa plants as materials, providing valuable resources for future functional genomics studies related to freezing stress [14,15]. The latest study found that chloroplasts store nutrients through photosynthesis to resist cold stress, and some genes are down-regulated or edited less efficiently [16].

However, most such studies have focused on a single species of alfalfa exposed to stress for less than 5 days, limiting the exploration of unique or shared cold-resistance genes and molecular mechanisms across species. In order to address the above knowledge gaps, cold stress was applied to MS and MF for 24 h and 120 h, respectively, at 4 °C. The physiological and metabolic changes of MS and MF in response to cold stress were measured, and then Gene Ontogeny (GO) enrichment and Kyoto Encyclopedia of Genes and Genomes (KEGG) pathway analysis were performed based on pan-transcriptional sequencing results. The purpose of this study was to independently analyze the genetic basis of the cold-stress response of MS and MF at the transcriptional level, and to compare them based on the results, aiming to provide potential genetic resources and valuable references for enhancing the cold resistance of alfalfa.

2. Results

2.1. Effects of Cold Stress on Morphological and Physiological Responses of MA and MF Seedlings

In the control group, the seedlings of both MS and MF plants had healthy leaves, and the plants of MF were shorter and had smaller leaves compared to MS. After 24 h of cold treatment, a small number of MS leaves showed signs of wilting and tissue softening (in the red circle of Figure 1A), while most of the MS plants in the 120 h treatment group showed slight stem drooping and a large number of leaves drooping, wilting, and yellowing, and only a few remained healthy (in the blue circle of Figure 1A), which was less common in MF leaves. With the increase of the duration of cold stress, leaf wilting and growth inhibition intensified, and the morphological changes of seedlings at the MS three-leaf stage were greater than those of MF.

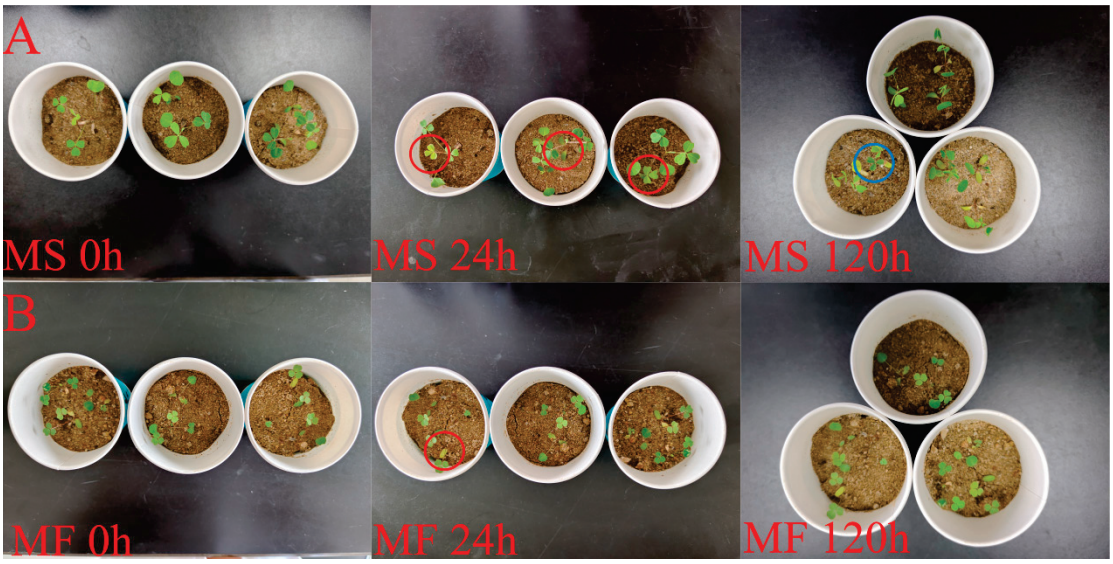


Figure 1. Morphological changes of MS and MF under cold stress. (**A**) MS was treated at 4 °C for 0 h, 24 h, and 120 h, respectively, and the leaves in the red circle were unhealthy while the leaves in the blue circle were healthy. (**B**) MF was treated at 4 °C for 0 h, 24 h, and 120 h, respectively, and the leaves in the red circle were unhealthy.

MDA levels significantly increased in both the MS and MF groups after 24 and 120 h of cold stress ($p < 0.05$), surpassing those of the control group (Figure 2A). SOD activity showed a significant increase after 24 h of cold stress ($p < 0.05$), followed by a decrease after 120 h ($p < 0.05$), though it remained higher than in the control group (Figure 2B). The SS content continued to rise in both alfalfa species under cold stress, although the SS content of the MS group was not significantly higher than that of the control group after 24 h ($p > 0.05$) (Figure 2C). Notably, MF exhibited a lower MDA content and higher SOD and SS contents than MS under cold-stress conditions for 0, 24, and 120 h.

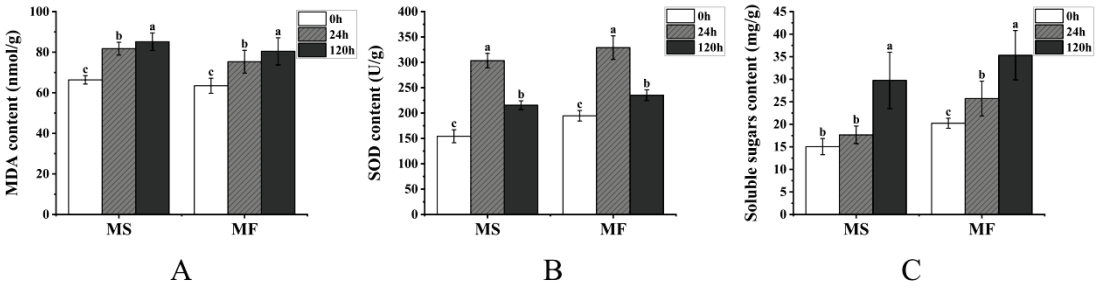


Figure 2. Contents of malondialdehyde (MDA), superoxide dismutase (SOD), and soluble sugar in the leaves of *Medicago sativa* L. and *Medicago falcata* L. under cold stress. (**A**) MDA content, (**B**) SOD content, and (**C**) soluble sugar content. Each value represents the mean of three replicates ± SD (standard deviation), represented by a vertical error bar. According to Duncan's multiple range test, different letters above the bar indicate significant differences at the 0.05 level. Among them, a, b and c are the results of single-factor ANOVA analysis, which can reflect the significant degree of differences between treatments.

2.2. RNA Sequencing and Transcriptome Assembly, Comparison, and Analysis

Eighteen cDNA libraries were constructed, yielding a total of 109.14 Gb of raw reads with an average of 6.06 Gb of reads per sample (Table 1). After filtering to remove redundant reads, a total of 108.40 Gb of clean reads were obtained, averaging 6.02 Gb per sample, yielding a mean Q30 of 93.96% and a mean Q20 of 98.02%. Alignment with the alfalfa reference genome resulted in an estimated 32,595,076 to 41,194,666 successfully mapped

clean reads, corresponding to an overall comparison rate ranging from 75.53% to 79.92%. Notably, the comparison rate of clean reads with unique genomic locations ranged from 71.20% to 76.20%, while those with multiple locations ranged from 3.58% to 4.41%. These findings highlight the high fidelity of the transcriptome data, enabling subsequent analyses.

Table 1. Statistics and comparison of sequencing data of each sample.

Sample	Raw Data (Gb)	Clean Data (Gb)	Clean Reads	Q30 (%)	Q20 (%)	GC (%)	Unique_Mapped (%)	Multiple_Mapped (%)	Total_Mapped (%)
CK-MS 1	5.62	5.59	36,485,352	94.05	98.10	42.44	74.64	3.71	78.35
CK-MS 2	6.35	6.31	40,096,186	93.99	98.04	42.95	74.32	3.58	77.90
CK-MS 3	5.47	5.44	32,595,076	94.35	98.19	43.21	74.73	3.80	78.53
CK-MF 1	6.31	6.27	40,325,286	93.88	97.99	42.09	72.73	3.71	76.44
CK-MF 2	6.27	6.22	39,122,956	94.62	98.29	43.11	72.38	3.61	75.99
CK-MF 3	6.28	6.23	37,066,462	94.21	98.10	43.32	71.57	4.06	75.63
MS 24 h 1	6.31	6.26	38,466,796	93.09	97.65	42.82	75.25	4.41	79.66
MS 24 h 2	6.24	6.20	41,194,666	93.89	97.99	42.21	76.20	3.72	79.92
MS 24 h 3	6.07	6.02	37,839,116	93.86	97.98	42.77	75.67	4.08	79.75
MF 24 h 1	6.22	6.18	40,993,790	93.80	97.93	42.25	72.91	3.86	76.76
MF 24 h 2	5.56	5.53	33,894,138	93.87	97.98	42.98	72.15	4.17	76.32
MF 24 h 3	6.16	6.13	39,815,090	93.88	97.99	41.94	72.90	3.98	76.88
MS 120 h 1	6.21	6.16	38,873,226	94.20	98.11	42.60	74.97	4.41	79.38
MS 120 h 2	6.27	6.22	38,736,768	94.09	98.05	43.00	74.53	4.11	78.64
MS 120 h 3	6.55	6.50	39,479,598	93.45	97.78	43.05	74.44	4.36	78.80
MF 120 h 1	5.50	5.46	34,913,352	93.94	98.04	42.39	72.12	4.04	76.15
MF 120 h 2	5.64	5.61	34,576,766	93.81	97.96	42.73	71.20	4.32	75.53
MF 120 h 3	6.10	6.06	39,593,770	94.30	98.18	42.05	72.24	4.06	76.30
Average	6.06	6.02	38,003,800	93.96	98.02	42.66	73.61	4.00	77.61

Note: CK-MS, MS 24 h, and MS 120 h represent 0 h, 24 h, and 120 h cold-stress treatment groups of *Medicago sativa* L., respectively. CK-MF, MF 24 h, and MF 120 h represent 0 h, 24 h, and 120 h cold stress treatment groups of *Medicago falcata* L., respectively. DEGs under cold stress.

Statistical analysis of the read distribution relative to the reference genome (Figure S1, Table S1) revealed that transcriptome data were predominantly mapped to exonic regions.

Both alfalfa species exhibited significant responses to cold stress, with a total of 57,080 DEGs detected, including 7915 encoded by novel genes (Table S2). The results of the comprehensive statistical analysis of gene-expression levels demonstrated consistent and uniformly distributed gene-expression levels across biological replicates, affirming the high quality of the 18 sequenced samples (Table 2 and Figure S2).

Table 2. Statistics on gene alignment.

Sample	Refer_Genes	Sequenced_Refer_Genes (%)	Novel_Genes	Sequenced_Novel_Genes (%)	Total_Genes	Sequenced_Total_Genes (%)
CK-MS 1	49,165	21,918 (44.58%)	7915	5171 (65.33%)	57,080	27,089 (47.46%)
CK-MS 2	49,165	21,401 (43.53%)	7915	4989 (63.03%)	57,080	26,390 (46.23%)
CK-MS 3	49,165	21,364 (43.45%)	7915	4963 (62.70%)	57,080	26,327 (46.12%)
CK-MF 1	49,165	21,775 (44.29%)	7915	5312 (67.11%)	57,080	27,087 (47.45%)
CK-MF 2	49,165	21,203 (43.13%)	7915	5003 (63.21%)	57,080	26,206 (45.91%)
CK-MF 3	49,165	21,410 (43.55%)	7915	4941 (62.43%)	57,080	26,351 (46.17%)
MS 24 h 1	49,165	22,001 (44.75%)	7915	5121 (64.70%)	57,080	27,122 (47.52%)
MS 24 h 2	49,165	21,823 (44.39%)	7915	5283 (66.75%)	57,080	27,106 (47.49%)
MS 24 h 3	49,165	22,141 (45.03%)	7915	5401 (68.24%)	57,080	27,542 (48.25%)
MF 24 h 1	49,165	21,113 (42.94%)	7915	5071 (64.07%)	57,080	26,184 (45.87%)
MF 24 h 2	49,165	21,271 (43.26%)	7915	5360 (67.72%)	57,080	26,631 (46.66%)
MF 24 h 3	49,165	21,473 (43.68%)	7915	5301 (66.97%)	57,080	26,774 (46.91%)
MS 120 h 1	49,165	21,296 (43.32%)	7915	4652 (58.77%)	57,080	25,948 (45.46%)
MS 120 h 2	49,165	21,258 (43.24%)	7915	4881 (61.67%)	57,080	26,139 (45.79%)
MS 120 h 3	49,165	21,520 (43.77%)	7915	5019 (63.41%)	57,080	26,539 (46.49%)
MF 120 h 1	49,165	20,948 (42.61%)	7915	5265 (66.52%)	57,080	26,213 (45.92%)
MF 120 h 2	49,165	21,137 (42.99%)	7915	5227 (66.04%)	57,080	26,364 (46.19%)
MF 120 h 3	49,165	21,524 (43.78%)	7915	5208 (65.80%)	57,080	26,732 (46.83%)
All	49,165	31,837 (64.76%)	7915	7915 (100.00%)	57,080	39,752 (69.64%)

Note: The numbers in the last row represent the sum of all the different genes.

The results of principal component analysis (PCA) showed that the biological replicates were almost identical between the treatment groups, and in subsequent analyses, we will focus on individuals with good reproducibility as references (Figure 3). The correlation between all cold-stress groups was strong, and the Pearson correlation coefficient was consistently above 0.9 (Figure S3). It is worth noting that the correlation between the

control group and the cold-stress group was always lower than 0.9, indicating that there were significant differences in gene-expression patterns between groups under cold stress.

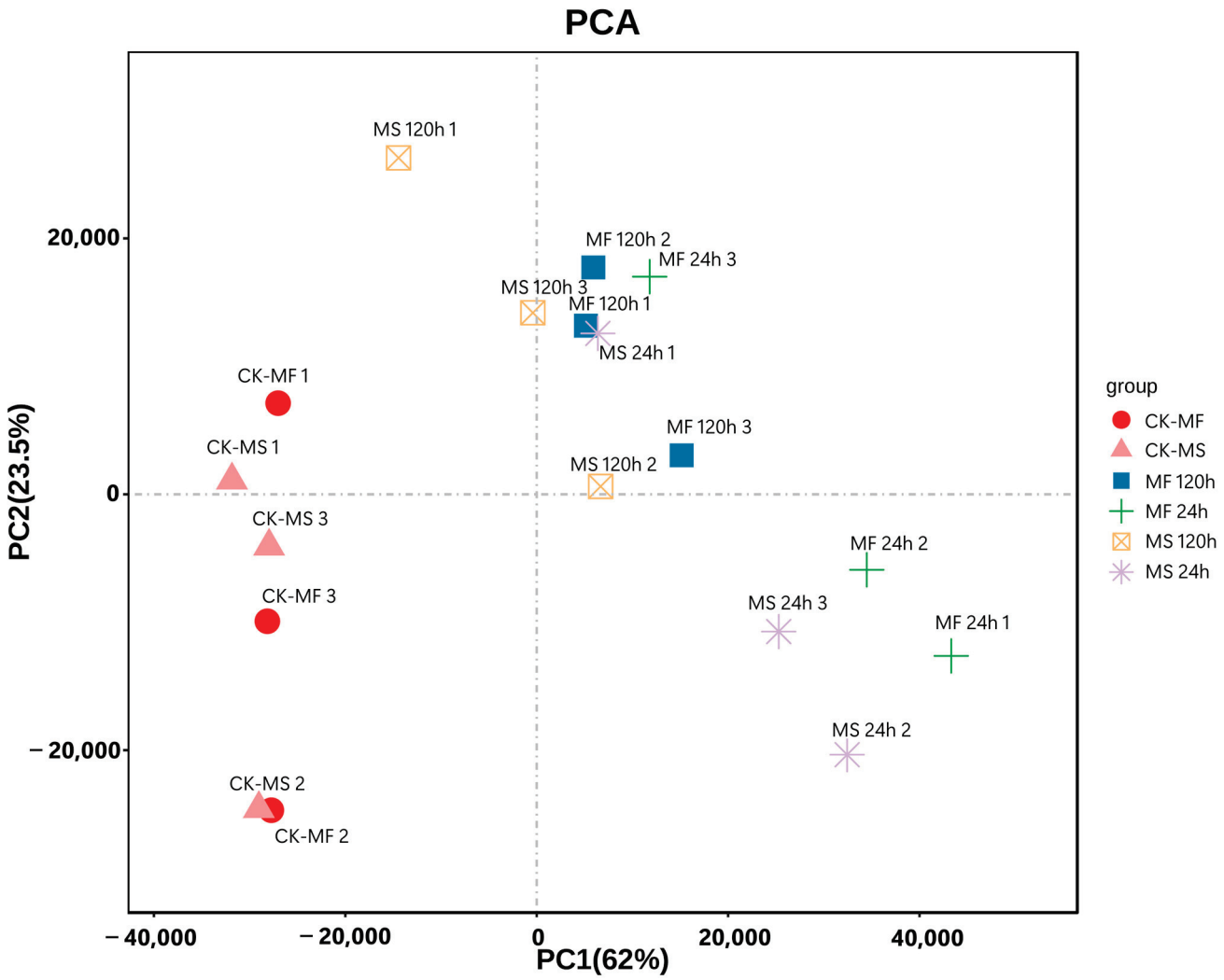


Figure 3. Principal component analysis (PCA) diagram of the sample. The PC1 coordinate represents the first principal component, and the percentage in parentheses indicates the contribution of the first principal component to the sample difference. The PC2 coordinates represent the second principal component, and the percentages in parentheses indicate the contribution of the second principal component to the sample variance. The colored dots in the diagram represent each sample.

The DEGs screening results (Figure 4A) highlight distinct responses to cold stress between the MS and MF cold-stressed groups at 24 h and 120 h compared to the control group. The comparison between the MS and control groups revealed 3175 DEGs (1176 up-regulated 1999 down-regulated) and 3070 DEGs (1508 up-regulated and 1562 down-regulated) at 24 h and 120 h, respectively (Tables S3 and S4). Similarly, the comparison between the MF and control groups yielded a higher number of down-regulated genes than up-regulated genes, including 5809 DEGs (2714 up-regulated and 3095 down-regulated) and 4962 DEGs (2403 up-regulated and 2559 down-regulated) at 24 h and 120 h, respectively (Tables S5 and S6).

Remarkably, inter-group comparisons revealed a higher prevalence of down-regulated genes across groups. Furthermore, 1274 genes in MS and 2983 genes in MF exhibited sustained significant regulation throughout the 120 h cold-stress period, denoted as MS-p and MF-p, respectively (Figure 4B, Table S7).

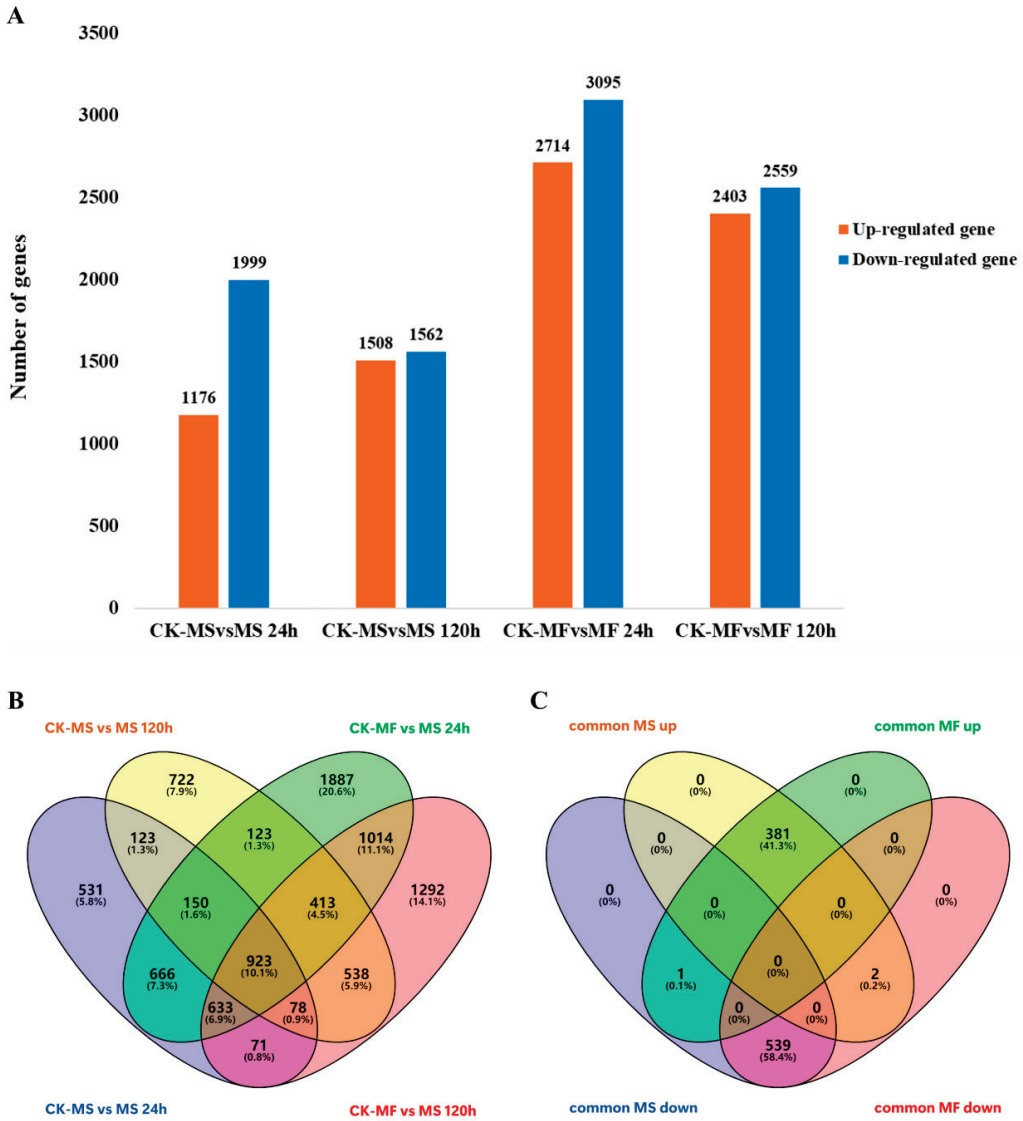


Figure 4. Analysis of DEGs. (**A**): Number of DEGs in each comparison group; (**B**): overlap of DEGs between two varieties compared with controls; and (**C**): overlap of two varieties co-expressed DEGs. Common MS up/down: up-regulated/down-regulated DEGs in *Medicago sativa* L.; common MF up/down: DEGs up-regulated/down-regulated in *Medicago falcata* L.

Differences in gene expression between MS and MF were evident, with 923 co-expressed genes identified as common cold-stress response genes across both species (Table S7). Notably, MF demonstrated a greater number of cold-stress response genes, with 2060 genes continuously regulated compared to 351 in MS. However, both varieties exhibited overlapping responses to cold stress, as indicated by the numerous cold-stress response genes common to both species.

Further analysis revealed that throughout the 120 h cold stress period, two genes were up-regulated in MS and down-regulated in MF, while one gene was down-regulated in MS and up-regulated in MF (Figure 4C). These findings suggest that nuanced regulatory mechanisms underlie the alfalfa response to cold stress.

2.3. Enrichment Analysis of DEGs

After annotation against the GO database, DEGs consistently implicated in the 120 h cold stress tolerance process in both MS and MF were categorized into three distinct classes (Figure 5, Tables S8 and S9). The most abundant GO terms for MS and MF in biological

processes were "oxidation-reduction process (GO:0055114)" and "external encapsulating structure organization (GO:0045229)", respectively. And the most numerous GO items in their cellular components and molecular functions were "membrane (GO:0016020)" and "catalytic activity (GO:0003824)". Among the top 20 GO terms in functional categories, Biological Process, Cellular Component, and Molecular Function, MS and MF shared 1, 14, and 5 common GO terms, respectively.

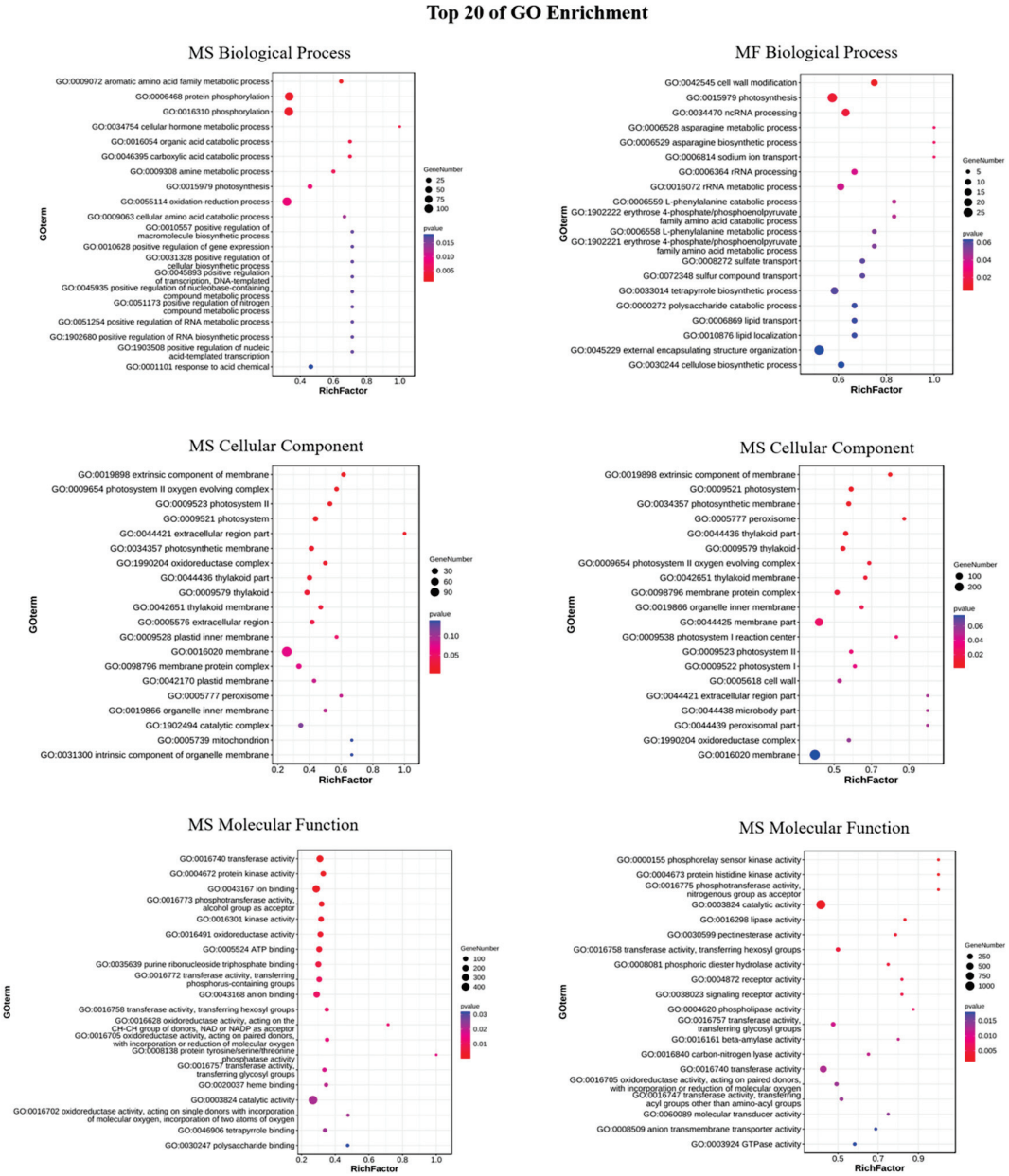


Figure 5. GO enrichment analysis of DEGs in *Medicago sativa* L. and *Medicago falcata* L. The GO enrichment bubble diagram of DEGs in MS and MF were plotted using the top 20 GO terms with the smallest Q values. The vertical coordinate was the GO term, and the horizontal coordinate was the enrichment factor (the number of differential genes in the GO term divided by all the numbers in the GO term). The size represented the number of genes, and the redder the color, the smaller the Q value).

Moreover, the 1274 genes consistently involved in 120 h cold-stress resilience in MS and MF were mapped to 30 and 44 KEGG pathways, respectively (Figure 6, Tables S10 and S11). The three pathways with the highest number of genes in MS and MF are "Metabolic pathways", "Protein processing in endoplasmic reticulum", and "Plant hormone signal

transduction". Notably, all identified MS pathways except for "Base excision repair" were observed in MF, with 29 pathways shared by MS and MF.

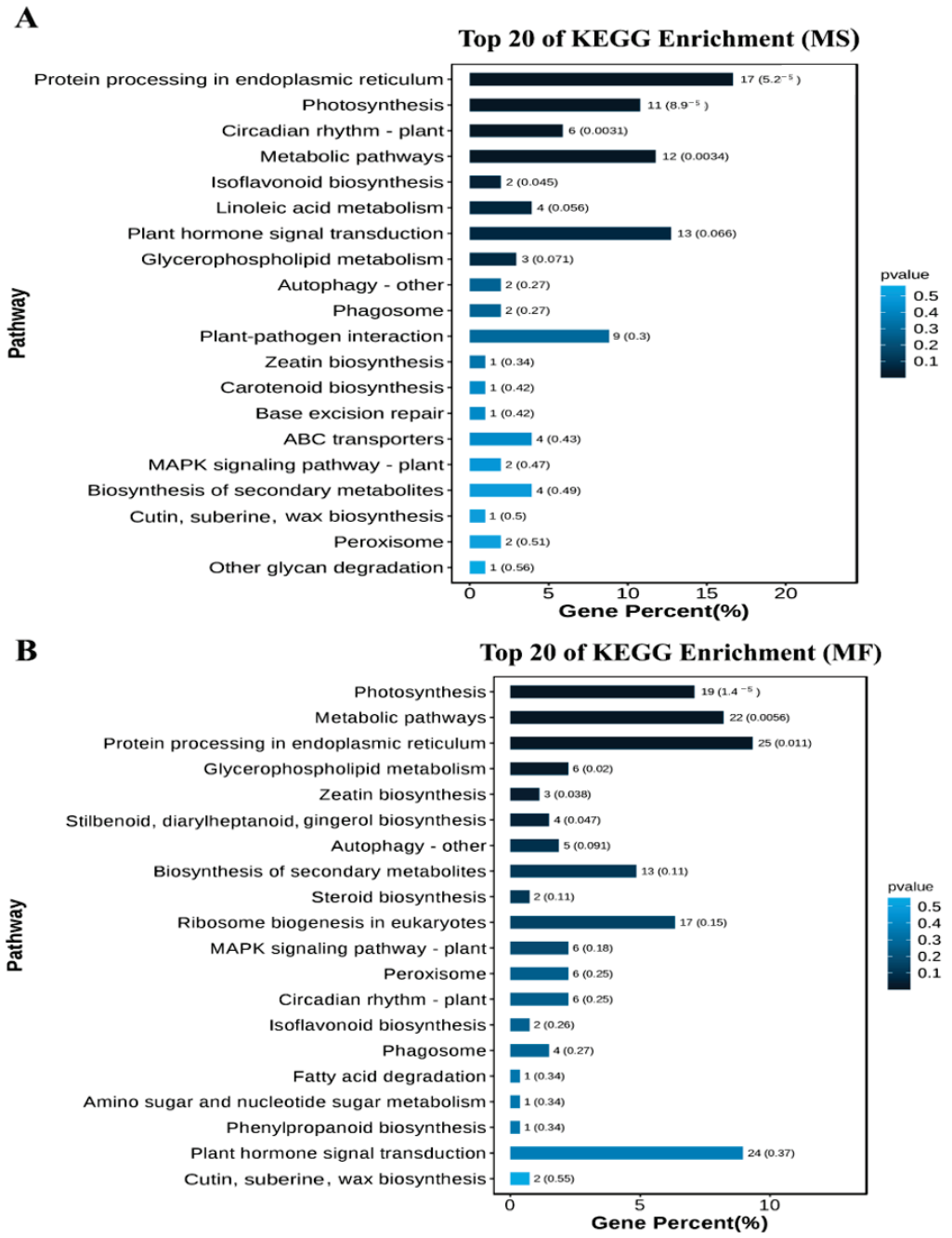


Figure 6. KEGG enrichment analysis of DEGs in *Medicago sativa* L. and *Medicago falcata* L. (**A**): The KEGG pathway enrichment of DEGs in *Medicago sativa* L. was mapped using the top 20 pathways with the smallest Q values. The ordinate is the pathway and the horizontal coordinate is the percentage of the number of this pathway in the number of all the different genes. The darker the color, the smaller the Q value, and the values on the column are the number and Q value of the pathway. (**B**): KEGG pathway enrichment of DEGs in *Medicago falcata* L.

2.4. TF Family Analysis

Functional annotation revealed the presence of 26 and 35 TF families among all significantly expressed DEGs implicated in the 120 h cold-stress responses in MS and MF, respectively (Table S1). Notably, 19 TF families were shared between both species.

In MS, the highest TF counts were associated with the AP2-EREBP and bHLH TF families, each boasting nine TFs. Following closely were the ARR-B and WRKY families, each comprising eight TFs. Conversely, in MF, the AP2-EREBP TF family predominated, with 25 TFs, followed by the ARR-B, bHLH, and NAC TF families, with 24, 14, and 13 TFs, respectively (Figure 7).

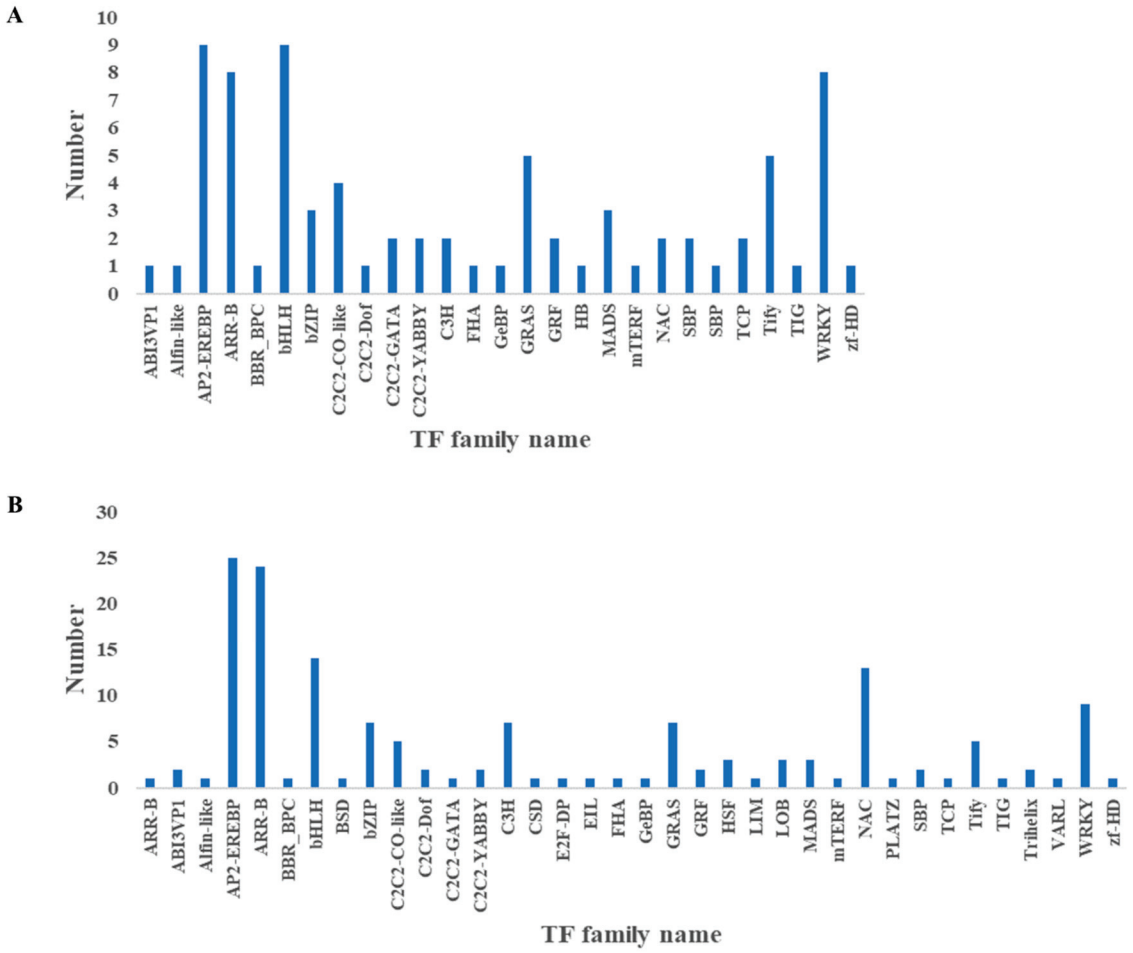


Figure 7. Family distribution of transcription factors in cold-stressed DEGs of *Medicago sativa* L. and *Medicago falcata* L. (**A**): Transcription factors in *Medicago sativa* L. (**B**): Transcription factors in *Medicago falcata* L.

Remarkably, the AP2-EREBP family TFs comprised the most abundant shared TFs, with seven TFs overlapping between the two species. Additionally, the bHLH and WRKY families contributed six TFs each, further underscoring their significance in the cold-stress response across MS and MF.

2.5. RNA-seq Expression Validation by RT-qPCR

Gene-expression profiling was performed using real-time reverse transcription quantitative PCR (RT-qPCR) to quantitatively determine the reliability of our transcriptome data. For this evaluation, six candidate cold-stress DEGs were monitored. The expression profiles of these selected DEGs were determined using qRT-PCR of duplicate biological samples processed in parallel. The results were in agreement with the RNA-seq values obtained using each method differed by a log2-fold difference (Figure 8). RNA-seq and qRT-PCR displayed a positive correlation with a Pearson coefficient $R^2 = 0.9981$ (*MsUBC2*) or $R^2 = 0.9982$ (*MsTUB*). Our results indicated that qRT-PCR expression profiles for the six selected DEGs were generally consistent with RNA-seq results.

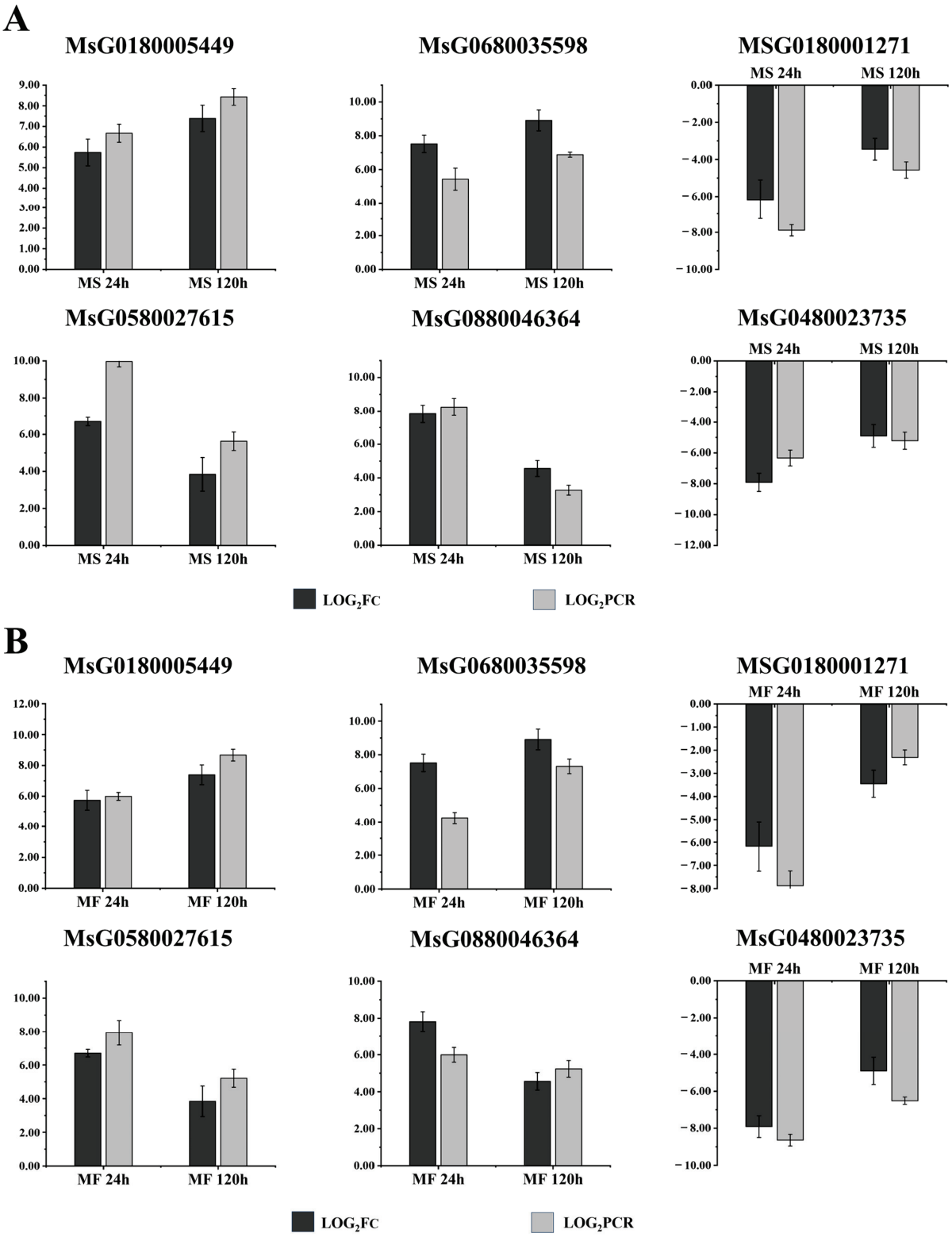


Figure 8. Validation of the RNA-seq data expression profile by qRT-PCR. The relative expression levels of six DEUs were calculated according to the $2^{-\Delta\Delta Ct}$ method using the *Medicago sativa* L. UBC2 and *Medicago sativa* L. TUB (GenBank accession no. L06967.1 and XM003630465) gene as an internal reference gene. We converted the obtained $2^{-\Delta\Delta Ct}$ values with the log formula to obtain what LOG_2FC and LOG_2PCR represented. Error bars represent standard deviations. (**A**) and (**B**) show the changes in genes in MS and MF, respectively. The x-axis indicates the various exposure durations of 4 °C cold stress: 24 h (MS/MF 24 h) and 120 h (MS/MF 120 h).

3. Discussion

3.1. Distinct MS and MF Morphological and Physiological Changes in Response to Low-Temperature Stress

Under normal growth conditions, MF plants typically exhibit a shorter height, smaller overall size, and smaller leaves than MS, with a creeping stem lying close to the ground as opposed to the upright stems of MS. Following stress exposure, MF leaves appeared heathier than those of MS, suggesting that MS may be more susceptible to cold stress compared to MF. This observation aligns with that of previous studies indicating that alfalfa varieties characterized by a lower plant height, shorter leaf length, and reduced biomass tend to demonstrate enhanced cold-stress resistance [17–19].

Cold hardiness in plants involves intricate physiological mechanisms aimed at mitigating damage, including alterations in plasma membrane properties, up-regulation of ROS-scavenging enzymes, and augmentation of osmoregulatory mechanisms [20,21]. In this study, we investigated the physiological and metabolic changes in two alfalfa species before and after exposure to cold stress.

Comparisons between healthy MS and MF plants revealed lower MDA levels and higher SOD and SS levels in MF plants compared to MS plants under normal conditions. However, both species exhibited increases in MDA levels following 24 h and 120 h of exposure to 4 °C stress, indicating membrane damage. Remarkably, MF consistently maintained lower MDA levels than MS, suggesting superior antioxidant capacity in this species. Meanwhile, SOD levels initially rose then declined in both species, indicating activation of the defense system in response to cold stress, although the protective efficacy of defense enzymes appeared limited, consistent with previous reports [22]. In contrast, the SS content of both species showed an upward trend, and that of MF showed a more significant increase under cold stress, indicating that soluble sugars accumulated under cold stress, alleviating water deficit and enhancing cold resistance under cold stress, which is consistent with previous studies [23].

Furthermore, MF consistently exhibited higher levels of defense enzymes and osmoregulatory substances compared to MS following 24 h and 120 h of 4 °C exposure, while maintaining lower MDA levels. These observations underscore the superior cold resistance of MF compared to MS, corroborating findings from previous studies [24,25].

3.2. Transcriptome Analysis of MS Seedlings under Low-Temperature Stress

Alignment of reads to various reference genome features, including introns and intergenic regions, offered insights into dynamic gene-expression changes in MS and MF under low-temperature stress. The overall comparison rates between the materials selected in this study and the alfalfa reference genome ranged from 75.53% to 79.92%, likely due to the cold-region specificity of the plant material we used being produced at 45 degrees north latitude. In this study, we used the group with better reproducibility of PCA results as the main analysis object, and the other group as a reference. Next, we will further refine the mechanism of alfalfa resistance to cold at the transcriptional level and increase the biological and technical replicates to improve the quality of the data. Intron region alignments may have stemmed from residual pre-mRNA or intron retention during variable shearing, while alignments with intergenic regions may have resulted from the transcription of unknown genes or non-coding RNA, providing a basis for subsequent expression analyses.

In MS, 1274 genes exhibited continuous regulation under 120 h of cold stress. GO enrichment analyses of these genes revealed significant enrichment of antioxidant-related terms such as “oxidation-reduction process” and “peroxisome”, indicating the key role of antioxidants in MS resistance to cold stress, consistent with the observed elevated SOD values after low-temperature exposure. Additionally, GO terms like “protein phosphorylation”, “photosynthesis”, and “membrane” were significantly enriched, aligning with prior transcriptome sequencing analyses of alfalfa’s response to cold stress [26]. Among them, protein phosphorylation is able to directly cause Ca^{2+} signaling coupling to the cold-specific transduction pathway [27]; chloroplasts are the site of photosynthesis in plants, but low

temperature will destroy the chloroplast structure, reduce the chlorophyll content, and, thus, reduce the photosynthetic efficiency, which is also an important cause of plant yellowing [28]; the metabolic level of plants will change when they are subjected to cold stress, and the up-regulation of the expression of catalytic activity-related genes will solve this problem to a certain extent [29]; and membranes are the first to sense low-temperature stress and, in response to [30], plants resist cold stress by maintaining membrane homeostasis by maintaining the unsaturation of membranous substances during cold stress [31].

KEGG pathway analysis highlighted the significant involvement of the "Peroxisome" pathway in MS's cold-stress response, affirming the pivotal role of defense enzymes in MS cold-stress tolerance. Moreover, the significant enrichment of "Plant hormone signal transduction" underscores the central regulatory role of hormones in MS cold-stress responses [14], while other enriched pathways identified in this study corroborate previously reported findings, including "Isoflavonoid biosynthesis", "Circadian rhythm—plant", and "Glycerophospholipid metabolism". Among them, isoflavones have antioxidant properties and can scavenge ROS under cold stress [32]; CBF expression is regulated by the circadian clock through the action of a central oscillator and also by day length (photoperiod) [33]; and glycerophospholipids are the main components of the plasma membrane, which help to maintain plasma membrane fluidity and cell function under low-temperature stress [34].

Notably, in this study, a total of 78 transcription factors from 26 families were found in significantly expressed DEGs, including *RAP2-1*, *ABF2*, *TIFY6B*, *GATA8*, and *SPL16*, encoding TFs belonging to AP2-EREBP, bZIP, Tify, C2C2-GATA, and SBP TF families that exhibited high-level expression. *RAP2-1* encodes the ethylene-responsive TF *RAP2-1*, a downstream regulator of C-repeat binding factors (CBFs) [35] that has been validated as a classical cold-responsive gene transcript in soybean [36]. *ABF2* encodes bZIP TF 46, which acts as an ABA-responsive element with a crucial role in cold resistance of crops, including strawberries [37]. *TIFY6B*, a member of the plant-specific TIFY TF family of adversity response regulators, encodes *TIFY6B*. In chili peppers, *TIFY6B* acts as a cold-stress-responsive element with shared functions with TFs CaTIFY7 and CaTIFY10b, members of the same TF family, which have been reported to enhance plant cold tolerance by inducing the expression of cold stress-related genes and triggering the ROS response [38]. *GATA8*, encoding GATA TF 8, has also been implicated in the cold-stress responses of Arabidopsis and rice [39], further underscoring the multifaceted regulatory network involved in MS's response to cold stress.

3.3. Transcriptome Analysis of MF Seedlings under Low-Temperature Stress

A total of 2983 genes displayed continuous regulation during 120 h of cold stress. GO enrichment analysis revealed the significant enrichment of antioxidant-related terms such as "oxidoreductase complex", "peroxisome", and "peroxisomal part", highlighting the crucial role of antioxidants in MF cold-stress tolerance. Moreover, the enrichment of cell wall-related terms like "pectinesterase activity", "cell wall modification", and "cell wall" underscores the importance of the dynamic cell wall polysaccharide network in providing stability and protection to plants under cold-stress conditions. Pectin esterases, ubiquitous cell wall-associated enzymes, which play key roles in shaping cell wall mechanical properties and porosity through the demethylation of pectin [40], have also been implicated in stress responses [41].

Furthermore, MF genes were enriched for numerous KEGG pathway terms related to resistance to cold stress, including "Peroxisome", which involves defense enzymes, and "Plant hormone signal transduction", which involves genes associated with the synthesis of JA, ABA, gibberellins, oleoresin steroids, and cytokinins, thereby affirming the role of phytohormones in the abiotic-stress response. Additionally, the pathway terms "Isoflavonoid biosynthesis" and "Circadian rhythm—plant" were also significantly enriched, consistent with previous studies.

In MF, a total of 154 TFs belonging to 35 TF families with potential roles in the cold stress response were identified, with genes encoding members of the plant-specific AP2-

EREBP TF family (*DREB1A*, *ERF110*, *ABR1*, and *WRI1*) and the ARR-B family (*APRR1*) exhibiting notably high expression levels. The AP2-EREBP family is known for its roles in plant development and responses to diverse biological and environmental stresses [42]. For example, overexpression of *DREB1A*, which encodes DREB-like protein 1A (*DREB1A*), endows plants with an enhanced tolerance to salinity, cold, and drought stress [43]. Similarly, *ERF110*, which encodes the ethylene-responsive TF *ERF110*, is involved in the rye drought stress response [44]. Another notable gene, *ABR1*, encodes the ethylene-responsive TF *ABR1*, which acts as an ABA-responsive repressor in *Arabidopsis thaliana* that participates in responses to cold, high salt, and drought stress [45]. *WRI1* encodes a well-known TF that regulates crop seed oil biosynthesis [46] and the expression of nonspecific lipid transfer proteins in response to nematode infections [47]. Additionally, *APRR1* encodes the two-component response regulator *APRR1*, a well-known TF that participates in regulating circadian rhythms [48].

3.4. Comparison of the MS and MF Transcriptomes under Low-Temperature Stress

The ICE1-CBF-COR pathway is the most widely studied cold-stress signaling pathway, which activates the expression of CBF through INDUCER OF CBF EXPRESSION 1 (ICE1) binding to the promoter region of CBF gene under cold-stress conditions, thereby improving the frost resistance of plants, and the role of this pathway has been emphasized in the participation of wheat crops in abiotic-stress response [49]. In this study, we analyzed the differential genes of MS and MF, and we found that the cold-resistance process of the materials used in this experiment was related to ICE1-CBF-COR pathway. The MsG0380016999 gene encoding the transcription factor ICE1 isoform X1 was significantly up-regulated in both alfalfa species after 24 h of cold stress, and it remained up-regulated until 120 h of cold stress. In addition, MsG0480021424, encoding CBF5, was significantly up-regulated after MF was subjected to cold stress for 24 h. The results of this study are consistent with the results suggesting that the overexpression of the ICE1 and CBF genes can confer high cold tolerance in plants [50,51], indicating that the ICE1–CBF–COR pathway plays an important role in the process of cold-stress resistance in alfalfa, especially in MF.

Aquaporin is the main channel of water transport in plant cells, and abiotic stress dehydrates cells by changing the water potential; it has been shown that aquaporin actively participates in regulating plant stress resistance [52]. In this study, we identified four isoforms of aquaporin: plasma membrane intrinsic proteins (PIPs), tonoplast intrinsic proteins (TIPs), nodulin 26-like proteins (NIPs), and small basic intrinsic proteins (SIPs). MsG0180000871 and MsG0780041015, which regulate TIP1 and TIP4, were significantly down-regulated in MS and MF after cold stress, while SIP1, which is regulated by MsG0780040029 and MsG0680031712, continued to be significantly up-regulated in MF, which was consistent with the situation found in maize and rice seedlings [53,54]. In addition, we found that MsG0180000871 was significantly down-regulated in MF earlier than it was in MS, indicating that MF responded more quickly to cold stress than MS. We also found that MsG0580029158 and MsG0480020797, which regulate PIP1 and PIP2, respectively, were down-regulated after 120 h of cold stress in both alfalfa species. Western blot analysis confirmed that Arabidopsis PIP1; 4 and PIP2; 5 was specifically up-regulated during cold acclimation, thereby increasing protein mass and total pip [55]. Our results of this experiment are inconsistent, and we suspect that the plasma membranes of both alfalfa species may have been damaged due to prolonged low-temperature stress, thus affecting the gene function. Interestingly, differential expression of MsG0780036261 encoding NIP2 and MsG0380011693 was detected in both alfalfa species; the former has been down-regulated and the latter has been up-regulated, but MsG0780036261 has been down-regulated in MS and less so in MF. Studies have shown that CaNIP1-5 and CaNIP4-1 are highly expressed in the aerial tissues of chickpea after low-temperature stress [56]; Overexpression of the VvNIP gene in grapes improved cold resistance [57]. However, some studies have suggested that the down-regulated expression of CsNIP5 in tea plants under low-temperature stress may be related to the ABA-dependent osmotic stress response [58].

There has still been no research on alfalfa, and we prefer that NIP2 should be gradually up-regulated under cold stress, while the reason for the down-regulation of MsG0780036261 in this study remains to be investigated.

Statistical analysis revealed a significantly higher number of genes that were consistently significantly regulated under 120 h of cold stress in MF compared to MS, encompassing most identified MS cold-stress resistance genes. This finding suggests that MF exhibits greater cold resistance than MS.

While most pathways enriched in MS were also present in MF, the absence of the "Base excision repair" pathway in MF is noteworthy, given its crucial role in protecting genomes from damage caused by intrinsic and environmental factors [59]. Several pathways that are only significantly expressed in MF have been shown to be associated with cold stress, including "Steroid biosynthesis" [60], "Fatty acid degradation" [61], "Amino sugar and nucleotide sugar metabolism" [62], "Phenylpropanoid biosynthesis" [63], "Oxidative phosphorylation" [64], "DNA replication" [65], "Nucleocytoplasmic transport" [66], "alpha-Linolenic acid metabolism" [67], "Nucleotide excision repair" [59], "RNA polymerase" [68], "Betalain biosynthesis" [69], "Protein export" [70], "Basal transcription factors" [71], and "Endocytosis" [72], among others. Additionally, pathways such as "Stilbenoid, diarylheptanoid, and gingerol biosynthesis" have reported roles in drought and alkali stress responses [73,74]. The "Basal transcription factors" pathway encompasses TAF12B, which encodes a TF belonging to the plant-specific ARR-B TF family and is known for its reported pivotal roles in plant processes [75], including the regulation of plant root growth in *A. thaliana* [76]. These two pathways may also contribute to the cold-stress response in alfalfa. In addition, TFs belonging to the HB TF family, which have been shown to coordinate phytohormone production during biotic stress responses and mechanical injury in sunflower [77], responded consistently to cold stress only in MS but not in MF, prompting us to speculate that HB family member expression in MS may participate in abiotic-stress responses.

Intriguingly, BSD, CSD, E2F-DP, EIL, HSF, LIM, LOB, PLATZ, and Trihelix were exclusively represented in the DEGs of MF. Particularly noteworthy is the PLATZ family, consisting of plant-specific zinc-finger TFs pivotal for plant growth, development, and responses to abiotic stresses. Moreover, in alfalfa, members of the Trihelix TF family have been implicated in responses to salt, cold, and drought stress [78,79], whereas copper/zinc SOD (CSD) TFs have been shown to be induced by cold stress [80]. These discoveries collectively suggest the significant contributions of PLATZ, Trihelix, and CSD TF family members to the sustained MF response to cold stress. Regarding other TF families, research on BSD TFs suggests their involvement in plant growth and development, particularly in fruit ripening [81]. Similarly, adjacent E2F-DP TF sequences may contribute to glutathione transferase-related detoxification functions. Additionally, the EIL TF family plays a pivotal role in the ethylene signaling pathway, which governs various plant growth and developmental processes, and responds differentially to dehydration, salinity, and phosphate starvation in soybean [82], while Lin-11, Isl-1, and Mec-3 (LIM) domain TFs are crucial in regulating fundamental plant biological processes. Although these TF families have not been directly linked to cold-stress responses, our findings suggest that they contribute to MF abiotic-stress tolerance by sustaining the 120 h cold-stress response in this species. Heat shock TF (HSF) family members are vital in plant growth, development, and stress responses, as evidenced by their negative roles in maize salt and drought-stress responses [83]; in addition, their antagonistic effects on methyl jasmonate (MeJA)-induced cold tolerance in banana [84]. Therefore, HSF TFs likely play negative roles in various abiotic-stress responses that include a significant role in the MF response to cold stress.

In addition to the abovementioned genes, our study identified two novel genes encoding the MtN19-like and DUF1997 family proteins that displayed consistent up-regulation in response to cold stress. Additionally, the *GmSGT3* gene, encoding soyasaponin III rhamnosyltransferase, exhibited up-regulation in MF and down-regulation in MS under cold stress conditions. While the functions of the former two proteins remain unreported, *GmSGT3* expression has been linked to saponin accumulation in soybean [85]. Nevertheless, despite

their differential regulation in response to cold stress in MS and MF, they hold potential as cold-stress-responsive genes.

Collectively, our findings highlight the nuanced differences between MF and MS in their sustained response to cold stress. While members of the AP2-EREBP, ARR-B, and bHLH TF families were highly expressed in both species, other TFs identified in MS and MF cold-stress transcriptomes also played crucial roles in regulating MF and MS transcriptional cold-stress responses. Therefore, we hypothesize that members of these three TF families and other TF families play pivotal roles in sustaining cold resistance across alfalfa species beyond those investigated in this study.

4. Materials and Methods

4.1. Plant Materials and Stress Treatment

This research was conducted at the Institute of Forage and Grassland Sciences, Heilongjiang Academy of Agricultural Sciences, located in Harbin, China (longitude: 126.53°, latitude: 45.80°). MS and MF experimental materials were grown under controlled conditions that included a photoperiod of 16 h of light followed by 8 h of darkness and a temperature of 22 °C. At the three-leaf stage of growth, alfalfa seedlings were subjected to cold stress in an artificial climate incubator set to maintain a light-dark cycle of 16-h light/8-h dark and a temperature of 4 °C. Three treatment groups were established for both MS and MF seedlings, consisting of two cold treatment durations of 24 h and 120 h, along with a control group at 0 h. For each treatment group, three biological replicates were carried out. Subsequently, all seedlings were harvested simultaneously then seedlings were photographed.

4.2. Physiological Index Determination

In this study, changes in Malondialdehyde (MDA), Superoxide dismutase (SOD), and Soluble sugar (SS) levels served as indicators for assessing both the extent of cell membrane damage and the ability of plants to adapt to cold stress. A total of 120 seedlings (20 seedlings per replicate for each species) were collected for the physiological experiments, with all treatment groups harvested at corresponding time points.

MDA content was determined using an MDA assay kit (Suzhou Keming Biotechnology Co., Ltd., Suzhou, China). MDA was condensed with thiobarbituric acid (TBA) to form a red product with a maximum absorption peak at 532 nm, and the content of lipid peroxide in the sample could be estimated after color comparison. At the same time, the absorbance at 600 nm was measured, and the difference between the absorbance at 532 nm and 600 nm was used to calculate the MDA content.

SOD content was determined using an SOD assay kit (Suzhou Keming Biotechnology Co., Ltd., Suzhou, China). Superoxide anion (O^{2-}) is produced by xanthine and xanthine oxidase reaction system, and O^{2-} can reduce nitrogen blue tetrazolium to form blue formazan, which is absorbed at 560 nm. SOD can scavenge O^{2-}, thereby inhibiting the formation of formazan; The darker the blue color of the reaction solution, the lower the SOD activity, and the higher the activity.

SS content was determined using an SOD assay kit (Suzhou Keming Biotechnology Co., Ltd., Suzhou, China). Based on the anthone method, furfural or hydroxymethylfurfural is further condensed with anthone reagent to produce a blue-green substance, which has the maximum absorption at the wavelength of 620 nm in the visible region, and its light absorption value is proportional to the content of sugar within a certain range.

Each experiment was repeated at least three times. Data analysis involved the use of Shapiro-Wilk test and one-way ANOVA test in SPSS v26, respectively, and plotting of data using Origin v2021.

4.3. RNA Extraction and cDNA Library Construction

After extracting total RNA from the samples, rRNA was removed, mRNA was enriched, and double-stranded cDNA was synthesized through reverse transcription. Subse-

quently, double-stranded ends were repaired and ligated then the resulting ligated DNA products were amplified via PCR to construct the cDNA library. To ensure sequencing quality, we assessed RNA integrity and DNA contamination of samples using agarose gel electrophoresis. Additionally, we assessed RNA purity based on OD260/280 and OD260/230 ratios using a NanoPhotometer spectrophotometer. RNA concentration was precisely quantified using a Qubit 2.0 fluorometer, and RNA integrity was accurately assessed using an Agilent 2100 Bioanalyzer.

Next, we employed fastp software version 0.22.0 [86] for quality control of raw reads. Reads containing adapters and low-quality data were filtered out, including the following: reads containing adapter sequences, reads with more than 10% undetermined bases (N), reads consisting entirely of A bases, and reads with over 50% of bases having quality scores (Q) $\leq$ 20. Subsequently, the remaining short reads were aligned to internal reference genes using the bowtie2 alignment tool [87], while HISAT2 software version 2.2.1 [88] was employed to map the reads to the reference genome. The data were plotted using the R (http://www.r-project.org/, accessed on 24 April 2024) ggplot2

The data processed by the PCA package version 4.4.0 beta were divided into 6 groups (CK-MF, CK-MS, MF 120 h, MF 24 h, MS 120 h, MS 24 h), and the data were visualized with the ggplot2 package version 3.4.2. The Corrplot package version 0.94 is used for Pearson correlation analysis and outputs heat maps.

4.4. Analysis of DEGs

After reconstructing complete transcripts using StringTie, genes identified in the sequencing results that were not present in the reference genome or reference gene set were classified as novel genes.

For differential expression analysis, we utilized DESeq2 version 1.30.1 [89] software. The analysis was conducted in three steps: read count normalization, calculation of hypothesis testing probability values (*p*-values) based on the model, and determination of false-discovery rate (FDR) values through multiple hypothesis testing. Significant DEGs were identified using the following criteria: FDR < 0.05 and $|\log2FC| > \log2(2)$, where FC represents the fold change in expression. Statistical mapping of DEGs genes was performed using Excel, while Venny2.1 (https://bioinfogp.cnb.csic.es/tools/venny/index.html, accessed on 12 December 2023) was employed to assess the degree of coincidence among statistically significant DEGs.

4.5. GO and KEGG Enrichment Analyses

DEGs were annotated using the GO database (http://www.geneontology.org/, accessed on 12 December 2023) to determine the number of genes associated with each term and to perform GO function statistics. Subsequently, a hypergeometric test was employed to identify significantly enriched GO terms among the DEGs as compared to background. Visualization of the results included the generation of a histogram and a bubble map depicting GO enrichment classifications.

For pathway analysis, the KEGG database (https://www.genome.jp/kegg/, accessed on 12 December 2023) was utilized to assess pathway significance enrichment. Using KEGG pathways as the unit, a hypergeometric test was conducted to identify pathways significantly enriched among the DEGs as compared to the entire background. The results were visualized through a KEGG enrichment bar plot.

4.6. Validation of RNA-seq Data by Real-Time qRT-PCR (Quantitative RT-PCR)

DEGs identified using methods described above were validated using qRT-PCR. We screened genes expressed in both MS and MF, and randomly selected 6 genes with obvious up-regulation or down-regulation of expression after 24 h and 120 h of cold stress for RT-qPCR (*MsG0180005449*, *MsG0680035598*, *MsG0180001271*, *MsG0580027615*, *MsG0880046364* and *MsG0480023735*). *Medicago sativa* L. UBC2 and *Medicago sativa* L. TUB (GenBank accession no.L06967.1 and XM003630465) were used as internal reference genes

to investigate the gene-expression levels of MS and MF after 24 h and 120 h of cold stress. Primer sets were designed using Primer Premier v6.24 (https://www.premierbiosoft.com/primerdesign/ accessed on 18 December 2023) and are listed in Additional file: Table S12. Reactions were performed using the following conditions: denaturation at 95 °C for 30 s followed by 40 cycles of amplification (95 °C for 5 s, 60 °C for 34 s). All samples were tested in triplicate.

5. Conclusions

Both MS and MF displayed morphological changes in response to under 24-h and 120-h cold stress exposure. However MF exhibited superior resilience after 120 h, as evidenced by consistently lower levels of MDA and higher levels of SOD and SS. Also of note, MF demonstrated a greater increase in MF SS compared to MS after 24 h of cold stress.

Transcriptome analysis revealed 1274 and 2983 genes consistently regulated under 120 h of cold stress in MS and MF, respectively, with 923 genes shared between the two species. GO enrichment and KEGG analyses unveiled significant differences in genes responsive to cold stress between MS and MF. Particularly noteworthy was the enrichment of cell wall-related GO terms in MF, including "pectinesterase activity", "cell wall modification", and "cell wall", emphasizing the role of the cell wall in providing stability and protection during cold stress.

Furthermore, while MS exhibited one unique pathway and one TF family member compared to MF, MF showcased 14 pathways and 9 TF family members absent in MS. Regardless, the expression of AP2-EREBP, ARR-B, and bHLH TFs was notable in both species, suggesting their potential role in conferring sustained cold resistance across other alfalfa species.

In summary, our comparative analysis of MS and MF cold stress responses provides valuable insights into molecular mechanisms underlying cold resistance in alfalfa. These findings significantly contribute to our understanding of cold stress tolerance in alfalfa and have far-reaching implications for breeding and genetic improvement efforts in related species within the clover genus.

Supplementary Materials: The following supporting information can be downloaded at: https://www.mdpi.com/article/10.3390/ijms251910345/s1.

Author Contributions: Conceptualization, J.W. (Jianzhong Wu); Methodology, J.W. (Jianzhong Wu); Software, Q.W. and Q.Z.; Validation, W.H.; Formal analysis, G.D.; Investigation, C.G.; Resources, J.W. (Jianzhong Wu); Data curation, Q.W.; Writing—original draft preparation, Q.W. and J.W. (Jianli Wang); Writing—review and editing, J.W. (Jianli Wang); Visualization, D.Z. and J.W. (Jianli Wang); Supervision, J.W. (Jianzhong Wu); Project administration, Z.S.; Funding acquisition, W.H. All authors have read and agreed to the published version of the manuscript.

Funding: This research was funded by the Science and Technology Innovation 2030-Major Project (2022ZD040120403).

Informed Consent Statement: Not applicable.

Data Availability Statement: Data is contained within the article and Supplementary Materials.

Conflicts of Interest: The authors declare no conflict of interest.

References

1. Huang, X.Z.; Lei, L.; Qiang, X.J.; Meng, Y.F.; Li, Z.Y.; Huang, F. Integrated Metabolomic and Transcriptomic Profiles Provide Insights into the Mechanisms of Anthocyanin and Carotenoid Biosynthesis in Petals of *Medicago sativa* ssp. Sativa and *Medicago sativa* ssp. Falcata. *Plants* **2024**, *13*, 700. [CrossRef] [PubMed]
2. Riday, H.; Charles, E.C.; Brummer; Moore, K.J. Heterosis of Forage Quality in Alfalfa. *Crop Sci.* **2002**, *42*, 1088–1093. [CrossRef]
3. Dong, W.K.; Ma, X.; Zhou, X.W.; Lu, X.P.; Wang, J.; He, J.; Wang, Y.; Ma, H.L. Effects of Exogenous Glycine Betaine on the Physiological Characteristics in *Medicago sativa* Seedlings under Low-Temperature Stress. *Acta Agrestia Sin.* **2019**, *27*, 130.

4. Heino, P.; Palva, E.T. Signal transduction in plant cold acclimation. In *Plant Responses to Abiotic Stress*; Springer: Berlin/Heidelberg, Germany, 2004.
5. Sharma, P.; Sharma, N.; Deswal, R. The Molecular Biology of the Low-Temperature Response in Plants. *BioEssays* **2005**, *27*, 1048–1059. [CrossRef]
6. Ara, N.; Nakkanong, K.; Yang, J.H.; Hu, Z.Y.; Zhang, M.F. Dissecting the Heat Stress-Induced Alterations in the Leaf Ultrastructure and Some Antioxidant Network Components in Interspecific (*Cucurbita maxima* × *Cucurbita moschata*) Inbred Line of Squash 'Maxchata' as to Its Parents Possessing Variable Heat Tolerance. *Plant Growth Regul.* **2015**, *76*, 289–301. [CrossRef]
7. Kim, K.Y. Molecular Cloning of Low-Temperature-Inducible Ribosomal Proteins from Soybean. *J. Exp. Bot.* **2004**, *55*, 1153–1155. [CrossRef]
8. Zhang, X.; Yang, H.; Li, M.; Bai, Y.; Chen, C.; Guo, D.; Guo, C.; Shu, Y. A Pan-Transcriptome Analysis Indicates Efficient Downregulation of the FIB Genes Plays a Critical Role in the Response of Alfalfa to Cold Stress. *Plants* **2022**, *11*, 3148. [CrossRef] [PubMed]
9. Zhao, W.; Song, J.; Wang, M.; Chen, X.; Du, B.; An, Y.; Zhang, L.; Wang, D.; Guo, C. Alfalfa MsATG13 Confers Cold Stress Tolerance to Plants by Promoting Autophagy. *Int. J. Mol. Sci.* **2023**, *24*, 12033. [CrossRef]
10. Zhang, L.L.; Zhao, M.G.; Tian, Q.Y.; Zhang, W.H. Comparative studies on tolerance of *Medicago truncatula* and *Medicago falcata* to freezing. *Planta* **2011**, *234*, 445–457. [CrossRef]
11. Wu, J.B. Research Progress on the Mechanism of Alfalfa Cold Resistance during Overwintering Period. *Agric. For. Fish.* **2015**, *4*, 300.
12. Zhu, J.K. Abiotic Stress Signaling and Responses in Plants. *Cell* **2016**, *167*, 313–324. [CrossRef] [PubMed]
13. Kanchupati, P.; Wang, Y.; Anower, M.R.; Boe, A.; Hu, T.; Wu, Y. The CBF-like gene family in alfalfa: Expression analyses and identification of potential functional homologs of Arabidopsis CBF3. *Crop Sci.* **2017**, *57*, 2051–2063. [CrossRef]
14. Zhang, S.; Shi, Y.; Cheng, N.; Du, H.; Fan, W.; Wang, C. De novo characterization of fall dormant and nondormant alfalfa (*Medicago sativa* L.) leaf transcriptome and identification of candidate genes related to fall dormancy. *PLoS ONE* **2015**, *10*, e0122170. [CrossRef] [PubMed]
15. Song, L.; Jiang, L.; Chen, Y.; Shu, Y.; Bai, Y.; Guo, C. Deep-sequencing transcriptome analysis of field-grown *Medicago sativa* L. crown buds acclimated to freezing stress. *Funct. Integr. Genom.* **2016**, *16*, 495–511. [CrossRef]
16. Zhang, T.; Chen, X.; Yan, W.; Li, M.; Huang, W.; Liu, Q.; Li, Y.; Guo, C.; Shu, Y. Comparative Analysis of Chloroplast Pan-Genomes and Transcriptomics Reveals Cold Adaptation in Medicago sativa. *Int. J. Mol. Sci.* **2024**, *25*, 1776. [CrossRef]
17. Brouwer, D.J.; Duke, S.H.; Osborn, T.C. Comparison of Seedling and Cuttings for Evaluating Winter Hardiness in Alfalfa. *Crop Sci.* **1998**, *38*, 1704–1707. [CrossRef]
18. Cunningham, S.M.; Volenec, J.J. Seasonal Carbohydrate and Nitrogen Metabolism in Roots of Contrasting Alfalfa (*Medicago sativa* L.) Cultivars. *J. Plant Physiol.* **1998**, *153*, 220–225. [CrossRef]
19. Schwab, P.M.; Barnes, D.K.; Sheaffer, C.C.; Li, P.H. Factors Affecting a Laboratory Evaluation of Alfalfa Cold Tolerance. *Crop Sci.* **1996**, *36*, 318–324. [CrossRef]
20. Korn, M.; Gärtner, T.; Erban, A.; Kopka, J.; Selbig, J.; Hincha, D.K. Predicting Arabidopsis Freezing Tolerance and Heterosis in Freezing Tolerance from Metabolite Composition. *Mol. Plant* **2010**, *3*, 224–235. [CrossRef]
21. Wang, X.C.; Zhao, Q.Y.; Ma, C.L.; Zhang, Z.H.; Cao, H.L.; Kong, Y.M.; Yang, Y.J. Global transcriptome profiles of *Camellia sinensis* during cold acclimation. *BMC Genom.* **2013**, *14*, 415. [CrossRef]
22. Tao, Y.; Sun, Q.Z. Dynamic variation of soluble sugar, tota l nitrogen and malondialdehyde in different alfalfa varieties and their effect on alfalfa's cold resistance. *Zhongguo Nongye Keji Daobao (J. Agric. Sci. Technol.)* **2008**, *10* (Suppl. S1), 56–60.
23. Zhao, Y.G.; Wu, Q.L.; Xu, L.R.; Peng, Q.Q. Changes of cold herdiness of yellow alfalfa and alfalfa in cool season. *Grassl. China* **1986**, *30*, 15–18. (In Chinese)
24. Pennycooke, J.C.; Cheng, H.M.; Stockinger, E.J. Comparative Genomic Sequence and Expression Analyses of *Medicago truncatula* and Alfalfa Subspecies *falcata COLD-ACCLIMATION-SPECIFIC* Genes. *Plant Physiol.* **2008**, *146*, 1242–1254. [CrossRef]
25. Zhang, Y.; Tan, J.; Guo, Z.; Lu, S.; He, S.; Shu, W.; Zhou, B. Increased abscisic acid levels in transgenic tobacco over-expressing 9 cis-epoxycarotenoid dioxygenase influence H_2O_2 and NO production and antioxidant defences. *Plant Cell Environ.* **2009**, *32*, 509–519. [CrossRef]
26. Shu, Y.J.; Li, W.; Zhao, J.Y.; Zhang, S.J.; Xu, H.Y.; Liu, Y.; Guo, C.H. Transcriptome Sequencing Analysis of Alfalfa Reveals CBF Genes Potentially Playing Important Roles in Response to Freezing Stress. *Genet. Mol. Biol.* **2017**, *40*, 824–833. [CrossRef]
27. Monroy, A.F.; Sarhan, F.; Dhindsa, R.S. Cold-Induced Changes in Freezing Tolerance, Protein Phosphorylation, and Gene Expression (Evidence for a Role of Calcium). *Plant Physiol.* **1993**, *102*, 1227–1235. [CrossRef] [PubMed]
28. Li, Y.; Zhu, J.; Xu, J.; Zhang, X.; Xie, Z.; Li, Z. Effect of cold stress on photosynthetic physiological characteristics and molecular mechanism analysis in cold-resistant cotton (ZM36) seedlings. *Front. Plant Sci.* **2024**, *15*, 1396666. [CrossRef]
29. Yu, L.; Dai, Z.; Zhang, Y.; Iqbal, S.; Lu, S.; Guo, L.; Yao, X. Proteome-wide identification of S-sulfenylated cysteines reveals metabolic response to freezing stress after cold acclimation in Brassica napus. *Front. Plant Sci.* **2022**, *13*, 1014295. [CrossRef] [PubMed]
30. Bowler, C.; Montagu, M.V.; Inze, D. Superoxide dismutase and stress tolerance. *Ann. Rev. Plant Physiol. Plant Mol. Biol* **1992**, *43*, 83–116. [CrossRef]

31. Zhang, D.; Zhang, Z.; Li, C.; Xing, Y.; Luo, Y.; Wang, X.; Li, D.; Ma, Z.; Cai, H. Overexpression of MsRCI2D and MsRCI2E Enhances Salt Tolerance in Alfalfa (*Medicago sativa* L.) by Stabilizing Antioxidant Activity and Regulating Ion Homeostasis. *Int. J. Mol. Sci.* **2022**, *23*, 9810. [CrossRef]
32. Posmyk, M.M.; Bailly, C.; Szafrańska, K.; Janas, K.M.; Corbineau, F. Antioxidant Enzymes and Isoflavonoids in Chilled Soybean (*Glycine max* (L.) Merr.) Seedlings. *J. Plant Physiol.* **2005**, *162*, 403–412. [CrossRef] [PubMed]
33. Maibam, P.; Nawkar, G.; Park, J.; Sahi, V.; Lee, S.; Kang, C. The Influence of Light Quality, Circadian Rhythm, and Photoperiod on the CBF-Mediated Freezing Tolerance. *Int. J. Mol. Sci.* **2005**, *14*, 11527–11543. [CrossRef] [PubMed]
34. Li, Z.S.; He, F.; Tong, Z.Y.; Li, X.L.; Yang, Q.C.; Hannaway, D.B. Metabolomic Changes in Crown of Alfalfa (*Medicago sativa* L.) during De-Acclimation. *Res. Sq.* **2022**, *12*, 14977. [CrossRef] [PubMed]
35. Zhou, M.Q.; Shen, C.; Wu, L.H.; Tang, K.X.; Lin, J. CBF-Dependent Signaling Pathway: A Key Responder to Low Temperature Stress in Plants. *Crit. Rev. Biotechnol.* **2010**, *31*, 186–192. [CrossRef] [PubMed]
36. Yamasaki, Y.; Randall, S.K. Functionality of Soybean CBF/DREB1 Transcription Factors. *Plant Sci.* **2016**, *246*, 80–90. [CrossRef]
37. Shen, J.C.; Liu, J.; Yuan, Y.G.; Chen, L.X.; Ma, J.X.; Li, X.; Li, J.M. The Mechanism of Abscisic Acid Regulation of Wild *Fragaria* Species in Response to Cold Stress. *BMC Genom.* **2022**, *23*, 670. [CrossRef]
38. Wang, X.; Li, N.; Zan, T.; Xu, K.; Gao, S.; Yin, Y.; Wang, F. Genome-wide analysis of the TIFY family and function of *CaTIFY7* and *CaTIFY10b* under cold stress in pepper (*Capsicum annuum* L.). *Front. Plant Sci.* **2023**, *14*, 1308721. [CrossRef]
39. Edrisi, M.K.; Farrokhi, N.; Samizadeh, L.H. Cold-responsive transcription factors in Arabidopsis and rice: A regulatory network analysis using array data and gene co-expression Network. *PLoS ONE* **2023**, *18*, e0286324. [CrossRef]
40. Goldberg, R.; Pierron, M.; Bordenave, M.; Breton, C.; Morvan, C.; Du Penhoat, C.H. Control of Mung Bean Pectinmethylesterase Isoform Activities: INFLUENCE of PH and CARBOXYL GROUP DISTRIBUTION along the PECTIC CHAINS. *J. Biol. Chem.* **2001**, *276*, 8841–8847. [CrossRef]
41. Phan, T.D.; Bo, W.; West, G.; Lycett, G.W.; Tucker, G.A. Silencing of the Major Salt-Dependent Isoform of Pectinesterase in Tomato Alters Fruit Softening. *Plant Physiol.* **2007**, *144*, 1960–1967. [CrossRef]
42. Riechmann, J.L.; Meyerowitz, E.M. The AP2/EREBP family of plant transcription factors. *Biol. Chem.* **1998**, *379*, 633–646. [PubMed]
43. Reuscher, S.; Akiyama, M.; Mori, C.; Aoki, K.; Shibata, D.; Shiratake, K. Genome-wide identification and expression analysis of aquaporins in tomato. *PLoS ONE* **2013**, *8*, e79052. [CrossRef] [PubMed]
44. Cheng, S.B.; Yang, X.Z.; Zou, L.; Wu, D.D.; Lu, J.L.; Cheng, Y.R.; Zhang, H.Q. Comparative physiological and root transcriptome analysis of two annual ryegrass cultivars under drought stress. *J. Plant Physiol.* **2022**, *277*, 153807. [CrossRef]
45. Pandey, G.K.; Grant, J.J.; Cheong, Y.H.; Kim, B.G.; Li, L.; Luan, S. ABR1, an APETALA2-Domain Transcription Factor That Functions as a Repressor of ABA Response in Arabidopsis. *Plant Physiol.* **2005**, *139*, 1185–1193. [CrossRef]
46. Kong, Q.; Yang, Y.; Guo, L.; Yuan, L.; Ma, W. Molecular Basis of Plant Oil Biosynthesis: Insights Gained from Studying the WRINKLED1 Transcription Factor. *Front. Plant Sci.* **2020**, *11*, 24. [CrossRef]
47. Song, X.; Li, E.; Song, H.; Du, G.; Li, S.; Zhu, H.; Sui, J. Genome-Wide Identification and Characterization of Nonspecific Lipid Transfer Protein (NsLTP) Genes in Arachis Duranensis. *Genomics* **2020**, *112*, 4332–4341. [CrossRef]
48. Kim, J.A.; Yang, T.J.; Kim, J.S.; Park, J.Y.; Kwon, S.J.; Lim, M.H.; Park, B.S. Isolation of Circadian-Associated Genes in Brassica Rapa by Comparative Genomics with Arabidopsis Thaliana. *Mol. Cells* **2007**, *23*, 145–153. [CrossRef] [PubMed]
49. Shi, Y.; Ding, Y.; Yang, S. Molecular Regulation of CBF Signaling in Cold Acclimation. *Trends Plant Sci.* **2018**, *23*, 623–637. [CrossRef]
50. Zuo, Z.F.; Kang, H.G.; Park, M.Y.; Jeong, H.; Sun, H.J.; Song, P.S.; Lee, H.Y. Zoysia japonica MYC type transcription factor ZjICE1 regulates cold tolerance in transgenic Arabidopsis. *Plant Sci. Int. J. Exp. Plant Biol.* **2019**, *289*, 110254. [CrossRef]
51. Skinner, J.S.; von Zitzewitz, J.; Szucs, P.; Marquez-Cedillo, L.; Filichkin, T.; Amundsen, K.; Stockinger, E.J.; Thomashow, M.F.; Chen, T.H.; Hayes, P.M. Structural, functional, and phylogenetic characterization of a large CBF gene family in barley. *Plant Mol. Biol.* **2005**, *59*, 533–551. [CrossRef]
52. Cheng, G.; Wang, M.; Zhang, L.; Wei, H.; Wang, H.; Lu, J.; Yu, S. Overexpression of a Cotton Aquaporin Gene *GhTIP1;1-like* Confers Cold Tolerance in Transgenic Arabidopsis. *Int. J. Mol. Sci.* **2022**, *23*, 1361. [CrossRef]
53. Zeng, R.; Zhang, X.; Song, G.; Lv, Q.; Li, M.; Fu, D.; Zhang, Z.; Gao, L.; Zhang, S.; Yang, X.; et al. Genetic variation in the aquaporin TONOPLAST INTRINSIC PROTEIN 4;3 modulates maize cold tolerance. *Plant Biotechnol. J.* 2024; *early view*. [CrossRef]
54. Miao, M.; Shi, X.; Zheng, X.; Wu, B.; Miao, Y. Characterization of SIPs-type aquaporins and their roles in response to environmental cues in rice (*Oryza sativa* L.). *BMC Plant Biol.* **2023**, *24*, 305. [CrossRef]
55. Rahman, A.; Kawamura, Y.; Maeshima, M.; Rahman, A.; Uemura, M. Plasma Membrane Aquaporin Members PIPs Act in Concert to Regulate Cold Acclimation and Freezing Tolerance Responses in Arabidopsis thaliana. *Plant Cell Physiol.* **2020**, *61*, 787–802. [CrossRef]
56. Deokar, A.A.; Tar'an, B. Genome-Wide Analysis of the Aquaporin Gene Family in Chickpea (*Cicer arietinum* L.). *Front. Plant Sci.* **2016**, *7*, 1802. [CrossRef]
57. Wu, Z.; Lu, S.X.; Ren, J.X. Genome-wide identification and expression analysis of the NlP gene family in grape. *Acta Bot.* **2021**, *41*, 1457–1466. (In Chinese)
58. Yue, C.; Cao, H.L.; Wang, Z. Cloning and expression analysis of aquaporin protein genes in tea pant (*Camellia sinensis*). *Acta Bot.* **2018**, *38*, 1419–1427. (In Chinese)

59. Córdoba-Cañero, D.; Morales-Ruiz, T.; Roldán-Arjona, T.; Ariza, R.R. Single-Nucleotide and Long-Patch Base Excision Repair of DNA Damage in Plants. *Plant J.* **2009**, *60*, 716–728. [CrossRef]
60. Xia, X.H.; Hao, L.L.; Sun, Y.F.; Lv, Y.Q.; Wang, Y.H.; Wu, H.Y.; Jiang, Z.J.; Li, X.R.; Yan, Y.H.; Chen, X.J.; et al. Unravelling Chilling-Stress Resistance Mechanisms in Endangered Mangrove Plant *Lumnitzera littorea* (Jack) Voigt. *Mar. Environ. Res.* **2023**, *192*, 106210. [CrossRef]
61. Wang, Y.; Wang, J.; Sarwar, R.; Geng, R.; Zhu, K.M.; Tan, X.L. Research progress on the physiological response and molecular mechanism of cold response in plants. *Front. Plant Sci.* **2024**, *15*, 1334913. [CrossRef]
62. Lin, M.; Sun, S.; Fang, J.; Qi, X.; Sun, L.; Zhong, Y.; Sun, Y.; Hong, G.; Wang, R.; Li, Y. BSR-Seq analysis provides insights into the cold stress response of Actinidia arguta F1 populations. *BMC Genom.* **2021**, *22*, 72. [CrossRef]
63. Li, D.; Lin, H.Y.; Wang, X.; Bi, B.; Gao, Y.; Shao, L.; Zhang, R.; Liang, Y.; Yang, Y.; Zhao, Y.P.; et al. Genome and whole-genome resequencing of Cinnamomum camphora elucidate its dominance in subtropical urban landscapes. *BMC Biol.* **2023**, *21*, 192. [CrossRef]
64. Liang, G.; Ma, Z.; Lu, S.; Ma, W.; Feng, L.; Mao, J.; Chen, B. Temperature-Phase Transcriptomics Reveals That Hormones and Sugars in the Phloem of Grape Participate in Tolerance during Cold Acclimation. *Plant Cell Rep.* **2022**, *41*, 1357–1373. [CrossRef]
65. Qu, Z.; Jia, Y.; Duan, Y.; Chen, H.; Wang, X.; Zheng, H.; Liu, H.; Wang, J.; Zou, D.; Zhao, H. Integrated Isoform Sequencing and Dynamic Transcriptome Analysis Reveals Diverse Transcripts Responsible for Low Temperature Stress at Anther Meiosis Stage in Rice. *Front. Plant Sci.* **2021**, *12*, 795834. [CrossRef]
66. Sinha, V.B.; Grover, A.; Singh, S.; Pande, V.; Ahmed, Z. Overexpression of Ran Gene from *Lepidium latifolium* L. (LlaRan) Renders Transgenic Tobacco Plants Hypersensitive to Cold Stress. *Mol. Biol. Rep.* **2014**, *41*, 5989–5996. [CrossRef]
67. Bertin, P.N.; Michotey, V.; Normand, P. Contributions of descriptive and functional genomics to microbial ecology. In *Environmental Microbiology: Fundamentals and Applications: Microbial Ecology*; Springer: Dordrecht, The Netherlands, 2015; pp. 831–846.
68. Yun, S.; Zhang, X. Genome-wide identification, characterization and expression analysis of AGO, DCL, and RDR families in Chenopodium quinoa. *Sci. Rep.* **2023**, *13*, 3647. [CrossRef]
69. Feng, Y.; Yan, X.; Guo, F.; Wang, S.; Liu, Z.; Long, W. Identification, Expression Analysis of Quinoa Betalain Biosynthesis Genes and Their Role in Seed Germination and Cold Stress. *Plant Signal. Behav.* **2023**, *18*, 2250891. [CrossRef]
70. John, A.; Krämer, M.; Lehmann, M.; Kunz, H.H.; Aarabi, F.; Alseekh, S.; Fernie, A.; Sommer, F.; Schroda, M.; Zimmer, D.; et al. Degradation of Fatty Acid Export Protein1 by Rhomboid-like Protease11 Contributes to Cold Tolerance in Arabidopsis. *BioRxiv (Cold Spring Harb. Lab.)* **2023**, *36*, 1937–1962. [CrossRef]
71. Ma, L.; Coulter, J.A.; Liu, L.; Zhao, Y.; Chang, Y.; Pu, Y.; Zeng, X.; Xu, Y.; Wu, J.; Fang, Y.; et al. Transcriptome Analysis Reveals Key Cold-Stress-Responsive Genes in Winter Rapeseed (*Brassica rapa* L.). *Int. J. Mol. Sci.* **2019**, *20*, 1071. [CrossRef]
72. Zhao, T.; Wu, T.; Zhang, J.; Wang, Z.; Pei, T.; Yang, H.; Li, J.; Xu, X. Genome-Wide Analyses of the Genetic Screening of C_2H_2-Type Zinc Finger Transcription Factors and Abiotic and Biotic Stress Responses in Tomato (*Solanum lycopersicum*) Based on RNA-Seq Data. *Front. Genet.* **2020**, *11*, 540. [CrossRef]
73. Jiao, Y.; Xie, R.J.; Jia, H.M. Identification of Potential Pathways of Morella Cerifera Seedlings in Response to Alkali Stress via Transcriptomic Analysis. *Plants* **2022**, *11*, 1053. [CrossRef]
74. Qian, H.; Xu, Z.; Cong, K.; Zhu, X.; Zhang, L.; Wang, J.; Wei, J.; Ji, P. Transcriptomic responses to drought stress in *Polygonatum kingianum* tuber. *BMC Plant Biol.* **2021**, *21*, 537. [CrossRef]
75. Yue, C.; Chen, Q.; Hu, J.; Li, C.; Luo, L.; Zeng, L. Genome-Wide Identification and Characterization of *GARP* Transcription Factor Gene Family Members Reveal Their Diverse Functions in Tea Plant (*Camellia sinensis*). *Front. Plant Sci.* **2022**, *13*, 947072. [CrossRef]
76. Kim, J.S.; Sakamoto, Y.; Takahashi, F.; Shibata, M.; Urano, K.; Matsunaga, S.; Yamaguchi-Shinozaki, K.; Shinozaki, K. *Arabidopsis* TBP-ASSOCIATED FACTOR 12 Ortholog NOBIRO6 Controls Root Elongation with Unfolded Protein Response Cofactor Activity. *Proc. Natl. Acad. Sci. USA* **2022**, *119*, e2120219119. [CrossRef]
77. Manavella, P.A.; Dezar, C.A.; Bonaventure, G.; Baldwin, I.T.; Chan, R.L. HAHB4, a sunflower HD-Zip protein, integrates signals from the jasmonic acid and ethylene pathways during wounding and biotic stress responses. *Plant J.* **2008**, *56*, 376–388. [CrossRef]
78. Li, X.; He, F.; Zhao, G.; Li, M.; Long, R.; Kang, J.; Yang, Q.; Chen, L. Genome-Wide Identification and Phylogenetic and Expression Analyses of the PLATZ Gene Family in *Medicago sativa* L. *Int. J. Mol. Sci.* **2023**, *24*, 2388. [CrossRef]
79. Li, K.; Fan, Y.; Zhou, G.; Liu, X.; Chen, S.; Chang, X.; Wu, W.; Duan, L.; Yao, M.; Wang, R.; et al. Genome-wide identification, phylogenetic analysis, and expression profiles of trihelix transcription factor family genes in quinoa (*Chenopodium quinoa* Willd.) under abiotic stress conditions. *BMC Genom.* **2022**, *23*, 499. [CrossRef]
80. Chen, Y.; Jiang, J.; Song, A.; Chen, S.; Shan, H.; Luo, H.; Gu, C.; Sun, J.; Zhu, L.; Fang, W.; et al. Ambient temperature enhanced freezing tolerance of *Chrysanthemum dichrum* CdICE1 Arabidopsis via miR398. *BMC Biol.* **2013**, *11*, 121. [CrossRef]
81. Ba, L.J.; Shan, W.; Zhao, Y.Y.; Chen, J.Y.; Lu, W.J.; Kuang, J.F. A Ripening-Induced Transcription Factor MaBSD1 Interacts with Promoters of MaEXP1/2 from Banana Fruit. *Plant Cell Rep.* **2014**, *33*, 1913–1920. [CrossRef]
82. Li, Q.; Shen, Y.; Guo, L.; Wang, H.; Zhang, Y.; Fan, C.; Zheng, Y. The *EIL* Transcription Factor Family in Soybean: Genome-Wide Identification, Expression Profiling and Genetic Diversity Analysis. *FEBS Open Bio* **2019**, *9*, 629–942. [CrossRef]
83. Wang, J.; Chen, L.; Long, Y.; Si, W.; Cheng, B.; Jiang, H. A Novel Heat Shock Transcription Factor (ZmHsf08) Negatively Regulates Salt and Drought Stress Responses in Maize. *Int. J. Mol. Sci.* **2021**, *22*, 11922. [CrossRef]
84. Ba, L.J.; Kuang, J.F.; Chen, J.Y.; Lu, W.J. MaJAZ1 attenuates the MaLBD5-mediated transcriptional activation of jasmonate biosynthesis gene MaAOC2 in regulating cold tolerance of banana fruit. *J. Agric. Food Chem.* **2016**, *64*, 738–745. [CrossRef]

85. Yano, R.; Takagi, K.; Tochigi, S.; Fujisawa, Y.; Nomura, Y.; Tsuchinaga, H.; Takahashi, Y.; Takada, Y.; Kaga, A.; Anai, T.; et al. Isolation and Characterization of the Soybean Sg-3 Gene That Is Involved in Genetic Variation in Sugar Chain Composition at the C-3 Position in Soyasaponins. *Plant Cell Physiol.* **2018**, *59*, 797–810. [CrossRef]
86. Chen, S.F.; Zhou, Y.Q.; Chen, Y.R.; Gu, J. Fastp: An Ultra-Fast All-In-One FASTQ Preprocessor. *Bioinformatics* **2018**, *34*, 1884–1890. [CrossRef]
87. Krumpelman, C.; Ghosh, J. Matching and Visualization of Multiple Overlapping Clusterings of Microarray Data. In Proceedings of the 2017 IEEE Symposium on Computational Intelligence and Bioinformatics and Computational Biology, Honolulu, HI, USA, 1–5 April 2007; IEEE: Piscataway Township, NY, USA, 2007. [CrossRef]
88. Kim, D.; Langmead, B.; L Salzberg, S. HISAT: A Fast Spliced Aligner with Low Memory Requirements. *Nat. Methods* **2015**, *12*, 357–360. [CrossRef]
89. Love, M.I.; Huber, W.; Anders, S. Moderated Estimation of Fold Change and Dispersion for RNA-Seq Data with DESeq2. *Genome Biol.* **2014**, *15*, 550. [CrossRef]

Disclaimer/Publisher's Note: The statements, opinions and data contained in all publications are solely those of the individual author(s) and contributor(s) and not of MDPI and/or the editor(s). MDPI and/or the editor(s) disclaim responsibility for any injury to people or property resulting from any ideas, methods, instructions or products referred to in the content.

International Journal of
Molecular Sciences

MDPI

Review

Harnessing the Potential of CRISPR/Cas in Targeted Alfalfa Improvement for Stress Resilience

Shugao Fan [1], Linyan Jia [2], Jiawei Wu [1] and Ying Zhao [1,*]

[1] School of Hydraulic and Civil Engineering, Ludong University, Yantai 264025, China; 3455@ldu.edu.cn (S.F.); wjw2097046621@163.com (J.W.)
[2] School of Resources and Environmental Engineering, Ludong University, Yantai 264025, China; j1251546376@163.com
* Correspondence: yzhao@ldu.edu.cn

Abstract: Alfalfa (*Medicago sativa*), recognized as the most valuable legume feed crop, faces significant challenges in enhancing both qualitative and quantitative production amidst the pressures of climate change. This review highlights these challenges, including the underutilization of genomic and genetic resources, while proposing potential solutions through genome editing. Our focus is on leveraging CRISPR/Cas technology in conjunction with decades of advancements in conventional breeding to expedite the improvement of alfalfa. By adopting this approach, we aim to overcome the limitations of traditional alfalfa improvement approaches and accelerate the development of improved cultivars capable of thriving in changing climates. Key candidate traits for CRISPR/Cas genome editing, as reviewed in the latest literature, include nutrient use efficiency, freezing tolerance, and resistance to pests and diseases. We dissect literature on potential gene pathways associated with these traits, providing molecular breeders with valuable insights for utilizing CRISPR/Cas genome editing. Furthermore, we propose editing modalities to expedite the development of stress-resilient, genome-edited alfalfa that can effectively cope with climate change.

Keywords: climate change; genome editing; abiotic stress; plant breeding

1. Introduction

Alfalfa is a perennial legume with promising economic prospects due to its versatile applications across multiple industries [1]. Primarily valued as a high-quality forage crop, alfalfa serves as a critical feed source for various livestock, contributing significantly to the profitability of the animal agriculture sector [2]. Its ability to fix nitrogen enriches soil fertility, reducing dependency on costly synthetic fertilizers and enhancing overall agricultural sustainability [3]. Additionally, alfalfa's adaptability extends to biofuel production, erosion control, and soil remediation efforts, amplifying its economic significance beyond traditional agricultural practices [4]. With increasing demand for nutritious animal feed and sustainable farming solutions, alfalfa remains a lucrative crop with ample opportunities for growth and innovation.

Like most crops, sustainable alfalfa improvement must be addressed from a climate change viewpoint with adoption of more effective technology. Genome editing holds significant potential to revolutionize alfalfa breeding by offering precise and targeted genetic modifications to improve desirable traits and address various challenges [5]. CRISPR genome editing accelerates the breeding process by enabling rapid, precise, and predictable genetic modifications without the need for traditional breeding methods. For example,

molecular breeders can use CRISPR to enhance traits such as yield, quality, stress tolerance, pest resistance, and nutrient efficiency, leading to the development of improved alfalfa cultivars. Technically breeders can introduce new functionalities, such as enhanced disease resistance, improved nutritional quality, or altered growth habits, by precisely engineering the alfalfa genome using CRISPR technology. Through a knockout approach CRISPR can be used to reduce or eliminate antiquality factors in alfalfa, such as lignin content or alkaloid levels, which can negatively impact forage digestibility and livestock performance [6].

2. Leveraging Genomic Resources for Alfalfa CRISPR Editing

Alfalfa exhibits significant intra-species genetic diversity [7]. This genetic heterogeneity complicates the breeding of polygenic traits like biomass yield, persistence, and disease resistance, leading to variability in trait expression and unpredictable outcomes in breeding crosses [8]. Conventional crop improvement strategies often struggle with this complexity, limiting predictable trait improvements. Advances in high-throughput sequencing, such as next-generation and long-read sequencing, have produced valuable genomic resources for alfalfa, including high-quality reference genomes, transcriptomic profiles, and detailed genetic maps [9]. These datasets provide crucial insights into the structure, organization, and function of the alfalfa genome, aiding in the identification of genes associated with important agronomic traits. CRISPR-mediated editing can exploit these resources by enabling the precise modification of key regulatory and coding regions, enhancing the efficiency of trait introgression and gene pyramiding in breeding programs. QTL mapping and genome-wide association studies (GWASs) have played critical roles in dissecting the genetic architecture of traits such as forage yield, persistence, and tolerance to biotic and abiotic stresses [10–12]. By combining CRISPR genome editing with QTL and GWAS data, we can validate candidate genes, introduce beneficial alleles, and fine-tune the expression of genes controlling key agronomic traits. This strategy overcomes the limitations of traditional marker-assisted selection (MAS), allowing for precise gene editing and faster phenotypic improvements [13]. Despite the availability of draft genome sequences, gaps in alfalfa's genome assembly and incomplete functional annotation remain significant obstacles to fully understanding the molecular mechanisms underlying important traits [14].

Further, integrating CRISPR genome editing with omics-based approaches, such as transcriptomics, proteomics, and metabolomics, will accelerate the identification of key metabolic pathways and regulatory networks controlling complex traits in alfalfa. This integrative approach will enable the fine-mapping of genotype–phenotype associations, the elucidation of gene-to-trait relationships, and the prioritization of candidate genes for breeding targets. The application of CRISPR-driven functional validation will not only enhance our understanding of the alfalfa genome but also aid in refining genome assemblies and improving the annotation of non-coding regulatory elements (Figure 1).

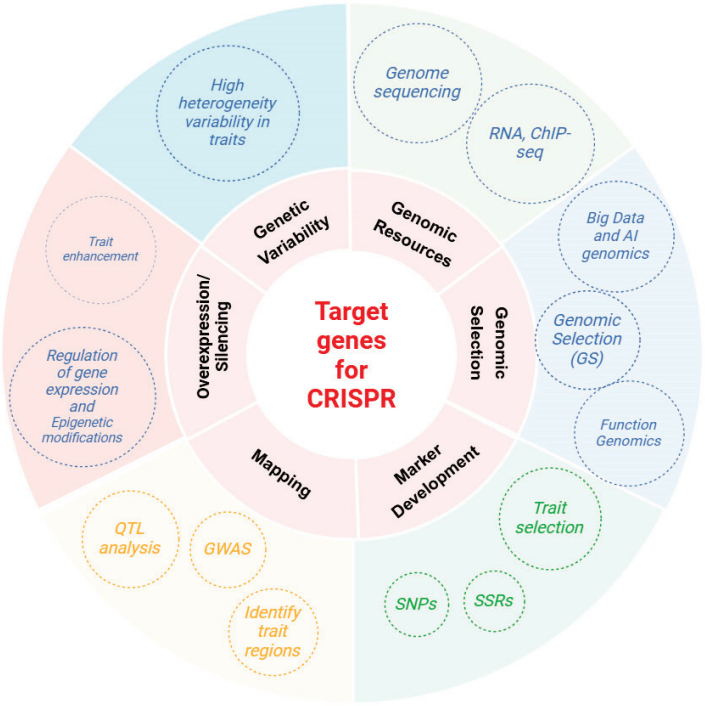


Figure 1. Overview of genomic pathways for alfalfa trait enhancement: integrating gene overexpression, genetic variability, genomic resources, and marker development to identify target genes for CRISPR.

3. Examples of CRISPR Target Traits and Editing Modalities

3.1. Knockout of Biotic Stress Tolerance Genes

Alfalfa is susceptible to a wide range of diseases and pests, which can significantly reduce yield and forage quality, leading to substantial economic losses for growers. Common pathogens include alfalfa mosaic virus, root rot, anthracnose, bacterial wilt, and various leaf spot diseases, while pests such as aphids, leafhoppers, and alfalfa weevils exacerbate crop damage [15,16]. Climate variability and shifting weather patterns further complicate disease and pest dynamics, making management efforts more unpredictable and challenging [17]. Breeding for resistance or tolerance to these biotic stresses is therefore critical for developing resilient alfalfa cultivars. However, this goal is challenging due to the complex host–pathogen interactions and the diversity of pathogens affecting alfalfa [18]. The application of CRISPR/Cas genome editing allows researchers to directly manipulate specific genes implicated in host defense mechanisms, thus bypassing the limitations of conventional breeding. For example, *AtEFR*, which confers resistance to bacterial wilt, and the lactoferrin gene, associated with resistance to bacterial stem blight, represent promising targets for CRISPR-mediated enhancement of disease resistance [19,20]. QTL mapping and gene discovery efforts have uncovered genes linked to resistance against *Phytophthora* root rot and *Aphanomyces* root rot, two of the most damaging root diseases in alfalfa [21,22]. These genes, particularly those with broad-spectrum resistance, are ideal candidates for CRISPR/Cas editing to develop cultivars with enhanced resistance. Functional genomics studies, such as the overexpression of *MtRAM2* resulting in increased susceptibility to *Phytophthora* root rot, provide further insights into potential susceptibility genes that can be targeted for knockout using CRISPR to mitigate vulnerability [23]. Research into the genetic basis of resistance to iron deficiency chlorosis and other abiotic stresses is also ongoing, with genes such as those identified by Zamboni [24] being potential targets for genome editing.

3.2. Multiplexing Towards Abiotic Stress Tolerance

Achieving abiotic stress tolerance in alfalfa while maintaining high yield and forage quality is a significant challenge due to the broad range of environmental conditions under which it is cultivated [25]. Traits such as stress tolerance, yield stability, and forage quality are all influenced by the interaction between genotype, environment, and management practices [26]. To ensure stable productivity, alfalfa must perform consistently across diverse climates and soils, making it essential to breed for broad adaptability. The challenge is to breed cultivars that can withstand abiotic stress while maintaining the high nutritional standards required by livestock producers [27]. The real potential of CRISPR lies in its ability to perform multiplex genome editing. Multiplex gene editing enables the simultaneous modification of multiple loci [28]. This is particularly valuable for polygenic traits like disease resistance, where multiple genes and pathways often contribute to the phenotype. One of the major challenges in breeding alfalfa for abiotic stress tolerance lies in the need to balance multiple traits simultaneously.

Multiplexing allows for the simultaneous modification of multiple genes, which is essential for addressing the polygenic nature of abiotic stress tolerance. Many abiotic stress responses in plants are governed by complex gene networks that regulate processes such as osmotic balance, stress signaling, and antioxidant defense. These networks involve numerous genes, each playing a role in the plant's ability to tolerate various stresses. With multiplex CRISPR editing, breeders can target multiple key genes across these networks in a single step, thereby accelerating the development of stress-tolerant cultivars.

Drought tolerance, for example, is a highly complex trait influenced by several physiological mechanisms, including stomatal regulation, water use efficiency, and root architecture. These processes are influenced by signaling pathways such as the MAPK and Ca^{2+} signaling pathways, the ABA-mediated signaling pathway, and key transcription factors (TFs) like MYB, WRKY, ERF, NAC, and bZIP [29]. Similarly, cold tolerance in alfalfa involves genetic pathways that regulate the plant's ability to mitigate oxidative stress and prevent cellular damage during freezing temperatures. This includes the Ca^{2+} signaling pathway and the cold-regulated (COR), inducer of CBF expression (ICE), and C-repeat binding factor (CBF) genes, which play crucial roles in cold acclimation and freezing tolerance. Recent research has identified genes linked to freezing tolerance, such as those involved in the reactive oxygen species (ROS) pathway and osmotic regulation [30]. Using multiplex CRISPR editing, these genes can be simultaneously modified to enhance cold hardiness without compromising other agronomic traits such as yield potential. Additionally, proteomic studies have identified proteins involved in heat stress adaptation, presenting further targets for multiplex editing to improve heat tolerance in alfalfa [31].

Another significant advantage of multiplex genome editing is the ability to improve broad-spectrum abiotic stress tolerance [32]. By simultaneously targeting key genes across different stress response pathways, breeders can develop cultivars with improved resistance to multiple stresses, including drought (DREB, AREB, PP2C, SnRK2), heat (Hsf, HSPs), cold (CBF, COR, ICE, LOS), and salinity (NHX, SOS1, HKT, AVP1). This broad-spectrum tolerance is essential for crops like alfalfa, which are cultivated across regions with highly variable climatic conditions. For example, germplasm evaluations have identified sources of drought tolerance, salinity resistance, and cold hardiness in wild relatives of alfalfa [33].

In addition to its applications in multiplex genome editing, CRISPR can be integrated with other advanced breeding techniques, such as genomic selection and marker-assisted breeding. Genomic selection leverages prediction models that combine genomic data with phenotypic information to estimate genomic estimated breeding values (GEBVs) for traits such as stress tolerance and yield stability [34]. By incorporating CRISPR-mediated edits into these models, breeders can accelerate the selection of individuals with optimal

trait combinations, reducing the reliance on extensive field trials. This integration of CRISPR with genomic selection enhances the efficiency of breeding programs by rapidly introgressing stress resistance alleles into elite breeding lines [35]. Moreover, the use of high-throughput phenotyping platforms can further streamline the selection process in alfalfa breeding programs. These platforms enable the rapid assessment of plant performance under various stress conditions, allowing breeders to screen large populations for desirable traits. When combined with CRISPR's precision, this high-throughput approach enhances the ability to select plants with superior stress tolerance and high yield potential.

CRISPR/Cas genome editing, particularly in its multiplex form, represents a powerful tool for overcoming the challenges associated with breeding alfalfa for abiotic stress tolerance. By enabling precise and simultaneous modifications of multiple genes, CRISPR allows breeders to address the polygenic nature of stress responses, leading to cultivars with improved resilience, yield stability, and forage quality. The integration of multiplex genome editing with advanced breeding technologies such as genomic selection further enhances the efficiency of breeding programs, paving the way for the development of alfalfa cultivars that can thrive in increasingly unpredictable environmental conditions.

3.3. Editing for Nutrient Uptake Efficiency

Fertilizer usage efficiency is a critical target trait for any crop improvement program [36]. While alfalfa can fix atmosphere nitrogen to meet its high production demands, optimum germination requires an initial fertilizer supply [37]. Plant nutrition should primarily focus on three critical nutrients: nitrogen (N), phosphorus (P), and potassium (K). Ensuring adequate levels of N, P, and K in the soil is crucial for optimizing crop yield and quality [38]. The nitrogen transporter *NRT1.1* gene serves as an auxin carrier that reduces auxin levels in the lateral root apex to limit lateral root extension in nitrogen-deficient soil [39]. In another study, it was reported that this process occurs upstream of the *ANR1* gene, which initiated a signaling cascade that promoted lateral root elongation towards the high-nitrogen zone in the rhizosphere [40,41]. Nitrogen deficiency in the soil like that caused by salt and drought causes the root to produce C-terminally encoded peptides (CEPs), which are transported to the shoot via the xylem and are recognized by two leucine-rich repeat (LRR) receptor kinases, CEP Receptor 1 and 2 (CEPR1/2) [42]. This causes the upregulation of Downstream1 and 2 (CEPD1/2), which are carried to the roots and foster nitrogen uptake by upregulating the high-affinity N transporter gene *NRT2.1* in nitrogen-deficient tissue [43].

Surprisingly, there is evidence demonstrating close relationships between nitrogen and phosphate (Pi) signaling to influence plant physiological and developmental processes [44,45]. The *GRAS* family transcription factor gene *HRS1* and its paralog *HHO1* have been shown to be transcriptionally induced by N but post-translationally regulated by Pi deficiency before coordinating a N-dependent primary root response to Pi deficiency [44]. Evidence also suggests that N and K signaling interact. For example, low K inhibits primary root growth, which is dependent on NH_4^+ [46]. Another N-K interaction aspect emerges in the control of lateral root branching. It was demonstrated that low nitrogen levels can effectively reduce secondary lateral root development driven by K deficiency [47]. An analysis of root systems in mutants deficient in genes known to be involved in K and N transport and/or signaling reveals that the N transporter *NTR1.1/NPF6.3* and the K channel *AKT1* play critical roles in this root response [47]. Also, *CIPK23* was shown to play a connective role that integrates N and K signals to control lateral root development via phosphorylation of *NTR1.1* and *AKT1* [47]. These observations incorporating N-P-K at the genetic level are important starting points in genome editing toward improved fertilizer uptake efficiency (Figure 2).

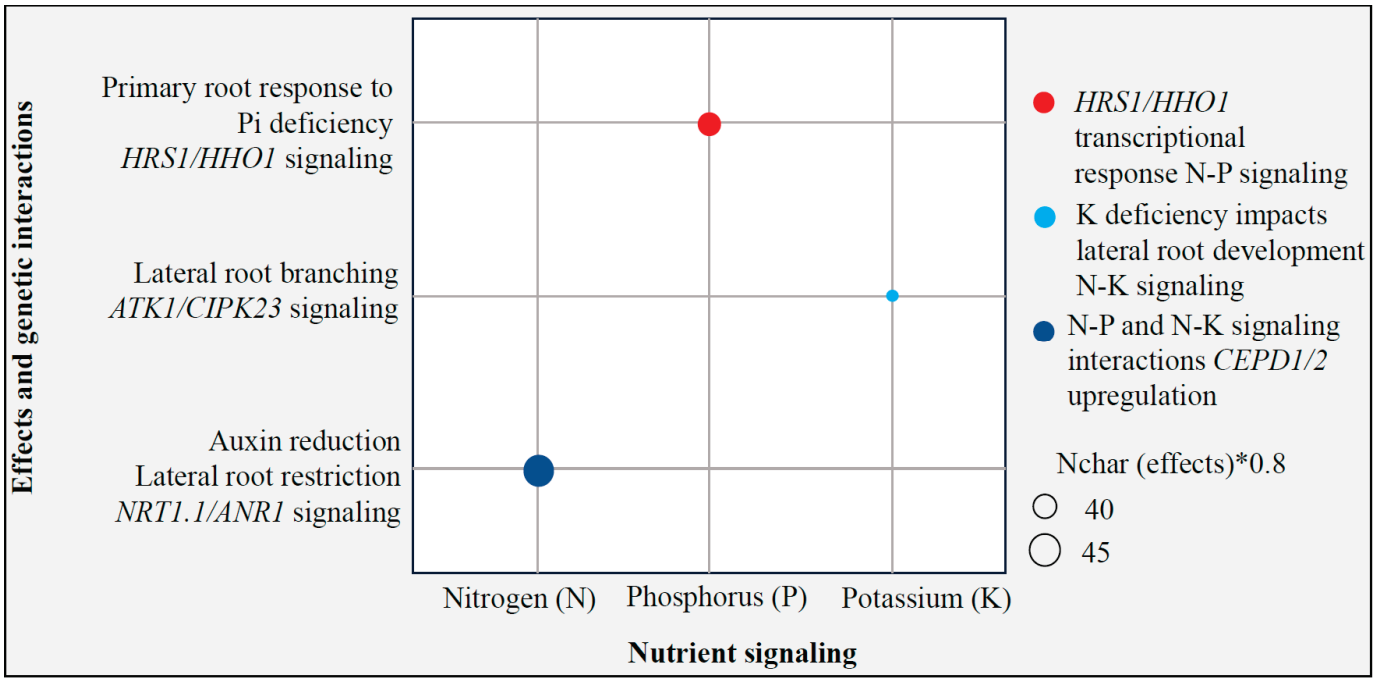


Figure 2. Bubble plot showing transcriptional regulation of N and P uptake to indicate that target genes for fertilizer uptake efficiency lie within the signal perception, transduction, and response mechanism to low N and P.

In the context of enhancing fertilizer use efficiency through nutrient signaling and uptake, several genes have emerged as promising targets for CRISPR-mediated genome editing. One such target is *NRT1.1* (*NPF6.3*), a nitrogen transporter involved in auxin transport and lateral root development, especially under nitrogen-deficient conditions. Editing this gene could improve nitrogen uptake and optimize root architecture in nitrogen-poor soils, potentially boosting crop performance in low-fertilizer environments. Another key candidate is *NRT2.1*, which plays a vital role in high-affinity nitrogen uptake. Enhancing its expression or modifying its nitrogen affinity could significantly increase nitrogen uptake efficiency, providing plants with better access to this essential nutrient [48].

Beyond nitrogen-related genes, the *AKT1* potassium channel is crucial for potassium transport within roots [49]. CRISPR editing of *AKT1* could enhance potassium uptake and strengthen plant resilience to potassium deficiency, ultimately improving overall fertilizer use efficiency. Additionally, the *HRS1* gene, which regulates plant responses to phosphate (Pi) deficiency, is a promising target. Its interaction with nitrogen signaling suggests that editing *HRS1* could optimize plant responses to both nitrogen and phosphorus deficiencies, promoting nutrient uptake and root growth [50]. Finally, the *CIPK23* gene integrates signals from nitrogen and potassium to regulate root development. Modifying *CIPK23* could fine-tune the plant's nutrient response, leading to increased crop yields and reduced reliance on excessive fertilizer inputs. Collectively, these targeted genetic modifications could pave the way for more efficient and sustainable agricultural practices (Figure 3).

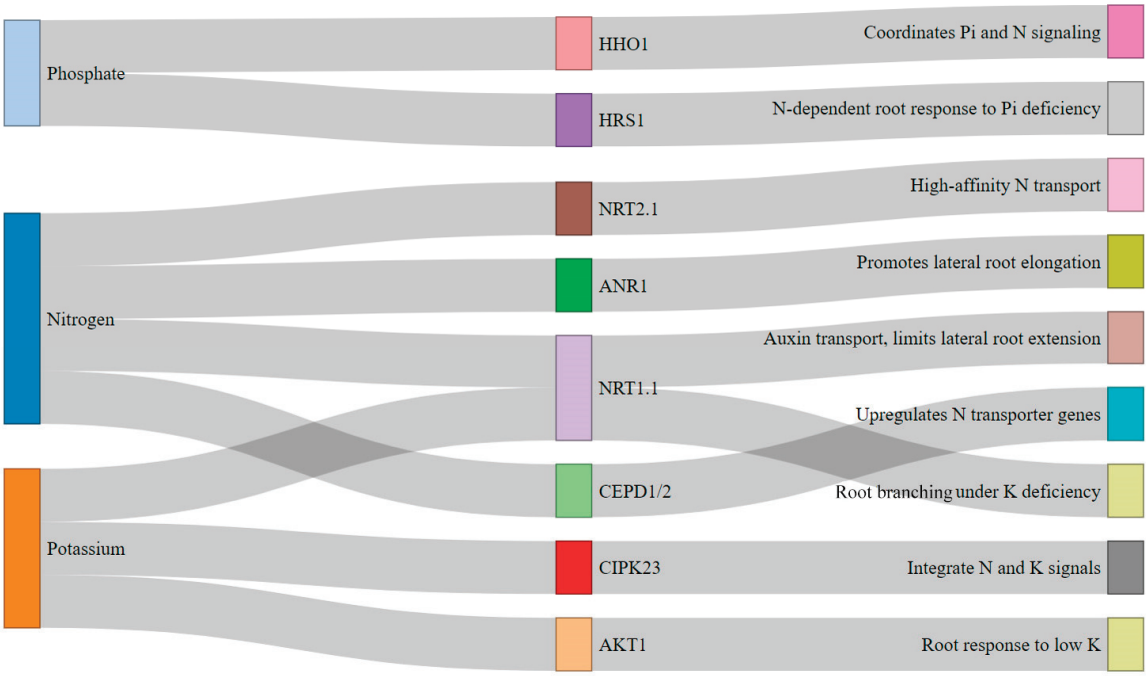


Figure 3. Alluvial plot showing pathways for modulating nitrogen, phosphate, and potassium signaling pathways: Key genes and their expected outcomes in root development and nutrient uptake in *Medicago sativa* (alfalfa). Key genes include Homeodomain leucine zipper protein 1 (*HHO1*), High-affinity phosphate transporter 1 (*HRS1*), Nitrate transporter 2.1 (*NRT2.1*), AUXIN RESPONSE FACTOR 1 (*ANR1*), Nitrate transporter 1 (*NRT1.1* 1), CEP domain-containing proteins 1 and 2 (*CEPD1/2*), CBL-interacting protein kinase 23 (*CIPK23*), and Arabidopsis potassium channel 1 (*AKT1*).

3.4. Antinutrient-Free Knockouts

Antinutrients are naturally occurring compounds found in plants that can interfere with nutrient absorption or digestion, potentially causing negative health effects. Alfalfa has antinutrients that cause foamy bloating in livestock [8]. Foamy bloating with alfalfa was associated with a high amount of saponin when ingested by both humans and livestock [51]. Together with other soluble proteins, when saponins are released into the stomach, they reduce smooth muscle activity, thereby reducing food mobility. This reduces the rumen digesta passage rate and may directly reduce or stop the eructation reflex [52]. Saponin biosynthesis requires three critical enzymes: oxidosqualene cyclases, which generate the basic triterpenoid skeletons; cytochrome P450 monooxygenases, which mediate oxidations; and uridine-diphosphate-dependent glycosyltransferases, which catalyze glycosylations [53]. In *Platycodon grandifloras*, the cytochrome P450 monooxygenase CYP716A141 was implicated in the biosynthesis of triterpenoid saponins [54]. Manipulation of saponin biosynthesis using RNAi revealed that β-amyrin synthase gene *BAS1* was positively involved in saponin biosynthesis in soybean as silenced lines were almost devoid of saponins without any other phenotypic penalties. Through a GWAS, the Sg-1 glycosyltransferase locus was found to regulate structural diversity of triterpenoid saponins of soybean [55]. Also, the biosynthesis of DDMP saponins in soybean is regulated by a distinct UDP-glycosyltransferase [56]. These findings pin-point key CRISPR KO to eliminate or reduce saponins without phenotypic penalties (Figure 4). Also, CRISPR-mediated genome editing enables the introduction of genetic changes that enhance alfalfa's resistance to diseases.

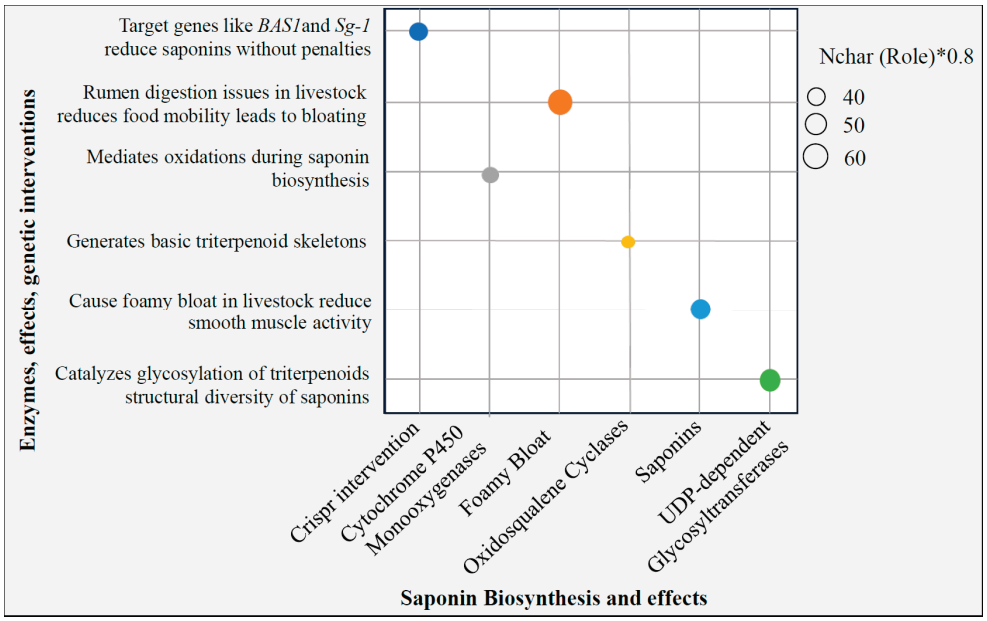


Figure 4. Bubble chart representing the CRISPR and Enzymatic Interventions in Saponin Biosynthesis: Targeting Genes, Enzyme Roles, and Their Effects on Livestock Health and Saponin Diversity. The different bubble colors represent distinct functional categories related to saponin biosynthesis and its effects.

4. Technical Bottlenecks and Advances in CRISPR/CAS Application in Alfalfa

Alfalfa (*Medicago sativa*) is characterized by a large and complex genome, presenting significant challenges for CRISPR-mediated genome editing [57]. Its polyploid nature, featuring multiple copies of each chromosome, complicates the precise targeting and editing of specific gene copies, resulting in potential off-target effects and unintended mutations [58]. The efficiency of CRISPR-mediated genome editing in alfalfa can vary based on the delivery method and the efficacy of introducing editing components into plant cells [59]. Conventional delivery methods, such as Agrobacterium-mediated transformation and particle bombardment, may face limitations in efficiency and scalability, particularly in large-scale editing endeavors [60]. Many agronomically important traits in alfalfa—including yield, forage quality, and stress tolerance—are governed by complex interactions among multiple genes [61]. The editing of these traits via CRISPR may necessitate the concurrent targeting of multiple genes or the modification of regulatory elements, which presents both technical and logistical hurdles. Alfalfa transformation typically relies on tissue culture techniques for the regeneration of whole plants from transformed cells. However, the recalcitrance of alfalfa tissue culture often results in the unavailability of efficient regeneration protocols for all genotypes or species, thus constraining the applicability of CRISPR across diverse genetic backgrounds [62].

Additionally, alfalfa genomes frequently harbor gene families with functional redundancy, wherein multiple genes can perform analogous functions [63]. Targeting a single gene within such a redundant family may not produce the desired phenotype due to compensatory mechanisms involving other family members. Consequently, the editing of multiple genes simultaneously may be essential to achieve specific trait modifications [64]. Addressing these challenges will require ongoing research and innovation in CRISPR technology, alongside advancements in alfalfa transformation protocols, genome sequencing, and bioinformatics tools (Figure 5). Current methodologies have incorporated helper genes, such as Wuschel2, and ultraistic plasmids to enhance editing efficiency. The authors of [65,66] detail comprehensive procedures for generating a non-homologous end-joining-

derived indel at a specific genomic locus in alfalfa utilizing CRISPR/Cas9. This method includes critical steps such as guide RNA design, binary CRISPR vector construction, Agrobacterium-mediated transformation of alfalfa explants, and molecular assessment of transformed genotypes for transgene integration and editing confirmation.

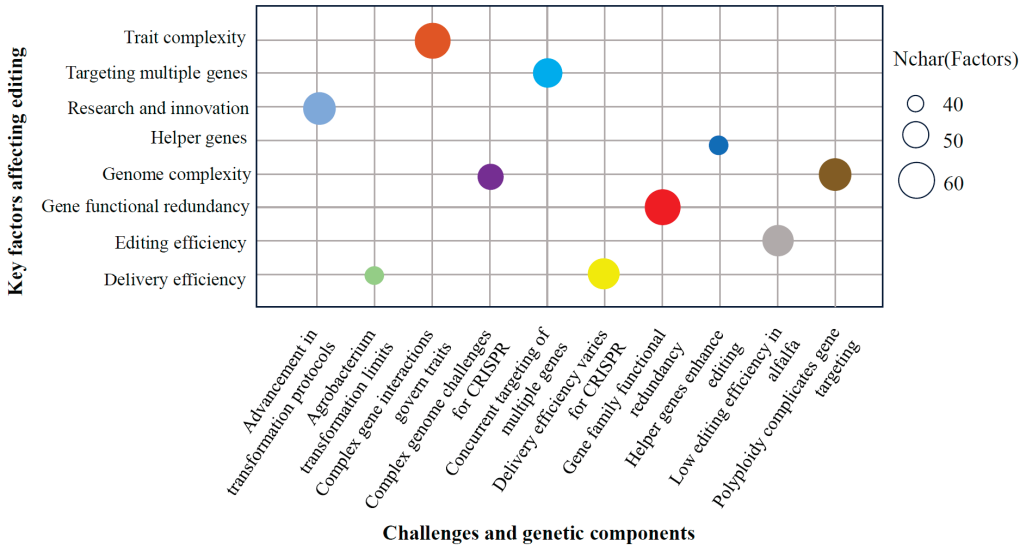


Figure 5. Bubble plot showing bottlenecks and advances in CRISPR genome editing in alfalfa. Different bubble colors represent various categories of challenges and genetic components influencing CRISPR efficiency, such as genome complexity, gene functional redundancy, and editing or delivery efficiency.

Despite these challenges, several breakthroughs have been achieved in alfalfa genome editing. Gao [67] successfully applied the CRISPR/Cas9 technique to induce mutations in the squamosa promoter-binding protein-like 9 (SPL9) gene in alfalfa. Due to the genome's complexity, they initially employed droplet digital PCR (ddPCR) for high-throughput screening of large populations of CRISPR-modified plants. Based on the genome editing rates obtained from ddPCR, plants with relatively high editing rates underwent further analysis through restriction enzyme digestion and PCR amplification. The resulting PCR products, encompassing the specific small, guided RNA target locus, were subcloned and sequenced to confirm successful genome editing. This successful application of the CRISPR/Cas9 system to edit the SPL9 gene within a multiplex genomic context provides valuable insights into the future application of this technology in alfalfa improvement. Nonetheless, the overall editing efficiency observed in the polyploid alfalfa genome was lower compared to that in less complex plant genomes, necessitating further refinement of CRISPR methodologies for enhanced genome editing efficacy in this species.

Wolabu [68] constructed multiplex gRNA-CRISPR/Cas9 vectors employing a polycistronic tRNA-gRNA approach targeting the *Medicago sativa stay-green* (*MsSGR*) gene. They demonstrated that substituting the CaMV35S promoter with the Arabidopsis ubiquitin promoter (*AtUBQ10*) to drive Cas9 expression in the multiplex gRNA system significantly enhanced genome editing efficiency. This optimized multiplex system achieved a genotypic mutagenesis efficiency of 75%, representing a 30-fold increase over single gRNA vectors. Importantly, phenotypic changes were readily observable in the mutants, with a phenotypic mutation efficiency of 68%. This highly efficient multiplex gRNA-CRISPR/Cas9 genome editing system enabled the generation of homozygous mutants with complete knockout of the four allelic copies in the T0 generation, effectively overcoming a major barrier to the utilization of genome editing for alfalfa improvement.

Subsequently, they investigated the potential for delaying flowering in alfalfa through multiplex CRISPR/Cas9-mediated mutagenesis of *FLOWERING LOCUS Ta1* (*MsFTa1*), a key floral integrator and activator gene. Four guide RNAs (gRNAs) were designed and clustered within a polycistronic tRNA-gRNA framework, which was then introduced into alfalfa via Agrobacterium-mediated transformation. Ninety-six putative mutant lines were identified through gene sequencing and characterized for delayed flowering time and associated desirable agronomic traits. Phenotypic assessment under long-day conditions revealed 22 independent mutant lines exhibiting delayed flowering compared to controls. Six independent MsFTa1 lines, harboring mutations in all four alleles of MsFTa1, displayed significantly enhanced forage biomass yields—up to a 78% increase in fresh weight and 76% in dry weight—relative to controls. Additionally, many of these lines exhibited reduced lignin, acid detergent fiber (ADF), and neutral detergent fiber (NDF) content, alongside significantly elevated crude protein (CP) and mineral contents, particularly in stem tissues.

Recently, Wolabu [69] demonstrated that mutating the *COUMARATE 3-HYDROXYLASE* gene in alfalfa using multiplex CRISPR/Cas9 leads to reduced lignin deposition and improved forage quality. These advancements underscore the potential of CRISPR technology for enhancing genetic improvement in alfalfa, facilitating the development of cultivars with superior traits for sustainable agricultural practices.

5. Conclusion and Future Perspectives

CRISPR/Cas genome editing presents a transformative approach for enhancing alfalfa breeding by precisely targeting genes involved in nutrient signaling and abiotic stress tolerance. Key genes like *AKT1*, *NRT1.1*, and *ANR1* can be edited to improve nutrient uptake efficiency and root development, optimizing alfalfa's adaptability to nutrient-deficient environments. Additionally, CRISPR's ability to fine-tune gene expression through targeted knockouts, such as those in promoter regions of *NRT2.1* and *NRT2.2*, offers a sophisticated method to enhance nitrogen uptake without completely disabling the gene. Furthermore, targeting genes like *CIPK23* and *HRS1* could boost the plant's resilience to potassium and phosphate deficiencies. Future research should focus on expanding beyond these targets to explore broader gene networks and utilize high-throughput phenotyping for novel gene discovery. As CRISPR techniques evolve, compliance with regulatory standards will be essential to enable the commercialization of CRISPR-modified alfalfa with enhanced stress tolerance, nutrient efficiency, and productivity.

An important consideration in the application of CRISPR/Cas genome editing is the potential risk of gene flow from cultivated alfalfa to its wild relatives. While gene-edited crops generally present a lower risk of unintended traits compared to traditional genetically modified crops, the possibility of gene transfer remains a concern, particularly for traits related to biotic and abiotic stress tolerance. Gene flow could potentially provide unintended advantages to wild populations, leading to ecological imbalances. To mitigate this risk, strategies such as isolation distances, containment measures, and ongoing monitoring are essential to limit the spread of edited traits. Furthermore, regulatory frameworks should be established to ensure responsible gene editing practices in alfalfa, including thorough environmental impact assessments. By adopting these precautionary measures, the benefits of CRISPR/Cas technology can be maximized while minimizing ecological risks.

Author Contributions: Conceptualization, Y.Z.; investigation, S.F. and L.J.; writing—original draft preparation, S.F. and J.W.; writing—review and editing, S.F. and Y.Z.; visualization, S.F.; supervision, Y.Z.; project administration, Y.Z.; funding acquisition, Y.Z. All authors have read and agreed to the published version of the manuscript.

Funding: This research was funded by Key Program of the National Natural Science Foundation of China for International Cooperation, grant number 42320104006.

Institutional Review Board Statement: Not applicable.

Informed Consent Statement: Not applicable.

Data Availability Statement: No new data were created or analyzed in this study. Data sharing is not applicable to this article.

Conflicts of Interest: The authors declare no conflicts of interest.

References

1. Soto-Zarazúa, M.G.; Bah, M.; Costa, A.S.G.; Rodrigues, F.; Pimentel, F.B.; Rojas-Molina, I.; Rojas, A.; Oliveira, M.B.P.P. Nutraceutical potential of new alfalfa (*Medicago sativa*) ingredients for beverage preparations. *J. Med. Food* **2017**, *20*, 1039–1046. [CrossRef] [PubMed]
2. Hadidi, M.; Orellana Palacios, J.C.; McClements, D.J.; Mahfouzi, M.; Moreno, A. Alfalfa as a sustainable source of plant-based food proteins. *Trends Food Sci. Technol.* **2023**, *135*, 202–214. [CrossRef]
3. Bouton, J. The economic benefits of forage improvement in the United States. *Euphytica* **2007**, *154*, 263–270. [CrossRef]
4. Fan, S.; Chen, J.; Mu, J.; Zhang, M. Genetic diversity and salt tolerance assessment of 51 alfalfa (*Medicago sativa*) varieties under saline soil conditions. *Front. Sustain. Food Syst.* **2023**, *7*, 1278913. [CrossRef]
5. Saini, H.; Thakur, R.; Gill, R.; Tyagi, K.; Goswami, M. CRISPR/Cas9-gene editing approaches in plant breeding. *GM Crops Food* **2023**, *14*, 1–17. [CrossRef] [PubMed]
6. Ghosh, G.; Padaria, J.C. Application of CRISPR/Cas9 in the improvement of industrially important crops. In *Industrial Crops Improvement: Biotechnological Approaches for Sustainable Agricultural Development*; Springer Nature: Cham, Switzerland, 2025; pp. 239–257.
7. Palumbo, F.; Pasquali, E.; Albertini, E.; Barcaccia, G. A review of unreduced gametes and neopolyploids in alfalfa: How to fill the gap between well-established meiotic mutants and next-generation genomic resources. *Plants* **2021**, *10*, 999. [CrossRef]
8. Wang, H.; Coulman, B.; Bai, Y.; Tar'an, B.; Biligetu, B. Genetic diversity and local adaption of alfalfa populations (*Medicago sativa* L.) under long-term grazing. *Sci. Rep.* **2023**, *13*, 1632. [CrossRef]
9. Hrbáčková, M.; Dvořák, P.; Takáč, T.; Tichá, M.; Luptovčiak, I.; Šamajová, O.; Ovečka, M.; Šamaj, J. Biotechnological perspectives of omics and genetic engineering methods in alfalfa. *Front. Plant Sci.* **2020**, *11*, 592. [CrossRef]
10. He, X.; Zhang, F.; He, F.; Shen, Y.; Yu, L.X.; Zhang, T.; Kang, J. Accuracy of genomic selection for alfalfa biomass yield in two full-sib populations. *Front. Plant Sci.* **2022**, *13*, 1037272. [CrossRef]
11. Long, R.; Zhang, F.; Zhang, Z.; Li, M.; Chen, L.; Wang, X.; Liu, W.; Zhang, T.; Yu, L.X.; He, F.; et al. Genome assembly of alfalfa cultivar Zhongmu-4 and identification of SNPs associated with agronomic traits. *Genom. Proteom. Bioinform.* **2022**, *20*, 14–28. [CrossRef]
12. Chen, H.; Zeng, Y.; Yang, Y.; Huang, L.; Tang, B.; Zhang, H.; Hao, F.; Liu, W.; Li, Y.; Liu, Y.; et al. Allele-aware chromosome-level genome assembly and efficient transgene-free genome editing for the autotetraploid cultivated alfalfa. *Nat. Commun.* **2020**, *11*, 2494. [CrossRef] [PubMed]
13. Maureira, I.; Osborn, T. Molecular markers in genetics and breeding: Improvement of alfalfa (*Medicago sativa* L.). In *Molecular Marker Systems in Plant Breeding and Crop Improvement*; Lörz, H., Wenzel, G., Eds.; Biotechnology in Agriculture and Forestry; Springer: Berlin/Heidelberg, Germany, 2004; Volume 55, pp. 239–257. [CrossRef]
14. Mejia-Guerra, M.; Zhao, D.; Sheehan, M. Genomic resources for breeding in alfalfa: Availability, utility, and adoption. In *The Alfalfa Genome*; Springer: Berlin/Heidelberg, Germany, 2021. [CrossRef]
15. Yang, B.; Zhao, Y.; Guo, Z. Research progress and prospect of alfalfa resistance to pathogens and pests. *Plants* **2022**, *11*, 2008. [CrossRef]
16. McNeill, M.; Tu, X.; Altermann, E.; Wu, B.; Shi, S. Sustainable management of *Medicago sativa* for future climates: Insect pests, endophytes, and multitrophic interactions in a complex environment. *Front. Agron.* **2022**, *4*, 825087. [CrossRef]
17. Singh, B.K.; Delgado-Baquerizo, M.; Egidi, E.; Guirado, E.; Leach, J.E.; Liu, H.; Trivedi, P. Climate change impacts on plant pathogens, food security and paths forward. *Nat. Rev. Microbiol.* **2023**, *21*, 640–656. [CrossRef] [PubMed]
18. Näpflin, K.; O'Connor, E.A.; Becks, L.; Bensch, S.; Ellis, V.A.; Hafer-Hahmann, N.; Harding, K.C.; Lindén, S.K.; Olsen, M.T.; Roved, J.; et al. Genomics of host-pathogen interactions: Challenges and opportunities across ecological and spatiotemporal scales. *PeerJ* **2019**, *7*, e8013. [CrossRef]
19. Pfeilmeier, S.; George, J.; Morel, A.; Roy, S.; Smoker, M.; Stransfeld, L.; Downie, J.A.; Peeters, N.; Malone, J.G.; Zipfel, C. Expression of the Arabidopsis thaliana immune receptor EFR in Medicago truncatula reduces infection by a root pathogenic bacterium, but not nitrogen-fixing rhizobial symbiosis. *Plant Biotechnol. J.* **2019**, *17*, 569–579. [CrossRef]

20. Stefanova, G.; Slavov, S.; Gecheff, K.; Vlahova, M.; Atanassov, A. Expression of recombinant human lactoferrin in transgenic alfalfa plants. *Biol. Plant* **2013**, *57*, 457–464. [CrossRef]
21. He, F.; Xu, M.; Liu, H.; Xu, Y.; Long, R.; Kang, J.; Yang, Q.; Chen, L. Unveiling alfalfa root rot resistance genes through an integrative GWAS and transcriptome study. *BMC Plant Biol.* **2025**, *25*, 58. [CrossRef] [PubMed]
22. Ma, Y.; Marzougui, A.; Coyne, C.J.; Sankaran, S.; Main, D.; Porter, L.D.; Mugabe, D.; Smitchger, J.A.; Zhang, C.; Amin, M.N.; et al. Dissecting the genetic architecture of aphanomyces root rot resistance in lentil by QTL mapping and genome-wide association study. *Int. J. Mol. Sci.* **2020**, *21*, 2129. [CrossRef]
23. Dai, H.; Zhang, X.; Zhao, B.; Shi, J.; Zhang, C.; Wang, G.; Yu, N.; Wang, E. Colonization of mutualistic mycorrhizal and parasitic blast fungi requires OsRAM2-regulated fatty acid biosynthesis in rice. *Mol. Plant-Microbe Interact.* **2022**, *35*, 178–186. [CrossRef]
24. Zamboni, A.; Zanin, L.; Tomasi, N.; Pezzotti, M.; Pinton, R.; Varanini, Z.; Cesco, S. Genome-wide microarray analysis of tomato roots showed defined responses to iron deficiency. *BMC Genom.* **2012**, *13*, 1. [CrossRef]
25. Fan, S.; Xu, X.; Chen, J.; Yin, Y.; Zhao, Y. Genome-wide identification, characterization, and expression analysis of m6A readers-YTH domain-containing genes in alfalfa. *BMC Genom.* **2024**, *25*, 18.
26. Greveniotis, V.; Bouloumpasi, E.; Skendi, A.; Korkovelos, A.; Kantas, D.; Zotis, S.; Ipsilandis, C.G. Modeling stability of alfalfa yield and main quality traits. *Agriculture* **2024**, *14*, 542. [CrossRef]
27. Buxton, D.R. Quality-related characteristics of forages as influenced by plant environment and agronomic factors. *Anim. Feed Sci. Technol.* **1996**, *59*, 37–49. [CrossRef]
28. McCarty, N.S.; Graham, A.E.; Studená, L.; Ledesma-Amaro, R. Multiplexed CRISPR technologies for gene editing and transcriptional regulation. *Nat. Commun.* **2020**, *11*, 1281. [CrossRef] [PubMed]
29. Basu, S.; Ramegowda, V.; Kumar, A.; Pereira, A. Plant adaptation to drought stress. *F1000Research* **2016**, *5*, 1554. [CrossRef]
30. Gao, R.; Wan, Z.-Y.; Jiang, C.; Zhang, J.-F.; Li, Y.-Y.; Wei, Z.-H.; Zhang, X.-Q. Quantitative trait locus analysis of freezing tolerance in alfalfa. *PLoS ONE* **2016**, *11*, e0161670. [CrossRef]
31. Yang, P.; Li, X.; Wang, X.; Chen, H.; Chen, F.; Shen, S.; Li, Y. Proteomic analysis of alfalfa response to heat stress. *PLoS ONE* **2015**, *10*, e0121853. [CrossRef]
32. Najera, V.A.; Twyman, R.M.; Christou, P.; Zhu, C. Applications of multiplex genome editing in higher plants. *Curr. Opin. Biotechnol.* **2019**, *59*, 93–102. [CrossRef]
33. Rahman, M.A.; Song, Y.; Hasan, M.M.; Jahan, M.S.; Siddiqui, M.H.; Park, H.S.; Lee, S.-H.; Singh, D.; Corpas, F.L.; Kabir, A.H.; et al. Mechanistic basis of silicon-mediated cold stress tolerance in alfalfa (*Medicago sativa* L.). *Silicon* **2024**, *16*, 1057–1069. [CrossRef]
34. Fernandes, C.; Barrios, S.; Santos, M.; Nunes, J.A.; Borges do Valle, C.; Jank, L.; Rios, E. Assessing genotype adaptability and stability in perennial forage breeding trials using random regression models for longitudinal dry matter yield data. *G3: Genes Genome Genet.* **2023**, *15*, jkae306. [CrossRef]
35. Sinha, D.; Maurya, A.K.; Abdi, G.; Majeed, M.; Agarwal, R.; Mukherjee, R.; Ganguly, S.; Aziz, R.; Bhatia, M.; Majgaonkar, A.; et al. Integrated genomic selection for accelerating breeding programs of climate-smart cereals. *Genes* **2023**, *14*, 1484. [CrossRef]
36. Govindasamy, P.; Muthusamy, S.K.; Bagavathiannan, M.; Mowrer, J.; Jagannadham, P.T.K.; Maity, A.; Halli, H.M.; Sujayanand, G.K.; Vadivel, R.; Das, T.K.; et al. Nitrogen use efficiency—A key to enhance crop productivity under a changing climate. *Front. Plant Sci.* **2023**, *14*, 1121073. [CrossRef]
37. Wan, W.; Liu, Q.; Li, K.; Zhao, K.; Qi, F.; Li, Y.; Sun, Z.; Li, H. Nitrogen fertilizer application for improving the biomass, quality, and nitrogen fixation of alfalfa (*Medicago sativa* L.) at different growth stages in a saline-alkali soil. *PeerJ* **2025**, *13*, e18796. [CrossRef] [PubMed]
38. Chrysargyris, A.; Tzortzakis, N. Optimizing nitrogen, phosphorus, and potassium requirements to improve Origanum dubium Boiss. growth, nutrient and water use efficiency, essential oil yield, and composition. *Ind. Crops Prod.* **2025**, *224*, 120291.
39. Wang, W.; Hu, B.; Li, A.; Chu, C. NRT1.1s in plants: Functions beyond nitrate transport. *J. Exp. Bot.* **2020**, *71*, 4373–4379. [CrossRef]
40. Remans, T.; Nacry, P.; Pervent, M.; Filleur, S.; Diatloff, E.; Mounier, E.; Tillard, P.; Forde, B.G.; Gojon, A. The Arabidopsis NRT1.1 transporter participates in the signaling pathway triggering root colonization of nitrate-rich patches. *Proc. Natl. Acad. Sci. USA* **2006**, *103*, 19206–19211. [CrossRef]
41. Bouguyon, E.; Brun, F.; Meynard, D.; Kubeš, M.; Pervent, M.; Leran, S.; Lacombe, B.; Krouk, G.; Guiderdoni, E.; Zažímalová, E.; et al. Multiple mechanisms of nitrate sensing by arabidopsis nitrate transceptor NRT1.1. *Nat. Plants* **2015**, *1*, 15015. [CrossRef]
42. Datta, T.; Kumar, R.S.; Sinha, H.; Trivedi, P.K. Small but mighty: Peptides regulating abiotic stress responses in plants. *Plant Cell Environ.* **2024**, *47*, 1207–1223.
43. Ohkubo, Y.; Tanaka, M.; Tabata, R.; Ogawa-Ohnishi, M.; Matsubayashi, Y. Shoot-to-root mobile polypeptides involved in systemic regulation of nitrogen acquisition. *Nat. Plants* **2017**, *3*, 17029. [CrossRef]
44. Medici, A.; Marshall-Colon, A.; Ronzier, E.; Szponarski, W.; Wang, R.; Gojon, A.; Crawford, N.M.; Ruffel, S.; Coruzzi, G.M.; Krouk, G. AtNIGT1/HRS1 integrates nitrate and phosphate signals at the Arabidopsis root tip. *Nat. Commun.* **2015**, *6*, 6274. [CrossRef] [PubMed]

45. Medici, A.; Szponarski, W.; Dangeville, P.; Safi, A.; Dissanayake, I.M.; Saenchai, C.; Emanuel, A.; Rubio, V.; Lacombe, B.; Ruffel, S.; et al. Identification of molecular integrators shows that nitrogen actively controls the phosphate starvation response in plants. *Plant Cell* **2019**, *31*, 1171–1184. [CrossRef]
46. Wang, X.; Kang, W.; Wu, F.; Miao, J.; Shi, S. Comparative transcriptome analysis reveals new insight of alfalfa (*Medicago sativa* L.) cultivars in response to abrupt freezing stress. *Front. Plant Sci.* **2022**, *13*, 798118. [CrossRef]
47. Kellermeier, F.; Armengaud, P.; Seditas, T.J.; Danku, J.; Salt, D.E.; Amtmann, A. Analysis of the root system architecture of Arabidopsis provides a quantitative readout of crosstalk between nutritional signals. *Plant Cell* **2014**, *26*, 1480–1496. [CrossRef] [PubMed]
48. Deng, Q.Y.; Luo, J.T.; Zheng, J.M.; Tan, W.F.; Pu, Z.J.; Wang, F. Genome-wide systematic characterization of the NRT2 gene family and its expression profile in wheat (*Triticum aestivum* L.) during plant growth and in response to nitrate deficiency. *BMC Plant Biol.* **2023**, *23*, 353. [CrossRef]
49. Hirsch, R.E.; Lewis, B.D.; Spalding, E.P.; Sussman, M.R. A role for the AKT1 potassium channel in plant nutrition. *Science* **1998**, *280*, 918–921. [CrossRef]
50. Singer, S.D.; Hannoufa, A.; Acharya, S. Molecular improvement of alfalfa for enhanced productivity and adaptability in a changing environment. *Plant Cell Environ.* **2018**, *41*, 1955–1971. [CrossRef] [PubMed]
51. Straub, T.; Ludewig, U.; Neuhäuser, B. The kinase CIPK23 inhibits ammonium transport in Arabidopsis thaliana. *Plant Cell* **2017**, *29*, 409–422. [CrossRef]
52. Patra, A.K.; Saxena, J. A new perspective on the use of plant secondary metabolites to inhibit methanogenesis in the rumen. *Phytochemistry* **2010**, *71*, 1198–1222. [CrossRef]
53. Sawai, S.; Saito, K. Triterpenoid biosynthesis and engineering in plants. *Front. Plant Sci.* **2011**, *2*, 25. [CrossRef]
54. Tamura, K.; Teranishi, Y.; Ueda, S.; Suzuki, H.; Kawano, N.; Yoshimatsu, K.; Saito, K.; Kawahara, N.; Muranaka, T.; Seki, H. Cytochrome P450 monooxygenase CYP716A141 is a unique β-amyrin C-16β oxidase involved in triterpenoid saponin biosynthesis in *Platycodon grandiflorus*. *Plant Cell Physiol.* **2017**, *58*, 874–884. [CrossRef]
55. Sayama, T.; Ono, E.; Takagi, K.; Takada, Y.; Horikawa, M.; Nakamoto, Y.; Hirose, A.; Sasama, H.; Ohashi, M.; Hasegawa, H.; et al. The *Sg-1* glycosyltransferase locus regulates structural diversity of triterpenoid saponins of soybean. *Plant Cell* **2012**, *24*, 2123–2138. [CrossRef] [PubMed]
56. Sundaramoorthy, J.; Park, G.T.; Komagamine, K.; Tsukamoto, C.; Chang, J.H.; Lee, J.D.; Kim, J.H.; Seo, H.S.; Song, J.T. Biosynthesis of DDMP saponins in soybean is regulated by a distinct UDP-glycosyltransferase. *New Phytol.* **2019**, *222*, 261–274. [CrossRef] [PubMed]
57. Mengstie, M.A.; Azezew, M.T.; Dejenie, T.A.; Teshome, A.A.; Admasu, F.T.; Teklemariam, A.B.; Mulu, A.T.; Agidew, M.M.; Adugna, D.G.; Geremew, H.; et al. Recent advancements in reducing the off-target effect of CRISPR-Cas9 genome editing. *Biol. Targets Ther.* **2024**, *18*, 21–28. [CrossRef]
58. Schaart, J.G.; van de Wiel, C.C.M.; Smulders, M.J.M. Genome editing of polyploid crops: Prospects, achievements, and bottlenecks. *Transgenic Res.* **2021**, *30*, 337–351. [CrossRef] [PubMed]
59. Zhao, H.; Zhao, S.; Cao, Y.; Jiang, X.; Zhao, L.; Li, Z.; Wang, M.; Yang, R.; Zhou, C.; Wang, Z.; et al. Development of a single transcript CRISPR/Cas9 toolkit for efficient genome editing in autotetraploid alfalfa. *Crop J.* **2024**, *12*, 788–795. [CrossRef]
60. Wolabu, T.W.; Mahmood, K.; Jerez, I.T.; Cong, L.; Yun, J.; Udvardi, M.; Tadege, M.; Wang, Z.; Wen, J. Multiplex CRISPR/Cas9-mediated mutagenesis of alfalfa FLOWERING LOCUS Ta1 (MsFTa1) leads to delayed flowering time with improved forage biomass yield and quality. *Plant Biotechnol. J.* **2023**, *21*, 1383–1392. [CrossRef]
61. Jia, C.; Zhao, F.; Wang, X.; Han, J.; Zhao, H.; Liu, G.; Wang, Z. Genomic prediction for 25 agronomic and quality traits in alfalfa (*Medicago sativa*). *Front. Plant Sci.* **2018**, *9*, 1220. [CrossRef]
62. Bottero, E.; Massa, G.; González, M.; Stritzler, M.; Tajima, H.; Gómez, C.; Frare, R.; Feingold, S.; Blumwald, E.; Ayub, N.; et al. Efficient CRISPR/Cas9 genome editing in alfalfa using a public germplasm. *Front. Agron.* **2021**, *3*, 661526. [CrossRef]
63. Shi, K.; Dong, H.; Du, H.; Li, Y.; Zhou, L.; Liang, C.; Şakiroğlu, M.; Wang, Z. The chromosome-level assembly of the wild diploid alfalfa genome provides insights into the full landscape of genomic variations between cultivated and wild alfalfa. *Plant Biotechnol. J.* **2024**, *22*, 1757–1772. [CrossRef] [PubMed]
64. Li, B.; Sun, C.; Li, J.; Gao, C. Targeted genome-modification tools and their advanced applications in crop breeding. *Nat. Rev. Genet.* **2024**, *25*, 603–622. [PubMed]
65. Che, P.; Wu, E.; Simon, M.K.; Anand, A.; Lowe, K.; Gao, H.; Sigmund, A.L.; Yang, M.; Albertsen, M.C.; Gordon-Kamm, W.; et al. Wuschel2 enables highly efficient CRISPR/Cas-targeted genome editing during rapid de novo shoot regeneration in sorghum. *Commun. Biol.* **2022**, *5*, 344. [CrossRef]
66. Subedi, U.; Burton Hughes, K.; Chen, G.; Hannoufa, A.; Singer, S.D. Eliciting targeted mutations in *Medicago sativa* using CRISPR/Cas9-mediated genome editing: A potential tool for the improvement of disease resistance. *Methods Mol. Biol.* **2023**, *2659*, 219–239. [CrossRef] [PubMed]

67. Gao, R.; Feyissa, B.A.; Croft, M.; Hannoufa, A. Gene editing by CRISPR/Cas9 in the obligatory outcrossing *Medicago sativa*. *Planta* **2018**, *247*, 1043–1050. [CrossRef]
68. Wolabu, T.W.; Cong, L.; Park, J.J.; Bao, Q.; Chen, M.; Sun, J.; Xu, B.; Ge, Y.; Chai, M.; Liu, Z.; et al. Development of a highly efficient multiplex genome editing system in outcrossing tetraploid alfalfa (*Medicago sativa*). *Front. Plant Sci.* **2020**, *11*, 1063. [CrossRef]
69. Wolabu, T.W.; Mahmood, K.; Chen, F.; Torres-Jerez, I.; Udvardi, M.; Tadege, M.; Cong, L.; Wang, Z.; Wen, J. Mutating alfalfa COUMARATE 3-HYDROXYLASE using multiplex CRISPR/Cas9 leads to reduced lignin deposition and improved forage quality. *Front. Plant Sci.* **2024**, *15*, 1363182. [CrossRef]

Disclaimer/Publisher's Note: The statements, opinions and data contained in all publications are solely those of the individual author(s) and contributor(s) and not of MDPI and/or the editor(s). MDPI and/or the editor(s) disclaim responsibility for any injury to people or property resulting from any ideas, methods, instructions or products referred to in the content.

MDPI AG
Grosspeteranlage 5
4052 Basel
Switzerland
Tel.: +41 61 683 77 34

International Journal of Molecular Sciences Editorial Office
E-mail: ijms@mdpi.com
www.mdpi.com/journal/ijms



Disclaimer/Publisher's Note: The title and front matter of this reprint are at the discretion of the Guest Editor. The publisher is not responsible for their content or any associated concerns. The statements, opinions and data contained in all individual articles are solely those of the individual Editor and contributors and not of MDPI. MDPI disclaims responsibility for any injury to people or property resulting from any ideas, methods, instructions or products referred to in the content.





Academic Open
Access Publishing

mdpi.com

ISBN 978-3-7258-8210-6